Analytical CHEMISTRY

JULY 1, 1987

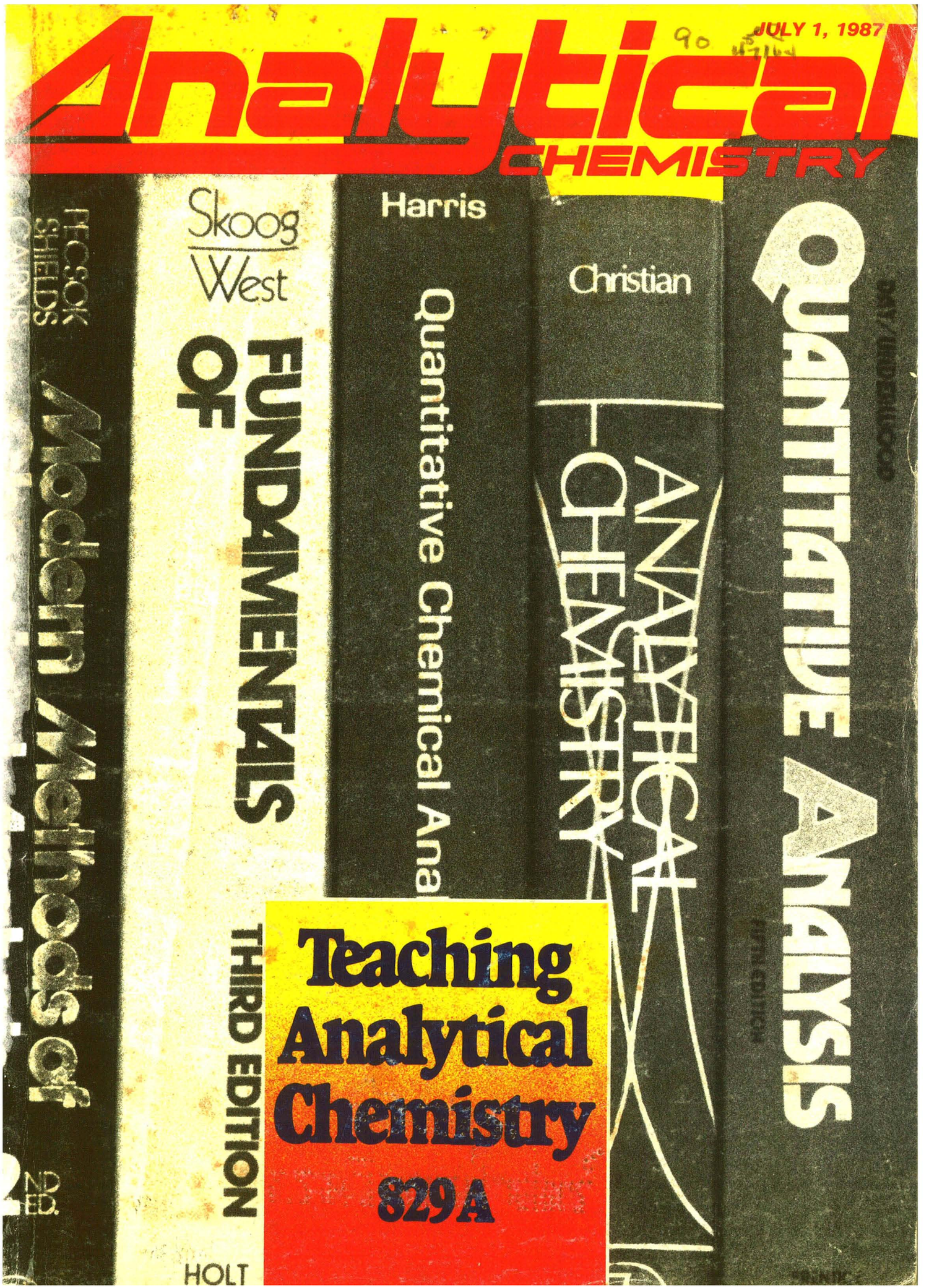

INVEST IN ONE OF OUR NEW FT-IR SPECTROMETERS.

IT'LL GROW ON YOU.

When you invest in a Digilab FT-IR spectrometer you're getting an instrument that's expandable with accessories and software to meet virtually any application you'll ever encounter.

For example, should you ever need expanded IR range, we have additional optical benches (and kits): one for near-IR, another for far-IR, and a vacuum bench for the most demanding far-IR work.

We cover the whole scope of applications by offering the largest range of accessories. These include photoacoustic, diffuse reflectance, three high performance FT-IR microscopes, and ATR for liquids and solids. Our high sensitivity GC/IR system, with full spectrum library search, characterizes complex mixtures rapidly and routinely.

Additional software packages apply four advanced quantitative algorithms to perform accurate multicomponent analyses.

As your laboratory's work load increases, we offer external sample compartments where additional accessories and experiments may be permanently set up. And with desktop Spectroscopic Productivity Centers, you can store and examine spectra with full software power without tying up the spectrometer.

So, when we say "it'll grow on you," we speak not just of your affection for your new FTS spectrometer. We refer as well to its seemingly endless capacity to meet your applications needs and solve your analytical problems.

Call (800) 225 1248 ext. 150 today (in Massachusetts call (617) 868 4330) for more information. Or write Bio-Rad, Digilab Division, 237 Putnam Avenue, Cambridge, MA 02139.

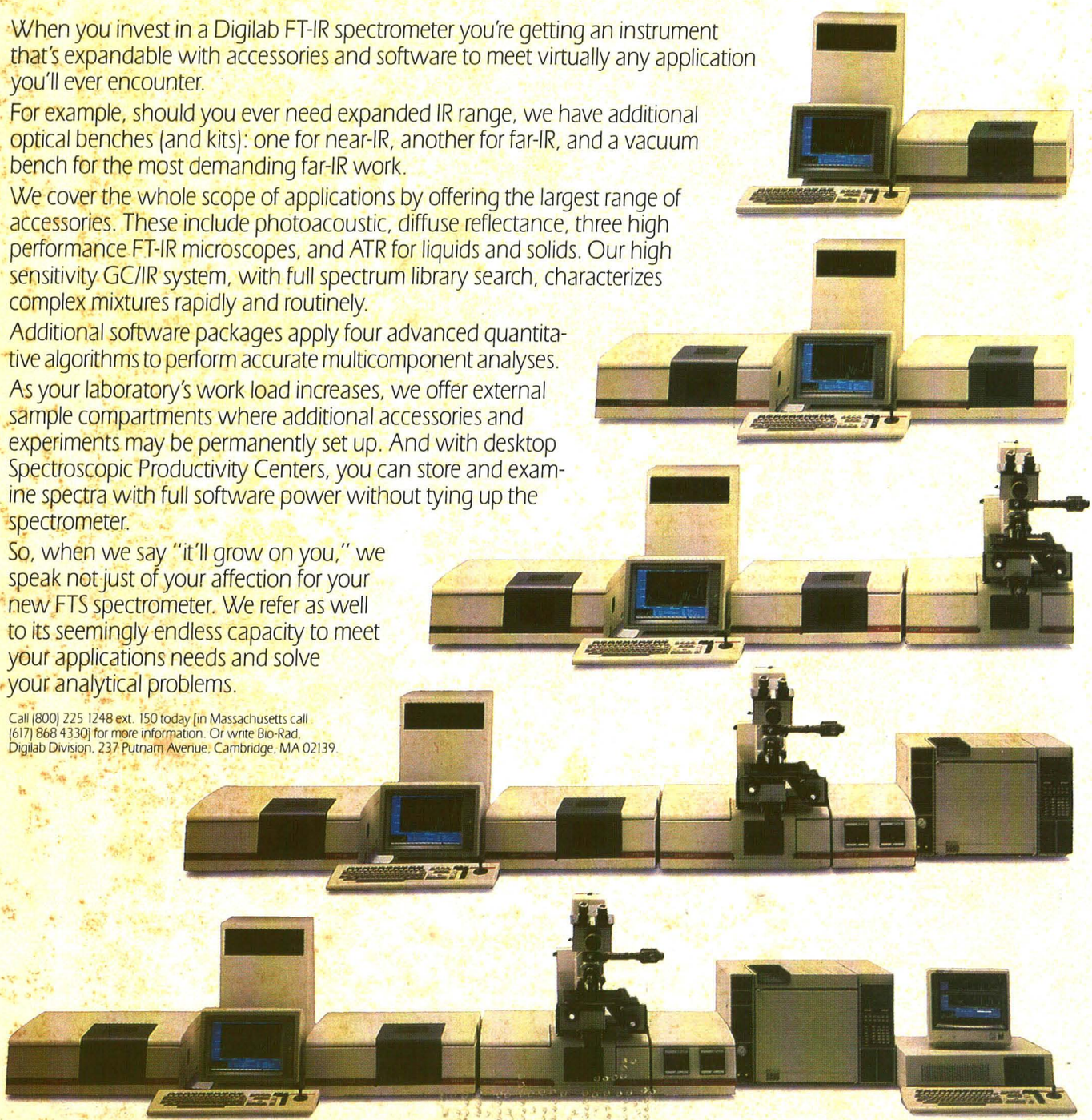

Another optical bench for near or far-IR.

The FTS 60 FT-IR Spectrometer, including research-grade optical bench and expandable data system.

External sample compartment and UMA 300 microscope.

High sensitivity GC/IR accessory (shown with Hewlett-Packard GC).

Spectroscopic Productivity Center for data storage and analysis.

BIO-RAD Digilab Division

CIRCLE 22 ON READER SERVICE CARD

How To Choose The Right Low Pressure LC System Even If It Isn't Ours

To simplify choosing the right peristaltic pump, detector and fraction collector for your LC System, review these guidelines and send for our free Low Pressure System Selection Worksheet:

1 Identify your separation goals.

Know the characteristics of your sample. What mass will you load on your column? What flow rate will you need to achieve optimal speed and resolution? At which wavelengths does your sample exhibit maximum absorbance? What size fractions will you collect? Are you interested in collecting peaks?

2 Examine the components' specs.

After you've identified the key operating parameters, take a look at the pump, detector and fraction collector specifications to be sure they meet your needs. To illustrate, let's look at specifications for components in the Gilson Low Pressure System.

The most important criteria used to select a peristaltic pump are smooth, stable flow and usable flow rate range. The Gilson system uses the new Minipuls 3 Pump. Stepper-motor drive and proven pump head design ensure smooth flow from 1 ul to 50 ml/min. A high flow head allows flow rates from 50 ml to 220 ml/min. Interchangeable pump heads with 1-, 2-, 4-, or 8 channels are available.

Wavelength specificity and ease-of-use are key considerations when choosing a detector. The Gilson 112 UV/VIS fixed-wavelength detector allows selection of wavelengths from 214 nm to 640 nm. A choice of five flow cells accommodates a wide range of flow rates and sample concentrations. A large digital readout and convenient autozero and event mark functions keep detector operation easy.

Select a fraction collector according to your collection mode, fraction volume, and multiple column collection needs. Gilson's FC 203 fraction collector allows drop, time, or peak collection modes with up to ten collection windows in each mode. The widest range of racks available—capable of handling as many as 128 fractions—makes the FC 203 suitable for almost any application.

3 Check for compatibility of components with each other and with your future needs.

At this point, you've identified components to meet basic needs, but also look at the components as a system. Were they designed to work together? Or will you need to buy complicated adapters and special plumbing? Working with a single supplier avoids the service and support problems often associated with a system assembled piece-by-piece.

You should also assess your future needs. An LC system may work fine for your current application. But will you need to change detection wavelengths or collection volumes later? Is an upgrade to HPLC a possibility? If so, consider modular equipment that adapts to your changing needs easily and inexpensively.

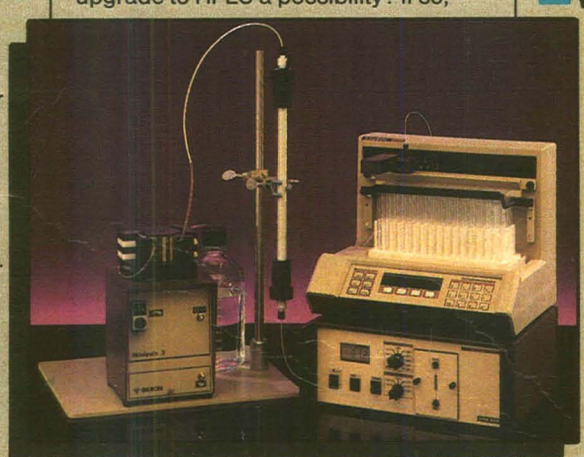

4 Look at each supplier's record of reliability, service and support.

After identifying suitable components, you narrow your choice by looking at each supplier's track record for reliable equipment and efficient service.

To evaluate the Gilson Low Pressure System, consider our reputation for fraction collectors and detectors. Gilson has a proven track record that began more than 35 years ago. More than 1000 FC 203s—introduced just 16 months ago—continue to display dependable, trouble-free operation.

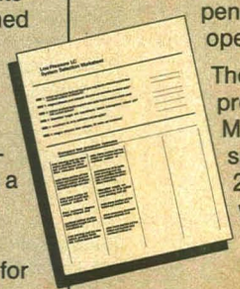

The Minipuls 2, the reliable predecessor to our new Minipuls 3, has earned spaces on more than 24,000 lab benches worldwide, making it the best-selling peristaltic pump.

5 Use our free Low Pressure LC System Selection Worksheet to gather and compare your options.

For the final step in choosing your system, compare the information you've gathered. To help, we've put together a selection worksheet to simplify the process.

This free worksheet lists major criteria to use in your comparisons. We've filled in information about the Gilson Low Pressure System and have left space for you to fill in specs from other suppliers.

Why do we encourage this comparison? Because it's the best way to buy a system matched to your needs. Plus, we're confident that in most cases your low pressure system will be a Gilson Low Pressure System.

So, for your free Low Pressure System Selection Worksheet, simply circle the number below on the magazine's reader service card. We'll see that you get your worksheet fast.

GILSON

Gilson Medical Electronics, Inc., Box 27, 3000 W. Beltline Hwy., Middleton, WI 53562 USA, Tel: (608) 836-1551, Telex: 26-5478
Gilson Medical Electronics (France) S.A., 72 Rue Gambetta, B.P. No. 45,95400, Villiers-Le-Bel, France, Tel: (1) 39.90.54.41, Telex: 696682

Circle 61 for free worksheet

Circle 62 for product literature

TOP GUN IN THE PURITY SHOOT OUT-

Burdick & Jackson

Talk is cheap. Anybody can say they're the leader in solvent purity. However, if you're more impressed with objective test results, only one company can prove they're the Top Gun in a recent solvent purity shootout. And that's Burdick & Jackson.

Here's the score.

SOLVENT COMPARISON DATA

SOLVENT	BRAND	ANALYSIS	RESULTS	BJ SPEC	TYPICAL B&J VALUE
Acetone	Competitor "E" Lot #6211 Lot #6245	Electron Capture	Failed	<10 ppt As Heptachlor Epoxide	2 ppt
Acetonitrile	Competitor "E" Lot #6248 Lot #6268	UV Absorbance	Failed	<0.01 A	0.007 A
Hexane HPLC-Grade	Competitor "F" Lot #860805	Electron Capture	Failed	<10 ppt As Heptachlor Epoxide	2 ppt
Methyl t-Butyl Ether	Competitor "E" Lot #5056	Electron Capture	Failed	<10 ppt EC As Heptachlor Epoxide	2 ppt
Methyl t-Butyl Ether HPLC-Grade	Competitor "F" Lot #856140	Electron Capture	Failed	<10 ppt As Heptachlor Epoxide	2 ppt
Methylene Chloride HPLC-Grade	Competitor "F" Lot #864521	Electron Capture	Failed	<10 ppt As Heptachlor Epoxide	2 ppt
Methylene Chloride	Competitor "B" Lot #617100	Water	Failed	<0.01%	0.005%
		Electron Capture	Failed	<10 ppt As Heptachlor Epoxide	2 ppt
Water	Competitor "B" Lot #626088	pH	Failed pH=8.8	pH Between 5.8 & 8.0	6.3
Water	Competitor "E" Lot #6225	pH	Failed pH=9.2	pH Between 5.8 & 8.0	6.3

In a recent competitive product study, 11 out of 20 lots tested failed to meet Burdick & Jackson quality assurance specifications.

For complete test results in the B&J solvent purity shootout, write: Burdick & Jackson, 1953 South Harvey Street, Muskegon, Michigan 49442. For additional technical assistance, please call us toll free at 800 368 0050.

Manufactured by
Burdick & Jackson
A Division of Travenol Laboratories, Inc.
1953 South Harvey Street
Muskegon, MI USA 49442
Telephone 616 726 3171
800 368 0050

Distributed Exclusively in USA by
American Scientific Products
A Division of Travenol Laboratories, Inc.
1430 Waukegan Rd.
McGaw Park, IL USA 60085
Telephone 312 689 8410

© 1987 Baxter Travenol Laboratories, Inc.

CIRCLE 20 ON READER SERVICE CARD

JULY 1, 1987
VOLUME 59
NUMBER 13

ANCHAM
59(13) 799A–866A/1585–1744 (1987)
ISSN 0003 2700

Registered in U.S. Patent and Trademark Office; Copyright 1987 by the American Chemical Society

ANALYTICAL CHEMISTRY (ISSN 0003-2700) is published semimonthly by the American Chemical Society at 1155 16th St., N.W., Washington, D.C. 20036. Editorial offices are located at the same ACS address (202-872-4600; TDD 202-872-8733). Second-class postage paid at Washington, D.C., and additional mailing offices. Postmaster: Send address changes to ANALYTICAL CHEMISTRY Membership & Subscription Services, P.O. Box 3337, Columbus, Ohio 43210.

Claims for missing numbers will not be allowed if loss was due to failure of notice of change of address to be received in the time specified; if claim is dated (a) North America: more than 90 days beyond issue date, (b) all other foreign: more than one year beyond issue date, or if the reason given is "missing from files."

Copyright Permission: An individual may make a single reprographic copy of an article in this publication for personal use. Reprographic copying beyond that permitted by Section 107 or 108 of the U.S. Copyright Law is allowed, provided that the appropriate per-copy fee is paid through the Copyright Clearance Center, Inc., 27 Congress St., Salem, Mass. 01970. For reprint permission, write Copyright Administrator, B&J Division, ACS, 1155 16th St., N.W., Washington, D.C. 20036.

Registered names and trademarks, etc., used in this publication, even without specific indication thereof, are not to be considered unprotected by law.

Advertising Management: Centcom, Ltd., 500 Post Rd. East, Westport, Conn. 06880 (203-226-7131)

1987 subscription rates include air delivery outside the U.S., Canada, and Mexico

	1 yr	2 yr
Members		
Domestic	$ 25	$ 42
Canada and Mexico	50	92
Europe	77	146
All Other Countries	104	200
Nonmembers		
Domestic	37	62
Canada and Mexico	62	112
Europe	127	231
All Other Countries	154	285

Three-year and other rates contact: Membership & Subscription Services, ACS, P.O. Box 3337, Columbus, Ohio 43210 (614-421-3776).

Subscription orders by phone may be charged to Visa, MasterCard, Barclay card, Access, or American Express. Call toll free at (800) ACS-5558 from anywhere in the continental United States; from Washington, D.C., call 872-8065. Mail orders for new and renewal subscriptions should be sent with payment to the Business Management Division, ACS, P.O. Box 57136, West End Station, Washington, D.C. 20037.

Subscription service inquiries and changes of address (Include both old and new addresses with ZIP code and *recent mailing label*) should be directed to the ACS Columbus address noted above. Please allow six weeks for change of address to become effective.

ACS membership information: Bebe Olsen, Washington address.

Single issues, current year, $5.00 except review issue and LabGuide, $10.00; **back issues and volumes and microform editions** available by single volume or back issue collection. For information or to order, call (800) ACS-5558 or write the Sales Department at the Washington address.

Nonmembers rates in Japan: Rates above do not apply to nonmember subscribers in Japan, who must enter subscription orders with Maruzen Company Ltd., 3–10 Nihonbashi 2-chome, Chuo-ku, Tokyo, 103, Japan. Tel: (03) 272-7211.

Analytical CHEMISTRY

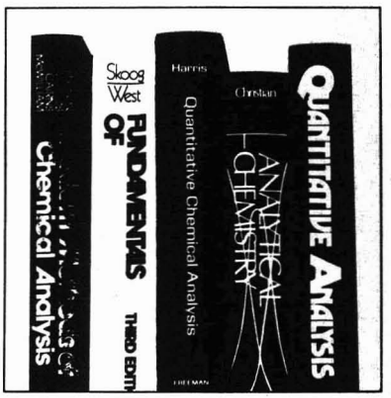

REPORT **823 A**

Teaching analytical chemistry—another view. Predominantly undergraduate institutions play a major role in the education of future analytical chemists. Royce C. Engstrom of the University of South Dakota urges those contemplating an academic career to consider the unique opportunities these schools offer

REPORT **829 A**

On the cover. **The curriculum in quantitative analysis.** What is being taught in quantitative analysis courses in the United States? William E. L. Grossman and David C. Locke of the City University of New York describe the results of a survey of approximately 300 colleges and universities and pose basic questions about the curriculum

BRIEFS **806 A**

EDITORIAL **815 A**

Quantitative analysis. Readers are invited to respond to the proposed new chemistry curriculum and to address in particular how much analytical chemistry should be included in the recommended three-year core curriculum

NEWS **817 A**

The Merck Award for Analytics will be presented for the first time in October 1988. ▸ **Hirschfeld Award in Near-Infrared Analysis:** nominations sought. ▸ **Coretech adopts R&D agenda action items**

MEETINGS **838 A**

The 26th Eastern Analytical Symposium will be held Sept. 13–18 in New York City's Hilton Hotel. The meeting will feature 340 papers, short courses, workshops, and an exposition of scientific equipment

BOOKS **852 A**

Critical reviews. Books on software applications in chemistry and on detectors for liquid chromatography are reviewed by Michael Delaney and Ira Krull

FOCUS **855 A**

LC/MS and SFC/MS: Will they replace GC/MS? was addressed at a symposium organized by Richard Browner of the Georgia Institute of Technology at this year's Pittsburgh Conference

NEW PRODUCTS & MANUFACTURERS' LITERATURE **860 A**

AUTHOR INDEX **1585**

FT-IR Computers: The Choice is Yours.

VAX, MicroVAX, VMS, LIMS/SM are registered trademarks of Digital Equipment Corporation.

Over a decade ago, Nicolet developed the first specialized laboratory computers for high-speed, high-accuracy FT processing. Since that time, more Nicolet computers have been utilized for FT spectroscopy than any other computer! Now, we have expanded our leadership in the computerized FT-IR laboratory in three important areas:

1. PC-based spectrometer systems. The outcome of Nicolet's acquisition of IBM Instruments' bench-top FT-IR

PC-IR main command menu.

systems earlier this year is a new series of PC-based spectrometer systems. These bench-top spectrometers combine the general purpose, cost-effective utility of the PC with the expanded application capabilities of Nicolet optics and accessories.

"Nicolet FT-IR computer workstations give you the advantages of high-speed interactive spectral processing, cost-effective, general-purpose PC control and integrated laboratory networking."

2. Laboratory networking. Nicolet is the first authorized FT-IR company to tie FT-IR into the Digital Equipment Corporation integrated laboratory network. With Nicolet's NIC-COM communication software, FT-IR spectroscopic information, quantitative analysis results and other information can be directly linked to the VAX LIMS/SM® environment as part of a complete laboratory information network. The Nicolet "VAX® Connection" also provides complete FT-IR data manipulation capabilities for VAX/VMS® computers.

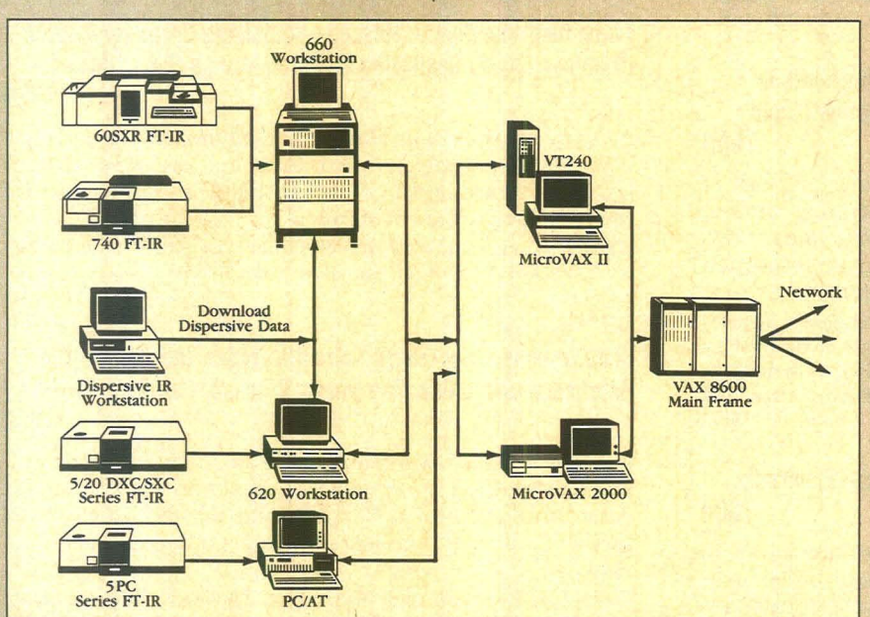

Nicolet brings it all together with communications software to tie FT-IR into the VAX LIMS/SM® network.

3. Dual-bus computer architecture. Nicolet's new 600 Series computers with dual-bus architecture further enhance your spectral processing capabilities by providing the perfect combination of high-speed interactive spectral processing functions (on the Nicolet Bus) and industry-standard interfacing (with the SCSI Bus) to the latest data system storage devices, peripherals, and accessories. Whether you need to download/integrate dispersive IR data into your FT-IR, interface

TGA-IR is one of many new hypenated techniques supported by the 600 Series workstation.

to your laboratory PC, or integrate your FT-IR systems into a laboratory network, the 600 Series has all the adaptability you need plus the unmatched real-time processing performance you'd expect from the FT-IR industry leader.

Let us demonstrate the application benefits of Nicolet FT-IR workstations in your laboratory. For more information, contact: Nicolet Analytical Instruments, 5225-1 Verona Road, Madison, WI 53711, Phone 608/271-3333.

digital™ Cooperative Marketing Program

Nicolet

INSTRUMENTS OF DISCOVERY

CIRCLE 110 ON READER SERVICE CARD

BRIEFS

Simulation of Carbon-13 Nuclear Magnetic Resonance Spectra of Substituted Cyclopentanes and Cyclopentanols 1586

Chemical shift models developed for conformationally flexible molecules simulate the spectra with sufficient accuracy for library search retrieval of the observed spectra for a set of similar compounds.

Debra S. Egolf and Peter C. Jurs*, Department of Chemistry, 152 Davey Laboratory, The Pennsylvania State University, University Park, Pa. 16802 *Anal. Chem., 59 (1987)*

Ion and Temperature Dependence of Electrical Conductance for Natural Waters 1594

The accuracy of four empirical equations describing the temperature dependence of electrical conductance of aqueous solutions is compared, and an improved equation applicable to environmental samples is evaluated.

John A. Sorensen, Department of Chemistry, University of Minnesota–Duluth, Duluth, Minn. 55812, and **Gary E. Glass***, Environmental Research Laboratory–Duluth, U.S. Environmental Protection Agency, 6201 Congdon Boulevard, Duluth, Minn. 55804 *Anal.Chem., 59 (1987)*

Effects of Blood Standards on Interlaboratory Variation in the Assay of Blood Selenium 1597

The benefits of using a common set of standards—preferably those of similar matrix and selenium concentration to the samples—in reducing interlaboratory CVs for determination of blood selenium are demonstrated.

Tee-Siaw Koh, Central Veterinary Laboratories, Department of Agriculture, IMVS, Frome Road, South Australia 5000, Australia *Anal. Chem., 59 (1987)*

Lithium/Sodium Ion Concentration Ratio Measurements in Blood Serum with Lithium and Sodium Ion Selective Liquid Membrane Electrodes 1600

A flow-through electrode system that requires ≤0.1 mL of sample is used to determine Li^+/Na^+ concentration ratios in serum samples from manic-depressive patients under lithium treatment. Results are compared with atomic absorption spectrometry–flame photometry measurements.

Erich Metzger, René Dohner, and Wilhelm Simon*, Department of Organic Chemistry, Swiss Federal Institute of Technology (ETH), CH-8092 Zürich, Switzerland, and **Dieter J. Vonderschmitt and Kurt Gautschi,** University Hospital, Zürich, Switzerland *Anal. Chem., 59 (1987)*

Selectivity Properties of Sodium Glass Membrane Electrodes under Non-Steady-State Conditions 1604

Sodium-selective glass membrane electrodes are shown to possess poor selectivity properties when used under non-steady-state conditions. Results indicate that "effective" selectivity coefficients are required when glass electrodes are used as detectors in automated systems.

Julie Wangsa and Mark A. Arnold*, Department of Chemistry, University of Iowa, Iowa City, Iowa 52242 *Anal. Chem., 59 (1987)*

Application of Polymer-Coated Glassy Carbon Electrodes in Anodic Stripping Voltammetry 1608

A Nafion perfluorosulfonate resin-coated mercury film electrode offers better resistance to organic interferences and, in some cases, higher sensitivity than does the conventional thin mercury film electrode.

Boy Hoyer, T. Mark Florence*, and Graeme E. Batley, CSIRO, Division of Energy Chemistry, Private Mail Bag 7, Menai, New South Wales 2234, Australia *Anal. Chem., 59 (1987)*

Repetitive in Situ Renewal and Activation of Carbon and Platinum Electrodes: Applications to Pulse Voltammetry 1615

In situ laser activation of solid electrodes leads to improved reversibility, lifetime, and reproducibility. Enhanced resolution is observed for laser-assisted voltammetric determination of several organic compounds, including phenol, dopamine, ascorbic acid, and hydroquinone.

Melanie Poon and Richard L. McCreery*, Department of Chemistry, The Ohio State University, 120 West 18th Avenue, Columbus, Ohio 43210 *Anal. Chem., 59 (1987)*

Maximum Likelihood Quantitative Estimates for Peaks: Application to Photoacoustic Spectroscopy 1620

The method of maximum likelihood is found to be suitable for quantitative interpretation of signal peaks in photoacoustic spectroscopy, in which it reduces detection limits by a factor of five over peak amplitude measurements.

P. E. Poston and J. M. Harris*, Department of Chemistry, University of Utah, Salt Lake City, Utah 84112 *Anal. Chem., 59 (1987)*

Trace Determination of Nitrogen-Containing Drugs by Surface Enhanced Raman Scattering Spectrometry on Silver Colloids 1626

Analytical calibration curves of *p*-aminobenzoic acid and 2-aminofluorene yield straight lines, and the slopes of their log–log plots are close to unity. Absolute detection limits for these compounds are 35 ng and 7 ng, respectively.

Edith L. Torres and J. D. Winefordner*, Department of Chemistry, University of Florida, Gainesville, Fla. 32611
Anal. Chem., 59 (1987)

Simultaneous Laser-Based Refractive Index and Absorbance Determinations within Micrometer Diameter Capillary Tubes 1632

A 1-mW helium–neon probe laser and a 2-mW helium–cadmium pump laser are employed to generate refractive index detection limits of 4×10^{-6} ΔRI and absorbance detection limits of 6.3×10^{-6} measured across a 50-μm diameter cuvette.

Darryl J. Bornhop and Norman J. Dovichi*, Department of Chemistry, University of Alberta, Edmonton, Alberta T6G 2G2, Canada *Anal. Chem., 59 (1987)*

* Corresponding author

Our newest Spectronic system withstands the tests of time.

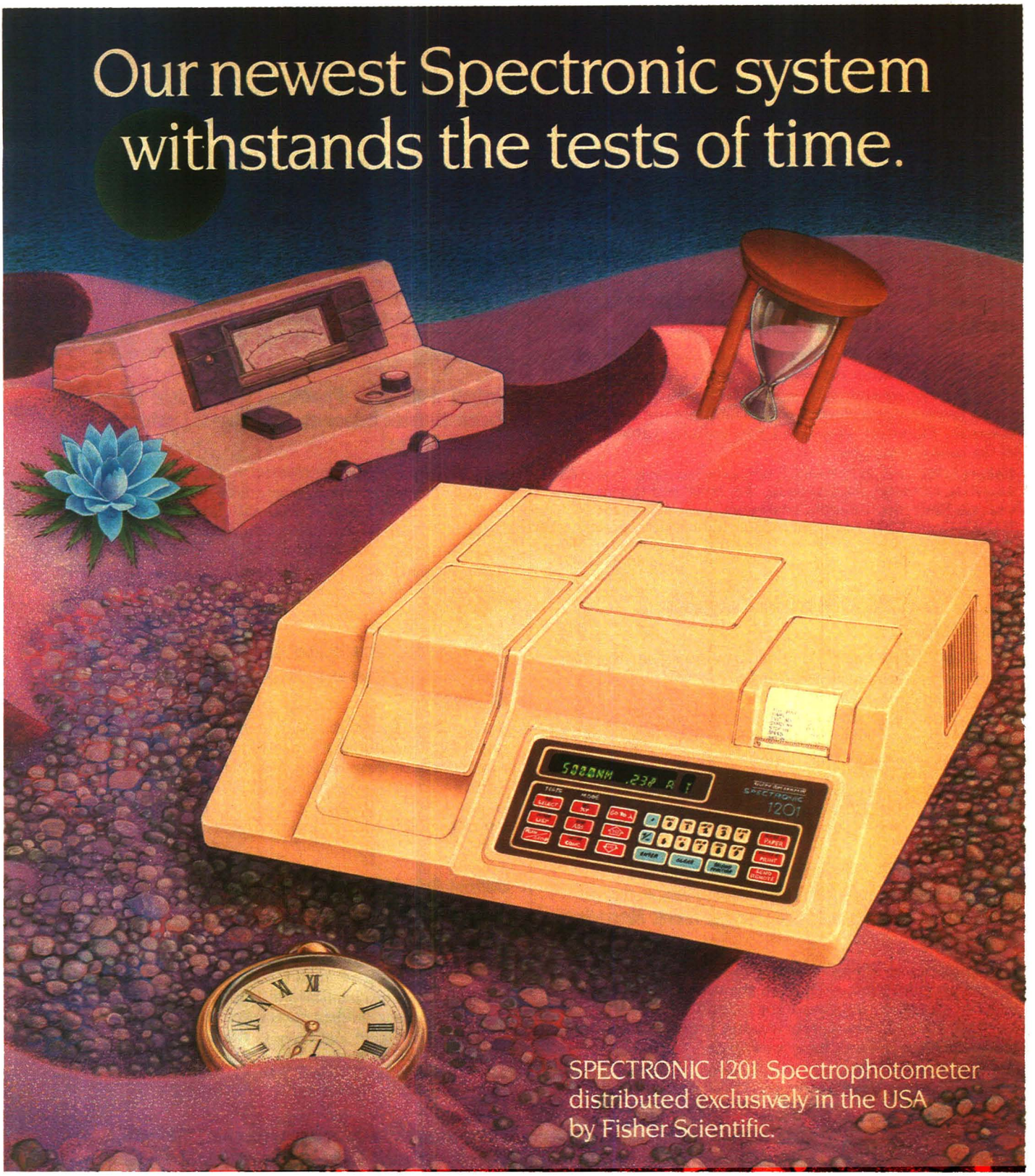

Time was, you had to program every test manually. No matter how often you needed to do it. • Now, the new SPECTRONIC® 1201 Spectrophotometer has features that save you testing time. And increase your productivity. • Start with automatic, preprogrammed test formats. You can repeat the same tests like linear and non-linear standard curves. Kinetics and absorbance ratio. Quickly, easily and accurately. At the touch of a button. • Add the SPEC 1201's unique dual-beam optical system which provides both stability *and* high energy for optimum reliability with greater sensitivity. So you'll have greater faith in your readings. And repeatability in your tests. Time after time. • Plus, the SPEC 1201's high-resolution wavelength scanning moves at speeds up to 3000 nm per minute. And it's ready to hook up with your computer or recorder. • Perhaps the best feature of the SPEC 1201 is one that withstands the true test of time. And that's the 35-year history of technical excellence and superior performance of its forerunner, the SPECTRONIC 20 Spectrophotometer. Some things will never change. Such as the quality and reliability you've come to expect from the SPECTRONIC name and Milton Roy. And the nationwide network of factory-trained service specialists who deliver prompt and complete instrument support. • High stability. Superior accuracy. Remarkable results. At an affordable price. • Call now for a free demonstration of the new SPEC 1201. 800-922-0826, 716-248-4000 in NYS.

2E029

MILTON ROY

CIRCLE 95 ON READER SERVICE CARD

BRIEFS

Fluorescence Emission as a Probe To Investigate Electrochemical Polymerization of 9-Vinylanthracene 1636

An in situ spectroelectrochemical technique that uses the photophysical property of the polymer to monitor the electropolymerization process is described. The technique should be useful for obtaining kinetic and mechanistic information about electropolymerization.

Prashant V. Kamat, Radiation Laboratory, University of Notre Dame, Notre Dame, Ind. 46556 *Anal. Chem., 59 (1987)*

Error Modeling and Confidence Interval Estimation for Inductively Coupled Plasma Calibration Curves 1639

Iteratively weighted error modeling for nonconstant variance ICP calibration curves is examined. Contributions of calibration bands and unknown sample measurement uncertainty levels are combined to obtain multiple-use confidence intervals. The effects of weighting are examined at both ends of the calibration curve.

Robert L. Watters, Jr.*, National Bureau of Standards, Center for Analytical Chemistry, Gaithersburg, Md. 20899, and **Raymond J. Carroll,** University of North Carolina at Chapel Hill, Chapel Hill, N.C. 27514, and **Clifford H. Spiegelman,** National Bureau of Standards, Center for Applied Mathematics, Gaithersburg, Md. 20899 *Anal. Chem., 59 (1987)*

External Heavy-Atom Effect in Room-Temperature Phosphorescence 1644

Time-resolved studies are conducted to investigate the RTP of dibenzo[*f*,*h*]quinoxaline adsorbed on filter paper substrate. The selective heavy-atom enhancement of vibronic bands of different symmetries in RTP analysis is discussed.

Georg W. Suter*, Alan J. Kallir, and Urs P. Wild, Physical Chemistry Laboratory, Swiss Federal Institute of Technology, ETH-Zentrum, CH-8092 Zurich, Switzerland, and **Tuan Vo-Dinh,** Advanced Monitoring Development Group, Health and Safety Research Division, Oak Ridge National Laboratory, Oak Ridge, Tenn. 37831-6101 *Anal. Chem., 59 (1987)*

Direct Experimental Evidence for in Situ Graphite and Palladium Selenide Formations with Improvement on the Sensitivity of Selenium in Graphite Furnace Atomic Absorption Spectrometry 1647

The presence of albumin on the surface of a pyrolitically coated graphite tube, along with the use of palladium as a matrix modifier, improves the selenium sensitivity of GFAAS. Electron microprobe studies present evidence for the mechanism behind these two effects.

Janet E. Teague-Nishimura and Takeshi Tominaga, Department of Chemistry, Faculty of Science, University of Tokyo, Hongo, Bunkyo-ku, Tokyo 113, Japan, and **Tsutomu Katsura,** Environmental Safety Center, Waseda University, Okubo, Shinjuku-ku, Tokyo 160, Japan, and **Kazuko Matsumoto*,** Department of Chemistry, School of Science and Engineering, Waseda University, Shinjuku-ku, Tokyo 160, Japan *Anal. Chem., 59 (1987)*

High-Performance Tandem Mass Spectrometry: Calibration and Performance of Linked Scans of a Four-Sector Instrument 1652

A method is developed for calibration of linked scans at constant B/E in a four-sector mass spectrometer. A single calibration curve from 0 to 3500 u yields product ion mass accuracies of better than 0.3 u for any precursor ion within this range.

Kimio Sato, Tohru Asada, Morio Ishihara, Fumio Kunihiro, Yoshihiro Kammei, and Eiji Kubota, JEOL, Ltd., Nakagami Akishima, Tokyo 197, Japan, and **Catherine E. Costello, Stephen A. Martin, Hubert A. Scoble, and Klaus Biemann*,** Department of Chemistry, Massachusetts Institute of Technology, Cambridge, Mass. 02139 *Anal. Chem., 59 (1987)*

Analysis of Molecular Orientational Order in Solid Samples by Nuclear Magnetic Resonance: Application to Lignin and Cellulose in Wood 1659

Two-dimensional Fourier transform solid state NMR is used to probe molecular orientation order of specific components in wood samples. Results for *Eucalyptus polyanthemus* reveal that there is no net molecular orientation order of lignin or cellulose over a macroscopic volume of about 0.9 cm^3.

Galen R. Hatfield, Mazier Sardashti, and Gary E. Maciel*, Department of Chemistry, Colorado State University, Fort Collins, Colo. 80523 *Anal. Chem., 59 (1987)*

Use of the Microwave-Induced Nitrogen Discharge at Atmospheric Pressure as an Ion Source for Elemental Mass Spectrometry 1664

Analytical characteristics for a MINDAP used as an ion source for elemental mass spectrometry are determined and compared with those obtained by ICP-MS. Detection limits for five elements range from 3 to 22 ng/mL.

Daniel A. Wilson, George H. Vickers, and Gary M. Hieftje*, Department of Chemistry, Indiana University, Bloomington, Ind. 47405 *Anal. Chem., 59 (1987)*

Collision-Activated Dissociation of Negative Ions in an Ion Trap Mass Spectrometer 1670

Polyatomic anions derived from several dinitrotoluene isomers, 2,4,6-trinitrotoluene, and 1,3,5-trinitro-1,3,5-triazocyclohexane are formed in an ion trap mass spectrometer by using negative ion chemical ionization and subsequently dissociated by using tandem mass spectrometric methods.

Scott A. McLuckey* and Gary L. Glish, Analytical Chemistry Division, Oak Ridge National Laboratory, Oak Ridge, Tenn. 37831, and **Paul E. Kelley,** Finnigan-MAT Corporation, 355 River Oaks Parkway, San Jose, Calif. 95134 *Anal. Chem., 59 (1987)*

Stable Isotope Dilution Thermospray Liquid Chromatography/Mass Spectrometry Method for Determination of Sugars and Sugar Alcohols in Humans 1674

Thermospray LC/MS allows identification and quantitation of saccharides and sugar alcohols in biological fluids without derivatization. Labeled glucose can be detemined in blood at tracer levels (< 1 % of total glucose) with an RSD of < 10%. Sorbitol concentration in amniotic fluid can be determined with an RSD of < 3%.

Nora V. Esteban, Daniel J. Liberato, James B. Sidbury, and Alfred L. Yergey*, Laboratory of Theoretical and Physical Biology, National Institute of Child Health, National Institutes of Health, Building 6, Room 136, Bethesda, Md. 20892
Anal. Chem., 59 (1987)

THE CHOICE OF SUPERCRITICAL CHEMISTS.

Sample introduction in SFC is critical. When you read a paper on Supercritical Fluid Chromatography you find that the same injector is mentioned over and over again . . . the Valco CI4W. The CI4W is specially made to withstand the high pressures required in HPLC, meet the more critical gas-tight standards of helium leak testing, and specially designed to minimize band-spreading. But the Valco CI4W is only one member of the world's largest family of rotary valves and injectors manufactured for HPLC, GC, and SFC; *all* designed to meet these standards.

CIRCLE 170 ON READER SERVICE CARD

VICI **Valco Instruments Co. Inc.**
P.O. Box 55603, Houston, TX 77255 USA
Telephone (713) 688-9345
Telefax (713) 688-8106 Telex 79-0033 VALCO HOU

VICI AG **Valco Europe**
Untertannberg 7 CH-6214 Schenkon, Switzerland
Telephone (045) 21 68 68
Telefax (045) 21 30 20 Telex 868342 VICI CH

Sales Calls 1-800-FOR-VICI

BRIEFS

Instrumentation, Applications, and Energy Deposition in Quadrupole Ion-Trap Tandem Mass Spectrometry 1677

An ion-trap mass spectrometer is adapted for tandem mass spectrometry. Ions are created within the trap, undesired ions are ejected from the trap, and the selected parent ion undergoes collisionally activated dissociation. Extremely high CAD efficiencies are readily achieved.

John N. Louris and R. Graham Cooks*, Department of Chemistry, Purdue University, West Lafayette, Ind. 47907, and **John E. P. Syka, Paul E. Kelley, and George C. Stafford, Jr.,** Finnigan MAT, 355 River Oaks Parkway, San Jose, Calif. 95134, and, **John F. J. Todd,** Chemical Laboratory, University of Kent, Canterbury, Kent, CT 27NH, U.K. *Anal. Chem., 59 (1987)*

Focused, Rasterable, High-Energy Neutral Molecular Beam Probe for Secondary Ion Mass Spectrometry 1685

A unique neutralization mechanism is employed to produce a focusable, fast neutral molecular beam probe for SIMS/FABMS. The beam is shown to be very effective for sputtering secondary ions from nonconductive samples. Application to FT-ICR SIMS is also discussed.

Anthony D. Appelhans, James E. Delmore*, and David A. Dahl, Idaho National Engineering Laboratory, EG&G Idaho, P.O. Box 1625, Idaho Falls, Idaho 83415 *Anal. Chem., 59 (1987)*

Effect of Sample-Charge Volume on the Sensitivity of Chromatographic Analysis 1692

A simple model makes it possible to quantify the gain in the sensitivity of the analyte-mass determination brought about by concentrating the sample. The theoretical results compare favorably with results obtained from an experimental test of the model.

Michal Roth* and Josef Novak, Institute of Analytical Chemistry, Czechoslovak Academy of Sciences, 61142 Brno, Czechoslovakia *Anal. Chem., 59 (1987)*

Identification of Mutagenic Methylbenz[*a*]anthracene and Methylchrysene Isomers in Natural Samples by Liquid Chromatography and Shpol'skii Spectrometry 1695

Twelve methylbenz[*a*]anthracenes and six methylchrysenes are identified in rock and air particulate matter by high-resolution Shpol'skii spectrometry. Characteristic low-temperature fluorescence emission peaks are reported.

Philippe Garrigues*, Marie-Pierre Marniesse, Stephen A. Wise, Jacqueline Bellocq, and Marc Ewald, Groupe d'Océanographie Physico-chimique, LA 348 CNRS, Université de Bordeaux I, 33405 Talence Cedex, France, and Organic Analytical Research Division, National Bureau of Standards, Gaithersburg, Md. 20899 *Anal. Chem., 59 (1987)*

Sampling of Airborne Polycyclic Aromatic Hydrocarbons 1701

Overall recoveries of greater than 90% and sampling precision of less than 10% RSD are generally obtained for 15 PAHs when NIOSH method P & CAM 183 is modified to include Tenax sorbent tubes.

Rein Otson*, Environmental Health Directorate, Health and Welfare Canada, Room B-19, E.H.C., Tunney's Pasture, Ottawa, Ontario, Canada K1A 0L2, and **John M. Leach and Lambert T. K. Chung,** B. C. Research, 3650 Wesbrook Mall, Vancouver, British Columbia, Canada V6S 2L2 *Anal. Chem., 59 (1987)*

Extraction and Recovery of Polycyclic Aromatic Hydrocarbons from Environmental Solids Using Supercritical Fluids 1705

Supercritical fluid extractions of urban dust, river sediment, and fly ash yield quantitative recovery of PAHs with extraction times as short as 30 min.

Steven B. Hawthorne* and David J. Miller, University of North Dakota Energy Research Center, Grand Forks, N.D. 58202 *Anal. Chem., 59 (1987)*

Simultaneous Determination of Linear Alkylbenzenesulfonates, Alkylphenol Polyethoxylates, and Nonylphenol by High-Performance Liquid Chromatography 1709

Relative standard deviations for all analytes in the different matrices studied do not exceed 6%. Detection limits with UV fluorescence detection are 95 ng for 4-nonylphenol, 80 ng for linear 4-alkylbenzenesulfonates, and 65 ng for 4-nonylphenol polyethoxylates with respect to injected amounts.

Antonio Marcomini and Walter Giger*, Swiss Federal Institute for Water Resources and Water Pollution Control (EAWAG), CH-8600 Dübendorf, Switzerland *Anal. Chem., 59 (1987)*

Determination of Water by Liquid Chromatography Using Conductometric Detection 1716

Addition of an acid to the nonaqueous eluent significantly improves sensitivity, which is limited at about 2.5 ppm. Examples are shown for the determination of water in samples that interfere with GC and/or Karl Fischer methods.

Timothy S. Stevens* and Karen M. Chritz, The Dow Chemical Company, U.S.A., Michigan Division Analytical Laboratories, 574 Building, Midland, Mich. 48667, and **Hamish Small,** 4176 Oxford Drive, Leland, Mich. 49654 *Anal. Chem., 59 (1987)*

Estrogen Conjugates in Late-Pregnancy Fluids: Extraction and Group Separation by a Graphitized Carbon Black Cartridge and Quantification by High-Performance Liquid Chromatography 1720

Biological samples are percolated through an experimental Carbopack cartridge, and five classes of estrogens are eluted. After solvent elimination, each class of conjugation is subfractionated and quantified by ion-pair HPLC.

Franca Andreolini, Claudio Borra, Federica Caccamo, Antonio Di Corcia*, and Roberto Samperi, Dipartimento di Chimica, Università "La Sapienza" di Roma, Piazza Aldo Moro, 00185 Roma, Italy *Anal. Chem., 59 (1987)*

Temperature Dependence of the Electron Spin Resonance Spectra of a Coal-Derived Vacuum Distillation Residue and Components 1726

An analysis of the effects of systematic errors on ESR intensity measurements shows that the materials listed in the title obey the Curie law exactly. Deviations lie within the predicted range of systematic errors.

Salvatore M. Castellano, William P. Chisholm, Richard F. Sprecher*, and Herbert L. Retcofsky, Division of Coal Science, Pittsburgh Energy Technology Center, Pittsburgh, Pa. 15236 *Anal. Chem., 59 (1987)*

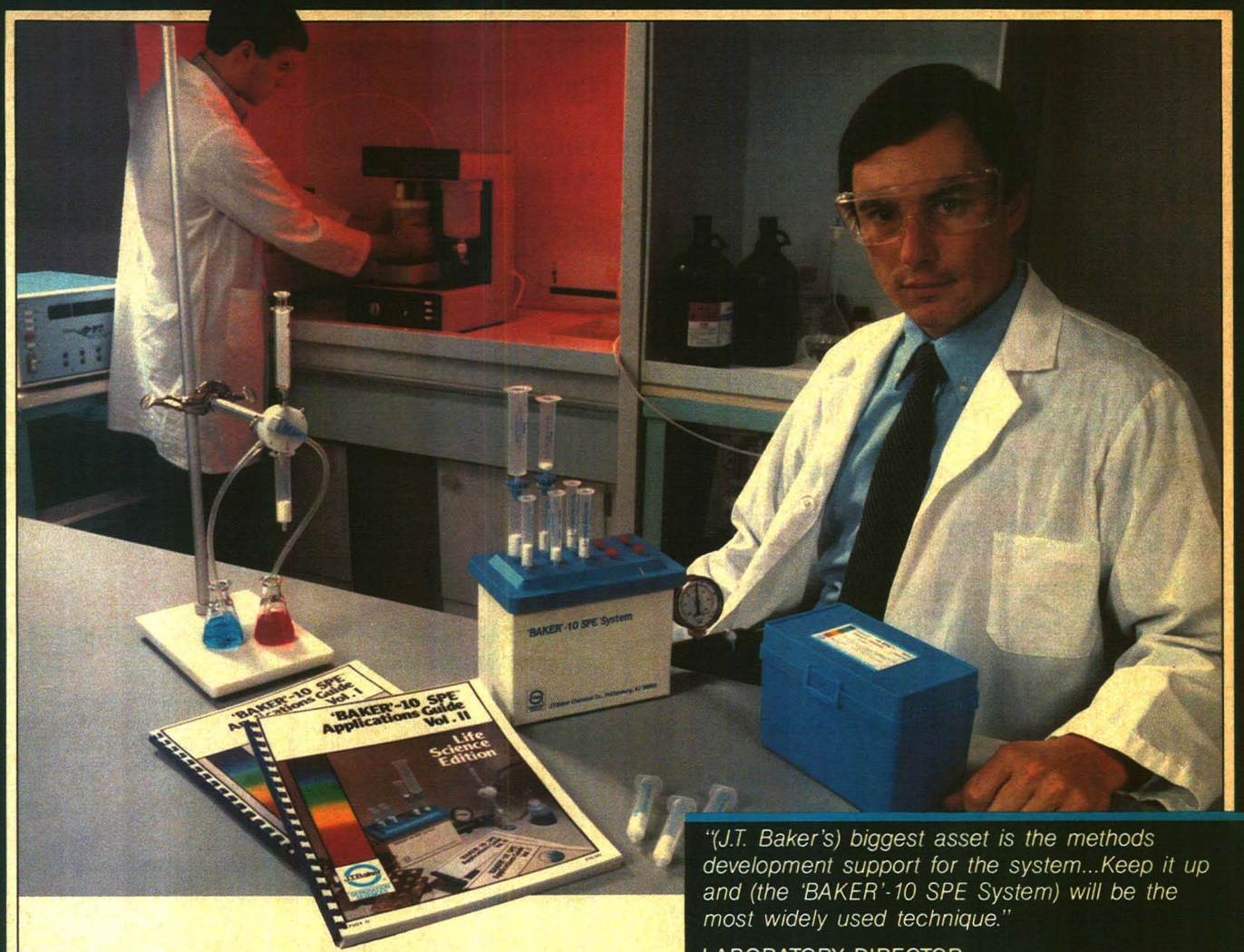

"(J.T. Baker's) biggest asset is the methods development support for the system...Keep it up and (the 'BAKER'-10 SPE System) will be the most widely used technique."

LABORATORY DIRECTOR

'BAKER'-10 SPE™

The Sample Preparation System That Comes With Built-In Applications Support.

Almost anyone can sell you a Solid Phase Extraction system to dramatically reduce the time you spend on sample preparation. Only J.T. Baker offers the applications support you need to make the technique work in your laboratory.

We developed the 'BAKER'-10 SPE™ family of products as alternatives to costly, time-consuming liquid/liquid extractions. With 'BAKER'-10, you can prepare samples 6 to 9 times faster. In minutes, your sample is ready for GC, HPLC, AA, UV, IR or RIA analysis.

But that's only part of the 'BAKER'-10 advantage. Through our knowledge of the chemistry and chromatographic principles behind the technique, we developed over 90 detailed procedures for preparing environmental, pharmaceutical, biological, food and cosmetic samples. You'll find these step-by-step procedures—and more—in Volumes I and II of the 'BAKER'-10 SPE Applications Guides. Plus, we offer courses in sample preparation, a Methods Development Kit, and a toll-free number you can call for solutions to specific sample preparation problems.

So if your application includes:

- Pesticides
- Herbicides
- PCB's
- PAH's
- PCB's in Transformer Oil
- Crude Oil
- Trace Metals
- Aflatoxins
- Caffeine
- Preservatives
- Nitrosamines
- Drugs and Metabolites
- Antibiotics
- Steroids
- Vitamins
- Catecholamines
- Nucleotides
- Carbohydrates
- Proteins
- Peptides

...and more...you can count on J.T. Baker to make Solid Phase Extraction work for you. Call us now for complete information.

CIRCLE 21 ON READER SERVICE CARD

J.T.Baker®

J.T. Baker Chemical Company
Research Products Division • 222 Red School Lane • Phillipsburg, NJ 08865 U.S.A.
Call Toll-Free: (800)582-2537 • In New Jersey or Canada: (201)859-2151 • FAX 201-859-2865 • Telex 299514 BAKR UR

Gross Gerau, West Germany • Deventer, Holland • Singapore • Mexico City, Mexico

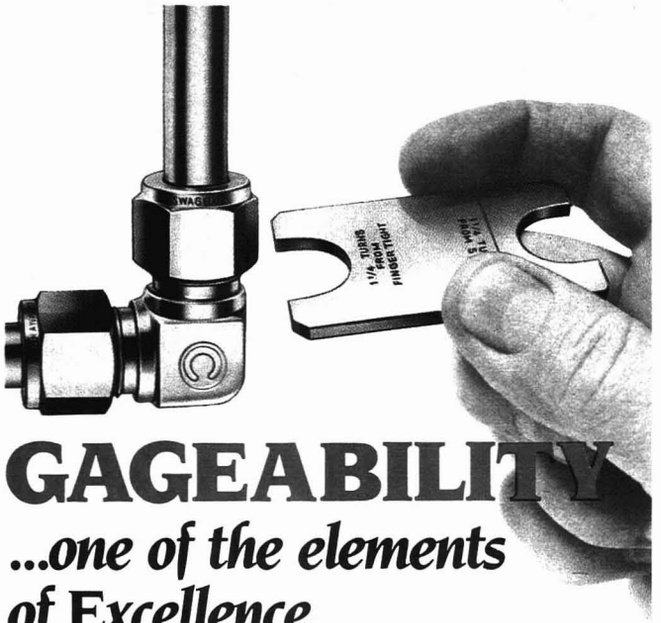

GAGEABILITY

...one of the elements of Excellence

Sufficient fitting pull-up assured with SWAGELOK Gap Inspection Gage.

Precision machining and unequaled quality control procedures make gageability a reality. Accumulation of tolerances, among four precision components, is minimized.

SWAGELOK Tube Fitting connections are made with a simple turn-and-a-quarter pull-up from finger tight.

Assist your installer or inspector, especially in critical systems or in difficult or inaccessible locations, by providing an additional degree of safety and reliability through gageability.

SWAGELOK Gap Inspection Gages assure sufficient fitting pull-up. If the gage will not fully enter the gap between the nut and body shoulder, fitting pull-up is sufficient. If the gage enters the gap, you'll know pull-up is incomplete.

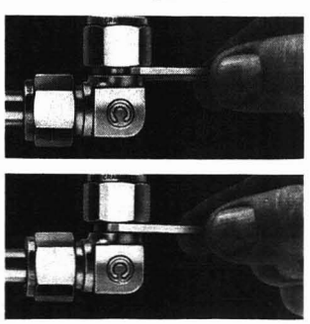

Only SWAGELOK Tube Fittings offer gageability of straight fittings and forged shaped elbows and tees in stainless steel and steel. Gages are available for 1/8" through 1" sizes.

The need for reliable performance is fully understood and respected by the tube fitting specialists who design, manufacture, sell and service SWAGELOK Tube Fittings.

FOUR PRECISION COMPONENTS

Gageability is made possible by manufacturing the SWAGELOK body, front ferrule, back ferrule and nut to exacting tolerances. Their precise interaction during make-up produces leak-free connections.

Swagelok® TUBE FITTINGS

Swagelok · WHITEY · CAJON · Sno-Trik · NUPRO

SWAGELOK Co., Solon, Ohio 44139
SWAGELOK Canada, Ltd., Ontario

© 1986 SWAGELOK Co. / all rights reserved C-35f

CIRCLE 30 ON READER SERVICE CARD

BRIEFS

Correspondence

Enantioselective Binding of 2,2,2-Trifluoro-1-(9-anthryl)ethanol on a Chiral Stationary Phase: A Theoretical Study 1731

Kenny B. Lipkowitz*, David A. Demeter, and Carol A. Parish, Department of Chemistry, Indiana–Purdue University, Indianapolis, Ind. 46223, and **Thomas Darden,** Laboratory of Molecular Biophysics, National Institute of Environmental Health Science, P.O. Box 12233, Research Triangle Park, N.C. 27709

Anal. Chem., 59 (1987)

Pulsed-Laser Photothermal Refraction Detection in Capillary Liquid Chromatography 1733

C. N. Kettler and M. J. Sepaniak*, Department of Chemistry, University of Tennessee, Knoxville, Tenn. 37996-1600

Anal. Chem., 59 (1987)

Aids for Analytical Chemists

Composite Ion Exchanger for Removal of Sodium-24 in Neutron Activation Analysis of Biological Materials 1737

Aleksander Bilewicz, Barbara Bartoś, and Jerzy Narbutt*, Department of Radiochemistry, Institute of Nuclear Chemistry and Technology, 03-195 Warsaw, Poland, and **Halina Polkowska-Motrenko,** Department of Analytical Chemistry, Institute of Nuclear Chemistry and Technology, 03-195 Warsaw, Poland

Anal. Chem., 59 (1987)

Recovery of Picloram and 2,4-Dichlorophenoxyacetic Acid from Aqueous Samples by Reversed-Phase Solid-Phase Extraction 1739

Martha J. M. Wells* and Jerry L. Michael, U.S. Forest Service, Southern Forest Experiment Station, Auburn University, Ala. 36849

Anal. Chem., 59 (1987)

Design and Evaluation of a Capillary Gas Chromatography–Atomic Absorption Spectrometer Interface 1742

Donald S. Forsyth, Food Research Division, Food Directorate, Health Protection Branch, Ottawa, Ontario, Canada K1A 0L2

Anal. Chem., 59 (1987)

Polaris/ICON™ FT/IR System— Flexible Enough For Any Demand; Tough Enough For Any User

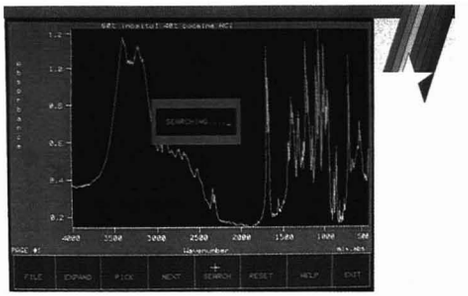

POLARIS™/ICON

As shown on the screen, above, ICON™ software adds sophisticated analytical routines to the solid FT-IR data of the Polaris spectrometer.

Mattson's versatile new Polaris/ICON teams together features as impressive alone as they are together.

As a stand-alone unit, the Polaris FT-IR lets even novice users run spectra *without* a computer. And the Polaris has other advantages you've come to expect from Mattson. Like the best optics in the business. Rugged construction that can stand up to the most demanding teaching or industrial environment. And ease of use that's appreciated by seasoned chemists and students.

Add on the new MS™/DOS based ICON FT-IR software, and you have a state-of-the-art system with exclusives you won't find anywhere else. Compatibility with any IBM-AT type computer. Elegant search capability supported by an extensive library of commercial spectra and Mattson's exclusive relationship with Fluka Chemicals. Mouse-control so you're free to do chemistry, not keypunching. High-resolution color graphics. And upgrade potential that means the Polaris/ICON can grow with your demands.

Find out more about the system flexible enough to fit your budgetary and analytical demands. The Polaris FT-IR and ICON FT-IR software. Impressive tools alone — an incredible system together.

Polaris/ICON — impressive alone, incredible together.

Polaris/ICON™ is a trademark of Mattson Instruments, Inc.
MS™ is a trademark of Microsoft, Inc.

Mattson Instruments, Inc.
1001 Fourier Court
Madison WI 53717 U.S.A.
Tel. (608) 831-5515
Telex: 262006

Mattson Instruments, Ltd.
Linford Forum
Rockingham Drive
Linford Wood
Milton Keynes MK 14 6LY
England
Tel. (0908) 679961
Telex: 82304 Forum G
Fax: 0908 668974

Mattson Instruments Pty. Ltd.
88 Station Street
Nunawading, 3131 Victoria
Australia
Tel. (03) 873 2177
Telex: 151823

Mattson

CIRCLE 94 ON READER SERVICE CARD

Introducing the new twice-monthly

Quality Research and News In Your Hands Twice as Fast

Analytical CHEMISTRY

Don't miss a single issue! The new, more timely ANALYTICAL CHEMISTRY, contains the same vital information in the field of measurement science. Twenty-four issues a year put the best in ANALYTICAL CHEMISTRY in your hands more often. You'll continue to find the same fine research articles, reports, special departments like Focus and A/C Interface, and the Annual Reviews and LabGuide issues.

There's never been a better time to subscribe

Call now and you can get your own subscription to the new twice monthly ANALYTICAL CHEMISTRY—including its sought-after annual "Application Reviews" and "LabGuide" issues.

SPECIAL RATES

Member*	1 Year	2 Years Save 15%	Nonmember	1 Year	2 Years Save 15%
U.S.	$ 25	$ 42	U.S.	$ 37	$ 62
Canada & Mexico	$ 50	$ 92	Canada & Mexico	$ 62	$112
Europe**	$ 77	$146	Europe**	$127	$231
All Other Countries**	$104	$200	All Other Countries**	$154	$285

*Member rates are for personal use only.
**Air service delivery included.

Call toll free: 800-424-6747

Or write: **American Chemical Society, Marketing Communications Department, 1155 Sixteenth Street NW, Washington, D.C. 20036**

This publication is available on microfilm, microfiche, and electronically through Chemical Journals Online on STN International.

EDITORIAL

Keeping Quantitative Analysis in Chemistry

The December 1986 REPORT, "Consider Teaching: It's Been Good to Us," by Peter T. Kissinger, R. Graham Cooks, and William R. Heineman brought a positive response from a number of our readers regarding various aspects of the teaching of analytical chemistry. This response led to my March 1987 editorial emphasizing the importance of the role of faculty at undergraduate institutions. In this issue we are following up with two REPORTS that explore this important topic. Royce C. Engstrom makes a strong case for the advantages of a career in teaching in "Teaching Analytical Chemistry—Another View." In a related area, David C. Locke and William E. L. Grossman provide important new data in "The Curriculum in Quantitative Analysis: Results of a Survey."

Both articles come at a particularly important time in view of the recent activities of the ACS Committee on Professional Training (CPT) chaired by Alice J. Cunningham of Agnes Scott College, Decatur, Ga. At the Denver ACS meeting in April the committee presented a new three-year core curriculum for eventual recommendation to the ACS. Chemistry in recent years has begun to overlap more effectively with other disciplines as fundamental understanding of new materials and more complex processes has improved, and the field continues to expand from its traditional beginnings to new and exciting areas. In view of this changing situation, CPT believes that new guidelines should allow for degrees that center on chemistry but emphasize specialized areas.

The minimum content of the recommended three-year core curriculum includes the following courses (and their semester credit hours): Fundamentals of Chemistry (4 or 8), Introduction to Organic and Biochemistry (8), Intermediate Inorganic Chemistry (4), Physical Chemistry (7), and Analytical Chemistry (4). The associated laboratory contact hours are 42 or 84, 84, 42, 42, and 84, respectively. The analytical course would be an upper-class course emphasizing instrumental analysis. The traditional sophomore quantitative analysis course has been eliminated. Although not explicitly stated, it has been suggested by some members of the committee that some of the material previously covered in quantitative analysis could be included in the laboratory portion of the Intermediate Inorganic Chemistry course during the second semester of the sophomore year. At this point, many inorganic chemists do not welcome this compromise in the content of their courses. Thus there is a real possibility that mastery of quantitative concepts and methods could be eliminated in the education of a chemist.

The various ACS divisions are being consulted about the proposed new curriculum. In view of its impact on the way we currently teach quantitative analysis, we strongly urge that our constituency respond to the proposed recommendations before the New Orleans ACS meeting in late August, when the CPT will present their revised guidelines. Please contact Alice Cunningham, Department of Chemistry, Agnes Scott College, Decatur, Ga. 30030.

G. H. Morrison

SGE PRESENTS THE AQ5-ULTRABORE SERIES CAPILLARY COLUMNS.

A range of aluminium coated fused silica capillary columns with an ID of 0.53mm for use in place of conventional capillary and packed columns.

OUTSTANDING FEATURES:

Superior chromatographic performance : highly inert and exhibiting excellent column to column reproducibility.

No breakdown of aluminium coating with temperature in your GC oven — No annoying unexplained column breakages. Extended column life.

Full range of popular bonded phases from low polarity BP1 (OV-1,SE30) to the more polar BP20 (CW20M) phases.

No outgassing of outer coating to interfere with highly sensitive detectors.

Outstanding flexibility : Can be fitted into the oven of any gas chromatograph: Supplied in 150mm diameter cages. The high thermal conductivity of aluminium provides optimum heat transfer to the phase coating during temperature programming: improved chromotographic performance.

Each column supplied with its own individual test Chromatogram and performance characteristics.

AQ Series columns can be used with existing instruments fitted with 0.53mm ID Capillary Adaptors.

Talk to SGE about their premium range of adaptors and connectors to convert your existing packed column chromatograph for use with capillary columns.

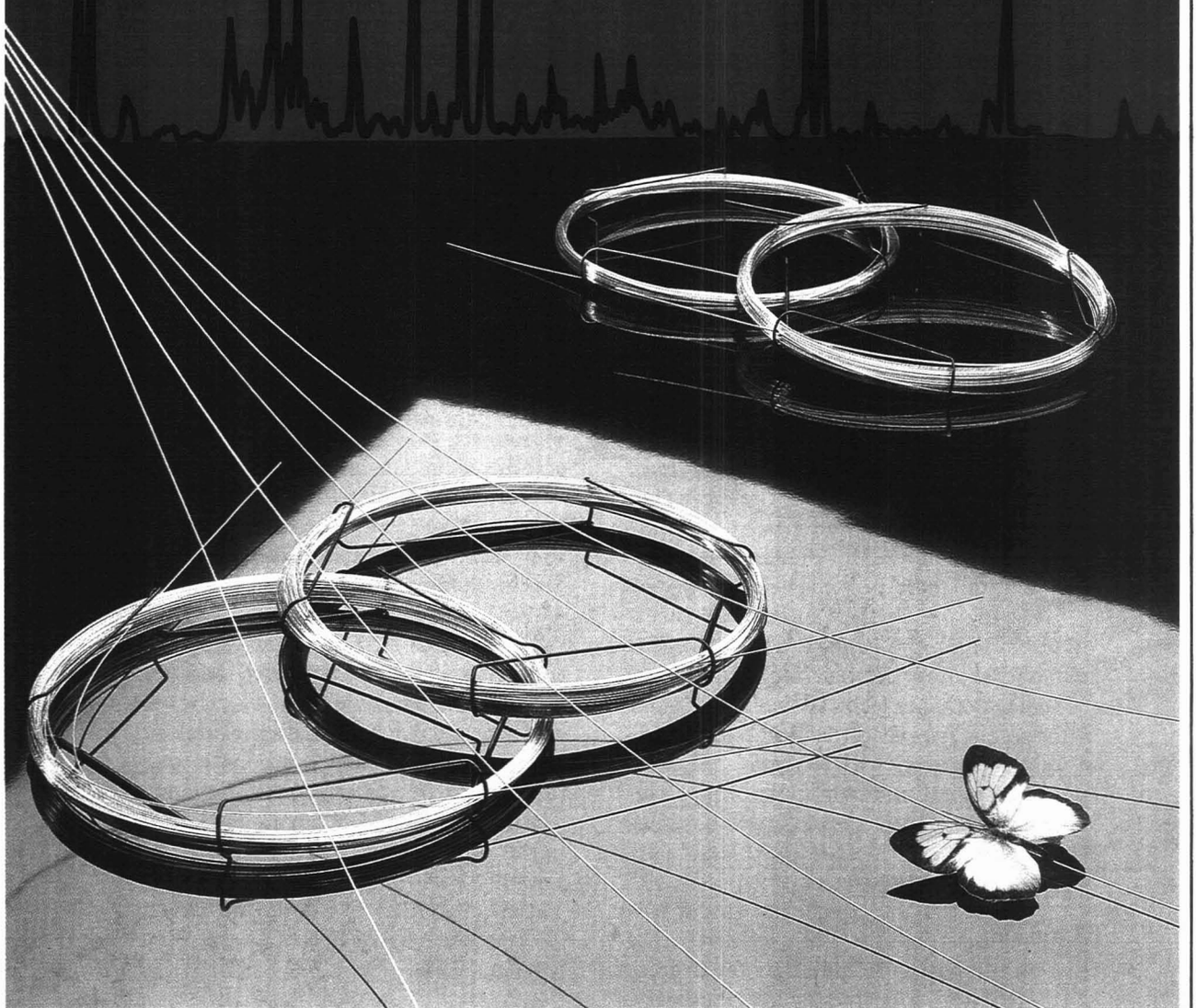

THE NEW PATH IN CAPILLARY COLUMN TECHNOLOGY

SGE

CONTACT YOUR NEAREST SGE OFFICE FOR DETAILS:
U.S.A. Sales Office: Scientific Glass Engineering Inc. 2007 Kramer Lane, Austin, Texas, 78758, U.S.A. Tel: 1 512 8377190, Tlx: 9108741358, Fax: 1 512 8369159
Australia-Head Office/International Sales: 7 Argent Place , Ringwood., Victoria, 3134, Australia., Tel: 613 8746333, Tlx: 33930, Fax: 613 8745672

SGE - cap 1

CIRCLE 150 ON READER SERVICE CARD

NEWS

Merck Award for Analytics

One of the first analytical reference works, named "Die Prüfung Chemischer Reagenzien auf Reinheit" ("The Testing of Chemical Reagents for Purity") was published 100 years ago by Carl Krauch, who had been a chemist with Merck at Darmstadt in Germany. The anniversary of this publication has prompted E. Merck Darmstadt to establish a new award for analytical chemistry that is named after the firm's founder. The Heinrich Emanuel Merck Award for Analytics, which will be awarded for the first time in October 1988 and every three years thereafter, recognizes recent contributions of younger chemists in the development and application of new methods of analysis, with an emphasis on wet chemical techniques and trace analytical sample preparation.

An international jury of specialists, including G. M. Hieftje (United States), A. Hulanicki (Poland), H. Malissa (Austria), A. Mizuike (Japan), G. Tölg (West Germany), and T. S. West (United Kingdom) will decide to whom the prize will be awarded. The jury is also entitled to decide to divide the prize among several nominees. Applicants are encouraged to submit papers that exemplify their research before Apr. 30, 1988, to Günther Tölg, Institut für Spektrochemie und Angewandte Spektroskopie, Post Box 778, Bunsen-Kirchhoff-Strasse 11, D-4600 Dortmund 1, F.R.G.

Nominations Sought for Hirschfeld Award

Nominations are now being sought for the Tomas Hirschfeld Award in Near-Infrared Analysis, sponsored by Technicon Industrial Systems Corp., a subsidiary of Bran + Luebbe, Inc. Nominees must be graduate students in a North American institution working in the field of near-infrared analysis and must be recommended by their major professor.

Professors should submit letters of recommendation, curriculum vitae, reprints of publications (if any), and other relevant supporting documents by Sept. 7, 1987, to William G. Fateley, P.O. Box 688, Manhattan, Kan. 66502. The award, which will be presented at the 1988 Pittsburgh Conference, consists of a $3000 check, a plaque, and expenses to attend the conference.

Coretech Adopts R&D Action Agenda

At its May board of directors meeting in Washington, D.C., the Council on Research and Technology (Coretech) voted unanimously to begin working immediately on a number of major goals to boost U.S. research and development, including the following:

- Congress extended the R&D Tax Credit under the 1986 Tax Reform Act until Dec. 31, 1988, but reduced its incremental rate from 25 to 20%. Because of the high-risk, long-term nature of R&D, Coretech is urging Congress to make the R&D tax credit permanent and restore it to a 25% incremental rate.
- Coretech supports increasing the National Science Foundation's fiscal year 1988 budget by 17%, the Reagan administration's requested amount, and considers it an important step toward doubling the agency's budget by 1992.
- Coretech strongly endorses H.R. 1905, "The University Research Facilities Revitalization Act of 1987," introduced on Apr. 1, 1987, by Representative Robert Roe of New Jersey. This legislation would authorize a $250-million university research facilities fund annually for 10 years to repair, renovate, or replace university scientific and engineering research facilities.

Coretech currently comprises 36 research-intensive corporations such as Du Pont, Hewlett-Packard, and Varian Associates; 73 major universities; 16 associations; 6 research institutes; and 6 affiliates. For further information on the council's program, write or phone Coretech at 1735 New York Ave., N.W., Suite 500, Washington, D.C. 20006-4759 (202-628-1700).

Holak Wins Wiley Award

Walter Holak, a career research chemist with the Food and Drug Administration (FDA) in Brooklyn, N.Y., is the 1987 Association of Official Analytical Chemists (AOAC) Harvey W. Wiley Award winner. The award will be presented at the 101st AOAC annual meeting in San Francisco this September.

An expert in regulatory analytical chemistry, Holak is receiving the award for his sustained contributions to the methodology necessary for the FDA to protect consumers, especially in the area of toxic substances in foods. Holak has made three contributions of particular significance: the development of a method to measure methyl mercury in seafood by liquid chromatography and atomic absorption spectrometry, the collaborative study of a method for determining free and bound sulfite in foods at the 10-ppm level, and the development of an accurate and sensitive method to measure iodine in foods, meeting a longstanding need in food analysis.

The $2500 Wiley Award is given annually to a scientist who has made outstanding contributions to the development of analytical methods of importance to AOAC's mission. Established in 1956 in honor of Harvey W. Wiley, the father of the 1906 Pure Food and Drug Act and a founder of AOAC, the award recognizes the scientist's role in protecting the consumer and environmental quality.

For Your Information

During a two-day program consisting of speeches, tours, and a banquet, the California Institute of Technology dedicated its new **Caltech Materials Research Group Laboratories** in May. The laboratories, which include facilities for new materials preparation and materials characterization and analysis, are funded by a three-year, $2.7-million start-up grant from the National Science Foundation and Caltech. Analytical instrumentation acquired for the new facility includes X-ray diffractometry equipment, an extended X-ray absorption fine-structure spectrometer, a

Rutherford backscattering spectrometer, a Mossbauer spectrometer, a differential scanning calorimeter, a differential thermal analyzer, and a 300-keV transmission electron microscope with scanning and analytical capabilities.

The National Science Foundation (NSF) has announced 151 grants totaling $6 million to small business to promote research and development on innovative commercial products and processes. The awards are Phase I grants under the 1986 solicitation for **NSF's Small Business Innovation Research program.** Phase I grants provide firms with up to $40,000 for six months to explore the technical feasibility of promising new ideas. The best projects to emerge from Phase I will receive approximately $200,000 from NSF for two years of Phase II research. Private investors then fund Phase III product development, manufacturing, and marketing efforts. This year's grants for analytical chemistry-related projects include one to Biode, Inc. for a surface acoustic wave SO_2 microsensor and two to Southwest Sciences, Inc. for an instrument for the in situ measurement of atmospheric water vapor and a very high-sensitivity spectrometer for atmospheric measurements.

Rohm and Haas Company has formed a new business venture with **Toyo Soda Manufacturing Company** of Japan to market analytical instrumentation and process equipment and supplies used for emerging applications that require isolation and purification of biological materials. Although this will be Rohm and Haas's initial effort in the sale of high-performance liquid chromatography systems, the firm points out that it already sells LC columns through its Supelco subsidiary and ultrafiltration membranes through its Romicon subsidiary.

In late April the Food and Drug Administration licensed a commercial test kit for screening blood and for validating an initial screening of donated blood for antibodies to the virus that causes AIDS (acquired immunodeficiency syndrome). The initial test of donated blood is currently conducted by an enzyme-linked immunosorbent assay (ELISA) screening test. To protect the public, the ELISA test was designed for maximum sensitivity to eliminate virtually all questionable blood and plasma. However, this increased sensitivity results in some nonspecific or false positive readings due to reactions to test components other than viral proteins or to other technical problems. A test called the Western blot can then be performed to validate the earlier finding of a positive ELISA test. Previously the **Western blot test** procedure had been used in a research setting **to identify specific AIDS antibodies.** The Western blot kit announced in April standardizes the procedure for use by blood bank personnel. The approved Biotech/Du Pont HIV Western blot kit will be manufactured by Biotech Research Laboratories Inc. of Rockville, Md. and distributed by E. I. du Pont de Nemours and Company. Robert Windom, Health and Human Services secretary for health, emphasized that individuals with antibody-positive Western blot results should be referred for medical evaluation, which may include additional testing. The significance of antibodies in an asymptomatic individual is not known. However, many people with AIDS virus antibodies will develop AIDS with the passing of time.

IBM Instruments Inc. ceased marketing supplies in May. The inventory of supply items, with the exception of silica-based HPLC columns, has been sold to Industrial Instrumentation and Instrument Supplies Inc. of Meriden, Conn. (800-243-3122; in Connecticut, 238-9191). The company will market the LC, electrochemistry, plotter, FT–IR, UV–vis, NMR, and EPR supplies formerly provided by IBM Instruments. The inventory of silica-based columns and related supplies has been sold to Jones Chromatography Ltd., Tir-y-Berth Industrial Estate, New Road, Hengoed, Mid-Glamorgan CFB 8AU, Great Britain. In the United States, write Jones Chromatography Inc., P.O. Box 620999, Littleton, Colo. 80162, or call 800-874-6244.

The manufacturing facilities and personnel of **EDAX International, Inc.,** an operating unit of Philips Electronic Instruments, will be moved from Prairie View, Ill., and combined with those of Philips Electronic Instruments, Inc. in Mahwah, N.J. The move was announced in May by Emile J. Geisenheimer, president of both Philips Electronic Instruments and EDAX International. Philips Electronic Instruments is a manufacturer of analytical X-ray diffraction and spectrometer systems, electron optics, and transmission and scanning electron microscopes. EDAX is a manufacturer of X-ray microanalytical equipment.

The board of directors of Mattson Instruments, Inc. (Madison, Wis.), has announced the election of founder **David R. Mattson** to the position of chairman and chief technical officer. He will be succeeded by **William J. Kennedy,** who will serve as president and chief executive officer. Kennedy previously served as president and chief executive officer of Alnor Instruments, Inc. (Chicago, Ill.).

Ronald E. Majors has been appointed general manager of chromatography business for EM Science, a manufacturer and marketer of laboratory reagents, solvents, and analytical systems in Cherry Hill, N.J. Majors will oversee the continued expansion of EM Science's chromatography business in the U.S. market. He will be responsible for the company's complete line of chromatography products as well as the development of new systems and products. Before joining EM Science, Majors spent more than 16 years at Varian Associates, most recently as life science marketing manager and before that as liquid chromatography marketing manager.

Analect Instruments, a division of Laser Precision Corp., has filed suit against Mattson Instruments, Inc. for **patent infringement.** The lawsuit charges that the optical design of Mattson's Cryolect matrix isolation sampling system is infringing on Analect's patent 4,473,295.

Varian Associates' joint venture with Siemens to manufacture and market NMR imaging spectroscopy systems has been named **Spectroscopy Imaging Systems Corporation.** The new company, to be located in Fremont, Calif., will be headed by Peter Llewellyn.

The mass spectrometry laboratory at Oak Ridge National Laboratory, which had been housed at ORNL's Y-12 plant in facilities that date back to the 1940s, will soon be joining the rest of the Analytical Chemistry Division at ORNL. After 15 years of planning, construction of a new mass spectrometry facility will begin this year, with completion expected in mid-1989. The new facility will house laboratories, offices, and support facilities. According to ORNL, it will contain the most comprehensive collection of mass spectrometers in the United States and will facilitate collaborative research with scientists worldwide.

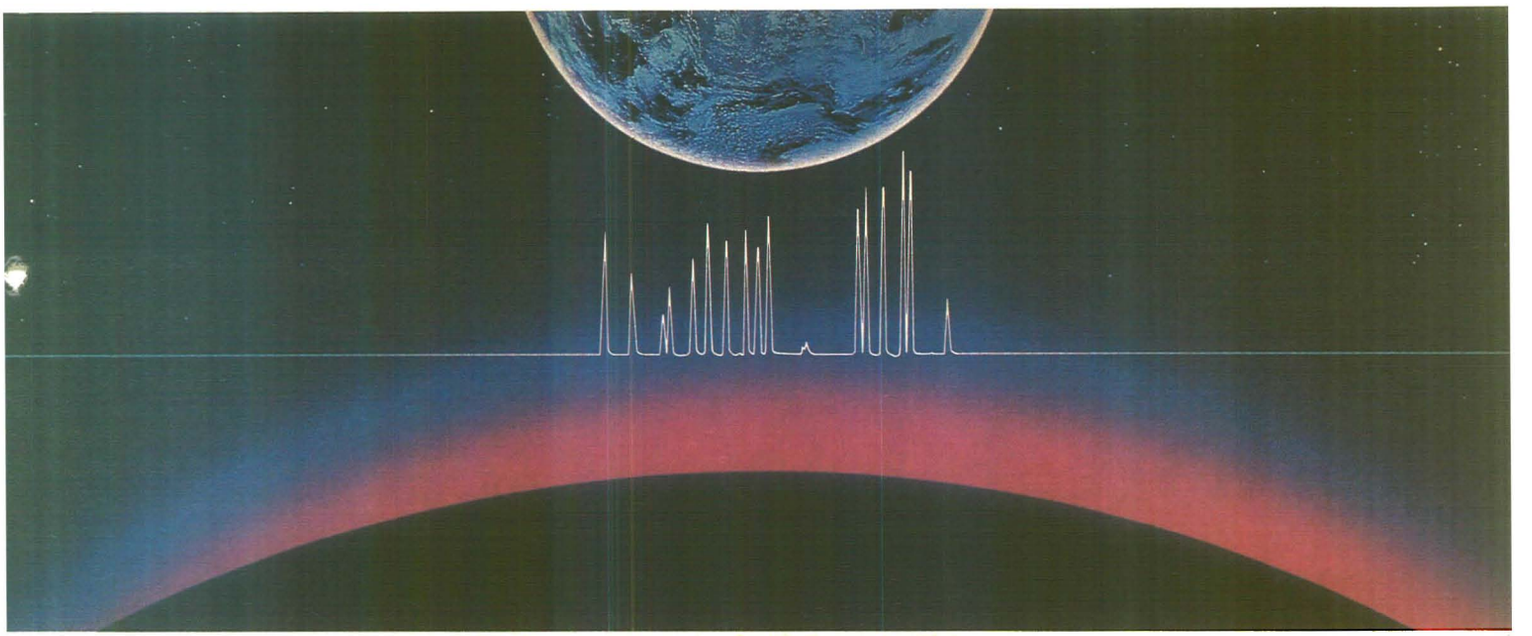

HPLC: 2002.

OMARS Project, 2002. Ten years in planning and 28 months under construction, the second Orbital Manufacturing and Research Station (OMARS) went on line with little public fanfare. Its purpose: zero-G manufacture of enzymes, and continuing study of the long-term effects of life in space.

Without HPLC, OMARS wouldn't have gotten off the ground. The space-tough, high tensile strength polymer composites used to construct the station were engineered using specialized GPC characterization methods. HPLC analysis of amino acids and other nutritional elements led to the development of super-efficient hydroponic produce that helps keep the project self-sufficient. On-line HPLC streamlines the genetic manufacturing process for maximum yield, and robotized Q.C. sampling saves precious man-hours. Automated monitoring of the artificial environment measures and identifies trace contaminants down to the parts per quadrillion level, to guarantee the safety of the orbital scientists. And instantaneous two-way data transmission links the HPLC power in space with the best minds on Earth.

Milford, Massachusetts, 1987. Waters is already meeting tomorrow's HPLC challenges. We're putting our technology to work in new ways, in new applications. From GPC characterization of space-age polymers to fast purification of bioactive proteins; from sensitive ion analysis of acid rain to metabolic mapping of therapeutic drugs. No one can predict exactly where HPLC will be fifteen years from now. But we plan to be there with you.

Whether you need an analytical result or a purified product, we can offer a range of solutions tailored to your needs and budget. And a guarantee you can't get anywhere else: whatever your application—simple, complex or "out of this world"—we'll keep working with you until you're successful. We've proven it thousands of times, in the lab, in the field, and on the production floor.

If you're putting HPLC to work, take your best shot at success and work with Waters. For immediate applications information, call toll-free (800) 252-HPLC; in Massachusetts, (617) 478-2000. Waters Chromatography Division, Millipore Corporation, 34 Maple St., Milford, MA 01757.

For a free poster of this illustration, circle Reader Service Card.

© 1987 Millipore Corporation

Waters
Division of MILLIPORE

CIRCLE 175 ON READER SERVICE CARD

We make your life easier by making

house calls.

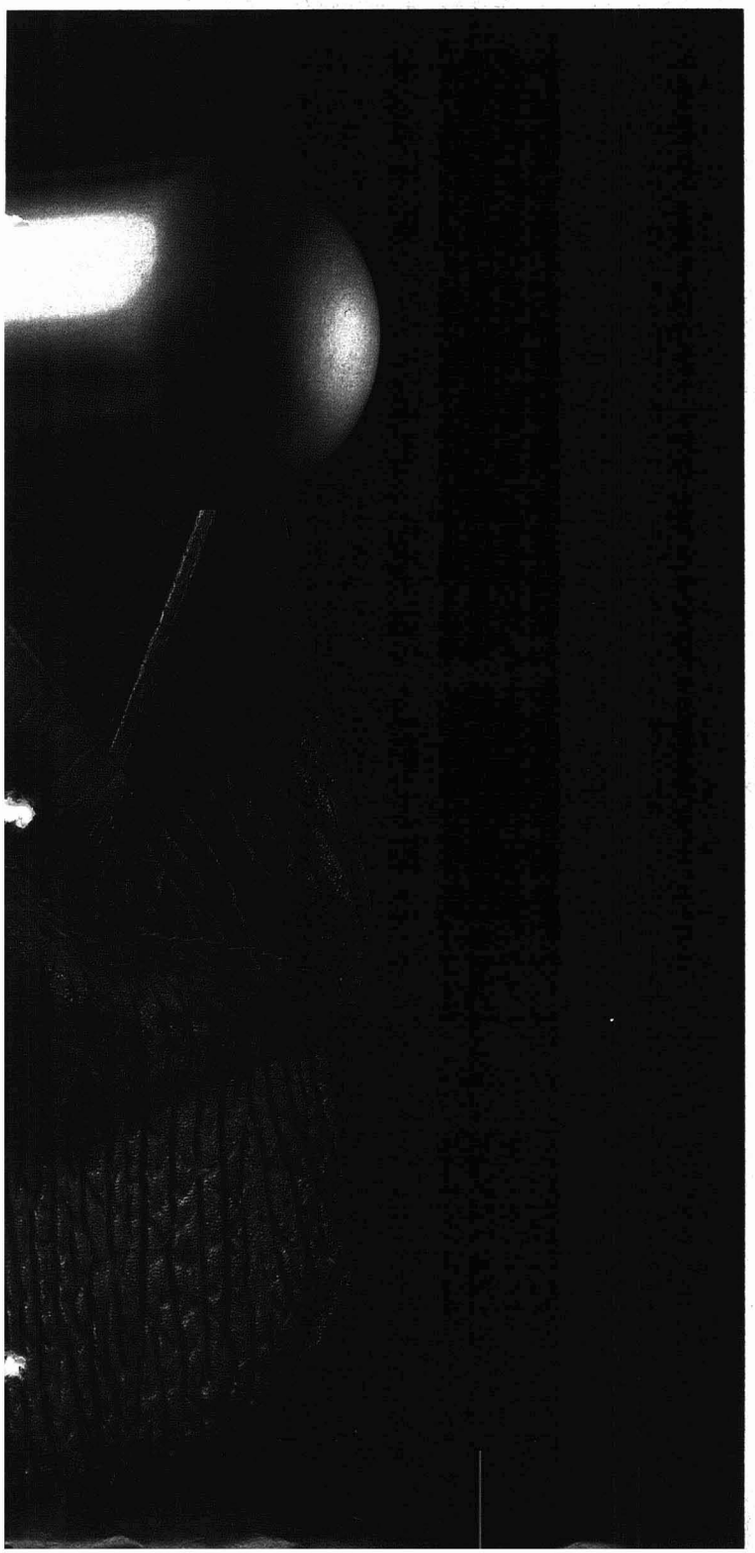

Now you don't have to suffer the uncertainty of a long-distance relationship with your special gases supplier. Because now you can get the high quality gases you need—and the personal service you want—from your local Airco distributor.

Instead of dealing with an order clerk on the phone, we'll send you a real, live gases expert. He'll get to know you, your lab and your requirements first hand. So if an emergency comes up he'll be right there to solve your problem.

By adding our distributors to our service capabilities, we've effectively added 300 stocking locations to our supply network. Each of our distributors is an expert in handling cylinder gases safely and efficiently. And since we don't have to rely on common carriers, you can expect uncommonly fast deliveries.

One thing, of course, hasn't changed. The special gases you get from our distributors are the same consistently high-purity gases you've come to expect from Airco. We're still sticklers about quality control. We still give our production and QC people the best training and equipment, so our customers get the best products. And we still use our specially designed Spectra-Seal® and Spectra-Steel® cylinders to keep your special gases pure.

As you can see, we're doing everything possible to help you win the war against rejects. Because we know that helping you increase your yield is the best way to win your business. Airco Gases, 575 Mountain Avenue, Murray Hill, NJ 07974. (201) 464-8100.

AIRCO

We're out to win your business.

CIRCLE 2 ON READER SERVICE CARD

Airco gases and application technology are also available through a nationwide network of authorized Airco gas distributors.

Have you ever had an idea that could change the world, only to have someone else beat you to it? After months of painstaking research, there's nothing more frustrating than reinventing the wheel. Again.

DIALOG® is the online information system that can give you a flying head start on your competition. Dialog goes right to the source, with 10 to 15 years of data on every subject, from aerospace to zoology. Even if you're in a specialized area of research, you never know when you'll need something from another field. With Dialog, it's all available instantly.

Anyone can learn to use Dialog, too. In fact, Dialog is so useful if it didn't already exist, you'd just have to invent it.

To find out about Dialog now, call 800-3-DIALOG. Or write: Dialog, 3460 Hillview Ave., Palo Alto, CA 94304.

DIALOG® INFORMATION SERVICES, INC.
A SUBSIDIARY OF LOCKHEED CORP
The world's largest online knowledgebank.

Guess who didn't use Dialog.

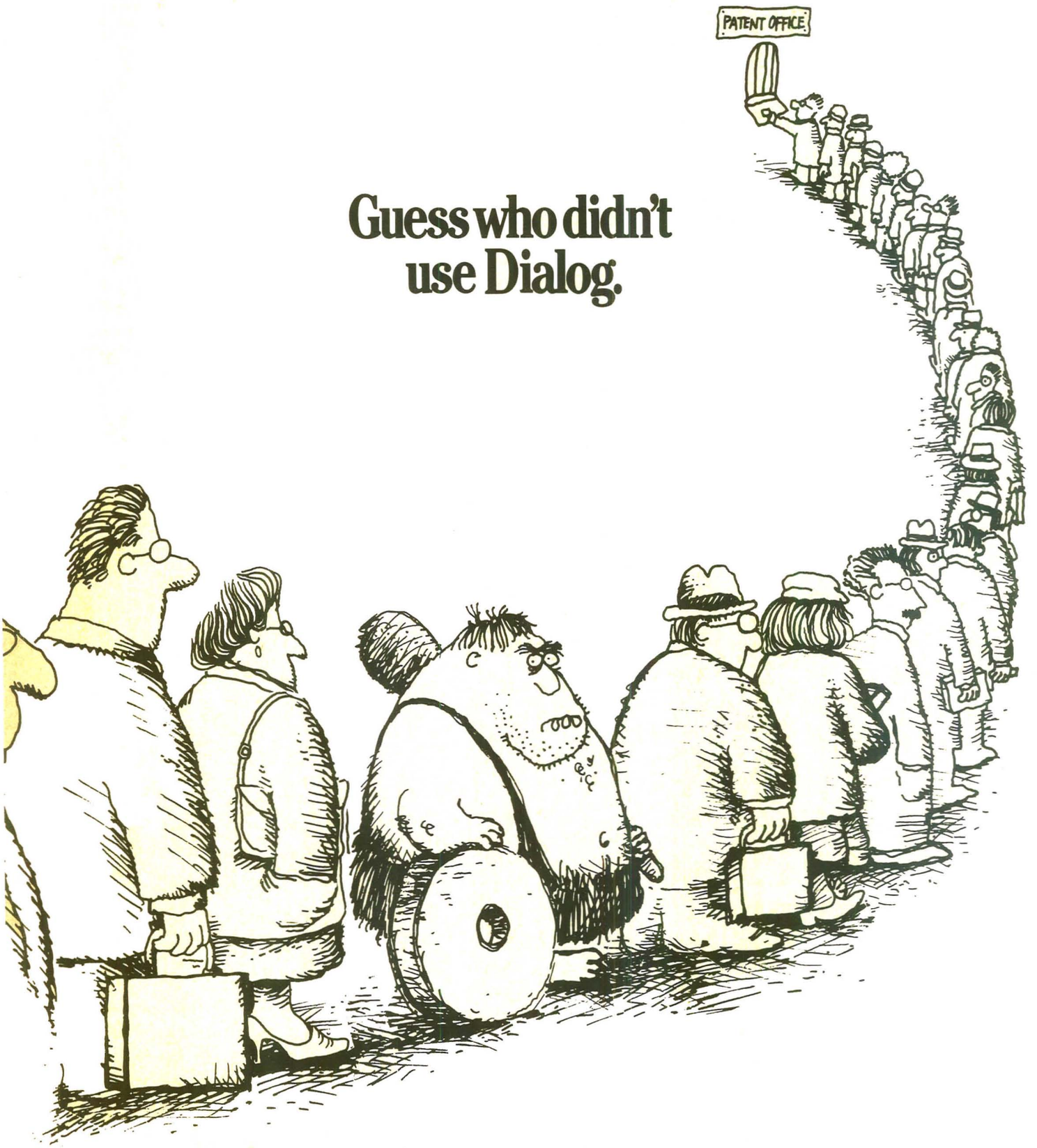

©Dialog Information Services, Inc. 1985

CIRCLE 32 ON READER SERVICE CARD

Royce C. Engstrom
Department of Chemistry
University of South Dakota
Vermillion, S.D. 57069

Teaching Analytical Chemistry—Another View

Bright, dedicated faculty at predominantly undergraduate institutions are essential for the continuing strength of the discipline

A recent REPORT in ANALYTICAL CHEMISTRY (*1*) evaluated the rewards and drawbacks of life in an academic setting and encouraged students of analytical chemistry to think about an academic career. The inspirational article was written from a unique perspective in that all of its authors are associated with major research institutions. An editorial in a later issue (*2*) reminded the readership of the important role undergraduate institutions play in the discipline of analytical chemistry. This REPORT is designed to give students additional information about academic careers and to emphasize the opportunities available at schools specializing in education at the undergraduate and perhaps at the master's level. We will call these schools predominantly undergraduate institutions (PUIs).

Two messages should be clear from this presentation. First, PUI departments play a major role in the education of future analytical chemists, and consequently there is a need for bright, dedicated faculty at those schools. Second, the unique opportunities and problems in PUI departments provide for certain people the setting that is most conducive to satisfying their scientific creativity, professional development, and personal goals. We should caution, however, that it is risky to generalize about PUIs because of their great diversity in mission and working conditions. The responsibilities, number of faculty, research capabilities, and degree of professional involvement among the faculty vary widely and warrant careful assessment by the prospective faculty member.

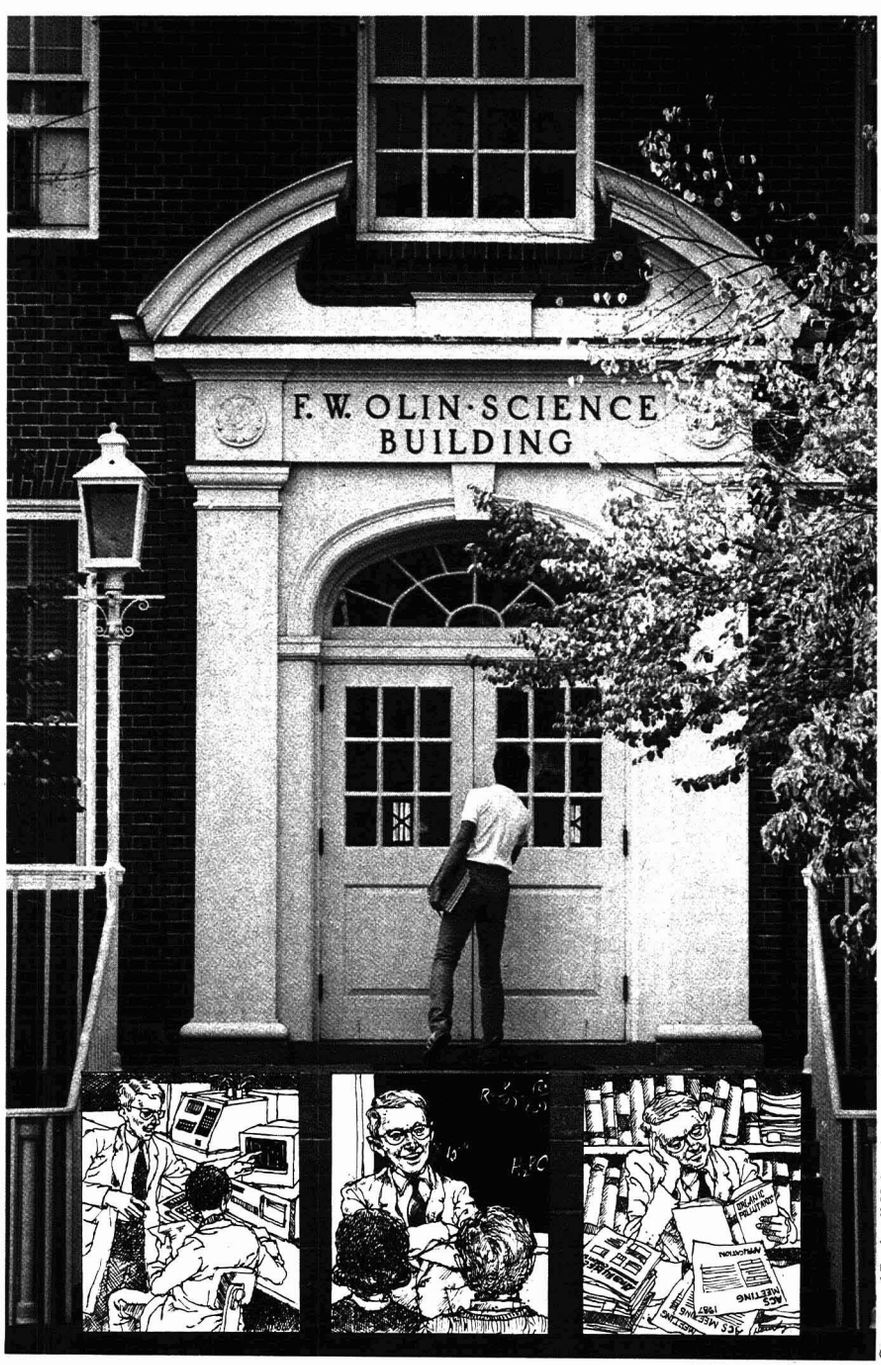

Courtesy of Bucknell University

Some facts

How many analytical chemists are there in PUI departments? The most recent directory of the ACS Division of Analytical Chemistry lists 1336 members in academic positions, 969 of whom have faculty positions. The *ACS Directory of Graduate Research 1985* shows 490 analytical chemists on the faculty at Ph.D.-granting institutions, which implies that 479 analytical chemists are faculty members at PUI institutions. The numbers should be considered estimates, because not all analytical faculty are necessarily members of the analytical division. But it is clear that there are practically equal

0003-2700/87/0359-823A/$01.50/0
© 1987 American Chemical Society

numbers of analytical faculty and, therefore, similar employment opportunities at both types of institutions. The distribution of analytical chemists among departments is, of course, different for the two types of schools. If we divide the number of faculty by the number of schools, we find that the average Ph.D.-granting department has between two and three analytical chemists (with a range from 0 to 9), whereas the average PUI department has one (with a range from 0 to 6).

The PUI departments produce a substantial portion of the country's bachelor-level chemists as well. The last annual report of the Committee on Professional Training (*3*) tabulated 3892 graduates with ACS-approved undergraduate degrees. Of those, 41% were from schools that do not have a Ph.D. program. Of the 5403 graduates with nonapproved chemistry degrees, 53% graduated from PUI departments. Of the master's graduates, 25% were from schools that offered the master's degree as their highest degree. There is no question about the need for well-trained and effective teachers at the undergraduate level and the importance of the role they play. A recent publication by the National Science Board (*4*) effectively addresses this point and should be prerequisite reading for anyone considering an academic career, regardless of the type of school.

Career flexibility

A faculty member's activities generally include teaching (i.e., lectures, laboratory supervision, and related preparation), research, service (both on- and off-campus), and advising. The fraction of time spent at each is a complex function of individual interest, institutional mission, time of year, and many other factors. Two lecture courses and laboratory supervision are a typical assignment for a PUI faculty member. Thus teaching obviously occupies a greater fraction of his or her time compared with that of a faculty member at a Ph.D.-granting institution. Survival in a PUI setting depends considerably less on the establishment of an internationally recognized research program; therefore, research and the financial support responsibilities that go with it do not have to be the dominant aspect of one's career. Primary attention can be focused on other areas, such as design of innovative teaching materials or development of laboratory experiments. Organizations such as the Bush Foundation, which operates in the North-Central region of the United States, support activities to promote effective teaching. If a person is so inclined, administrative positions are fairly accessible at small schools where there are relatively few people waiting in line for them.

The extent to which a faculty member is free to choose a career direction depends on a number of factors. For example, the emphasis PUI departments place on research varies considerably, and the time available for it may be nonexistent or comparable with that of a small Ph.D.-granting school. If none of the current faculty are engaged in research, it is likely that other duties completely consume their time or that research is not stressed at that school. An excellent starting point for identifying research-active PUI departments is *Research in Chemistry at Undergraduate Institutions*, a directory published by the Council on Undergraduate Research (available from Brian Andreen, Council on Undergraduate Research, 6840 E. Broadway Blvd., Tucson, Ariz. 85710-2815). Service commitments at small schools can be quite heavy; these schools have many, if not most, of the committees of their Ph.D.-granting counterparts and usually fewer faculty members to staff them. Many schools now are placing increased emphasis on advising, and much of the responsibility goes to the faculty.

Being an analytical chemist in a small department, where you are likely to be the only one, has both desirable and undesirable aspects. You have a high degree of freedom in designing the analytical curriculum (see the related REPORT, p. 829 A), but you also are responsible for staying in touch with the entire field of analytical chemistry.

(The ACS Committee on Professional Training publishes guidelines for all subdisciplines, including analytical chemistry.) You can teach all aspects of the discipline that your department offers, but you are less likely to teach a course in your specialty area (i.e., chromatography, spectroscopy, electrochemistry). The analytical chemist often bears major responsibility for upkeep and acquisition of instrumentation, and although to a degree this task is necessary and appropriate, it can be time-consuming and it usually counts for little in promotion or tenure decisions.

Many time-consuming activities can provide a bonus as well. Direct laboratory supervision provides an excellent opportunity for one-on-one teaching,

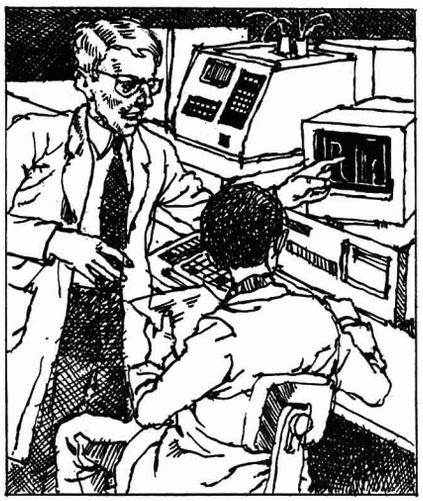

for monitoring student progress, and for getting to know the students. In my experience, informal conversation in the lab has been an important factor in many students' decisions to pursue chemistry as a career. The service commitments at a smaller school permit faculty from across campus to interact, and they provide the opportunity for an individual to have significant input into the direction and policies of the school.

Teaching, research, service, and advising may represent the official aspects of an academic position, but faculty at PUI departments have another task that isn't directly reflected in any of those categories. They must provide their students with ample opportunities to discover the excitement of analytical chemistry and of doing creative work, and they must send a clear message that their work is enjoyable and challenging. Relatively few students enter college knowing they want to pursue chemistry as a career, and most have little, if any, idea of what analytical chemistry is. The task of increasing the number of analytical chemists lies very much with the undergraduate departments and represents a challenging and rewarding endeavor for a potential faculty member.

Research

Potential faculty at PUI departments are usually concerned with whether or not it is possible to have an active research program. The answer is, yes! In 1986, ANALYTICAL CHEMISTRY published 30 papers showing authors associated with PUI departments. There are unique rewards in doing research in a PUI setting. For example, if you enjoy

Linking Value to Performance.

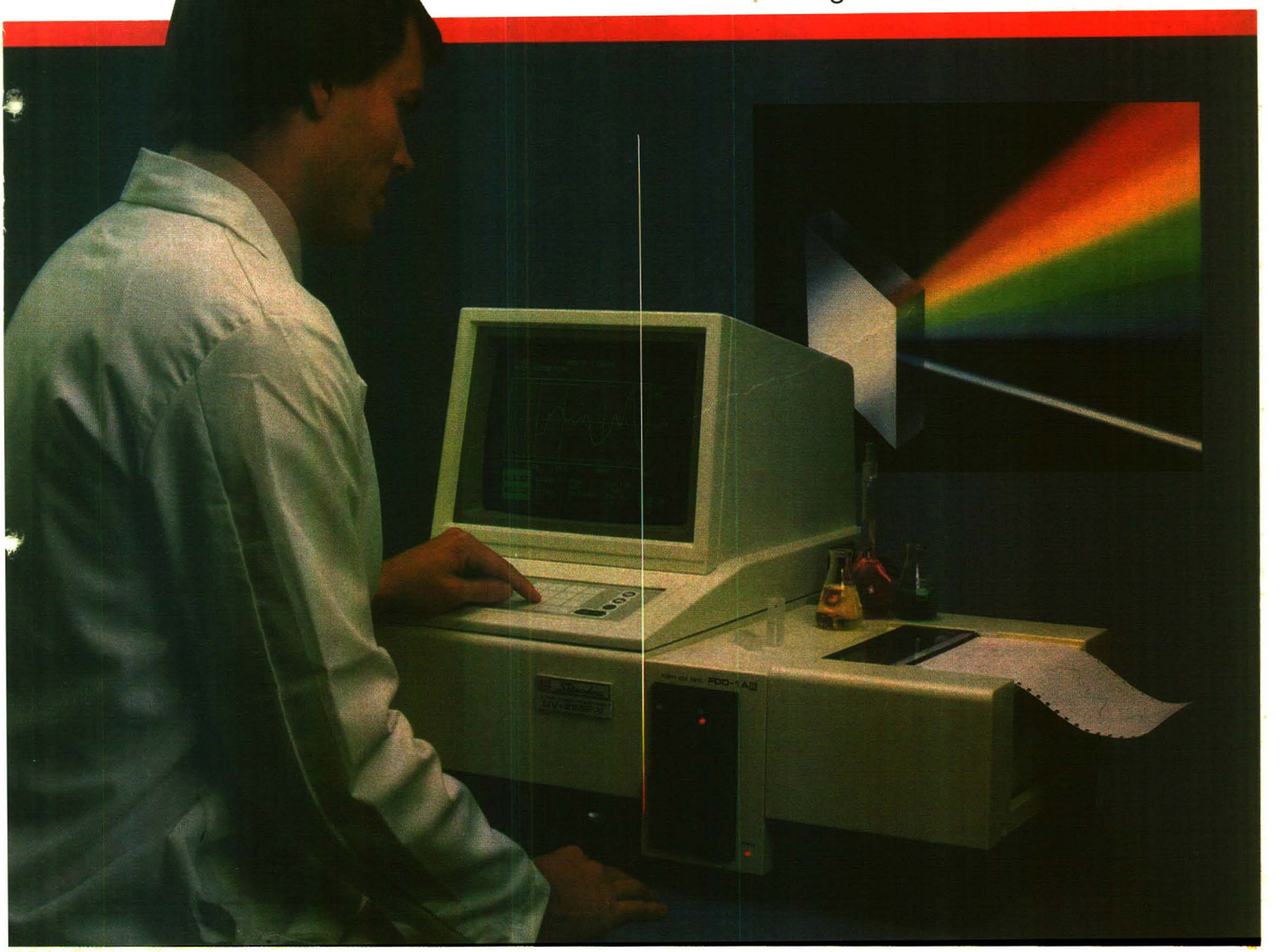

The new UV-265: a UV-VIS with a fundamental difference.

Good, basic optics. Since good spectroscopy has to start with good optics, we've put our best "back-to-basics" thinking into our advanced UV-VIS model UV-265. Fully-sealed optics and completely separate lamphouse without a mirror for *long term integrity of results*; proven symmetrical, double beam design for a flat baseline—every time; a blazed, holographic grating for increased energy throughput; and adjustable slits ensure high spectral resolution (better than 0.1nm)

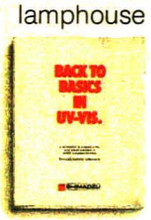

Advanced software power. To fully utilize the information obtained from the UV-265 high-resolution optics and integrated recording system, we've added complete microprocessor control, comprehensive applications software, a full line of accessories and the largest memory yet. A full 2.4 Mbyte memory lets you store and retrieve up to 75 spectra or over 200 parameters and calibration sets per disk. And, of course, it comes with IBM PC/Apple II interface.

So, compare the fundamental differences in UV-VIS instrumentation, write or call for our "Back-to-basics in UV-VIS" booklet and details on the new UV-265.

Shimadzu Scientific Instruments, Inc.
7102 Riverwood Drive, Columbia, MD 21046
(301) 381-1227

SHIMADZU

Shimadzu Corporation International Marketing Div.: Shinjuku-Mitsui Building, 1-1, Nishishinjuku 2-chome, Shinjuku-ku, Tokyo 160, Japan. Tel: Tokyo 03-346-5641 Telex: 0232-3291 SHMDT J.
Shimadzu (Europa) GmbH: Acker Strasse 111, 4000 Düsseldorf, F.R. Germany. Tel: (0211) 666371 Telex: 08586839

Circle 152 for literature. Circle 153 for a call from our representative.

being directly involved in experimental work on a day-to-day basis, then the relative freedom from research administrative duties permits that involvement. The faculty member can (and usually must) spend time doing experiments, working up data, and (not so rewarding) washing the glassware. Students and faculty spend a considerable amount of time working side by side, and watching a student get "turned on" to research for the first time is one of the most satisfying aspects of teaching. There are, of course, a number of potential barriers to research, including relative lack of support staff, students who don't stay in the research group very long, and the ever-present teaching commitments. However, the excitement of research for faculty and students alike, and the effectiveness of research as a teaching medium, make the effort to overcome these barriers well worthwhile.

Funding is important for a healthy research program in analytical chemistry in a PUI setting. Few areas of modern analytical research do not rely on instrumentation to some extent, and start-up funds in PUI departments range from none available to $15,000–$20,000. Clearly one has to be realistic about the type of research that can be started. Generation of external funding is important for providing equipment, your own summer salary, and support for students who are full-time researchers in the summer or part-time during the academic year and for attending scientific meetings. (A single national meeting can more than wipe out your departmental travel allotment!)

Fortunately, the situation with respect to research funding of scientists in PUI departments has improved in recent years. Research Corporation, the Petroleum Research Fund Type B Program of the ACS, and the Research at Undergraduate Institutions (RUI) program of the National Science Foundation (NSF) all target PUI scientists and should be investigated by new faculty members. According to Henry Blount, program director for chemical analysis and surface chemistry at NSF, there are currently seven analytical faculty with research support under the RUI program, and the success rate is similar to that in the regular NSF channels. There is no specific limit or quota on the number of grants to PUI faculty. In addition, NSF has initiated a program aimed at undergraduates called "Research Experiences for Undergraduates" (see *Anal. Chem.* **1987,** *59,* 293 A). Although that program is not restricted to applications from PUI departments, it does reflect the realization that undergraduate research involvement is a necessary and productive activity.

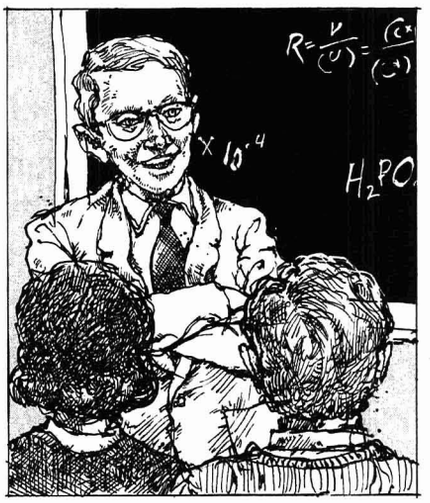

An excellent source of information on undergraduate research is the newsletter published by the Council on Undergraduate Research (available from Michael Doyle, Department of Chemistry, Trinity University, San Antonio, Tex. 78284). The newsletter periodically contains a listing of funding sources, articles on the history of research in PUI departments, comments on various funding agencies, and otherwise generally inspiring articles regarding undergraduate research. A subscription should be deemed a necessary investment by any PUI department that is involved in research, and the student considering an academic career might benefit from reading the newsletter as well. Some philosophies about undergraduate research also have been presented in a series of articles that resulted from a symposium on that topic a few years ago (*5*).

Professional involvement

Being the only analytical chemist in a department can make it easy to lose touch with your field unless you make a determined effort to maintain communication with other analytical chemists. Choose a department with a faculty that attends meetings, presents papers, and plays an active role in local, regional, and national professional organizations. If a department doesn't place priority on professional development, it will be difficult for a new faculty member to do so. Sabbaticals and brief visits to larger institutions are inspirational and educational from a technical point of view and can provide stimulating discussion at a level your undergraduates can't give. Those visits also give you a firsthand look at what Ph.D.-granting departments expect of their incoming graduate students.

Small-school atmosphere

Difficult to define but nonetheless important is the sense of community that a smaller school can provide. A faculty member at a small school interacts with people from physical plant to central administration and often knows every chemistry major in the department. Divisional structure within the department is usually unnecessary, and one faculty member can keep abreast of what the others are doing. An individual can have input into most departmental matters and into a large number of college and university matters. Access to campus policy makers is relatively easy, and in many places it is still possible to visit with the college president in the coffee shop. Although life can still be hectic at a PUI school, it is perhaps less so than at a large, major university.

Your career—your choice

The important thing to keep in mind is that you are free to decide how your professional and personal life develop, and that with a little imagination and perseverance, you can create an atmosphere that can satisfy whatever level of challenge or creativity you want. Both industry and academics, either at a small or large school, have their unique opportunities and problems. A PUI setting may provide the best overall environment for your personality and interests and no doubt can provide you with an exciting career in a position that is vitally important to the field of analytical chemistry.

References

(1) Kissinger, P. T.; Cooks, R. G.; Heineman, W. R. *Anal. Chem.* **1986,** *58,* 1399 A.
(2) Morrison, G. H. *Anal. Chem.* **1987,** *59,* 375 A.
(3) *Chem. Eng. News.* **1987,** *65*(20), 59.
(4) "Undergraduate Science, Mathematics and Engineering Education," 86-100; National Sci. Bd; National Science Foundation: Washington, D.C., 1986.
(5) Mohrig, J. R.; Wubbels, G. G. *J. Chem. Educ.* **1984,** *61,* 507.

Royce C. Engstrom received his B.S. in 1975 from the University of Nebraska at Omaha and his Ph.D. in 1979 from the University of Wisconsin–Madison. He is currently an associate professor and chairman of the chemistry department at the University of South Dakota. His research interests are in electroanalytical chemistry and in the characterization of surfaces and interfaces using techniques with high spatial resolution.

Turbochrom brings you the best views of the future.

Introducing Turbochrom with Microsoft Windows.™

It's the PC-based chromatography data system for multi-tasking power through Microsoft Windows—the choice of IBM™ and other computer leaders.

This powerful chromatography software gets results. Acquire data from 15 instruments simultaneously, while using your computer to generate custom reports, optimize acquisition parameters, or run other programs.

Turbochrom networks easily to other PCs, and connects with Nelson's lab information management products. Contact Nelson Analytical, Inc., 10040 Bubb Road, Cupertino, CA 95014. (408) 725-1107.

nelson ANALYTICAL

We're Always Thinking Ahead.

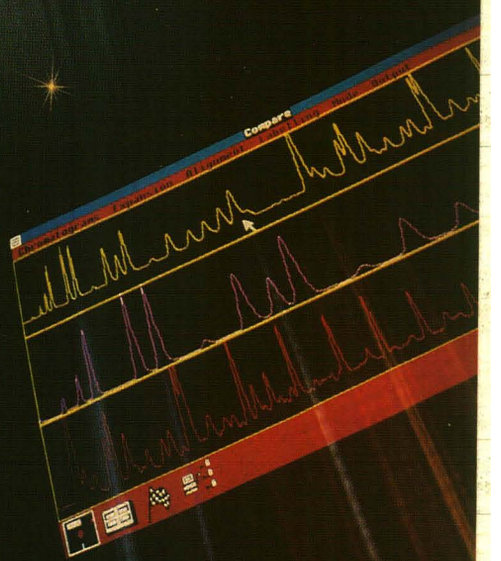

Windows is a registered trademark of Microsoft Corp.
IBM is a registered trademark of International Business Machines Corp.

CIRCLE 112 ON READER SERVICE CARD

In LC sample injection, "just right" is all wrong.

Rheodyne explains why.

Why not load a 20-μL sample into a 20-μL sample loop? Seems just right. But it's all wrong.

It's wrong because loading a volume of sample equal to the volume of the loop produces the worst accuracy and precision. Much more sample—or much less—is better.

This is one of several important facts about LC sample injection not immediately apparent to those who use liquid chromatographs. All are explained in our one-page bulletin, "Tips on LC Injection." It clears up many common misconceptions. And helps you get better quantitative results.

For a copy contact Rheodyne, Inc., P.O. Box 996, Cotati, California, 94928, U.S.A. Phone (707) 664-9050.

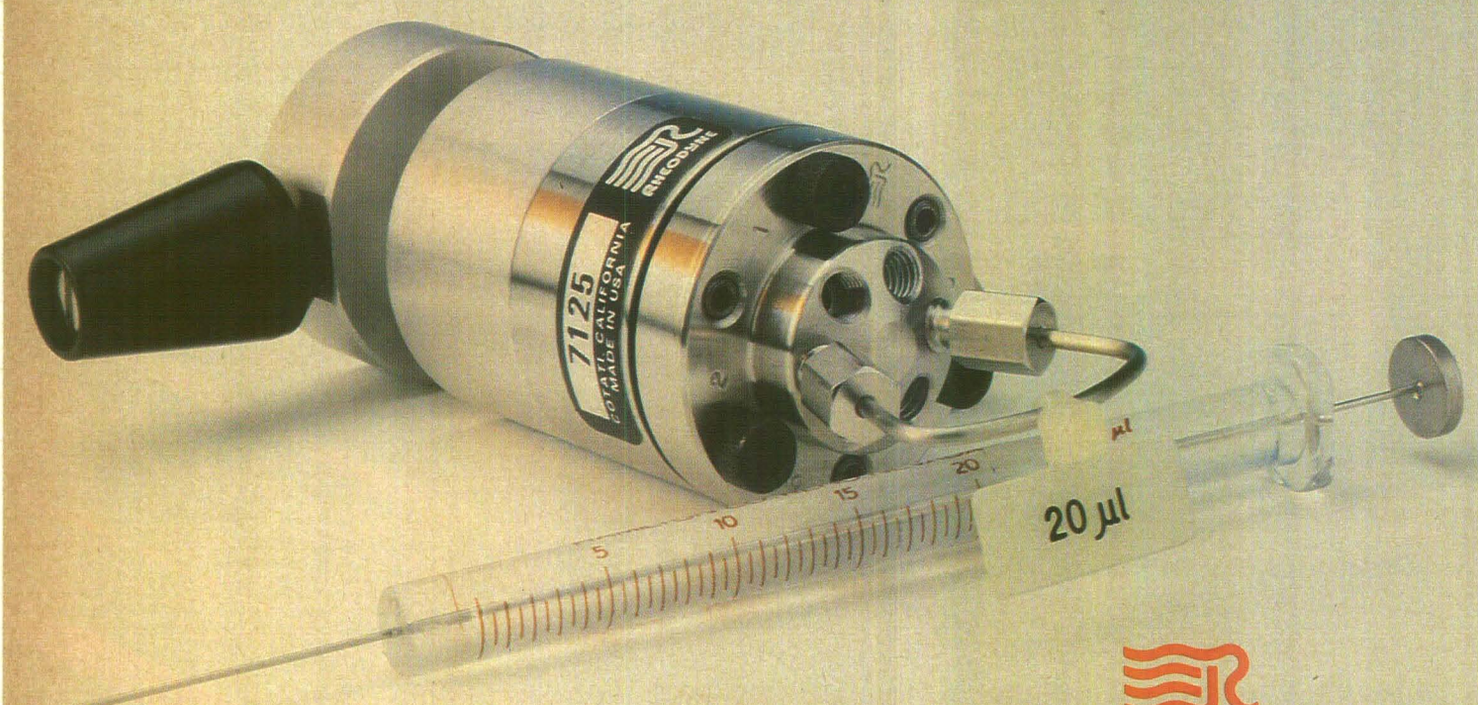

RHEODYNE

THE LC CONNECTION COMPANY

CIRCLE 140 ON READER SERVICE CARD

David C. Locke
Chemistry Department
Queens College, CUNY
Flushing, N.Y. 11367

William E. L. Grossman
Chemistry Department
Hunter College, CUNY
New York, N.Y. 10021

The Curriculum in Quantitative Analysis: Results of a Survey

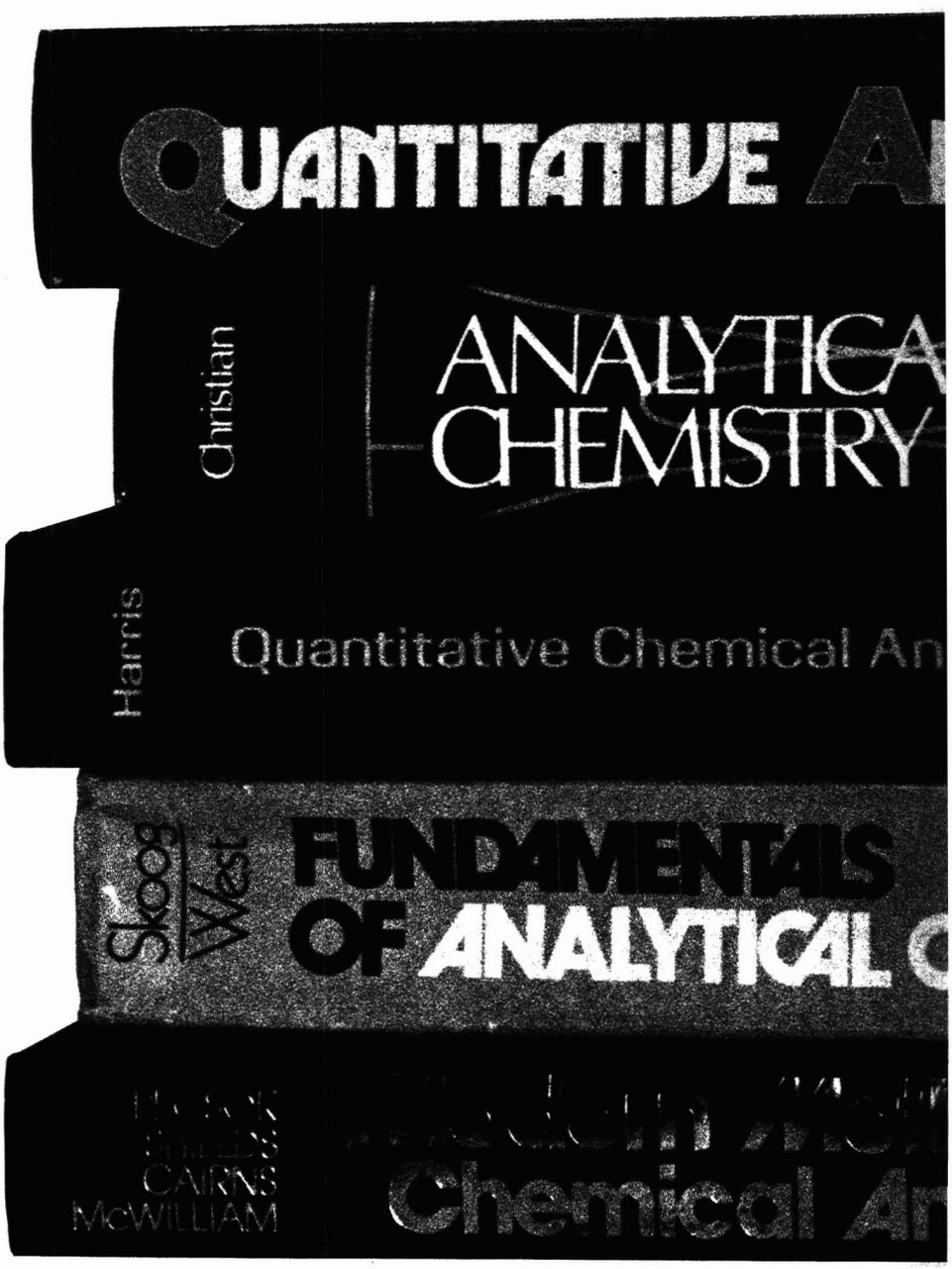

During the course of undergraduate studies, every chemistry major is introduced to the concepts of quantitative analysis. As instructors of sophomore-level quantitative analysis courses at the City University of New York, we wanted to learn whether the content of our courses was similar to that of others in the United States. We developed a short questionnaire to determine which topics our colleagues teach, how much weight they give these topics, and which experiments they use in the laboratory. We also wanted to discover how closely the ACS examination in quantitative analysis (*1*) matches the typical course curriculum. This REPORT describes the questionnaire and the results we obtained and poses some basic questions about the curriculum in quantitative analysis.

Questionnaire, distribution, and response

The three-page questionnaire contained three parts. The first part asked for demographic and general course information. The second part asked for an estimate of the number of lecture hours devoted to a given set of topics. This set was essentially the table of contents of Day and Underwood's text (*2*) plus a few additional topics; any of the popular current texts include virtually the same topics. We also requested estimates of the number of lecture hours spent on these same topics in the instrumental analysis and general chemistry courses, primarily to determine where subjects not discussed in the quantitative analysis course were covered, if at all. However, responses to this question were insufficient for meaningful conclusions to be drawn. The third part asked about the laboratory experiments performed in the quantitative analysis course and in the other two courses; the list of experiments was drawn from the Day and Underwood laboratory manual (*3*) and from our own experience. Space for listing additional topics was provided, and comments were solicited.

The questionnaire was sent to approximately 300 colleges and universities in the United States. The addressees either were known by us to be ana-

0003-2700/87/0359-829A/$01.50/0
© 1987 American Chemical Society

Table I. Textbooks used in quantitative analysis courses

Textbook authors	% of Respondents using[a]
Skoog & West	31.1
Harris	23.6
Day & Underwood	11.3
Fritz & Schenck	7.5
Christian	5.7
Ramette	4.7
Kennedy	3.8
Flaschka, Bernard, & Sturrock	2.8
Harris & Kratochvil	1.9
Kenner & Busch	1.9
Brewer	0.9
Guenther	0.9
Pecsok, Shields, Cairns, & McWilliam	0.9
Peters, Hayes, & Hieftje	0.9

[a] $n = 104$

lytical chemists or were listed in the ACS *College Chemistry Faculties* (*4*) as specialists in analytical chemistry. The specific colleges were chosen somewhat arbitrarily, but we attempted to strike a balance among two-year community colleges, four-year colleges, and research-oriented universities. The surveys were mailed out in June 1986; those returned to us by October 1986 are included in this summary.

Of the 300 questionnaires sent out, 119 were returned, and 109 of them contained usable information. However, because only three of the approximately 50 two-year schools that received the questionnaire responded, the effective rate of return is 109 out of 250, or about 40%. This high response rate—and the fact that nearly every respondent requested a copy of the survey results—indicates to us that academic analytical chemists are greatly interested in the content of quantitative analysis courses.

Respondent profile

From the general information section we learned that the respondents were predominantly (98%) from four-year colleges and universities; 83% of the schools offer a one-semester course, 16% a one- or (rarely) a two-quarter course, and only one a trimester course. The course size varied considerably; 44% of the schools typically register 20 or fewer students per course; 41% between 21 and 50; and 15% have 51–150 registrants. Two-thirds of the quantitative analysis courses are scheduled for 3 hours of lecture per week; one-third have 2 lecture hours. A few have either 1 or 4 hours of lecture. In the laboratory, 6–10 experiments are done in three-quarters of the courses; 90% schedule 3–6 hours of lab per week (3 or 5 lab hours, 12.5% each; 4 hours, 20%; 6 hours, 45%), and a few have 7–9 hours. However, if we group responses by number of lab hours and separately average the number of experiments done by each group, the average number, 8.9 experiments, is almost independent of the number of scheduled lab hours.

The textbooks used in the respondents' courses are listed in Table I. Editions were usually not specified, but presumably the most recent editions were used. Two-thirds of the respondents used one of only three texts, and 90% used one of eight texts.

Course content

The most important information obtained from this survey concerns the content of the courses, which we express as the relative amount of lecture time spent on various subjects ordinarily considered to be in the domain of the quantitative analysis course. The results are presented in Table II. The data supplied (hours of lecture per topic) were converted to a percentage of the total lecture time, and these percentages were averaged. We used this parameter, rather than hours of lecture, to normalize for the variable number of lecture hours per week and weeks per course. We also calculated the percentage of respondents who reported spending more than one-third of a lecture hour on each subject (the column in Table II headed "% Courses"). The relative lecture times hold few surprises, although the variations (expressed as % SD [standard deviation]) from one instructor to another are significant. In the typical course, 3% of lecture time is equivalent to about 1 lecture hour. Topics covered in less than 1 hour on the average can be considered specialty topics, and the greater apparent variations in coverage of subjects from activity concept on down the list merely reflect the absence of coverage of the topic in many courses. This is evident from the "% Courses" column in Table II. For example, every instructor covers experimental error and acid–base and redox equilibria. Most instructors spend between 7% and 15% of total lecture time on acid–base equilibria, but the range is from 3% to 38%. On the other hand, 10% of the respondents spend 0.5 hours lecturing on fluorescence spectroscopy; 11% give the topic 1 hour, and 3%, 2 hours; but 76% don't mention the subject at all in this course. Presumably the topics covered in quantitative analysis vary from institution to institution at

Table II. Quantitative analysis course lecture topics

Topic	% Lecture	% SD	% Courses	% ACS standardized test questions
Acid–base equilibria	12.3	54	100	14
Redox equilibria	7.1	49	100	14
Advanced acid–base equilibria	6.3	60	100	0
Complexometric titrations	5.6	52	96	12
Review of chemical equilibria	5.3	72	90	0
Statistical methods	5.2	63	94	10
Spectrophotometry	5.2	73	86	16
Gravimetric analysis	5.1	65	85	6
Introduction to volumetric analysis	4.8	75	95	0
Solubility equilibria	4.8	69	88	2
Potentiometry/pH	4.6	61	88	0
Application of redox titrations	4.0	65	90	2
Experimental error	3.6	64	100	0
Activity concept	2.8	89	83	0
Introduction to separations	2.8	103	60	0
Precipitation titrations	2.6	96	71	4
Ion-selective electrodes	2.2	86	67	2
Gas chromatography	2.1	143	44	4
UV spectrophotometry	1.9	128	47	0
Sampling for chemical analysis	1.7	100	69	0
Atomic spectroscopy	1.7	88	36	0
Nonaqueous pH/titrations	1.6	113	56	2
Solvent extraction	1.4	143	42	4
HPLC	1.4	150	38	2
Polarography	1.0	210	27	0
Coulometry	0.9	156	29	0
Electrogravimetry	0.8	188	28	0
Fluorescence spectroscopy	0.6	217	24	2

Think Small.

Maximize ICP Productivity With ARL's New Mini-Torch.

Meet the mini-torch: the most compact and efficient plasma torch ever devised. It makes ARL's 3410 ICP Spectrometer ideal for the small lab. Or, for the big lab with a small budget.

Because it can save you $10,000 a year in ICP overhead.

With the 3410, less is definitely more. It offers smaller operating costs: the mini-torch cuts both argon and power consumption by a full 50%. It means smaller space requirements: the compact system sits on its own integrated storage cabinet. And, it boasts a smaller purchase price—the smallest of any complete ICP system.

Better yet, the 3410 combines these cost savings with analytical performance that's absolutely unsurpassed.

For the big picture on this small wonder, call ARL at 818-352-6011. And cut your overhead down to size.

ARL

Applied Research Laboratories

9545 Wentworth St., P.O. Box 129, Sunland, CA 91040
(818) 352-6011
For more sales information, call ARL toll-free at: 800-551-8741 Interstate and 800-631-6841 in California.

CIRCLE 4 ON READER SERVICE CARD

Table III. Lecture vs. text coverage, by textbook used

Topic	Skoog & West (n = 32)			Harris (n = 25)			Day & Underwood (n = 14)		
	% Text	% Lecture	% SD[a]	% Text	% Lecture	% SD[a]	% Text	% Lecture	% SD[a]
Acid–base equilibria	10.2	12.8	47	12.0	14.3	48	5.7	10.1	54
Redox equilibria	9.6	7.6[b]	46	6.8	7.3	61	6.1	7.7[b]	30
Advanced acid–base equilibria	2.7	7.1[b]	72	6.5	6.5	55	4.0	6.0[b]	48
Complexometric titrations	3.8	6.5[b]	55	3.8	5.7[b]	55	4.6	4.6	57
Review of chemical equilibria	3.4	6.6[b]	68	4.8	6.2[b]	56	5.1	3.9	66
Statistical methods	5.4	5.9	53	3.4	4.1	65	5.1	4.5	61
Spectrophotometry	9.0	4.7[b]	89	6.2	4.9[b]	46	8.3	4.8[b]	67
Gravimetric analysis	5.0	5.3	56	3.4	4.6	72	5.2	4.9	73
Introduction to volumetric analysis	4.2	4.7	62	0	4.3[b]	72	4.6	4.1	66
Solubility equilibria	4.4	5.0	73	3.2	5.4[b]	56	4.3	4.7	63
Potentiometry/pH	6.3	4.4[b]	67	3.4	4.9[b]	57	3.8	5.6	89
Applications of redox titrations	5.4	4.1[b]	66	5.5	3.5[b]	91	4.9	5.0	42
Experimental error	2.9	4.0[b]	75	2.4	3.3[b]	63	2.2	3.0	52

[a] % SD = % standard deviation in lecture hours.
[b] Difference between % lecture and % text is significant at the 95% level.

least in part as the coverage of subjects varies among other chemistry courses at that institution. However, our data are too sparse to draw a firm conclusion.

We thought there might be a relationship between the relative amount of time spent on a topic in lecture and the relative emphasis in the textbook used. To test this, we separated questionnaires according to textbook used and determined for the three most popular texts the percentage of lecture time spent on the 13 topics to which more than 1 hour of lecture was devoted on the overall average (Table II). The differences for each topic were subjected to t tests. These results are given in Table III. The variation among lecturers is again large. Although it is clear, and hardly surprising, that lecturers do not feel constrained to follow slavishly the emphases in their assigned texts, the range of topics clearly does follow the textbooks.

Textbook evolution

We also thought it would be of interest to trace text content through the years. We counted pages in four earlier quan-

Table IV. Subjects covered by % text pages

Topic	Harris (*11*)	Kolthoff et al. (*5*)	Kolthoff & Sandell (*6*)	Rieman et al. (*7*)	Willard & Furman (*8*)
Acid–base equilibria	12.0	9.5	7.9	15.6	12.3
Redox equilibria	6.8	3.6	3.4	6.9	7.0
Advanced acid–base equilibria	6.5	1.1	—	—	—
Complexometric titrations	3.8	9.5	—	—	—
Gravimetric analysis	3.4	11.9	44.1	28.7	28.6
Review of chemical equilibria	4.8	4.0	5.4	—	3.4
Statistical methods	3.4	5.9	6.5[a]	1.7	2.2[a]
Spectrophotometry	6.2	7.7	5.7	4.5	2.4
Introduction to volumetric analysis	—	2.2	2.2	4.8	4.8
Solubility equilibria	3.2	5.9	3.6	—	—
Potentiometry/pH	3.4	1.5	1.4	7.7	—
Application of redox titrations	5.5	9.1	10.4	14.4	16.5
Experimental error	2.4	1.1	[a]	1.7	[a]
Activity concept	2.0	0.6	0.4	1.2	0.7
Introduction to separations	2.6	0.6	—	2.4	1.9
Precipitation titrations	4.3	1.4	4.7	3.3	6.8
Ion-selective electrodes	1.7	—	—	—	—
Gas chromatography	3.2	2.5	—	—	—
Sampling for chemical analysis	—	—	—	0.2	0.7
Atomic spectroscopy	3.4	1.0	0.7	—	—
Nonaqueous pH/titrations	0.3	1.0	—	—	—
Solvent extraction	2.9	5.5	1.1	—	—
HPLC	4.3	6.6[b]	0.5[b]	—	—
Polarography	6.8	4.6	—	1.0	—
Coulometry	1.1	1.2	—	—	—
Electrogravimetry	3.6	4.3	5.2	6.0	12.6
Fluorescence	1.5	1.4	0.5	—	—
Total no. of pages	585	724	558	418	413

[a] Includes experimental error and statistics.
[b] Column chromatography.

ARL has a new source of excitement.

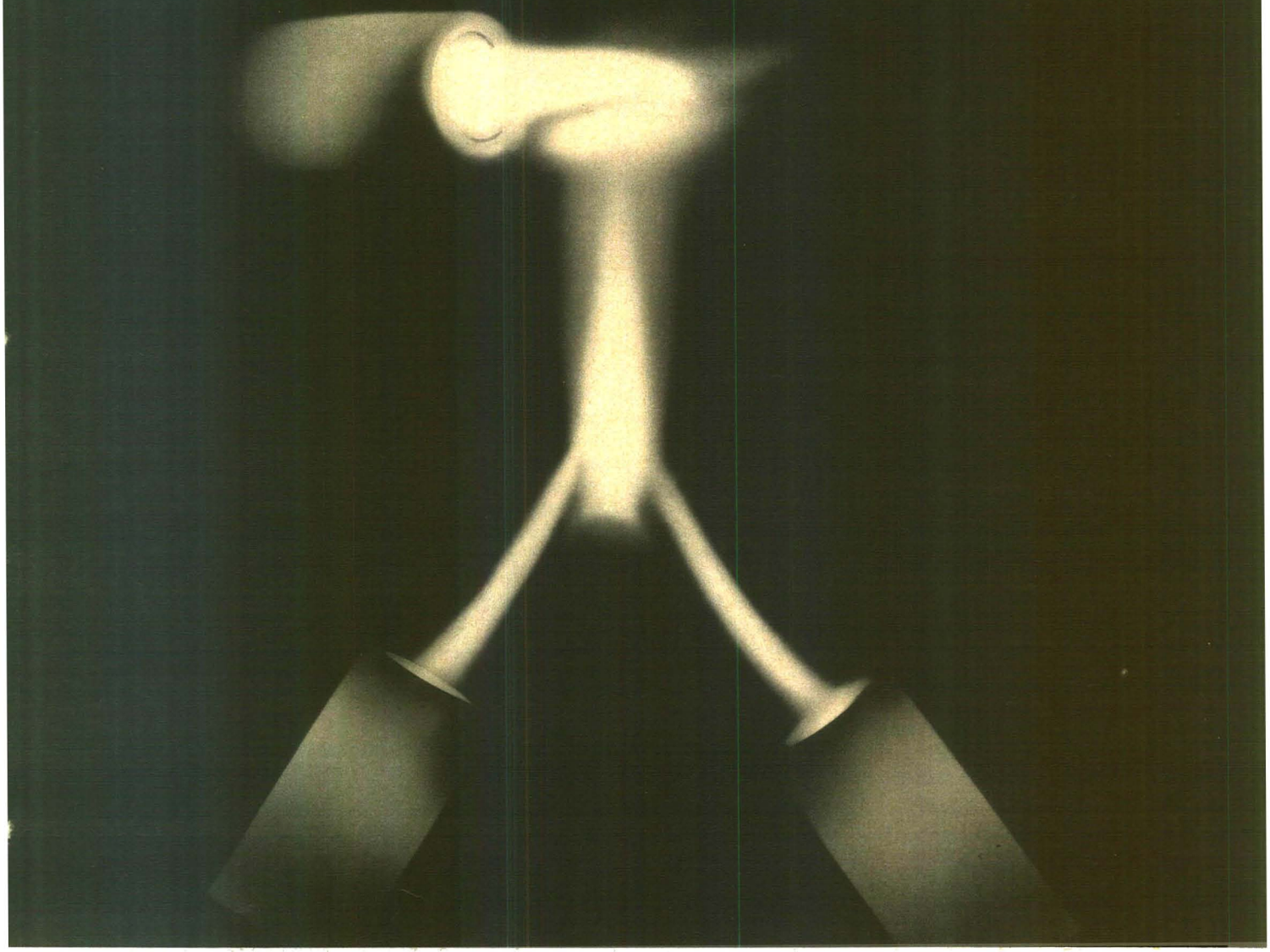

DC Plasma, for complex matrices, nasty samples and tight budgets.

Meet our new plasma. ARL is now your exclusive source for SpectraSpan DC Plasma Spectrometers. But we warn you. You may find their performance, and price irresistible.

To begin with, the SpectraSpan DCP is famous for its ruggedness and reliability. It tackles high solids, organic solvents, viscous samples, and complex matrices as a matter of course. Plus, its Echelle Spectrometer covers a broad 190 nm to 800 nm range, with extremely high resolution.

Operation is easy. And so is the price, with a single element sequential for less than $25,000 and a 20-element simultaneous unit for about $75,000.

Exciting? Yes. Perfect for everyone? No. Which is why ARL offers more elemental analysis choices than anyone else. We have written a paper to help you decide which technology... AA, ICP or DCP... is right for you. Send or call for your copy today.

ARL

Applied Research Laboratories

9545 Wentworth Street, P.O. Box 129, Sunland, California 91040

For more sales and marketing information, call ARL toll-free at: 800-551-8741 Interstate and 800-631-6841 in California.

CIRCLE 3 ON READER SERVICE CARD

SUPER-QUIET XENON LAMPS FOR PHOTOMETRIC INSTRUMENTS

Outstanding luminance from UV to IR

Hamamatsu flash mode Super-Quiet Xenon Lamps provide a minimum of 10^9 flashes! Arc stability is 5 times higher, service life 10 times longer than conventional lamps. Available in three sizes for:

- Stroboscopes
- Chromatographs
- Photoacoustic Spectroscopes
- Strobe Cameras
- Photomasking Devices
- Fluorospectrophotometers
- Color and SO_2 Analyzers
- Other light-sensitive instruments

For Application Information, Call 1-800-524-0504
1-201-231-0960 in New Jersey

HAMAMATSU

HAMAMATSU CORPORATION
360 FOOTHILL ROAD
P. O. BOX 6910
BRIDGEWATER, NJ 08807
PHONE: 201/231-0960
International Offices in Major Countries of Europe and Asia.

© Hamamatsu Photonics, 1986

CIRCLE 63 ON READER SERVICE CARD

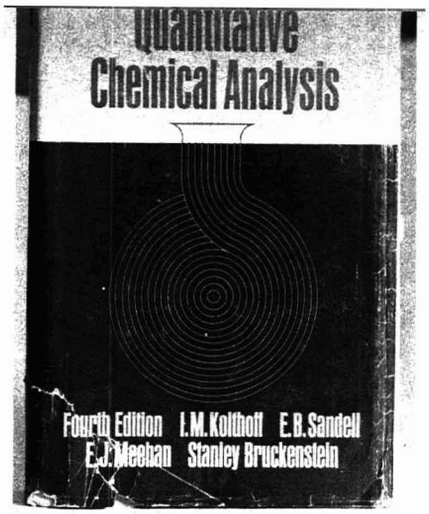

A well-used fourth edition of Kolthoff's quantitative analysis text.

titative analysis texts: Kolthoff et al. (1969) (*5*); Kolthoff and Sandell (1952) (*6*); Rieman, Neuss, and Naiman (1951) (*7*); and Willard and Furman (1940) (*8*). We were unable to locate a copy of the 1936 (1st) edition of Kolthoff and Sandell (*9*), perhaps the granddaddy of quantitative analysis texts (*10*). The results are compared in Table IV. Although there was far greater emphasis on gravimetric analysis and applications of redox titrations, the distribution of pages among the other topics generally is not too different from that in contemporary texts. However, the earlier texts are qualitatively different: in particular, the experimental aspects of analysis are far more closely integrated with the theoretical descriptions. In modern textbooks the experimental directions are in a wholly separate section or even a separate manual, with some footnotes. As has been thoughtfully noted by Williams and Bromund (*10*), these earlier texts reflect what analytical chemists then actually practiced professionally: gravimetric and volumetric analyses. Contemporary quantitative analysis textbooks certainly do not reflect what analytical chemistry is, nor what analytical chemists do or are expected to know today. Rather, current texts seem to have evolved directly from their predecessors, with expanded coverage of statistical methods and the addition of discussions of some instrumental techniques, which for the most part are covered in other courses anyway.

ACS examination

We determined the percentage of questions on the ACS Examinations Committee's standardized test in quantitative analysis (*1*) that fall into each of our topic categories. The percentages are shown in Table II. Eighty percent of the questions concern the major lecture topics (those to which one or more lecture hours are devoted on the average). However, the attention paid in the standardized exam to redox equilibria, complexometric titrations, statistical methods, spectroscopy, experimental error, and solvent extraction seems somewhat out of line with the emphasis in lectures and texts.

Laboratory experiments

We requested information on the experiments performed in the laboratory portions of the respondents' quantitative analysis courses, without regard to the relative amount of time spent on

Table V. Laboratory experiments

Experiment	No. of respondents[a] performing experiment in: Quantitative analysis	Instrumental analysis	Introductory chemistry
Acid–base indicator titration	95	1	11
Spectrophotometry	87	13	4
Complexometric titration	85	4	2
Redox indicator titration	83	2	8
Acid–base potentiometric titration	82	10	3
Gravimetric determination	79	0	12
Precipitation titration	59	2	2
Calibration of glassware	51	2	5
Potentiometric redox titration	44	18	2
Ion exchange	40	9	4
Calibrate balance	30	0	3
Gas chromatography	27	52	0
Electrogravimetry	21	17	0
Grans plot titration	16	9	0
HPLC	13	52	0
Coulometric titration	12	33	1
Infrared spectroscopy	5	56	1
NMR spectroscopy	1	40	1

[a] Total no. of respondents = 95.

Fun Physical Science Activities for Children and Adults to Do Together

- colorful comic book format
- useful at home or in classrooms
- reinforces language and math skills
- relates science concepts to technology
- aimed at 4th through 6th graders

Price per subscription (one-year, four-issues)		
To continental U.S. addresses	1–4	$4.00 each
	5–19	$3.00 each
	20 or more	$2.00 each
To addresses outside the continental U.S.	50 or more (minimum)	$3.00 each

For subscription information write or call:

American Chemical Society
Prehigh School Science Program
1155 Sixteenth St., N.W.
Washington, DC 20036

(202) 452-2113

-MICROANALYSIS-

- **CAPSULES** PRESSED CAPSULES, SMOOTH WALLED CAPSULES, BOATS AND PANS IN ALUMINIUM, TIN, SILVER, NICKEL OR PLATINUM
- **SILICAWARE** COMBUSTION, REDUCTION, SCRUBBING TUBES, MAGNETIC LADLES, SWARF CRUCIBLES, CONVERSION TUBES FOR ELEMENTAL ANALYSERS
- **REAGENTS** COMBUSTION CATALYSTS, CONTACT CARBONS, METALS, REDUCTION REAGENTS, SILICA CHIPS AND WOOL, SILVER GAUZE AND WOOL, COLUMN PACKING MATERIALS, COMBUSTION ADDITIVES, DOPING AGENTS, ORGANIC ANALYTICAL STANDARDS FOR ELEMENTAL ANALYSIS
- **PLATINUMWARE** BOATS, DISHES, CRUCIBLES, BASKETS, FLAGS AND GAUZE CATALYST STRIPS IN PLATINUM
- **SUNDRIES** 'O' RINGS, FORCEPS, MICRO-DESICCATORS, BALANCE BRUSHES, MICRO-PIPETTES, GELATIN CAPSULES, MICRO-SPATULAS, OXYGEN FLASKS, TUBING FITTINGS, NYLON AND COPPER TUBING

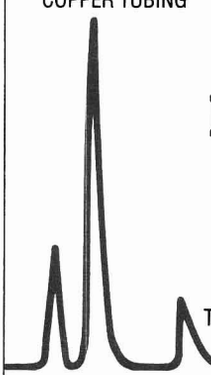

ELEMENTAL MICROANALYSIS LIMITED

EXETER ROAD INDUSTRIAL ESTATE
OKEHAMPTON · DEVON · ENGLAND · EX20 1QA
TELEPHONE: (0837) 4446/7
TELECOM GOLD MAILBOX 87 WQQ090
TELEX 265871 MONREF G QUOTING REF: WQQ090

CIRCLE 42 ON READER SERVICE CARD

each. Table V lists the experiments and courses in which they are performed. Again, the traditional determinations seem to continue to be the mainstays of the laboratory part of the course. Although presumably they are emphasized less than in days of yore, gravimetric analyses still are carried out. Even more surprising to us is the number of institutions at which balances and glassware are calibrated!

Conclusion

This survey has given us a good idea of what *is* being taught in contemporary quantitative analysis courses. What *should* be taught is another question. To what extent must we concern ourselves with teaching fundamental principles and laboratory skills, and how far can we go toward showing students modern analytical practices? Are the skills taught in the labs, and the principles enunciated in texts and lectures, sufficiently fundamental to everything we do to justify the time and intellectual effort expended on them? Are we being fair to our students or to ourselves by hanging onto a curriculum outlined half a century ago? These questions clearly are worth addressing, and an appropriate forum might be found at meetings widely attended by analytical chemists. We believe a wide-ranging discussion of the content of the analytical chemistry component of the undergraduate chemistry major is long overdue.

Acknowledgment

We thank all those who completed and returned the questionnaires.

References

(1) Examinations Committee, Division of Chemical Education, American Chemical Society. *ACS Examination in Analytical Chemistry, Form 1982;* American Chemical Society: Washington, D.C., 1982.
(2) Day, R. A.; Underwood, A. L. *Quantitative Analysis*, 5th ed.; Prentice-Hall: Englewood Cliffs, N.J., 1986.
(3) Day, R. A.; Underwood, A. L. *Quantitative Analysis, Laboratory Manual*, 5th ed.; Prentice-Hall: Englewood Cliffs, N.J., 1986.
(4) American Chemical Society. *College Chemistry Faculties;* American Chemical Society: Washington, D.C., 1984.
(5) Kolthoff, I. M.; Sandell, E. B.; Meehan, E. J.; Bruckenstein, S. *Quantitative Chemical Analysis;* MacMillan: New York, 1969.
(6) Kolthoff, I. M.; Sandell, E. B. *Textbook of Quantitative Inorganic Analysis*, 3rd ed.; MacMillan: New York, 1952.
(7) Rieman, W.; Neuss, J. D.; Naiman, B. *Quantitative Analysis*, 3rd ed.; McGraw-Hill: New York, 1951.
(8) Willard, H. H.; Furman, W. H. *Quantitative Analysis;* Van Nostrand: Princeton, N.J., 1940.
(9) Kolthoff, I. M.; Sandell, E. B. *Textbook of Quantitative Inorganic Analysis;* MacMillan: New York, 1936.
(10) Williams, T. R.; Bromund, R. H. *J. Chem. Educ.* **1979**, *56*, 98–99.
(11) Harris, D. C. *Quantitative Chemical Analysis;* Freeman: New York, 1982.

David C. Locke (right) is professor of chemistry at Queens College of the City University of New York. His research interests include analytical applications of supercritical fluids, physical measurements using chromatography, HPLC, and environmental chemistry.

William E. L. Grossman is associate professor of chemistry at Hunter College of the City University of New York. He is interested in the analytical applications of Raman spectroscopy and in keeping dry.

Multiply your UV/VIS capabilities:

Design a system for optimum performance.
Start with one of our highly reliable Lambda UV/VIS Spectrophotometers. Add the optimum mix of Perkin-Elmer accessories to suit your needs. Then choose one or more of our application-specific software packages. The result? The perfect system to multiply the UV/VIS capabilities of your lab.

A system for nearly every application.
No matter what your application—biological sciences, industrial quality control, pharmaceutical research or food analyses—there's a Perkin-Elmer UV/VIS system that will satisfy your requirements. And with our full line of accessories, such as cell holders, temperature controllers and sample holders, you can equip each instrument to fit your exact specifications.

Advanced software, additional versatility.
Our software makes our hardware even more versatile. We offer programs for kinetics, quantitative analysis, tablet dissolution, multicomponent analysis, spectral manipulation and protein and nucleic acid quantitation. And

The Lambda Series from Perkin-Elmer.

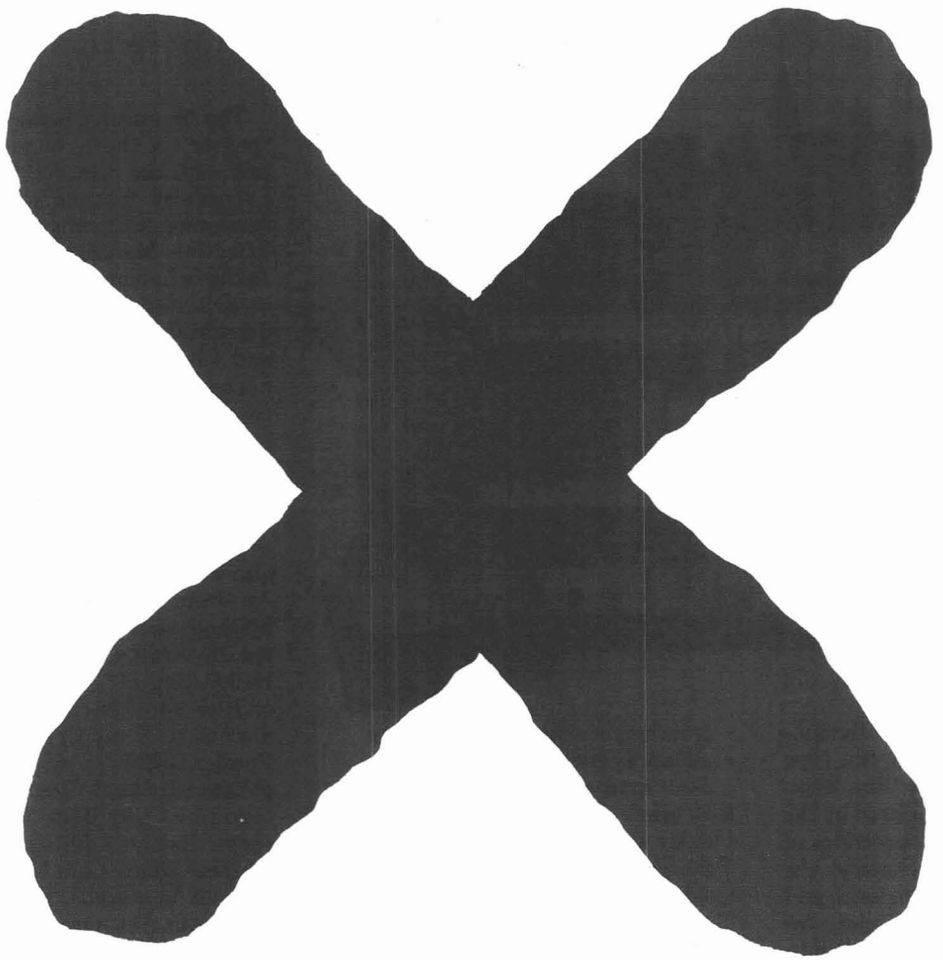

we're constantly developing new applications software to multiply our spectrophotometers' capabilities.

Comprehensive service.
To ensure your Lambda Series' effectiveness, Perkin-Elmer provides specialized service just about anywhere around the globe. Our Technical Specialists, for example, assist you with informed UV/VIS applications and software backup. Our Service Engineers are highly trained to give you fast, efficient on-site service. And customer training courses are available to help you get the most out of our UV/VIS instruments.

If you're ready to multiply your UV/VIS capabilities, consider all the benefits the Lambda Series offers. Then call your Perkin-Elmer Technical Representative for more details. Or, for literature in the U.S., please call 1-800-762-4000.

Perkin-Elmer Corp., 761 Main Ave.
Norwalk, CT 06859-0012 U.S.A.
Tel: (203) 762-1000. Telex 965-954.

Bodenseewerk Perkin-Elmer & Co., GmbH,
Postfach 1120, 7770 Ueberlingen,
Federal Republic of Germany. Tel: (07551) 810.

Perkin-Elmer Ltd., Post Office Lane,
Beaconsfield, Bucks HP9 1QA, England.
Tel: Beaconsfield (049 46) 6161.

1937 50 1987

PERKIN-ELMER

CIRCLE 128 ON READER SERVICE CARD

MEETINGS

The 26th Eastern Analytical Symposium (EAS) will be held at the New York Hilton in New York City, Sept. 13–18. The meeting is sponsored by the North Jersey and New York sections of the American Chemical Society; the Delaware Valley, New England and New York sections of the Society for Applied Spectroscopy; and the American Microchemical Society.

The technical program consists of 55 oral and four poster sessions. Session topics include the following:

- advances in HPLC
- environmental chemistry: reliability, techniques, and economics
- developments in near-IR
- chemometrics
- thermal characterization of polymeric materials
- microwave techniques
- analytical chemistry in the regulatory milieu
- advances in the applications of NMR spectroscopy
- current issues in drug testing
- problem solving in pharmaceutical research and development
- computer hardware and its applications in the laboratory
- fluorescence spectroscopy
- modern methods in electroanalytical chemistry
- frontiers in analytical toxicology
- advances and trends in FT–IR

Four symposia will be held to honor this year's award recipients. William Fateley will be the recipient of the New York Society for Applied Spectroscopy Gold Medal on Wednesday, Sept. 16. The EAS award in chromatography will be presented to Haleem J. Issaq on Wednesday, Sept. 16. Velmer Fassel will receive the EAS award for outstanding achievements in analytical chemistry at a symposium held on Thursday, Sept. 17. Finally, the American Microchemical Society's Benedetti-Pichler Award will be presented to David Hercules on Friday, Sept. 18.

An exposition of scientific instruments and supplies will also take place in the New York Hilton. In addition, 10 workshops sponsored by the exhibitors will be offered on the following topics: atomic spectroscopy, GC–SFC, near-IR, chemical microscopy, LC–GC sample preparation, FT–IR, LIMS, ICP, calibration of DSC and TGA, and HPLC detection. Those interested in preregistering should use the form on p. 842 A. For further information on the workshops, contact Mary Lynn Grayeski, Department of Chemistry, Seton Hall University, South Orange, N.J. 07079 (201-761-9042).

The American Chemical Society will sponsor six short courses in conjunction with the meeting: Electronics for Laboratory Instrumentation, Quality Assurance of Chemical Measurements, Effective Management of Chemical Analysis Laboratories, Thermal Analysis in Materials Characterization, Fundamentals of Experimental Design, and Analytical IR Spectroscopy: Techniques, Applications, Computer Methods. For additional information, contact the Department of Educational Materials, American Chemical Society, 1155 16th St. N.W., Washington, D.C. 20036 (202-872-4508).

Six EAS-sponsored short courses also will be offered: Near-IR Analysis: An Industrial Tool (Sept. 12–13), Methods and Principles of Intermediate 2D-NMR (Sept. 13), Advances in HPLC (Sept. 13–14), Solid State NMR and Its Applications (Sept. 14), Introduction to X-ray Crystallography and Powder Diffraction (Sept. 15), and Applications of High-Resolution Chromatography, Capillary GC, and SFC (Sept. 16–17). Additional information on these courses can be obtained from Vincent Venturella, EAS short course chairman, Anaquest/BOC Group, 100 Mountain Ave., Murray Hill, N.J. 07974 (201-771-6392). The form on p. 842 A can be used for preregistration.

An employment service will be available during the meeting. For details, contact Margot Myers, EAS Employment Chairman, Brookside Apts. B-6, Laurel Street, Rye, N.Y. 10580 (914-967-5001).

The symposium dinner reception will be held on Wednesday, Sept. 16, in the Grand Ballroom of the New York Hilton Hotel. It is complimentary to all regular registrants, exhibitors, and speakers.

The EAS has reserved a block of rooms for conferees at the New York Hilton Hotel. To obtain special rates, rooms must be reserved through the EAS. Reservation forms can be obtained from Ken Fleischer, EAS Room Reservations Committee, RD #1, Box 730, Valatie, N.Y. 12184 (518-758-6431).

To preregister, send the completed

ACS SHORT COURSES

(Sponsored by the Colorado Section of the ACS)

to be held in conjunction with the

IN

DENVER

Basic Laboratory Electronics for Scientists

Instructor: James B. Calvert, Ph.D., P. E., July 30-31, 1987, Tuition: $300 ($250 for members of ACS, RMCDG, SAS)

This two day intensive course will take the student from the basic physics of electronics and electrical circuits to the design and troubleshooting of transistor and op-amp circuits, power supplies and the control of electromagnetic actuators. No previous knowledge of electronics is assumed. The course will be both quantitative and experimental. You will work with a kit of components, making circuits and testing them with electronic instruments. You will become familiar with common electronic components and learn how to assemble them. The course will familiarize you with the fundamental concepts useful in electronics, such as impedance levels, single-time constant circuits, feedback, and working models for semiconductor devices. These concepts will allow you to understand and use electronics with increased confidence.

Contaminants in Ground Water and Potable Water: Sources, Transformations, Detection and Quantitation

Instructors: E. Thurman, Ph.D. and M. Reddy, Ph.D., July 30-31 and August 1, 1987, Tuition: $425 ($375 for members of ACS, RMCDG, SAS)

This course will review current sampling methods for organic and inorganic contaminants in water; discuss recent advances dealing with the sources, movement, distribution and removal of contaminants in surface and ground water; and evaluate current and developing analytical methodology for major ions, trace elements and organic contaminants in water. The objective of the course is to present the requirements of a comprehensive contaminant investigation, through lectures, notes, slides, handouts and field trips to an advanced water treatment facility and a hazardous waste disposal site in the Denver area. The course will examine a wide range of topics to benefit both beginners and experienced professionals involved in the study of contaminants in the environment.

Basic Principles of Mass Spectrometry and Interpretation of Organic Mass Spectra

Instructors: J. A. Zirrolli, Ph.D. and C. M. Moynihan, July 29-31, 1987, Tuition: $325 ($275 for members of ACS, RMCDG, SAS)

This course will describe the principles of modern mass spectrometry and apply them to the identification of organic compounds. Sample introduction methods (GC, vapor, direct probe), ionization processes (positive, negative, FAB, chemical, electronic), mass analysis and detection will be discussed with emphasis on molecular ion analysis and simple fragmentation processes. The course will develop an approach to the determination of elemental composition and diagnostic fragmentation patterns, and the student will become familiar with the mass spectra characteristic of common organic compound classes, drugs, pesticides and pollutants. The course is based upon and uses as a reference the text, Interpretation of Organic Mass Spectra, Third Edition by F. W. McLafferty, University Science Books, 1980.

ADDITIONAL SHORT COURSES

APPLIED STATISTICAL METHODS IN CHEMISTRY
Dr. Robert A. Crovelli
2 Days: August 6-7, 1987
Tuition: members $325, non-members $375

SMALL CHEMICAL BUSINESSES: INS AND OUTS
Dr. D. Stull, Dr. R. Daughenbaugh and Mr. W. Paukert
1 Day: August 6, 1987
Tuition: members $200, non-members $250

SAMPLING OF PARTICULATE CHEMICALS: THEORY AND PRACTICE
Mr. Francis F. Pitard
3 Days: August 5-7
Tuition: members $375, non-members $425

Registration deadline for all courses is July 17, 1987. For information contact:

Joseph A. Zirrolli
Dept. of Pharmacology
Box C236
4200 E. 9th Avenue
Denver, CO 80262
(303) 394-8961

or

Larry D. Becker
USGS-NWQL
5293-B Ward Road
Arvada, CO 80002
(303) 236-5345

CONFERENCE SYMPOSIA

CHROMATOGRAPHY Honoring Harold Walton

SUPERCRITICAL FLUID CHROMATOGRAPHY

ION CHROMATOGRAPHY

INDUCTIVELY COUPLED PLASMA/MASS SPECTROMETRY

NUCLEAR MAGNETIC RESONANCE

ELECTRON PARAMAGNETIC RESONANCE

CHEMILUMINESCENCE

ENVIRONMENTAL CHEMISTRY

INFRARED SPECTROSCOPY

ATOMIC SPECTROSCOPY

MASS SPECTROMETRY

COMPUTER APPLICATIONS

QUALITY ASSURANCE

For preliminary program write to: Sandy Grande
8780 W. Quarto Circle
Littleton, CO 80123

MEETINGS

Symposium Officers

General Chairman: *S. David Klein*, Merck & Company
Chairman-Elect: *Harvey Gold*, E. I. du Pont de Nemours & Company
Past Chairman: *Walton Caldwell*, Berlex Laboratories
Secretary: *Genevieve Bonini*
Treasurer: *Richard Saferstein*, N.J. State Police
Archives Chairman: *Kenneth Fleischer*
Arrangements Chairman: *Hal Ferrari*
At-Large: *Evelyn Sarnoff*, U.S. FDA
Awards Chairman: *Robert Weinberger*, ABI Analytical/Kratos
Employment Chairman: *Margot Myers*
Exhibit Chairman: *Norman Gardner*
Exposition Chairman: *James McDivitt*, Ethicon
Housing Chairman: *Stephen Scypinski*, Varian Instruments
Legal Chairman: *Robert Vetrecin*, Ethicon
Message Center Chairman: *Waldemar Palaitis*, Merck & Company
Parliamentarian: *Kenneth Fleischer*
Printing and Direct-Mail Chairman: *J. P. Luongo*, AT&T Bell Laboratories
Program Chairman: *Peter Keliher*, Villanova University
Publicity Chairman: *S. David Klein*, Merck & Company
Registration Chairman: *Irene Nurkiewicz*
Short Courses Chairman: *Vincent Venturella*, Anaquest Corporation
Special Functions Chairman: *Sandra Hankin*, GTE
Technical Films Chairman: *Richard Soltero*, Berlex Laboratories
Workshops Chairman: *Mary Lynn Grayeski*, Seton Hall University

Photos courtesy of the N.Y. Convention & Visitors Bureau

Times Square

form on p. 842 A to Irene Nurkiewicz, EAS Registration, 16 Fairbanks Lane, Basking Ridge, N.J. 07920. Preregistration forms must be postmarked by Aug. 15. For further information on the symposium, contact J. P. Luongo, AT&T Bell Labs, 1A-352, Murray Hill, N.J. 07974 (201-846-1582, EAS hotline).

Program

MONDAY MORNING

Advances in HPLC

Chaired by C. Horvath, Yale U

8:30 Purification of Oligonucleotides. **L. Haff,** Perkin-Elmer Corp.
9:00 MS for Identification of Peptides from Tryptic Digests of Proteins. **W. S. Hancock,** Genentech
9:30 Impact of Structural Changes in Protein HPLC. **B. L. Karger,** Northeastern U
10:30 Relationship Between Protein Structure and Chromatographic Retention. **F. E. Regnier,** Purdue U
11:00 Rapid Protein Analysis by HPLC. **C. Horvath,** Y. F. Maa, and K. Kalghatgi, Yale U

Environmental Chemistry: Reliability, Techniques, and Economics

Chaired by A. Bober, Maryland Dept. of Health and Mental Hygiene

8:30 Quality Assurance in Environmental Analytical Chemistry. **C. Jones, Jr.,** U.S. EPA
9:10 A States' Viewpoint of Environmental Chemistry Techniques. **A. Bober,** Maryland Dept. of Health and Mental Hygiene
10:30 Instrumental Methods for Environmental Analyses. **E. G. Brame, Jr.,** Crippen Consulting Associates
11:10 Economic Considerations of Environmental Analysis: Program Issues vs. Laboratory Operations. **B. D. Lowman,** S. J. Simon, and M. T. Homsher, Lockheed Engineering and Management Co.

Computational Chemistry as a Companion to Analytical Chemistry

Chaired by S. W. Topiol, Berlex Laboratories

8:30 Response Properties of Polymeric Materialism. **A. Ratner,** Northwestern U
9:10 Calculation of Thermochemical Properties of Gas-Phase Molecules Using the BAC-MP4 Method. **C. F. Melius,** Sandia National Laboratories
10:30 Free Energy Calculations by Molecular Simulation. **D. L. Beveridge,** Wesleyan U
11:10 Computational Studies of Drug/Receptor Interactions: Implications for Chromatographic Separation Simulations. **S. W. Topiol,** Berlex Laboratories

Thermal Characterization of Polymeric Materials—I

Chaired by E. A. Turi, Polytechnic U

8:30 Introduction. **E. A. Turi,** Polytechnic U
8:35 Thermal Characteristics of Multicomponent Polymers. **W. M. Prest, Jr.,** Xerox Corp.
9:15 Thermal Stability of Substituted Aramides. S. S. Kim, **E. M. Pearce,** and S. Narang, Polytechnic U
10:25 Thermal Behavior of Epoxy Encapsulated Integrated Circuits. **H. E. Bair,** A. Hale, and S. Matsuoka, AT&T Bell Laboratories, and C. W. Macusko, U of Minnesota
10:55 Viscoelastic Properties of Amorphous Polymers Containing Platelet Fillers. **R. P. Chartoff** and D. M. Porter, U of Dayton, and E. H. Eriksen, Porsgrunn, Norway

New Developments in NIR—I

Chaired by D. E. Honigs, U of Washington

8:30 Baseline and Scatter Correction by a Quantum Mechanical Filter. **C. Miller** and D. E. Honigs, U of Washington
9:10 Reference Spectra in the NIR. **E. Stark,** New York
10:30 Analysis of Polymers by NIR Spectroscopy. **F. DeThomas,** Pacific Scientific
11:10 Analysis of Parenteral Dosage Forms by NIR. **E. Ciurczak,** College of St. Elizabeth

Advances in Chromatography—I

Chaired by D. Shelley, Stevens Institute of Technology

8:30 Comparison of GC Capillary Injection Modes in Drug Screening. **Z. Penton,** Varian Instrument Group
8:50 Cold Direct Injection as an Alternative to On-Column Injection in High-Resolution Capillary Chromatography. **J. R. Berg,** Varian Instrument Group
9:10 Assessment of Chromatographic Efficiency Through Statistical Bandshape Analysis. A. Onwubuya and **J. T. Maloy,** Seton Hall U
9:30 An Investigation of the Distribution of Chlorobenzenes in Urban Surface Soils.

MEETINGS

K. M. Aldous, D. R. Hilker, S. Connor, H. Valente, and W. H. Ding, New York State Dept. of Health

10:20 Polychlorinated Dibenzo-*p*-dioxide and Polychlorinated Dibenzofuran Production in Various Operating Stages of a Resource Recovery Incinerator. **D. R. Hilker,** K. M. Aldous, P. W. O'Keefe, R. M. Smith, H. Valente, D. Spink, S. Connor, J. Jurusik, and W. H. Ding, New York State Dept. of Health

10:40 Quantitative Pyrolysis GC in Polymer Analysis. **T. P. Wampler,** Chemical Data Systems

11:00 Recent Advances in Reversed-Phase Alumina Supports. **L. F. Wieserman,** C. M. Conroy, and J. W. Novak, Jr., Alcoa Laboratories

Poster Session
Computers

MONDAY AFTERNOON

Preparative HPLC

Chaired by H. Colin, Varex Corp.

1:30 Simulation of the Elution and Separation of Overlapping Bands on Overloaded LC Columns. **G. Guiochon,** S. Ghodbane, and S. Golshan-Shirazi, Georgetown U

2:10 System Integration in Multidimensional Chromatography of Proteins. **F. E. Regnier** and R. Stringham, Purdue U

3:30 Recent Developments in Process Scale HPLC. **K. Jones,** U of Manchester, U.K.

4:10 Displacement Chromatography of Biopolymers. **C. S. Horvath,** A. Liao, and B. Chen, Yale U

Chemometrics

Chaired by S. D. Brown, U of Delaware

1:30 Computer-Assisted Prediction of Chromatographic Retention Indices. **P. C. Jurs,** R. H. Rohrbaugh, and M. N. Hasan, Pennsylvania State U

2:10 Validation Strategies for Multicomponent Analysis of Pharmaceuticals. **R. Roman,** Smith Kline and French Laboratories

3:30 Chemometrics as a Process Analysis Tool. **D. Osten,** 3M Labs

4:10 Digital Filters for Kinetic Analysis in Flow Systems. **S. D. Brown,** U of Delaware

Thermal Characterization of Polymeric Materials—II

Chaired by E. A. Turi, Polytechnic U

1:30 How to Design Miscible Polymer Blends. **F. E. Karasz,** U of Massachusetts

2:10 Phase Relationships in Ternary Polymer Blends. **J. R. Fried,** U of Cincinnati, and A. C. Su, National Sun Yat-sen U, Taiwan

3:20 Transitions vs. Properties of Thermosetting Systems. **J. K. Gillham,** Princeton U

3:50 DSC and DMA Analysis of the Primary Transition of Biphasic, PVC-Based Systems. **M. T. Shaw** and H.-K. Boo, U of Connecticut

WE KEEP YOU RUNNING

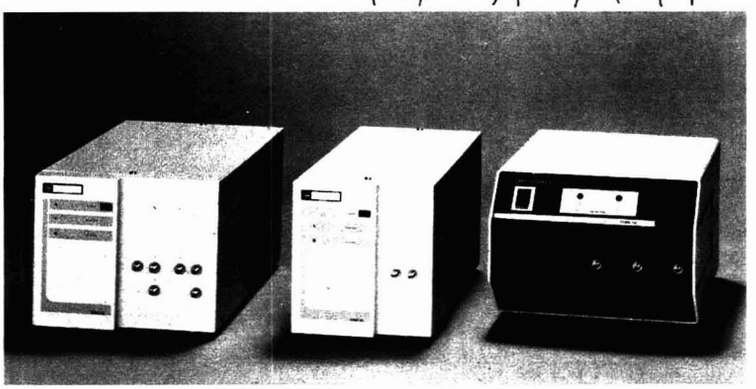

ERC-3000 Series
Continuous On-Line Degassers

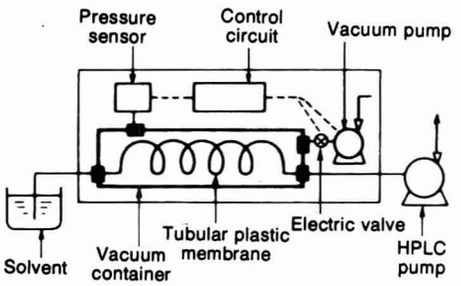

The Erma **ERC-3000 SERIES ON-LINE DEGASSERS** allow rapid, continuous solvent degassing. *Constant Operation* is assured after a simple, one-time installation — unlike traditional methods, which are time consuming and require constant monitoring and interruptions.

The solvent passes through a tubular plastic membrane within a vacuum container. Gas escapes through surface pores while the solvent volume remains constant, increasing retention time reproducibility. Pump cavitation is eliminated, assuring more reliable pump performance. The unit is compact and self-contained, eliminating cumbersome components.

Keep Your Solvents Running.
For more information, contact ANSPEC — the *Exclusive* ERMA distributor for the U.S.A.
Call **800-521-1720;** in Michigan 800-482-3452

Erma TOKYO — ANSPEC

P. O. Box 7730 • Ann Arbor, MI 48107 • 313-665-9666

CIRCLE 44 ON READER SERVICE CARD

Preregistration

Eastern Analytical Symposium
September 13–18, 1987

Make checks payable to "Treasurer, EAS" and mail this form to Irene Nurkiewicz, EAS Registration Chairman, 16 Fairbanks Lane, Basking Ridge, N. J. 07920.

Deadline for preregistration is Aug. 15, 1987.

Preregistrations postmarked after Aug. 15, 1987, will be charged the full at-meeting rates.

Fees:	Preregistration	At-Meeting
Regular	$ 40	$ 55
Student	$ 10	$ 15
Workshop*	$ 25	$ 40
1-day EAS Short Course**	$250	$250
2-day EAS Short Course**	$350	$350

*Fee for workshops is in addition to the registration fee.
**Fee for short courses includes registration fee.

Name _____
Last First Initial

Address _____

City _____ State _____ Zip _____

Business phone _____

Check applicable: ☐ This is my first EAS.
☐ Note change of address.

Check one: Mailing address is ☐ Home ☐ Business

Check the appropriate box and indicate the fee in blank spaces:

Registration: Regular ☐ Student ☐ ..... $ _____

Workshops:

Atomic Spectroscopy (Sept. 14 P.M.) ..... $ _____
Near Infrared (Sept. 15 A.M.) ..... $ _____
Chemical Microscopy (Sept. 15 A.M.) ..... $ _____
GC–SFC (Sept. 15 P.M.) ..... $ _____
Calibration of DSC & TGA (Sept. 15 P.M.) ..... $ _____
FT–IR (Sept. 16 A.M.) ..... $ _____
LIMS (Sept. 16 A.M.) ..... $ _____
ICP (Sept. 16 P.M.) ..... $ _____
LC–GC Sample Preparation (Sept. 17 A.M.) ..... $ _____
HPLC Detection (Sept. 17 P.M.) ..... $ _____

EAS Short Courses:

Methods and Principles of Intermediate 2D–NMR ..... $ _____
Solid-State NMR and Its Applications ..... $ _____
Near Infrared Analysis, An Industrial Tool ..... $ _____
Advances in HPLC ..... $ _____
Applications of High-Resolution Chromatography, Capillary GC and SFC ..... $ _____
Introduction to X-ray Crystallography & Powder Diffraction ..... $ _____

Total Amount Enclosed ..... $ _____

Payment must accompany preregistration form.

MEETINGS

Microwave Techniques

Chaired by H. M. Kingston and L. B. Jassie, National Bureau of Standards

1:30 Digestion and Trace Metal Analysis of Environmental Samples—A Comparison of Microwave and EPA Procedures. **T. Copeland** and W. Charlton, ERCO-Div. ENSECO
2:00 Microwave Acid Dissolutions at High Temperatures and High Pressures. H. M. Kingston and **L. B. Jassie,** National Bureau of Standards
2:30 Manual and Robotically Controlled Microwave Pressure Dissolution at Kidd Creek Mines: A Review. **J. Labreque,** Kidd Creek Mines Ltd., Canada
3:30 Novel Analytical Applications for Microwave Heating and Drying. **M. J. Collins** and E. D. Neas, CEM Corp.
4:00 Rapid Organic Synthesis Using Microwaves. **R. Gedye,** K. Westaway, and F. Smith, Laurentian U, Canada

New Developments in NIR—II

Chaired by D. E. Honigs, U of Washington

1:30 Combining NIR with Imaging. **J. Callis,** C. Barlow, and J. Kelly, U of Washington
2:10 Programmed Random Access NIR Spectroscopy with Acoustically Tuned Optical Filters. **D. Wetzel,** A. Eilert, and G. Kemeny, Kansas State U
3:30 NIR Fiber-Optic Sampling Probes. **P. Cooper** and D. Webster, Pacific Scientific
4:10 Theoretical and Experimental Development of the NIR Laplace Transform Spectrometer. **J. Perkins** and D. E. Honigs, U of Washington

TUESDAY MORNING

The Maturing of Supercritical Fluid Chromatography

Chaired by D. E. Martire, Georgetown U

8:30 Advances in SFC Instrumentation and Applications. **F. Yang,** Lee Scientific
9:10 Advances in the Practice of SFC with Packed and Capillary Columns. **D. R. Gere,** Suprex Corp.
10:30 Theory of Solute Retention in SFC and Its Applications. **D. E. Martire,** Georgetown U
11:10 Ancillary Methods of SFC. **M. Novotny,** Indiana U

Advances in the Applications of NMR Spectroscopy—I

Chaired by G. N. Chmurny, NCI-Frederick Cancer Research Facility

8:30 Handyman's Guide to One- and Two-Dimensional NMR Techniques. **R. H. Bible,** G. D. Searle Co.
9:10 Probing Heavy Petroleum Materials with NMR Spectroscopy. **K. D. Rose** and M. A. Francisco, Exxon Research and Engineering
10:30 NMR Studies of Intracellular Drug Transformations and Studies of Cyclophosphamide and Ifsofamide. **W. Egan** and S. M. Ludiman, FDA, National Institutes of Health
11:10 NMR in Physiology. **I.C.P. Smith,** National Research Council, Canada

Current Issues in Drug Testing

Chaired by M. Stajic, New York State Dept. of Health

8:30 Anatomy of Drug Testing. **S. J. Mule,** New York State DSAS
9:10 Post Mortem Drug Testing. **Y. H. Caplan,** Maryland Office of the Chief Medical Examiner
10:30 Quality Assurance and Proficiency Testing. **P. H. Field,** Wisconsin State Laboratory of Hygiene
11:10 Courtroom Toxicology. **F. Rieders,** National Medical Services, Inc.

Lasers in Analytical Chemistry

Chaired by R. G. Michel, U of Connecticut

8:30 Laser-Excited Atomic Spectrometry in Graphite Tube Furnaces. **R. G. Michel,** D. J. Butcher, J. P. Dougherty, and F. R. Preli, Jr., U of Connecticut
9:10 Resonant Two-Photon Ionization of Small Biological Molecules Using Pulsed-Laser Desorption into Supersonic Beam–MS. **D. M. Lubman,** U of Michigan
10:30 Combining Laser Spectroscopy and Chromatography in Chemical Analysis. **E. S. Yeung,** Iowa State U
11:10 Real-Time Correlation Filters Applied to Pulsed-Laser-Excited Photothermal Spectroscopy. **S. E. Bialkowski,** Utah State U

New Computer Hardware and Its Applications in the Laboratory

Chaired by G. C. Levy, Syracuse U

8:30 Utilization of New Computer Architectures in Analytical Chemistry. **G. C. Levy,** Syracuse U
9:10 Multiprocessor Laboratory Workstation Computers. **J. LaRoc,** MASSCOMP
10:30 Graphics Supercomputers in Scientific Research. **I. Reed,** Stellar Computers
11:10 Bringing Instrumentation into the Laboratory Local Area Network. **J. T. Currie, Jr.,** Digital Equipment Corp.

Recent Advances in Fluorescence Spectroscopy

Chaired by L. J. Cline Love, Seton Hall U

8:30 Mathematical Methods for Enhancement of Fluorescence Spectroscopic Detection for Chromatography. **S. Rutan,** D. D. Gerow, G. E. Hartmann, and C. B. Motley, Virginia Commonwealth U
9:10 Chemical Sensing Based on Surface-Bound Fluorescent Probes. **R. Seitz** and Z. Shaksher, U of New Hampshire
10:20 Phase Fluorometry Using UHF-Modulated Mode Locked Lasers. **M. Wirth,** U of Delaware

Poster Session
NMR

TUESDAY AFTERNOON

Multidimensional Chromatography

Chaired by R. S. Hartwick, Rutgers U

1:30 Multidimensional Micro-LC/TLC. **D. Shelley,** Stevens Institute of Technology
2:00 Coupled-Column/Gradient Elution HPLC. **S. A. Tomellini** and C. F. Buck, U of New Hampshire
2:30 Automated Multidimensional GC for Complex Mixture Analysis. **B. Gordon,** R. J. Reynolds Tobacco Co.
3:30 Multidimensional LC/GC for Routine Complex Mixture Analysis. **T. V. Raglione** and R. A. Hartwick, Rutgers U
4:00 Multidimensional Separations: Matching the Solution to the Problem. **J. C. Giddings,** U of Utah

Advances in Atomic Fluorescence Spectrometry with ICPs and Furnaces

Chaired by A. Montaser, George Washington U

1:30 Pulsed Lasers and Hollow Cathode Source Atomic Fluorescence Spectrometry in the ICP. **J. D.**

ENVIRONMENTAL ANALYSIS
with Tekmar® Purge & Trap Concentrators

- Is in strict compliance with EPA protocols.
- Operates with wide bore capillary columns. An optional cryofocusing unit is available for narrow bore columns.
- Includes a "no compromise" automatic sampler with ten discrete samplers which provide true minimum carry-over.
- Is able to run any type of purge and trap sample: water, soils, sludge, slurries and air samples.

Since 1975 Tekmar *Purge and Trap Concentrators* have been used for the trace analysis of volatile organic compounds in environmental samples. Over the years Tekmar Concentrators have become the industry standard for their reliability and for providing the best reproducibility available. Most importantly, our products are supported by an integrated network of technical salespeople, application specialists, service engineers, and product managers with a level of experience greater than all of our competitors combined! ***Call us today for answers to your environmental analysis needs!***

Tekmar® *The world's leader in Purge & Trap Technology.*

Tekmar Company, P.O. Box 371856, Cincinnati, Ohio 45222-1856
Call (800) 543-4461 / In Ohio (800) 344-8569 / Telex No. 21-4221 / Telefax (513) 761-5183
In Canada, call Technical Marketing Associates (416) 826-7752

CIRCLE 157 ON READER SERVICE CARD

Winefordner, U of Florida

2:00 Comparison of Excitation Sources and Sample Introduction Systems for Hollow Cathode Lamp Excited ICP Atomic Fluorescence Spectrometry. **D. Demers,** Baird Corp.

2:30 Studies with an ICP–Atomic Fluorescence Spectrometer: Effects of Various Organic Solvents on Signal-to-Noise and on Detection Limits. **S. F. Zhu,** R. H. Clifford, H. Wang, and P. N. Keliher, Villanova U

3:30 Diagnostic Studies of ICP Discharges with Atomic Fluorescence Spectrometry. **A. Montaser,** S. Chan, and H. Tan, George Washington U

4:00 Background Correction for Atomic Fluorescence Spectrometry. **R. G. Michel,** U of Connecticut

LIMS—Users' Perspectives Postinstallation

Chaired by N. H. Woo, Merck & Co.

1:30 LIMS in the Control Division at Upjohn. **E. Cooper,** Upjohn Co.

1:45 LIMS in Analytical Research at Merck. **I. Chapple,** Corporate Computer Resources, and S. D. Klein, and J. A. McCauley, Merck & Co.

2:00 LIMS in Environmental Chemistry at N.J. Public Health. **J. Wallin,** N.J. Dept. of Public Health

2:15 LIMS in Analytical Chemistry at Calgon. **A. Nakagawa,** Calgon Analytical Laboratories

2:30 LIMS in Analytical Chemistry at Exxon. **P. Tyne,** Exxon Chemical Co.

Frontiers in Analytical Toxicology

Chaired by S.H.Y. Wong, U of Connecticut

1:30 Capillary SFC for Drug Analysis. **F. Yang,** Lee Scientific

2:10 GC/MS for Clinical Drug Analysis. **D. G. Deutsch,** State U of New York, Stony Brook

3:30 Robotics for Clinical Drug Analysis. **G. Schmidt,** Perkin Elmer Corp.

4:10 Antidepressant-Monitoring Methodologies: LC and Immunoassays. **S.H.Y. Wong,** U of Connecticut

Advances and Trends in FT–IR

Chaired by I. M. Hamedeh, Perkin-Elmer Corp.

1:30 FT–IR Reflection Spectroscopy of Surfaces by Center-Burst Suppression. **P. Griffiths,** U of California, Riverside

2:10 FT–IR Studies of Bio-Organic Systems. **K. Nakanishi** and B. McGuiness, Columbia U

3:30 Continuous Recording of FT–IR Spectra of Components Separated by Reverse-Phase HPLC. **J. Gagel** and K. Biemann, Massachusetts Institute of Technology

4:10 Multivariate Calibration for Quantitative FT–IR Analysis of Glass. **E. Thomas** and D. Haaland, Sandia Labs

WEDNESDAY MORNING

New York SAS Award Symposium

Chaired by C. M. Paralusz, Permacel, Avery International

8:30 Introduction. **L. J. Cline Love,** Seton Hall U

8:40 Photoacoustic and Diffuse-Reflectance FT–IR: A New Perspective. **P. Griffiths,** U of California, Riverside

9:20 Applications of Variable-Temperature ATR to Polymer Systems. **J. A. Graham,** Hercules, Inc.

10:30 Regular and Anomalous Particle Size Effects in NIR Spectroscopy. **D. E. Honigs,** U of Washington

11:10 Is Spectroscopy Useful? **B. J. Bulkin,** Standard Oil

Drug Monitoring: Direct Plasma Injection HPLC

Chaired by T. R. Koziol, Berlex Laboratories

8:30 HPLC Analysis of Drugs by Direct Plasma Injection Using Internal Surface Reverse-Phase Columns. **T. Pinkerton,** Upjohn Co.

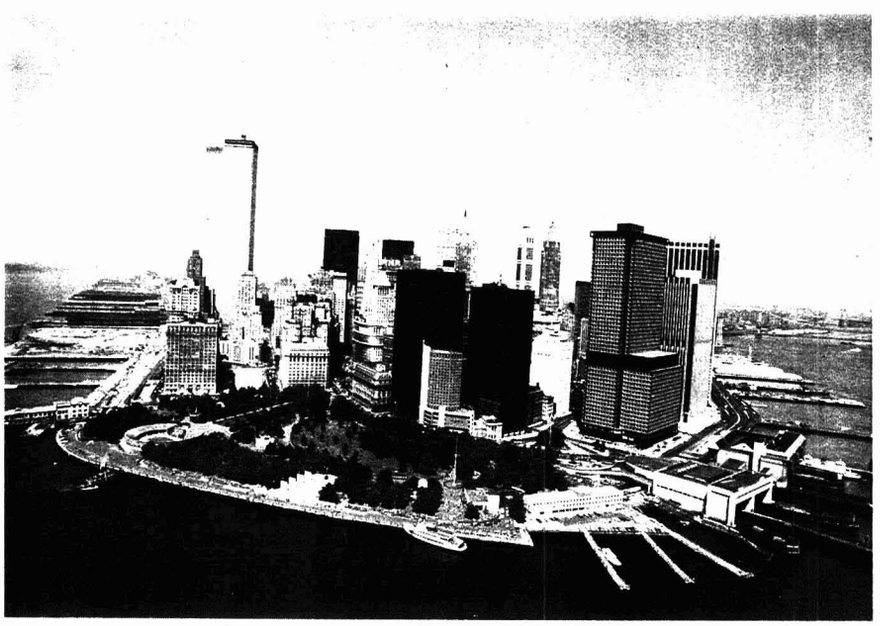

Manhattan

9:00 Column-Switching HPLC Methods for Drug Analysis from Biological Fluids. **J. Veals,** C. Lin, and G. Durante, Schering-Plough

9:30 Direct Plasma Injection HPLC, Analysis of Drugs Using Conventional Mobile Phases with Column Switching. **E. Woolf** and T. Koziol, Berlex Laboratories

10:40 Direct Serum Injection: Use of Micellar Cleanup with Column Switching for the Determination of Drug Substances by HPLC. **J. Posluszny** and R. Weinberger, ABI Analytical

11:10 Quantitation of Drug Substances Using Direct Serum Injection HPLC with Micellar Mobile Phases. **L. J. Cline Love** and J. Fett, Seton Hall U

EAS Chromatography Award Symposium: Chromatography—The Next Decade—I

Chaired by J. Cazes, Sanki Laboratories, Inc.

8:30 Introduction. **J. Cazes,** Sanki Laboratories, Inc.

8:35 Mesomorphic Polysiloxane Stationary Phases for Capillary GC. **G. Janini,** Kuwait U, Kuwait, and R. J. Laub, San Diego State U

9:05 Laser Fluorescence Detection in Capillary LC and Electrophoresis. **V. L. McGuffin,** Michigan State U

9:35 Chromatographic Signal Transformations. **P. Kucera,** Lederle Laboratories, Inc.

10:30 Cyclodextrins in Separations. **D. W. Armstrong,** Texas Tech U

11:05 Presentation of the Award to Haleem J. Issaq

11:05 Mixed Columns and Column Supports for LC Separations. **H. J. Issaq,** Frederick Cancer Research Facility

Optimization of Instrumentation and Parameters for One- and Two-Dimensional NMR Spectroscopy

Chaired by P. L. Rinaldi, Varian Instrument Group

8:30 Optimization of Acquisition and Processing Parameters for One-Dimensional NMR Spectroscopy. **R. Santini,** Purdue U

9:10 Optimization of Two-Dimensional J and Chemical Shift Correlation and Experiments. **P. L. Rinaldi,** Varian Associates

10:30 Optimization of Two-Dimensional NOE-Related Experiments. **A. Pardi,** Rutgers U

Trace Metal Speciation—I

Chaired by I. S. Krull, Northeastern U

8:30 Overview of Chromatography-Element Selective Detection. Interfacing of GC with Microwave-Induced Plasma Emission Detection. **P. Uden,** U of Massachusetts, Amherst

9:10 Trace Metal Speciation via Mobile-Phase Ion Chromatography–Postcolumn Oxinate Formation-Fluorescence/ICP Detection. I. S. Krull and **B. Karger,** Northeastern U

10:30 Sample Introduction for Plasma—MS. **J. A. Caruso,** U of Cincinnati, and F. Fricke, U.S. FDA

11:10 HPLC–ICP and HPLC–GFAAS Systems for the Determination of Organometallic Compounds in Environmental Samples. **K. Irgolic,** Texas A&M U

Advances in Spectroscopy

Chaired by D. Gerth, Betz Laboratories

8:30 Recent Advances in Automation of EPA Contract Laboratory Program Inorganics Analyses. **M. E. Tatro,** SPECTRA Spectroscopy and Chromatography Specialists

8:50 Studies of the Transitions Involved in the Production of Graphite Fibers from Polyacrylonitrile Fibers by Diffuse-Reflectance Spectroscopy in the IR and UV. **F. J. DeBlase,** Harrick Scientific Corp., and E. M. Pearce and H. Dodiuk, Polytechnic U

9:10 Evaluation of Improved Coatings for an Integration Sphere. **J. Steensrud,** Varian Instrument Group

9:30 Analytical Performance of Glow Discharge, Conventional ICP, and Spark Ablation-ICP Atomic Emission Spectrometries for Analysis of Geological and Related Materials. **I. B. Brenner,** Geological Survey of Israel, Israel, A. Lamarchand, P. Grosdaillon, and Y. Lang, Jobin Yvon Instruments SA, France, and J. Lerner, ISA Inc.

10:30 Performance and Operating Characteristics of a Multi-Element Glow Discharge AA Spectrophotometer. **A. E. Bernhard,** T. S. Scuitto, and T. Mickle, Analyte Corp., and E. H. Piepmeier, Oregon State U

10:50 Systematic Approach to Matrix Modification in Graphite Furnace AAS. **T. M. Rettberg,** L. M. Beach, and D. E. Shrader, Varian Instrument Group

11:10 Totally Automated Determination of Cisplatin in Biological Fluids by LC–AAS. **S. Scypinski** and A. J. Hockman, Varian Instrument Group

11:30 Former Impossible Identification, Qualification, and Quantitation of Polymers by Near IR Analysis. **F. A. DeThomas,** Pacific Scientific

Poster Session
Spectroscopy

WEDNESDAY AFTERNOON

New York SAS Award Symposium

Chaired by A. Melveger, Ethicon, Inc.

1:30 Presentation of the Award to William G. Fateley.

1:35 The Wave of the Future. **W. G. Fateley,** Kansas State U

2:15 Biology, Bugs, and Bill. **R. J. Jakobsen,** Mattson Institute for Spectroscopic Research

3:30 FT-Raman Spectroscopy: The Better Approach to Hadamard. **B. Chase,** E. I. du Pont de Nemours and Co.

4:10 Infrared Measurements of Oriented States. **J. L. Koenig,** Case Western Reserve U

Chromatography—The Next Decade—II

Chaired by H. J. Issaq, NCI-Frederick Cancer Research Facility

1:30 Definition of a Set of Stationary Phases for GC: Prediction, Frustration, and Triumph. **R. J. Laub,** San Diego State U

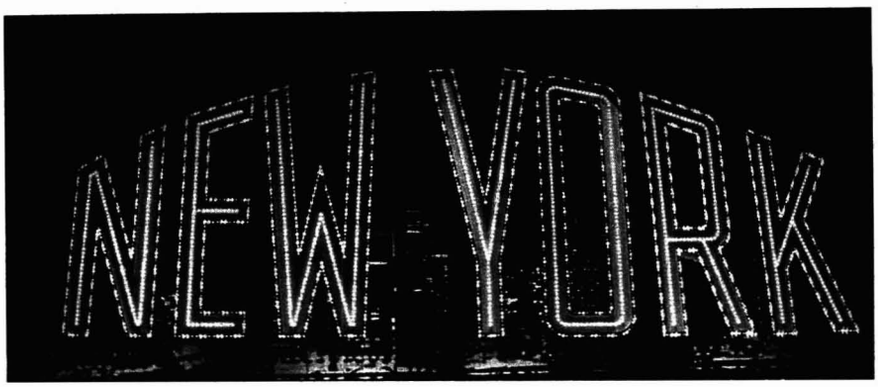

2:00 Metal Chelate Interaction Chromatography of Proteins. **Z. El-Rassi** and C. Horvath, Yale U

2:30 Simple, Efficient, Low-Cost, and Reliable—The Chromatograph of the Future. **R.P.W. Scott,** Georgetown U

3:30 Process Scale LC. **L. Snyder,** L. C. Resources, Inc.

4:00 Therapeutic Drug Monitoring and Toxicology. **S.H.Y. Wong,** U of Connecticut

Quantitative Structure Determination by NMR

Chaired by R. A. Byrd, FDA, National Institutes of Health

1:30 Methods and Examples of Protein Structure Determination by NMR. **P. L. Weber,** Smith Kline and French Laboratories

2:10 Confirmation of Peptides in Solution by Combined Use of NMR and Energy Minimization Methods. **J. A. Ferretti,** National Heart, Lung, and Blood Institute

3:30 NMR-Pseudo Energy Approach to the Structure of Glycolipids. **J. H. Prestegard,** Yale U

4:10 Detailed Structure of DNA in Solution Using 2D-NMR and Molecular Mechanics. **T. L. James,** U of California, San Francisco

Trace Metal Speciation—II

Chaired by I. S. Krull, Northeastern U

1:30 Interfacing of LC with ICP/MS Detection. **R. S. Houk,** Iowa State U

2:10 Future of Intelligent Spectrometers in Chemical Analysis. **M. B. Denton,** U of Arizona

3:30 Interfacing of Microbore and Capillary LC Techniques with a Microscopic Epifluorescence Imaging Detector. **F. Brinkman,** National Bureau of Standards

4:10 Long-Term Monitoring of Trace Metals by Automated HPLC with Electrochemical Detection. **A. Bond,** Deakin U, Australia

Analytical Chemistry at the Interdisciplinary Interface—I. The Interface with Biological Science

Chaired by W. R. Heineman, U. of Cincinnati

1:30 Electroanalytical Chemistry at the Interface with Biochemistry. **W. R. Heineman,** U. of Cincinnati

2:10 Piezoelectric Biosensors. **G. J. Bastiaans,** Integrated Chemical Sensors

3:30 Bioanalytical Applications of Fluorescence Spectroscopy. **F. V. Bright,** Indiana U

4:10 Nano-Scale Separations and Biotechnology. **J. W. Jorgenson,** U of North Carolina, Chapel Hill

THURSDAY MORNING

EAS Award Symposium for Outstanding Achievements in Analytical Chemistry

Chaired by P. N. Keliher, Villanova U

8:30 ICP–AES in the Analysis of Ceramics and Related Materials. **X. Shen,** Shanghai Institute of Ceramics, China

9:00 Comparative Performances of Inert Gas Plasma Excitation Sources. **A. T. Zander,** Perkin-Elmer Corp.

10:20 Sample Presentation in ICP Emission Spectrometry: Practical Applications from Fundamental Studies. **R. F. Browner,** Georgia Institute of Technology

11:00 Presentation of the Award to Velmer A. Fassel

11:05 Successful New Analytical Techniques: What Are the Magical Ingredients? **V. A. Fassel,** Iowa State U

Modern Methods in Electroanalytical Chemistry—I

Chaired by K. M. Kadish, U of Houston

8:30 EXAFS Spectroelectrochemistry. **W. R. Heineman,** R. C. Elder, D. M. Caster, C. E. Lunte, U of Cincinnati, and H. D. Dewald, Ohio U.

9:10 High-Sensitivity Spectroscopic Probes of Electroactive Events. **R. McCreery,** R. Parkard, and C. C. Jan, Ohio State U

10:30 Molecular Adsorption Studies at Electrode Surfaces by Electron Energy Loss Spectroscopy. **A. Hubbard,** G. N. Salaita, D. G. Frank, D. A. Stern, L. L. Davidson, N. Batina, E. Wellner, and D. C. Zapien, U of Cincinnati

11:10 Electroanalytical Chemistry at the Liquid–Liquid Interface. **E. Wang,** Chinese Academy of Sciences, China

Advances in Experimental NMR Methods

Chaired by R. H. Bible, Searle R&D

8:30 Nonseparative Structural Analysis of Complex Mixtures by Ultrahigh Resolution NMR. **A. Allerhand** and S. R. Maple, Indiana U

9:10 NMR Studies of Molecules in Shear Flow. **J. B. Grutzner,** Purdue U

10:30 Indirect Detection of ^{13}C and ^{15}N: Technical Considerations. **D. Cowburn,** Rockefeller U
11:10 Current Numerical Methods and Applications of Super-Mini to Mainframe Computers in NMR Spectroscopy. **R. A. Byrd,** FDA, National Institutes of Health

Problem Solving in Pharmaceutical Research and Development: Symposium Honoring the Memory of Takeru Higuchi

Chaired by A. F. Fell, U of Bradford, U.K.

8:30 Tribute to Takeru Higuchi. **L. A. Sternson,** Smith Kline and French Laboratories
8:35 LC/MS and SFC in Pharmaceutical Research and Development. **D. E. Games,** University College, Cardiff, U.K.
9:10 Strategies for Postcolumn Reaction Detection in HPLC. **R. Weinberger,** ABI Analytical
10:30 Novel Techniques for Drug Analysis in Biological Fluids by HPLC. **L. J. Cline Love,** Seton Hall U
11:10 Interlaboratory Transfer of HPLC Methods: Problems and Solutions. **J. Kirschbaum,** Squibb Institute for Medical Research

Analytical Chemistry at the Interdisciplinary Interface—II. The Interface with Materials Science

Chaired by D. M. Hercules, U of Pittsburgh

8:30 Analytical Chemistry at Surfaces. **D. M. Hercules,** U of Pittsburgh
9:10 Use of Ultrahigh Vacuum Surface Analytical Methods in Understanding Higher-Pressure Catalytic Reactions. **C. T. Campbell,** Indiana U
10:30 FT-Raman Spectrometry: A Useful Tool for Characterizing Sensor Surfaces. **D. E. Honigs,** U of Washington
11:10 Thermal Waves and Surface Characterization. **R. M. Miller,** Unilever Research, U.K.

Advances in Chromatography—II

Chaired by V. Berry, Salem State College

8:30 Novel Method for Packing Columns Using Common Low-Flow LC Pumps. **V. Berry,** Salem State College, and K. Lawson, U of Pretoria, South Africa
8:50 Performance Appraisal of Acid–Hydrolysis Stabilized Bonded C-4 Silica Stationary-Phase Materials by HPLC. **N. Sagliano, Jr.,** and R. A. Hartwick, Rutgers U
9:10 On-Line Sampling Selectivity in Capillary Column HPLC. **J. Rusik** and J. C. Gluckman, U of Vermont
9:30 Recent Development of Microcolumn HPLC in Japan. **T. Miki** and D. Ishii, Tokyo U of Agriculture, Japan
10:20 Centrifugal Partition Chromatography—LC Without a Solid Support. **J. Cazes,** W. Murayama, and H. Nunogaki, Sanki Laboratories Inc.
10:40 Characteristics and Use of 2.1-mm ID Microbore HPLC Columns. **R. C. Ludwig,** R. Eksteen, and L. T. Peter, Supelco Inc.
11:00 New Alternative to Normal-Phase HPLC Automation Using Methylene Chloride Mobile Phases: A Synchronized Dual Switching Valve Loop Injection System. **E. M. Fujinari,** E. I. du Pont de Nemours and Co.

Poster Session
Chromatography, General Analytical Chemistry

THURSDAY AFTERNOON

EAS Award Symposium for Outstanding Achievements in Analytical Chemistry

Chaired by R. M. Barnes, U of Massachusetts, Amherst

1:30 ICPAS: What Comes Next? **R. M. Barnes,** U of Massachusetts, Amherst
2:10 Development of a Microwave Plasma Ionization Detector for GC. **Q. Jin,** Jilin U, China
3:30 Sampling ICPs for Mass and Optical Spectroscopy. **R. S. Houk,** Iowa State U
4:10 ICP–FTS: Where Are We in the Seven Ages of Its Lifetime? **M. W. Routh,** Applied Research Laboratories

Advances in Electrophoresis

Chaired by S. D. Spotts, LKB Instruments, Inc.

1:30 Preparative Purification of Proteins Using Immobilized pH Gradients. **L. J. DeLucas,** H. A. Slocum, and D. Moore, U of Alabama, Birmingham
2:10 Pulsed-Field Gel Electrophoresis of Large DNA Molecules. **C. L. Smith,** Columbia U
3:30 Overview of Recent Directions in Analytical Electrophoresis. **D. J. Reeder** and J. J. Edwards, Center for Analytical Chemistry
4:10 High-Performance Capillary Electrophoresis. **B. L. Karger,** A. Cohen, and A. Paulis, Northeastern U

Modern Methods in Electroanalytical Chemistry—II

Chaired by K. M. Kadish, U of Houston

1:30 Unifying Approach to Analytical Voltammetry. **A. Bond,** Deakin U, Australia
2:10 Electroanalytical Techniques with Ultramicroelectrodes. **M. R. Wightman,** Indiana U
3:30 Multiple Electron Transfer Reactions of Organometallic Compounds. **W. E. Geiger,** U of Vermont
4:10 Electrosynthesis and Electrochemistry of Metalloporphyrins Containing a Metal–Metal or a Metal–Carbon Bond. **K. M. Kadish,** U of Houston

Advances in the Applications of NMR Spectroscopy—II

Chaired by W. J. Boyko, Villanova U

1:30 Solid-State NMR of High-Performance Polymers. **J. A. Bonesteel,** E. I. du Pont de Nemours and Co.
2:10 Structure and Dynamics of Insoluble Plant Polyesters: Complementary Use of CP–MAS, FT–MAS, and Spin Relaxation Techniques. **R. E. Stark** and T. Zlotnik, CUNY, Staten Island
3:30 Preparation and NMR Spectroscopic Analysis of Species at the Surface of a Heterogeneous Catalyst. N. Bansal, D. Barbino, L. Hesselbring, C. Tirendi, C. Tsiao, and **C. Dybowski,** U of Delaware
4:10 Protein Structure and Dynamics by NMR Spectroscopy. **S. Opella,** U of Pennsylvania

Problem Solving in Pharmaceutical Research and Development: Symposium Honoring the Memory of Takeru Higuchi

Chaired by D. E. Games, U of Wales, U.K.

1:30 Impact of Biotechnology on Pharmaceutical Industry: Challenges and New Perspectives. **L. A. Sternson,** Smith Kline and French Laboratories
2:10 Digital Techniques for Rapid-Scanning UV and Luminescence HPLC. **A. F. Fell,** U of Bradford, U.K.
3:30 Bioequivalent and Generic Pharmaceuticals. **A. P. DeSilva,** Zenith Pharmaceutical Laboratories
4:10 Chiral Separation in the Pharmaceutical Industry. **D. W. Armstrong,** Texas Tech U

George Washington Bridge

FRIDAY MORNING

Benedetti-Pichler Award Symposium

Chaired by P. Hicks, Cabot Corp.

8:30 Examining the State of the Art in Scanning Auger Microanalysis. **L. Salvati, Jr.,** Perkin-Elmer Corp.
9:00 Developments of the Raman Microprobe Mole—Instrumentation and Applications. **F. Adar,** Instruments SA, Inc.
9:30 Ion Microprobe Analysis of Technical Materials. **M. Grasserbauer,** Technical U of Vienna, Austria
10:30 Experiments with Micro-Sized Beams for Materials Analysis. **K. H. Purser,** General Ionex Corp.
11:00 Presentation of the Award to David M. Hercules
11:05 Laser Microprobe MS: The Past, Present, and Future. **D. M. Hercules,** U of Pittsburgh

LC/MS

Chaired by R. F. Browner, Georgia Institute of Technology

8:30 Strengths, Limitations, and Potential of Magic-LC/MS. **R. F. Browner** and D. D. Perkins, Georgia Institute of Technology
9:10 Role of Chromatographic Separation in Conjunction with Tandem MS. **R. A. Yost** and M. F. Lee, U of Florida
10:20 Atmospheric Pressure Ionization LC/MS/MS: No Heat, No Hassle. **J. D. Henion** and E. Lee, Cornell U
11:00 Comparison of Thermospray and Magic-LC/MS. **A. Apfel** and P. Goodley, Hewlett-Packard
11:40 Studies of Peptides Using a New Particle Beam Liquid Chromatograph–Mass Spectrometer. **R. C. Willoughby,** S. Mitrovich, J. D. Buchner, and F. Poeppel, Extrel Corp.

Recent Advances in GC

Chaired by H. M. McNair, Virginia Polytechnic Institute and State U

8:30 Recent Advances in GC. **H. M. McNair,** Virginia Polytechnic Institute and State U
9:10 Conformational Analysis Using Megabore Columns in Parallel. **W. Jennings** and R. Freeman, J&W Scientific, Inc.
10:20 New Directions in GC Selectivity—Retention and Detection. **M. Lee,** R. Skelton, C. Rouse, P. Farnsworth, and K. Markides, Brigham Young U
11:00 High-Temperature Capillary GC. **J. Hinshaw,** Perkin-Elmer Corp.

Analytical Chemistry in the Regulatory Milieu

Chaired by A. Bober, Maryland Dept. of Health and Mental Hygiene

8:30 Introduction. **A. Bober,** Maryland Dept. of Health and Mental Hygiene
8:35 Analysis of Controlled Substances for Legal Purposes. **H. L. Schlesinger,** DEA
9:20 Analytical Technology and Regulatory Analysis. **R. L. Ellis,** USDA
10:35 NIOSH—Odd Man In. **J. Posner,** NIOSH

Electron and Optical Microscopy

Chaired by T. J. Hopen, McCrone Research Institute

8:30 Isolation and Electron-Beam Characterization of Light-Scattering Centers from Fiber-Optic Glasses. **J. Bradley,** McCrone Associates
9:10 Chemical Microscopy with FT–IR Microspectrometry. **J. Reffner,** Spectra-Tech
10:20 Volume Percentage Determination in Asbestos Analysis. **D. Mefford,** DCM Science Lab, Inc.
11:00 Microscopical Characterization of Inorganic Explosives. **T. J. Hopen,** McCrone Research Institute

Ultrasensitive X-ray Microprobe Techniques Using Synchrotron Radiation

Chaired by K. W. Jones, Brookhaven National Laboratory

8:30 Ultrasensitive Determination and Localization of Trace Elements with Synchrotron Radiation. **B. M. Gordon,** Brookhaven National Laboratory
9:10 Measurement of Trace Element Distributions in Geological Samples. **M. L. Rivers,** U of Chicago and Brookhaven National Laboratory

Discover NIR, the New Spectroscopy

NIR Spectroscopy offers superior performance for Quantitative IR Analysis. The Model 6250 Near Infrared Research Spectrophotometer is the premium system for utilizing the tremendous potential of NIRS. Make sure your choice in a Rapid Scanning NIRS Instrument has these essential features:

- **SUPERIOR INSTRUMENT PERFORMANCE.** Average noise between 1100–2500 nm for 50 scans: 0.000025 log 1/R. Wavelength precision, better than 0.015 nm.
- **FAST SCANNING.** 0.4 seconds per scan.
- **WAVELENGTH RANGE.** 1100–2500 nm PbS; 600–1100 nm Silicon.
- **VERSATILITY.** Diffuse Reflectance; Transmission; Transmission/Reflectance Interaction.
- **FLEXIBILITY IN SAMPLING.** Small as 0.2 cm^2 and Large as 50 cm^2 Area Illumination; Moving Sample Mechanism; Fiber Optic Accessories.
- **SOFTWARE CAPABILITY**—IBM PC/ATE. Three regression programs; Oracle 1—Data Translation; Spectral Matching; Spectral Library; P.L.S.; FTNIR; Process Control Software.

Your laboratory has UV-Vis and FTIR . . . the Model 6250 fills the gap—NIRS.

For more information and a free brochure on the Pacific Scientific Model 6250 System, call 800-638-2790 toll-free.

PACIFIC® SCIENTIFIC
INSTRUMENT DIVISION

2431 Linden Lane, Silver Spring, MD 20910 (301) 495-7000 800-638-2790
4 First Ave., Globe Park, Marlow Bucks, England SL7 1YA (06284) 74074

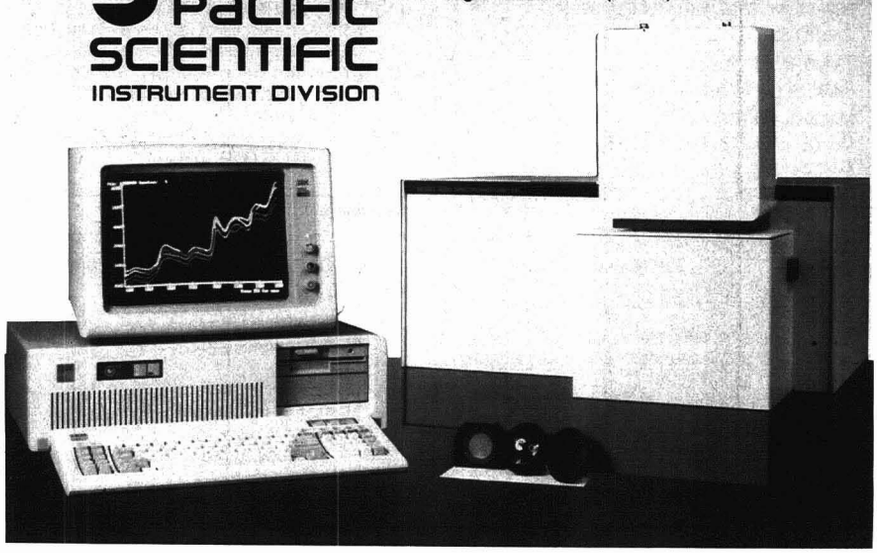

CIRCLE 125 ON READER SERVICE CARD

New Directions in Electrophoretic Methods

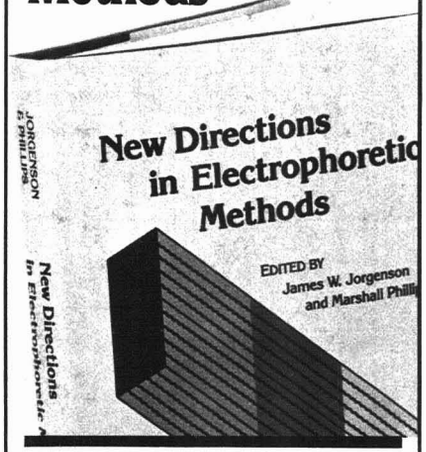

Electrophoresis is the most powerful process available for the separation and analysis of complex mixtures of charged biopolymers. This new book offers scientists the latest developments in electrophoretic separations and state-of-the-art electrophoretic technology and applications. It covers both the basic theory and development of electrophoretic methods and the separation and identification tools used by developers. The sixteen chapters in this book focus on several electrophoretic methods:

- isotachophoresis
- zone electrophoresis
- isoelectric focusing
- two-dimensional electrophoresis
- pulsed electrophoresis

Specific topics discussed with these methods include:

- polyacrylamide gels
- immobilized pH gradients
- silver-stain detection of proteins
- agarose gels
- synthetic ion-containing polymers

Electrophoretic methods play a major role in scientific advances in medicine, agriculture, chemistry, and biotechnology. This book will prove a valuable reference for anyone working with electrophoretic methods.

James W. Jorgenson, *Editor, University of North Carolina*

Marshall Phillips, *Editor, U.S. Department of Agriculture*

Developed from a symposium sponsored by the Divisions of Agricultural and Food Chemistry and Analytical Chemistry of the American Chemical Society

ACS Symposium Series No. 335
284 pages (1987) Clothbound
LC 87-1777 ISBN 0-8412-1021-7
US & Canada $64.95 Export $77.95

Order from: **American Chemical Society**
Distribution Office Dept. 52
1155 Sixteenth St., N.W.
Washington, DC 20036

or CALL TOLL FREE

800-227-5558

and use your credit card!

MEETINGS

9:40 Measurement of the Distribution of Trace and Toxic Elements in Biological Materials. **J. G. Pounds,** Brookhaven National Laboratory

10:40 Applications of Synchrotron X-ray Fluorescence to the Analysis of Trace Elements in Meteorites. **J. Delaney,** American Museum of Natural History

11:10 Chemical Speciation of Chromium on Aluminum Surfaces. **H. S. Issacs,** Brookhaven National Laboratory

FRIDAY AFTERNOON

Analytical Chemistry in the Regulatory Milieu

Chaired by A. Bober, Maryland Dept. of Health and Mental Hygiene

1:30 Special Aspects of Regulatory Analysis at the Food and Drug Administration. **E. Sarnoff,** U.S. FDA

2:15 Considerations in the Analysis of Workplace Air Samples. **M. Shulski,** OSHA

3:15 Analytical Chemistry in the Environmental Protection Agency. **P. Freidman,** U.S. EPA

Forensic Science

Chaired by C. R. Midkiff, Bureau of Alcohol, Tobacco & Firearms

1:30 Is It Conclusive? Gunshot Residue Determination by a Combination of HPLC and Graphite Furnace AA. D. B. Dahl and **P. F. Lott,** U of Missouri

2:10 Gunshot Residue Analysis in the SEM/EDX. Present and Future. **S. Basu,** New York State Police HQ Crime Laboratory

3:10 Gunshot Primer Residue Program in the FBI Laboratory. **D. Habekost,** FBI Laboratory

3:50 Building a Single Fiber Library Using Micro FT-IR. **H. Q. Le,** Michigan State U

FAB/MS

Chaired by B. S. Larsen, E. I. du Pont de Nemours and Co.

1:30 Desorption Ionization, Analysis of Glycopeptides. **C. Fenselau,** Johns Hopkins U

2:00 Applications of FAB to Pharmaceutical Impurity Problems. **F. Crow,** R. H. Robins, and W. K. Duholke, Upjohn Co.

2:30 Sequence Analysis of Proteins by Tandem Magnetic Deflection MS. **S. A. Carr,** M. E. Hemling, G. D. Roberts, and R. J. Anderegg, Smith Kline and French Laboratories

3:20 Glycoconjugate Structure—Function Relationship. **V. N. Reinhold,** Harvard School of Public Health

3:50 Analysis of Biopolymers by FAB/MS. **B. Larsen,** E. I. du Pont de Nemours and Co.

Polymorphism in Pharmaceuticals

Chaired by J. A. McCauley, Merck & Co.

1:30 Thermodynamics and Detection of Polymorphism. **J. A. McCauley,** Merck Sharp & Dohme Research Laboratories

2:10 Polymorphs and Solvates of Drugs—A Molecular View. **S. Byrn,** Purdue U

3:10 Polymorphs, Hydrates, and Solvates—Pharmaceutical Case Histories. **E. E. Fiese,** Pfizer Central Research

3:50 Characterizing Polymorphic Forms of Drug Candidates Utilizing Thermal Methods of Analysis and Scanning Electron Microscopy. **M. Cotton,** B. Down, and E. Vadas, Merck Frosst Laboratories, Canada

Advances in Chromatography—III

Chaired by G. Pearse, LeMoyne College

1:30 PTH-Amino Acids Resolved from Sequencer Impurities on a Deactivated C-18 Column. **M. A. Eighme,** R. C. Ludwig, and R. Eksteen, Supelco Inc

1:50 Use of a NIR On-Line Analyzer as a Preparative LC Detector in the Pharmaceutical Industry. **B. Thompson,** Pacific Scientific

2:10 Determination of Mebezonium Iodide in a Pharmaceutical Dosage Form Using HPLC. **N. F. Cappuccino,** B. A. Styler, and L. E. Ericson, Hoechst-Roussel Pharmaceuticals, Inc.

2:30 "Fast" HPLC in the Pharmaceutical Analysis of Desipramine Hydrochloride and of Other Tricyclic Antidepressants. **N. Strojny,** R. Williams, and G. Severin, Danbury Pharmacal Inc.

3:10 Isolation and Purification of Plant Storage Proteins by HPLC. **R. W. Blain,** N. Sagliano, Jr., and R. A. Hartwick, Rutgers U

3:30 HPLC Separation and Detection of Phytic Acid and Other Inositolphosphate Isomers Using a Metal Complex Mobile Phase Additive. **S. K. Henderson** and K. Griffin, Quinnipiac College and D. E. Henderson, Trinity College

3:50 Comparative Study of Co(II), Zn(II), and Eu(II) Beta Diketone Complexes for Enhanced UV Detection of Sugar Phosphates in Isocratic and Gradient Elution Reversed-Phase HPLC. **D. E. Henderson** and S. J. Saltzmann, Trinity College, and S. K. Henderson, Quinnipiac College

YOUR PROBLEM	THE AMICON SOLUTION		COMBINED RESULTS	AMICON MATREX PRICE 60Å MATERIAL (GERMAN MARKS) (1987 ave. European prices. Discounts available for bulk quantities)	
Resolution α	Matrex Silica μm	Amicon N-Pack Column mm	Efficiency Obtained N (TP/m)	DM/kg (100 kg order)	DM/kg (>1 ton order)
1.05	15	50 x 500 300 x 500	27700 25800	950	850
1.10	20	50 x 500 300 x 500	19000 18000	200	180
1.15	35-70	50 x 500 300 x 500	10500 10000	29	24
1.20	70-200	50 x 500 300 x 500	5000 4800	21	15

WHEN YOU START WITH AMICON CHROMATOGRAPHY TECHNOLOGY YOU STOP RELATING EFFICIENCY TO PARTICLE SIZE AND START SAVING MONEY.

In liquid chromatography, the equation states that the greater the efficiency required, the smaller the media particle size and, therefore, the greater the cost. In the past, this has led many people to consider preparative chromatography as an expensive separation technique or even to dismiss it completely.

New AMICON* technology is changing all that, by allowing a larger particle size to be used to achieve the required efficiency. This not only opens up a new era in efficiency vs. economy, but also makes the purity, speed and performance of chromatography a viable alternative for numerous new applications.

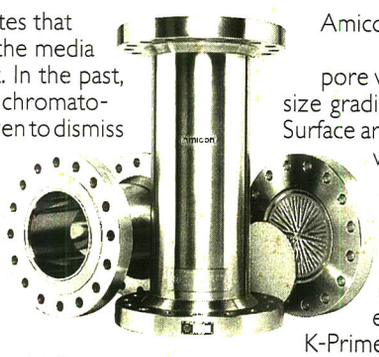

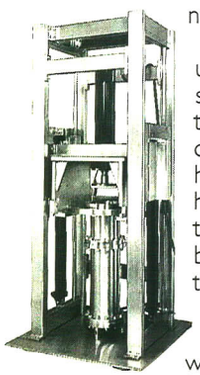

N-Pack 300AL

It starts with the new Amicon N-Pack packing/unpacking system. Used in conjunction with Amicon stainless steel chromatography columns, it eliminates the problem of uneven column packing which dictates the need to use small particle sizes to achieve high efficiency. The N-Pack's packing speed creates a high velocity in the exiting solvent stream, improving the packing density of particles at the bottom of the bed and ensuring uniform and homogenous packing throughout the column. Immediately, larger particle sizes can be used and costs reduced.

However, Amicon chromatography efficiency with economy is not just the sum of one new technology. It also covers the quality and cost of Amicon MATREX™ silica packings themselves.

Firstly, rigid control of chemical purity, surface area, pore volume, pore size distribution and selective particle size grading ensures consistently reproducible characteristics. Surface area and pore volume are controlled to within ±2% within lots and batch-to-batch reproducibility is maintained to within ±5%.

Secondly, as a member of the W. R. Grace & Co. group of companies, Amicon is the world's largest single source of silica media. As well as the ability to supply a comprehensive range, that means obvious economies, especially for bulk buyers. Add to that the K-Prime chromatograph, and you can even enjoy all those Amicon advantages in a single automated package.

But if you're already using chromatography, don't take our word for it. Check the efficiency vs. cost figures above against your own. Alternatively, if you're in pharmaceuticals, biotechnology or fine chemicals recovery and have been hesitant about the economic viability of chromatography in the past, have a word with our international applications team by ringing one of the offices below.

We only do it if we do it better.

amicon®

Division of W. R. Grace & Co.

AMICON® and MATREX™ are registered trademarks of W. R. Grace & Co.

FRANCE 37.28.91.00. ITALY (02) 9332500. NETHERLANDS 010.411.96.90. SCANDINAVIA - SWEDEN (042) 26.14.60. SWITZERLAND (01) 830.44.03. UK (045 382) 5181. W. GERMANY (02302) 80.19.96. OTHER COUNTRIES: SWITZERLAND (021) 499 111.

0145E/AC

CIRCLE 1 ON READER SERVICE CARD

Learn how to protect yourself and minimize your risk from chemicals and hazards in the laboratory

Laboratory Safety and Health

An Audio Course Produced by the American Chemical Society

An important concern for every industrial and academic laboratory is an effective safety and occupational health program. This new audio course helps you meet this vital need.

With this course, you'll become familiar with the basic guidelines for safe laboratory practices and master prudent safety methods. You'll also discover the *secrets* of laboratory safety and

- be able to minimize your risk of exposure
- know about the law and how it protects you
- effectively use safety equipment and protective facilities

You'll also cover a variety of safety- and health-related topics, including safety philosophy, federal regulations, occupational illness, known carcinogens, and more. You'll gain an understanding of the necessary guidelines for dealing with accidents in the lab and for making health and safety an integral part of effective lab practices.

Intended for bench chemists, science teachers, upperclass undergraduates, graduate students, and others involved with the use of chemicals, this course will enable management and supervisory personnel to develop an effective safety program.

Brief Course Outline

- Introduction: Overview of Course; Safety Philosophy
- Scope of the Problem: Life's Hazards; Hazard vs Risk; Deaths, Accidents, and Illness
- The Question of Liability: Negligence and the Prudent Person; Case Studies
- Hazards in the Laboratory: Chemical; Mechanical; Electrical; Radiation; Pressure and Vacuum Operations; Biological; Noise; Physical
- Working with Chemicals: Ordering; Manipulations; Inventory; Storage; Waste Disposal
- Safety Rules and Recommended Practices
- Protective Equipment: Glasses, Goggles, and Face Shields; Lab Coats; Shoes; Hearing Protection; Gloves; Respirators
- Protective and Emergency Facilities: Eyewash Fountains; Safety Showers; Fire Blankets; Fume Hoods; Fire Fighting Equipment
- Responding to Emergencies: Evacuation; Obtaining Assistance; Temporary Care; Fires; Chemical Spills
- Reporting Incidents and Accidents
- Introduction to Industrial Hygiene and Toxicology
- Federal Regulations: OSHA/NIOSH; EPA; NRC
- The Reference Library: Publications; Federal Agencies, Associations, and Professional Societies
- Summary: The Effective Safety Program

About the Instructor

Dr. James Kaufman is Professor of Chemistry at Curry College in Milton, Massachusetts, and a laboratory safety consultant. He authored *Laboratory Safety Guidelines* when he worked at Dow Chemical Company and which has been widely distributed to industry and academe. He is a member of the ACS Council Committee on Chemical Safety and is active in the ACS Division of Chemical Health and Safety.

Unit (Catalog No. C-87)

Four cassettes (4.0 hours playing time) and 168-page manual: $295.00, U.S. & Canada; $354.00, export. Additional manuals: $20.00 each, U.S. & Canada; $24.00 each, export.

To place your order, use the coupon below or CALL TOLL FREE 800-424-6747 and use your credit card or purchase order number. Please use the Priority Code and Catalog Number when ordering.

No-Risk Guarantee

All ACS Audio Courses come to you with a money-back guarantee. If you are not completely satisfied, return the course within ten days for a full refund or cancellation of invoice.

American Chemical Society, Distribution Office, Priority Code 40, 1155 Sixteenth Street, N.W., Washington, DC 20036

Yes! Please send me the following:

Qty. Total

_____ Complete course(s), *Laboratory Safety and Health* at $295.00 each (U.S. & Canada) or $354.00 each (export). Catalog No. C-87 $ _____

_____ Additional manuals at $20.00 each (U.S. & Canada) or $24.00 each (export). $ _____

TOTAL $ _____

☐ Payment enclosed (make checks payable to the American Chemical Society.

☐ Purchase order enclosed. P.O. # _____

Charge my ☐ MasterCard ☐ VISA ☐ American Express ☐ ACCESS ☐ Barclaycard ☐ Diners Club/Carte Blanche

Account # _____

Expires _____ Interbank # _____ (MC and ACCESS only)

Name of cardholder _____

Signature _____

Ship to: _____

Name _____

Title _____

Organization _____

Address _____

City, State, ZIP _____

ACS SHORT COURSES

(Sponsored by the Colorado Section of the ACS)
to be held in conjunction with the

IN

DENVER

Applied Statistical Methods in Chemistry

Instructor: Robert A. Crovelli, Ph.D., August 6-7, 1987, Tuition: $375 ($325 for members of ACS, RMCDG, SAS)

This course stresses how to think statistically by studying the definitions, terminology, notations, assumptions, concepts, principles, applications and examples of basic statistical methods in chemistry. The student will learn how to use the methods without an emphasis on proofs. The course consists of the following topics: probability concepts, random variables, probability distributions, sampling principles, descriptive statistics, statistical estimation, statistical quality control, tests of hypotheses, nonparametric statistics, analysis of variance, design of experiments, factorial experiments, simple linear regression, multiple linear regression and statistical computer programs.

Small Chemical Businesses: Ins and Outs

Instructors: D. Stull, Ph.D., R. Daughenbaugh, Ph.D. and W. Paukert, August 6, 1987, Tuition: $250 ($200 for members of ACS, RMCDG, SAS)

This one day course will present a practical roadmap for small chemical businesses, from inception to operation. Topics on chemical entrepreneuring, starting the new business, proprietary technology, governmental regulations, and growth will be discussed along with practical tips, real world examples and proven technologies. Participants will be involved in the process of conceiving and operating their own chemical business and each participant will receive a workbook/resource guide.

Sampling of Particulate Chemicals: Theory and Practice

Instructor: Mr. Francis F. Pitard, August 5-7, 1987, Tuition: $425 ($375 for members of ACS, RMCDG, SAS)

This advanced course presents a general theory on the sampling of particulate materials as applied to chemicals and pharmaceuticals. An entirely new concept of trace constituents is presented with suggestions for a revision and modernization of current standards. Many practical examples encountered in real situations are presented and step by step case studies are examined for the optimization of sampling protocols. A demonstration will be presented on how to use four user friendly programs to rapidly solve most sampling problems encountered in current practice. The course is recommended for analytical chemists, quality control managers, production statistics engineers, research scientists and everyone in quest of commercial equity.

ADDITIONAL SHORT COURSES

BASIC LABORATORY ELECTRONICS FOR SCIENTISTS
Dr. James B. Calvert, P.E.
2 Days: July 30-31, 1987
Tuition: members $250, non-members $300

CONTAMINANTS IN GROUND WATER AND POTABLE WATER: SOURCES, TRANSFORMATIONS, DETECTION AND QUANTITATION
Dr. E. M. Thurman and Dr. M. M. Reddy
3 Days: July 30-31, August 1, 1987
Tuition: members $375, non-members $425

BASIC PRINCIPLES OF MASS SPECTROMETRY AND INTERPRETATION OF ORGANIC MASS SPECTRA
Dr. J. A. Zirrolli and Ms. C. M. Moynihan
3 Days: July 29-31, 1987
Tuition: members $275, non-members $325

Registration deadline for all courses is July 17, 1987. For information contact:

Joseph A. Zirrolli
Dept. of Pharmacology
Box C236
4200 E. 9th Avenue
Denver, CO 80262
(303) 394-8961

or

Larry D. Becker
USGS-NWQL
5293-B Ward Road
Arvada, CO 80002
(303) 236-5345

CONFERENCE SYMPOSIA

CHROMATOGRAPHY Honoring Harold Walton

SUPERCRITICAL FLUID CHROMATOGRAPHY

ION CHROMATOGRAPHY

INDUCTIVELY COUPLED PLASMA/MASS SPECTROMETRY

NUCLEAR MAGNETIC RESONANCE

ELECTRON PARAMAGNETIC RESONANCE

CHEMILUMINESCENCE

ENVIRONMENTAL CHEMISTRY

INFRARED SPECTROSCOPY

ATOMIC SPECTROSCOPY

MASS SPECTROMETRY

COMPUTER APPLICATIONS

QUALITY ASSURANCE

For preliminary program write to: Sandy Grande
8780 W. Quarto Circle
Littleton, CO 80123

Use of Computers in the Examination of Chemical Data

Computer Software Applications in Chemistry. Peter Jurs, xiv + 253 pp. John Wiley & Sons, 605 Third Ave., New York, N.Y. 10158. 1986. $34.95

Reviewed by Michael Delaney, Chemometrics Section Manager, Cambridge Analytical Associates, 1106 Commonwealth Ave., Boston, Mass. 02215

This book introduces chemists to the different ways that computers are used to assist in the examination of chemical data. Jurs, a renowned researcher in this field, notes that chemists now need sufficient computer skills to practice their profession. This book is not concerned with interfacing instruments to computers, but rather with what a chemist will do with the large amounts of data that computerized instruments are capable of generating.

Topics range from traditional, numerical techniques to newer, nonnumerical topics of expert systems and chemical structure handling. The level of coverage is introductory, thus chemists interested in chemical applications of computers will find this book to be a suitable starting point. The book is divided into four parts, each of which has several chapters. Part 1, Introduction, describes the important concepts in computerized hardware and software, discusses the propagation of errors, and makes some suggestions about writing successful computer codes. Part 2, Numerical Methods, consists of seven chapters that address topics such as curve fitting, Monte Carlo simulation, and simplex optimization. Part 3, Nonnumerical Methods, discusses chemical structure handling, molecular mechanics, pattern recognition, expert systems, and spectroscopic library searching. Part 4, Graphics, has two chapters on the display of data and the display of molecules.

Each chapter includes useful references, and some chapters group references by topic. Unfortunately, the text does not mention the word "chemometrics," although the pattern recognition chapter does include reference to the extensive chemometrics reviews in ANALYTICAL CHEMISTRY.

A unique feature is the inclusion of more than 20 FORTRAN computer programs that illustrate the techniques covered in the book. Readers can type these programs into their computers and try them out with their own data. Examples of input and output are included with each program so that readers can see what the program does and can verify the successful operation of a typed-in program. Programs are written in the older "GO TO" style of FORTRAN, so it should be possible to execute the programs by using virtually any compiler. Unfortunately, this style of programming makes the programs difficult to follow or modify.

Aside from the brevity of the book, I have few criticisms. The pattern recognition chapter could have been strengthened by devoting more than just one paragraph each to the important topics of cluster analysis and the SIMCA technique. Also, the example used in this chapter was based on simulated data with no chemical basis. It may be hard for some readers to grasp the goal of pattern recognition.

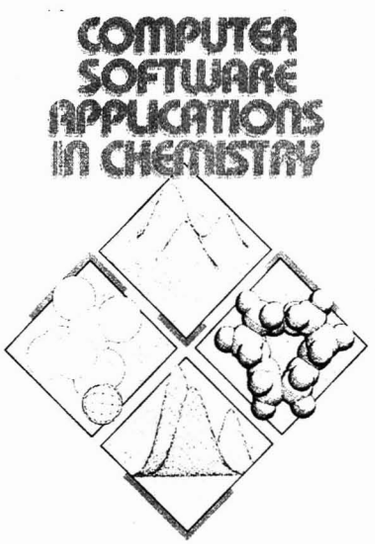

As a survey of applications, this book is successful. Supplemental material would be required to make it useful as a textbook. The book is easy to read and will not intimidate chemists who are not computer-literate. A wide range of topics is covered, but each topic is only addressed at a somewhat superficial level. Because the book is a survey of applications, it could have included a few other topics such as computerized organic synthesis, X-ray crystallography, and signal processing.

In summary, I found this book to be quite useful for its intended audience. It brings together a large number of topics in a very readable way. I hope the book will get wide circulation, because it could be of benefit to many chemists.

Detectors for Liquid Chromatography. Edward S. Yeung, Ed. ix + 366 pp. John Wiley & Sons, 605 Third Ave., New York, N.Y. 10158. 1986. $54.95

Reviewed by Ira Krull, Barnett Institute of Chemical Analysis, Northeastern University, 341 MU, 360 Huntington Ave., Boston, Mass. 02115

This is a text that lacks a true beginning and an end but offers a tremendous amount of useful, interesting information. It is an edited text, which usually implies a certain lack of cohesiveness and confluence, as opposed to one written by a single author or multiple authors working closely together. Several books have recently appeared that deal specifically with detectors for liquid chromatography (LC). Books by Scott (authored) and Vickrey (edited) are illustrative. Perhaps there is something positive to be said about an authored text. Chapters seem to lead from one to the next, without effort, and information flows from one section to another, with a definite and clear relationship. Edited texts, on the other hand, too often lack this fluency, this flow of information and ideas, and thus don't always hang close to the central theme. This is not really a serious fault, but it makes for difficult reading unless one examines the book chapter by chapter.

What this book really lacks is an introductory chapter that discusses detection in flowing streams in a broad sense. What is a concentration-sensitive versus mass-flow-sensitive detector? What are sources of detector

noise? What is response index? What is linearity of response? What about similar areas that are covered so well in authored texts about LC detectors? There is no real introduction; the book just begins with a chapter on refractive index detection. Why start here?

Similarly, there is no unified central theoretical discussion of the relationships between LC and detection, variance due to the detector, the detector relationship between peak shape and asymmetry, flow rate effects on detector response, series–parallel detection, requirements for microbore–capillary LC detection, fast LC detection, pre-

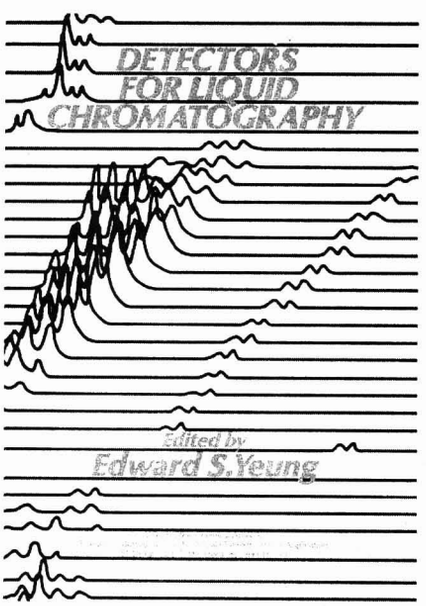

parative LC detector requirements, and so on. There is relatively little discussion of the chromatography end of high-performance liquid chromatography (HPLC) detection; emphasis is placed almost entirely on detection, as if the invited authors were really spectroscopists or electrochemists, and not specialist chromatographers. However, this varies from chapter to chapter, depending on the particular author's interests and expertise.

The editor, a well-known expert in laser spectroscopic detection for flowing solutions, especially LC, has selected a number of other well-known experts in specific detection approaches, such as Steve Weber (electrochemistry), Jack Henion (mass spectrometry), and Michael Sepaniak (fluorescence detection). However, some areas of current interest and importance, such as reaction detection and derivatizations and data handling and computer interfacing, have been omitted without explanation. Several approaches have been lumped together under a miscellaneous methods chapter, almost as an afterthought, when in reality they can be very useful and important. It might have made more sense to expand into a full chapter element-selective detectors or light-scattering detectors, especially when so many of these are already commercially available and routinely used in LC. Separate chapters devoted to FT–IR, thermal lens detection, photoacoustic spectroscopy, and polarimetry seem a bit out of place as there are no commercial systems available specifically for LC interfacing. Also, these areas are still research-oriented rather than applications- or routine use-oriented.

Not to overemphasize the negative aspects of an otherwise quite useful and comprehensive text, I would point out that the remainder of the book has been well written. As expected, there are chapters on UV–vis and fluorescence, indirect photometric detection, electrochemical detection, and mass spectrometry, plus a miscellaneous category. All the chapters are well written. References are recent and comprehensive, and most are easy to follow and understand. There is a strong emphasis on lasers for LC detection, despite the fact that very few laser-based detectors for LC are commercially available. Indeed, Low-Angle Laser Light Scattering may be the only commercially available laser-based detector that is compatible with size exclusion chromatography or HPLC, but it is never discussed.

Perhaps two of the best chapters are those by Sepaniak (on LC/fluorescence) and Henion (on LC/MS), because they are so comprehensive and clearly written. They are thorough, evenhanded, well-balanced overviews of each area. Each chapter begins with theoretical concepts and background. The influences of environmental factors, HPLC mobile phases, salt content, temperature, organic content, and so on, are discussed as they affect detector signal response. Basic instrumentation, always accompanied by schematic or actual diagrams or figures, operational parameters, available cell dimensions or interfaces, and commercial instrumentation are discussed. Even approximate prices are indicated for potential buyers. Sensitivity, analyte selectivity, linearity of response, detection limits, and related analytical figures of merit are illustrated and elucidated. Specific applications with illustrative chromatograms and quantitative data are provided, and future research areas and applications are enumerated. All of the information of interest is included in a logical, systematic sequence. These chapters were particularly pleasurable and enjoyable, perhaps because they were so thorough, clearly written, and comprehensive, but not long-winded.

Other chapters were not nearly as comprehensive; they tended to emphasize one aspect or a few aspects, especially theory, principles, fundamentals, and equations, and often little else. An overview of all areas related to detection approaches would have been more informative and interesting, as well as practical and useful. Some chapters were too theoretical and academic, offering little indication of how specific detection approaches might be used for certain types of samples at certain detection limits.

In this regard, it is hard to discern the specific audience for this book. Was it intended for the novice or advanced analytical chemist–chromatographer, graduate or undergraduate student, researcher or general practitioner, or laboratory worker? The level of each chapter is advanced and includes currently available and research-grade approaches and instruments, which suggests that the book is not for any undergraduate or graduate students but rather for those already specialized or about to be specialized in HPLC detection. It is surely not a fundamental book on chromatography, detectors, or detection approaches, because it assumes that the reader has quite a bit of background information. It is a research-oriented text, not a general reference book, and as such serves its purpose rather well. It is difficult to recommend the book to the ordinary reader, but it can be heartily recommended to anyone specializing in detection approaches for LC who already is well-versed in chromatography and detection principles.

Books Received

NMR for Liquid Fossil Fuels. Leonidas Petrakis, David Allen. x + 242 pp. Elsevier Science Publishing, 52 Vanderbilt Ave., New York, N.Y. 10017. 1986. $70

Surfactant Solutions: New Methods of Investigation. Raoul Zana, Ed. xii + 479 pp. Marcel Dekker, 270 Madison Ave., New York, N.Y. 10016. 1987. $99.75

High-Performance Liquid Chromatography. Vol. 4. Csaba Horvath, Ed. ix + 321 pp. Academic Press, 111 Fifth Ave., New York, N.Y. 10003. 1987. $70

Electrochemistry, Sensors and Analysis. Malcolm Smyth, Johannes Vos, Eds. xviii + 419 pp. Elsevier Science Publishing, 52 Vanderbilt Ave., New York, N.Y. 10017. 1986. $118

Your chance in '87! Don't miss these popular

HANDS-ON COURSES!

ACS Short Courses to be held at VPI, Blacksburg, Virginia

LIQUID CHROMATOGRAPHY
THEORY AND PRACTICE

Monday–Thursday, December 14–17, 1987

This state-of-the-art, hands-on course provides the training you need to effectively and efficiently work with this important analytical method. Through lectures and the do-it-yourself learning experience, you will

☞ learn important fundamentals of high-speed, high-efficiency liquid chromatography

☞ cover theory, instrumentation, and applications

☞ focus on BPC (partition), LSC (adsorption), reverse phase, and gel permeation

☞ work with commercially available equipment as well as several modular systems

☞ have free lab time to use or experiment with equipment

Faculty
Dr. Harold McNair (Course Director), Professor of Analytical Chemistry, Virginia Polytechnic Institute and State University, Blacksburg, VA. Guest lecturers from industry, instrument companies, and universities will participate.

Fee
ACS Members: $815.00;
Nonmembers: $895.00 (Includes tuition, lecture and laboratory materials, and all lunches.)

THE COMPUTER-INTEGRATED LABORATORY
A HANDS-ON EXPERIENCE IN LAB AUTOMATION

Sunday–Friday, September 20–25, 1987

Essential for all scientists who need or want to learn how computers operate at the machine/assembler level. This highly-rated course gives you hands-on, problem-solving experience that will enable you to

☞ find the right lab information management system for your needs

☞ integrate your old analog instruments with your new intelligent ones into a network environment

☞ help your management and computing center understand the problems of the scientific lab and show them how the electronic lab is fiscally and legally essential

Faculty
Dr. Raymond E. Dessy, Professor of Chemistry, Virginia Polytechnic Institute and State University, Blacksburg, VA, and the VPI and SU Chemistry Department Computer-Aided Research Group.

Fee
ACS Members: $845.00;
Nonmembers: $925.00 (Includes tuition, lecture and laboratory materials, and all lunches.)

GAS CHROMATOGRAPHY
PACKED AND CAPILLARY COLUMNS

Monday–Friday, September 28–October 2, 1987

Chemists and technicians—develop a comprehensive understanding of the theory and practice of gas chromatography. Through lectures and hands-on laboratory sessions in this basic course, you will

☞ master the necessary fundamentals to understand techniques and instrumentation

☞ gain practical experience working with GC equipment

☞ learn specialized techniques

☞ be able to try out new ideas or repeat experiments

No previous GC experience is required for this course. Registrants with technical questions regarding the course content may contact Dr. McNair directly: (703) 961-6579. Because of the amount of lab work performed by the participants, enrollment is limited to 24, so we urge early registration.

Faculty
Dr. Harold McNair, Professor of Chemistry, Virginia Polytechnic Institute and State University, Blacksburg, VA, is one of the most highly praised instructors in the ACS Short Course program.

Fee
ACS Members: $915.00;
Nonmembers: $995 (Includes tuition, lecture and laboratory materials, and all lunches).

The Site
All three courses will be held at Virginia Polytechnic Institute and State University (VPI) in Blacksburg, VA. Further specifics, including information on accommodations, will accompany confirmation of registration.

American Chemical Society • Education Division • 1155 Sixteenth Street, N.W. • Washington, DC 20036

Please register me in the following ACS Short Course at VPI:

Liquid Chromatography: Theory and Practice
☐ December 14–17, 1987
☐ ACS Member $815.00 ☐ Nonmember $895.00

The Computer-Integrated Laboratory:
A Hands-On Experience in Lab Automation
☐ September 20–25, 1987
☐ ACS Member $845.00 ☐ Nonmember $925.00

Gas Chromatography: Packed and Capillary Columns
☐ September 28–October 2, 1987
☐ ACS Member $915.00 ☐ Nonmember $995.00

NOTE: PREPAYMENT REQUIRED FOR CONFIRMATION.

DO NOT MAIL this form if less than two weeks remain before course starting date. Call (202) 872-4508 to confirm that space is available.

Name _____
Title _____
Organization _____
City, State, ZIP _____
Home Phone _____
Business Phone _____

LC/MS and SFC/MS: Will They Replace GC/MS?

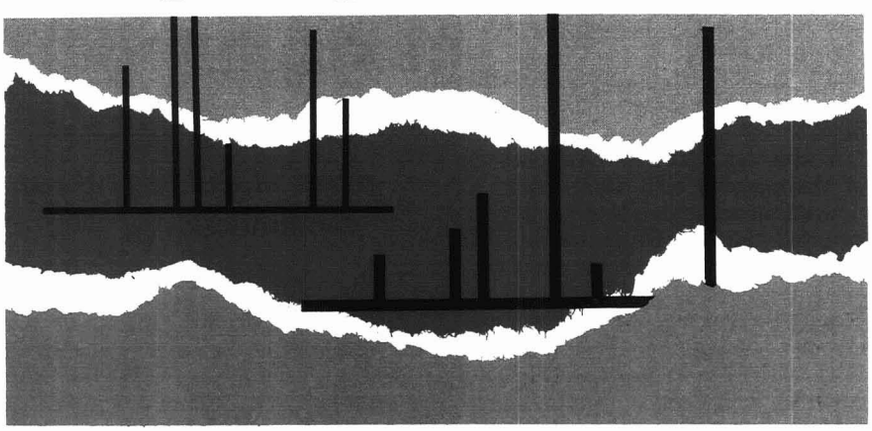

Will LC/MS and SFC/MS eventually replace GC/MS as the method of choice for organic trace analysis? This question was addressed at a symposium organized by Richard Browner of the Georgia Institute of Technology at this year's Pittsburgh Conference in Atlantic City, N.J. The symposium, one of the best-attended technical sessions at this year's meeting, featured presentations by Browner, Ron Hites of Indiana University, Jack Henion of Cornell University, Dick Smith of Battelle's Pacific Northwest Laboratory, and Marvin Vestal of The University of Houston.

Hites, whose topic was "Recent Developments in GC/MS—It's Not Dead Yet," described how far gas chromatography–mass spectrometry (GC/MS) has come in the past 25–30 years and indicated that progress is still being made in both instrumentation and methods. GC/MS was one of the first hyphenated techniques, dating back to the work of Klaus Biemann in the early 1960s, and is a natural combination, said Hites, because both techniques deal with volatile and semivolatile compounds, both work well with sample sizes in the nanogram range, and both work best with thermally stable compounds.

Although the first GC/MS experiments were performed more than 25 years ago, Hites continued, GC/MS did not become popular until devices were developed to separate the carrier gas from organic compounds and until computers were available for acquiring and processing the data. Technological improvements over the past 15–20 years, including the development of fused-silica capillary GC columns, high-speed pumps, and microprocessors, have also greatly increased the popularity and availability of GC/MS systems. Continued innovations in the computer industry have resulted in microcomputer-based data systems with a price-to-performance ratio of 100 to 1000 times that of early systems. Whereas the early systems were very large and expensive (a typical GC/MS in the late 1960s or early 1970s took up two rooms and cost about $900,000), bench-top GC/MS systems are now available for about $60,000. "While this is still a lot of money," said Hites, "GC/MS is now available to almost anyone—it is truly mass spectrometry for the masses."

Even though GC/MS has been an established technique for quite a while, said Hites, progress is still being made. Although most GC/MS is done using electron impact (EI) ionization (which is useful for compound identification because of the large mass spectral libraries that are available both on line and in the literature), said Hites, EI may not be the optimum ionization method for all problems. He believes, therefore, that alternate ionization, such as negative ion GC/MS and positive chemical ionization, is the most important recent innovation in GC/MS.

Negative ion GC/MS, which involves ionizing with very low energy electrons and measuring negative ions, is useful in both environmental and biomedical research, according to Hites, and has been routinely used to determine chlorinated compounds in sediment and fish samples with a detection limit of a few picograms. Although negative ion GC/MS significantly improves both the sensitivity and selectivity of the analysis, the spectra are notoriously temperature- and concentration-dependent and are only moderately reproducible from lab to lab. Hites's research group is currently working on these problems, and they have discovered that careful control of several ion source parameters solves most of them. They also are studying the combination of positive chemical ionization with charge-exchange ionization for isomer-specific identification of polycyclic aromatic hydrocarbons. This technique, says Hites, is particularly valuable because no standard compounds are required.

But GC/MS is not necessarily the most appropriate method for every type of analysis. Henion, whose topic was "LC/MS, SFC/MS, and GC/MS: When, Where, and Why?" explained that GC/MS remains the undisputed analytical technique for identifying and quantifying organic analytes of interest after suitable sample workup has been performed. As long as the analytes of interest are amenable to GC (i.e., thermally stable, volatile, and nonpolar) either with or without suitable derivatization, GC/MS provides the best combination of sensitivity, selectivity, and speed of analysis.

For compounds that are not thermally stable, volatile, or nonpolar enough to be amenable to GC, however, alternative chromatographic techniques are required. Thus, although GC/MS is still the method of choice for many drugs and their metabolites, pesticides, herbicides, and various compounds that may be derivatized by common methods, liquid chromatography–mass spectrometry (LC/MS) or supercritical fluid chromatography–mass spectrometry (SFC/MS) are preferred for ther-

mally labile compounds, compounds that are difficult to quantitatively derivatize because of steric hindrances, and higher molecular weight compounds that are too volatile to be amenable to GC. For example, said Henion, LC/MS clearly is preferred for determination of very polar sulfonated azo dyes in wastewater, and SFC/MS or LC/MS is preferred over GC/MS for analysis of samples containing thermally labile *N*-nitroso compounds (which are believed to be related to carcinogenicity from nitrites in cooked foods).

LC/MS

Vestal, whose topic was "Optimization of Thermospray LC/MS for Difficult Samples," agreed that LC/MS is preferable for some applications. "For samples amenable to GC/MS, and there are many," he said, "there is no need to explore alternatives. But for nonvolatile or thermally labile compounds such as proteins, samples that require derivatization for determination by GC/MS, samples that are difficult to extract from a matrix that is incompatible with GC, when less extensive clean-up is required for LC analysis, or when LC procedures are already available, such as determination of impurities in samples, LC/MS may be desirable."

"Even though GC/MS has been an established technique for quite a while, progress *is* still being made."

"LC/MS has all the power of GC/MS without the limitations," said Vestal. "MS makes a good detector for LC; it is sensitive, it can provide molecular weight and structural information, it is universal and selective, and it has a fast response." Both Henion and Vestal agree, however, that LC as an inlet for MS has some problems. Coupling of LC and MS is difficult, said Vestal, because of differences in phase and temperature. And Henion pointed out that direct introduction of LC effluent into a mass spectrometer ion source creates a large volume of gas that is too much for the conventional MS vacuum pumping system to handle. Because most mass spectrometers must maintain a high vacuum for normal operation, changes must be made to the instrument for LC to be compatible with mass spectrometry.

Several different approaches to this problem have been taken, including two discussed at the symposium: the thermospray interface developed by Vestal and the monodisperse aerosol generation (MAGIC) interface developed by Browner.

In thermospray LC/MS, gas-phase ions are produced by field-assisted evaporation from charged liquid droplets or solid particles. Ionization of neutrals also occurs by gas-phase ion molecule reactions, and external sources of ionization, such as a heated filament or an electrical discharge, may be used to supplement the direct ionization process.

Vestal demonstrated the application of thermospray to several classes of nonvolatile compounds several years ago, but the sensitivities obtained in some of the more difficult cases were several orders of magnitude poorer than those typically obtained on smaller, more volatile molecules. Recent work with several classes of difficult samples including peptides, nucleotides, sulfonated azo dyes, underivatized sugars, and large hydrocarbons, said Vestal, has established that the optimum operating conditions for thermospray depend strongly on characteristics of both the sample and the solvent. Fine-tuning these parameters, which include the diameter of the vaporizer nozzle, length of the heated zone, degree of vaporization of the solvent, geometry and temperature profiles along the channel connecting the vaporizer to the ion-sampling orifice, and the potential applied to the electrodes within the ion source, should lead to improved performance of thermospray LC/MS.

MAGIC LC/MS involves desolvation of the LC effluent followed by flash vaporization of the dry particles in the ion source area. Because it is transport-based, MAGIC LC/MS leaves the choice of ionization technique (either EI or CI) open to the user, said Browner. Both standard and microbore columns with either normal or reversed-phase separations can be accommodated, and gradient elution is routinely simple.

In addition to the thermospray and MAGIC interfaces, two new interfaces, Extrel's ThermaBeam and VG's Plasmaspray, were introduced at this year's Pittsburgh Conference (see the June 1 FOCUS, p. 769 A, for more details on commercial instrumentation for LC/MS). The ThermaBeam operates on a principle similar to that of the MAGIC interface; the primary difference is the way in which the aerosol is generated. The Plasmaspray directs the aerosol from a thermospray unit through a plasma discharge in an effort to break up the species in the aerosol and provide more structural information. The appearance of new interfaces indicates that interest in LC/MS is growing and that the problems of LC/MS interfacing have not yet been completely solved.

SFC/MS

Smith, whose topic was "SFC/MS—Principles and Promise," agreed that GC/MS, LC/MS, and SFC/MS all have their places in the analytical laboratory. "It is generally agreed that GC/MS is superior to LC/MS in terms of detection limits and selectivity and should be the method of choice, given a problem equally amenable to both techniques," he said. "It would also appear that similar considerations, though not as nearly clear-cut, should govern the choice between SFC/MS and LC/MS. This issue, however, has been clouded by the greater maturity of HPLC [high-performance liquid chromatography] compared to SFC. The limitations of SFC are less defined due to the more modest experience with and understanding of supercritical fluids, especially for highly polar analytes, where the most widely used fluids (CO_2 and pentane) have insufficient solvating power. But for amenable analyte mixtures, SFC provides high-speed or high-resolution separations superior to HPLC. And while the flame ionization detector [FID] provides excellent sensitivity for a wide range of thermally labile or less volatile compounds, its application is limited to the small number of amenable supercritical fluids (and their low polarity) that do not give an FID response.

"LC/MS has all the power of GC/MS without the limitations."

"MS, however, provides an almost perfect complement for SFC," he continued. "It is applicable to essentially any fluid or fluid mixture and has both sensitivity and selectivity that approach GC/MS. Direct interfacing of SFC and MS, however, is not trivial (as is often stated), but must be based on an understanding of supercritical fluid solvation phenomena and processes inherent in the expansion to the low-pressure environment necessary for

Finnigan MAT TSQ® 70 Quadrupole MS/MS: A Generation Ahead

Ahead in high mass performance by a quadrupole MS/MS. FAB ionization with the TSQ 70 yields unsurpassed resolution of the molecular ion cluster from biomolecules like bovine glucagon (MW 3480). Get the facts in Technical Report #601: "High Mass Analysis Using FAB Ionization with the TSQ 70."

Ahead in combining the specificity of MS/MS with the sensitivity to measure dioxins at low picogram levels in complex matrices (Technical Report #602: "MS/MS Analysis of Dioxins").

Ahead in Instrument Control Language (ICL)* so advanced, it makes real-time data-dependent decisions that provide maximum information from a minimum of sample (Technical Report #603: "Data-Dependent Instrument Control on the Finnigan MAT TSQ 70").

Others *tell* you they have a new generation of MS/MS performance. We welcome the chance to *prove* what the TSQ 70 can do for you. Look at the data in these technical reports, and ask for a demonstration. See for yourself why the TSQ 70 is a generation ahead, again.

Mass spectrometry:
We make the difference.

Finnigan MAT

U.S.A., 355 River Oaks Parkway, San Jose, CA 95134. (408) 433-4800
Benelux, Landjuweel 7, 3905 PE Veenendaal. 08385 27266
France, 69, rue de Paris, F-91400 Orsay (1) 69 28 52 53
Italy, Via Valadier, 37B, 00193 Rome. (06) 316000
Japan, Shiozaki Bldg., 2-7-1 Hirakawa-cho, Chiyoda-ku, Tokyo 102. (03) 221-1
Sweden, Årstaänsvagen 1C, 117 43 Stockholm. (08) 190480
U.K., Paradise, Hemel Hempstead, Herts HP2 4TG. (0442) 233555
W. Germany, Postfach 14 40 62, D-2800 Bremen 14. (0421) 54 93-0

*patent applied for

Circle 58 for literature.
Circle 59 to have a representative call.

ionization, such as the effects of pressure and temperature on fluid-phase solubilities and the nucleation and precipitation processes during expansion of the fluid. These considerations become increasingly important as compound polarity increases and volatility decreases. Thus the pressure restrictor and the fluid expansion process through the restrictor, in conjunction with the specific ionization method, will largely define the limits of applicability for direct MS detection. Similar, but not identical, restraints are also imposed by the solvating power of supercritical fluids which may be practical for SFC. Thus the ultimate limitations of SFC/MS for polar or high molecular weight compounds are not currently well defined."

One interesting possibility for extension of SFC to very polar and ionic compounds, said Smith, involves the use of reverse micelle supercritical fluid mobile phases. "With these mobile phases SFC can be extended, and even enzymes such as cytochrome-*c* (with a molecular weight of about 13,000) can be addressed. However, the ultimate utility of the combination with mass spectrometry is certainly questionable due to the presence of the typically nonvolatile surfactant used to form reverse micelles."

"While neither LC/MS nor SFC/MS seems destined to *replace* GC/MS, they will become increasingly important tools in the analytical laboratory."

Browner concluded that neither LC/MS nor SFC/MS will replace GC/MS—at least not yet. "To the practicing analytical chemist," he said, "the choice of acronyms required to solve the problem at hand is largely irrelevant. The questions of real importance are as follows: Is the technique required to solve the problem available? Is it economically feasible at a reasonable cost per sample? Is it routinely simple to operate and reliable on a regular basis? On all three of these points, GC/MS scores very highly. So why is there so much discussion in the analytical community on the prospects for alternative means of coupling chromatographic techniques to mass spectrometric detectors?

"The answer follows from the nature of many new analytical problems which are being presented to mass spectroscopists. GC/MS is a mature technique; its ability to handle a wide range of sample types with relative ease is well established. However, many samples of environmental, biochemical, or clinical origin contain compounds that are too involatile or thermally labile to allow separation by GC. This has led to the 'demand pull' to create alternative techniques, such as LC/MS and SFC/MS, that can handle them effectively."

The consensus among the speakers at the symposium was that although neither LC/MS nor SFC/MS seems destined to *replace* GC/MS, they will become increasingly important tools in the analytical laboratory. When asked whether LC/MS will replace GC/MS, Vestal exclaimed, "No, of course not! Will it become as important as GC/MS? Yes, probably within 4 or 5 years. And will it replace GC/MS for some applications? Definitely!"

Mary Warner

GAIN

The Professional Edge

WITH MEMBERSHIP IN THE AMERICAN CHEMICAL SOCIETY

- Keep up-to-date with weekly copies of *CHEMICAL AND ENGINEERING NEWS*
- Enjoy substantial discounts on subscriptions to ACS's internationally respected, authoritative journals and publications
- Network with your fellow scientists at local, regional and national meetings
- Enhance your career opportunities with ACS employment services
- Save on insurance and retirement plans and tax deferred annuity programs
- Discover the latest advances in your discipline with a first-year-free Division membership

. . . and this is just the beginning.

Learn why 9 out of 10 ACS members renew year after year. Gain the Professional Edge: Join ACS now. For further information write or send the coupon below or call TOLL FREE 1-800-424-6747

American Chemical Society
1155 Sixteenth St., N.W.
Washington, DC 20036

YES! Please send information on the advantages of joining the ACS.

Name _____

Address _____

_____

_____

I am most interested in the following science(s): _____

_____

Look. Light element performance with an XRF spectrometer.

Revolutionary.

The new ultrathin window in our Quantum Detector* is able to pass even soft X-rays. Giving you, for the first time ever, high-speed, light element performance at the low cost of energy dispersive XRF.

With Quantum, you can determine elements lighter than sodium. Nitrogen for instance. Plus get greatly improved detection limits for Na, Mg, and Al. And with the ability to detect lighter elements, you can quantify heavier elements more accurately.

Available in our Delta XRF Analyst system, the Quantum Detector—coupled with our exclusive Secondary Target capabilities—comprises the industry's most complete XRF package.

Quantum also shines in SEM analyses where its rugged window can withstand simultaneous venting of your SEM to one atmosphere.

Take a Quantum leap forward. Call Kevex today.

Kevex Corporation 1101 Chess Drive, Foster City, CA 94404
415/573-5866 1-800-227-0277

Kevex Affiliate (Getac GmbH) Tel 49-6131-40091 Kevex Canada, Ltd. Tel 416-731-2161
Kevex France (Fondis, S.A.) Tel 33-1-34810024 Kevex UK Tel 44-582-400596

*Patent Pending

Example of Minimum Detection Limits

Elements	Conventional Detector	Quantum X-ray Detector
N	not detectable	1.6 wt %
O	not detectable	1.0 wt %
F	not detectable	0.7 wt %
Na	0.11 wt %	244 ppm
Mg	292 ppm	84 ppm
Al	340 ppm	245 ppm
Si	166 ppm	157 ppm

*MDL's will vary with matrix, time of analysis and excitation conditions.

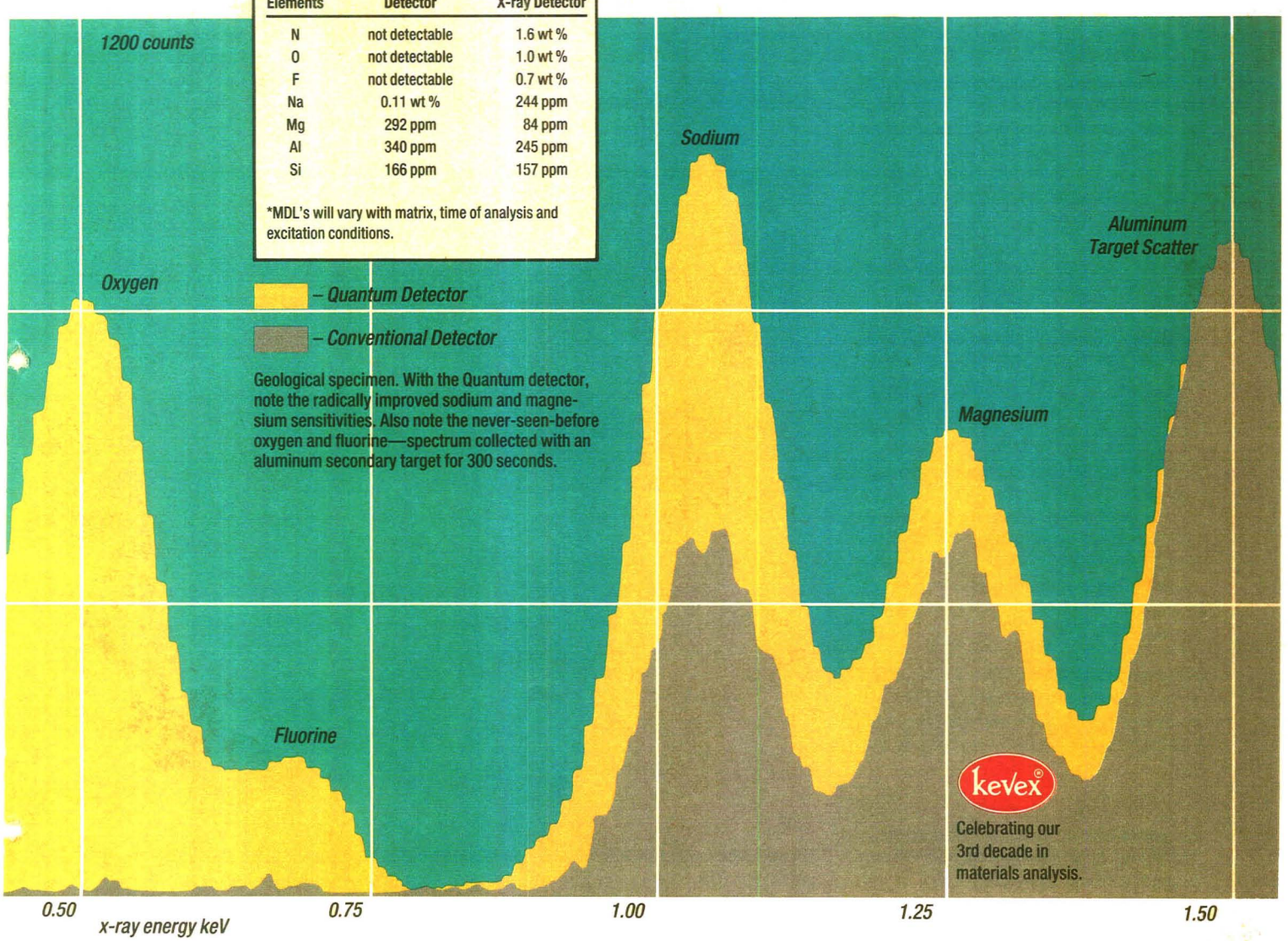

Geological specimen. With the Quantum detector, note the radically improved sodium and magnesium sensitivities. Also note the never-seen-before oxygen and fluorine—spectrum collected with an aluminum secondary target for 300 seconds.

kevex®

Celebrating our 3rd decade in materials analysis.

CIRCLE 85 ON READER SERVICE CARD

NEW PRODUCTS

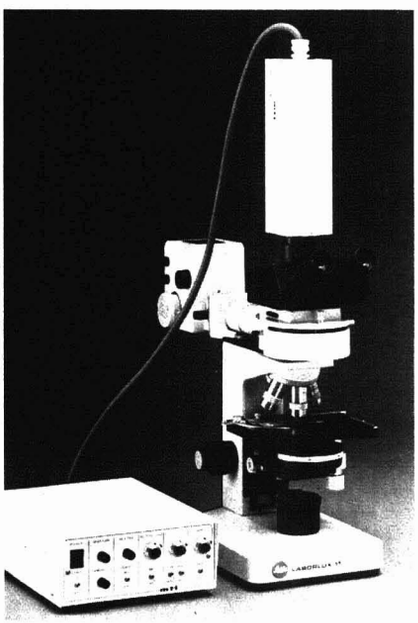

70 series video microscopy camera interfaces with computers for digital imaging and resolves problems associated with bright field, dark field, and polarized light. A compact remote head features up to 1200 lines of resolution. DAGE-MTI **401**

UV–vis. Series 5000 double-beam scanning computing spectrophotometer features a "talk-back" video display that shows all selected parameters and updates the instrument status. Automatic base-line correction and wavelength calibration also are included. Cecil **403**

SIMS. MIQ Model 256 ion microprobe features a compact ultra high-vacuum system and three ion sources (liquid metal gallium, duoplasmatron, and cesium). A variety of samples, including metals, insulators, semiconductors, biological materials, and minerals, can be analyzed. Riber **404**

Pharmaceutical testing. Dissolution sampler automates pharmaceutical analysis by collecting and automatically transferring samples to either the flow cell of a spectrophotometer or injection loop of an HPLC. The unit can handle up to 19 sets of six samples and can be programmed for up to 100 hours-long protocols. ISCO **405**

DNA synthesis. 7500 DNA Synthesizer, an integrated combination of hardware, software, and optimized beta-cyanoethyl phosphoramidite chemistry, can be controlled by an IBM PC-AT or compatible computer. DNA fragments of 100-, 120-, and 140-mer can be synthesized. Milligen **406**

UV–vis/Near–IR. Cary 2400 spectrophotometer extends from the UV–vis to near-IR region (185–3152 nm). The instrument is designed to analyze difficult solid samples often found in photonic applications. A dual double-pass grating monochromator is featured. Varian **407**

ICP/MS. Elan inductively coupled plasma mass spectrometer combines the ion generation characteristics of ICP with the low noise detection capability of MS. The instrument is used for low-level multi-element determination in a wide range of sample matrices. The detection limit for a one-minute analysis is ~1 μg/L. Perkin-Elmer **410**

Microtome. Microcut H1200 microtome prepares samples for electron microscopy and is designed for cytochemistry, neuroscience research, and histological studies. The microtome's vibrating blade cuts sections of fresh or fixed tissue in thicknesses of 10 μm to 1,000 μm with minimal structural damage. Bio-Rad/Polaron **411**

Ultracentrifuge. Model L7-65 ultracentrifuge spins samples at 65,000 rpm (485,000 g) and can be used to isolate plasmids, DNA, or RNA using cesium chloride gradients. The ultracentrifuge features automatic soft-start, two-stage braking, thumb wheel control

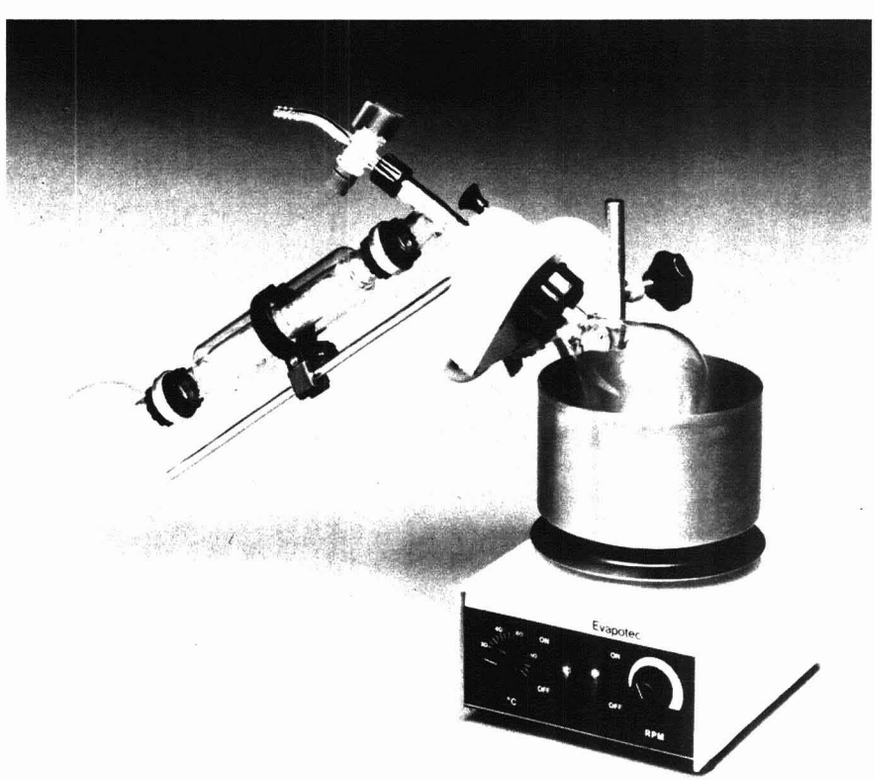

Micro rotary evaporator features a stainless steel bath, three sizes of evaporating flasks (50-, 100-, and 250-ml), and variable speed control (80–200 rpm) for evaporation of viscous solutions. Haake Buchler **402**

For more information on listed items, circle the appropriate numbers on one of our Readers' Service Cards

THE LATEST GREATEST PLATE IS OURS

Diamond Series TLC Plate. All New and Readily Available to Meet Today's Laboratory Needs.

The Whatman technologically advanced Diamond Series is the latest plate on the market. Yet, it already promises to make all others obsolete.

In laboratory tests, it has shown the no-nonsense characteristics you've been waiting for . . . like a superior hard and reflective surface, a quality organic binder, and uniform particle size and distribution.

So what you end up with, of course, is a great plate. One that doesn't flake, can be easily written on, gives off less background noise, isn't reactive towards reagents, is highly efficient and offers fast development time.

And, just as great, a plate that can be delivered in the quantities you want . . . where you want them . . . when you want them.

Why not put our "latest and greatest" claim to the test today. Contact your nearest Whatman chromatography distributor or call our special Diamond Series line. We'll give you a plate you can depend on and service to match. (800) 922-0361 or in N.J. (201) 773-5800, Ext. 219.

Whatman®

CIRCLE 178 ON READER SERVICE CARD

sets, digital readouts, built-in diagnostics, and a vacuum-encased induction drive system. Beckman **412**

Moisture detection. KFS-186 Karl Fischer aquametry system can be used with any pH meter for detecting moisture in food; grain; paint; paper and petroleum products; drugs; and chemicals. The system uses a solid-state circuit that generates its own polarizing current and displays the end point directly on a pH meter. Lazar **408**

HPLC detector. Spectromonitor 3100 variable wavelength LC detector features linear operation from 2.0 to 0.001 AUFS. Absorbance can be measured throughout the UV–vis range (190–700 nm). A 10-mm path length high-efficiency and pressure maxN series fluid cell is included. LDC/Milton Roy **409**

Software

Safety. Saf-T-Manager software is used to retrieve and print material safety data sheets; access information on spill–response procedures, recommended protective clothing and equipment and related health hazards; maintain a chemical inventory; and track employee progress through company training programs. The software is designed for any IBM PC, PC-XT, or compatible computer. J.T. Baker **415**

Graphics. Wisconsin Interactive Molecule Processor software generates publication-quality chemical structures and diagrams using the Apple laser-writer printer, HP laser jet, HP7475A, or compatible plotters. The software can be used with any IBM PC or compatible computer. Aldrich **416**

Manufacturers' Literature

Electrophoresis. Brochure describes different types of precast polyacrylamide gradient and isoelectric focusing gels. Gel casting supplies, electrophoresis units, reagents, and accessories also are listed. A chart is included to indicate the appropriate gel to be used with specific electrophoresis equipment. 12 pp. Isolab **418**

LC/MS. The first issue of *TSP Report*, a monthly publication concerning the most recent developments and applications of LC/MS and LC/MS/MS, previews the latest developments in collision-induced dissociation thermospray LC/MS. 4 pp. Finnegan MAT **421**

Scales. Brochure describes weighing equipment used in cosmetic and pharmaceutical industries. Applications of scales and weighing systems are described for receiving and shipping, central weighing and dispensing, quality control and analysis, and fill-control batch-weighing. Mettler **419**

Detector. Brochure describes the 112 UV–vis detector, which is designed for life science and industrial laboratories and can be used for HPLC, gravity flow, and low-pressure chromatography. A chart lists available sensitivity ranges as a function of path length. 6 pp. Gilson Medical Electronics **420**

Applications note. Electrochemical techniques that evaluate the corrosion resistance of metal finishes are described. Corrosion rate determination, porosity measurements, polishing evaluation, localized corrosion failures, and coating tests by electrochemical impedance techniques are presented. 8 pp. EG&G Princeton Applied Research **422**

Catalogs

Reagents. Catalog lists more than 500 immunochemicals and reagents. Descriptions and specifications of products including Nephelometric grade antisera and calibrators for in vitro diagnostics as well as a range of immunochemicals for research and development applications are provided. 60 pp. Sigma **424**

Radiochemistry. Catalog features scintillation counting supplies, radiochemicals, and radiation survey equipment. Also included are biotechnology products, chromatography supplies, electrophoresis equipment, desiccators, liquid-handling equipment, and safety supplies. 160 pp. Research Products International **425**

Spectral interpretation. Catalog describes audio-visual programs for infrared, NMR, Raman, ESR, and mass spectral interpretation. Also included are presentations on Beilstein, Gmelin, chemical abstracts, and the library sciences. Science Media **426**

Air monitoring. Catalog describes instrumentation for measuring air velocity, relative humidity, temperature, RPM, pressure, dew point, pH, conductivity, and dissolved oxygen. Handheld digital display units, multiple-function instruments, and meters with data-logging and computer-interfacing capabilities are featured. Solomat **427**

PURGE AND TRAP

Introducing the new Model 4460 sample concentrator:

- Wide bore capillary capability at no extra cost.
- Full compliance with EPA protocols for standard methods.
- Microprocessor for easy, automated operation. Fully programmable.
- Times and temperatures for standard methods (including EPA 502.1/601 and 524.1) are default programmed.
- Autosampler optional. Up to 76 vials, auto rinse.

Write or call for details. Phone (409) 690-1711.
P. O. Box 2980, College Station, TX 77841.

O·I·CORPORATION

CIRCLE 120 ON READER SERVICE CARD

ENVIRONMENTAL SCIENCE & TECHNOLOGY

ES&T

The premiere research publication in the environmental field.

Environmental science continues to be one of the fastest growing fields. And ES&T has grown right along with it!

ES&T continues to give you the practical, hard facts you need on this science . . . covering research, techniques, feasibility, products and services.

Essential reading for environmental scientists both in the business and academic world . . . ES&T has increased its emphasis on peer-reviewed research dealing with water, air, and waste chemistry in addition to adding critical reviews of important environmental science issues—all relevant to understanding the management of our natural environment.

Also included are discussions on environmental analyses, governmental regulations, current environmental lab activities, and much more!

For rate information, and to subscribe, call toll free:

(800) 424-6747

TEMPUNIT® & TEMPETTE®

CIRCULATORS

THE *ORIGINALS* AND STILL THE BEST

Once you buy a Tecam® Circulator, either an original Tempunit or its younger brother the Tempette, you'll never want to own any other. Reports from our own customers prove that over 98% recommend our circulators to their colleagues. That's why we sell our same customers over and over again and why our customer base is continuously expanding. The reason? In two words: Reliability and Performance. When you receive our catalog, check the specification *and price* with the leading competition and talk to your colleagues. Then your choice will be 'no choice'. Because the Tempunit and Tempette circulators are clearly the best.

TRANSFORM YOUR BATH INTO A PRECISE THERMOSTATIC SYSTEM

Techne

Techne Incorporated
3700 Brunswick Pike
Princeton, NJ 08540
Telephone (609) 452-9275

CIRCLE 156 ON READER SERVICE CARD

LABORATORY SERVICE CENTER

ONEIDA RESEARCH SERVICES, INC.

SYNTHETIC COMPOUND ANALYSES

2-DAY SERVICE FOR:

- Molecular Weights
- C, H, N Microanalyses
- Structural Mass Spectra
- X-ray Elemental Scans

One Halsey Rd., Whitesboro, NY 13492
Telephone (315) 736-3050

FREE DATA, FAST

To quickly amass data on all of the products you need, consult the Lab Data Service section on our *Analytical Chemistry* reader reply card insert.

HELP WANTED ADS

ROP display at ROP rates. Rate based on number of insertions within contract year. Cannot be combined for frequency.

Unit	1-TI	6-TI	12-TI
1″ (25 mm)	$160	$140	$135
	24-TI	**48-TI**	**72-TI**
	$125	$120	$115

CALL OR WRITE JANE GATENBY

ANALYTICAL CHEMISTRY
500 Post Road East
P.O. Box 231
Westport, CT 06880
203-226-7131

Laboratory Service Center (Equipment, Materials, Services, Instruments for Leasing), Maximum space — 4 inches per advertisement. Column width, 2-3/16″; two column width, 4-9/16″. Artwork accepted. No combination of directory rates with ROP advertising. Rates based on number of inches used within **12** months from first date of first insertion. Per inch: **1″ — $141; 12″ — $139; 24″ — $136; 36″ — $131; 48″ — $128.**

CALL OR WRITE JANE GATENBY

ANALYTICAL CHEMISTRY
500 Post Road East
P.O. Box 231
Westport, CT 06880
203-226-7131

Use Laboratory Service Center

MOST USED

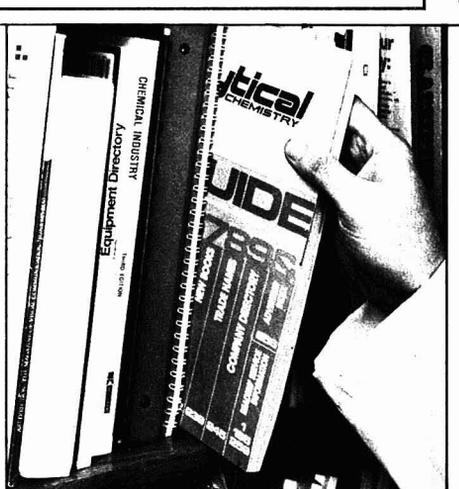

....because it's the most useful.

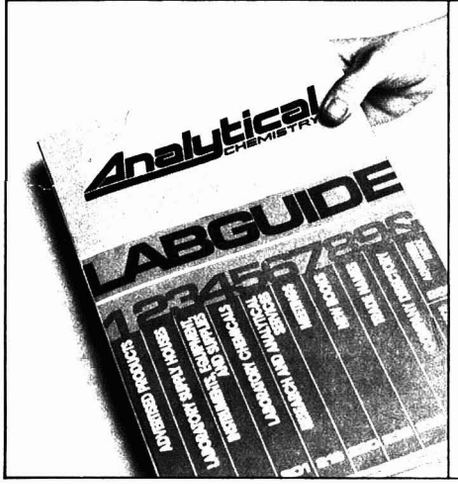

Published since 1955, the annual *LabGuide* leads all others in advertising pages and in reader usage (22,000 references daily). It's the true one-stop buying source where most manufacturers say with their ads, "Here we are. Compare our products with those of our competitors." That's why in more than six out of ten purchases by the 277,000 users it serves, the *LabGuide* is consulted before the purchase is made.

INDEX TO ADVERTISERS IN THIS ISSUE

CIRCLE INQUIRY NO.	ADVERTISERS	PAGE NO.
2	*Airco Special Gases Hammond Farrell, Inc.	820A–821A
1	**Amicon Hedges & Hughes Limited	850B
3–4	Applied Research Laboratories Eric Mower & Associates	831A, 833A
21	J. T. Baker Chemical Company Steigler, Wells & Brunswick, Inc.	811A
22	*Bio-Rad Digilab Division	IFC
20	Burdick & Jackson Nordstrom/Cox Marketing	802A
30	*Crawford Fitting Company/ A Swagelok Company Falls Advertising Company	812A
32	Dialog Information Services Humpal, Leftwich & Sinn, Inc.	822A
42	Elemental Microanalysis Limited	835A
44	Erma, Inc. F.S.C. Advertising Ltd.	841A
58–59	Finnigan MAT Corporation Lena Chow, Inc.	857A
61–62	*Gilson Medical Electronics, Inc.	801A
63	Hamamatsu Corporation Mandabach & Simms, Inc.	834A
85	*Kevex Corporation Technical Marketing Programs	859A
90	*Leco Corporation	OBC
94	Mattson Instruments, Inc. Bjork, Cunningham & Welch	813A
95	*Milton Roy Company/ Analytical Products Division Blair Advertising, Inc.	807A
112	Nelson Analytical Hayes/Rothwell	827A
110	*Nicolet Instrument Corporation Nicolet Advertising	804A–805A
120	*O. I. Corporation	862A
125	Pacific Scientific Barrett Advertising	847A
128	*Perkin-Elmer Corporation AC&R Advertising, Inc.	836A–837A
140	*Rheodyne, Inc. Bonfield Associates	828A
150	*Scientific Glass Engineering, Inc. Arden Advertising Agency	816A
152–153	*Shimadzu Scientific Instruments, Inc. Techmarketing, Inc.	825A
156	*Techne, Inc. Brunswick Advertising	863A
157	Tekmar Kenyon Hoag Associates	843A
170	*Valco Instruments Company, Inc. Technical Advertising Associates	809A
175	Waters Chromatography/Division of Millipore Millicom, Inc.	819A
178	Whatman, Inc. Northeast Communications Associates	861A

Directory section, see page 864A.

** See ad in ACS Laboratory Guide.*

*** Company so marked has advertisement in Foreign Regional edition only.*

Advertising Management for the American Chemical Society Publications

CENTCOM, LTD

President
Thomas N. J. Koerwer

Executive Vice President **James A. Byrne**
Senior Vice President **Benjamin W. Jones**
Alfred L. Gregory, *Vice President*
Clay S. Holden, *Vice President*
Robert L. Voepel, *Vice President*
Joseph P. Stenza, *Production Director*

500 Post Road East
P.O. Box 231
Westport, Connecticut 06880
(Area Code 203) 226-7131
Telex No. 643310

ADVERTISING SALES MANAGER
James A. Byrne, VP

ASSISTANT ADVERTISING SALES MANAGER
Bruce E. Poorman

ADVERTISING PRODUCTION MANAGER
Jane F. Gatenby

SALES REPRESENTATIVES

Philadelphia, PA . . . Patricia O'Donnell, CENTCOM, LTD., GSB Building, Suite 725, 1 Belmont Avenue, Bala Cynwyd, Pa. 19004. Telephone: 215-667-9666

New York, NY . . . Dean A. Baldwin, CENTCOM, LTD., 60 East 42nd St., New York, N.Y. 10165. Telephone: 212-972-9660

Westport, CT . . . Edward M. Black, CENTCOM, LTD., 500 Post Road East, P.O. Box 231, Westport, Ct. 06880. Telephone: 203-226-7131, Telex 643310

Cleveland, OH . . . Bruce E. Poorman, John C. Guyot, CENTCOM, LTD., 325 Front St., Suite 2, Berea, Ohio 44017. Telephone: 216-234-1333

Chicago, IL . . . Michael J. Pak, CENTCOM, LTD., 540 Frontage Rd., Northfield, Ill. 60093. Telephone: 312-441-6383

Houston, TX . . . Michael J. Pak, CENTCOM, LTD., Telephone: 312-441-6383

San Francisco, CA . . . Paul M. Butts, CENTCOM, LTD., Suite 1070, 2672 Bayshore Frontage Road, Mountain View, CA 94043. Telephone: 415-969-4604

Los Angeles, CA . . . Clay S. Holden, CENTCOM, LTD., Newton Pacific Center, 3142 Pacific Coast Highway, Suite 200, Torrance, CA 90505. Telephone: 213-325-1903

Boston, MA . . . Edward M. Black, CENTCOM, LTD., Telephone: 203-226-7131

Atlanta, GA . . . Edward M. Black, CENTCOM, LTD., Telephone: 203-226-7131

Denver, CO . . . Paul M. Butts, CENTCOM, LTD., Telephone: 415-969-4604

United Kingdom

Reading, England . . . Malcolm Thiele, Technomedia Ltd., Wood Cottage, Shurlock Row, Reading RG10 OQE, Berkshire, England. Telephone: 073-434-3302, Telex #848800

Lancashire, England . . . Technomedia Ltd., c/o Meconomics Ltd., Meconomics House, 31 Old Street, Ashton Under Lyne, Lancashire, England. Telephone: 061-308-3025

Continental Europe . . . Andre Jamar, International Communications, Inc., Rue Mallar 1, 4800 Verviers, Belgium. Telephone: (087) 22-53-85, Telex #49263

Tokyo, Japan . . . Shuji Tanaka, International Media Representatives Ltd., 2-29 Toranomon, 1-Chome Minato-ku Tokyo 105 Japan. Telephone: 502-0656, Telex #22633

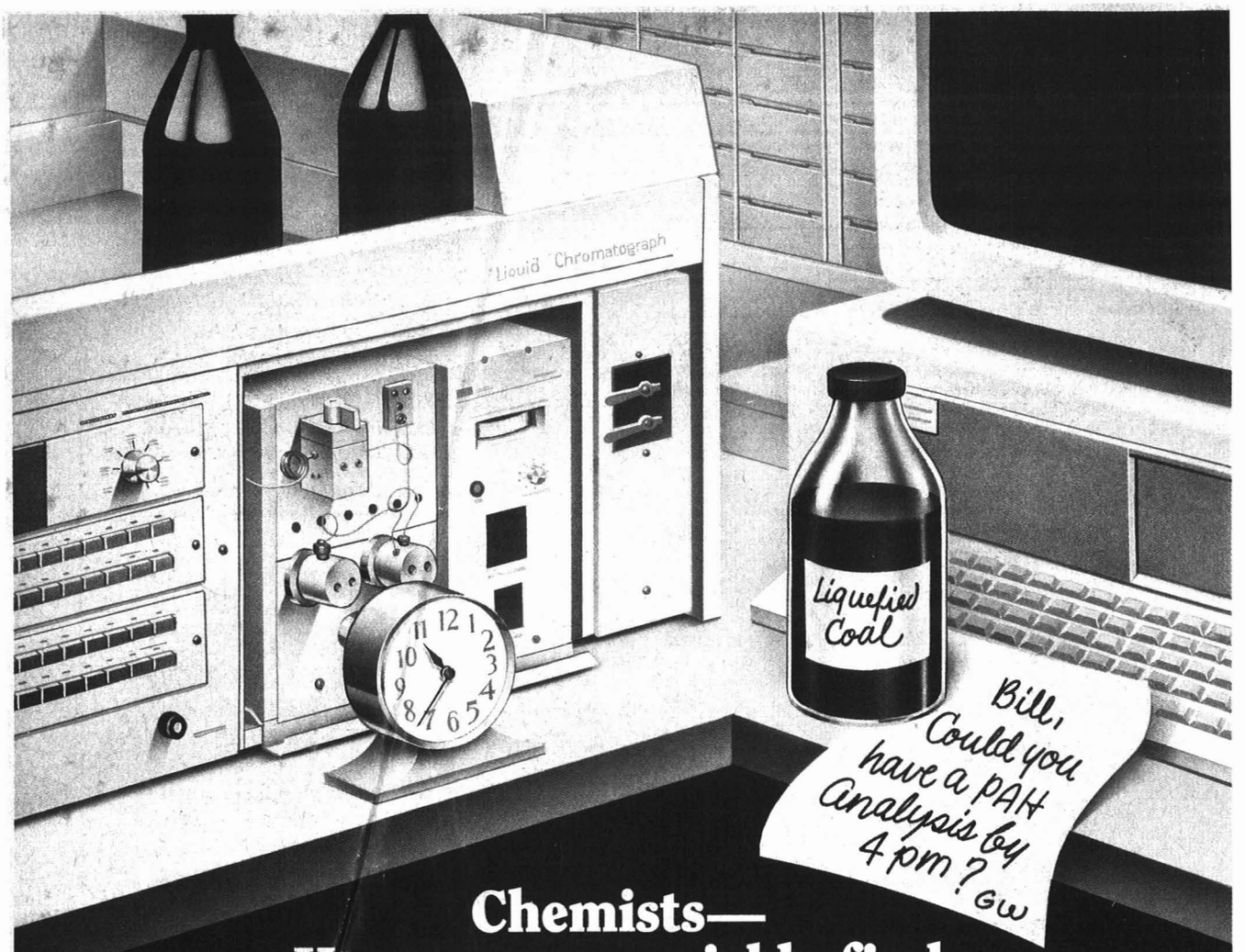

Chemists— How can you quickly find an analytical procedure to solve this problem?

Search CHEMICAL JOURNALS ONLINE.

CHEMICAL JOURNALS ONLINE is the new powerful information search system that permits you to quickly search over 45,000 journal articles and display:

Experimental Procedures • Experimental Data • Preparation Techniques • New Chemical Names • Synthesis Information

• PLUS CROSSOVER CAPABILITIES WITH CAS ONLINE

As part of STN, International, CHEMICAL JOURNALS ONLINE provides you with the unique ability to instantaneously cross over from CAS ONLINE to the full-text of appropriate journals.

CHEMICAL JOURNALS ONLINE is not only precise in its searching but also cost effective. In minutes you can save yourself days of tedious work.

CHEMICAL JOURNALS ONLINE contains:

- The American Chemical society's 18 primary journals with over 45,000 articles dating back to 1982.
- A learning file for training and teaching purposes for one low connect hour charge.
- John Wiley & Son's Polymer Journals Online dating back to 1984. (Available Summer 1987)
- Other publisher's journals in the future.

To put CHEMICAL JOURNALS ONLINE to work for you, call an American Chemical Society sales representative today at **800-424-6747**. The call is free.

Or write, Sales Office, American Chemical Society, 1155 Sixteenth Street, N.W., Washington, D.C. 20036.

Your Research Is Not Complete Until You Search **CHEMICAL JOURNALS ONLINE**

Analytical CHEMISTRY

EDITOR: **GEORGE H. MORRISON**

ASSOCIATE EDITORS: **Klaus Biemann, Georges Guiochon, Fred E. Lytle, Robert A. Osteryoung, John A. Smith**

Editorial Headquarters
1155 Sixteenth St., N.W.
Washington, D.C. 20036
Phone: 202-872-4570
Teletype: 710-8220 151

Managing Editor: Sharon G. Boots
Associate Editors: Stuart A. Borman, Rani A. George, Louise Voress
Assistant Editors: Mary D. Warner, Grace K. Lee
Production Manager: Leroy L. Corcoran
Art Director: Alan Kahan
Designer: Sharon Harris Wolfgang
Production Editor: Elizabeth E. Wood
Circulation: Cynthia G. Smith
Editorial Assistant, LabGuide: Joanne Mullican

Journals Dept., Columbus, Ohio
Associate Head: Marianne Brogan
Associate Editor: Rodney L. Temos

Advisory Board: Shier S. Berman, Brian S. Bidlingmeyer, Henry N. Blount, Gary D. Christian, Harry V. Drushel, Larry R. Faulkner, Peter R. Griffiths, Gary M. Hieftje, Nobuhiko Ishibashi, Mary A. Kaiser, David L. Nelson, Erno Pungor, Dennis Schuetzle, Nicholas Winograd, Edward S. Yeung, Andrew T. Zander

Instrumentation Advisory Panel: Howard G. Barth, Richard F. Browner, James B. Callis, Richard S. Danchik, Thomas C. Farrar, Joel M. Harris, John F. Holland, Ronald E. Majors, Linda B. McGown

The Analytical Approach Advisory Panel: Edward C. Dunlop, Robert A. Hofstader, Wilbur D. Shults

Published by the
AMERICAN CHEMICAL SOCIETY
1155 16th Street, N.W.
Washington, D.C. 20036

Books and Journals Division
Director: D. H. Michael Bowen
Journals: Charles R. Bertsch
Research and Development: Lorrin R. Garson

Manuscript requirements are published in the January 1, 1987 issue, page 219. Manuscripts for publication (4 copies) should be submitted to ANALYTICAL CHEMISTRY at the ACS Washington address.

The American Chemical Society and its editors assume no responsibility for the statements and opinions advanced by contributors. Views expressed in the editorials are those of the editors and do not necessarily represent the official position of the American Chemical Society.

AUTHOR INDEX

Andreolini, F., 1720
Appelhans, A. D., 1685
Arnold, M. A., 1604
Asada, T., 1652

Bartoš, B., 1737
Batley, G. E., 1608
Bellocq, J., 1695
Biemann, K., 1652
Bilewicz, A., 1737
Bornhop, D. J., 1632
Borra, C., 1720

Caccamo, F., 1720
Carroll, R. J., 1639
Castellano, S. M., 1726
Chisholm, W. P., 1726
Chritz, K. M., 1716
Chung, L. T. K., 1701
Cooks, R. G., 1677
Costello, C. E., 1652

Dahl, D. A., 1685
Darden, T., 1731
Delmore, J. E., 1685
Demeter, D. A., 1731
Di Corcia, A., 1720
Dohner, R., 1600
Dovichi, N. J., 1632

Egolf, D. S., 1586
Esteban, N. V., 1674
Ewald, M., 1695

Florence, T. M., 1608
Forsyth, D. S., 1742

Garrigues, P., 1695
Gautschi, K., 1600
Giger, W., 1709
Glass, G. E., 1594
Glish, G. L., 1670

Harris, J. M., 1620
Hatfield, G. R., 1659
Hawthorne, S. B., 1705
Hieftje, G. M., 1664
Hoyer, B., 1608

Ishihara, M., 1652

Jurs, P. C., 1586

Kallir, A. J., 1644
Kamat, P. V., 1636
Kammei, Y., 1652
Katsura, T., 1647
Kelley, P. E., 1670, 1677
Kettler, C. N., 1733
Koh, T.-S., 1597
Kubota, E., 1652
Kunihiro, F., 1652

Leach, J. M., 1701
Liberato, D. J., 1674
Lipkowitz, K. B., 1731
Louris, J. N., 1677

Maciel, G. E., 1659
Marcomini, A., 1709
Marniesse, M.-P., 1695
Martin, S. A., 1652
Matsumoto, K., 1647
McCreery, R. L., 1615
McLuckey, S. A., 1670
Metzger, E., 1600
Michael, J. L., 1739
Miller, D. J., 1705

Narbutt, J., 1737
Novák, J., 1692

Otson, R., 1701

Parish, C. A., 1731
Polkowska-Motrenko, H., 1737
Poon, M., 1615
Poston, P. E., 1620

Retcofsky, H. L., 1726
Roth, M., 1692

Samperi, R., 1720
Sardashti, M., 1659
Sato, K., 1652
Scoble, H. A., 1652
Sepaniak, M. J., 1733
Sidbury, J. B., 1674
Simon, W., 1600
Small, H., 1716
Sorensen, J. A., 1594
Spiegelman, C. H., 1639
Sprecher, R. F., 1726
Stafford, G. C., Jr., 1677
Stevens, T. S., 1716
Suter, G. W., 1644
Syka, J. E. P., 1677

Teague-Nishimura, J. E., 1647
Todd, J. F. J., 1677
Tominaga, T., 1647
Torres, E. L., 1626

Vickers, G. H., 1664
Vo-Dinh, T., 1644
Vonderschmitt, D. J., 1600

Wangsa, J., 1604
Watters, R. L., Jr., 1639
Wells, M. J. M., 1739
Wild, U. P., 1644
Wilson, D. A., 1664
Winefordner, J. D., 1626
Wise, S. A., 1695

Yergey, A. L., 1674

Simulation of Carbon-13 Nuclear Magnetic Resonance Spectra of Substituted Cyclopentanes and Cyclopentanols

Debra S. Egolf and Peter C. Jurs*

Department of Chemistry, 152 Davey Laboratory, The Pennsylvania State University, University Park, Pennsylvania 16802

The carbon-13 nuclear magnetic resonance spectra of substituted cyclopentanes and cyclopentanols have been simulated with computer-assisted methods. Linear model equations relate the chemical shift values to calculated molecular structural descriptors that represent the surroundings of the carbon centers. Sets of equations were developed that simulate the spectra with sufficient accuracy for library search retrieval of the observed spectra for a set of similar compounds.

Carbon-13 nuclear magnetic resonance spectroscopy (^{13}C NMR) is a valuable analytical tool used for organic structure elucidation. Interpretation of ^{13}C NMR spectra is often based on comparison with standard reference spectra stored in libraries. When suitable spectra are not available for comparison, other methods must be employed to evaluate complex experimental spectra (*1*). Spectrum simulation is one method that chemists can utilize to produce spectra that approximate the observed spectra of organic compounds.

One approach to spectrum simulation is to develop linear models based on structural parameters that describe carbon environments. These models have the form

$$S = b(0) + b(1)x(1) + b(2)x(2) + ... + b(p)x(p) \quad (1)$$

where S is the predicted chemical shift of a given carbon atom, the $x(i)$ are numerical descriptors that encode structural features of the chemical environment of the atom, the $b(i)$ are coefficients determined from a multiple linear regression analysis of a set of observed chemical shifts, and p denotes the number of descriptors in the model.

This approach was first tested on linear and branched alkanes (*2*, *3*) and later extended to include compounds with heteroatoms and unsaturations (*4*, *5*). Further investigations of this approach became feasible through the development of an interactive computer system which aids in the model construction and evaluation (*6*, *7*). Large numbers of descriptors for complex molecules can now be handled conveniently as shown in spectral simulation studies for various structural classes: cyclohexanols and decalols (*8*), steroids (*9*), and some cyclopentanes (*10*).

Chemical shift is a measure of the chemical environment of a particular carbon center, which is highly dependent on the conformation of the molecule. Conformation can be expressed through geometrical descriptors. For a conformationally locked molecule the chemical environments of the atoms can be approximated by a single set of descriptor values. On the other hand, for a geometrical descriptor to adequately describe a particular property of a flexible molecule, it should ideally be calculated for several conformations of that molecule.

Obtaining a continuum of conformations and their corresponding geometrical descriptor values even with a computer is costly and time-consuming. Several issues therefore need to be investigated. For small molecules is it appropriate to approximate conformationally mobile molecules with a static molecular structure? More importantly, does a static structure, which implies a unique geometry, gravely affect geometrical descriptor values, and therefore chemical shift models? This paper addresses the above questions concerning the applicability of this simulation system to conformationally flexible molecules. Various statistics are also presented as numerical measures of the durability of the chemical shift models.

EXPERIMENTAL SECTION

Figures 1 and 2 show the 50 cyclopentanes and cyclopentanols used in this study. The set of compounds used in the formation of chemical shift models consists of 32 substituted cyclopentanes with 9 epimeric structural pairs and substituents ranging from methyl and hydroxyl to propyl and *tert*-butyl. The spectra for structures **1–16** were obtained from a paper by Roberts and co-workers (*11*). A spectrometer operating at 15.1 MHz provided the proton decoupled spectra. These spectra were reported relative to carbon disulfide (CS_2) and were corrected to a tetramethylsilane (Me_4Si) standard by using a conversion factor of 192.8 ppm. All of the compounds were measured as 20–30% (v/v) solutions in dioxane. The spectra for compounds 17 and 18 were taken from ref 12. The spectra were scanned on a Varian CFT-20 spectrometer and reported relative to (Me_4Si). These compounds were measured in a solution of deuteriated chloroform. The spectra for compounds **19–32** were taken from data published by Schneider and co-workers (*13*). Decoupled spectra were obtained with a spectrometer by scanning at 22.63 MHz in PFT mode. The chemical shifts of ring carbons were measured relative to cyclopentane; but substituent chemical shifts were compared to a Me_4Si standard. These compounds were measured in a solution of 25–35% deuteriated chloroform with 10% Me_4Si.

The prediction set contains three topologically equivalent dimethylcyclopentanols and *n*-propylcyclopentane. The spectra for compounds **33–35** were taken from the Schneider data set previously discussed (*13*), and the spectrum for compound **36** was taken from a collection compiled by Johnson and Jankowski (*14*). This spectrum was taken on an XL-100 spectrometer in the Fourier transform mode. This compound was measured in a 1 mL/2 mL solution of deuteriated chloroform with chemical shift values being measured relative to Me_4Si.

A set of 15 hydroxyl-substituted cyclopentanes was utilized in the second study. Compounds 8 and **37–50** are less structurally diverse than the set of compounds discussed above. The spectra for these compounds were taken from a paper by Perlin and co-workers (*15*). Chemical shifts were recorded with a Varian HA-100 CW spectrometer operating at 25.15 MHz. These spectra were measured relative to methyl iodide but reported relative to Me_4Si. All of the compounds were measured as aqueous solutions.

To begin our study, the 50 chemical structures were entered into the computer disk files by using the graphical input procedures of the ADAPT software system (*16*, *17*). Approximate three-dimensional coordinates were obtained by using an interactive molecular mechanics program (*18*). Allinger's MM2 program (*19*, *20*) has been interfaced to our software system and was used for further structural manipulation.

The computer programs used in this analysis are written in FORTRAN and implemented on a PRIME 750 computer operating in the Department of Chemistry at The Pennsylvania State

0003-2700/87/0359-1586$01.50/0 © 1987 American Chemical Society

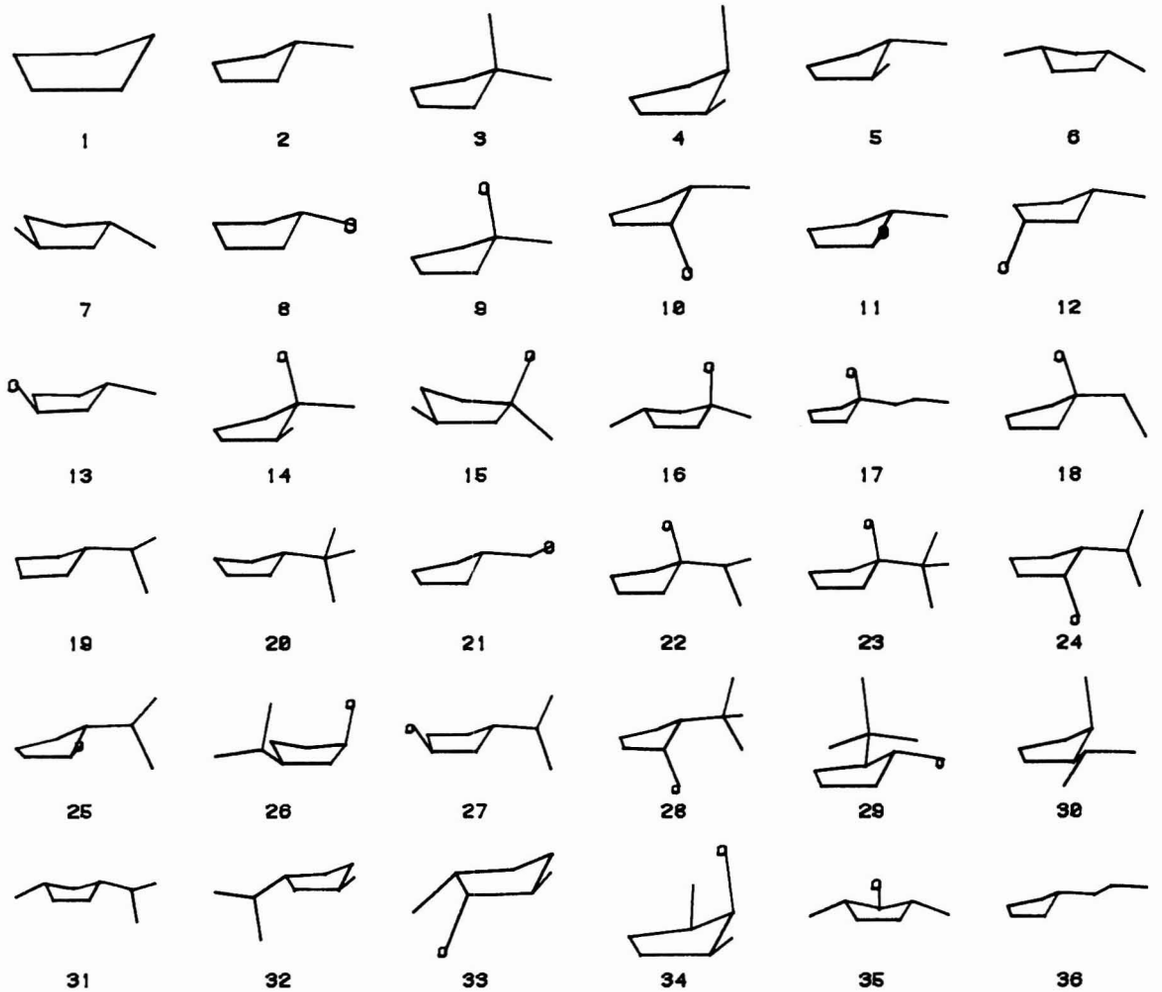

Figure 1. The compounds used in the first study. Compounds **1–32** comprise the reference set and compounds **33–36** comprise the prediction set: **1**, cyclopentane; **2**, methylcyclopentane; **3**, 1,1-dimethylcyclopentane; **4**, *cis*-1,2-dimethylcyclopentane; **5**, *trans*-1,2-dimethylcyclopentane; **6**, *cis*-1,3-dimethylcyclopentane; **7**, *trans*-1,3-dimethylcyclopentane; **8**, cyclopentanol; **9**, 1-methyl-1-cyclopentanol; **10**, *cis*-2-methyl-1-cyclopentanol; **11**, *trans*-2-methyl-1-cyclopentanol; **12**, *cis*-3-methyl-1-cyclopentanol; **13**, *trans*-3-methyl-1-cyclopentanol; **14**, 1,*c*-2-dimethyl-*r*-1-cyclopentanol; **15**, 1,*c*-3-dimethyl-*r*-1-cyclopentanol; **16**, 1,*t*-3-dimethyl-*r*-1-cyclopentanol; **17**, 1-propyl-1-cyclopentanol; **18**, 1-ethyl-1-cyclopentanol; **19**, isopropylcyclopentane; **20**, *tert*-butylcyclopentane; **21**, cyclopentylmethanol; **22**, 1-isopropyl-1-cyclopentanol; **23**, 1-*tert*-butyl-1-cyclopentanol; **24**, *cis*-2-isopropyl-1-cyclopentanol; **25**, *trans*-2-isopropyl-1-cyclopentanol; **26**, *cis*-3-isopropyl-1-cyclopentanol; **27**, *trans*-3-isopropyl-1-cyclopentanol; **28**, *cis*-2-*tert*-butyl-1-cyclopentanol; **29**, *trans*-2-*tert*-butyl-1-cyclopentanol; **30**, *cis*-1-isopropyl-2-methylcyclopentane; **31**, *cis*-1-isopropyl-3-methylcyclopentane; **32**, *trans*-1-isopropyl-3-methylcyclopentane; **33**, *t*-2,*c*-5-dimethyl-*r*-1-cyclopentanol; **34**, *c*-2,*c*-5-dimethyl-*r*-1-cyclopentanol; **35**, *t*-2,*t*-5-dimethyl-*r*-1-cyclopentanol; **36**, *n*-propylcyclopentane.

University. Tektronix PLOT-10 software provides the graphics capabilities for these studies.

RESULTS AND DISCUSSION

The conformational attributes of the compounds being investigated will be considered first. The problem of conformational stability of molecules with regard to developing parametric models with the ADAPT software has been considered previously (*8*). In that study a set of conformationally rigid cyclohexanols and decalols was used to form parametric equations, which subsequently were used to predict, with excellent results, the chemical shifts of conformationally mobile cyclohexanols. However, to take the experiment one step further, what would happen if the equations were generated by using conformationally mobile molecules? Could reasonable regression models be obtained to approximate the chemical shifts, and if so, would it then be feasible to predict the chemical shifts of other molecules not originally used in the creation of these models?

Cyclopentane is found to exist in two general conformations of comparable energy: the envelope and half-chair forms. It has been determined that in solution cyclopentane undergoes changes between these two conformations in what is called a pseudorotation circuit (*21*). The circuit consists of twenty distinct conformations alternating between the envelope and half-chair forms. Thus, one conformation would not accurately define the state in which this molecule exists. Adding substituents to the molecule modifies this pseudorotation circuit by causing increases in the energy required to obtain particular conformations. For methylcyclopentane the largest difference in energy of two conformations is approximately 1.5 kcal/mol (*13*). Molecules with bulkier substituents should exhibit larger barriers to pseudorotation. These molecules, however, still oscillate between several different, yet energetically similar, conformational structures.

In order to gain a perspective on the conformational stability of the cyclopentyl molecules of this study, the energies of various conformations of structures 1–32 were determined. Several initial conformers of each molecule were generated by using the ADAPT interactive molecular mechanics program. Following this, MM2 returned the final coordinates and strain energies. In all cases except four, different stable conformers were obtained for each molecule. For structure **19**, three conformers were readily determined. As can be seen in Table I, seven of the conformers are within 0.5 kcal/mol of each other, and only nine are over 2.0 kcal/mol different in energy. Thus, a significant number of the compounds have at least two favorable low-energy conformations. Because structures

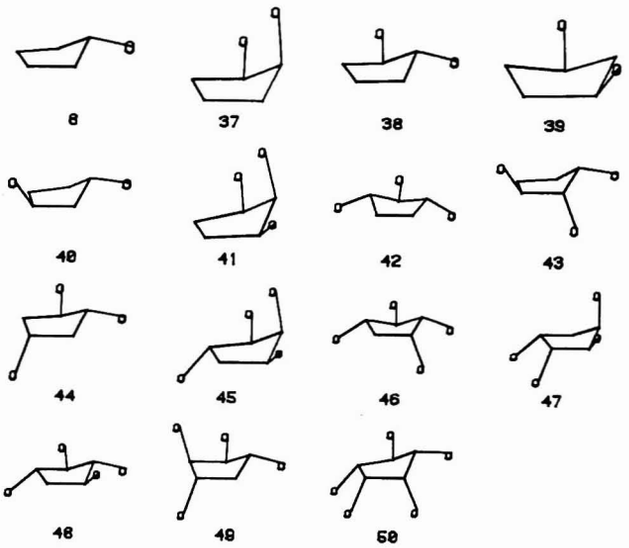

Figure 2. The compounds used in the second study: **8**, cyclopentanol; **37**, *cis*-1,2-cyclopentanediol; **38**, *trans*-1,2-cyclopentanediol; **39**, *cis*-1,3-cyclopentanediol; **40**, *trans*-1,3-cyclopentanediol; **41**, *r*-1,*c*-2,*c*-3-cyclopentanetriol; **42**, *r*-1,*t*-2,*c*-3-cyclopentanetriol; **43**, *r*-1,*c*-2,*t*-3-cyclopentanetriol; **44**, *r*-1,*t*-2,*c*-4-cyclopentanetriol; **45**, *r*-1,*c*-2,*c*-3,*t*-4-cyclopentanetetrol; **46**, *r*-1,*c*-2,*t*-3,*c*-4-cyclopentanetetrol; **47**, *r*-1,*c*-2,*t*-3,*t*-4-cyclopentanetetrol; **48**, *r*-1,*t*-2,*c*-3,*t*-4-cyclopentanetetrol; **49**, *r*-1,*t*-2,*t*-3,*c*-4-cyclopentanetetrol; **50**, *r*-1,*c*-2,*c*-3,*c*-4,*t*-5-cyclopentanepentol.

Table I. Energy Differences of MM2 Generated Conformers (kcal/mol)

compd	low-energy conformer[a]	energy difference[b]	compd	low-energy conformer	energy difference
1	11.40		**17**	15.53	1.42
2	11.56	1.20	**18**	16.33	0.04
3	13.00		**19**	15.35	0.16/1.02
4	13.86		**20**	16.60	3.44
5	12.19	2.12	**21**	12.58	2.02
6	11.84		**22**	18.02	0.25
7	12.01	1.19	**23**	20.22	3.14
8	12.71	0.16	**24**	17.98	2.14
9	13.43	0.91	**25**	17.03	0.05
10	13.42	1.04	**26**	16.73	0.30
11	12.96	1.20	**27**	16.58	1.14
12	12.72	1.29	**28**	19.33	3.91
13	12.79	1.16	**29**	18.61	2.74
14	14.44	1.99	**30**	16.09	4.41
15	13.72	1.04	**31**	15.55	0.30
16	13.75	1.23	**32**	15.74	2.60

[a] The low-energy conformations were the ones used in this study. [b] Energy difference = (energy of higher energy conformer) − (energy of lower energy conformer).

1, **3**, **4**, and **6** exhibit only one conformational preference, it is probable that the pseudorotation circuit has just one low-energy well, whereas for all of the other structures, there must be at least two low-energy wells either of comparable or significantly different energies. Without obtaining the complete energy profiles, these hypotheses, however, cannot be verified. It is necessary only to realize that, indeed, the molecules are conformationally flexible.

Definition of the First Study. Compounds **1**–**36**, depicted in Figure 1, comprise the first study to be discussed. Each compound is represented by its lowest energy conformation. The reference set of structures, compounds **1**–**32**, contain 234 carbon atoms. Carbon-13 chemical shift values were input to the computer disk files. By use of the data reduction method previously described (*9*), duplicate atoms, those in equivalent environments, were removed from the atom list so that only carbon atoms with unique properties comprise the data set. Following this procedure, 178 carbon atoms remain. Simple topological, topological electronic, and geometrical descriptors were calculated for these carbon centers. A descriptor containing the chemical shift values corresponding to the remaining unique carbon centers was created to serve as the dependent variable for the regression analyses.

Ideally, subsets of atoms in similar chemical environments lead to better parametric models of chemical shift values than the atom set as a whole (*3*). Two different, yet complementary schemes for partitioning the atoms into appropriate subsets will be compared and contrasted in this study. One criterion for determining the classification of the atom centers is the multiplicity of the atom center; while the other criterion employed is the atom's location within the molecule. Linear models were generated for each subset and statistics and prediction results are presented.

Atom Grouping by Multiplicity. Grouping the atoms by multiplicity produces five subsets: (1) 35 primary, (2) 82 secondary, (3) 36 tertiary, (4) 11 tertiary with hydroxyl substituents, and (5) 13 quaternary carbon atoms. The quaternary subset contains five centers without a hydroxyl substituent and eight centers with a hydroxyl substituent. One atom failed to fall into any of these subsets because it is the only secondary carbon with an attached hydroxyl group; thus, it was excluded from the study.

Model Formation. Each of the five atom subsets was considered separately for the formation of regression models. Only statistically significant descriptors were retained for consideration in the regression procedure (*7*, *8*). Several regression models were then computed for each atom subset and were evaluated on the basis of various statistics (*22*–*25*). The best models obtained are presented in Table II. The descriptor labels are defined and mean, standard deviation, regression coefficient, and mean effect on predicted chemical shifts are presented for each descriptor in the model. The mean effect is a measure of the shielding or deshielding effects of each descriptor.

The model for the primary carbons is comprised of one geometrical, one topological electronic, and two simple topological descriptors. The secondary carbon model is composed of three geometrical, one topological electronic, and two simple topological descriptors. The best model for the tertiary carbon atoms without hydroxyl substituents employs only two topological descriptors, one simple and the other electronic. The tertiary carbon atom set with hydroxyl substituents and the quaternary atom set are each described by univariate models containing a geometrical descriptor and a topological descriptor, respectively. The tertiary and quaternary models will be limited in their application to configurational isomers since they only encode topological properties. In fact, the single descriptor in the quaternary model is only an indicator of α attachment of a hydroxyl group.

Model Evaluation. Table III presents a summary of the regression model statistics with the low, high, mean, and standard deviation of the chemical shift values for each atom group. The statistics presented for each model are as follows: n, the number of observations; p, the number of descriptors in the model; R, the multiple correlation coefficient for the predicted vs. observed chemical shifts; R(adj), multiple correlation coefficient adjusted for degress of freedom; s, the standard error of estimate for the predicted chemical shifts (in parts per million); and F, the F value for the statistical significance of the regression model.

The first four models show standard errors on the order of 1 ppm, but the quaternary model has a standard error of 3 ppm. Although the range of chemical shift values for the quaternary model is 31.91–87.14 ppm, the chemical shifts actually cluster in two subgroups of smaller ranges of

Table II. Chemical Shift Models

P	descriptor[a]	mean	SD[b]	coeff	mean effect, ppm
			Primary Carbons (Group 1)		
1	TCON 2	1.48	0.18	25.7 ± 0.9	37.9 ± 1.4
2	TOCG 3	0.234	0.183	−3.56 ± 1.02	−0.832 ± 0.239
3	AVC2 2	0.971	0.891	0.925 ± 0.176	0.899 ± 0.171
4	CXVD 1	−0.0822	0.0416	−15.3 ± 4.2	1.26 ± 0.34
5	intercept			−17.5	−17.5
			Secondary Carbons (Group 2)		
1	HXI3 1	0.108	0.036	121 ± 8	13.1 ± 0.9
2	AVC1 2	0.744	0.767	3.84 ± 0.39	2.86 ± 0.29
3	TOCG 3	0.271	0.242	−6.71 ± 0.71	−1.82 ± 0.19
4	AVC3 1	0.683	0.646	1.45 ± 0.24	0.987 ± 0.163
5	HXVD 1	0.0941	0.3049	−4.60 ± 1.15	−0.433 ± 0.108
6	OSTR 1	0.136	0.127	5.05 ± 1.31	0.688 ± 0.178
7	intercept			17.0	17.0
			Tertiary Carbons (Group 3)		
1	ICON 2	1.48	0.73	11.1 ± 0.3	16.3 ± 0.5
2	NTCG 3	−0.159	0.212	3.29 ± 1.15	−0.523 ± 0.183
3	intercept			24.6	24.6
			Tertiary Carbons with Attached Hydroxyl (Group 4)		
1	HHI3 2	0.103	0.052	35.0 ± 6.4	3.62 ± 0.66
2	intercept			71.2	71.2
			Quaternary Carbons (Group 5)		
1	NNOX 1	0.615	0.506	47.2 ± 1.7	29.0 ± 1.1
2	intercept			34.8	34.8

[a] Descriptor definition: AVC1 2, number of primary carbons located two bonds from the carbon center; AVC2 2, number of secondary carbons located two bonds from the carbon center; AVC3 1, number of tertiary carbons attached to the carbon center; CXVD 1, van der Waals energy due to interactions between the carbon center and other heavy atoms; HHI3 2, average of sum of inverse cubed throughspace distances from the hydrogens attached to the carbon center to hydrogens three bonds from the carbon center; HXI3 1, average of sum of inverse cubed throughspace distances from the hydrogens attached to the carbon center to heavy atoms two bonds from the carbon center; HXVD 1, van der Waals energy due to interactions between hydrogens attached to the carbon center and heavy atoms in the molecule; ICON 2, the molecular connectivity index computed over the bonds two bonds from the carbon center; NNOX 1, number of oxygen atoms attached to the carbon center; NTCG 3, sum of σ charges of heavy atoms three bonds from the carbon center; OSTR 1, van der Waals energy of the nearest oxygen divided by the distance from the oxygen to the carbon center; TCON 2, sum of the molecular connectivity index terms for one and two bonds from the carbon center; TOCG 3, sum of the absolute values of σ charges for atoms three bonds away from the carbon center. [b] SD = standard deviation.

Table III. Summary of Model Statistics

	obsd chemical shifts									
group	low	high	mean	SD[a]	n	p	R	R(adj)	s	F
1	9.00	29.90	21.70	4.94	35	4	0.987	0.985	0.86	275
2	18.20	51.00	32.39	7.44	82	6	0.991	0.990	1.05	660
3	28.21	59.40	40.38	8.45	36	2	0.988	0.988	1.33	688
4	73.38	80.11	74.86	2.07	11	1	0.877	0.877	1.05	30
5	31.91	87.14	63.83	24.07	13	1	0.993	0.993	3.00	764

[a] SD = standard deviation.

31.91–39.20 and 79.30–87.14 ppm. The single descriptor only takes on values of 0 and 1; thus only two chemical shift values, 34.80 and 81.98 ppm, can be predicted. This model is not sensitive to small chemical shift differences. All models, except the tertiary with hydroxyl model, have excellent correlation coefficients. The high value of the correlation coefficient for the quaternary model is misleading because of its dependence on the large overall range of the shift values. Likewise, the correlation coefficient for the tertiary with hydroxyl model is deceiving because of the small range of chemical shift values under consideration, 73.38–80.11 ppm. Thus, an abnormally low correlation coefficient of 0.88 was obtained. The F values for all of the models are excellent.

A principal concern is our ability to accurately approximate genuine spectra. Therefore, the chemical shifts simulated by the five linear models were combined to form complete spectra for each compound. To determine the degree of similarity of the spectra, the residual mean square (rms) error of the predicted vs. the observed spectrum for each compound was computed. The mean error over the 32 compounds is 1.26 ppm with a low error of 0.28 ppm and a high of 3.22 ppm. Twenty-three of the spectra have a rms error below 1.5 ppm; however, seven of the spectra with greater errors include at least one signal for a quaternary carbon atom. Consequently, due to the poor simulation of the quaternary carbon shifts, the mean rms value is higher than might otherwise be expected.

To better determine the significance of the rms statistic, a library search was performed. The object of the search procedure is to retrieve the top five spectra that most closely resemble each predicted spectrum when the Euclidean distance metric is used as the method of comparison. The library is composed of 261 spectra including the spectra of this data set. Cyclopentylmethanol was the only compound for which the observed spectrum was not retrieved as any of the top five best matches. This was to be expected since one of its

Table IV. Chemical Shift Differences between Epimeric Pairs

compd no.	compd pair	C1	C2	C3	C4	C5	other carbons
4, 5	1,2-diMe	5.1	5.1	1.8	0.1	1.8	CH_3, 3.6
6, 7	1,3-diMe	−1.9	−1.9	−1.9	0.9	0.9	CH_3, 0.3
10, 11	1-OH, 2-Me	4.6	2.4	0.8	−0.6	−0.6	CH_3, 4.6
12, 13	1-OH, 3-Me	0.0	0.2	−1.1	0.3	−0.2	CH_3, −0.4
15, 16	1-OH, 1,3-diMe	−0.4	−0.4	0.8	0.1	0.7	1-CH_3, 0.3; 3-CH_3, 0.5
24, 25	1-OH, 2-*i*-Pr	3.13	1.04	0.66	0.91	0.91	CH, 2.60; CH_3, −0.65
26, 27	1-OH, 3-*i*-Pr	0.13	0.06	−1.17	0.45	0.00	CH, −1.74; CH_3, 0.00
28, 29	1-OH, 2-*t*-Bu	0.00	3.12	4.22	2.37	1.43	C, −1.74; CH_3, −1.56
31, 32	1-*i*-Pr, 3-Me	2.29	2.15	−0.59	−0.45	0.00	CH, 0.00; *i*-CH_3, 0.00; 3-CH_3, 0.00

chemical shifts was removed from the study as noted earlier. Of the remaining 31 predicted spectra, 26 were matched with their corresponding observed spectrum. The five incorrectly matched spectra of compounds **15**, **24**, **27**, **28** and **32** were each matched with the spectrum of the compound's configurational isomer. In each case, the second best match was the correct match. The observed chemical shifts of the epimeric pairs of compounds contained in this study are compared in Table IV. As can be seen, often differences between chemical shift pairs are negligible, especially for 1,3-substituted compounds, with respect to the standard errors of the model equations. Thus, the search results are not surprising.

Due to the high residual standard error incurred by the quaternary model, it is possible that the shifts simulated by this model, in fact, hinder the accurate identification of simulated spectra. Thus, an attempt was made to determine the usefulness of the chemical shift values simulated by particular models for the precise definition of predicted spectra. If these regression models are sufficiently discriminating when simulating chemical shifts, a predicted spectrum lacking one shift can potentially be correctly identified through association of the remaining shifts with library spectra. For example, exclusion of the quaternary carbon shift predictions from the simulated spectra leaves 11 spectra short one shift and one spectrum minus two shifts. In addition, compound **21** is also missing one predicted chemical shift. Comparison of observed spectra containing one more chemical shift than the predicted spectrum can be accomplished by removing the unmatched shift from each spectrum. Now each simulated spectrum with n predicted signals is compared with all observed spectra containing n or $n + 1$ signals, effectively increasing the number of possible matches for most of the predicted spectra. When the simulated quaternary shifts are excluded, the predicted spectrum of compound **23** lacks two shifts; thus, a correct identification of this spectrum is not anticipated. A library of just the observed spectra for the 32 compounds in the study was searched and 24 of the other 31 spectra were correctly identified. Now the corresponding observed spectra for compounds **3**, **21**, and **28** are the third best matches, and the spectra for compounds **15**, **24**, **27**, and **32** are still second choice matches.

For comparison, a library search was performed while withholding the chemical shift values for the tertiary carbons with hydroxyl substituents instead of the quaternary values. In this case, no simulated spectra are missing more than one signal; thus, all have the possibility of being correctly matched with their corresponding observed spectra. The results show that 26 of the 32 spectra were correctly matched. However, the spectra for compound **21** was accurately identified as the third best match; and the spectra for compounds **15**, **24**, **27**, **28** and **32** correspond to the second choice matches.

None of the other sets of predicted chemical shifts can be withheld from the spectra without poor characterization of the individual spectra of several compounds. When the predicted values for the tertiary carbons with hydroxyl substituents were withheld, the search was just as successful as when they were included. On the other hand, when the quaternary shifts were not included in the spectra, some of the spectra lost valuable information that differentiate them from other spectra. Therefore, although the standard error for the quaternary model is high, the information present is significant enough to be useful in the simulation of approximate spectra for differentiation between these compounds.

Atom Grouping by Location. An alternative approach to classification of the data was considered in an effort to improve the simulations of the chemical shift values. First the drawbacks of the above simulations are noted; then the relative merits of this classification method are discussed.

A disadvantage of grouping the atoms by multiplicity is that the quaternary chemical shift values are not well described. Inclusion of a second descriptor in the model would significantly decrease the standard error. However, a five-to-one ratio of observations to parameters, the number of descriptors plus one, must be maintained to uphold the validity of the regression model. Consequently, to increase the number of descriptors in the model the number of observations must also be increased. The composition of the quaternary atom set must also be considered. Just as the tertiary carbon centers were separated based on the presence of a hydroxyl substituent, so also should the quaternary carbon centers. Unfortunately, both subsets contain too few atoms from which even univariate regression models can be developed.

Furthermore, the chemical shifts for the tertiary atoms without hydroxyl substituents were only described by two topological descriptors in the regression model. Thus the shift predictions for this atom set also are not sensitive to geometry. During model formation and subsequent statistical testing, other candidate models including more descriptors, some encoding geometry, were tested. All of those models either performed poorly or possessed grave multicollinearities.

The new atom classification method was generated to alleviate the lack of sensitivity and robustness of the previous models. The primary and secondary atom sets were retained while the other three subsets were regrouped. The new atom groupings take into consideration both the influence of the hydroxyl substituent and the location of the atom centers in either the cyclopentane ring backbone or as part of a side chain. Atoms within the ring backbone are, in general, more restricted in movement than those atoms located in the *tert*-butyl and isopropyl moieties; thus, it is probably beneficial to model them separately. Therefore, all carbon atoms with an attached hydroxyl substituent—8 quaternary, 11 tertiary, and the single secondary atom originally excluded from the study—were combined as a group. The 27 tertiary and single quaternary carbon centers contained in the backbone cyclopentane rings were grouped together, as were the 9 tertiary and 4 quaternary carbon centers located in side chains attached to the backbones. Subsets 6–8 of 20, 28 and 13 atoms were formed.

Model Formation. Regression models of 3, 4, and 1 descriptors, respectively, were constructed for each new atom set as presented in Table V. The model for the set of carbon

Table V. Chemical Shift Models

p	descriptor[a]	mean	SD[b]	coeff	mean effect, ppm
		Carbons with Attached –OH (Group 6)			
1	ACON 1	0.436	0.0417	−122 ± 7	−53.3 ± 2.9
2	CHVD 1	−0.0648	0.135	10.0 ± 2.1	−0.648 ± 0.138
3	HXVD 1	0.000466	0.152	6.79 ± 1.71	0.00316 ± 0.00080
4	intercept			131	131
		Ring Carbons (Group 7)			
1	AVC1 2	1.32	1.34	5.43 ± 0.26	7.18 ± 0.34
2	AVC3 1	0.643	0.678	1.98 ± 0.50	1.27 ± 0.32
3	CCHG 1	−0.0273	0.00917	110 ± 28	−3.00 ± 0.77
4	OSTR 3	0.0114	0.0142	−46.7 ± 18.9	−0.658 ± 0.267
5	intercept			37.8	37.8
		Side Chain Carbons (Group 8)			
1	HRD3 2	0.155	0.0360	58.2 ± 10.2	9.04 ± 1.57
2	intercept			24.1	24.1

[a] Descriptor definition: ACON 1, the molecular connectivity index computed over bonds one bond from the carbon center divided by the number of bonds one bond away; AVC1 2, number of primary carbons located two bonds from the carbon center; AVC3 1, number of tertiary carbons attached to the carbon center; CCHG 1, σ charge on the carbon center; CHVD 1, van der Waals energy due to interactions between the carbon center and hydrogens in the molecule; HRD3 2, sum of inverse cubed throughspace distances from the carbon center to hydrogens three bonds away; HXVD 1, van der Waals energy due to interactions between hydrogens attached to the carbon center and heavy atoms in the molecule; OSTR 3, van der Waals energy of the nearest oxygen divided by the cubed distance from the oxygen to the carbon center. [b] SD = standard deviation.

Table VI. Summary of Model Statistics

	obsd chemical shifts									
group	low	high	mean	SD[a]	n	p	R	R(adj)	s	F
6	67.01	87.14	77.31	4.87	20	3	0.979	0.976	1.08	122
7	32.20	59.40	42.72	8.16	28	4	0.989	0.988	1.31	258
8	28.21	37.31	33.18	2.42	13	1	0.866	0.866	1.26	33

[a] SD = standard deviation.

centers with hydroxyl substituents contains one simple topological and two geometrical descriptors. The ring carbon model combines two simple topological, one topological electronic, and one geometrical descriptor; and the chemical shifts for the side chain carbons are modeled by a single geometrical descriptor.

Model Evaluation. Table VI presents the statistics for each new model. The range of the chemical shift values for each of the three groups is relatively small; therefore, small shift differences are being encoded by the descriptors. The R values are quite good and the standard errors for all three models fall below 1.5 ppm, a significant improvement over the error for the quaternary model. The F values again are excellent.

The simulated spectra from these new models were combined with the spectra for the primary and secondary models to form complete spectra for each compound. A comparison was made between the simulated and observed spectra of each compound yielding low and high rms errors of 0.28 and 2.42 ppm and a mean value over all 32 spectra of 0.99 ppm, 0.3 ppm less than that of the other simulation. Twenty-nine of the 32 are simulated with an rms error of less than 1.5 ppm.

A search of the spectral library for the closest match to each predicted spectrum was performed and only 26 of the 32 spectra were matched with their corresponding observed spectra. The other six predicted spectra for compounds **5**, **13**, **24**, **27**, **28** and **32** were each matched with the spectrum of the configurational isomer of the compound and, in each case, the corresponding spectrum was the second choice. Although the standard errors for the new models were improved over those of the original models, the only apparent advantage of these simulated spectra, as determined from the comparison and search results, is the suitable encoding of the atom previously removed from the study.

Simulation of Prediction Set Spectra. As a final test, the chemical shifts for the external prediction compounds, three epimeric 2,5-dimethylcyclopentanols and *n*-propylcyclopentane, were simulated by using both sets of regression models with descriptor values calculated for those four compounds. The chemical shift values for the three epimers were assigned to the incorrect compounds in the paper from which they were obtained (*13*), as verified by Schneider (*26*). For the evaluation of the simulation, the revised assignment of chemical shift values was used as the observed spectra for the compounds. Comparison of the predicted spectrum with the observed spectrum of each compound leads to some interesting results. For the predicted spectra from the original models, the antisymmetric epimer has an rms error value of 1.72 ppm; while the cis/cis and trans/trans spectral comparisons have error values of 5.03 and 2.94 ppm, respectively. *n*-Propylcyclopentane has an error value of 2.02 ppm. Use of the other models for determining the predicted spectra gives error values of 1.96, 5.21, 3.68, and 3.35 ppm for the four spectra.

By use of the predicted spectra from the original models, the spectral library of 261 spectra was searched for the best matches. The predicted spectra for compounds **33** and **36** were matched with their corresponding observed spectra; however, the observed spectrum for compound **35** was matched with the predicted spectrum for **34** and vice versa for the predicted spectrum of compound **35**. A search for the best matches to the predicted spectra for the new models gives the same results except that the observed spectrum for compound **36** is chosen as the second best match for the corresponding predicted spectrum, while the first choice is a spectrum for a compound outside of the cyclopentane data set. The chemical shift for the tertiary atom for *n*-propylcyclopentane is predicted quite poorly in both simulations.

Due to the trends of the chemical shift values in the data

Table VII. Chemical Shift Models

p	descriptor[a]	mean	SD[b]	coeff	mean effect, ppm
		Secondary Carbons (Group 9)			
1	NTCG 2	−0.497	0.358	−19.9 ± 0.4	9.89 ± 0.20
2	intercept			24.3	24.3
		Tertiary Carbons with Attached Hydroxyl (Group 10)			
1	HHVD 1	0.865	0.520	−3.02 ± 0.85	−2.61 ± 0.74
2	CXVD 1	−0.0425	0.0391	24.9 ± 5.6	−1.06 ± 0.24
3	HXVD 1	0.248	0.277	6.13 ± 1.35	1.52 ± 0.37
4	NTCG 2	−0.527	0.338	−2.34 ± 0.85	1.23 ± 0.45
5	OSTR 3	0.182	0.073	7.11 ± 3.07	1.29 ± 0.56
6	intercept			75.7	75.7

[a] Descriptor definition: CXVD 1, van der Waals energy due to interactions between the carbon center and other heavy atoms; HHVD 1, van der Waals energy due to interactions between hydrogens attached to the carbon center and other hydrogens in the molecule; HXVD 1, van der Waals energy due to interactions between hydrogens attached to the carbon center and heavy atoms in the molecule; NTCG 2, sum of σ charges of heavy atoms two bonds from the carbon center; OSTR 3, van der Waals energy of the nearest oxygen divided by the cubed distance from the oxygen to the carbon center. [b] SD = standard deviation.

set as confirmed by the prediction of the shifts for compounds **34** and **35**, it is possible that the spectra for the two compounds should be assigned to the opposite compound. With this alternate shift assignment, a comparison of rms errors for the two different sets of models produces 0.85 and 2.78 ppm for the original models and 1.82 and 2.10 ppm for the new models. Even with the spectra switched, the prediction errors are high; but it appears that the original set of models predicts chemical shift values for compounds outside the original data set with greater success than the second set of models. However, it should be noted that no quaternary carbon atoms were present in the prediction set compounds.

Assessment of Conformational Effects. A direct test of the effect of conformation on the simulation of chemical shifts was performed through utilizing the other conformers generated for the data set. Initially, the descriptors on which the regression models were based were developed from the lowest energy structures obtained for each compound. However, conformers that differ from the lowest energy structures by less than 1.5 kcal/mol should still have a significant effect on the average chemical shift values of these compounds. Referring back to Table I, it can be seen that conformers within 1.5 kcal of the lowest energy conformers were generated for compounds **2**, **7**, **8**, **9**, **10**, **11**, **12**, **13**, **15**, **16**, **17**, **18**, **19**, **22**, **25**, **26**, **27**, and **31**. These structures, along with the lowest energy conformers of the other 14 structures, were used to create new descriptor values for this set of conformations. These descriptor values then replaced those in the original regression equations but the same coefficients were retained. From these equations new simulated chemical shift values were obtained and combined to form complete spectra for each compound.

The simulated spectra for the atom sets grouped by multiplicity were first considered. The rms error incurred when these simulated spectra are compared with the observed spectra is 1.33 ppm. This error is almost 0.1 ppm greater than the error for the original simulation. Twenty-one of the spectra have errors below 1.5 ppm as compared with the previous number of 23. More significant, however, is the performance of the new spectra in a library search. The search is executed with the same library of spectra as before. Again, the same six spectra are mismatched; but two additional simulated spectra, 11 and 12, match their corresponding observed spectra as the second best match.

Similarly, the simulated spectra for the atom sets grouped according to atom location were examined. The rms error is 1.19 ppm, 0.2 ppm greater than the error for the original data. Only 22 spectra have rms errors below 1.5 ppm as compared to 29 previously. The results of the library search are much as before with the following exceptions. The spectrum for compound **13** is now accurately identified, although three additional spectra—**12**, **15**, and **16**—are not matched with their corresponding observed spectra as the best match.

This test seems to indicate that the regression models are fairly specific to the conformations of the structures used to develop the descriptors. Although the geometrical descriptors are necessary to separate configurational isomers, these descriptors may not be providing enough information to accurately separate the spectra of those isomers when the structures themselves are conformationally flexible. If, on the other hand, the lowest energy conformation of flexible molecules is determined to be the dominant conformation, geometrical descriptors calculated for these molecules should be useful in spectrum simulation and the subsequent identification of configurational isomers.

Definition of the Cyclopentanol Study. The second study involves the set of 15 cyclopentanol structures depicted in Figure 2, compounds **8** and **37–50**. This data set was chosen to study the parametrization of a more homogeneous set of structures and their simulated chemical shifts. Less structural diversity among the compounds should lead to more uniform chemical shift variations, which are more easily encoded with linear regression models.

Due to the small number of compounds, a prediction set is not feasible. Thus, internal tests will define the success/failure of the simulation programs to determine chemical shift values accurately. Although compounds with multiple hydroxyl substituents have not previously been studied under this simulation system, it was hypothesized that the descriptors currently available would sufficiently characterize the molecules and prove useful in predicting their chemical shift values.

The data set is composed of 29 secondary carbon centers and 46 tertiary centers with an attached hydroxyl substituent. Unique carbon centers based on topology and geometry were perceived. The two subsets to be parametrized, groups 9 and 10, now contain 21 distinct secondary and 32 tertiary carbon centers. The spectra for all of the carbon centers were entered into disk files, and simple topological, topological electronic, and geometrical descriptors were calculated. The chemical shift values of the compounds were merged with the unique carbon centers to form the dependent variable for the regression analyses.

Model Formation. Regression models were generated for both the secondary and tertiary carbon centers as presented in Table VII. The chemical shifts for the subset of secondary carbon centers are best described by a single topological electronic descriptor. On the other hand, the chemical shifts of the tertiary carbon centers with attached hydroxyl groups are characterized by five descriptors—one topological elec-

Table VIII. Summary of Model Statistics

	obsd chem shifts									
group	low	high	mean	SD[a]	n	p	R	R(adj)	s	F
9	20.30	44.90	34.15	7.14	21	1	0.996	0.996	0.64	2450
10	69.50	85.10	76.12	4.06	32	5	0.968	0.963	1.11	77

[a] SD = standard deviation.

tronic, and four geometrical, including three van der Waals descriptors.

Model Evaluation. The regression model statistics are presented in Table VIII. As can be seen, the standard error of 0.64 for the secondary carbon model is quite low, indicating that in this case, the geometry of the carbon centers has little effect on the values of the chemical shifts. The standard error of the tertiary model is also quite good. The correlation coefficient and F statistic again show the statistical significance of each model.

The complete simulated spectrum for each compound was generated by combining the simulated spectra of the two models. These spectra were then compared with the observed spectra of each compound. Of the 15 spectra generated, 14 of those compared to the observed spectra within 1.5 ppm with an average error of 0.91 ppm and low and high values of 0.41 and 1.92 ppm, respectively.

A library search of the 15 observed spectra for the best spectral match for each predicted spectrum produced a success rate of 14 out of 15 chosen correctly. The predicted spectrum for compound **39** was matched with the observed spectrum for compound **40** and the second best match was with the correct spectrum. These two compounds are an epimeric pair and their corresponding chemical shifts differ by only 0.3 ppm. Thus, it is not likely that any method would differentiate between the two spectra enough to permit an accurate assignment. A general library search for these spectra was not performed since the spectra of these compounds are significantly different from those of all others in the library; thus, obtaining an accurate assignment of the predicted spectra to the observed would be trivial.

CONCLUSIONS

This spectral simulation system is effective when utilized for the prediction of conformationally averaged spectra of flexible molecules. The linear models derived by relating the chemical shift values to the structural descriptors are, in general, robust and sensitive to small structural changes. Therefore, the simulated spectra can be used to accurately identify structures topologically, and in many cases, geometrically as well.

Grouping of the carbon centers by different classification schemes was valuable in this study, and alternative methods of atom subsetting may be applicable in future studies. Atom grouping by multiplicity leads to better predictive models for the four prediction compounds, although the models for the atom groups based on location more accurately simulate the spectra of the reference set. To truly assess the merits of one classification scheme over the other for this structural class, a larger data set, in particular more atoms for the external prediction set, is essential.

Finally, as was anticipated, linear models generated for less structurally diverse atom sets appear to have better predictive capabilities than those models based on the atomic environments of compounds with an assortment of substituents. Again, due to the lack of data, any definitive conclusions about the predictive abilities of the models for the hydroxyl substituted compounds cannot be corroborated. Ideally, compounds with a common structural backbone and simple substitutions are the best candidates for spectral simulation studies.

Registry No. **1**, 287-92-3; **2**, 96-37-7; **3**, 1638-26-2; **4**, 1192-18-3; **5**, 822-50-4; **6**, 2532-58-3; **7**, 1759-58-6; **8**, 96-41-3; **9**, 1462-03-9; **10**, 25144-05-2; **11**, 25144-04-1; **12**, 5631-24-3; **13**, 5590-95-4; **14**, 16467-04-2; **15**, 33642-39-6; **16**, 33642-40-9; **17**, 1604-02-0; **18**, 1462-96-0; **19**, 3875-51-2; **20**, 3875-52-3; **21**, 3637-61-4; **22**, 1462-05-1; **23**, 69745-48-8; **24**, 85982-42-9; **25**, 85982-43-0; **26**, 85982-44-1; **27**, 85982-45-2; **28**, 40557-25-3; **29**, 40557-26-4; **30**, 61868-01-7; **31**, 61828-02-2; **32**, 61828-03-3; **33**, 65378-78-1; **34**, 65404-79-7; **35**, 63057-29-4; **36**, 2040-96-2; **37**, 5057-98-7; **38**, 5057-99-8; **39**, 16326-97-9; **40**, 38551-62-1; **41**, 34361-69-8; **42**, 56570-86-6; **43**, 29782-96-5; **44**, 42142-32-5; **45**, 16329-22-9; **46**, 28948-03-0; **47**, 16329-19-4; **48**, 16329-20-7; **49**, 14003-71-5; **50**, 18939-02-1.

LITERATURE CITED

(1) Gray, N. A. B. *Prog. Nucl. Magn. Reson. Spectrosc.* **1982**, *15*, 201–248.
(2) Grant, D. M.; Paul, E. G. *J. Am. Chem. Soc.* **1964**, *86*, 2984–2990.
(3) Lindeman, L. P.; Adams, J. Q. *Anal. Chem.* **1971**, *43*, 1245–1252.
(4) Ejchart, A. *Org. Magn. Reson.* **1980**, *13*, 368–371.
(5) Ejchart, A. *Org. Magn. Reson.* **1981**, *15*, 22–24.
(6) Smith, D. H.; Jurs, P. C. *J. Am. Chem. Soc.* **1978**, *100*, 3316–3321.
(7) Small, G. W.; Jurs, P. C. *Anal. Chem.* **1983**, *55*, 1121–1127.
(8) Small, G. W.; Jurs, P. C. *Anal. Chem.* **1983**, *55*, 1128–1134.
(9) Small, G. W.; Jurs, P. C. *Anal. Chem.* **1984**, *56*, 2307–2314.
(10) Egolf, D. S.; Jurs, P. C. In *Chemical Pattern Recognition Methods in Analytical Spectroscopy*; Meuzelaar, H. L. C., Ed.; Plenum: New York, in press.
(11) Christl, M.; Reich, H. J.; Roberts, J. D. *J. Am. Chem. Soc.* **1971**, *93*, 3463–3468.
(12) *Sadtler Standard C-13 NMR Spectra*; Sadtler Research Laboratories: Philadelphia, PA, 1976.
(13) Schneider, H.-J.; Nguyen-Ba, N.; Thomas, F. *Tetrahedron* **1982**, *38*, 2327–2337.
(14) Johnson, L. F.; Jankowski, W. C. *Carbon-13 NMR Spectra*; Wiley-Interscience: New York, 1972.
(15) Ritchie, R. G. S.; Cyr, N.; Korsch, B.; Koch, H. J.; Perlin, A. S. *Can. J. Chem.* **1975**, *53*, 1424–1433.
(16) Brugger, W. E.; Jurs, P. C. *Anal. Chem.* **1975**, *47*, 781–783.
(17) Stuper, A. J.; Jurs, P. C. *J. Chem. Inf. Comput. Sci.* **1976**, *16*, 99–105.
(18) Stuper, A. J.; Brugger, W. E.; Jurs, P. C. *Computer Assisted Studies of Chemical Structure and Biological Function*; Wiley-Interscience: New York, 1979; pp 83–90.
(19) Burkert, U.; Allinger, N. L. *Molecular Mechanics*; ACS Monograph 177; American Chemical Society: Washington, DC, 1982.
(20) Clark, T. *A Handbook of Computational Chemistry: A Practical Guide to Chemical Structure and Energy Calculations*; Wiley: New York, 1985; Chapters 1 and 2.
(21) Fuchs, B. In *Topics in Stereochemistry*; Eliel, E. L., Allinger, N. L., Eds.; Wiley: New York, 1978; Vol. 10, pp 1–94.
(22) Draper, N. R.; Smith, H. *Applied Regression Analysis*, 2nd ed.; Wiley-Interscience: New York, 1981.
(23) Belsley, D. A.; Kuh, E.; Welsch, R. E. *Regression Diagnostics: Identifying Influential Data and Sources of Collinearity*; Wiley-Interscience: New York, 1980.
(24) Allen, D. M. Technical Report No. 23, 1971; Department of Statistics, University of Kentucky, Lexington, KY.
(25) Snee, R. D. *Technometrics* **1977**, *19*, 415–427.
(26) Schneider, H.-J., Universitat des Saarlandes, Saarbrucken, West Germany, personal communication, 1986.

RECEIVED for review December 1, 1986. Accepted March 13, 1987. This work was supported by the National Science Foundation under Grant CHE-8503542. The PRIME 750 computer was purchased with partial financial support of the National Science Foundation. Portions of this paper were presented at the First Symposium on Pattern Recognition Methods in Analytical Spectroscopy, Snowbird, Salt Lake City, UT, June 1986, and at the 38th Annual Meeting, Pittsburgh Conference and Exposition on Analytical Chemistry and Applied Spectroscopy, Atlantic City, NJ, March 1987.

Ion and Temperature Dependence of Electrical Conductance for Natural Waters

John A. Sorensen

Department of Chemistry, University of Minnesota—Duluth, Duluth, Minnesota 55812

Gary E. Glass*

Environmental Research Laboratory—Duluth, U.S. Environmental Protection Agency, 6201 Congdon Boulevard, Duluth, Minnesota 55804

Four empirical equations describing the temperature dependence of electrical conductance of aqueous solutions are compared for the case of single electrolytes. The best method uses a modified Walden product where the log of the ratio between the conductances at two temperatures is assumed to be proportional to the log of the corresponding ratio of viscosities, that is, log $(X_{t_1}/X_{t_2}) = K$ log (η_{t_2}/η_{t_1}). A basis for predicting the constant of proportionality for mixed systems given the ion concentrations is proposed and the dependence of ionic strength effects and ion association is discussed. The value of K may also be estimated from the hydrogen ion concentration (in micromoles per liter) where $K = 0.941 - 0.00639[H^+]$ as found by regression of data for 692 lakes. A case study of time trend data for lakes is presented.

One of the most common of all measurements of water quality is electrical conductance. The usefulness of such a measure has been exploited recently as a powerful tool used for the quality assurance of ion concentration measurements in the USEPA ERL-D water quality acid rain database (*1*) and has been used to evaluate historical data (*2–4*). Since electrical conductance is a strong function of temperature and measurements cannot always be at a standard temperature (usually 25 °C) it is necessary to apply a temperature conversion formula before meaningful comparisons can be made for most applications. The four most common methods for their conversions are all empirical and are evaluated here for accuracy.

The methods or equations considered here for expressing conductance at 25 °C are as follows:

$$X_{25} = X_t(\eta_t/\eta_{25})^{K_1} \quad (1)$$

$$X_{25} = X_t[1 + K_2(25 - t)] \quad (2)$$

$$X_{25} = X_t K_3^{(25-t)} \quad (3)$$

$$X_{25} = \frac{X_t}{1 - K_4(25 - t)} \quad (4)$$

where X_t is the conductance at temperature t in °C, η_t is the viscosity of water at temperature t, and K_i is the appropriate constant for eq i (method i).

Method 1 uses the modified Walden product (*5*) as proposed by Wagner (*6*) where, for any ion, he assumed $\lambda^\circ\eta^{K_1}$ is constant. Here λ° represents the limiting conductance of the ion. Method 2 is commonly recommended by industry (*7*) and elsewhere (*8*), method 3 is a modified version of method 2, and method 4 is recommended by ref 9.

Wagner showed that eq 1 describes environmental samples (mixed electrolytes) very well for a suitable choice of K_1, which varies with sample type. In this work we show that eq 1 is the method of choice for the case of single electrolytes and we also describe a method of predicting the value of K_1 for a given mixed system of up to 11 ions. The dependency of K_1 on ionic strength and ion association is also considered.

RESULTS AND DISCUSSION

Method Comparisons—Single Electrolytes. To test the four methods for accuracy we begin by using KCl limiting conductance vs. temperature data from literature (*5*, *10*, *11*). Considering a practical temperature range from about 0 to 45 °C we first define constants K_i such that eq 1–4 hold true exactly at some temperature sufficiently different from 25 °C. If we choose 10 °C, the resulting values are $K_1 = 0.866$, $K_2 = 0.0263$, $K_3 = 1.0224$, and $K_4 = 0.0188$. Next, for each method in turn, we calculate $(X_{25}/X_t)_M - (X_{25}/X_t)_L$ for several temperatures where $(X_{25}/X_t)_M$ is the conductivity ratio according to the method and $(X_{25}/X_t)_L$ is the ratio according to literature values.

Figure 1 shows a plot of the resulting conductivity ratio differences vs. temperature for each method. Method 1 follows the KCl literature remarkably well as indicated by a near zero difference over the temperature range and is clearly the method of choice here. The ranking from best to worst agreement with literature, for the other 3 methods, is 4, 3, and 2. Although not shown here, we also examined HCl and $CaSO_4$ in the same way and obtained similar results with different constants K_i.

Determination of Constant K for Method 1. Having decided on method 1, we turn to the determination of K (the subscript indicating method number will now be dropped for brevity) for the mixed electrolytes in typical lake water systems. Equation 1 was proposed by Wagner assuming $\lambda^\circ\eta_t^{K^\circ}$ is a constant where λ° is the limiting conductance of the ion at temperature t and K° is the corresponding limiting value of K. Taking the log we may write

$$\ln \lambda^\circ = -K^\circ \ln \eta_t + \text{constant} \quad (5)$$

Plotting ln λ° vs. $-\ln \eta_t$ for η_t's over a range of temperatures will yield K° as the slope. Table I shows the results of calculating the slopes K° for 11 of the most prominent ions found in lake water by using a least-squares regression.

Note that for H^+, Na^+, Ca^{2+}, Mg^{2+}, OH^-, and SO_4^{2-} the regressions were also done without the $t = 0$ °C data as that point appeared slightly aberrant when plotted. Subsequent analyses presented here use the later results since the data in our studies are sufficiently above 0 °C. The r^2 values from the table indicate that Wagner's assumption is valid for these ions.

Ionic Strength Effects—Single Electrolytes. The constants given in Table I and their application to eq 1 are valid only for low ionic strength solutions. To approximate what effect the ionic strength has on temperature conversion we consider a symmetric electrolyte where we may write the

0003-2700/87/0359-1594$01.50/0 © 1987 American Chemical Society

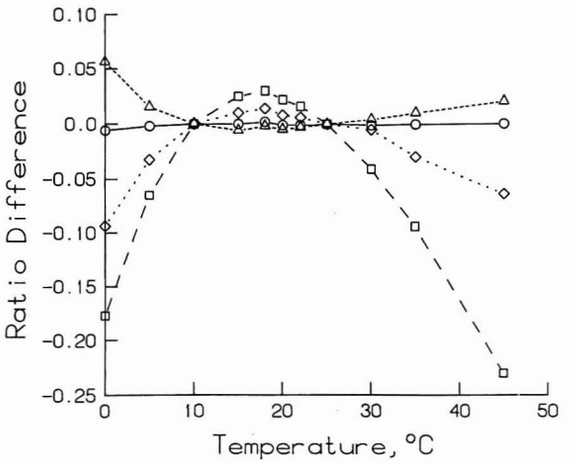

Figure 1. Difference between calculated and literature conductivity ratios for KCl at several temperatures for each method: (O) method 1; (□) method 2; (◇) method 3; (△) method 4. The points are connected by lines for visual clarity.

Table I. Regression Results[a] for ln λ° vs. -ln η

ion	$K°$ ± SD	r^2	temp data used, °C
H^+	0.615 ± 0.007	0.999	0, 5, 15, 18, 25, 35, 45
	0.608 ± 0.007	0.999	5, 15, 18, 25, 35, 45
Na^+	0.938 ± 0.007	1.000	0, 5, 10, 15, 18, 25, 35, 45
	0.950 ± 0.002	1.000	5, 10, 15, 18, 25, 35, 45
K^+	0.850 ± 0.001	1.000	0, 5, 10, 15, 18, 25, 35, 45
NH_4^+	0.869 ± 0.004	1.000	0, 18, 25, 35
Ca^{2+}	0.956 ± 0.015	0.999	0, 10, 15, 18, 25, 35, 45
	0.984 ± 0.009	1.000	10, 15, 18, 25, 35, 45
Mg^{2+}	0.871 ± 0.042	0.999	0, 10, 18, 25
	0.967 ± 0.013	1.000	10, 18, 25
OH^-	0.841 ± 0.042	0.998	0, 15, 18, 25, 35, 45
	0.736 ± 0.002	1.000	15, 18, 25, 35, 45
Cl^-	0.889 ± 0.002	1.000	0, 5, 10, 15, 18, 25, 35, 45
HCO_3^-	0.949 ± 0.002	1.000	0, 15, 35, 38
NO_3^-	0.834 ± 0.002	1.000	0, 18, 25, 35
SO_4^{2-}	0.943 ± 0.007	1.000	0, 10, 15, 18, 25, 35, 45
	0.928 ± 0.002	1.000	10, 15, 18, 25, 35, 45

[a] All values are based on Robinson and Stokes (*5*) except for HCO_3^- data (12), SO_4^{2-} data at 15, 35, 45 °C (13), and all data at 10 °C (14, 15).

equivalent conductance by using the Onsager and Fuoss equation (*16*)

$$\Gamma = \gamma\Lambda°[1 - g(\gamma I)^{1/2}] \tag{6}$$

where γ is the fraction of dissociated ions, $\Lambda°$ is the equivalent conductance at zero ionic strength, I is the ionic strength for total dissociation, and g is given by

$$g = \frac{8.205 \times 10^5 Z^2}{(\epsilon T)^{3/2}} + \frac{82.50Z}{\Lambda°\eta(\epsilon T)^{1/2}} \tag{7}$$

where Z is the absolute value of the charge on each ion, ϵ is the dielectric constant of water, η is the viscosity of water in poise, and T is the absolute temperature. For two temperatures T_1 and T_2 we may write

$$(\eta_1/\eta_2)^K = \Lambda_2/\Lambda_1 \tag{8}$$

or

$$\left(\frac{\eta_1}{\eta_2}\right)^K = \frac{\gamma_2\Lambda_2°[1 - g_2(\gamma_2 I)^{1/2}]}{\gamma_1\Lambda_1°[1 - g_1(\gamma_1 I)^{1/2}]} \tag{9}$$

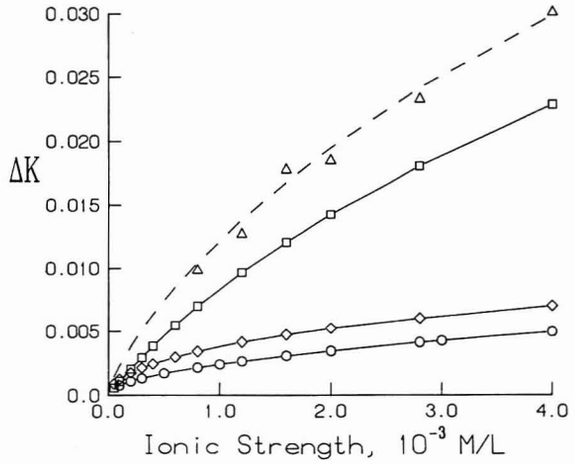

Figure 2. ΔK computed at several ionic strengths (at total dissociation) for both $CaSO_4$ and KCl solutions. Equation 11 calculations: (O) KCl, (□) first term for $CaSO_4$, (◇) second term for $CaSO_4$, (broken line) both terms for $CaSO_4$, (△) based on literature conductance values for $CaSO_4$. The lines connect points of computation for visual clarity.

where the subscripts denote the appropriate temperature. Using the relation $(\eta_1/\eta_2)^{K°} = \Lambda_2^0/\Lambda_1^0$ we get

$$\left(\frac{\eta_1}{\eta_2}\right)^K = \left(\frac{\eta_1}{\eta_2}\right)^{K°} \frac{\gamma_2[1 - g_2(\gamma_2 I)^{1/2}]}{\gamma_1[1 - g_1(\gamma_1 I)^{1/2}]} \tag{10}$$

taking logs and rearranging

$$\Delta K = \frac{\ln\left(\frac{\gamma_1}{\gamma_2}\right)}{\ln\left(\frac{\eta_1}{\eta_2}\right)} + \frac{\ln\left[\frac{(1 - g_1(\gamma_1 I)^{1/2})}{(1 - g_2(\gamma_2 I)^{1/2})}\right]}{\ln\left(\frac{\eta_1}{\eta_2}\right)} \tag{11}$$

where $\Delta K = K° - K$.

Both terms in Eq 11 predict a decrease in K with increasing ionic strength. The first term arises from equilibrium changes while the second term primarily represents the ionic strength effect on conductance. Figure 2 shows the magnitude of these terms calculated for $CaSO_4$ and KCl solutions where temperatures 1 and 2 are 10 and 25 °C, respectively. The two lower curves represent the second term for each electrolyte where the difference between them is due primarily to the Z value. The upper solid curve is the first term for $CaSO_4$ where the values for γ were computed based on a dissociation constant of −2.176 and an enthalpy of 1.46 kcal/mol as determined by Katayama (*13*). The individual points (△) represent ΔK values computed directly from conductivity measurements also from Katayama by the following

$$\Delta K = \frac{\ln\left(\frac{\Lambda_2°}{\Lambda_1°}\frac{\Lambda_1}{\Lambda_2}\right)}{\ln\left(\frac{\eta_1}{\eta_2}\right)} \tag{12}$$

Note that, as expected, the sum of the two terms in eq 11 for $CaSO_4$, shown by the broken curve, approximates the individual points (△).

Mixtures. We assume that the total conductivity for a mixture of the 11 ions at 25 °C can be computed by a simple sum of eq 1 over all the ions. That is,

$$X_{25} = \sum_{i=1}^{11}(X_t)_i\left(\frac{\eta_t}{\eta_{25}}\right)^{K_i} \tag{13}$$

or

$$X_{25} = X_t \sum_{i=1}^{11} f_i \left(\frac{\eta_t}{\eta_{25}}\right)^{K_i} \quad (14)$$

where f_i is the ith ions fractional contribution to the total conductivity at temperature t and K_i is its K value. Expanding $(\eta_t/\eta_{25})^{K_i}$ about $K_i = a$ we get

$$\left(\frac{\eta_t}{\eta_{25}}\right)^{K_i} = \left(\frac{\eta_t}{\eta_{25}}\right)^{a} \left[1 + \ln\left(\frac{\eta_t}{\eta_{25}}\right) \times (K_i - a) + \frac{\left(\ln\left(\frac{\eta_t}{\eta_{25}}\right)\right)^2 (K_i - a)^2}{2} + \ldots \right] \quad (15)$$

If we let $a = 0.61$ (lowest value in Table I), $K_i = 0.98$ (highest value in Table I), and $t = 10$ °C then $\ln(\eta_t/\eta_{25}) = 0.384$ and we get

$$\left(\frac{\eta_t}{\eta_{25}}\right)^{K_i} \approx \left(\frac{\eta_t}{\eta_{25}}\right)^{0.61} [1 + 0.14 + 0.01 + \ldots] \quad (16)$$

To a good approximation we therefore neglect the third and higher order terms. Note that eq 16 represents somewhat of an extreme test for the validity of this approximation for the choices of K_i and a. Performing the sum yields

$$X_{25} \approx X_t \left(\frac{\eta_t}{\eta_{25}}\right)^{a} \left[1 + \ln\left(\frac{\eta_t}{\eta_{25}}\right)(\bar{K} - a) \right] \quad (17)$$

where $\bar{K} = \sum^{11}_{i=1} f_i K_i$, the conductivity weighted average for K. Finally, we note that this result in equivalent to

$$X_{25} \approx X_t (\eta_t/\eta_{25})^{\bar{K}} \quad (18)$$

Equation 18 is the final result for dilute mixed electrolytes. There is no simple way to modify this equation to account for ionic strength effects as was done for the case of single electrolytes by using eq 11. However, a direct calculation of the conductance based on the ion concentrations is possible by using the complex results of Quint and Viallard (*17*). The calculation is valid for any temperature provided the necessary constants at that temperature are known. The most important of these are the viscosity and the limiting conductance for each ion, which may be calculated by rearranging eq 1 and by using Table I. The calculation may also be carried out to terms involving $I^{3/2}$ for applicability to more concentrated solutions. Note that the derivation of eq 11 uses only $I^{1/2}$ terms. An appropriate $\bar{K}$ value for a given nondilute solution for use in eq 18 may be found by directly calculating the conductances at two temperatures and solving for $\bar{K}$ by rearranging eq 18.

Uncertainty Considerations. The resulting percent error in calculating the conductivity ratio X_{25}/X_t by using eq 1 due to an error in estimating K can be found by writing

$$\frac{\Delta F}{F} = \left| 1 - \left(\frac{\eta_t}{\eta_{25}}\right)^{\delta K} \right| \quad (19)$$

where $(\Delta F/F) \times 100$ is the percent error and δK is the error in estimating K. Table II shows the magnitude of such errors for various temperatures t.

Together, Table II and Figure 2 show that neglecting the second term in eq 11 gives rise to an error of less than 0.3 % for typical temperature conversions over the range of concentrations suggested by the figure.

Application to the USEPA ERL-D Water Quality Data Base. The USEPA ERL-D water quality data base (*1*) contains concentration data for all 11 ions along with many other

Table II. The Relationship at Various Temperatures between the Percent Error $[(\Delta F/F) \times 100]$ in Calculating X_{25}/X_t Given the Error δK in Estimating K

	$\Delta F/F \times 100\%$				
δK	0 °C	5 °C	10 °C	15 °C	20 °C
0.001	0.07	0.05	0.04	0.02	0.01
0.005	0.35	0.27	0.19	0.12	0.06
0.010	0.70	0.54	0.38	0.25	0.12
0.050	3.5	2.7	1.9	1.2	0.59
0.100	7.2	5.5	3.9	2.5	1.2
0.300	23.2	17.4	12.2	7.7	3.6

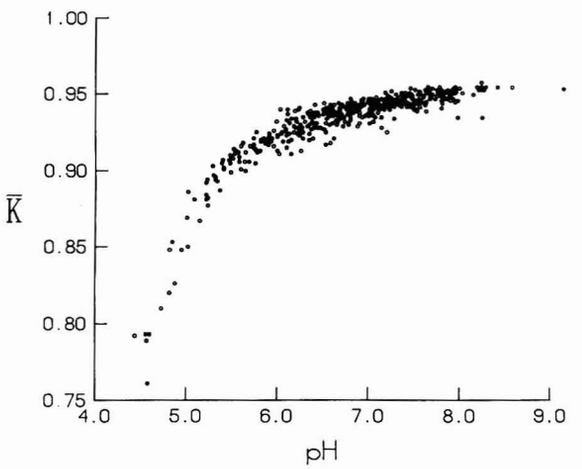

Figure 3. Estimated value of $\bar{K}$ as a function of pH for 692 lakes in Minnesota, Wisconsin, and Michigan.

measurements for 692 lake sites in Minnesota, Wisconsin, and Michigan over a 5-year period. The data base permits us to calculate $\bar{K}$ for each lake by using the results of Quint and Viallard and the discussion above after correcting ion concentrations for sulfate species. It is interesting to note that the average $\bar{K}$ value calculated for the lakes in this study was about 0.936 while Wagner (*6*) reports an experimental value of 0.935 for the lakes in his study. Also, a $\bar{K}$ value of 0.936 corresponds to using a value of 0.0201 in eq 4 (for $t = 10$ °C) while 0.0200 and 0.0191 are recommended for use by ref 9 in the 14th and 15th editions, respectively.

Figure 3 shows a plot of $\bar{K}$ vs. pH for these lakes. At high pH (high alkalinity) we see the expected dominance of HCO_3^-, Ca^{2+}, and Mg^{2+}. Table I shows that each of these ions has a relatively high K value with an average of about 0.97. At lower pH values other ions with lower $\bar{K}$ values become more important, with the extremely low K value for H^+ having an increasing influence.

Due to the complexity of rigourously calculating $\bar{K}$ for any example, we offer the following estimation based on a linear regression of $\bar{K}$ vs. $[H^+]$. The relationship is nearly linear ($r^2 = 0.81$) and may be written overall as

$$\bar{K} = 0.941 - 0.00639[H^+] \quad (20)$$

where $[H^+]$ is expressed in micromoles per liter.

Application to Historical Data Base. During 1926 to 1931 Birge and Juday (*2*) made extensive water quality studies of many lakes in northern Wisconsin. We are presently analyzing this data in relation to modern studies done on the same lakes. A key measurement is conductivity and one of the issues is to verify that the historical values, which are reported at 20 °C, were accurately converted from the actual field measurements.

First we adopt a maximum temperature difference procedure that assumes that the conductivities were originally measured at the reported lake temperatures. Next we convert the reported conductivities (916 values for 242 lakes) to the

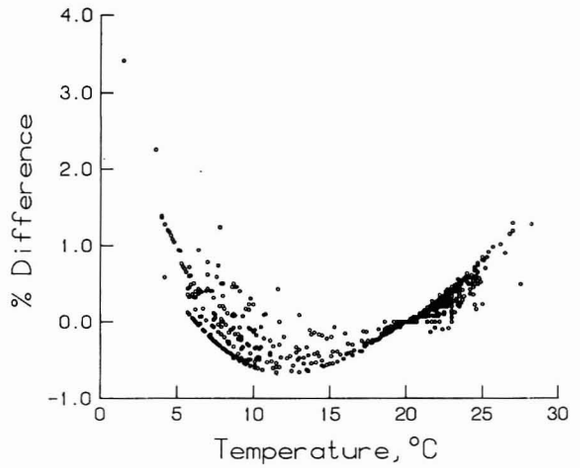

Figure 4. Percent correction as a function of temperature needed for adjusting reported historical conductivity values to account for the temperature conversion method originally used.

lake temperature by rearranging the equation used by Birge and Juday (*18*) (which was essentially method 4), that is

$$X_T = X_{20}(1 - 0.022(20 - t)) \qquad (21)$$

Finally we convert to 20 °C by using the appropriate $\bar{K}$ value for each lake.

Figure 4 shows the percent difference between this result and the originally reported conductivity plotted as a function of lake temperature. The plot illustrates three points: (1) The effect of the variation in $\bar{K}$ values from lake to lake is expressed by the spread in the vertical direction at a given temperature. (2) The general error in the temperature conversion method used by Birge and Juday is shown by the overall shape of the curve, similar to Figure 1. (3) The average absolute percent difference is roughly 0.3% and is within the precision of the original measurements.

A comparison of data from 233 lakes common to both the historical and modern data sets shows an average increase in conductivity of 4.3 ± 5.6 (standard deviation) μS/cm over the 50 year period. This difference has a highly significant T test value of 11.7.

LITERATURE CITED

(1) Glass, G. E.; Sorensen, J. A.; Liukkonen, B. W.; Rapp, G. R., Jr.; Loucks, O. L. *Water, Air, Soil Pollut.* **1986**, *31*, 1–15.
(2) Juday, C.; Birge, E. A. *Acad. Sci. Arts Lett.* **1933**, *28*, 205–259.
(3) Juday, C.; Birge, E. A. *Acad. Sci. Arts Lett.* **1938**, *31*, 223–276.
(4) Eilers, J. M.; Glass, G. E.; Pollack, A. K.; Sorensen, J. A., submitted for publication in *Can. J. Fish. Aquat. Sci.*
(5) Robinson, R. A.; Stokes, R. H. *Electrolyte Solutions*, 2nd ed.; Butterworths: London, 1968; 571 pp.
(6) Wagner, I. W. *Vom Wasser* **1971**, *38*, 27–48.
(7) Dionex Corporation Technical Note No. 9, Sunnyvale, CA, 1981.
(8) *Handbook of Common Methods in Limnology*, 1st ed.; C. V. Mosby: St. Louis, MO, 1974; p 74.
(9) *Standard Methods for the Examination of Water and Wastewater*, 15th ed.; R. R. Donnelly and Sons: Springfield, VA, 1980; p 73.
(10) Li, C. C.; Fang, H. *Anal. Chem.* **1942**, *64*, 1544–1547.
(11) Bremner, R. W.; Thompson, T. G., Utterback, C. L. *Anal. Chem.* **1939**, *61*, 1219–1223.
(12) Shedlovsky, T.; MacInnes, D. A. *Anal. Chem.* **1935**, *57*, 1705–1710.
(13) Katayama, S. *J. Solution Chem.* **1976**, *5*, 241–248.
(14) Broadwater, T. L.; Evans, D. F. *J. Solution Chem.* **1974**, *3*, 757–769.
(15) Kay, R. L.; Evans, D. F. *J. Phys. Chem.* **1966**, *70*, 2325–2335.
(16) Onsager, L.; Fuoss, R. M. *J. Phys. Chem.* **1932**, *36*, 2689–2778.
(17) Quint, J.; Viallard, A. *J. Solution Chem.* **1978**, *7*, 533–548.
(18) Evershed, S. *Digby and Biggs Dionic Water Tester*, 2nd ed.; Evershed and Vignoles Ltd.: London, 1910; 34 pp.

RECEIVED for review December 15, 1986. Accepted March 2, 1987. The research described in this article has been funded in part by the U.S. Environmental Protection Agency through Cooperative Agreement CR809412 to the University of Minnesota—Duluth and was conducted at the U.S. EPA Research Laboratory—Duluth.

Effects of Blood Standards on Interlaboratory Variation in the Assay of Blood Selenium

Tee-Siaw Koh

Central Veterinary Laboratories, Department of Agriculture, IMVS, Frome Road, South Australia 5000, Australia

To determine the effects of using a common set of blood selenium (Se) standards in reducing the interlaboratory coefficient of variation (CV) for the assay of blood Se, 43 laboratories from 12 countries participated in a survey involving the assay of Se in three blood samples (0.2–2.9 μmol of Se/L) using either a set of blood Se standards as supplied or their own aqueous standards. When aqueous standards were used for calibration, the interlaboratory CV's were 82% and 143% at 0.5 and 0.2 μmol of Se/L, respectively. These CV's were reduced to about 29% when the blood standards were used. The study demonstrated the benefit of a common set of standards, preferably those of similar matrix and Se concentrations to the samples, in reducing interlaboratory CV's.

The assay of selenium (Se) in biological specimens including blood is commonly undertaken to determine the Se status of man and animals. In a recent survey (*1*) of the determination of Se in blood, it was found that the interlaboratory coefficient of variation (CV) was unsatisfactory at blood Se concentrations below 0.5 μmol/L and that at about 0.2 μmol/L, the CV was up to 57%. This analytical variation is of concern in the diagnosis of marginal Se deficiency in livestock where the blood Se concentrations of interest are in the range 0.15–0.50 μmol/L (*2*). This gross analytical variability prevented any agreement between laboratories in different countries as to the absolute Se concentration in blood at which Se deficiency occurs. This report concerns an interlaboratory study on the effectiveness of a common set of blood standards in reducing the interlaboratory CV's at these blood Se levels.

EXPERIMENTAL SECTION

Preparation of Blood Samples. Four blood samples from the previous survey (*1*) were used as a common set of blood standards for all laboratories. On the basis of the results reported in the survey, the mean blood Se concentrations (μmol/L) of these four samples, namely, RM1-Se-A, RM1-Se-B, RM1-SeC, and

0003-2700/87/0359-1597$01.50/0 © 1987 American Chemical Society

Table I. Statistical Findings for Blood Se (μmol/L) Assay Using Aqueous and Blood Standards for Calibrations[a]

	no. of labs	Adelaide-4		Adelaide-5		Adelaide-6	
		aqueous	blood	aqueous	blood	aqueous	blood
				Percent of Outliers			
all[b]	44	13.6	6.8	7.0	2.3	11.4	4.5
fluoro[c]	26	15.4	11.5	4.0	4.0	11.5	7.7
hyd gen[d]	12	0.0	0.0	0.0	0.0	8.3	0.0
				Mean			
all	44	0.52 (0.42)	0.46 (0.44)	2.80 (2.81)	2.86 (2.81)	0.25 (0.18)	0.20 (0.19)
fluoro	26	0.53 (0.43)	0.47 (0.43)	2.76 (2.83)	2.91 (2.82)	0.22 (0.18)	0.20 (0.19)
hyd gen	12	0.42 (–)	0.45 (–)	2.77 (–)	2.83 (–)	0.17 (0.16)	0.19 (–)
				Minimum			
all	44	0.18 (0.30)	0.32 (0.33)	1.13 (1.89)	2.23 (2.23)	0.00 (0.06)	0.10 (0.10)
fluoro	26	0.18 (0.33)	0.32 (0.37)	2.07 (2.07)	2.23 (2.23)	0.06 (0.06)	0.10 (0.10)
hyd gen	12	0.30 (–)	0.35 (–)	1.89 (–)	2.48 (–)	0.11 (0.11)	0.13 (–)
				Maximum			
all	44	2.41 (0.53)	1.17 (0.53)	5.07 (3.64)	4.94 (3.37)	2.41 (0.30)	0.42 (0.28)
fluoro	26	2.32 (0.53)	1.17 (0.51)	3.64 (3.64)	4.94 (3.37)	0.73 (0.29)	0.42 (0.28)
hyd gen	12	0.52 (–)	0.52 (–)	3.36 (–)	3.31 (–)	0.30 (0.21)	0.24 (–)
				95% Confidence Interval			
all	44	0.39–0.65 (0.41–0.44)	0.41–0.50 (0.43–0.45)	2.62–2.97 (2.70–2.92)	2.73–2.98 (2.73–2.88)	0.14–0.35 (0.16–0.19)	0.18–0.21 (0.18–0.20)
fluoro	26	0.37–0.69 (0.41–0.45)	0.40–0.53 (0.42–0.44)	2.56–2.96 (2.68–2.98)	2.70–3.11 (2.71–2.93)	0.16–0.27 (0.16–0.20)	0.18–0.23 (0.17–0.21)
hyd gen	12	0.38–0.46 (–)	0.42–0.47 (–)	2.52–3.02 (–)	2.70–2.96 (–)	0.14–0.20 (0.14–0.18)	0.17–0.21 (–)

[a] Figures in brackets have outliers excluded and (–) indicates no outliers in that category. [b] All: All methods including gas chromatography and graphite furnace AAS in addition to fluorometry and hydride generation AAS. [c] fluoro: fluorometry. [d] hyd gen: hydride generation AAS.

RM1-Se-D were 0.24, 0.54, 1.48, and 2.64, respectively. Three additional blood samples designated Adelaide-4, Adelaide-5, and Adelaide-6 were prepared as described previously (*1*) and were treated as unknowns. The Se in the blood samples was metabolically incorporated and was not added in vitro as Se compounds.

Invitation to Participate. Invitations to participate in the survey were sent to 54 laboratories, 40 of these participated in the previous survey (*1*). Each laboratory was sent a sufficient quantity of blood to permit at least triplicate determinations on each sample. Each participant was required to determine the concentration of Se in the three unknown samples based on calibration with aqueous Se standards normally used in his/her laboratory and with the four blood standards supplied. Participants were given 8 weeks to return the two sets of results and the value of regression coefficient for each method of calibration.

Homogeneity Test of Blood Samples. Twenty vials each of the three unknown blood samples were randomly selected for Se assay giving a CV of less than 2% in all cases. The CV's for Se content of the four blood standards were previously found to be less than 2% (*1*).

Statistical Analysis. Grubb's test, coefficient of skewness, and coefficient of kurtosis were concurrently applied to each set of data to detect outliers at 5% level of probability (*3*). Differences in mean Se values between calibration methods were examined by paired Student's *t* test and values between fluorometry and hydride generation methods examined by the two sample Student's *t* test.

RESULTS AND DISCUSSION

Forty-three laboratories from 12 countries returned results with a median turn-around time of about 9 weeks. All results were received within 24 weeks. The 12 countries (and the number of participants) were Australia (5), Belgium (1), Canada (2), China (5), Finland (7), German Democratic Republic (1), Federal Republic of germany (1), New Zealand (6), Norway (1), Spain (1), United kingdom (3), and United States (10). One laboratory reported results based on two analytical methods. The four analytical methods used by (and the percentage of) the participants were fluorometry (60), hydride generation atomic absorption spectrophotometry (AAS) (28), gas chromatography (7), and graphite furnace AAS (5).

Table II. Effects of Aqueous and Blood Standards Calibrations on Mean Blood Se Concentrations (μmol/L) by All Methods, Graphite Furnace AAS, and Gas Chromatography

	Adelaide-4		Adelaide-5		Adelaide-6	
no. of labs	aqueous	blood	aqueous	blood	aqueous	blood
			All Methods[a]			
44	0.52	0.46	2.80	2.86	0.25	0.20
			Graphite Furnace AAS[b]			
2	*0.18*	0.46	*1.66*	2.89	*0.00*	0.12
	0.35	0.33	2.78	2.74	0.18	0.20
			Gas Chromatography[b]			
3	0.39	0.41	2.84	2.70	0.23	0.22
	0.42	0.51	2.95	2.84	0.11	0.22
	2.41	0.53	*5.07*	2.41	*2.41*	0.16

[a] All methods includes fluorometry and hydride generation AAS in addition to graphite furnace AAS and gas chromatography. [b] Data are mean values reported by individual laboratories. Results which are outliers are italicized.

The effects of analytical techniques and use of aqueous or blood standards on the incidence of outlying results, the mean, and ranges of Se values are given in Table I. There was no significant difference between the mean Se values for the three unknown samples obtained by calibration with aqueous or blood standards (paired Student's *t* test, $P > 0.05$) although the percentage of outlying results was lower when using the blood standards. Mean Se values obtained with fluorometry

Table III. Intralaboratory and Interlaboratory Coefficient of Variation (%) of Mean Blood Se Concentrations (μmol/L) by Various Methods Using Aqueous and Blood Standards Calibrations[a]

method	no. of labs	Adelaide-4		Adelaide-5		Adelaide-6	
		aqueous	blood	aqueous	blood	aqueous	blood
				Intralaboratory			
all[b]	44	7.5	8.0	4.3	3.7	11.2	11.9
fluoro[c]	26	7.3	8.6	4.4	3.4	10.4	12.3
hyd gen[d]	12	5.8	6.5	4.4	4.2	12.6	11.4
				Interlaboratory			
all	44	81.9 (11.8)	28.6 (9.8)	20.5 (12.2)	13.9 (8.3)	142.6 (28.5)	28.7 (21.1)
fluoro	26	75.4 (10.1)	34.5 (7.7)	17.5 (12.3)	17.0 (9.2)	60.8 (28.4)	33.9 (24.2)
hyd gen	12	14.5 (–)	9.5 (–)	14.3 (–)	7.3 (–)	30.7 (21.1)	15.1 (–)

[a] Results in parentheses have outliers excluded and (–) indicates no outliers in that category. [b] All methods including fluorometry, hydride generation AAS, graphite furnace AAS, and gas chromatography. [c] fluoro: fluorometry. [d] hyd gen: hydride generation AAS.

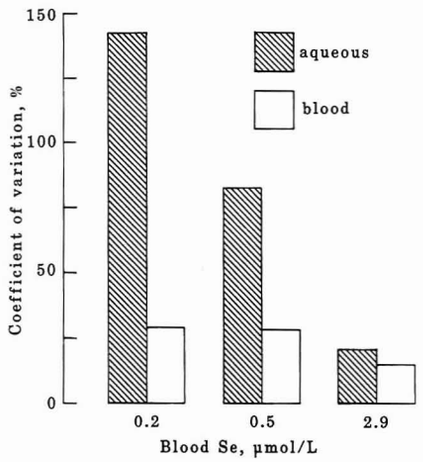

Figure 1. Effect of calibration using aqueous or blood standards on the interlaboratory coefficient of variation for blood selenium determination.

and hydride generation AAS were similar ($P > 0.05$) but the former gave a higher percentage of outlying results than the latter. The data supplied by individual laboratories using graphite furnace AAS and gas chromatography were insufficient for statistical analysis but are given in Table II.

Mean intralaboratory CV is not related to analytical techniques and calibration methods but it is an inverse function of blood Se concentration and is acceptable in all cases with a maximum of about 12% (Table III). In contrast, interlaboratory CV's are unacceptably high at about 82% and 143% at Se concentrations (μmol/L) of 0.5 (Adelaide-4) and 0.2 (Aldelaide-6), respectively, when calibration was based on aqueous standards. These high CV's were markedly reduced when blood standards were used (Table III and Figure 1). The reduction in interlaboratory CV's was noteworthy at Se concentrations of about 0.2 μmol/L (Adelaide-6) where the CV of about 143% was reduced to 29%.

About 60% of the participants reported the implementation of quality control (QC) schemes through either the assay of standard reference materials or regular interlaboratory collaborations. It is reasonable to assume that the participants in this group were likely to have taken appropriate steps to ensure accurate preparation of their aqueous standards. Examination of the effects of calibration methods on interlaboratory CV's between these laboratories revealed similar patterns to those of the overall data, indicating that variation in aqueous standards among laboratories, if any, was unlikely to have contributed to the difference in CV's between the two calibration methods. In addition, participants generally reported satisfactory regression coefficients (r^2) with an overall mean value of 0.999 for the aqueous and the blood standards. Consequently, it is believed that the reduction in interlaboratory CV's with the blood standards was due to the similarity in matrix and in Se concentration between the standards and the unknown samples. The necessity of matching matrix and Se concentration was further demonstrated by the results of one participant who reported the concurrent assay of NBS SRM bovine liver 1577 with the survey samples. With the two calibration methods, the participant obtained a mean value of 13.4 μmol/kg (certified value, 13.9 ± 1.4) for SRM 1577 but two sets of differing Se values for the three unknown blood samples: 2.41 (Adelaide-4), 5.07 (Adelaide-5), and 2.41 (Adelaide-6) with the aqueous standards and 0.53, 2.41, and 0.16 with the blood standards. When subject to outliers exclusion tests, the results which were calibrated against aqueous standards were regarded as outliers whereas those with blood standards were not.

This study demonstrated the benefits of a common set of standards, preferably similar in matrix and elemental concentration to the samples for quality control. This method of calibration is particularly to be recommended at trace-element concentrations where reliable results could not be achieved with the conventional method of calibration.

ACKNOWLEDGMENT

The author thanks the participants for their cooperation and R. Dolby of Invermay Agricultural Research Centre (New Zealand) and H. F. Mayland of USDA-ARS, Idaho, for distribution of the survey samples in their countries.

LITERATURE CITED

(1) Koh, T.-S. *Trace Elem. Anal. Chem. Med. Biol., Proc. Int. Workshop, 3rd* **1984**, *3*, 201–206.
(2) Judson, G. J. *Proc. Post-Grad. C'ttee Vet. Sc. (Australia)* **1984**, *71*, 157–168.
(3) Dybczynski, R.; Tugsavul, A.; Suschny, O. *Analyst (London)* **1978**, *103*, 733–744.

RECEIVED for review July 28, 1986. Accepted March 11, 1987.

Anal. Chem. 1987, 59, 1600–1603

Lithium/Sodium Ion Concentration Ratio Measurements in Blood Serum with Lithium and Sodium Ion Selective Liquid Membrane Electrodes

Erich Metzger, René Dohner, and Wilhelm Simon*

Department of Organic Chemistry, Swiss Federal Institute of Technology (ETH), CH-8092 Zürich, Switzerland

Dieter J. Vonderschmitt and Kurt Gautschi

University Hospital, Zürich, Switzerland

A flow-through electrode system requiring ≤0.1 mL of sample solution has been developed to determine Li^+/Na^+ concentration ratios in aqueous solutions and blood serum by using a cell assembly consisting of a Li^+-selective and a Na^+-selective liquid membrane electrode. Assays in serum samples of manic-depressive patients under lithium treatment were executed and the results were compared with atomic absorption spectrometry/flame photometry measurements.

Very recently the efforts to develop Li^+-selective electrodes for the determination of Li^+ activities in blood serum of patients under a lithium treatment of manic-depressive psychosis have been intensified (for a review see ref 1). Only a few of the proposed ionophores can be utilized in clinically relevant sensors (*1–6*).

The ionophore *N,N*-dicyclohexyl-*N'*,*N'*-diisobutyl-*cis*-cyclohexane-1,2-dicarboxamide (ETH 1810, **1** in Figure 1) exhibits the best Li^+/Na^+ selectivities in clinically relevant sensors found to date (log K^{Pot}_{LiNa} = −2.45 in *o*-NPOE (*o*-nitrophenyl octyl ether)/KT-*p*-ClPB (potassium tetrakis(*p*-chlorophenyl)borate)/PVC (poly(vinyl chloride)) membranes) (*3, 5*). Sensors based on this ionophore allow absolute Li^+ assays in blood serum within the clinical Li^+ concentration range by using a fixed ion background calibration method (*5*). The use of a relatively polar plasticizer of low lipophilicity (*o*-NPOE, **4** in Figure 1) however imposes certain limitations in respect to sensor response time and membrane lifetime (*1, 7, 8*).

Li^+ electrodes based on the ionophore 5-butyl-*N,N,N',N'*-tetracyclohexyl-5-ethyl-3,7-dioxaazelaic acid diamide (ETH 2137, **2** in Figure 1) show a lower Li^+/Na^+ selectivity (log K^{Pot}_{LiNa} = −1.9 in BBPA (bis(1-butylpentyl) adipate)/PVC membranes) but have the advantage of fast electromotive force (emf) response, high electrode potential stability, and improved membrane lifetime due to the use of a more lipophilic plasticizer (BBPA, **5** in Figure 1) (*1*).

The highest Li^+/Na^+ selectivities so far achieved are still considerably away from the value that is required for a contribution of less than 1% by the activity of the interfering ion (Na^+) to the activity of the primary ion (Li^+) (log K^{Pot}_{LiNa} = −4.3 (*9*), see Nikolsky–Eisenman equation (*10*)). The clinical Li^+ concentration range (0.7–1.5 mM (*11–13*)) therefore covers the curved part of the electrode response function of these sensors. With the use of the Li^+ ionophores of the highest known (so far) Li^+/Na^+ selectivity, this range is slightly above the detection limit (*1, 5, 10, 14*) so that Li^+ assays are possible if a fixed ion background calibration is used. Due to the curvature of the electrode response function in the clinical Li^+ concentration range, the emf difference between a Li^+ concentration of 0.7 and 1.5 mM decreases from ideally 19.3 mV (no Na^+ interference) to 13.0 mV and 7.2 mV for ETH 1810/KT-*p*-ClPB/*o*-NPOE/PVC membranes and ETH 2137/BBPA/PVC membranes, respectively. As a consequence, high requirements with respect to the reproducibility of the cell emf have to be met (*1*). This is achieved for both types of membranes; membranes based on ETH 2137 being superior.

Even if a fixed ion background (140 mM Na^+) calibration is used, there remain uncertainties in the emf of the sensor cell assembly of up to about 0.74 mV (ETH 1810) and 1.3 mV (ETH 2137) due to varying sodium levels in blood over the normal physiological range of 135–150 mM (*1, 5*). This results in uncertainties in the Li^+ assay of up to about 5.1% (ETH 1810) and 18.0% (ETH 2137). This problem can be overcome if no longer the absolute Li^+ activity but the Li^+/Na^+ concentration ratio is determined. A cell assembly consisting of a Li^+-selective electrode and a Na^+-selective electrode as a reference (instead of a conventional reference electrode with liquid junction) exhibits an emf which depends on the Li^+/Na^+ concentration ratio. The Li^+/Na^+ concentration ratio seems to be even the more distinctive parameter in clinical lithium therapy because a patient with a low sodium level in blood reaches a dangerous lithium ion concentration at lower lithium levels than someone normal in sodium (*11–13, 15*).

Here we report on Li^+/Na^+ concentration ratio measurements in aqueous solutions and blood serum by using different Li^+ sensors, which are based on our most promising ionophores, and a suitable Na^+-selective solvent polymeric membrane electrode. Blood serum samples of patients under Li^+ treatment were assayed and the results were compared with measurements by atomic absorption spectrometry and flame photometry.

EXPERIMENTAL SECTION

Reagents, Sample Preparation. The aqueous electrolyte solutions for the potentiometric measurements were prepared with doubly quartz distilled water and chloride salts of high purity (purum p.a. or puriss. p.a., Fluka AG, Buchs, Switzerland, and pro analysis, E. Merck, Darmstadt, Germany). The blood serum for the measurement of the electrode response functions (three samples of about 100 mL) was pooled serum from the Medico-Chemical Central Laboratory, University Hospital, Zürich, Switzerland, where sodium, potassium, total calcium, and magnesium ion concentrations were determined by flame photometry (AES) or atomic absorption spectrometry (AAS). The serum was proven to be less than 3×10^{-5} M in Li^+. The serum samples were then prepared for the measurements by multiple addition of small volumes of an aqueous solution being 0.05 M in LiCl and 0.135 M in NaCl to the same serum stock solution. After each addition and a short mixing period, volumes of 0.1 mL were taken for emf measurements. The comperative studies of measurements with ISE's (ion selective electrodes) and with AAS/AES were executed with blood serum samples of patients suffering from manic-depressive psychosis and under lithium treatment. Their Li^+ concentrations were determined by AAS and the Na^+ concen-

0003-2700/87/0359-1600$01.50/0 © 1987 American Chemical Society

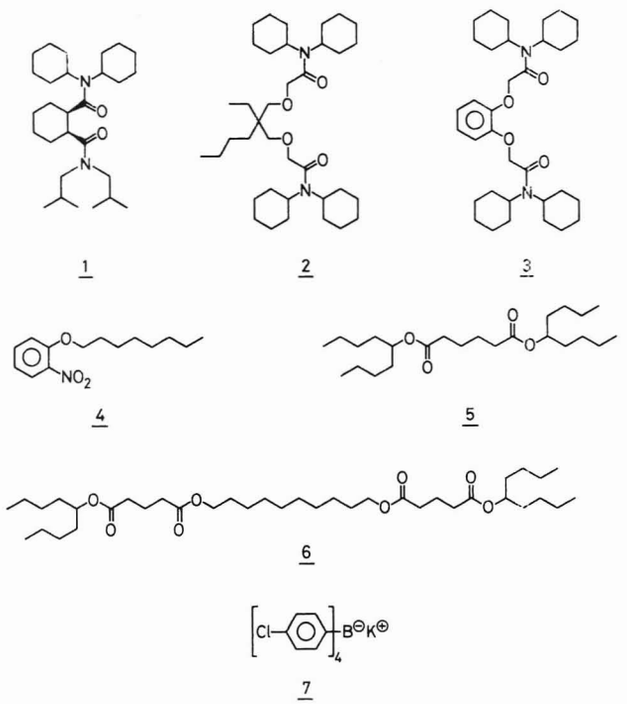

Figure 1. Structures of the Li^+ ionophores (**1** (ETH 1810) and **2** (ETH 2137)), the Na^+ ionophore (**3** (ETH 2120)), the membrane plasticizers (**4** (*o*-NPOE), **5** (BBPA), and **6** (ETH 469)), and the membrane additive (**7** (KT-*p*-ClPB)).

trations by AES. The calibration solutions for the corresponding ISE assays were prepared from serum stock solutions by adding small volumes of LiCl 0.05 M/NaCl 0.135 M.

Poly(vinyl chloride) (PVC S704 hochmolekular) originated from Lonza AG, Visp, Switzerland (now available from Fluka AG); *o*-nitrophenyl octyl ether (*o*-NPOE, puriss. p.a., **4** in Figure 1), bis(1-butylpentyl) adipate (BBPA, purum p.a., **5** in Figure 1), decane-1,10-diyl bis[(1-butylpentyl) glutarate] (ETH 469, **6** in Figure 1), and potassium tetrakis(*p*-chlorophenyl)borate (KT-*p*-ClPB, purum p.a., **7** in Figure 1) were supplied by Fluka AG. The synthesis of the Li^+ ionophores **1** and **2** (Figure 1) is described in refs 5 and 1, respectively. The preparation of the Na^+ ionophore **3** (Figure 1) is given in ref *16*.

Cell Assemblies for the emf Measurements. All emf studies were performed with the cell (see Figure 2)

Ag; AgCl, internal filling solution||
Na^+-selective membrane||sample solution||
Li^+-selective membrane||internal filling solution,
AgCl; Ag (i)

The Li^+-selective [9], the Na^+-selective [6], and a common (platinum wire) [4] poly(methyl methacrylate) electrode module are mounted together with a fourth poly(methyl methacrylate) module [10] (equipped with a Cheminert (LDC/Milton Roy, Riviera Beach, FL) drain tube junction [12, 13]) on an aluminum plate [11]. The actual flow-through electrode system (Figure 2) has a volume of 15 μL (modules [4, 6, 9]). The sample solutions are injected through a platinum net [3] with a glass syringe and fill the vertical sample channel (0.8-mm i.d.) and the tube [13], which is fixed at the end of the channel and is bent upward. The sample is thus contacted simultaneously with the platinum wire of the common electrode [19], the Na^+-selective membrane [18], and the Li^+-selective membrane [17]. The sample volume required is about 0.1 mL. The solution is removed by applying vacuum.

The internal filling solutions of the ISE's are 0.001 M LiCl/0.14 M NaCl in aqueous 0.5% Agar [7] and are in contact with the chlorinated silver wires and the plugs [16] (Lemo S.A., 1110 Morges, Switzerland). Buna-nitrile O-rings [5, 14, 15] are employed for sealing purposes. The whole system is shielded and grounded by an aluminum cylinder [2, 8, 11] and an aluminum cap [1], which is placed during the emf measurements.

Three different Li^+-selective membranes of the following approximate compositions were used: (a) 2.6 wt % carrier ETH 1810 (**1**), 0.4 wt % KT-*p*-ClPB (**7**), 64.7 wt % *o*-NPOE (**4**), 32.3 wt % PVC; (b) 2.6 wt % carrier ETH 1810 (**1**), 0.6 wt % KT-*p*-ClPB (**7**), 64.5 wt % ETH 469 (**6**), 32.3 wt % PVC; (c) 2.0 wt % carrier ETH 2137 (**2**), 65.6 wt % BBPA (**5**), 32.4 wt % PVC. The composition of the Na^+-selective membrane was as follows: (d) 1.0 wt % carrier ETH 2120 (**3**), 66.0 wt % ETH 469 (**6**), 33.0 wt % PVC. The preparation of the membranes and of the flow-through ion selective electrode modules is described in ref *17*. The electrodes were conditioned before use for about 8 h with an aqueous LiCl (0.001 M)/NaCl (0.14 M) solution reinjected several times into the sample channel.

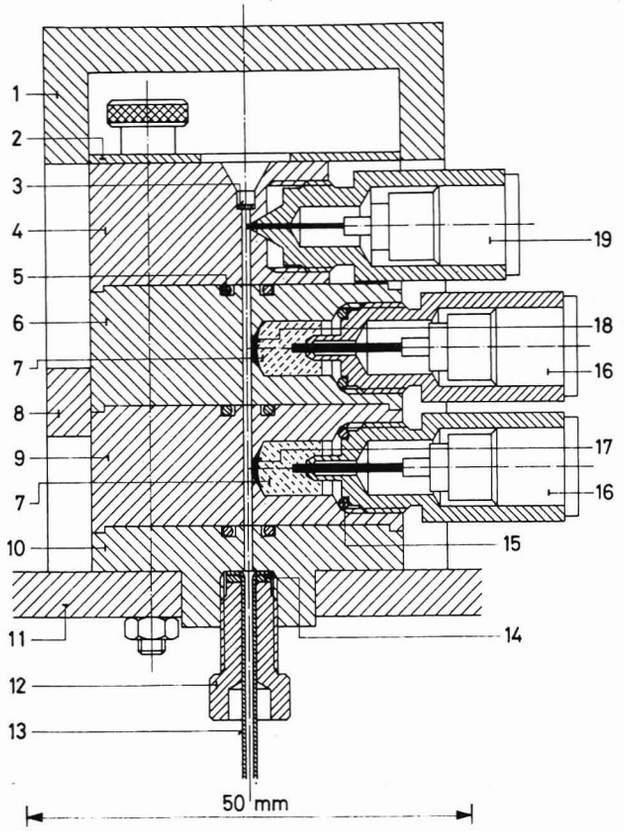

Figure 2. Li^+/Na^+ flow-through electrode system for the concentration ratio measurements (schematic): [1] aluminum cap; [2] aluminum plate; [3] platinum net; [4] common electrode (platinum wire) module; [5] buna-nitrile O-rings; [6] Na^+-selective electrode module; [7] internal filling solutions; [8] aluminum cylinder; [9] Li^+-selective electrode module; [10] fourth module; [11] aluminum plate; [12] drain tube junction; [13] drain tube; [14] buna-nitrile O-ring; [15] buna-nitrile O-rings; [16] chlorinated silver wires, plugs; [17] Li^+-selective membrane; [18] Na^+-selective membrane; [19] common electrode (platinum wire), plug.

emf Measurements. They were performed by using the common mode rejection technique (*17*). The flow-through system was first rinsed with one or two sample injections. The emf for the sample injected afterward was measured during 4 min at 21–23 °C, taking readings in 20-s intervals. The mean of the last six values was taken for further evaluation (see results and discussion).

Determination of Li^+ Concentrations in Serum by AAS. The serum sample was diluted 10-fold with 0.2 M 2-amino-2-methyl-1-propanol/0.01 M ethylenediaminetetraacetic acid, containing 1‰ by volume of a 30% solution of Brij 35, and directly aspirated into the flame. The measurements were carried out on a Varian atomic absorption spectrophotometer, Model AA-875, at 670.8 nm. The enhancement of the signal by Na^+ and K^+ was compensated by employing lithium standards containing these ions in physiological concentrations.

Determination of Na^+ Concentrations in Serum by AES. The Na^+ concentrations were determined by AES in the same way as K^+ in ref 18.

RESULTS AND DISCUSSION

Based on Nicolsky–Eisenman equations (*10*) for the re-

Table I. Parameters Obtained with Three Different Li^+-Selective Membranes in Li^+/Na^+ Concentration Ratio Measurements[a]

	cell response function						reproducibility of cell emf (std dev, mV)	
	log K^{Pot}_{LiNa}		residual std dev, mV		response time,[b] s			
membrane	aqueous	undil serum	aqueous	undil serum	aqueous	undil serum	aqueous	undil serum
a	−2.2	−2.2	0.3	0.6	~100	~100	0.2	0.2
b	−1.8	−1.7	0.06	0.2	15–20	20–25	0.05	0.07
c	−1.9	−1.9	0.1	0.06	30	15–20	0.03	0.03

[a] The Na^+-selective membrane d was used. [b] The time to reach the final emf to within a value being equivalent to a 5-fold subdivision of the clinical range with a 95% confidence limit (*19*) (0.5, 0.3, and 0.4 mV for membranes a, b, and c, respectively). The concentration changes covered the clinical range.

Table II. Li^+/Na^+ Concentration Ratio Determinations in Human Blood Serum by ISE's (Membranes c/d) and AAS/AES[a]

sample	c_{Li}/c_{Na} by cell (i) × 10^3	error calcd for uncertainty in emf of 0.1 mV, %	c_{Li} by AAS, mM (std dev, 0.03 mM)	c_{Na} by AES, mM (std dev, 3 mM)	c_{Li}/c_{Na} by AAS/AES × 10^3	rel accuracy, % (ISE vs. AAS/AES)
1	4.19 (0.4)[e]	1.7	0.64	144	4.44 (5.1)[c]	−5.7
2	3.25 (0.4)	2.1	0.52	147	3.54 (6.1)	−8.2
3	5.48 (0.3)	1.4	0.81	143	5.66 (4.3)	−3.3
4	2.64 (3.5)	2.5	0.41	142	2.89 (7.6)	−8.5
5	4.64 (0.1)	1.6	0.59	135	4.37 (5.6)	6.1
6	4.63 (0.6)	1.6	0.67	145	4.62 (4.9)	0.2
7	1.83 (0.0)	3.4	0.24	143	1.68 (12.7)	8.9
8	4.51 (0.7)	1.6	0.68	144	4.72 (4.9)	−4.5
9	1.99 (4.7)	3.1	0.31	144	2.15 (9.9)	−7.7
10	4.46 (0.2)	1.6	0.56	130	4.31 (5.8)	3.5
11	negative (−)		<0.03	146	$<2 \times 10^{-4}$	
12	5.17 (0.2)	1.5	0.71	140	5.07 (4.7)	2.0
13	3.69 (0.4)	1.9	0.57	147	3.88 (5.6)	−4.8
14	11.62 (0.7)	0.9	1.59	146	10.89 (2.8)	6.7
15	4.30 (1.7)	1.7	0.62	145	4.28 (5.3)	0.5
16	6.32 (0.7)	1.3	0.95	139	6.83 (3.8)	−7.6
17	1.71 (3.3)	3.6	0.26	141	1.84 (11.7)	−7.1
18	4.05 (0.9)	1.7	0.55	139	3.96 (5.9)	2.3
19	4.54 (1.0)	1.6	0.65	146	4.45 (5.1)	1.9
20	2.54 (0.9)	2.5	0.34	135	2.52 (9.1)	0.9
21	5.38 (0.0)	1.4	0.81	142	5.70 (4.3)	−5.6
22	9.78 (0.4)	1.0	1.38	143.7	9.60 (3.0)	1.8
23	8.97 (0.2)	1.0	1.27	142.5	8.91 (3.2)	0.6
24	8.00 (0.1)	1.1	1.157	141.3	8.19 (3.4)	−2.3

[a] Calibration of the electrodes with pooled blood serum spiked with 0.05 M LiCl/0.135 M NaCl. Residual standard deviation of the calibration function: 0.03 mV ($N = 5$). [b] Mean of two measurements with relative standard deviation in percent given in parentheses. [c] Errors in the AAS/AES concentration ratio measurement calculated from the uncertainties of ±0.03 mM (AAS) and ±3 mM (AES) in percent given in parentheses.

sponse of the Li^+-selective and the Na^+-selective half cells, respectively, we obtain for the emf of cell assembly i:

$$\text{emf [mV]} = E_0 + s \log \left(\frac{a_{Li}}{a_{Na}} + K^{Pot}_{LiNa} \right) \qquad \text{(ii)}$$

where $s = 2.303\,RT/F = 59.16$ mV (25 °C), K^{Pot}_{LiNa} is a selectivity factor for the Li^+-selective electrode (preference of Na^+ over Li^+ by the Li^+-selective membrane), a_{Li} and a_{Na} are activities of Li^+ and Na^+ in the sample solution, and E_0 is a constant emf difference (temperature dependent). To derive eq ii the following assumptions are made: (1) the Li^+- and Na^+-selective half cells exhibit theoretical Nerstian response in pure Li^+ and Na^+ salt solutions. (2) The Na^+-selective electrode shows no interference by other ions. (3) The Li^+-selective electrode exhibits interference only by Na^+ ions, specified by K^{Pot}_{LiNa}. Assuming further equal single ion activity coefficients for Li^+ and Na^+, the emf of cell i can be described by

$$\text{emf [mV]} = E_0 + s \log \left(\frac{c_{Li}}{c_{Na}} + K^{Pot}_{LiNa} \right) \qquad \text{(iii)}$$

with c_{Li} and c_{Na} being the concentrations of Li^+ and Na^+ in the sample solution.

Measurements of Li^+/Na^+ concentration ratios have been performed with the three Li^+-selective membranes a, b, and c and the Na^+-selective membrane d (see Experimental Section, flow-through electrodes in Figure 2). The nonlinear response in aqueous solutions and blood serum strictly corresponds to eq iii; the curvature is given by K^{Pot}_{LiNa}. Relevant parameters are summarized in Table I. As expected, the selectivity of membrane c is lower than that of membrane a. It, however, is superior in respect to response time and reproducibility of the cell emf and was therefore preferred for further studies. Figure 3 shows a typical response of cell assembly i with membranes c/d to the Li^+/Na^+ concentration ratio in undiluted blood serum. The response curve matches eq iii with a residual standard deviation of 0.06 mV. The curvature corresponds to log $K^{Pot}_{LiNa} = -1.9$ (see Table I). The reproducibility of a single emf value is better than 0.1 mV (standard deviation). Therefore Li^+/Na^+ concentration ratios can be determined down to Li^+ concentrations of 0.2 mM in blood serum if an adequate calibration is made. An uncertainty of 0.1 mV in the emf at this Li^+ level leads to an error in the ratio measurement of about 4%. At a Li^+ level of 1

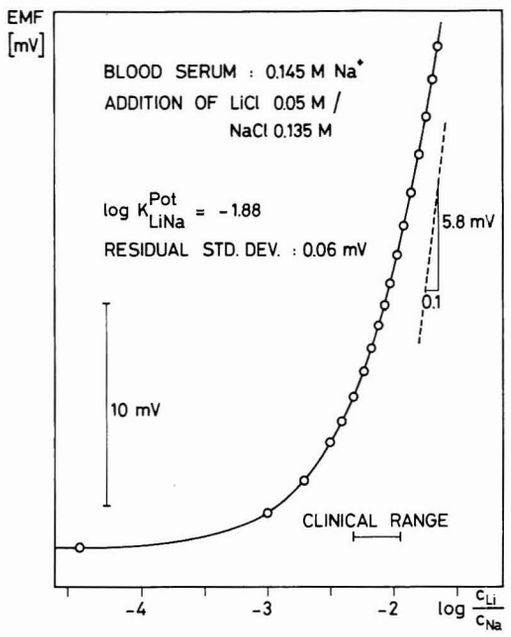

Figure 3. emf response function of the Li^+/Na^+ concentration ratio flow-through cell assembly (membrane c and d) for blood serum. Residual standard deviation was 0.06 mV.

mM this error is about 1.2%.

Table II summarizes results obtained with membranes c/d in the concentration ratio assays on serum samples of patients under lithium treatment. The comparison with AAS/AES measurements (clinical routine analysis) shows a mean deviation of 4.4%. The main contribution seems to be the uncertainty in the AAS/AES determination observed in routine analysis at the university hospital (see Table II).

The procedure of determining concentration ratios potentiometrically described here shows a surprisingly high accuracy and precision, which is probably mainly due to the absence of reference electrodes with liquid junctions. The ratio procedure eliminates problems related to the controversy between direct (undiluted blood, plasma, or serum sample) and indirect (diluted sample) measurements, which is partly linked to effects ascribable to the presence of remarkable amounts of proteins and lipids in blood (*20*). When normal blood or serum samples are spiked with known concentrations of Li^+, very reliable assays of Na^+, K^+, and other ions are also at hand.

LITERATURE CITED

(1) Metzger, E.; Aeschimann, R.; Egli, M.; Suter, G.; Dohner, R.; Ammann, D.; Dobler, M.; Simon, W. *Helv. Chim. Acta* **1986**, *69*, 1821.
(2) Kimura, K.; Kitazawa, S.; Shono, T. *Chem. Lett.* **1984**, 639.
(3) Metzger, E.; Ammann, D.; Schefer, U.; Pretsch, E.; Simon, W. *Chimia* **1984**, *38*, 440.
(4) Kitazawa, S.; Kimura, K.; Yano, H.; Shono, T. *Analyst (London)* **1985**, *110*, 295.
(5) Metzger, E.; Ammann, D.; Asper, R.; Simon, W. *Anal. Chem.* **1986**, *58*, 132.
(6) Xie, R. Y.; Christian, G. D. *Anal. Chem.* **1986**, *58*, 1806.
(7) Oesch, U.; Anker, P.; Ammann, D.; Simon, W. In *Ion-Selective Electrodes*; Pungor, E., Buzâs, I., Eds.; Akadémiai Kiadó: Budapest, 1985; Vol. 4, pp 81–101.
(8) Gadzekpo, V. P. Y.; Hungerford, J. M.; Kadry, A. M.; Ibrahim, Y. A.; Xie, R. Y.; Christian, G. D. *Anal. Chem.* **1986**, *58*, 1948.
(9) Oesch, U.; Ammann, D.; Schefer, U.; Metzger, E.; Simon, W. Proceedings of the International Symposium on Ion-Selective Electrodes, June 10–14, 1985, Shanghai, People's Republic of China, in press.
(10) Guilbault, G. G.; Durst, R. A.; Frant, M. S.; Freiser, H.; Hansen, E. H.; Light, T. S.; Pungor, E.; Rechnitz, G.; Rice, N. M.; Rohm, T. J.; Simon, W.; Thomas, J. D. R. *Pure Appl. Chem.* **1976**, *48*, 127.
(11) Amdisen, A. *DMB Dan. Med. Bull.* **1975**, *22*, 277.
(12) Amdisen, A.; Schou, M. *Münch. Med. Wochenschr.* **1975**, *117*, 1417.
(13) Samuel, D.; Gottesfeld, Z. *Endeavour* **1973**, *32*, 122.
(14) Morf, W. E. *The Principles of Ion-Selective Electrodes and of Membrane Transport*; Akadémiai Kiadó: Budapest (and Elsevier: Amsterdam and New York), 1981.
(15) Johnson, F. N. in *The Psychopharmacology of Lithium*; Macmillan: London, 1984; p 5.
(16) Maruizumi, T.; Wegmann, D.; Suter, G.; Ammann, D.; Simon, W. *Mikrochim. Acta*, in press.
(17) Osswald, H. F.; Dohner, R. E.; Meier, T.; Meier, P. C.; Simon, W. *Chimia* **1977**, *31*, 50.
(18) Osswald, H. F.; Asper, R.; Dimai, W.; Simon, W. *Clin. Chem.* (*Winston-Salem*, N.C.) **1979**, *25*, 39.
(19) Ammann, D.; Anker, P.; Metzger, E.; Oesch, U.; Simon, W. In *Ion Measurements in Physiology and Medicine*; Kessler, M., Höper, J., Harrison, D. K., Eds.; Springer-Verlag: Berlin, Heidelberg, New York, and Tokyo, 1985; pp 102–110.
(20) Oesch, U.; Ammann, D.; Simon, W. *Clin. Chem.* (*Winston-Salem, N.C.*) **1986**, *32*, 1448.

RECEIVED for review January 8, 1987. Accepted March 12, 1987. This work was partly supported by E. I. du Pont de Nemours & Co., Inc., and by Ciba Corning Diagnostics Corp.

Selectivity Properties of Sodium Glass Membrane Electrodes under Non-Steady-State Conditions

Julie Wangsa and Mark A. Arnold*

Department of Chemistry, University of Iowa, Iowa City, Iowa 52242

Sodium-selective glass membrane electrodes display poor selectivity properties when operated under non-steady-state conditions. This poor selectivity is caused by long-lived transitory potential excursions exhibited by glass membranes in response to activity steps of interfering cations. Relative errors caused by potassium are commonly as large as 800%. Other examined cations, which include lithium, ammonium, magnesium, calcium, strontium, and barium, also generate considerable electrode inaccuracies. Experimental parameters of interfering ion to primary ion concentration ratio, glass hydrated layer thickness, pH, ionic strength, and solution flow rate have been examined with respect to their individual effects of the non-steady-state selectivity of glass electrodes. Results indicate that, even under optimal experimental conditions, "effective" selectivity coefficients are required for accurate detection with glass electrode detectors in automated systems.

Ion-selective membrane electrodes are commonly used as detectors in both segmented and nonsegmented automated systems. The convenience of using membrane electrodes as detectors comes from their rapid response, low cost, simple instrumentation requirements, nondestructive nature, and high selectivity. An example is the sodium-selective glass membrane electrode, which has been widely employed as a detector in automated analyzers for clinical, nutritional, industrial, and agricultural situations (*1–3*).

As reported by several researchers, glass (*4–7*), solid-state (*8, 9*), and polymer (*10, 11*) membrane electrodes can display time-dependent selectivities in response to sudden ion activity steps. The potential–time curve shown in Figure 1 is a typical response of a sodium glass electrode to a potassium ion activity step (*12*). Initially, the electrode is equilibrated with a pH 7.5, 0.1 M Tris–HCl buffer that contains 1 mM sodium chloride (position A). At position B, the potassium ion activity is rapidly stepped from 0 to 50 mM with no change in either the hydrogen or sodium ion activities. This potassium ion activity step causes a large potential excursion where the potential initially changes in a positive direction before reaching a maximum and then slowly decaying to a steady-state value. When the potassium ion activity is stepped back from 50 to 0 mM (position C), a second transitory potential excursion of similar magnitude and duration is observed, but this latter excursion is in the opposite direction. Similar transitory responses have been reported for the other classes of membrane electrodes, but the duration of the transient decay is typically much faster than for glass membrane electrodes. Overall, these time-dependent responses can be interpreted as time-dependent selectivities, where the electrode initially displays little or no selectivity for the interfering ion and the selectivity is restored to an expected equilibrium value after some time.

As suggested by Pungor and co-workers (*8, 9*), time-dependent selectivities can complicate the response of membrane electrode detectors in flow systems where the electrode potential is measured under non-steady-state conditions. Of primary importance is the extent to which this time-dependent selectivity phenomenon contributes to the inaccuracy of such detectors. The purpose of our investigation has been to determine the effect of the time-dependent selectivity on the inaccuracy of the sodium selective glass membrane electrode under non-steady-state conditions. Several experimental parameters have been examined to establish their significance with respect to electrode inaccuracy.

EXPERIMENTAL SECTION

Apparatus and Materials. The electrochemical cell was composed of a flow-through, tubular glass membrane electrode in combination with a single junction silver/silver chloride reference electrode. The glass electrode was prepared by using sodium-selective glass (Corning NA 0152), which was purchased from Microelectrodes, Inc., Londonberry, NH. The reference electrode (Model 9001) was purchased from Orion Research, Inc., Cambridge, MA. Electrode potentials were monitored with a Fisher Accumet pH/mV potentiometer (Model 620) in combination with a Sargent-Welch strip chart recorder (Model XKR). A Fisher temperature bath (Model 80) was used with glass-jacketed cells to maintain solution temperatures.

All solutions were prepared with distilled-deionized water from a Milli-Q three-house water purification unit. All salts were of analytical grade purity and were appropriately dried before use.

Procedures. A schematic representation of the experimental arrangement is shown in Figure 2. Flow-through glass electrodes were constructed by placing a short length (approximately 1 cm) of the sodium-selective glass tubing through a plastic test tube (see insert in Figure 2). This glass tubing was held in place with epoxy. An internal solution composed of 0.1 M sodium chloride and an internal silver/silver chloride reference electrode were added to complete the electrode assembly. After passing through the sodium electrode, the solution of interest flowed through a short length (approximately 5 cm) of poly(vinyl chloride) (PVC) tubing into a large reservoir of 0.1 M Tris–HCl, pH 7.5 buffer. The single junction silver/silver chloride reference electrode was also immersed in this same reservoir of buffer to complete the elctrochemical cell. A Faraday cage was positioned around the entire electrochemical cell to reduce noise. Potentials were obtained either by following the potentiometer directly or by extrapolating from the strip chart recording.

The flow arrangement included a Technicon AutoAnalyzer II autosampler and proportioning pump. Solutions flowed through small diameter Teflon tubing (0.5 mm i.d.; 1.8 mm o.d.) with a short strand of microporous Teflon tubing (Gore & Associates, Elkton, MD) positioned just before the electrode to remove air bubbles (*12, 13*). Unless otherwise noted, the system flow rate was 1.26 mL/min.

Data were collected in either a steady-state or non-steady-state mode. In the steady-state mode, the autosampler was not used and the solution of interest was continually pumped through the electrode until a steady-state potential was attained. In the non-steady-state mode, the solution of interest was sampled for a set time interval followed by the wash buffer. A 15-s sampling time, which corresponds to 315 μL of sample, was employed with a 105-s wash period between samples. Unless otherwise indicated, the background or wash buffer was composed of 0.1 M Tris–HCl at pH 7.5.

RESULTS AND DISCUSSION

The effect of steady-state vs. non-steady-state measurements with the sodium glass electrode in the presence of potassium is seen by comparing the response curves presented in Figures 3 and 4. These figures show the steady-state

0003-2700/87/0359-1604$01.50/0 © 1987 American Chemical Society

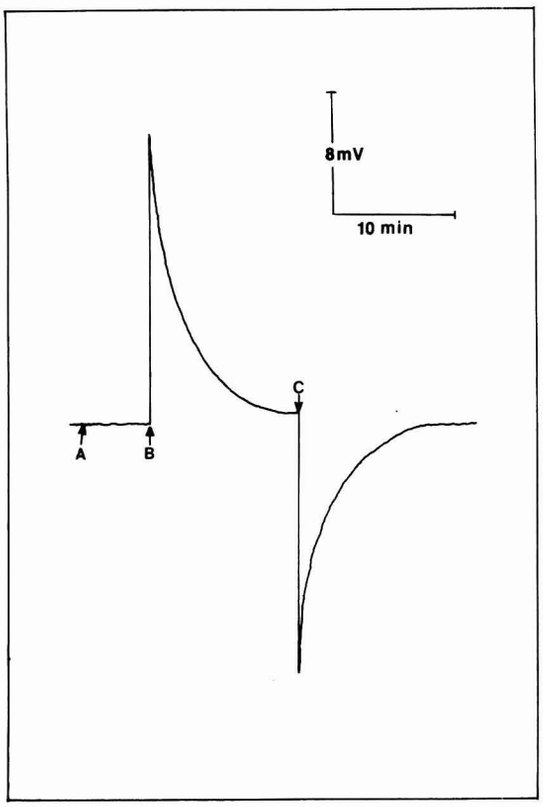

Figure 1. Transitory response to potassium ion activity steps by a sodium selective glass membrane electrode: (A) 0.1 M Tris–HCl + 1 mM sodium chloride, pH 7.5; (B) potassium activity step from 0 to 50 mM with no change in sodium or hydrogen activities; (C) potassium activity step back from 50 to 0 mM.

(Figure 3) and non-steady-state (Figure 4) response of the glass electrode with and without 0.1 mM potassium present. As expected, the electrode response is only slightly affected by the presence of potassium in the steady-state mode. This small effect is expected because of the well-documented selectivity of this membrane composition for sodium over potassium (*4*, *14*). In contrast, the presence of potassium dramatically alters the electrode response at low sodium concentrations in the non-steady-state mode. Large deviations in the response curves are obtained in the presence of potassium. These deviations are caused by the time-dependent selectivity of the glass membrane and represent significant inaccuracies in the electrode response.

Electrode inaccuracy can be expressed as the relative error caused by potassium. This relative error is calculated by comparing the recorded potential for a sodium standard in the presence of potassium with a standard curve prepared with potassium-free sodium standards. For the results presented in Figures 3 and 4, the relative error caused by 0.1 mM potassium with 0.1 mM sodium in the non-steady-state mode is 800%; whereas the relative error in the steady-state measurement under the same conditions is only 28.8%.

Figure 5 illustrates how the transient response causes the observed errors in the non-steady-state mode. This figure shows the individual steady-state and non-steady-state potentiometric responses to sodium alone and the transitory response to a sample with both sodium and potassium. The effect of the transitory response to potassium on the sodium measurement in the steady-state mode is minimal because the potential decays to an equilibrium value and the potential before equilibrium is of no concern. The response to sodium in the non-steady-state mode, however, does not reach an equilibrium value and the magnitude of the transitory response to potassium can be significant. Figure 5A represents the situation where the potassium activity is relatively high

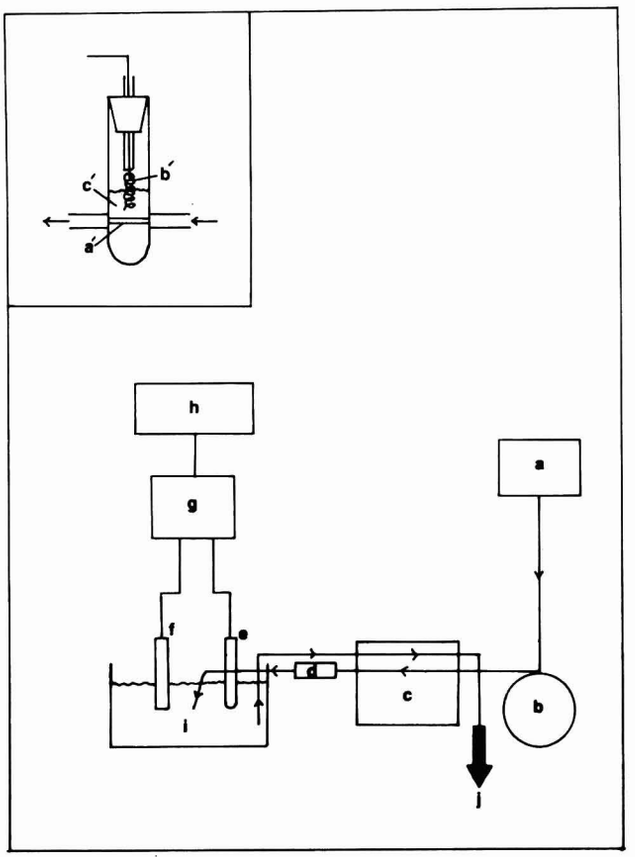

Figure 2. Schematic of experimental arrangement: (a) reservoir of wash buffer; (b) autosampler with test solutions; (c) proportioning pump; (d) microporous Teflon tubing; (e) flow-through glass electrode; (f) reference electrode; (g) potentiometer; (h) strip chart recorder; (i) reservoir of wash buffer; (j) waste. The insert is a close-up of a flow-through glass electrode: (a′) sodium selective glass tubing; (b′) internal silver/silver chloride electrode; (c′) 0.1 M sodium chloride internal reference solution.

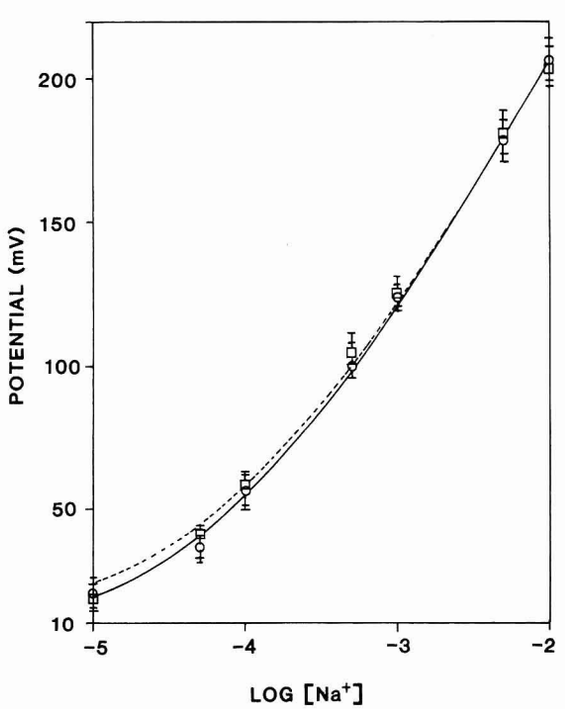

Figure 3. Sodium response curves in the steady-state mode without (–□–) and with (--O--) 0.1 mM potassium present. Error bars represent ±1 standard deviation about the mean of at least three measurements.

in comparison to the sodium activity. Under these conditions, the component of the electrode response due to potassium (the

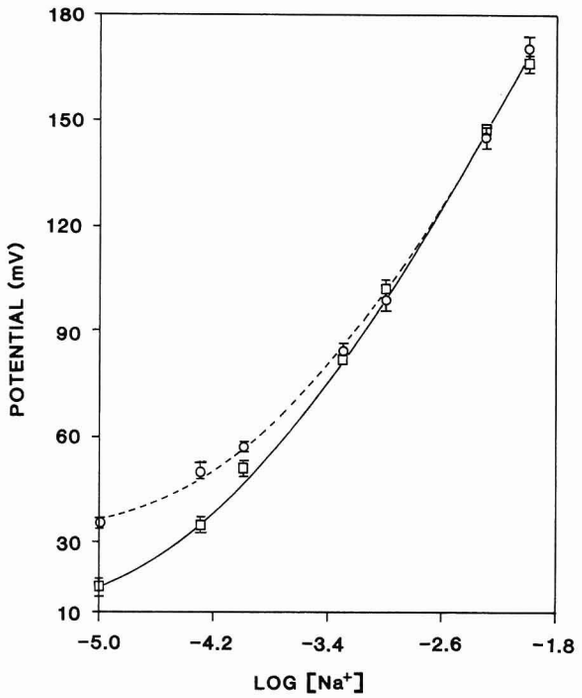

Figure 4. Sodium response curves in the non-steady-state mode without (–□–) and with (--O--) 0.1 mM potassium present. Error bars represent ±1 standard deviation about the mean of at least three measurements.

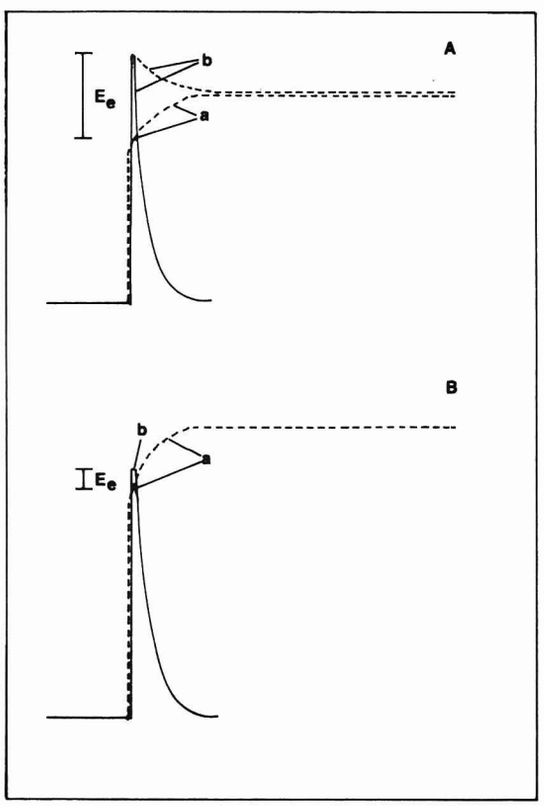

Figure 5. Potential–time traces for electrode responses in steady-state (- - -) and non-steady-state (——) modes without (a) and with (b) potassium present. Conditions established for small (A) and large (B) responses to sodium with respect to the magnitude of the transitory response to potassium. E_e represents the measured potential error.

transitory response) is large with respect to the response to sodium alone. The error in the measurement is the value E_e. On the other hand, larger signals are attained for higher sodium activities and the magnitude of the transitory response is less significant, which results in smaller errors (see Figure 5B).

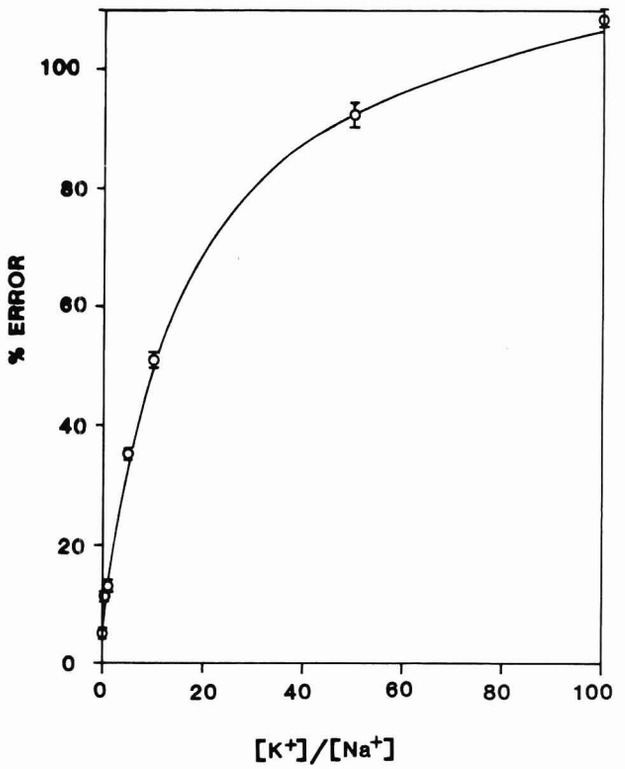

Figure 6. Dependency of relative error on potassium-to-sodium activity ratio. Error bars represent ±1 standard deviation about the mean of at least three measurements.

The above discussion implies that the degree of inaccuracy is affected by the ratio of interfering to primary cation activities. Greater relative amounts of the primary ion generate large signals, which render the transitory peak height less significant. Figure 6 shows the results of a study in which the relative error is measured as a function of potassium-to-sodium activity ratio. In this experiment, the sodium ion activity has been maintained at 0.1 mM while the potassium level is varied from 0.01 to 10 mM. These results indicate that the relative error, or inaccuracy, increases with an increase in the potassium-to-sodium ratio. A maximum error is obtained as this activity ratio increases.

For optimal selectivity it is important to minimize electrode inaccuracies by minimizing electrode transitory responses to interfering cations. An attempt to identify experimental parameters that significantly affect the magnitude of the transient response has been made.

The first parameter of interest is the thickness of the glass hydrated layer. The hydrated layer thickness has been identified as a major component in the transient response (*12*). The effect of hydrated layer thickness has been studied by measuring transitory responses at different thicknesses. Hydrated layer thicknesses have been varied by exposing the electrode surface to a solution of 1 mM ammonium bifluoride for specific time intervals. Longer time intervals result in more etching and thinner hydrated layers. Table I summarizes the transient response data from this experiment. Thinner hydrated layers result in smaller transient peak heights, which should translate to smaller relative errors and greater selectivity. No transient response is observed with the complete removal of the hydrated layer (*15*, *16*).

Another factor related to thinner hydrated layers that helps to reduce the inaccuracy of the glass electrode is the enhanced dynamic response to the primary ion. Thinner hydrated layers respond faster to sodium alone, which leads to larger potential changes during a specific sample/electrode residence time. Overall, thinner hydrated layers result in less transient response to interfering ions and greater response to the primary

Table I. Magnitude of Potential Excursion as a Function of Glass Hydrated Layer Thickness[a]

exposure time,[b] min	magnitude of potential excursion, mV: potassium stepped from 0 to 0.1 mM	potassium stepped from 0.1 to 0 mM
0	31.0	−23.2
0.5	26.8	−19.8
1.0	25.0	−20.0
2.0	24.3	−17.6
4.0	25.0	−17.7
8.0	20.2	−15.7

[a] Hydrated layer thickness decreases with increasing exposure time. [b] Exposure of glass membrane to 1 mM ammonium bifluoride.

ion. The overall effect is an enhancement in the non-steady-state selectivity.

No transitory response to interfering ions and maximum response to the primary ion are obtained when the glass hydrated layer is completely removed by prolonged etching. Although maximal non-steady-state selectivity is anticipated under these conditions, use of such a glass membrane electrode for analytical purposes is not practical because immediately after the hydrated layer is removed, it begins to re-form.

Because the hydrated layer thickness alters the non-steady-state selectivity, it is important that a constant thickness is used during subsequent characterization studies. To control the hydrated layer thickness, electrodes have been treated with 1 mM ammonium bifluoride for 5 min at the beginning of each day. This etching treatment establishes a reproducible thickness at the beginning of each experiment. The rate of hydration is slow enough that consistent electrode responses can be obtained for at least 8 h after this pretreatment. Without the etching treatment, considerable variation in the non-steady-state response is observed from day to day. Throughout these studies, electrodes have been stored between experiments in the 0.1 M Tris–HCl, pH 7.5, buffer at room temperature.

Figure 7 shows the effect of pH on the relative errors measured in the non-steady-state mode. In this experiment, a Tris–citric acid buffer system has been employed to cover the pH range from 5.0 to 9.5. Potassium-free sodium standards have been used to construct sodium calibration curves at each pH. The response to a 0.01 mM sodium solution has been compared to that for a solution with 0.01 mM sodium and 0.1 mM potassium. A decrease in pH results in an increase in the relative error or an increase in the electrode inaccuracy. This effect of pH is explained by considering that the sodium-selective glass membrane electrode responds to hydrogen ions. As the pH increases, the effective detection limit for sodium is enhanced, and larger potential responses for sodium in the non-steady-state mode are observed. The magnitude of the transient response is not pH dependent, however. Hence, at higher pH values, transitory responses to potassium are less significant with respect to the larger signals for sodium, and smaller errors are obtained (see Figure 5).

The effect of ionic strength on the magnitude of electrode inaccuracy has been examined by measuring the relative error caused by buffer solutions with ionic strengths that ranged from 0.04 to 0.16 M. Ionic strengths have been adjusted by using various concentrations of Tris in the buffer. Unfortunately, it is not possible to alter the ionic strength without also changing the cation concentration in the solution. In this experiment, the $Tris^+$ concentration increased with ionic strength. Results show that an increase in ionic strength, with the corresponding increase in $Tris^+$ concentration, gives an increase in the relative error. The magnitude of this ionic

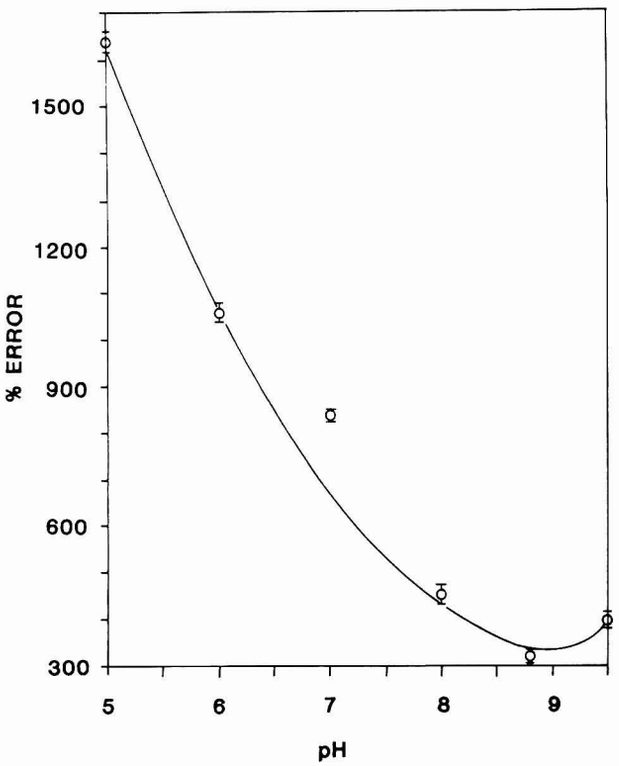

Figure 7. Relative error as a function of solution pH. Error bars represent ±1 standard deviation about the mean of at least three measurements.

Table II. Selectivity of Sodium Glass Electrode in Non-Steady-State Mode

cation[a]	potential difference, mV: 0.01 mM sodium	1 mM sodium	% rel error: 0.01 mM sodium	1 mM sodium
Li^+	1.0 ± 0.2	2.2 ± 0.4	48 ± 0.1	17.5 ± 2.7
NH_4^+	7.8 ± 0.2	5.1 ± 0.2	368 ± 21.8	44.1 ± 3.8
K^+	18.8 ± 0.2	9.1 ± 0.1	1600 ± 37.8	87.9 ± 7.1
Mg^{2+}	0.6 ± 0.2	1.3 ± 0.3	23.1 ± 2.2	12.7 ± 2.6
Ca^{2+}	4.3 ± 0.4	2.7 ± 0.8	174.7 ± 20.3	24.0 ± 8.5
Sr^{2+}	5.3 ± 0.2	3.4 ± 0.1	231.3 ± 15.8	31.9 ± 0.6
Ba^{2+}	12.1 ± 0.5	5.8 ± 0.9	746.2 ± 44.9	59.0 ± 9.3

[a] Cation concentration is 0.1 mM.

strength effect is greater at lower sodium concentrations. The explanation for this ionic strength effect is similar to that given for the pH effect. Although this glass electrode is known to possess excellent selectivity for sodium over $Tris^+$, the detection limit to sodium is adversely affected by high $Tris^+$ concentrations. As the $Tris^+$ concentration increases, the electrode response to sodium is less, which results in a greater effect from the transitory response to potassium and greater electrode inaccuracy.

The effect of solution flow rate has been studied over the range from 0.38 to 1.55 mL/min. No significant differences in the extent of error due to potassium have been found over this range. No effect of solution flow rate suggests that the transitory phenomenon occurs in the glass hydrated region of the electrode as opposed to the aqueous diffusion layer at the electrode/solution interface (*12*).

Finally, the selectivity pattern for the sodium-selective glass membrane electrode in the non-steady-state mode has been determined. Electrode responses to solutions that contain sodium and a cation of interest have been compared to the signal from the same solution without the cation of interest. The potential differences and their corresponding percent

relative errors are summarized in Table II.

For monovalent cations, potassium shows the largest errors followed by ammonium and then lithium. It is well-known that divalent cations elicit minimal response in the steady-state mode with glass membranes of the type used here. This lack of response to divalent cations is thought to be a function of their slow mobilities within the glass membrane matrix (*17*). As shown in Table II, however, large transitory responses to divalent cations cause significant errors in the non-steady-state mode. The relative selectivity pattern is $Mg^{2+} < Ca^{2+} < Sr^{2+} < Ba^{2+}$, which follows the pattern commonly associated with cation exchangers. These results suggest that the transient phenomenon is associated with an ion-exchange process with the hydrated region of the glass membrane. Such an ion-exchange process has been proposed in this regard (*10*, *12*). For all cations, the magnitude of the inaccuracy is lower at higher sodium concentrations.

Results presented in this paper clearly demonstrate significant inaccuracies in the response of the sodium glass membrane electrode when operated in a non-steady-state mode. The time-dependent selectivity of the glass membrane, caused by rapid activity steps of cations, appears to be responsible for these inaccuracies. As a result, this electrode must be used with caution and optimal experimental conditions must be established for each particular application to minimize this time-dependent selectivity phenomenon. Several experimental parameters have been identified that can be used in such optimization studies. Even under optimal conditions, however, the use of "effective" selectivity coefficients in the non-steady-state mode must be considered for glass membrane electrodes.

LITERATURE CITED

(1) Arnold, M. A.; Meyerhoff, M. E. *Anal. Chem.* **1984**, *56*, 20R-48R.
(2) Fricke, G. H. *Anal. Chem.* **1980**, *52*, 2589R-275R.
(3) Florence, E. *Analyst (London)* **1986**, *111*, 571-573.
(4) Eisenman, G.; Bates, R.; Mattock, G.; Friedman, S. M. *The Glass Electrode*; Interscience; New York, 1966.
(5) Friedman, S. M.; Jamieson, J. D.; Nakashima, M.; Friedman, C. L. *Science* **1959**, *130*, 1252-1254.
(6) Rechnitz, G. A.; Kugler, G. C. *Anal. Chem.* **1967**, *39*, 1682-1688.
(7) Akimoto, N.; Hozumi, K. *Bunseki Kagaku* **1976**, *25*, 554-560.
(8) Toth, K.; Fucsko, J.; Lindner, E.; Feher, Z.; Pungor, E. *Anal. Chim. Acta* **1986**, *179*, 359-370.
(9) Gratzl, M.; Lindner, E.; Pungor, E. *Anal. Chem.* **1985**, *57*, 1506-1511.
(10) Rechnitz, G. A. Ed. *NBS Special Publ. (U.S.)* **1969**, *No. 314*.
(11) Pacey, G. E.; Miami University, personal communication, 1985.
(12) Arnold, M. A.; Zisman, S. A.; Hise, S. M. *Anal. Chim. Acta* **1986**, *187*, 17-29.
(13) Martin, G. B.; Cho, H. K.; Meyerhoff, M. E. *Anal. Chem.* **1984**, *56*, 2612-2613.
(14) Eisenman, G. *Glass Electrodes for Hydrogen and Other Cations, Principles and Practice*; Marcel Dekker: New York, 1967.
(15) Vitiello, J. D.; Kearney, S. D.; Czaban, J. D.; Cormier, A. D. *Clin. Chem. (Winston-Salem, NC)* **1980**, *26*, 1021.
(16) Karlberg, B. *J. Electroanal. Chem. Interfacial Electrochem.* **1973**, *42*, 115-126.
(17) Eisenman, G. *NBS Special Publ. (U.S.)* **1969**, *No. 314*.

RECEIVED for review December 23, 1986. Accepted March 23, 1987. Acknowledgment is made to the donors of the Petroleum Research Fund, administered by the American Chemical Society, for support of this research.

Application of Polymer-Coated Glassy Carbon Electrodes in Anodic Stripping Voltammetry

Boy Hoyer,[1] T. Mark Florence,* and Graeme E. Batley

CSIRO, Division of Energy Chemistry, Private Mail Bag 7, Menai, New South Wales 2234, Australia

This paper describes the use of glassy carbon electrodes coated with Nafion perfluorosulfonate resin in anodic stripping voltammetry. The coating procedure, performed by applying a solution of the polymer to the electrode surface, is convenient and fast. Subsequently, mercury is plated onto the electrode. The thickness of the polymer film is so low that it does not impede mass transport of the analytes. In comparison with the conventional mercury film electrode, the main advantages of the modified electrode are improved resistance to interference from surface-active compounds, increased sensitivity when used in conjunction with differential voltammetric methods, and better mechanical stability of the mercury film. The analytical utility of the polymer-coated electrode is demonstrated by application to untreated urine samples.

One of the most common problems in anodic stripping voltammetry (ASV), when applied to the direct analysis of biological samples or polluted waters, is the interference effects caused by organic constituents of the sample matrix. Adsorption of surface-active compounds onto the working electrode can interfere with the diffusional transport of the analyte and usually results in peak depression (*1*). Moreover, adsorption/desorption processes of organic compounds can yield tensammetric peaks which can interfere with or be mistaken for the metal peaks (*2*). Extraneous peaks can also be caused by redox processes of nonanalyte matrix constituents. Obviously, these interference effects greatly complicate the interpretation of stripping voltammograms, particularly in speciation analysis where sample pretreatment must be kept to a minimum.

Recently, coating of the working electrode with permselective membranes has been introduced as a means of circumventing the organic interferences in ASV. The function of the membrane is to prevent the organic interferents from reaching the interface at which the deposition/stripping process takes place. Obviously, a compromise between exclusion of organic matter and the unhindered transport of the metal ions must be sought. Stewart and Smart (*3*, *4*) covered a glassy carbon electrode with a bulk dialysis membrane (1000 nominal molecular weight cutoff) through which a thin mercury film electride was plated. For cadmium, excellent resistance toward organic interferences was obtained although the dialysis membrane to some extent interfered with the mass transport of the analyte. Owing to their thickness, bulk

[1] Permanent address: Department of Chemistry, Aarhus University, 8000 Aarhus C, Denmark.

0003-2700/87/0359-1608$01.50/0 © 1987 American Chemical Society

membranes suffer from the general drawback that the time required for equilibration with the contacting solution is of the same order of magnitude as the duration of a typical ASV experiment, and the response time of the electrode can become a limiting factor. Wang and Hutchins-Kumar (*5*) coated a thin mercury film electrode (TMFE) with a cellulose acetate membrane and also obtained good resistance toward organic interference. However, this electrode modification procedure requires at least 70 min, which is inconvenient for practical ASV work. In both approaches, the membrane becomes the limiting factor to mass transport of the analyte.

In this paper, we report on the characteristics of a Nafion-coated thin mercury film electrode (NCTMFE) for use in ASV. Nafion, a non-cross-linked perfluorosulfonate cation-exchange resin, has recently been used for electrode coating in a great variety of electrochemical studies, mostly in conjunction with immobilization of positively charged redox couples within the film coating (*6*, *7*). The Nafion polymer is chemically inert, nonelectroactive, hydrophilic, and insoluble in water and thus possesses almost ideal properties for preparation of modified electrodes. The coating can be recast from a solution of the polymer which makes the electrode modification procedure convenient and fast. Moreover, ultrathin coatings can be prepared which pose minimum resistance to diffusion of the analyte and yet discriminate against organic species. Also, with very thin films, the "dead volume" within the polymer film is minimized which allows rapid electrode response to changed solution conditions (e.g., standard additions).

In this study, the practical utility of the NCTMFE has been assessed by application to trace metal analysis in untreated urine samples.

EXPERIMENTAL SECTION

Apparatus. Square-wave and differential pulse measurements were performed with a Metrohm 646 voltammetric processor, while a Princeton Applied Research Model 174 polarographic analyzer was used for linear sweep measurements. In all experiments, a laboratory-built electrochemical cell was used. The cell consisted of a 50-mL cylindrical Perspex beaker screwed into a Perspex cover in which were mounted the nitrogen delivery tube, a Metrohm 628-10 rotating glassy carbon electrode (3 mm diameter), a platinum coil counter electrode, and a Ag/AgCl (3 M KCl) reference electrode.

Reagents. All buffers and supporting electrolyte solutions were prepared from Merck Suprapur reagents and distilled water, while other chemicals were of analytical grade. The protein standard solution (Sigma) contained 0.5 g/L albumin and 0.3 g/L globulin. The sample of Nafion-125 obtained from E. I. du Pont de Nemours an Co. was dissolved in a 1/1 ethanol–water mixture according to the procedure previously described (*8*). The content of the Nafion in the resulting stock solution determined by evaporation of a small aliquot was found to be 0.21% (w/v).

Procedure. The glassy carbon working electrode was coated by applying a droplet of the Nafion solution to the electrode surface with a microliter pipet. In this study, three film thicknesses were investigated, prepared by applying (a) 2 μL of a 1:1 dilution of the stock solution, (b) 2 μL of the stock solution, and (c) 4 μL of the stock solution. These coatings are referred to as low-, medium-, and high-thickness films, respectively. The solvent was allowed to evaporate, whereafter the formed film was dried with a hair-dryer for 60 s. As previously noted (*9*), this heat treatment step improves the stability and electrochemical performance of the Nafion-coated electrode. Mercury was deposited on the glassy carbon/Nafion substrate by adding 5×10^{-5} M mercury(II) nitrate to the supporting electrolyte medium and depositing at –800 mV vs. Ag/AgCl for 5 min. Mercury deposition was done in situ except in the analysis of urine samples in which preformed films were used.

Unless otherwise stated, a medium containing 0.07 M acetate buffer, pH 4.0 (prepared from sodium acetate and nitric acid), and 0.05 M NaCl was used in the electrochemical experiments. Solutions and samples were deaerated with nitrogen for 5 min prior to ASV. Electrode rotation was stopped prior to recording of the stripping signal.

Urine samples were diluted 1/3 with water and analyzed by ASV shortly after sampling. For cadmium and lead determinations, the pH was adjusted to 5.5, while copper determination was carried out at pH 1.0. In both cases, pH adjustment was done with aliquots of concentrated hydrochloric acid.

The instrumental settings for square-wave anodic stripping voltammetry (SWASV) were as follows: modulation amplitude, 25 mV; modulation frequency, 125 Hz; effective scan rate, 30 mV/s. The instrumental settings used for differential pulse anodic stripping voltammetry (DPASV) were as follows: modulation amplitude, 50 mV; pulse repetition time, 1 s; effective scan rate, 6 mV/s. In the experiments with linear sweep anodic stripping voltammetry (LSASV), the scan rate was 50 mV/s.

RESULTS AND DISCUSSION

Microscopy Studies of Nafion Films. Visually, the Nafion coatings were transparent and appeared somewhat more dull than the bare glassy carbon electrode. Two zones were clearly discernible: a dull ring zone and a highly refractive center zone. The formation of the refractive pattern followed the gradual retraction of the evaporating Nafion solution during the preparation of the coating. The extent of the refractive zone decreased with high film thickness.

In an optical microscope (500 and 1000× magnification), the low- and medium-thickness Nafion films appeared smooth and uniform with very few macroscopic holes. With the high-thickness Nafion film, cracks in the coating extending down to the glassy carbon surface were observed. The cracks, the largest of which could be seen with the naked eye, developed during the evaporation of the Nafion solution and were mostly confined to the edge of the coating. However, these cracks were relatively few and well separated, and the fraction of the glassy carbon exposed by them was insignificantly small. Under the microscope, the general appearance of the coating was still uniform and smooth.

Plating of mercury onto the Nafion-coated electrodes changed the microscopic appearance dramatically, and a pattern of finely dispersed droplets was observed. From the photomicrographs it was not possible to determine whether the mercury was deposited below, within or on top of the Nafion film.

Mercury Deposition. Mercury electrodeposited onto the glassy carbon/Nafion substrate from mercury(II)-containing solutions could clearly be seen as a grayish deposit which first formed in the refractive center zone and gradually expanded toward the edge of the electrode with longer deposition times. The amount of mercury plated onto the NCTMFE was determined by performing the electrodeposition in a solution spiked with radioactive mercury-203 (total mercury, 2.2×10^{-5} M; 10-min deposition at –900 mV vs. Ag/AgCl). Subsequently, the electrode was rinsed and the mercury deposit dissolved in concentrated nitric acid. A low-thickness NCTMFE incorporated approximately half as much mercury as a bare glassy carbon electrode (33 300 ± 2800 counts/min for a bare electrode vs. 18 100 ± 1300 counts/min for a Nafion-coated electrode (n = 3 for both measurements)). This result was quite surprising and encouraging, as a much higher depression of the mercury plating efficiency was expected in the presence of the polymer film. The amount of mercury deposited on the low-thickness NCTMFE was 3.2×10^{-9} mol, corresponding to an average thickness of 66 Å assuming uniform coverage of the electrode area. By comparison, the average thickness of the Nafion coating is approximately 2000 Å, assuming equal densities of the recast Nafion film and the bulk membrane (1.98 g/cm^3 (*10*)). In practice, however, the density of the recast polymer will be somewhat lower owing to water uptake during the radical dissolution procedure, and the calculated thickness should therefore be considered as a minimum value.

Table I. Effects of Nafion Coating on the ASV Peak Currents of Lead, Cadmium, and Copper

	I_p(Cd)/μA			I_p(Pb)/μA			I_p(Cu)/μA		
	SW[a]	DP[b]	LS[c]	SW	DP	LS	SW	DP	LS
TMFE	0.6	3.5	1.1	1.5	6.2	1.4	5.2	1.3	0.9
low-thickness NCTMFE	5.2	9.7	1.2	8.2	11.0	1.3	1.8	2.0	0.9
medium-thickness NCTMFE	4.1	10.3	1.0	6.6	11.9	1.1	2.6	2.6	1.0
high-thickness NCTMFE	0.2	2.8	1.3	0.7	7.5	1.2	5.8	3.5	1.2

[a-c] SW, DP, and LS are square wave, differential pulse, and linear sweep anodic stripping voltammetry, respectively. Experimental conditions were as follows: 2.0×10^{-7} M metal ion; preelectrolysis for 60 s at −900 mV vs. Ag/AgCl.

Hence, even for the low-thickness NCTMFE, the Nafion film is considerably thicker than the mercury layer. However, it cannot be concluded on the basis of the calculated nominal thicknesses that the mercury is fully contained within the polymer as the mercury may fill up the pores of the Nafion coating and extend beyond it.

Next, the question of the distribution of the mercury within the Nafion film was addressed. Although unusual charge propagation properties have been suggested for the Nafion polymers (*11*), it was believed that the reduction of the mercuric ions and the growth of the mercury phase took place at the glassy carbon/Nafion interface. This hypothesis was strongly supported by two observations. First, in a radiotracer experiment, a mercury-plated Nafion electrode was immersed in dimethyl sulfoxide (Me_2SO) which removed the Nafion quantitatively, leaving a clearly visible mercury deposit on the electrode. After removal of the remaining mercury with nitric acid, it was found that the mercury activity was distributed between the Me_2SO and the nitric acid in the ratio 3:7. The Me_2SO fraction is probably even overestimated because the rinsing water applied to the electrode after the film dissolution was pooled with the Me_2SO before the counting, and this water may have dislodged mercury droplets from the glassy carbon surface. It appears highly unlikely that the Nafion film could be dissolved without removing the bulk of the deposited mercury unless the mercury droplets are attached directly to the glassy carbon surface. Second, as discussed below, the NCTMFE showed considerably higher resistance toward interference from surface-active agents than the conventional TMFE, indicating that the polymer hinders the transport of the interferents to the mercury surface. Obviously, this protective mechanism can only be operative if the mercury is confined beneath or within the polymer film.

At the high-thickness NCTMFE, no visible mercury deposition was observed in the cracks which formed in the coating.

The Nafion coating stabilizes the formed mercury phase mechanically and prevents the coalescence or dislodgement of mercury droplets which may take place at the TMFE. In an experiment in which an eccentric and slightly vibrating rotating electrode was used, large areas of bare glassy carbon quickly developed at the normal TMFE, whereas no change in the visual appearance or performance of a NCTMFE was observed after prolonged use with the damaged rotator. Moreover, a NCTMFE withstands gentle wiping with filter paper, whereas this treatment completely ruins a TMFE. The improved mechanical stability of the NCTMFE is a major advantage if the analysis is carried out under strongly convective conditions or if the sample contains particulate matter.

ASV Response Characteristics of NCTMFE. As shown in Figure 1, the NCTMFE gives rise to well-defined SWASV signals for cadmium, lead, and copper. For comparison, the stripping signals were also recorded with DPASV and LSASV, and the peak currents obtained are given in Table I. Although repetitive preparations of the Nafion coating resulted in considerable variation in the ASV sensitivity of the electrode (see below), the data in Table I are qualitatively representative

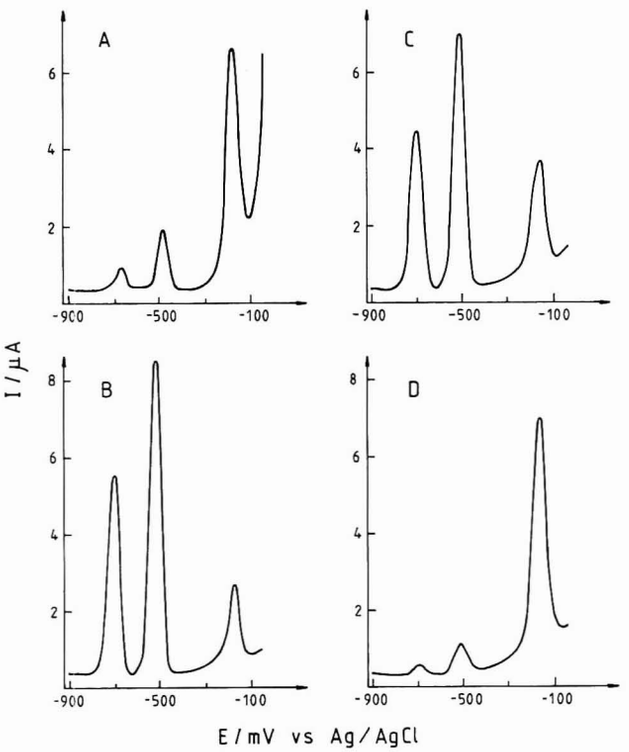

Figure 1. Square-wave stripping signals obtained with (A) TMFE and (B–D) low-, medium-, and high-thickness NCTMFE, respectively: 2×10^{-7} M cadmium, lead, and copper; preelectrolysis for 60 s at −900 mV vs. Ag/AgCl; electrode rotation rate, 500 rpm.

except that a high-thickness NCTMFE usually produced a lower copper signal than a medium-thickness NCTMFE. The unusual order of sensitivity for cadmium, lead, and copper obtained with SWASV at the uncoated TMFE, i.e., with the copper signal being much higher than those of the other two metals when present in equal molarity, differs from the order obtained with DPASV and requires a comment. It was found that the enhancement of the copper signal was related to the chloride concentration of the medium: instead of the usual decrease of the copper wave with chloride concentration observed in DPASV (*12*), it was found that chloride concentrations in the range 0.02–0.1 M caused enhancement of the SWASV copper signal. The effect was not investigated further but is probably kinetic in nature since the frequency of the potential waveform applied to the working electrode differed considerably between DPASV and SWASV (in the present study: 1 Hz and 125 Hz, respectively). The enhancement effect was not observed with low- and medium-thickness NCTMFE, but reappeared with a high-thickness NCTMFE.

Several interesting observations can be made from Table I:

(a) Coating of the glassy carbon electrode with a low-thickness Nafion film resulted in a startling increase in the lead and cadmium signal when recorded with SWASV and, to a lesser extent, with DPASV. With higher film thicknesses,

Table II. Effect of Nafion Coating on the Peak Potential and Peak Width in SWASV

	Cd		Pb		Cu	
	E_p[a]/mV	$W_{1/2}$[b]/mV	E_p/mV	$W_{1/2}$/mV	E_p/mV	$W_{1/2}$/mV
TMFE	−660	54	−474	54	−170	64
low-thickness NCTMFE	−689	59	−508	59	−160	56
medium-thickness NCTMFE	−689	64	−508	60	−160	64
high-thickness NCTMFE	−689	69	−508	69	−155	69

[a] Potentials are given relative to Ag/AgCl. [b] $W_{1/2}$ peak width at half maximum. Experimental conditions are given in Table I.

the signals decreased and with a high-thickness NCTMFE, the sensitivities for lead and cadmium were lower than those observed at a conventional TMFE.

(b) For copper, a low-thickness Nafion coating caused a moderate increase of the DPASV signal, whereas the SWASV signal was decreased; however, the latter effect is probably caused by the abovementioned enhancement of the SWASV signal of copper at the TMFE. Indeed, in the absence of chloride in the electrolyte medium a low-thickness NCTMFE also caused enhancement of the SWASV signal of copper. Highest sensitivity was usually obtained with a medium-thickness film and the signals diminished with further increases in film thickness. (As mentioned above, the copper signals in Table I measured with the high-thickness NCTMFE are unusually large.)

(c) With the exception of the SWASV signal of copper at the TMFE, the magnitudes of the square-wave and differential-pulse signals generally followed the same trend as a function of Nafion film thickness although the changes in the square-wave signals were much more dramatic than those seen in the differential-pulse signals.

(d) The magnitude of the linear-sweep voltammetric signals only varied slightly as a function of film thickness for either of the metals. In theory, the LSASV signal is a direct measure of the amount of metal accumulated in the mercury phase during deposition. Therefore, this result indicates that the relationship between the peak heights measured with the differential techniques and the thickness of the Nafion film cannot be accounted for by differences in preelectrolysis efficiency.

In Table II, the peak potentials and peak widths of the SWASV signals for cadmium, lead, and copper at the TMFE and the NCTMFE are given. A low-thickness Nafion coating shifted the peak potentials of cadmium and lead approximately 30 mV in a negative direction relative to those at the uncoated electrode, indicating that the coating indeed constitutes a separate phase which interacts with the stripping process. For copper, a small positive peak shift was observed. Further increases in the Nafion film thickness did not affect the peak potentials noticeably. For lead and cadmium, Nafion-coating resulted in some peak broadening which increased with film thickness. For copper, a low-thickness NCTMFE yielded a slightly sharper peak than the TMFE; however, with increasing film thickness, the peak was again broadened.

The effects of Nafion coating on the peak potentials and peak widths in DPASV and LSASV followed the same trends as those described for SWASV.

The relatively constant values of the LSASV peak heights in the absence and presence of Nafion films indicate that the membrane coating does not significantly hinder the transport of metal ions to the electrode surface during deposition. Calculation of the diffusion layer thickness δ at the RDE with conditions typical for the present study (diffusion coefficient of metal ion, 10^{-5} cm^2/s; kinematic viscosity of electrolyte medium, 10^{-2} cm^2/s; rotation speed, 500 rpm) yields a value for δ of 2×10^{-3} cm. Thus, the Nafion coatings are considerably thinner than the diffusion layer. The data available on diffusion of metal ions in bulk Nafion (e.g., ref 13) show that the diffusion coefficients in the polymer phase are somewhat lower than those in aqueous solution. However, owing to the radical procedure used to dissolve the bulk Nafion, the recast films will undoubtedly be more hydrated than the bulk phase and will not hinder diffusion to the same extent. Experimentally, the transport properties of the Nafion coating were investigated by recording Levich plots (i.e., signal magnitude as a function of (rotation rate)$^{1/2}$). In the range of rotation speeds available (500–3000 rpm) the stripping signals increased with the rate of rotation, and correlation coefficients of 0.985, 0.988, and 0.988 were obtained for cadmium, lead, and copper, respectively. Thus, in spite of the Nafion coating, the limiting step in the overall mass transport during deposition is still the convective-diffusive transport of analyte in the solution.

Most likely, the enhancement of the SWASV and DPASV signals at the low-thickness NCTMFE is due to more efficient replating of metal ions when the applied pulse ceases as the film coating will confine the newly oxidized ions to the immediate vicinity of the electrode surface. This explanation also accounts for the fact that greater enhancement is seen with SWASV than with DPASV as the pulse repetition rate is much faster in the former method, allowing the analyte to undergo more redox cycles during the stripping scan.

However, the fall-off in signal observed between a medium- and high-thickness film indicates that other effects are operative. It is interesting to note that the SWASV signals obtained with the high-thickness film NCTMFE in two ways resembled those measured at the conventional TMFE. First, the order of the peak heights of cadmium, lead, and copper when measured with SWASV (i.e., $I_{Cu} > I_{Pb} > I_{Cd}$) was the same, whereas the order was different with the low- and medium-thickness NCTMFE. Second, the unusual effect of chloride concentration on the SWASV peak height of copper at the TMFE reappeared at the high-thickness NCTMFE but was not seen at the thinner Nafion coatings. These findings strongly indicate, that the electrode process at the high-thickness NCTMFE is more susceptible to solution chemistry effects than at the thinner coatings. No experimental evidence was obtained which could further elucidate this phenomenon, but a plausible explanation is simply that a partial opening of the polymer structure takes place between the medium- and high-thickness NCTMFE, leaving the mercury phase more exposed. Also, the loss in sensitivity for cadmium and lead in SWASV and DPASV at the high-thickness NCTMFE can be accounted for in this manner, as a larger fraction of the newly oxidized metal will escape from the vicinity of the electrode surface before the pulse is reversed, and the sensitivity gain accruing from multiple deposition/stripping cycles of the analyte will diminish. Furthermore, the hypothesis is supported by the fact that macroscopic cracks appeared in the high-thickness NCTMFE which implies that contractive forces are present in the polymer film. With increasing film thickness, these forces become stronger in comparison with the Nafion/glassy carbon interaction, and the polymer sheet is under stress.

The cracks observed at the high-thickness NCTMFE did not affect the performance of the electrode as it exhibited the

peak shifts typical of Nafion coating and showed much greater insensitivity to surface-active compounds than the TMFE.

Nafion coating was not found to affect the size and shape of the ASV background signal noticeably in chloride-free solutions. However, in chloride-containing media, the commencement of the oxidation wave of chloride was shifted positively (cf. Figure 1), thus expanding the useful potential range. In the standard medium employed, containing 0.05 M chloride, the potential shift observed in the SWASV voltammograms was approximately 100 mV. The reason for this effect is probably that the Nafion coating to some extent repels anions and therefore lowers the effective chloride activity at the electrode surface.

Being an ion-exchange resin, Nafion is capable of preconcentrating metal ions on its own. Thus, prior to the application of the preelectrolysis potential, the Nafion coating may already have accumulated an amount of trace metal ions which to some extent will be amalgamated once the reductive plating potential is imposed on the electrode. In order to assess the significance of this mechanism relative to the direct diffusion of metal ions through the membrane, an experiment was performed in which a NCTMFE without any applied potential was allowed to equilibrate with a solution containing 2×10^{-7} M cadmium, lead, and copper. Subsequently, a square-wave scan from 0 V to −900 mV was performed in order to measure the amount of metal incorporated in the Nafion. In the absence of Nafion coating no metal reduction wave was seen, indicating that the metal ion concentrations are too low to be determined by the direct voltammetric method. In the presence of Nafion, signals from cadmium, lead, and copper (in particular the latter) were clearly discernible. However, the peak currents obtained in this manner were, at the most, 5% of those obtained in an SWASV experiment performed on the same sample with 60 s deposition at −900 mV vs. Ag/AgCl. It can therefore be concluded that, with the very thin Nafion coatings employed, the cation-exchange preconcentration mechanism is insignificant in comparison to diffusion of metal ions through the film during the deposition step in ASV.

The sensitivity in SWASV of different NCTMFEs prepared with the same procedure (i.e., coating of the glassy carbon electrode and subsequent deposition of mercury) could vary by a factor as high as 3. This finding indicates that the formation of the Nafion phase during the evaporation of the applied polymer solution plays a significant role in the performance of the electrode. Two correlations between the visual appearance of the Nafion coating and the sensitivity were observed. First, sensitivity tended to increase with the extent of the central, refractive zone. Second, an irregular refraction pattern in the central zone resulted in higher sensitivity than a regular, concentric pattern. The microscopic reason for this behavior is not known.

Once prepared, the NCTMFE showed excellent reproducibility. Repetitive DPASV signals ($n = 8$) measured with 30-s preelectrolysis at −1.0 V vs. Ag/AgCl in a solution containing 1.0×10^{-7} M of cadmium, lead, and copper resulted in relative standard deviations of the peak currents of 4.2%, 4.2%, and 5.0%, respectively.

The linearity of the responses was examined with DPASV at a low-thickness NCTMFE. In the first experiment, the metal ion concentrations were varied between 1 and 80 nM with the experimental conditions $E_{dep} = -1000$ mV, $t_{dep} = 120$ s, and pulse amplitude = 50 mV. In a second experiment, the metal concentrations were varied between 0.1 and 2.0 μM with the instrumental parameters $E_{dep} = -1000$ mV, $t_{dep} = 10$ s, and pulse amplitude = 10 mV. The correlation coefficients obtained in the first and second experiment (in parentheses) were 0.9995 (0.994), 0.997 (0.998), and 0.990 (0.996) for cadmium, lead, and copper, respectively. At concentrations higher than 2 μM, nonlinearity (i.e., saturation effects) became evident. In conclusion, the NCTMFE exhibits linear response and is analytically useful over a wide concentration range.

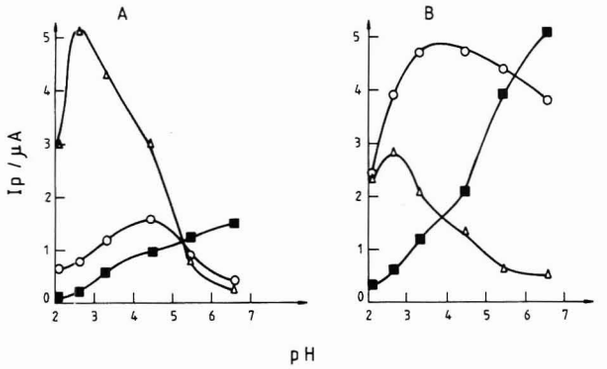

Figure 2. Effect of pH on the SWASV peak current of cadmium (■), lead (O), and copper (Δ) at (A) TMFE and (B) low-thickness NCTMFE: 2.0×10^{-7} M metal ion; preelectrolysis for 60 s at −900 mV vs. Ag/AgCl; initial medium composition, 0.02 M NaAc, 0.05 M NaCl. pH-variation was obtained by titration with concentrated nitric acid.

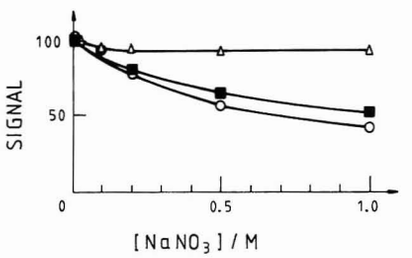

Figure 3. Effect of ionic strength on SWASV peak currents of cadmium (■), lead (O), and copper (Δ). Peak currents are given relative to those obtained with no added sodium nitrate. Experimental conditions were as follows: 2×10^{-7} M metal ion; preelectrolysis for 60 s at −900 mV vs. Ag/AgCl; initial medium composition, 0.07 M acetate buffer, 0.05 M sodium chloride.

Figure 2 shows the pH dependence of the stripping peak currents of cadmium, lead, and copper at the TMFE and the NCTMFE. With both electrodes, cadmium shows a steady decrease in sensitivity with decreasing pH, while lead and copper show maximum sensitivity at intermediate pH values. For lead, the pH values of the maximum differ somewhat between the TMFE and the NCTMFE (pH 4.3 and 3.8, respectively). The effect of ionic strength on the response of Nafion-coated electrodes was tested by addition of an inert electrolyte to the standard medium. At the TMFE, addition of up to 1 M sodium nitrate did not produce any significant change in the peak currents of cadmium, lead, and copper, whereas the signals decreased with increasing ionic strength at the NCTMFE, in particular for cadmium and lead (Figure 3). The explanation for the latter observation is probably that the diffusion coefficients of counterions in ion-exchange materials normally increase with the ionic strength of the contacting solution (*14*). Consequently, during the stripping step in the differential ASV techniques the newly oxidized analyte will diffuse further away from the electrode surface before the pulse is reversed, and the signal enhancement owing to multiple plating/stripping cycles of the analyte will be diminished. Another possible explanation is simply that the morphology and the geometrical parameters of the Nafion microstructure change as a function of the ionic strength of the contacting solution (*15*).

Effect of Surfactants on the ASV Response of the NCTMFE. The effect of surface-active organic compounds on the ASV response at the NCTMFE was examined by using cadmium as test analyte. For comparison, the surfactant effect

Table III. Effect of Surfactants on the SWASV Peak Current of Cadmium for the TMFE and the NCTMFE

surfactant	electrode type	Δi_p (%) at the following surfactant concn				
		1 ppm	2 ppm	5 ppm	10 ppm	20 ppm
Triton X-100	TMFE	+4	−11	−41	−66	*a*
	NCTMFE	+2	+6	−11	*b*	−16
sodium dodecyl sulfate	TMFE	0	−11	*b*	*b*	−33
	NCTMFE	+4	−1	−2	*b*	−7
dodecylpyridinium chloride	TMFE	−68	*a*	*a*	*a*	*a*
	NCTMFE	+8	−12	*b*	*b*	−60
gelatin	TMFE	−18	−40	*b*	*b*	−54
	NCTMFE	−1	−5	−7	*b*	−6
protein standard solution	TMFE	−45	−85	−89	−100	−100
	NCTMFE	0	−3	−11	*b*	−16
octanol	TMFE	+2	+12	+11	*b*	−4
	NCTMFE	0	+1	−2	*b*	−5

[a] Signal poorly defined or interfered with by tensammetric peaks. [b] Signal not measured at this surfactant concentration. Experimental conditions: [Cd(II)] = 2.0×10^{-7} M, preelectrolysis for 60 s at −90 mV vs. Ag/AgCl; electrode rotation rate, 500 rpm. High-thickness NCTMFEs were used except for protein standard solution (low thickness).

on the conventional TMFE was also recorded. The six surfactants chosen were nonionic (Triton X-100), anionic (sodium dodecyl sulfate), and cationic (*n*-dodecylpyridinium chloride) detergents, a colloidial protein (gelatin), a protein standard solution (albumin and globulin in the weight ration 5:3), and a long-chained alcohol (1-octanol).

As seen in Table III, the NCTMFE is much less susceptible to peak depression than the TMFE in the presence of detergents, especially with Triton X-100 and dodecylpyridinium chloride. Whereas the latter caused severe peak depressions at the TMFE in concentrations as low as 1 ppm, much higher concentrations could be tolerated with the NCTMFE. In addition, the signal quality is higher at the NCTMFE. For instance, with Triton X-100 present in concentrations higher than 5 ppm, a tensammetric peak strongly interfered with the cadmium signal at the TMFE, whereas no such effect was seen at the NCTMFE (Figure 4).

It is interesting to observe that the extent of peak depression at the NCTMFE caused by detergents is in the order cationic > nonionic > anionic. Other things being equal, this sequence would be expected from the cation-exchange properties of Nafion in that cations more easily penetrate a negatively charged membrane than do neutral molecules or—in particular—anions. Moreover, it has been shown that Nafion has a remarkably high affinity for hydrophobic cations (*16*), which probably accounts for the fact that dodecylpyridinium chloride causes larger peak depression at the NCTMFE than any of the other surfactants tested. The NCTMFE also showed a better response than the TMFE in the presence of protein. Indeed, with the protein standard solution the difference in performance was remarkable; whereas 1 ppm protein almost halved the cadmium signal at the TMFE, addition of 8000 ppm protein only caused a 60% signal reduction at the NCTMFE. However, at this concentration level of organic matter it cannot be said whether the peak depression is caused by the interaction of the protein with the electrode process or by secondary effects such as complexation of the analyte and changes in the viscosity of the medium.

1-Octanol did not affect the cadmium signal significantly, either in the presence or absence of a Nafion coating on the electrode.

Application of NCTMFE in Analysis of Urine Samples. The analytical utility of the NCTMFE was assessed by applying it to the determination of trace metals in untreated urine. This matrix poses considerable problems in electroanalysis due to its high organic content and it also affected the performance of the NCTMFE. Addition of urine to a 0.5 M hydrochloric acid solution resulted in a drop in sensitivity for cadmium, lead, and copper. At the low pH of this medium,

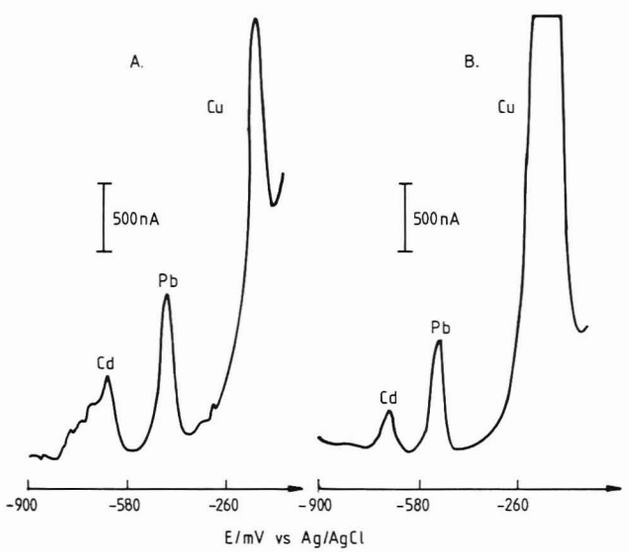

Figure 4. Square-wave stripping signals obtained with (A) TMFE and (B) high-thickness NCTMFE in solution containing 5 ppm Triton X-100. Experimental conditions are as given in Table III except that the sample was also spiked with 2×10^{-7} M Pb(II) and 2×10^{-7} M Cu(II).

complexation of the trace metals by constituents of the urine matrix is unlikely, and the signal depression can therefore be attributed to adsorption of organic matter on the working electrode. Direct analysis of undiluted urine samples with the TMFE or the NCTMFE did not prove feasible as adsorption of organic matter took place to the extent that a brownish tinge developed on the cell walls and on the RDE. Although well-defined stripping signals could be obtained, the signal magnitude decreased during repetitive ASV scans in the urine matrix. However, the interference effects could largely be remedied by 1/3 dilution of the urine sample with water. Figure 5 shows stripping voltammograms of cadmium, lead, and copper obtained under such conditions. Generally, in order to release bound trace metals, sample acidification is desirable for total metal determination but the loss of sensitivty for cadmium at low pH (cf. Figure 2) was found to be prohibitive. However, it has been shown previously (*17*, *18*) that the cadmium and lead responses measured in urine at pH 4–6 reflect total metal. The lead content of the undiluted urine sample was found to be 25 nM, while the cadmium signal, although discernible, was not a significantly higher than the blank signal. At pH 5.5, no sensible recovery of copper spikes could be obtained in the urine samples, probably due to solution chemistry effects. Acidification to pH 1.0 greatly increased the copper signal, and it responded to standard

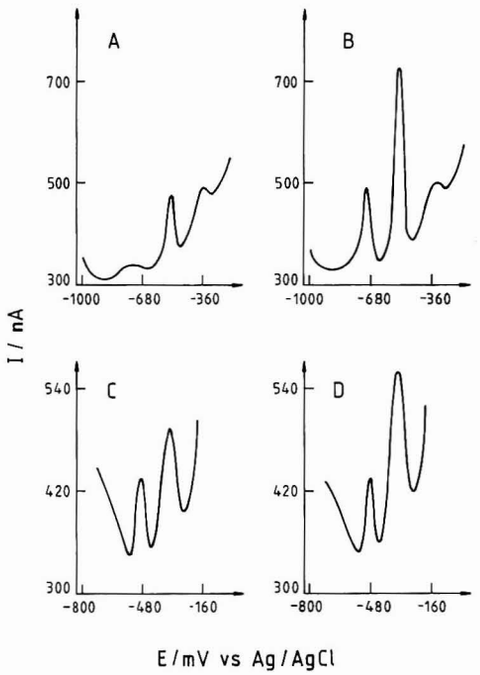

Figure 5. DPASV signals of cadmium, lead, and copper obtained with high-thickness NCTMFE in an untreated, diluted urine sample: (A) pH 5.5, preelectrolysis for 60 s at −1000 mV vs. Ag/AgCl; (B) as (A) spiked with 5 nM Cd(II) and 12.5 nM Pb(II); (C) pH 1.0, preelectrolysis for 60 s at −800 mV; (D) as (C) spiked with 50 nM Cu(II).

additions at this pH. The copper concentration of the urine sample was found to be 0.33 μM, which is in reasonable agreement with the value obtained by inductively coupled plasma spectroscopy (0.29 μM). Occasionally, crazing of the polymer coating occurred when low-thickness Nafion films were exposed to the acidified urine matrix. This problem did not occur with the high-thickness NCTMFE, which therefore was preferred for this application.

Although the NCTMFE was not insensitive to the organic constituents of the urine matrix, its performance was far superior to that of the TMFE. With the latter, a noisy background signal was obtained, and the cadmium and copper signals were often interfered with by unidentified peaks, probably due to redox processes or adsorption/desorption of sample constituents. At the NCTMFE, no such phenomena were observed, and the quality of the ASV signals was higher. At present, further research is being carried out to assess the utility of the NCTMFE for routine analysis of clinical samples.

CONCLUSION

The above results show that the application of the NCTMFE in stripping analysis is very promising. The electrode modification not only offers considerably higher resistance to organic interferences than the TMFE but also yields higher sensitivity when used in conjunction with superimposed differential waveforms. Another important advantage of the NCTMFE is the mechanical stabilization of the mercury film. At present, work on the preparation of Nafion films with improved properties is under way. In particular, recast films which reconstitute the properties of the bulk polymer would be desirable as the latter is completely insoluble in organic solvents at ambient temperature and pressure. Recent progress in this area has been reported (*19*).

However, it must be appreciated that membrane coating of the working electrode cannot possibly eliminate all organic interferences in ASV. Even if the interfering species are prevented from reaching the electrode surface and thus cannot give rise to tensammetric waves or redox signals, they may still deposit on the outside of the membrane and affect mass transport. For ASV analysis of samples with high organic contents, electrode regeneration between each measurement may therefore be inevitable. As recently reported (*20*), this approach can be fully automated with the conventional TMFE when implemented in a flow system. In the case of the NCTMFE the renewal of the Nafion coating cannot be automated, but rinsing of the electrode surface with a suitable solvent may prove sufficient.

Registry No. Cd, 7440-43-9; Pb, 7439-92-1; Cu, 7440-50-8; C, 7440-44-0; Hg, 7439-97-6; Nafion, 39464-59-0; Triton X-100, 9002-93-1; sodium dodecyl sulfate, 151-21-3; dodecylpyridinium chloride, 104-74-5; 1-octanol, 111-87-5.

LITERATURE CITED

(1) Brezonic, P. L.; Brauner, P. A.; Stumm, W. *Water. Res.* **1976**, *10*, 605.
(2) Batley, G. E.; Florence, T. M. *J. Electroanal. Chem.* **1976**, *72*, 121.
(3) Stewart, E. E.; Smart, R. B. *Anal. Chem.* **1984**, *56*, 1131.
(4) Smart, R. B.; Stewart, E. E. *Environ. Sci. Technol.* **1985**, *19*, 137.
(5) Wang, J.; Hutchins-Kumar, L. D. *Anal. Chem.* **1986**, *58*, 402.
(6) Martin, C. R.; Rubinstein, I.; Bard, A. J. *J. Am. Chem. Soc.* **1982**, *104*, 4817.
(7) White, H. S.; Leddy, T.; Bard, A. T. *J. Am. Chem. Soc.* **1982**, *104*, 4811.
(8) Martin, C. R.; Rhoades, T. A.; Ferguson, J. A. *Anal. Chem.* **1982**, *54*, 1639.
(9) Nagy, G.; Gerhardt, G. A.; Oke, A. F.; Adams, R. N.; Moore, R. B.; Szentirmay, H. N.; Martin, C. R. *J. Electroanal. Chem.* **1985**, *188*, 85.
(10) *Product Information on Nafion*; Du Pont: Wilmington, DE, 1980.
(11) Buttry, D. A.; Anson, F. C. *J. Am. Chem. Soc.* **1983**, *105*, 685.
(12) Florence, T. M.; Batley, G. E.; *J. Electroanal. Chem.* **1977**, *75*, 791.
(13) Lopez, M.; Kipling, B.; Yeager, H. L. *Anal. Chem.* **1977**, *49*, 629.
(14) Helfferich, F. *Ion Exchange*; McGraw-Hill: New York, 1962.
(15) Mauritz, K. A.; Hopfinger, A. J. In *Modern Aspects of Electrochemistry*; Brockris, T. O'M., Conway, B. E., White, R. E., Eds.; Plenum: New York, 1982; Vol. 14, pp 425–508.
(16) Moore, R. B.; Wilkinson, J. E.; Martin, C. R. *Anal. Chem.* **1984**, *56*, 2572.
(17) Copeland, T. R.; Christie, J. H.; Osteryoung, R. A.; Skogerboe, R. K. *Anal. Chem.* **1973**, *45*, 2171.
(18) Lund, W.; Eriksen, R. *Anal. Chem. Acta* **1979**, *107*, 37.
(19) Moore, R. B.; Martin, C. R. *Anal. Chem.* **1986**, *58*, 2569.
(20) Hoyer, B.; Kryger, L. *Talanta* **1986**, *33*, 883.

RECEIVED for review December 16, 1986. Accepted March 16, 1987. A research fellowship (to B.H.) from Aarhus University, Denmark, and a travel grant (No. 11-5773) from the Danish Natural Science Research Council are gratefully acknowledged.

Repetitive in Situ Renewal and Activation of Carbon and Platinum Electrodes: Applications to Pulse Voltammetry

Melanie Poon and Richard L McCreery*

Department of Chemistry, The Ohio State University, 120 West 18th Avenue, Columbus, Ohio 43210

Glassy carbon and platinum electrodes were renewed and activated in situ by using a previously reported technique involving pulsed laser light. The laser pulse delivered directly in the solution of interest was able to repeatedly remove passivating films or oxide layers and result in an active, reproducible solid electrode surface. A differential pulse voltammetry technique was developed in which the electrode is laser activated before each potential pulse during a conventional potential scan. This laser-assisted voltammetric experiment provided enhanced resolution and greatly extended electrode life for the voltammetry of several organic species, including phenol, dopamine, ascorbic acid, and hydroquinone. Some physical effects of repetitive laser pulses were observed and local melting and ablation were possible at higher laser powers. Laser activation may be useful for exploiting the wide potential window of solid electrodes, while improving their reproducibility, lifetime, and electron transfer kinetics.

The prominence of the dropping mercury electrode (DME) in analytical applications of voltammetric techniques stems largely from its renewable, reproducible surface. In a wide range of applications, the continually exposed fresh mercury surface and the entirely new drop every few seconds are important for maintaining an analytically useful response. In contrast to the DME, solid electrodes are often deactivated by either species in solution or those generated by a redox process. The result is passivation of the surface which can cause highly irreproducible measurements. In extreme cases, the charge transfer process is completely inhibited and the electrode must typically be removed from solution and restored by one of a number of pretreatment methods. Poor stability can interfere with the performance of solid electrodes to the point where their advantages of mechanical rigidity and wide potential window are difficult to realize. Two general approaches have been pursued to activate and stabilize solid electrodes for analytical or electrocatalytic applications. First, the electrode may be protected by a selectively permeable membrane which excludes deactivating materials. The Clark oxygen electrode is a classical example, and electrodes protected by Nafion (*1*, *2*) or cellulose (*3*, *4*) are more recent cases. Second, a carbon or platinum electrode may be reactivated by a variety of procedures, most of which involve removal from the cell.

Numerous procedures for cleaning and activating carbon (*5–26*) or platinum (*27–35*) electrodes have been presented and reviewed (*10*) and include polishing (*5–7*, *10*), plasma treatment (*24*), heat treatment (*22*, *23*), laser activation (*25*, *26*), flaming (*30*, *35*), electrochemical cycling (*13*, *14*, *17–19*, *21*), and various chemical reactions (*20*, *30*). These procedures drastically affect electrode performance, with, for example, rate constants for the $Fe(CN)_6^{3-/4-}$ electron transfer rate varying by 3 orders of magnitude on carbon (*10*) and 2 orders of magnitude on platinum (*30*) as a function of pretreatment procedure. The majority of these procedures are fairly tedious and time-consuming, with most requiring meticulous attention to cleanliness. An exception is carbon paste, where a new surface may be prepared quickly, albeit outside the cell (*31*). A few of these procedures may be carried out in situ, including laser activation of glassy carbon (GC) (*25*, *26*), electrochemical cycling of platinum by pulse (*33*, *34*) or scanning waveforms (*28*, *35–37*), and mechanical removal of electrode material (*32*).

We have reported a new in situ method for electrode pretreatment that uses a short laser pulse to irradiate the electrode directly in the solution of interest (*25*), and we discussed a particular application to glassy carbon (*26*). The objectives of the present work are two, both directed primarily at analytical voltammetry using solid electrodes. First, laser activation was investigated as a means to repeatedly renew solid electrodes passivated by adsorbed or polymeric materials. Second, we sought to improve analytical voltammetry by enhancing the electron transfer rate using laser activation.

EXPERIMENTAL SECTION

The electrochemical cell, optical arrangement, and lasers have been described previously (*26*). For some of the present work, the fundamental output of the Nd:YAG laser (1064 nm) was frequency doubled by using a standard potassium dihydrogen phosphate crystal and separated from the 532-nm light with a dichroic mirror. For both wavelengths, a He–Ne pilot beam was coincident with the Nd:YAG beam to aim the laser onto the electrode. The laser pulse duration was 7–10 ns, with total energy ranging from 5 to 60 mJ, and only the center of the unfocused Nd:YAG beam impinged on the electrode. In addition to the Nd:YAG laser, a small N_2 laser (Laser Science VSL 337, pulse duration 3–4 ns, peak power 40 kW) was used for one experiment with its beam focused to a 200-μm diameter spot. The electrochemical cell was constructed of Teflon and was able to accommodate electrodes of varying diameter sealed in glass. Platinum electrodes were made by sealing Pt wire (Engelhard or Goodfellow Metals) in type 0120 potash soda lead glass (Corning) followed by annealing. The glassy carbon working electrode design used previously was changed due to the entrapment of gas bubbles in the Teflon washer after a large number of laser pulses. Glassy carbon (GC20-s, Tokai) was cut with a low-speed diamond saw (Buehler) into small rectangular pieces of approximately 1 × 1 × 5 mm and sealed in the same Corning glass with Torr seal (Varian Associates), leaving the 1 × 1 mm surface exposed. Electrical connections to electrodes were made with silver epoxy. All electrochemical experiments using GC were performed with the 1 × 1 mm exposed area, which was fully illuminated by the laser pulse. For scanning Auger and profilometer experiments, a large (ca. 1 × 1 cm) GC square was illuminated on a ca. 1 mm diameter area, to permit comparison between illuminated and dark regions. Cyclic voltammetry was performed with a CV-1B (Bioanalytical Systems) potentiostat with Ag/AgCl (3 M NaCl) reference and a Pt wire auxiliary electrode. The reference electrode was isolated from the cell by a sintered glass frit (Porosity E, Ace Glass). As explained below, laser activation was combined with differential pulse voltammetry (DPV) by preceding the potential pulse with a laser pulse. Due to fundamental aspects of Nd:YAG laser design, it is not simple to trigger the laser at will; however the Q-switch may be gated by a TTL pulse. With the laser flashlamp running continuously at 10 Hz, the drop knocker pulse from a PAR 174A polarograph was used to trigger a 100-ms monostable vibrator, which gated the Q switch. The result was a laser light pulse arriving at the electrode within 0–100 ms after the drop knocker signal. Since the "drop time" on the polarograph was set to 1 s, a laser pulse preceded each potential pulse by 0.9–1.0 s. For all DPV experiments reported here, the modulation amplitude was 10 mV and the dc scan rate was 2 mV/s.

0003-2700/87/0359-1615$01.50/0 © 1987 American Chemical Society

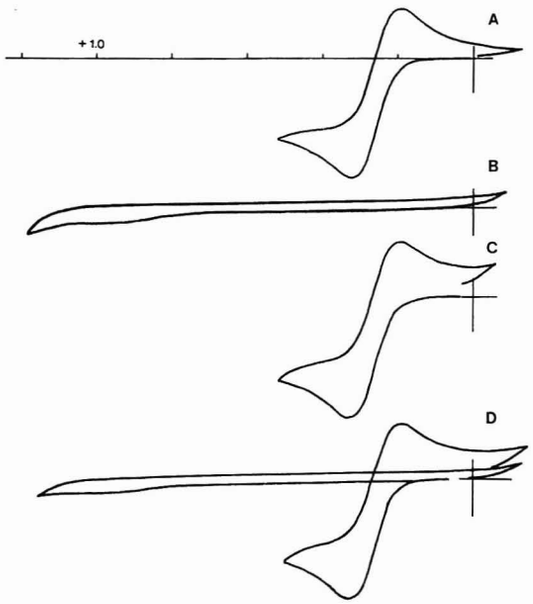

Figure 1. Voltammetry of 3 mM ferrocyanide in the presence of 3 mM phenol in 1 M KCl at a 125 μm diameter Pt electrode. Curve A is prior to and curve B is after phenol film formation by phenol oxidation. Curve C is after a single 30 MW/cm^2 laser pulse (532 nm). The curves labeled D were taken after 40 film formation and removal cycles.

Electrodes were polished conventionally with 600 grit SiC paper followed by 1.0-, 0.3-, 0.05-μm deagglomerated alumina (Baikalox) in a slurry with Nanopure water on a Texmet polishing cloth (Buehler). For the experiment demonstrating Pt oxide removal, the electrode was also cleaned in hot concentrated sulfuric acid before potential cycling. In all cases, thorough rinsing and sonication were performed with Nanopure water.

Ascorbic acid, phenol, hydroquinone, eugenol, *o*-chlorophenol, potassium ferrocyanide, sodium dihydrogen phosphate, sodium monohydrogen phosphate, and potassium chloride were reagent grade and used as received. Dopamine hydrochloride and serotonin hydrochloride were obtained from Sigma Chemical Co. All solutions were prepared fresh daily with Nanopure water (Sybron Barnstead, 16 MΩ) and degassed with nitrogen.

Auger analysis was performed on a Model 595 physical electronic scanning Auger microprobe with an accelerating voltage of 3 kV and a base pressure of 1×10^{-9} torr. The sensitivity factors for appropriate peaks are C (270 eV) = 0.2, O (510 eV) = 0.5, and Cl (180 eV) = 1.0. The scanning electron microscope and profilometer have been described previously (*26*).

RESULTS AND DISCUSSION

Three examples of laser renewal of modified electrode surfaces will be presented here: removal of phenoxy films from GC and Pt, removal of the oxide film from GC formed during electrochemical anodization, and removal of an oxide layer from Pt. In all cases, the laser pulse(s) were delivered in situ without cell disassembly or changing solutions. After discussion of these examples, a solid electrode analogue of the DME will be presented, involving laser activation before each potential pulse in a differential pulse voltammetry experiment. Finally, the long-term effects of laser activation on GC and Pt surfaces will be discussed.

The oxidation of phenol at a Pt electrode results in a phenoxy radical which couples to form a passivating polymeric film on the electrode. After only one potential scan from –0.1 to +1.2 V in the presence of phenol, the oxidation of solution species is completely inhibited. Previous methods of restoring such a passivated electrode involved treatment with a flame (*38*), anodic polarization in an acidic solution of ferric chloride (*39*), or polishing. Figure 1 demonstrates repeated renewal of the polyphenoxy-coated electrode by in situ laser irradiation. A Pt electrode was immersed in a solution containing $Fe(CN)_6^{3-/4-}$ and phenol, and voltammetric scans were conducted

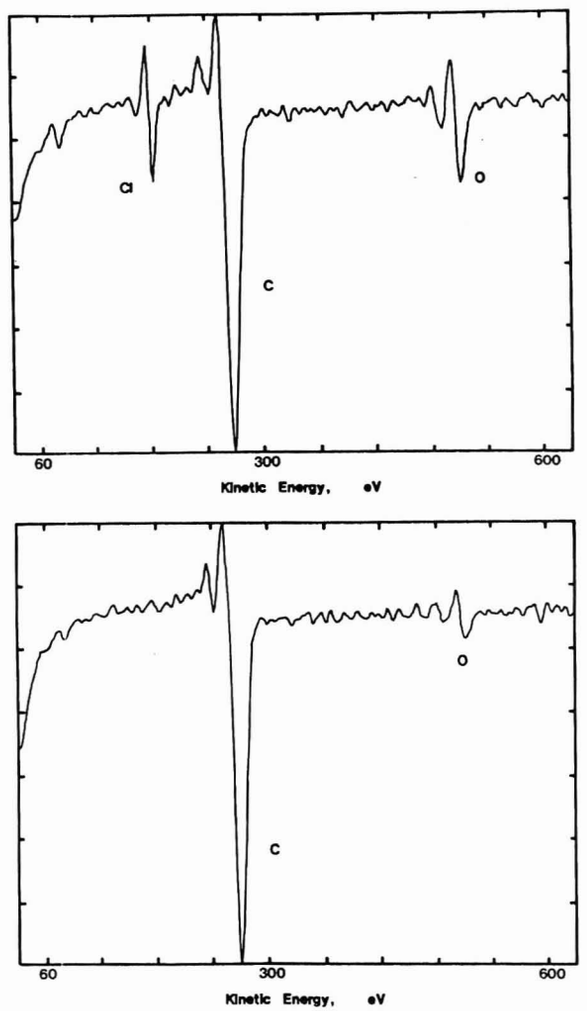

Figure 2. Scanning Auger microprobe survey spectra of nonirradiated (upper) and irradiated (25 MW/cm^2) (lower) regions of GC which had been coated with a film of *o*-chlorophenol. Irradiated region was about 1 mm^2 in area.

either in the $Fe(CN)_6^{3-/4-}$ potential range (–0.1 to +0.5 V vs. Ag/AgCl) or through the phenol oxidation (–0.1 to +1.2 V). The $Fe(CN)_6^{3-/4-}$ couple thus acted as a marker of electrode activity toward solution components. The first two curves are voltammograms prior to (curve A) and after (curve B) phenol film formation. After curve B, the electrode was subjected to a single 30 MW/cm^2 laser pulse in situ,after which the $Fe(CN)_6^{3-/4-}$ couple reappeared (curve C). The voltammograms in Figure 1D are similar to those in B and C but were obtained after 40 complete cycles of film formation and removal. Each cycle consisted of the following steps: seven voltammetric scans from –0.1 to 1.2 V, to deposit a phenol film and passivate the electrode, a single 30 MW/cm^2 laser pulse delivered in situ at 532 nm, a single voltammetric scan from –0.1 to +0.5 V to observe the $Fe(CN)_6^{3-/4-}$ couple. Film removal was demonstrated for 40 cycles at a Pt electrode and the voltammogram looks essentially the same even after 1000 consecutive laser pulses. Throughout the 40 film formation and removal cycles and subsequent 1000 laser pulses, the $Fe(CN)_6^{3-/4-}$ peak current had a relative standard deviation of 3%. For a similar reactivation of a GC electrode, a slightly lower power density is required (24 MW/cm^2) to remove the phenol film. With cycle repetition on GC, there also appears to be a small steady increase in the background and anodic peak current for ferrocyanide (variation ±5% for 35 cycles).

The elemental composition of a glassy carbon electrode surface was determined by scanning Auger microscopy before and after phenol film removal by laser treatment. An electrode

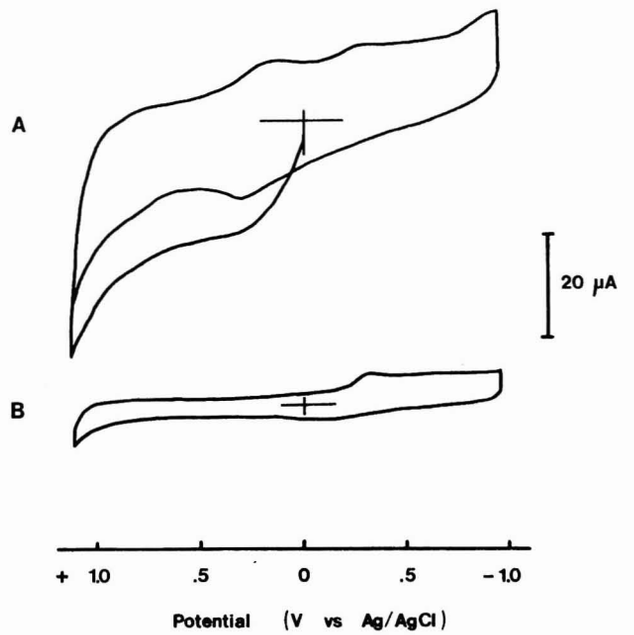

Figure 3. Removal of surface film and redox couple from electrochemically pretreated GC. Voltammogram A is after 5 min at +1.75 V vs. Ag/AgCl in 0.1 M KNO_3. Voltammogram B is after subsequent treatment with three 25 MW/cm^2 laser pulses. Scan rate was 100 mV/s.

was coated with a polymeric film of *o*-chlorophenol by scanning to +1.2 V, then laser irradiated. The chlorophenol derivative was chosen as a marker because the oxygen signal may result from untreated carbon (*13*, *17*, *40*) and the Auger signal displayed by chlorine is relatively strong. Figure 2 shows Auger survey spectra of the irradiated and nonirradiated areas of a chlorophenol film on GC. Comparison of these spectra shows considerable reduction of oxygen in the laser-treated area as reported earlier (*26*) and no detectable Cl in the laser-treated region. It cannot be stated from these results that laser irradiation leaves the electrode surface atomically clean, but from the voltammetry and the Auger spectra, we can conclude that the passivating effects of the film have been removed, and the presence of the chlorine marker was reduced to immeasurable levels on the laser-treated surface.

Electrochemical oxidation of GC surfaces has been shown to enhance electron transfer rates for a variety of redox couples, and good evidence exists for formation of an oxygen-rich surface film (*13*, *17*, *19*, *21*). This film results in a higher background current and may be responsible for enhanced charge transfer. Figure 3 demonstrates that laser treatment can remove the effects of electrochemical pretreatment of GC (5 min at +1.75 V in 0.1 M KNO_3) at GC. Laser treatment reduces background current and results in the loss of the surface waves at ca. +0.3 V usually attributed to quinoid species. The PtOH film formed on Pt during positive potential scans may also be removed with laser activation. After the film was formed during a positive scan to +1.4 V, the potential was held at +0.60 V, where the PtOH film was not yet reduced. As shown in Figure 4, three 10-ns pulses of 60 mJ results in removal of most of the PtOH film as demonstrated in the subsequent potential scan from +0.6 to 0 V. It was necessary to hold the electrode at +0.6 V for approximately 5 s during laser treatment, but a control experiment in the absence of laser treatment showed negligible decrease in PtOH reduction current.

These examples demonstrate fast, facile, in situ, repeated renewal of platinum and GC electrode surfaces under a variety of conditions. When combined with pulse voltammetry, laser renewal would provide a DME analogue for solid electrodes with a repetitively renewed electrode surface free of history

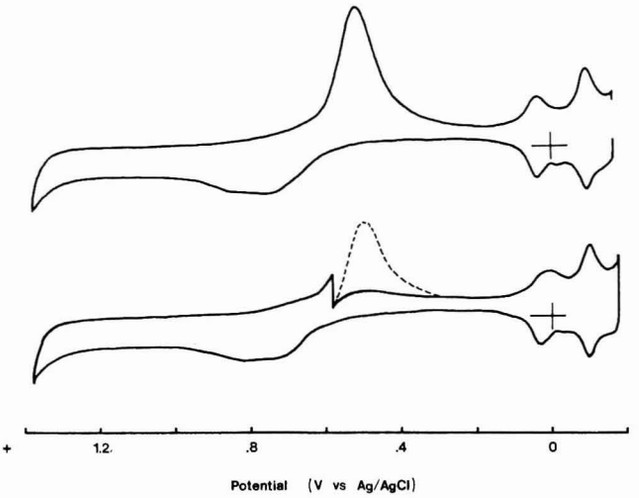

Figure 4. Removal of PtOH layer by laser irradiation. Upper curve is a typical voltammogram of Pt in 1 M H_2SO_4 at a scan rate of 50 mV/s. Lower curve solid line shows effects of three 45 MW/cm^2 laser pulses delivered while the potential was held at +0.6 V after scanning to +1.4 V. Lower curve dashed line is a control experiment where the electrode was held at +0.6 V for 5 s after PtOH formation and then scanned negatively with no laser treatment.

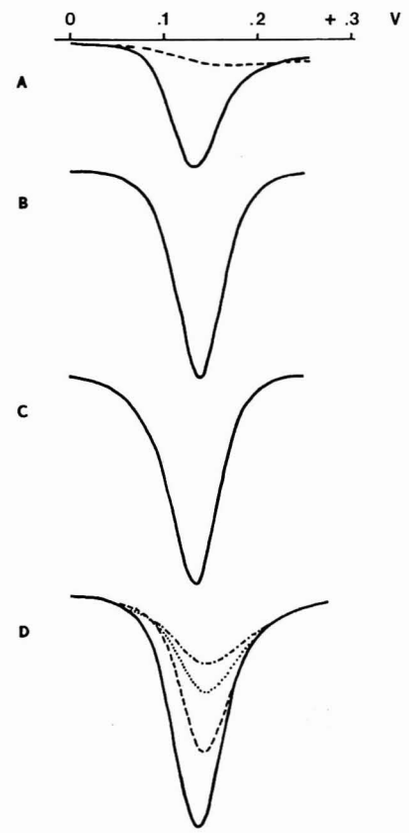

Figure 5. Differential pulse voltammetry of 1 mM dopamine in 0.1 M phosphate, pH 7.4 on GC. Curve A solid line is first scan with no laser treatment and dotted line is the second scan. Curve B is the first scan with a 20 MW/cm^2 laser pulse preceding each potential pulse. Curve C is the 24th scan with the laser on. Curve D shows the decay of the DPV response after the laser is turned off.

effects. Figure 5, curve A, shows an ordinary differential pulse voltammogram of dopamine at a GC electrode at pH 7.4. The electrode response decays rapidly with time due to filming of the products of the oxidation reaction (*41*), and after only one scan, severe passivation has occurred. Scan B and C of the same figure are the results of an experiment designed so that a laser pulse is delivered to the electrode at the time corresponding to the new Hg drop for a DME, such that each potential pulse occurs on a freshly activated surface. As shown

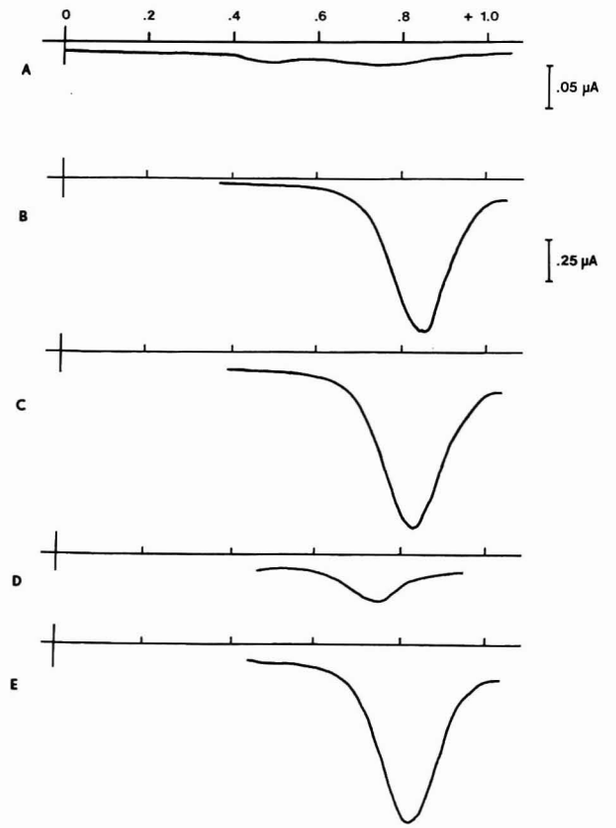

Figure 6. Differential pulse voltammetry of 2 mM phenol in 1 M KCl on GC. Curve A is with no laser treatment. Curve B is the first scan with 25 MW/cm^2 laser pulses before each potential pulse. Curve C is the 22nd such scan. Curve D is the first scan with the laser turned off. Curve E is the first scan after the laser treatment is resumed. Curves B–E have the same vertical scale.

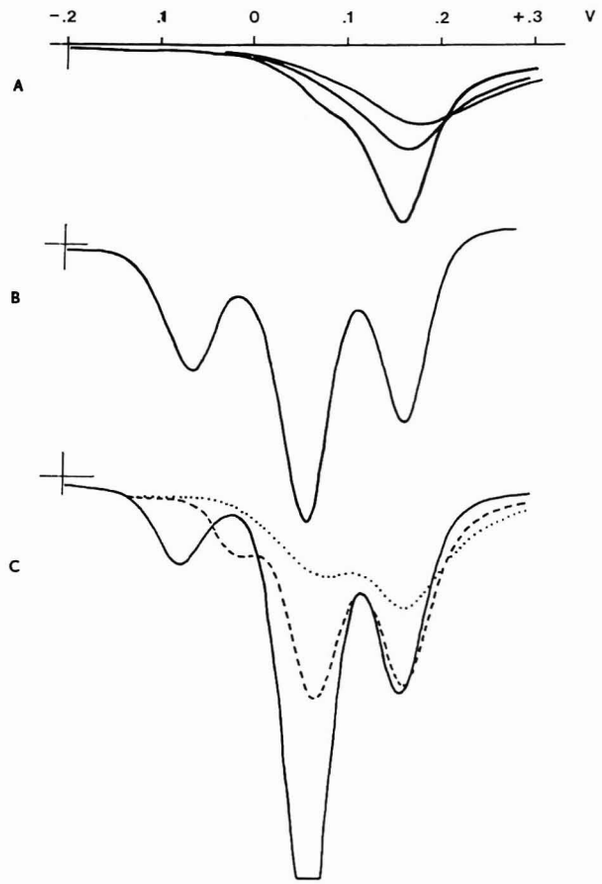

Figure 7. Differential pulse voltammetry of 1 mM ascorbic acid, hydroquinone, and dopamine in 0.1 M phosphate, pH 7.4 on GC. Curve A shows the decaying response for three scans of the mixture with no laser treatment. Curve B is a voltammogram with 25 MW/cm^2 laser pulses preceding each potential pulse. Curves C are the first (solid), second (dashed), and third (dotted) voltammograms after the laser was turned off.

in Figure 5 no degradation of response was observed on successive scans, with 30 voltammetric scans yielding an average peak response of 0.518 ± 0.027 μA. The same behavior was observed for the oxidation of serotonin on GC, with an ordinary electrode lasting for one scan and a laser-renewed surface lasting for at least 28 scans. Once the laser was turned off, the response rapidly degraded. For the phenol oxidation with DPV, the first scan exhibits very poor response, due to electrode passivation during the voltammetric scan. As shown in Figure 6, excellent response is possible on a repetitive basis with laser activation.

More dramatic effects of the combination of laser activation with DPV are apparent in the voltammetry of a mixture of dopamine, hydroquinone, and ascorbic acid, shown in Figure 7. On an ordinary polished GC electrode the three species are severely overlapped due to slow heterogeneous electron transfer kinetics. When a laser pulse precedes each potential pulse, the three components are resolved and peak potentials are close to the thermodynamic values. The improvement in resolution provided by activation has been noted previously for both highly polished GC (*10*) and laser-activated GC (*26*) and results from the increase in electron transfer rate from the activation procedure. The additional features apparent in Figure 7 are two: longevity and effects on adsorption. First, the laser effects are persistent, lasting at least tens of scans and thousands of potential or laser pulses, whereas a polished surface would require disassembly and renewal. Second, the laser reduces adsorption by decreasing the time available for reactants to adsorb. As shown in curve C hydroquinone can exhibit anomalously large peaks due to reactant adsorption after the laser is turned off. In the presence of laser pulses the peak height for hydroquinone is reduced significantly, since any adsorbed material is removed with each laser pulse.

The cumulative physical effects of many laser pulses on the electrode surface during the above experiments were examined with a profilometer and a scanning electron microscope. Figure 8 shows a profilometer trace of a 1 × 1 cm GC piece after 3000 laser pulses at several power densities were applied at a rate of 10 Hz to a 1 mm diameter area of the electrode immersed in water. A well-defined crater with a diameter equal to that of the laser spot was observed, indicating removal of GC from the substrate. The crater depth was power density dependent, but at powers employed for film removal (ca. 25 MW/cm^2) the average ablation rate was about 10 Å/laser pulse. Thus 3000 pulses resulted in a crater of 3 μm depth. A profilometer trace on a laser-treated Pt surface did not show net ablation of the surface but rather surface roughening to the extent of a few micrometers (Figure 9). Note that the abscissa in the profilometer traces is severely compressed relative to the ordinate, so the peaks and valleys are much more gradual than they appear in the traces. While ablation of GC or melting of Pt occur at higher powers, they are not necessarily required for activation or film removal. The power density required to remove polyphenoxy films as shown in Figures 1 and 2 (25 MW/cm^2) causes no observable change in the Pt surface at the profilometer or SEM level. Most of the beneficial effects of laser pulses on GC were at power densities which produce some ablation, but it is not yet clear that ablation is necessary for activation. We are presently attempting to accurately correlate physical and chemical surface effects of lasers with electrochemical performance.

The cost of the Nd:YAG laser used up to this point is high, in the range of $30–35K. The high pulse energy (5–100 mJ)

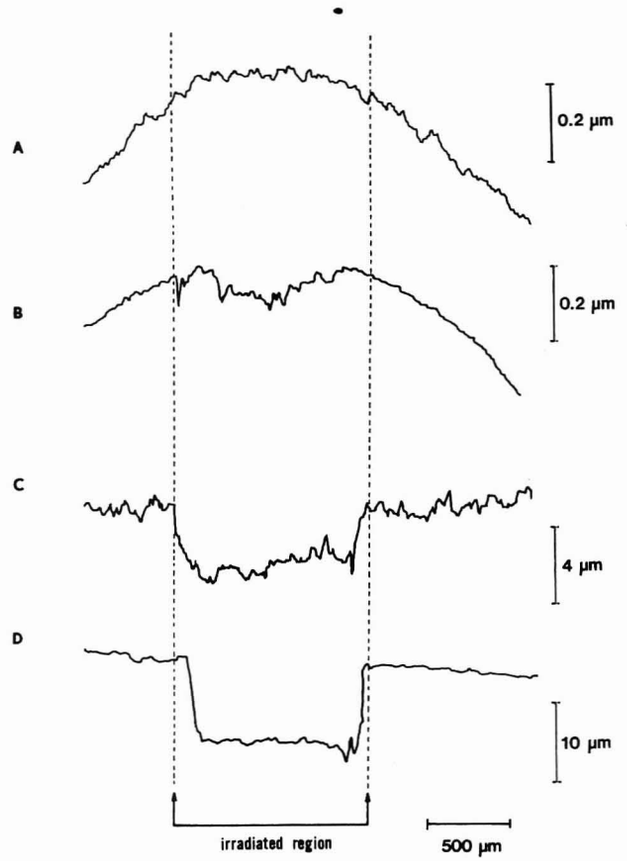

Figure 8. Profilometer traces of GC surface treated with 3000 laser pulses in water: trace A, 10 MW/cm^2; trace B, 13 MW/cm^2; trace C, 22 MW/cm^2; trace D, 44 MW/cm^2.

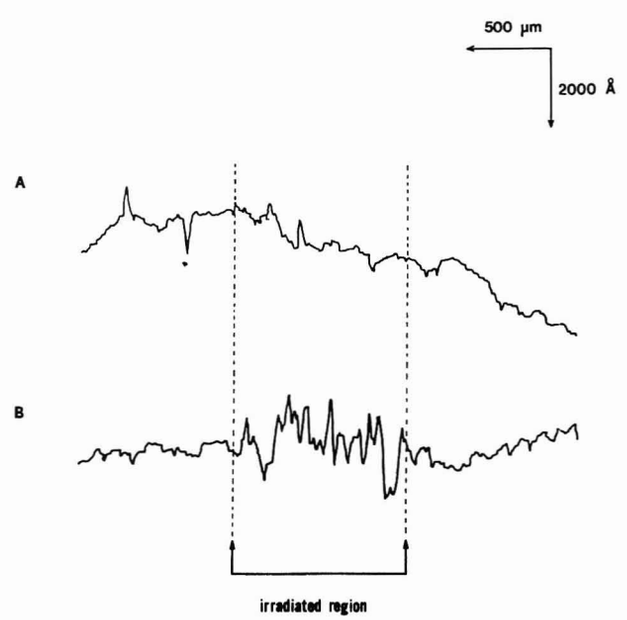

Figure 9. Profilometer traces of a Pt surface treated with 3000 laser pulses in water: curve A, 44 MW/cm^2; curve B, 66 MW/cm^2.

used here is sufficient to achieve the ca. 30 MW/cm^2 power density over a typical voltammetric electrode with a diameter of a few millimeters. It is useful for the present work because the center 1 mm of the beam could be used to maximize the uniformity of the power density. If a smaller, less even beam is acceptable, much smaller lasers may be used. Figure 10 shows laser activation of a 3 mm diameter GC electrode activated by 150-μJ pulses from a small N_2 laser (Laser Scientific VSL 337, list price \$3K) focused to a spot of 200 μm diameter. To produce the bottom voltammogram, approximately 100 laser pulses were distributed over the electrode surface during

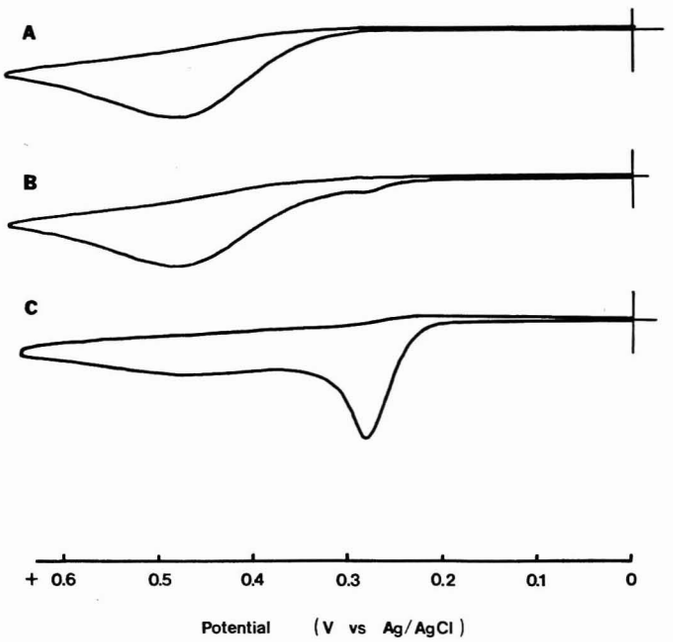

Figure 10. Effect of N_2 laser irradiation on voltammetry on 1 mM ascorbic acid in 0.1 M H_2SO_4. Curve A is a conventionally polished electrode. Curve B is after irradiation of a small fraction (ca. 5%) of electrode area. Curve C is after irradiation of a large fraction of the total electrode area by ca. 100 laser pulses.

a period of ca. 5 s. The ca. 30–90 MW/cm^2 power densities achieved with this small laser were sufficient to activate the oxidation of ascorbic acid where the laser spot impinged on the electrode. If the electrode size were 200 μm, single laser pulses from a small N_2 laser should produce effects comparable to those observed with the Nd:YAG system used for most of the work reported here.

CONCLUSION

Laser pulses from a Nd:YAG laser can repeatedly renew and activate solid electrode surfaces. It is also shown that similar effects can be observed when a low-cost N_2 laser is focused down to a small area on the electrode. The approach is fast (10 ns), in situ, and repeatable on a 100-ms time scale, for a total of at least several thousand repetitions. When combined with differential pulse polarography, several benefits result compared to conventional DPV on solid electrodes. First, history effects from potential pulse to potential pulse are removed, permitting voltammetry on severely passivating materials. Second, the laser pulse activates electron transfer permitting more redox systems to exhibit close to their thermodynamic potentials and in many cases improve resolution. Third, electrode stability is greatly improved due to repetitive renewal of the surface. For a 1 mm thick GC electrode and a 25 MW/cm^2 power density, the electrode would last about 10^6 laser pulses, or 10^3–10^4 DPV scans.

The results reported here indicate that a variety of films and superficial substrate layers may be removed by in situ laser treatment. The excellent behavior of GC or Pt electrodes after thousands of pulses implies negligible long-term degradation of electrode performance, at least in terms of analytical response and electron transfer rate. In addition, it does not appear likely that laser-desorbed materials are returning to the surface in quantities sufficient to affect electrode performance.

The SAM results on chlorophenol films indicate effective removal of the chlorine marker, at least to levels below the SAM sensitivity of about 1 atom % on the surface. Without further spectroscopic data, it is not possible to determine how completely various films or adsorbates are removed, except to say they have no observable effects on the electroanalytical

response. In the case of extremely strongly adsorbed materials on GC, it should always be possible to increase laser power until substrate ablation removes all surface adsorbates. Any technique involving a research quality Nd:YAG laser will be expensive and would not be considered routine. However, the N_2 laser results indicate promise for reducing cost and complexity of a laser activated pulse voltammetry method for small electrodes. Perhaps a more fundamental long-term result of this work will be a better understanding of the relationship between surface properties and electrochemical performance. The effects of laser activation on carbon surface chemistry are presently under investigation.

LITERATURE CITED

(1) Gerhardt, G. A.; Oke, A. F.; Nagy, F.; Moghaddam, B.; Adams, R. N. *Brain Res*. **1984**, *290*, 390.
(2) Nagy, F.; Gerhardt, G. A.; Oke, A. F.; Rice, M. E.; Adams, R. N.; Moore, R. B.; Szentirmay, N. M.; Martin, C. R. *J. Electroanal. Chem*. **1985**, *188*, 85.
(3) Wang, J.; Hutchins-Kumar, L. D. *Anal. Chem*. **1986**, *58*, 402.
(4) Wang, J.; Hutchins-Kumar, L. D. *Anal. Chem*. **1985**, *57*, 1536.
(5) Rusling, J. F. *Anal. Chem*. **1984**, *56*, 575.
(6) Kumau, G. N.; Willis, W. S.; Rusling, J. F. *Anal. Chem*. **1985**, *57*, 545.
(7) Thornton, D. C.; Corby, K. T.; Spendel, V. A.; Jordan, J.; Robbat, A.; Rutstrom, D. J.; Gross, M.; Ritzler, G. *Anal. Chem*. **1985**, *57*, 150.
(8) Laser, D.; Ariel, M. *J. Electroanal. Chem. Interfacial Electrochem*. **1974**, *52*, 291.
(9) Gunsingham, J.; Fleet, B. *Analyst (London)* **1982**, *107*, 896.
(10) Hu, I. F.; Karweik, D. H.; Kuwana, T. *J. Electroanal. Chem. Interfacial Electrochem*. **1985**, *188*, 59.
(11) Plock, C. E. *J. Electroanal. Chem. Interfacial Electrochem*. **1969**, *22*, 185.
(12) Taylor, R. J.; Humffray, A. A. *J. Electroanal. Chem. Interfacial Electrochem*. **1973**, *42*, 347.
(13) Engstrom, R. C.; Strasser, V. A. *Anal. Chem*. **1984**, *56*, 136.
(14) Blaedel, W. J.; Jenkins, R. A. *Anal. Chem*. **1974**, *46*, 1952.
(15) Moiroux, J.; Elving, P. J. *Anal. Chem*. **1978**, *50*, 1056.
(16) Wightman, R. M.; Paik, E. C.; Borman, S.; Dayton, M. A. *Anal. Chem*. **1978**, *50*, 1410.
(17) Cabaniss, G. E.; Diamantis, A. A.; Murphy, W. R., Jr.; Linton, R. W.; Meyer, T. J. *J. Am. Chem. Soc*. **1985**, *107*, 1845.
(18) Wang, J.; Hutchins, L. D. *Anal. Chim. Acta* **1985**, *167*, 325.
(19) Gonon, F. G.; Fombarlet, C. M.; Buda, M. J.; Pujol, J. F. *Anal. Chem*. **1981**, *53*, 1386.
(20) Rice, M. E.; Galus, Z.; Adams, R. N. *J. Electroanal. Chem*. **1983**, *143*, 89.
(21) Falat, L.; Cheng, H. Y. *J. Electroanal. Chem*. **1983**, *157*, 393.
(22) Stutts, K. J.; Kovach, P. M.; Kuhr, W. G.; Wightman, R. M. *Anal. Chem*. **1983**, *55*, 1632.
(23) Fagan, D. T.; Hu, I. F.; Kuwana, T. *Anal. Chem*. **1985**, *57*, 2759.
(24) Evans, J.; Kuwana, T. *Anal. Chem*. **1979**, *51*, 358.
(25) Hershenhart, E.; McCreery, R. L.; Knight, R. D. *Anal. Chem*. **1984**, *56*, 2256.
(26) Poon, M.; McCreery, R. L. *Anal. Chem*. **1986**, *58*, 2745.
(27) Bishop, E.; Hitchcock, P. H. *Analyst (London)* **1973**, *98*, 475.
(28) Kinoshita, K. In *Modern Aspects of Electrochemistry*; Bockris, J. O'M., Conway, B. E., White, R. E., Eds.; Plenum: New York, 1982; Vol. 14, p 557, and references therein.
(29) Arnatore, C.; Saveant, J. M.; Tessier, D. J. *J. Electroanal. Chem. Interfacial Electrochem*. **1983**, *146*, 37.
(30) Goldstein, E. L.; Van de Mark, M. R. *Electrochim. Acta* **1982**, *27*, 1079.
(31) Adams, R. N., *Electrochemistry at Solid Electrodes*; Marcel Dekker: New York, 1969.
(32) Petrii, O. A.; Khomchenko, I. G. *J. Electroanal. Chem. Interfacial Electrochem*. **1980**, *106*, 277.
(33) Austin, D. S.; Polta, J. A.; Polta, T. Z.; Tang, A. P. C.; Cabelka, T. D.; Johnson, D. C. *J. Electroanal. Chem. Interfacial Electrochem*. **1984**, *168*, 227.
(34) Neuberger, G. G.; Johnson, D. C. *Anal. Chim. Acta* **1986**, *179*, 381.
(35) Gilman, S. In *Electroanalytical Chemistry. A Series of Advances*; Bard, A. J., Ed.; Marcel Dekker: New York, 1967, Vol. 2, p 111.
(36) Conway, B. E.; et al. Anal. *Chem*. **1973**, *45*, 1331.
(37) Hoare, J. P. *Electrochim. Acta* **1982**, *27*, 1751.
(38) Hedenburg, J. F.; Freiser, H. *Anal. Chem*. **1953**, *25*, 1355.
(39) Koile, R. C.; Johnson, D. C. *Anal. Chem*. **1979**, *51*, 741.
(40) Van der Linden, W. E.; Dieker, J. W. *Anal. Chim. Acta* **1980**, *119*, 1.
(41) Lane, R. F.; Hubbard, A. T. *Anal. Chem*. **1976**, *48*, 1287.

RECEIVED for review January 2, 1987. Accepted March 23, 1987. This work was supported by the donors of the Petroleum Research Fund, administered by the American Chemical Society, and by the OSU Materials Research Laboratory. Partial support from The Chemical Analysis Division of the National Science Foundation is also acknowledged.

Maximum Likelihood Quantitative Estimates for Peaks: Application to Photoacoustic Spectroscopy

P. E. Poston and J. M. Harris*

Department of Chemistry, University of Utah, Salt Lake City, Utah 84112

The method of maximum likelihood provides an optimum technique for combining measurements of differing uncertainty. The method is appropriate for the quantitative interpretation of peaks from analytical measurements where the peak shape is known or can be measured. Maximum likelihood estimates of sample concentration are derived in this work for several classes of noise having both homogeneous and inhomogeneous variance. The theory is tested by using numerically simulated data and then applied to detection of weak absorbances in liquids using pulsed laser-excited photoacoustic spectroscopy. Maximum likelihood estimates produce detection limits which are a factor 5 lower than a gated measurement at the peak maximum, in agreement with theoretical predictions.

A large fraction of the data produced by analytical chemistry methods appears in the form of peaks rising from a base line as a function of time, wavelength, or applied voltage. Numerous examples could be listed from spectroscopy, chromatography, voltammetry, and flow injection analysis. To determine the amount of sample or analyte responsible for the observed signal is a standard goal of a quantitative analytical procedure. For data that appears in the form of peaks, a number of strategies may be implemented to obtain an estimate of the sample concentration. The most straightforward approach is a measurement at a single point, usually at the signal maximum, corresponding to the peak height (*1*); this strategy may be adequate when the signal-to-noise ratio is large. Recently, the theory and practice of peak integration or peak area measurement were investigated for improving quantitation in chromatographic applications (*2–4*). Since integration has the property of averaging noise while summing up the available signal, it is a simple but potentially powerful method for reducing detection limits when flicker ($1/f$) noise is not predominating.

The effectiveness of a data processing strategy generally improves as more "a priori" knowledge is utilized in the analysis. The concept has been implemented in quantitation

0003-2700/87/0359-1620$01.50/0 © 1987 American Chemical Society

of signal peaks by use of a "matched filter" where the expected shape of a peak is cross-correlated with the raw data (*5–8*). The zero-displacement value of this correlation function yields an optimal estimate of signal magnitude or sample concentration when the noise in the data is constant, that is, when the variance of the error distribution is independent of signal amplitude. The fact that cross-correlation of the data with the model peak shape is an optimal quantitative estimate can be shown either by minimizing the squared deviations in the time domain (*6, 8*) or by maximizing the signal-to-noise ratio in the frequency domain (*7–9*).

In this paper, we derive maximum likelihood or weighted least-squares estimates for the sample quantity of concentration responsible for an observed peak given an expected peak shape. The result of this time domain strategy to fitting signal peaks is equivalent to the frequency domain, "matched filter" approach when the noise power or signal variance is constant; however, the maximum likelihood approach can provide optimal quantitation estimates even with noise sources which depend on signal amplitude such as shot noise or proportional noise. Maximum likelihood estimates of sample concentration are derived for each of the above classes of noise, as well as mixed noise sources. The theory is first tested by using numerically simulated data with pseudorandom Gaussian noise. The technique is then applied to improving detection of weak absorbances in liquids using pulsed laser-excited photoacoustic spectroscopy, the signals from which are characterized by a mix of constant and proportional noise. Maximum likelihood estimates of sample concentration produce detection limits which are a factor 5 lower than gated measurement at the peak maximum, in agreement with theoretical predictions.

THEORY

For a series of n independent measurements of a sample concentration, c_i, each having an uncertainty given by a standard deviation, σ_{c_i}, the estimate of the mean concentration, $\hat{c}$, which maximizes the likelihood of having made the n observations (*10*) is

$$\hat{c} = \sum_i (c_i/\sigma_{c_i}^2)/\sum_i (1/\sigma_{c_i}^2) \quad (1)$$

This least-squares expression weights each measurement by the inverse of the measurement variance. The uncertainty of this weighted average is characterized by a variance $\sigma_{\hat{c}}^2$, which can be found by using propagation of errors (*10*)

$$\sigma_{\hat{c}}^2 = 1/\sum_i (1/\sigma_{c_i}^2) \quad (2)$$

The maximum likelihood formalism can be used to obtain optimal concentration estimates from signal peaks when some known signal shape is expected from the measurement. The signal shape may be obtained by modeling the physical process responsible for the measurement (*11*), obtained by linear regression from a series of standard samples (*12*), or by averaging the signal from a single pure standard (*8*). The use of weighted linear least squares to obtain a concentration estimate requires that the signal, z_i, from a sample having a true concentration, $\bar{c}$, be proportional to a shape function, g_i, which is independent of concentration, such that $z_i = \bar{c}g_i + e_i$, where e_i is the error in the signal. Under this condition, each data point in time provides an independent measure of the sample concentration

$$c_i = z_i/g_i \quad (3)$$

the uncertainty of which depends on the nature of the errors, e_i, in the measured signal.

Constant Noise. When the amplitude of the noise or error is independent of the signal amplitude, then the signal standard deviation is constant, $\sigma_{z_i} = \sigma_z$. The uncertainty of the concentration as determined at each point, i, using eq 3 can be found by a simple propagation of errors, $\sigma_{c_i} = \sigma_z/g_i$. Substituting these values of the standard deviation into the weighted least-squares formula of eq 1, provides a maximum likelihood estimate of the sample concentration

$$\hat{c} = \sum_i z_i g_i/\sum_i (g_i^2) \quad (4)$$

This result corresponds to calculating the zero-displacement value of the cross-correlation between the signal and the shape function, divided by a constant which is proportional to the mean square value of the shape function. This result is identical with the "matched filter" estimate of signal magnitude, previously described (*5–8*). The power of the maximum likelihood strategy becomes more evident when dealing with noise sources having inhomogeneous variance, such as shot or proportional noise described in the following sections.

Shot Noise. If a signal peak arises from a very weak current or a faint optical signal, then the signal uncertainty may be dominated by the small number of electrons or photons being detected. Under these circumstances, the standard deviation of the signal is predicted by Poisson statistics (*10*) to be proportional to the square root of the mean signal amplitude, $\sigma_{z_i} = k'(\bar{z}_i)^{1/2} = k'(\bar{c}g_i)^{1/2}$. The uncertainty in concentration at each point, i, is found by propagation of errors through eq 3, where $\sigma_{c_i} = k'(\bar{c}/g_i)^{1/2}$. The concentration uncertainty for shot noise limited signals depends on the square root of the inverse peak shape amplitude rather than simply the inverse of the amplitude as in the constant noise case. Substituting this concentration uncertainty relationship into eq 1 yields the following optimal estimate of sample concentration:

$$\hat{c} = \sum_i z_i/\sum_i g_i \quad (5)$$

When the signal uncertainty is dominated by shot noise, therefore, the maximum likelihood estimate for the concentration is the area divided by a constant corresponding to the area of the peak shape function.

Proportional Noise. When the predominant noise present in a signal arises from fluctuations in the measurement sensitivity, such as amplifier gain noise or excitation source noise, the rms noise amplitude or standard deviation of the signal increases in proportion to signal size, $\sigma_{z_i} = k\bar{z}_i = k(\bar{c}\, g_i)$. The corresponding uncertainty in the concentration obtained at each point using eq 3 can again be found from propagation of errors. This yields a simple result, $\sigma_{c_i} = \sigma_{z_i}/g_i = k\bar{c}$, indicating that the error in concentration is constant, independent of i. Substituting this result into eq 1 shows that the concentration measurements, c_i, are unweighted in the maximum likelihood estimate, which corresponds to weighting the observed signal values, z_i, by the *inverse* of the peak shape function

$$\hat{c} = (1/N)\sum_i c_i = (1/N)\sum_1 (z_i/g_i) \quad (6)$$

Mixed Noise Sources. While proportional noise may dominate the uncertainty of a signal in regions where the signal amplitude is large, it is unusual to find the entire waveform governed by proportional noise particularly in regions where the amplitude is small. In the vicinity of the base line with either a small value of g_i or $\bar{c}$, it is probable that signal uncertainty will not continue to decrease in proportion to signal amplitude but will rather reach a constant noise limit. Since the proportional noise and constant noise would, in general, be derived from different, independent sources, their contributions tothe overall signal variance would equal the sum of the two noise variances

$$\sigma_{z_i}^2 = k^2\bar{z}_i^2 + \sigma_z^2 \quad (7)$$

This somewhat more complex form of the signal variance can be propagated through eq 3 to determine the concentration uncertainty which is substituted into eq 1. The resulting weighted least-squares estimate of the sample concentration is given by

$$\hat{c} = \frac{\sum[z_i g_i/(k^2\bar{z}_i^2 + \sigma_z^2)]}{\sum_i[g_i^2/(k^2\bar{z}_i^2 + \sigma_z^2)]} \quad (8)$$

For mixed proportional and constant noise, therefore, the signal contribution to maximum likelihood estimate varies between being weighted inversely with the peak shape amplitude and being weighted in proportion to the peak shape amplitude depending on the relative size of the two noise sources. This model for mixed proportional and constant noise was found to accurately describe the uncertainty in pulsed laser-excited photoacoustic spectroscopy, where proportional noise is related to shot-to-shot variation in the laser pulse energy and the acoustic sensitivity while a constant amplitude noise from the detector electronics dominates when the sample absorbance is small.

Error Estimates. For any of the above methods of concentration or amplitude estimation, the uncertainty of the estimate can be determined by using eq 2, where the concentration variance associated with each data point in the peak, $\sigma_{c_i}^2$, depends on the uncertainty of the signal, $\sigma_{c_i}^2 = \sigma_{z_i}^2/g_i^2$. For mixed constant and proportional noise, the concentration estimate determined using Equation 8 should exhibit a variance given by

$$\sigma_{\hat{c}}^2 = 1/\sum_i[g_i^2/(k^2\bar{z}_i^2 + \sigma_z^2)] \quad (9)$$

This formula is appropriate for predicting the concentration variance with any relative fraction of constant and proportional noise. It provides a theoretical basis to test the improvement in precision which a maximum likelihood approach affords for peak quantitation in general and for photoacoustic detection in particular.

EXPERIMENTAL SECTION

Numerical Simulations. Numerical studies were carried out on a Leading Edge Model D personal computer running Fortran 77. A Gaussian distributed pseudo-random-number generator from the NAG subroutine library was used to produce model noise having a mean of zero and a standard deviation of unity. Different sequences were added to each data set and scaled to the desired signal-to-noise ratio. Constant noise, the standard deviation or root mean square (rms) amplitude of which is independent of signal intensity, was modeled by multiplying the output from the random number generator by a single scaling factor before adding it to model signals. Proportional noise was scaled in proportion to the signal magnitude.

Photoacoustic Measurements. The diagram of the photoacoustic spectroscopy experiment, used to test the above concepts in maximum likelihood estimation, is shown in Figure 1. A Nd:Yag laser pumped dye laser system (QuantaRay Model DCR-2) was used for sample excitation. The 1.06-μm, 20-Hz output of the Nd:YAG laser was frequency doubled to 532 nm and used to pump the dye laser which was operated at 560 nm and a pulse energy of 3 mJ. The dye laser beam was focused with a 45-cm focal length lens. The sample cell was positioned approximately 5 cm before the beam waist to avoid nonlinear optical effects, dielectric breakdown, and bubble formation.

The cylindrical sample cell was constructed of 15 mm i.d. Pyrex tubing, 5.0 cm in length, with two glass tee sections on top to accommodate the piezoelectric transducer assembly and filling port, respectively. To a third tee section below the cell was attached a standard Teflon stopcock. An aspirator was connected to the stopcock to facilitate easy changing of samples during data collection. This also ensured that the cell remained in exactly

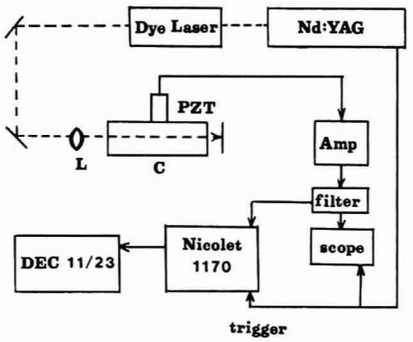

Figure 1. Block diagram of pulsed-laser excited photoacoustic spectrometer: L is a 45-cm focal length lens, C is the sample cell, and PZT is the piezoelectric transducer. Details of the instrumentation are described in the text.

the same position relative to the laser beam throughout the experiment. The piezoelectric transducer assembly was based on the design of Tam and Patel (*13*).

The output from the piezoelectric transducer was amplified with a 3-MHz bandwidth preamplifier having a voltage gain of approximately 200, as previously described (*14*). Background signals arising from ambient acoustic noise and vibrations were removed with a four-pole active filter having a low frequency cutoff at approximately 10 kHz, constructed from Analog Devices Model 509 operational amplifiers. The signal from the filter was fed to a 60-MHz oscilloscope (Tektronix Model 2213) for monitoring and a signal averager (Nicolet Model 1170) for data acquisition. The signal was digitized at 5 MHz for 256 channels using a flash converter plug-in unit (Nicolet Model 1134); 256 photoacoustic transients were collected and averaged for each experiment. The averaged transient signal was transferred via a serial interface (DEC Model D1V11-J) to a DEC 11/23 microcomputer for analysis. All data analyses were performed on the 11/23 using Fortran IV routines.

Azulene (Aldrich) was chosen as a sample analyte for this study due to its high photostability in the visible region. The solvent, carbon tetrachloride, glass distilled, was vacuum degassed in an ultrasonic cleaner prior to mixing solutions. Degassing was virtually complete after about 10 min. Solutions were made by dilution of a single stock solution, the absorbance of which was verified with a Cary 17D spectrophotometer. Sample solutions were filtered with PTFE 0.5-μm-pore filters made by Millipore, which resulted in greatly reduced stray light from particulates.

A typical data gathering and manipulation sequence is as follows. First, six replicates of the solvent blank were acquired. In general, six replicates were taken since F values and Student's t values do not change significantly beyond this point. This was followed by the lowest absorbing sample (six replicates), and then another set of solvent blank measurements was made. The two blank data sets were averaged together, and this background signal was subtracted from the sample signal. This procedure was repeated for successively higher absorbance samples. Continuous blank measurements were made to avoid uncertainties from any slowly changing background signal level.

All data were corrected for dc offset by determining the average of the transient and subtracting that value from the entire transient. The data were also converted to the piezoelectric signal in volts by dividing by the preamplifier gain, the sensitivity of the flash converter plug-in unit, and by the number of averages. The first 10 μs of the fitting function, before the arrival of the first acoustic pulse, was arbitrarily set to zero to avoid having rf noise from the Q switch influence the quantitative results.

RESULTS AND DISCUSSION

Numerical Studies. The use of maximum likelihood estimates for quantitation of analytical peaks was first evaluated by using numerically generated data so that the noise characteristics could be controlled. Peaks were simulated as Gaussian functions having an arbitrary maximum of unity and differing amounts of proportional and constant noise. Two examples are shown in Figure 2, parts a and b, where the ratios of the rms proportional noise amplitude and the rms constant

Table I. Maximum Likelihood Concentration Estimates for Numerically Simulated Peaks

kz_p/σ_z[a]	$(S/N)_p$[b]	$\sigma_{\hat{c}}$[c]	$s_{\hat{c}}$[d]	σ_{c_p}[e]	s_{c_p}[d]	$\sigma_{c_p}/\sigma_{\hat{c}}$[f]
10	3.8	2.2×10^{-2}	3.1×10^{-2}	2.1×10^{-1}	2.6×10^{-1}	9.2
	8.5	1.1×10^{-2}	1.6×10^{-2}	1.4×10^{-1}	1.2×10^{-1}	12.7
	12.7	7.4×10^{-3}	1.0×10^{-2}	9.6×10^{-2}	7.8×10^{-2}	12.9
	21.2	4.5×10^{-3}	6.2×10^{-3}	5.9×10^{-2}	4.7×10^{-2}	13.2
	29.6	3.2×10^{-3}	4.4×10^{-3}	4.2×10^{-2}	3.4×10^{-2}	13.2
2	4.2	2.1×10^{-2}	3.9×10^{-2}	1.7×10^{-1}	2.4×10^{-1}	8.3
	5.3	1.7×10^{-2}	3.1×10^{-2}	1.5×10^{-1}	1.9×10^{-1}	8.7
	6.2	1.6×10^{-2}	2.9×10^{-2}	1.6×10^{-1}	1.6×10^{-1}	9.9
	9.3	1.0×10^{-2}	1.9×10^{-2}	1.1×10^{-1}	1.1×10^{-1}	10.2
	15.6	6.3×10^{-3}	1.2×10^{-2}	6.5×10^{-2}	6.4×10^{-2}	10.4

[a] Ratio of proportional to constant noise at peak maximum. [b] Signal-to-noise ratio at peak maximum. [c] Relative standard deviation of weighted least-squares concentration estimate determined using eq 9. [d] Sample relative standard deviation of concentration estimates, n = 10. [e] Relative standard deviation of peak height concentration estimate determined using eq 10. [f] Improvement in precision of maximum likelihood estimate over peak height measurement.

noise amplitude at the peak maximum are 10.0 and 2.0, respectively. Comparing these plots shows that the signal-to-noise ratio of the data dominated by proportional noise is considerably more independent of signal amplitude. For both examples, the weighted least-squares fit is also plotted given by $\hat{z}_i = \hat{c}g_i$, where the concentration estimated, $\hat{c}$, is determined from eq 8. For an ideal fit, the weighted residuals, $(\hat{z}_i - z_i)/\sigma_{z_i}$, should form a uniform distribution about zero spanning the t limits of the Gaussian distribution. While a few outliers are found, the residuals are generally random and confined to a range of $\pm 3\sigma_{z_i}$, as shown by the example in Figure 2c.

As a test of the theory developed in the section above, the uncertainty of the concentration estimate predicted by eq 9 can be compared to a sample standard deviation obtained from replicated numerical results. For two relative fractions of proportional and constant noise and five different signal to noise ratios, this comparison was made with ten replicates at each condition to determine the sample standard deviation; the results are reported in Table I. In all cases, the predicted and observed standard deviations were indistinguishable at 95% confidence, according to an F test (*10*).

A second goal of these numerical simulations was to determine the improvement in precision of a maximum likelihood estimate relative to a more naive concentration determination, such as a measurement of peak height. The concentration estimate derived from the peak height, $c_p = z_p/g_p$, is drawn from a population having a variance

$$\sigma_{c_p}^2 = (k^2\bar{z}_p^2 + \sigma_z^2)/g_p^2 \qquad (10)$$

which is a single term at the maximum or peak value, $i = p$, from the error expression given in eq 9. This prediction of the variance in the concentration estimate for single measurements of peak height was compared to the sample variance of replicated numberical results, listed in Table I as their corresponding standard deviations. The predicted and observed variances were again indistinguishable at the 95% confidence level according to an F test.

The validity of the variance predictions of eq 9 and 10, evident from the numerical studies, allows one to evaluate the improvement in precision of the maximum likelihood estimate over a simple peak height measurement. The improvements in precision are calculated from the ratios of concentration standard deviations, $\sigma_{c_p}/\sigma_{\hat{c}}$, and are also listed in Table I. The main trend found in these results is that the maximum likelihood method is more effective for signals increasingly dominated by proportional noise. This is to be expected since, for the 100% proportional noise case, the signal to noise ratio of each point in the peak is constant and contributes at equal concentration precision to the concentration estimate. Under these circumstances, one expects that the improvement in concentration standard deviation over a peak height measurement would reach a limiting value of $n^{1/2}$, corresponding to $256^{1/2} = 16$ for these studies; this result was indeed observed in a numerical simulation by setting the constant noise var-

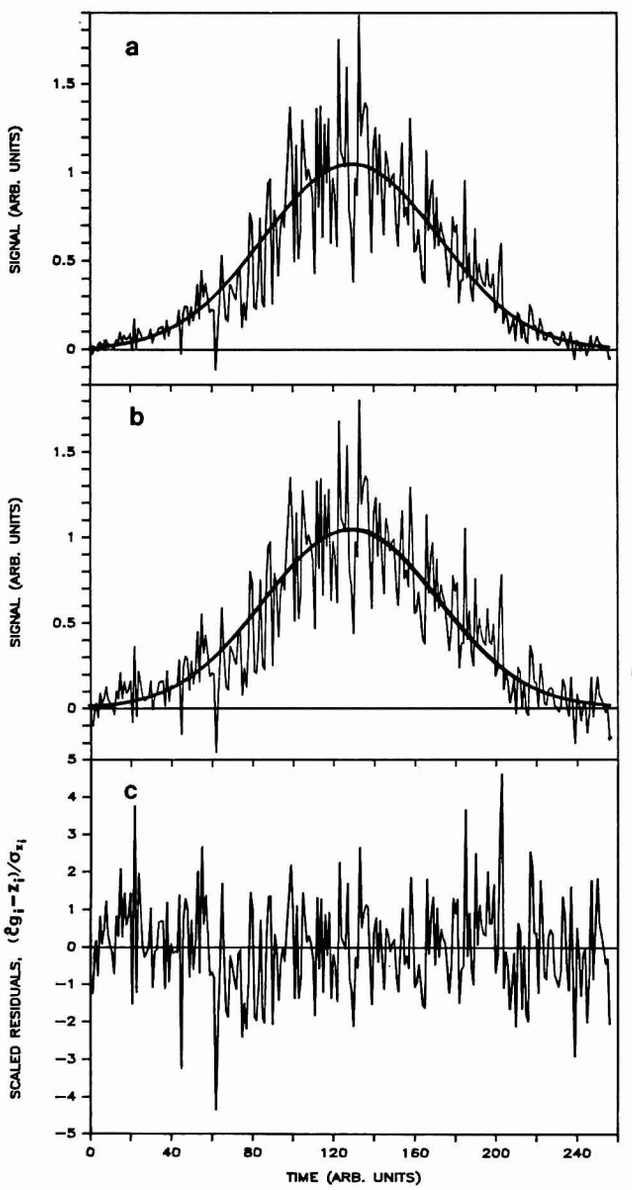

Figure 2. Maximum likelihood quantitative estimates for numerically simulated peaks. The ratios of the rms proportional noise amplitude and the rms constant noise amplitude at the peak maximum are 10.0 and 2.0 for parts a and b, respectively; the heavy line indicates the best fit of the data ($\hat{c}g_i$). Part c shows the scaled residual error for part b $[(\hat{c}g_i - z_i)/\sigma_{z_i}]$.

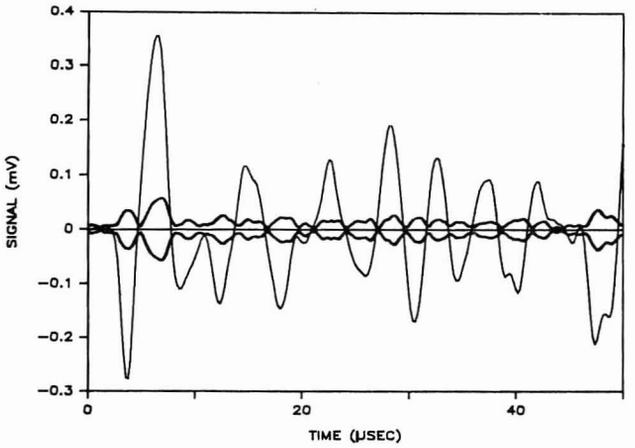

Figure 3. Average photoacoustic transient for azulene in CCl_4, $Z = 4.7 \times 10^{-4}$ cm^{-1}. The standard deviations of each of the 256 points are plotted as symmetric error bounds about the origin using a heavy line.

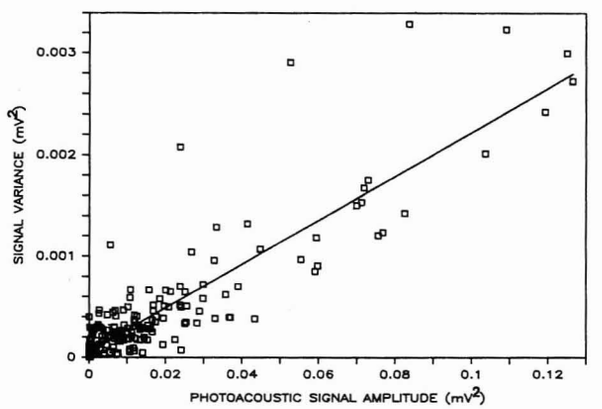

Figure 4. Photoacoustic signal variance vs. the square of signal magnitude. Heavy line is the linear least squares best fit to eq 7.

iance in the simulation equal to zero.

Application to Photoacoustic Measurements. In order to apply weighted least squares analysis to photoacoustic data, the linearity of the measurement must be established. Photoacoustic data were gathered on six azulene samples prepared in carbon tetrachloride uniformly spanning the absorbance range of 1.9×10^{-5} to 4.7×10^{-4} cm^{-1}. Measuring the amplitude at the maximum of the largest photoacoustic peak yielded a linear calibration plot having a correlation coefficient for an unweighted linear least squares fit, $r = 0.987$, and no systematic deviation from linearity. The slope of the calibration line was 0.70 ± 0.05 V/AU and the intercept was 5 ± 11 μV, indicating that the line passes through the origin within experimental error.

To properly compute a maximum likelihood estimate of sample concentration from an experimental data set, unlike the numerical simulation studies where the magnitudes of the proportional and constant noise were known in advance, one must determine the magnitudes of these errors from replicate measurements. This task was accomplished by averaging six replicates of the photoacoustic measurement on the highest absorbing sample, $A = 4.7 \times 10^{-4}$ cm^{-1}, and determining the reproducibility of each point along the photoacoustic transient. A plot of the average signal and the standard deviation shown as error bounds in Figure 3 reveals significant proportional character in the noise along with a small constant noise contribution which keeps the error bounds from vanishing when the signal size is small. If the proportional and constant noise sources are independent, then one would expect the signal variance to follow the relationship of eq 7. This was assessed by rearranging the data from Figure 3 as a histogram of signal

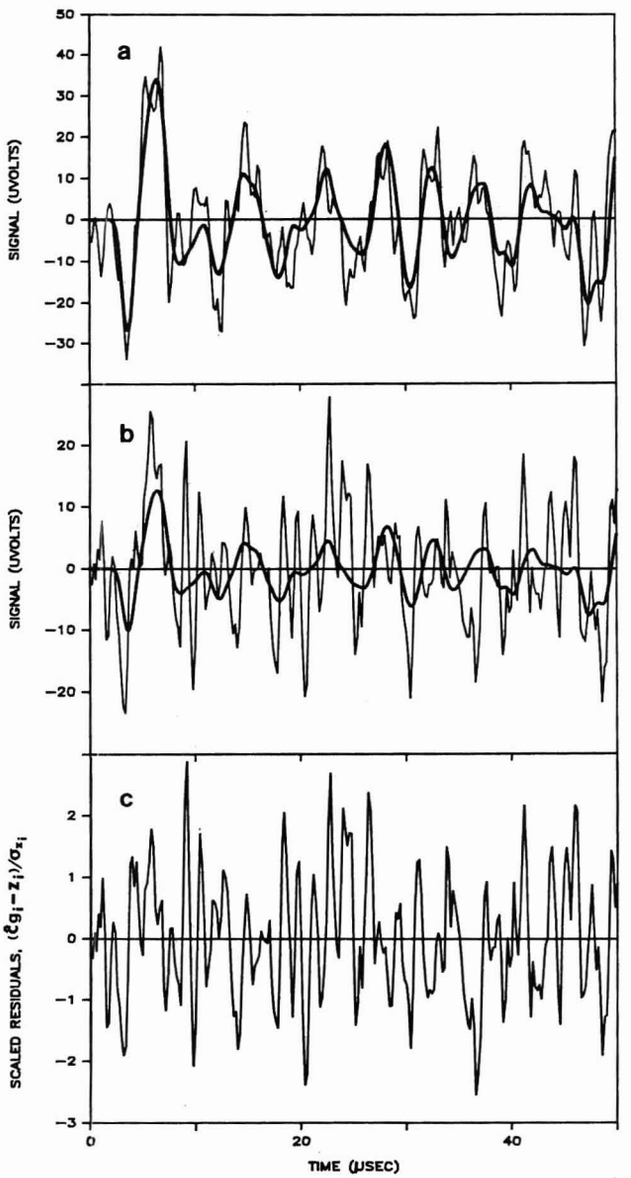

Figure 5. Maximum likelihood absorbance estimates for photoacoustic signals. Photoacoustic transients from azulene in CCl_4 in parts a and b have absorbances $A = 4.7 \times 10^{-5}$ cm^{-1} and 1.9×10^{-5} cm^{-1}, respectively; the best fits to the data ($\hat{c}g_i$) are shown as heavy lines. Part c shows the scaled residual error for part b $[(\hat{c}g_i - z_i)/\sigma_{z_i}]$.

variance plotted vs. the square of the signal magnitude as shown in Figure 4. The slope of this plot is the proportionality factor, k^2, for the proportional noise variance, the square root of which is $k = 0.21 \pm 0.01$. The intercept is the constant noise variance, the square root of which is $\sigma_z = 7.8$ μV. The primary source of the constant noise was traced to the piezoelectric detector and its amplification electronics since nearly the same level of constant noise was observed with the laser beam blocked. Some of the proportional noise appears to be related to pulse-to-pulse fluctuations in the laser energy; if the Q switch hold-off voltage is adjusted to be less than optimal, leading to erratic pulse energy fluctuations, the proportional noise factor increases significantly. Proportional noise can also arise from convection, driven by laser heating of the illuminated region, giving rise to gradients in the solvent density which would affect the photoacoustic response (*13*).

The average photoacoustic transient for the highest concentration sample plotted in Figure 3 was also used as the model for the shape function, g_i, in order to obtain maximum likelihood quantitative estimates for lower concentration samples including several sets of replicates of the solvent blank. The results of these studies are summarized in Figure

Table II. Maximum Likelihood Absorbance Estimates for Photoacoustic Signals[a]

A, cm^{-1}	$\hat{A}$, cm^{-1}	$\sigma_{\hat{A}}$, cm^{-1}	$s_{\hat{A}}$, cm^{-1}	σ_{A_p}, cm^{-1}	s_{A_p}, cm^{-1}	LOD$_{\hat{A}}$[b]	LOD$_{A_p}$[b]	$\sigma_{A_p}/\sigma_{\hat{A}}$	$s_{A_p}/s_{\hat{A}}$
$4.7\ (\pm 0.1) \times 10^{-5}$	4.7×10^{-5}[c]	2.2×10^{-6}	2.7×10^{-6}	1.4×10^{-5}	8.3×10^{-6}	1.1×10^{-5}	3.4×10^{-5}	6.2	3.0
$1.9\ (\pm 0.2) \times 10^{-5}$	1.5×10^{-5}[c]	2.0×10^{-6}	2.3×10^{-6}	1.2×10^{-6}	7.8×10^{-6}	9.2×10^{-6}	3.2×10^{-5}	6.0	3.4
solvent blank 1	6.0×10^{-6}	2.2×10^{-6}	2.3×10^{-6}	1.2×10^{-5}	6.1×10^{-6}	9.4×10^{-6}	2.4×10^{-5}	5.4	2.6
solvent blank 2	5.4×10^{-6}	2.1×10^{-6}	2.3×10^{-6}	1.2×10^{-5}	1.6×10^{-5}	9.2×10^{-6}	6.2×10^{-5}	5.7	6.9
solvent blank 3	4.0×10^{-6}	2.1×10^{-6}	1.6×10^{-6}	1.2×10^{-5}	6.0×10^{-6}	6.7×10^{-6}	2.4×10^{-5}	5.7	3.7
solvent blank 4	1.8×10^{-6}	2.0×10^{-6}	1.7×10^{-6}	1.2×10^{-5}	1.1×10^{-5}	7.2×10^{-6}	4.4×10^{-5}	5.8	6.7

[a] The results for each sample represent six replicate trials. For definitions of terms, see footnotes in Table I. [b] Limits of absorbance detection defined as (*14*), LOD$_A$ = $2t$(one-sided)S_A. [c] Results represent the net sample absorbance since the blank was subtracted from these photoacoustic signals.

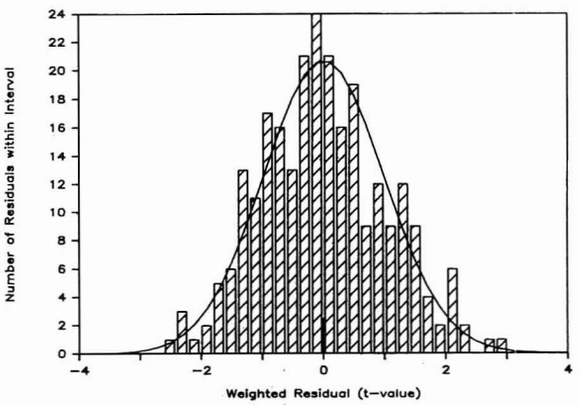

Figure 6. Histogram of the scaled deviations from photoacoustic transient of Figure 5c. Solid line is the model Gaussian error distribution with no adjustment of parameters (zero mean, unit standard deviation, area equals 256 observations).

5 and Table II. In order to assess the impact of the data analysis on the detection of weak absorbing solutions, the quantitative results are presented not in terms of concentration of the particular chromophore detected but rather in terms of absorbance per unit path length, which is equal to the product of molar absorptivity and concentration. Path length is factored out of the sample absorbance since the magnitude of the acoustic signal does not depend on path length as long as it exceeds the diameter of the piezoelectric transducer, which is 0.4 cm in this work.

The capability of a maximum likelihood estimate to extract quantitative information from noisy data is illustrated by the results in Figure 5. For the 1.9×10^{-5} cm^{-1} sample in Figure 5b; for example, the maximum likelihood estimate is in error by only 20% despite the peak signal to noise ratio being only 1.6. The scaled residuals, shown in Figure 5c, are random and of a magnitude expected for the experimental error, indicating that most of the quantitative information has been successfully extracted. As a test of the Gaussian model for the error distribution used as the underlying basis to obtain a maximum likelihood estimate of eq 1, a histogram of the scaled deviations of Figure 5c is plotted in Figure 6 along with the model error distribution with no adjustment of parameters (zero mean, unit standard deviation, area equals number of observations). The noise of the photoacoustic signals is remarkably Gaussian, which accounts in part for the agreement between the experimental results and theoretical predictions described below.

The experimental results are quantitatively summarized in Table II where standard deviations of peak height and maximum likelihood estimates, predicted by eq 9 and 10, respectively, are compared with sample standard deviations obtained from replicate measurements. As with the simulation studies, the expected errors could not be distinguished, using an F test at 95% confidence, from those predicted by theory. The sample standard deviations of peak height measurements, s_{A_p}, appear to be more erratic than those derived from fitting the complete photoacoustic transient, $s_{\hat{A}}$, probably due to the dependence of the former on the small number of particular data points drawn into the sample.

The limits of absorbance detection (*14*) for maximum likelihood and peak height determinations are also reported in Table II based on the observed sample standard deviations of the replicated results. There does not appear to be a significant increase in the limits of detection for absorbance measurements made with samples exhibiting absorbance background as high as 5×10^{-5} cm^{-1} which is consistent with the predictions of eq 9 and 10. The improvement in quantitative precision at the blank level over a peak height measurement given by a maximum likelihood estimate of the complete transient record was predicted by eq 9 and 10 to be a factor of 5.6 (±0.2) on average while the observed improvement based on replicate measurements was found to average about 5.0 (±2). The uncertainty of this latter result is related to the rather erratic behavior of the peak height standard deviations, discussed above.

The photoacoutstic transients making up the four sets of solvent blank replicates were processed without any background or blank subtraction step. The four determinations of the blank absorbance, $\hat{A}$, each of which is the average of six measurements, exceed the decision limit (*14*) for detecting nonzero absorbance, $[t(\text{one-sided})s_{\hat{A}}/6^{1/2}]$, in all four trials. If the four results are averaged together, the absorbance of carbon tetrachloride at 560 nm may be estimated, $A = 4.3\ (\pm 0.8) \times 10^{-6}$ cm^{-1}. This is similar in magnitude to results obtained at 514.5 nm using thermal lens methods which produced an average value of $5.6\ (\pm 0.6) \times 10^{-6}$ cm^{-1} (*17*, *18*).

As a final test of the stability of the signal background and its influence on the results, the target fitting function, g_i, was first orthogonalized against the blank signal using a Gram–Schmidt orthonormalization procedure (*15*, *16*) before application of the weighted least-squares fit. Orthonormalization has been shown to be a powerful method for discriminating against large fluctuating backgrounds from signals having characteristic time behavior different than an absorption signal, such as stray light on the transducer or rf noise (*15*). Such a fitting function can be adapted to a maximum likelihood estimate if the weighting factors from the noise distribution are derived independently of the orthonormalized model to which the data will be fit. The photoacoustic data were carried through this procedure and compared with the results in Table II; the precision and accuracy of the estimated sample absorbances, however, were indistinguishable from those obtained without prior orthogonalization of g_i. One can conclude that fluctuations in the background signal in this particular case are not dominating the uncertainty of the results.

CONCLUSIONS

The method of maximum likelihood provides an optimum technique for combining measurements of differing uncertainty which is appropriate for the quantitative interpretation of peaks from analytical measurements where the peak shape is known or can be measured. A propagation of errors cal-

culation allows one to predict both the uncertainty in the quantitative results produced by this method and the improvement in precision relative to other methods. The importance of maintaining a reproducible peak shape for this approach to data analysis should not be overlooked. In our early attempts to apply the method to photoacoustic detection, we used a sample cell which was removed between measurements to change samples. This procedure did not maintain a reproducible spatial relationship between the excitation beam and the piezoelectric transducer and produced random phase shifts in the acoustic waveform between measurements. In retrospect, it is not surprising that these earliest attempts to apply the method of maximum likelihood met with little success since the peak shape was not stable.

ACKNOWLEDGMENT

The authors wish to express their appreciation to D. Heisler, D. Plumb, and M. Scott for their help with the detector electronics and data acquisition. H. Morrow is acknowledged for his fabrication of the photoacoustic cell.

LITERATURE CITED

(1) Sweileh, J. A.; Cantwell, F. F. *Can. J. Chem.* **1985**, *63*, 2559–2563.
(2) Taraszewski, W. J.; Haworth, D. T.; Pollard, B. D. *Anal. Chim. Acta* **1984**, *157*, 73–82.
(3) Laeven, J. M.; Smit, H. C. *Anal. Chim. Acta* **1985**, *176*, 77–104.
(4) Synovec, R. E.; Yeung, E. S. *Anal. Chem.* **1985**, *57*, 2162–2167.
(5) Mann, C. K.; Goleniewski, J. R.; Sismandis, C. A. *Appl. Spectrosc.* **1982**, *36*, 223.
(6) Lam, R. B. *Appl. Spectrosc.* **1983**, *37*, 567–569.
(7) Dyer, S. A.; Hardin, D. S. *Appl. Spectrosc.* **1985**, *39*, 655–662.
(8) Nickolaisen, S. L.; Bialkowski, S. E. *J. Chem. Inf. Comput. Sci.* **1986**, *26*, 57–59.
(9) Papoulis, A. *Probability, Random Variables, and Stochastic Processes*; McGraw-Hill: New York, 1965.
(10) Bevington, P. R. *Data Reduction and Error Analysis for the Physical Sciences*; McGraw-Hill: New York, 1969.
(11) Carreira, L. A.; Antcliff, R. R. In *Advances in Laser Spectroscopy*; Garetz, B. A., Lombordi, J. R., Eds.; Heyden: London, 1982; Chapter 6.
(12) Honigs, D. E.; Hieftje, G. M.; Hirschfeld, T. *Appl. Spectrosc.* **1984**, *38*, 317–322.
(13) Tam, A. C.; Patel, C. K. N. *Appl. Opt.* **1979**, *18*, 3348–3357.
(14) Currie, L. A. *Anal. Chem.* **1968**, *40*, 586–593.
(15) Bialkowski, S. E. *Anal. Chem.* **1986**, *58*, 1706–1710.
(16) Brown, C. W.; Obremske, R. J.; Anderson, P. *Appl. Spectrosc.* **1986**, *40*, 734–742.
(17) Dovichi, N. J.; Harris, J. M. *Anal. Chem.* **1981**, *53*, 106–109.
(18) Carter, C. A.; Harris, J. M. *Appl. Opt.* **1984**, *23*, 476–481.

RECEIVED for review November 17, 1986. Accepted March 5, 1987. This work was funded in part by the National Science Foundation under Grant CHE85-06667. Fellowship support (to J.M.H.) from the Alfred P. Sloan Foundation is also acknowledged.

Trace Determination of Nitrogen-Containing Drugs by Surface Enhanced Raman Scattering Spectrometry on Silver Colloids

Edith L. Torres[1] and J. D. Winefordner*

Department of Chemistry, University of Florida, Gainesville, Florida 32611

The evaluation of surface enhanced Raman scattering (SERS) spectroscopy on silver colloids as an analytical technique is presented. The use and performance of a simple and inexpensive device for Raman studies are evaluated by taking advantage of the enhanced signals observed in this new technique. The results demonstrate that SERS on silver colloids can be successfully used for the qualitative determination of N-containing drugs such as *p*-aminobenzoic acid (PABA), phenytoin, uracil, and uracil derivatives as well as N-containing polynuclear aromatic hydrocarbons, such as 2-aminofluorene. Analytical calibration curves of PABA and 2-aminofluorene yield straight lines with the slopes of their log–log plots close to unity. The absolute limits of detection for these compounds were 35 and 7 ng, respectively. Reasons for the rather poor correlation between signal and concentration for the other adsorbates studied are discussed. For some compounds, SERS has the high identification power inherent in all vibrational techniques, with the added advantage of being nearly as sensitive as many luminescence techniques presently used for trace analytical purposes.

Since the discovery of the technique now known as surface enhanced Raman scattering (SERS) spectroscopy in 1974 most of the research reported has been oriented towards the understanding of the phenomenon itself (*1–7*). Little attention has been given to the development of the technique as an analytical method for the identification and quantitation of molecular species present at trace concentration levels. The technique of SERS consists of observing the regular Raman process at or near metallic surfaces, which are properly roughened, detecting in this way Raman bands, which can be amplified by factors ranging from 3 to 6 orders of magnitude. Its sensitivity, therefore, is similar to that of luminescence techniques with the added advantage of spectral selectivity.

The simplicity of instrumentation needed to perform Raman studies, i.e., UV–visible sources, UV–visible monochromators, UV–visible detectors, glass and quartz optics, and cells, and a wide range of solvents including aqueous solutions make Raman spectrometry and especially SERS a valuable analytical method. Recently, Pemberton and Buck (*8*) reported the detecton of the anion diphenylthiocarbazone adsorbed at the surface of a silver electrode. By use of the multiplicative effects of surface enhancement and resonance enhancement, concentration levels as low as 10^{-9} M were reported to give spectra with acceptable signal-to-noise (S/N) ratios. Following this line, Tran (*9*) reported subnanogram detection of dyes spotted on filter paper that was previously treated with colloidal silver hydrosols. Detection limits were in the picogram range level and the calibration plots exhibited linear responses.

Vo-Dinh et al. (*10–12*), however, have directed their research toward the development of practical substrate materials that can be easily prepared and that can provide data with sufficient reproducibility and accuracy for analytical purposes.

[1] Present address: Smith Kline & French Lab. Co., Call Box SKF, Cidra, PR 00639.

0003-2700/87/0359-1626$01.50/0 © 1987 American Chemical Society

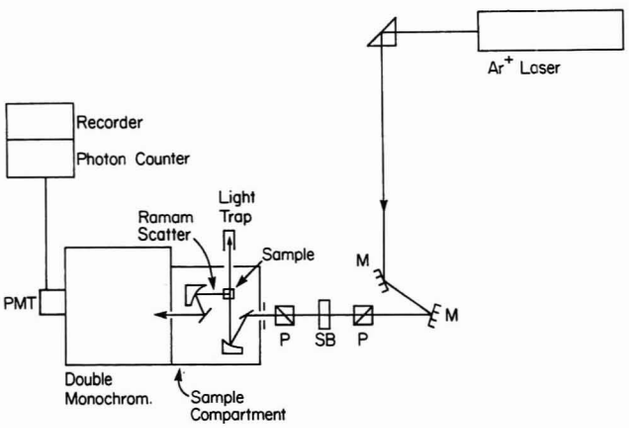

Figure 1. Experimental arrangement for SERS studies: M, mirrors; P, polarizers; SB, Soleil-Babinet compensator, and PMT, photomultiplier tube.

They have also applied the technique for the detection of nitro polynuclear aromatic hydrocarbons (*13*). Specific applications of SERS as an analytical technique include the determination of copper and zinc phthalocyanine complexes on silver island films (*14*) and of tributyl phosphate after adsorption on silver hydrosols (*15*). Finally, more recently, Sheng et al. (*16*) have classified silver hydrosols by evaluation of sedimentation upon the SERS signal.

As an extension of these studies, additional qualitative and quantitative SERS results are presented in this work for several adsorbates on silver colloidal hydrosols. Various reasons for using colloidal hydrosols as substrates for the observation of SERS can be pointed out. First, they are easily prepared by chemical techniques, which are simpler than the generation of properly roughened electrodes or electrochemically deposited surfaces. Secondly, the costly instrumentation used to produce and characterize vacuum-deposited metal island films is not needed. The silver colloidal hydrosols are easily characterized by their adsorption spectra. Finally, colloidal hydrosols provide the possibility of continuous renewal of the sample by flow through a laser beam. This not only minimizes sample decomposition and colloidal instability but also offers the possibility of developing the technique as a detector for flow-through systems, such as flow injection analysis and high-performance liquid chromatography.

The specific purposes of this study were three-fold: first, to evaluate the use and performance of a simple and inexpensive spectrometric system for Raman studies, which could significantly increase the applicability of the SERS technique; second, to perform SERS measurements with this system on molecules of current interest, such as drugs and polynuclear aromatic hydrocarbons; third, to develop the technique as an analytical method for the measurement of small amounts or concentrations of analytes.

EXPERIMENTAL SECTION

Instrumentation. The Raman system used in this study is shown in Figure 1. It consisted of an argon ion laser (Model 171, Spectra-Physics), illuminating homogeneously the entrance slit of a single-beam sample compartment from the Fluorolog 2 series spectrofluorometers (Spex Industries). The sample compartment was mated to a double monochromator (Model 1680B, Spex), which was driven by a wavelength control module (Model CD2A, Spex).

The polarization of the laser was changed with a Soleil–Babinet compensator (Model K1148, Karl-Lambrecht Corp.) and chosen to be perpendicular to the direction of observation by a couple of Glan–Foucault polarizers (Karl-Lambrecht). For all measurements, the intensity of the 514.5-nm laser line was 500 mW at the laser head, resulting in 100 mW reaching the sample due to transmission losses. The Raman scatter was collected at 90° to the excitation beam and measured with a thermoelectrically cooled (by a refrigerated chamber Model TE 177RF-005, Products for Research, Inc.) photomultiplier tube (R-928, Hamamatsu) operated at 800 V and a photon counting system (Model 1105/1120, SSR Instruments, Inc.). The samples were placed in standard 1-cm × 1-cm liquid sample cells. The absorption (extinction) spectra were measured with a Perkin-Elmer (Model 330) UV–visible spectrophotometer. The depolarization ratios ($p = I_a/I_b$) were determined by rotating the polarization direction of the incident laser beam and measuring the Raman intensity when it was perpendicular (I_b) and parallel (I_a) to the direction of observation of the scatter signal.

Procedure. All reagents ($AgNO_3$ and $NaBH_4$) were purchased from Fisher Scientific and Eastman Kodak. The analytes *p*-aminobenzoic acid, uracil, uridine 6-aminouracil, naphthalene, 2-naphthol, 2-aminonaphthaline, fluorene, and 2-aminofluorene were purchased from Fisher, Sigma Chemical Co., Aldrich Chemical, Mallinckrodt Chemical Works, or Nutritional Biochemical Corp. The surfactants, poly(vinyl alcohol), cetylpyridinium chloride, and sodium dodecyl sulfate were purchased from Eastman Kodak, Sigma, and Sigma, respectively. The silver hydrosols were prepared according to the procedure previously described by Creighton et al. (*17*). Typically, 20 mL of 1×10^{-3} M of $AgNO_3$ was added dropwise to 60 mL of vigorously stirred (ice cooled) 2×10^{-3} M $NaBH_4$ aqueous solution to yield a light yellow colloid, which slowly turned brownish at around 15 °C while it was reaching room temperature. It is very important that the colloid does not appear to be turbid when viewed under oblique illumination as this is an indication of particles that have grown to diameters greater than 50 nm. Their appearance should be that of colored solutions. The cleanliness of the glassware and purity of the materials used are important factors that determined the reproducibility and stability of the colloids. For this reason, all the glassware used for the sols had been previously soaked in a 1:1 HNO_3:H_2O solution and rinsed several times with deionized water (Barnstead Sybron Co.). All the solutions were made with triply distilled water.

Stock solutions of 500 μg/mL of the analytes listed in Table I were prepared in ethanol (except for uracil, uridine, and 6-aminouracil for which triply distilled water was used). For Raman measurements, the sols were aged for 2 h, after which the necessary volume of analyte needed to give the desired concentration in sols was added to it. After being allowed to stand for 30 min, the mixture was ready for experimental study. Hydrosols older than 3 h were not used.

RESULTS AND DISCUSSION

Qualitative Study. In order to assess the identification power of the SERS spectra obtained with the instrumental system described above, several adsorbates were studied. The adsorbates (analytes) studied included several pyrimidine derivatives of ribonucleic acid (RNA) and the amino derivative of one of them. In the past, reseachers have successfully studied the SERS spectra of nucleic acid components of deoxyribonucleic acid (DNA) and some of their derivatives at rough silver electrode surfaces (*18–20*) and on colloidal silver suspensions (*22–24*) at concentration levels as low as a few micrograms per milliliter. Of the N-containing bases of RNA, uracil is the only one which is not present in DNA (thymine takes its place). Although its biological importance in the process of protein synthesis is clear, its SERS spectrum has not yet been reported in the literature.

The SERS spectrum of uracil is shown in Figure 2. The band positions together with their vibrational mode assignments appear in Table I. Due to the very low NRS (normal Raman scatter) intensities and to the experimental arrangement used in this study, no NRS spectrum could be observed for the molecule when dissolved in water. For comparison purposes, however, the data obtained from ref 21 for thymine in water are also included in Table I.

In the ring bending mode region, only two bands appear at 578 and 603 cm^{-1}. Four other bands have been reported (*21*) at lower energies, but in this study, the intense Rayleigh line limits their observation. At 796 cm^{-1}, the totally sym-

Table I. SERS Results for Uracil[a]

$\overline{\Delta\nu}_{Ag}$[b]	$\overline{\Delta\nu}_{Ag}$[c]	$\overline{\Delta\nu}_{H_2O}$[d]	calcd[e]	line shift[f]	assignments
578 (0.20)	586	565		13	$N_1C_2N_3^B - C_2N_3C_4^B$
603 (0.20)	632		614		$N_1C_2O^B + N_3C_4O^B$
796 (1.0)	776	750	795	46	ring breathing
1040 (0.13)					stretching motion of the ring's
1094 (0.11)					C–N bonds[h]
1207 (0.40)	1184	1169	1200	7	$-C_6H^B + C_2N_3^S$
1267 (0.49)	1275	1238		29	$ring^S + CH^B$
1381 (0.50)	1344	1360	1375	21	$N_3H^B - C_4 = O^S$
1511 (0.23)	1504	1503		8	NH^B
1559 (0.07 Sh)	1562				
1582 (0.11)	1584	*g*	1562		$N_3C_4^S + N_1C_2^S + C_6H_5^S - N_1C_6^S$
1610 (0.30)	1652	1657		-47	$C_4 = O^S + C_5 - C_6^S$
		1691			$C_2 = O^S$

[a] Abbreviations used: S = stretching, B = bending, Sh = shoulder. All numbers are in cm^{-1}. [b] SERS in this study, values in parentheses are relative intensities. [c] SERS from ref 21. [d] NRS (normal Raman scatter) from ref 21. [e] Calculated values from ref 25. [f] Line shift = $\overline{\Delta\nu}_{Ag}$[b] – $\overline{\Delta\nu}_{H_2O}$[d]. [g] Could not be seen due to solvent interference. [h] From ref 26.

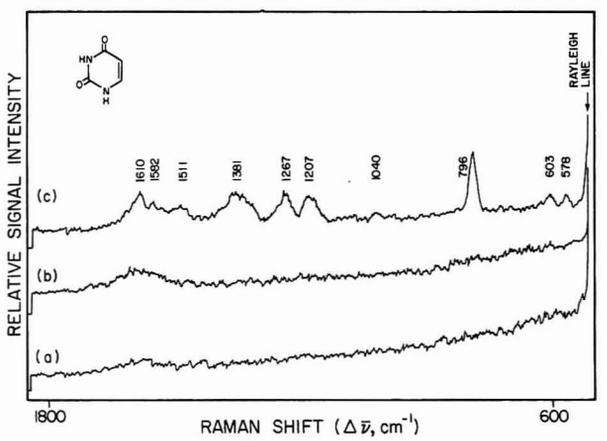

Figure 2. Scattered intensity (1 cm = 130 counts/s) vs. Raman shift ($\overline{\Delta\nu}$, cm^{-1}) of (a) 500 μg/mL uracil in water, (b) the silver hydrosols showing the continuum background radiation, and (c) 5 μg/mL uracil in silver hydrosols (SERS spectrum).

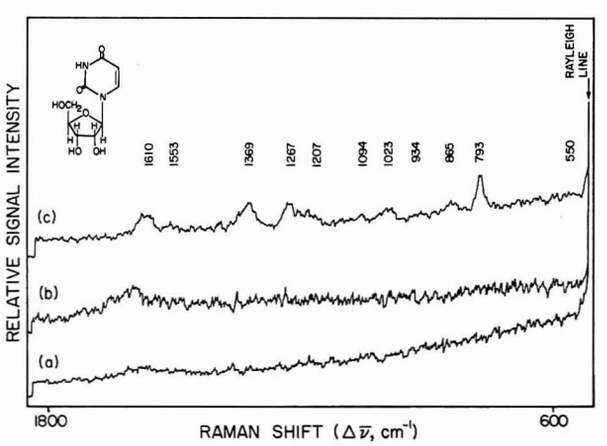

Figure 3. Scattered intensity (1 cm = 130 counts/s) vs. Raman shift ($\overline{\Delta\nu}$, cm^{-1}) of (a) 500 μg/mL uridine in water, (b) the silver hydrosols, and (c) 5 μg/mL uridine in silver hydrosols (SERS spectrum).

metric ring stretching vibration appears. In addition to its high intensity, this band was also found to have a high depolarization ratio ($p > 0.75$), whereas for aqueous uracil, the corresponding band is almost completely polarized ($p \leq 0.25$) (*26*); this suggests that the molecule is actually adsorbed on the silver surface.

Table II and Figure 3 show that the Raman spectra of uracil (see Table II) and uridine are very similar because the Raman lines of ribose are very weak compared to those of the pyridine nucleus. Two new bands appear at 865 and 934 cm^{-1}, which have been attributed to C–O stretching mode in the ribose residue. All the other bands agree well with the already assigned uracil bands.

Table II. SERS Results for Uridine and 6-Aminouracil[a]

band positions/cm^{-1}[b]			
$\overline{\Delta\nu}_{Ag}$(uracil)	$\overline{\Delta\nu}_{Ag}$(uridine)	$\overline{\Delta\nu}_{Ag}$(6-amino-uracil)	assignment
578 (0.20)	550 (0.16)	568 (0.12)	$N_1C_2N_3^B - C_2N_3C_4^B$
796 (1.0)	793 (1.0)	684 (1.0)	ring breathing
	865 (0.27)		$C–O^S$ ribose[c]
		972 (0.06)	$C_6 - N^S$
	934 (0.16)		$C–O^S$ ribose[c]
1040 (0.13)	1023 (0.25)	1040 (0.11)	stretching motion of the ring's
1094 (0.11)	1094 (0.14)		C–N bonds
1207 (0.40)	1207 (0.20 Sh)		$-C_6H^B + C_2N_3^S$
1267 (0.49)	1267 (0.64)	1260 (0.08)	$ring^S + CH^B$
1381 (0.50)	1369 (0.61)	1389 (0.08)	$N_3H^B - C_4 = O^S$
1511 (0.23)		1485 (0.07)	NH^B
1559 (0.07 Sh)	1553 (0.11)	1550 (0.13)	
1610 (0.30)	1610 (0.43)		$C_4 = O^S + C_5C_6^S$

[a] Abbreviations as in Table I. [b] Values in parentheses are relative intensities. [c] From ref 26.

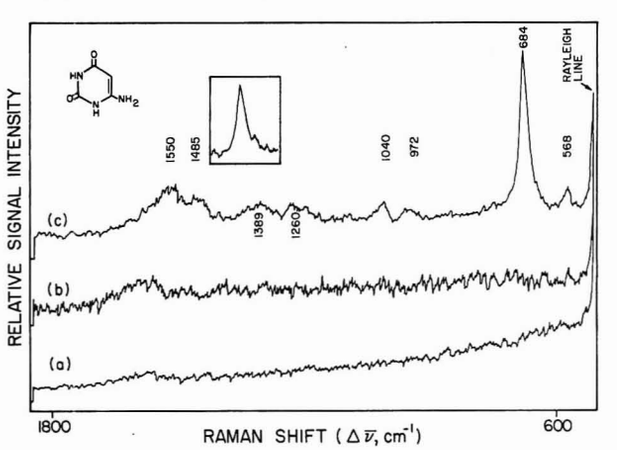

Figure 4. Scattered intensity (1 cm = 130 counts/s) vs. Raman shift ($\overline{\Delta\nu}$, cm^{-1}) of (a) 500 μg/mL 6-aminouracil in water, (b) the silver hydrosols, and (c) 50 μg/mL 6-aminouracil in silver hydrosols (SERS spectrum). The insert figure corresponds to the 684-cm^{-1} surface-enhanced band of 5 μg/mL 6-aminouracil.

The SERS results obtained for 6-aminouracil are shown in Figure 4 and Table II. The ring breathing mode has shifted

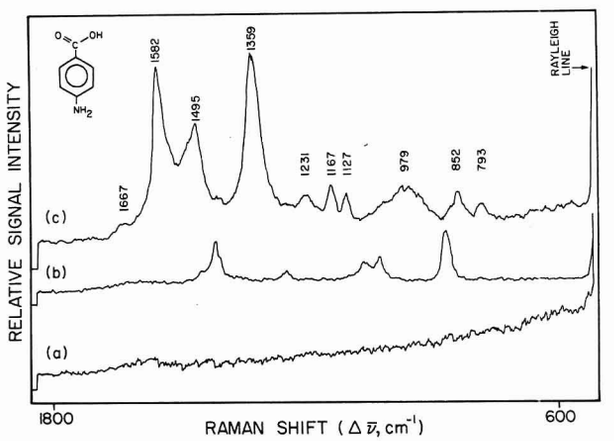

Figure 5. Scattered intensity vs. Raman shift of (a) the silver hydrosols (3 cm = 390 counts/s), (b) 80 μg/mL PABA in water (1 cm = 390 counts/s), and (c) SERS spectrum of 50 μg/mL PABA in silver hydrosols (1 cm = 390 counts/s).

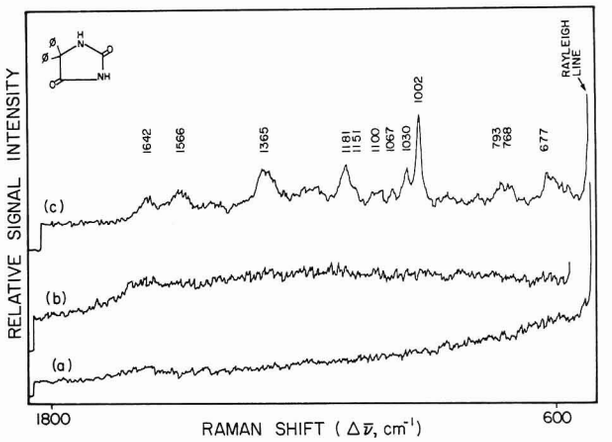

Figure 6. Scattered intensity (1 cm = 130 counts/s) vs. Raman shift of (a) the silver hydrosols, (b) 0.75 μg/mL phenytoin in water, and (c) 0.75 μg/mL phenytoin in silver hydrosols (SERS spectrum).

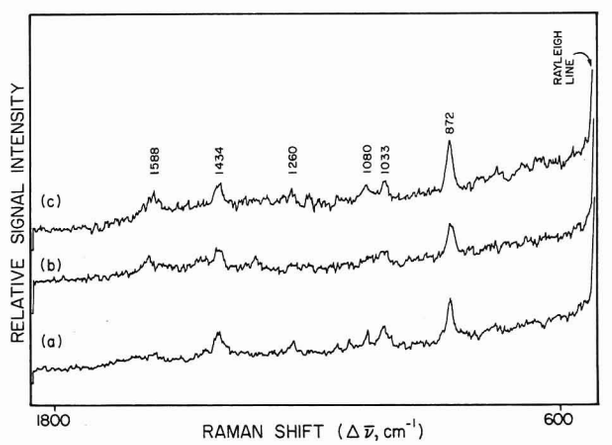

Figure 7. Scattered intensity (1 cm = 130 counts/s) vs. Raman shift of (a) 50 μg/mL naphthalene in silver hydrosols, (b) 50 μg/mL naphthol in silver hydrosols, and (c) 50 μg/mL 2-aminonaphthalene in silver hydrosols.

to a lower frequency from 793 to 684 cm^{-1}. Only one new band appears at 972 cm^{-1}, which could be assigned to either the C_6–N stretching vibration or the N–H bending vibration; for a definite assignment, a deuterated derivative has to be studied. The band associated with the C_6H bending vibration (at ~1207 cm^{-1}) in uracil and uridine disappears in the 6-aminouracil spectrum. This is as expected since the amino group is now replacing the hydrogen. The other bands that disappear are those assigned to the C_4=O (at 1610 cm^{-1}) and C_6C_5 (at 1582 cm^{-1}) stretching vibrations. There is a possibility that the molecule is no longer bound to the surface through the C=O group but instead through the amino group at C_6. Other vibrations of the $-NH_2$ group itself do not show up because they occur at frequencies higher than the ones shown in the spectrum ($\overline{\Delta\nu} > 2000$ cm^{-1}, e.g., at ~3000 cm^{-1}, one finds the antisymmetric and symmetric NH stretching vibration, and at 1600 cm^{-1}, one finds the NH_2 bending (scissors) vibration, which is a weak band (*27*)).

The high-quality SERS spectra shown in section c of Figures 2–4 in the presence of the silver hydrosols greatly exceed those obtained from a solution in the absence of the colloidal particles (compare sections a and c of Figures 2–4); good S/N ratios were obtained in all of the SERS cases. In section b of Figures 2–4, the continuous inelastic scattering of the silver hydrosols (before the analyte is added) is shown; the only noticeable feature of these scans is about 1600 cm^{-1}, which is assigned to the –OH bending vibration of the water molecules.

Four other molecules were studied by SERS in order to further demonstrate the potential analytical utility of the technique. These were *p*-aminobenzoic acid (PABA), phenytoin, 2-aminofluorene, and 2-aminonaphthalene. The first of these, PABA, is a drug extensively used in pharmaceutical and nutritional products. Its SERS spectrum is shown in Figure 5. The most prominent bands appear at 1582 and 1495 cm^{-1} corresponding to C–C stretching vibrations of the benzene ring and at 1395 cm^{-1} corresponding to a stretching vibration of the COO^- group. Following in intensity are a band at 1167 cm^{-1}, which could be assigned to C–H in plane bending, and a band at 1127 cm^{-1}, probably due to NH_2 bending. The bands that appear at frequencies lower than 1000 cm^{-1} are assignable to benzene ring modes. The absence of a Raman mode in the 1700-cm^{-1} region corresponding to vibration of the COO–H group together with the appearance of a strong band at 1359 cm^{-1}, which above was assigned to a stretching vibration of the COO^- group, suggests that the molecule is adsorbed in its anionic form. The predominant species at the pH used (pH ≈9) is the anion. Suh et al. (*28*) have argued that considering the aminobenzoate anion to be almost planar, it is likely to be π-bonded to the silver surface in a flat orientation rather than perpendicular to the surface. Binding could also occur through the lone pairs on either the carboxylate or amine group. They further suggested that this might explain the dominance of benzene vibrations in the SERS spectrum. For comparison purposes, Figure 5 also contains the NRS spectrum for a dilution of the ethanolic stock solution of PABA in water. The bands at around 872, 1033, 1080, 1260, and 1434 cm^{-1} are all assigned to ethanol vibrational modes.

Phenytoin is a drug which is widely prescribed for the treatment of epilepsy (*29*). Traditional methods for its identification include time-consuming screening tests, which also give a positive response for molecules such as barbiturates, bemegride and primidone (*30*). Therefore, the development of a method that will allow a rapid identification of the drug is desirable. The SERS spectrum of phenytoin appears in Figure 6. The frequencies at which the bands appear are included in the spectrum to facilitate future reference. No attempts were made to assign the bands to specific vibrational modes of the molecule but the spectrum correlates well with its published NRS spectrum (*31*).

The two other molecules studied are polycyclic aromatic hydrocarbons (PAHs). These are molecules formed during incomplete combustion of organic materials. It has been known for many years that certain PAHs possess carcinogenic properties. For this reason, analytical methodology for the identification and quantitation of these compounds has undergone rapid growth and development in the past years. Luminescence techniques are very sensitive for PAH deter-

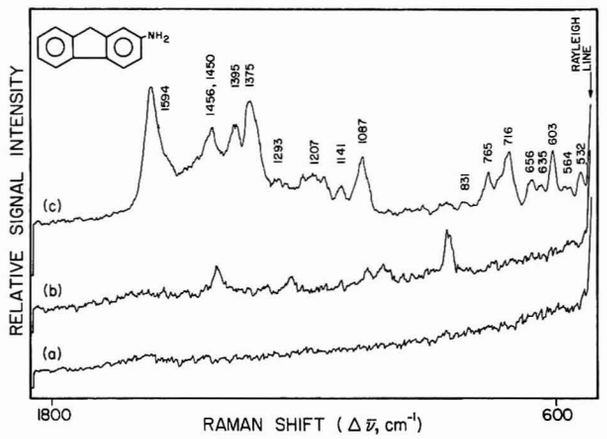

Figure 8. Scattered intensity vs. Raman shift of (a) the silver hydrosols (1 cm = 130 counts/s), (b) 50 μg/mL fluorene in silver hydrosols (1 cm = 130 counts/s), and (c) 10 μg/mL 2-aminofluorene in silver hydrosols (1 cm = 390 counts/s).

minations. However, the broad overlapping bands observed in fluorescence and phosphorescence spectra render limited applicability of these techniques for structure identification.

Figure 7 shows the SERS of naphthalene and two of its derivatives, 2-naphthol and 2-aminonaphthalene. The stronger bands of these spectra could only be assigned to vibrations of the ethanol molecule. The hydrosols did not change color upon addition of these analytes; i.e., no coagulation occurred. Therefore, it can be assumed that no adsorption took place as has been previously reported for benzene in silver colloids (*32*).

Fluorene and 2-aminofluorene, on the other hand, exhibit very different SERS spectra as shown in Figure 8. The spectrum of 2-aminofluorene is a very intense one which correlates well with its structure. The fluorene spectrum, however, resembles those of naphthalene and its derivatives. The amino group in the fluorene molecule induces adsorption onto the silver surface, while it has no effect on the adsorption of naphthalene. This can be explained by the greater delocalization of the lone-electron pair of the nitrogen atom in the π system of naphthalene, which decreases the possibility of interaction with the silver surface. It is interesting to note that selective adsorption of 2-aminofluorene instead of fluorene and naphthalene derivatives provides an interesting potential for the selectivity of SERS.

Quantitative Study. The dependence of the intensity of the 1005 cm^{-1} SERS band of phenytoin on concentration was studied under different experimental conditions. In all of the experiments performed, a poor correlation between signal intensity and analyte concentration was found for phenytoin. Nevertheless, this study was valuable as it determined the optimum conditions for further experimentation. It was found that higher signals are obtained if the hydrosols were aged for just 2 h prior to their mixing with the analytes. The longer the aging period of the hydrosols, the higher the concentration of analyte needed to induce aggregation in a given period of time. This is because the stabilizing ions on the surface of the particles are less easily displaced. In the same way, for a constant analyte concentration, the time elapsed after analyte addition in order to obtain a given signal intensity increased as the aging period of the hydrosol increased (since the signal intensity depended on the extent of the aggregation induced by the analyte addition on the colloidal particles). So, for a phenytoin concentration of 80 μg/mL in the sols, the following was observed:

(i) A comparable signal intensity was obtained 10 min after mixing with the sols if they were aged for 24 h.

(ii) A comparable signal intensity was obtained 40 min after mixing with the sols if they were aged for 48 h.

(iii) No aggregation was induced at this analyte concentration if the sols were aged for 4 days.

If the same experiment was repeated for hydrosols aged for just 2 h, a comparable signal intensity as for the above cases is obtained in just 30 min for a phenytoin concentration of only 0.75 μg/mL in the sols.

The color of the colloidal dispersions prior to analyte addition also plays an important role in the intensity of the SERS bands of the analytes. As it is widely known, the color of the colloidal solution is an indication of the size of the dispersed particles. A more clear tone of yellow is indicative of smaller particles in solution, while a brownish yellow indicates bigger particles and an even darker color of the sols is accompanied by turbidity of the solution. An experiment was performed with three colloidal solutions, each differing from the other in the initial color of the colloidal suspension. Again, for a phenytoin concentration of 80 μg/mL, the following were found:

(i) For the initially clear yellow suspension, a $S/N = 60$ is obtained 2 h after adding the analyte to the colloidal solution.

(ii) For the initial brownish yellow suspension, a $S/N = 60$ is obtained 10 min after adding the analyte to the colloidal solution.

(iii) For the initially turbid suspension, precipitation of the colloid was induced by the analyte addition, and no SERS was observed.

These results are explained on the basis that a certain degree of aggregation is needed in order to observe the surface enhanced effect on colloidal suspensions. For the clear yellow sols, initially containing smaller particles in solution, more time needed to elapse after analyte addition in order for the particles to form the linear strings of aggregates. The growth process will bring the particles into resonance with the laser line, which will excite their surface plasmon polaritons, a condition that is essential for the observation of the SERS effect. On the other hand, if precipitation of the silver occurs in the initially turbid colloidal suspension, the SERS effect is suppressed.

The main problem in the quantitation study of phenytoin arose from the interaction that this particular adsorbate has with the silver hydrosols. For low concentrations of adsorbate (<0.75 μg/mL), the SERS effect was not observed, presumably because the concentration was too low to induce chain formation. In the concentration range between 0.75 and 1.25 μg/mL, aggregation was induced by this adsorbate, and a good correlation between signal intensity and analyte concentration was found. Higher concentrations of analyte, however, caused further coagulation of the colloids leading to the precipitation of metallic silver as could be inferred by the observation of visible particles. This was accompanied by a decrease in the signal while the supernatant solution completely clarified.

Two solutions to quantitation problem are possible. In the first approach, it is known that, at least under some circumstances, an adsorbed polymer stabilizes a dispersion against flocculation. In fact, organic molecules with large nonpolar groups are known to adsorb strongly to the surface of metal colloids, which enables the observation of their SERS spectra (*33–36*). Thus, a series of experiments were performed in which three different stabilizers, namely, poly(vinyl alcohol) (PVA) at 0.1% (v/v) concentration, sodium dodecyl sulfate (SDS) at 5×10^{-2} M concentration, and cetylpyridinium chloride at 1.2×10^{-3} M concentration were used as protective agents. These were added to the colloidal suspensions up to the above mentioned concentrations either before or after analyte addition. In all cases the analyte could not displace the stabilizers from the colloidal surface, and thus no SERS spectrum could be observed from it.

Table III. Effect of the Concentration of Silver Hydrosol on the SERS Signal of 0.75 μg/mL Phenytoin

concn of silver sols, M	SERS rel signal intens	concn of silver sols, M	SERS rel signal intens
2.5×10^{-5}	1.3	2.5×10^{-4}	13.0
1.5×10^{-4}	15.0	5.0×10^{-4}	3.0

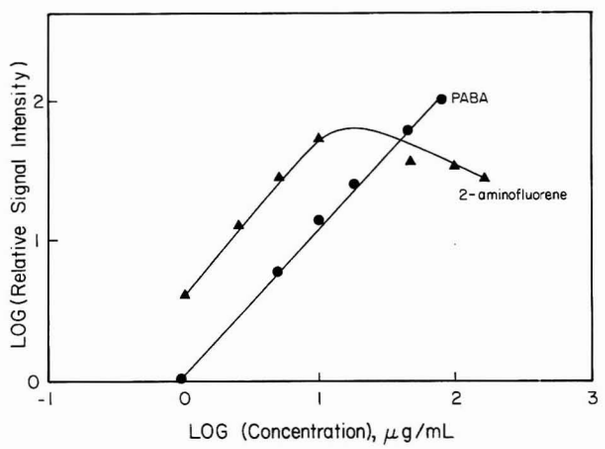

Figure 9. Logarithmic calibration plot for PABA at the 1359-cm^{-1} Raman band and for 2-aminofluorene at the 1594-cm^{-1} Raman band.

The second approach was to change the initial concentration of the reagents used to prepare the colloidal suspension so as to change the final number of available silver sites in solution. Lower concentrations of reagents are expected to produce a smaller number of larger particles in solution, while more concentrated reagents should produce larger number of smaller particles. As a first inference, it seems rather logical to suppose that a diluted silver hydrosol would require less analyte to bring about aggregation than a concentrated one since there is a smaller number of particles to be acted upon by the analyte. There are, however, other factors to be considered. Upon dilution of the hydrosol, the suspended particles become more widely separated, and, as a result, the probability of collisional interaction is decreased. The predominance of one or the other of these processes defines the effect of the concentration of the sols. It can be inferred from Table III that better signals are obtained at intermediate concentrations of hydrosols where these effects can be regarded as nearly equal. At the lowest sol concentration, lower signals are obtained, reflecting the predominance of the dilution effect. Similarly, at higher sol concentrations, even though there are more silver sites available for analyte adsorption, the particles are closer together and the addition of the analyte brings about complete coagulation and thus a decrease in the SERS intensity.

A quantitative study was also performed on the other adsorbates reported in the previous section. Uracil and its derivatives behaved similarly to phenytoin, and at concentrations as low as 5 μg/mL, complete coagulation of the hydrosols was observed. However, good calibration curves were obtained for PABA and 2-aminofluorene. In Figure 9, the logarithmic calibration plots of these compounds are shown. The data were obtained with the 1359- and 1594-cm^{-1} Raman bands of PABA and 2-aminofluorene, respectively. For both compounds, the curves are linear over nearly 2 orders of magnitude. No attempts were made here to evaluate other analytical figures of merit such as accuracy, selectivity, and precision. However, it has been shown (*37*) that a careful attention to the sample preparation procedure gives precisions within ±10% (RSD) of the signal in the SERS spectrum of PABA. From the linear calibration plots and the noise

Table IV. SERS Limits of Detection[a] and Calibration Sensitivities for PABA and 2-Aminofluorene

	PABA	2-amino-fluorene
calibratn sensitivities, RSI[b]/μg/mL	1.21	5.44
C_L, μg/mL	0.5	0.1
corrn coeff	0.997	0.993
slope of log–log calibratn curve	1.05	1.13

[a] $C_L = 3\sigma_B/m$, where C_L is the limit of detection in μg/mL, σ_B = 1/5 peak to peak noise and m is the slope of the linear calibration curve (i.e., the calibration sensitivity). [b] Relative Signal Intensity.

measurements, the detection limits are in the sub-microgram-per-milliliter range (see Table IV). Considering that the laser beam was illuminating only a 0.071-cm^3 cuvette volume, the absolute limits of detection are 35 and 7 ng for PABA and 2-aminofluorene, respectively. It should be mentioned at this point that better limits of detection should be obtained by tuning the laser to the peak absorption maximum of the surface plasmon polaritons, at which point the maximum surface enhancement effect would be obtained.

The maximum signal obtained as the concentration of analyte is increased reflects saturation of available interaction sites at the silver surface as has been pointed out by others (*10*, *16*). This is accompanied by the precipitation of metallic silver as discussed earlier. The concentration at which the maximum signal is reached is characteristic of the particular analyte under study, thus reflecting the different extent of colloidal aggregation as a result of the adsorbates. In fact, the SERS signal produced by a given concentration of 2-aminofluorene is roughly 50% higher than that produced by the same concentration of PABA (Figure 9). Analytical calibration curves for concentrations under this limiting value should have a linear response. The intensity of the Raman band under study will slowly decrease toward the unenhanced value as the concentration is increased further.

Finally, since the NRS spectrum could not be measured with the spectrometer used, no enhancement factors could be calculated for the molecules where SERS was observed. However, for the most intense band of all the molecules studied, a depolarization ratio (p) greater than 0.7 could be deduced from the depolarization study, which is typical for SERS bands.

Final Comments. The experimental results clearly demonstrate that an analytical method based on SERS provides high spectral selectivity and identification power as well as high analytical sensitivity and detection power for the study of N-containing drugs and PAHs. The experimental arrangement used throughout this work possessed several advantages. First of all, the system is roughly 3 times less expensive than the conventional ones used for Raman studies. For the SERS studies, in which large signals limited by background shot noise are observed, an improvement in the measured S/N can be obtained at the expense of a small loss in resolution. A very large gain in measurement time is also obtained since the instrument can scan at faster speeds, which is a very important prameter to consider when developing an analytical technique. The system used is simple and no time-consuming precise optical adjustments are necessary to maximize the scatter of Raman radiation into the monochromator.

Overall, the technique is still in its infancy and many figures of merit, including limits of detection, precision, linear dynamic range, selectivity, sensitivity, and reproducibility, remain to be reported for the various adsorbates of current analytical interest. For the future, we can foresee that SERS spectroscopy will likely be applied as a selective detector for high-performance liquid chromatography (HPLC). Such

studies are under way in the authors' laboratory.

ACKNOWLEDGMENT

The authors thank S. G. Schulman of the School of Pharmacy, University of Florida for the phenytoin.

Registry No. PABA, 150-13-0; uracil, 66-22-8; uridine, 58-96-8; 6-aminouracil, 873-83-6; naphthalene, 91-20-3; 2-naphthol, 135-19-3; 2-aminonaphthaline, 91-59-8; 2-aminofluorene, 153-78-6; phenytoin, 57-41-0; silver, 7440-22-4.

LITERATURE CITED

(1) Fleischmann, M.; Hendra, P. J.; McQuillan, A. J. *Chem. Phys. Lett.* **1974**, *26*, 163-166.
(2) Jeanmarie, D. L.; van Duyne, R. P. *J. Electroanal. Chem. Interfacial Electrochem.* **1977**, *84*, 1-20.
(3) Albrecht, M. G.; Creighton, J. A. *J. Am. Chem. Soc.* **1977**, *99*, 5215-5217.
(4) *Surface Enhanced Raman Scattering*; Chang, R. K., Furtak, T. E., Eds.; Plenum: New York, 1982.
(5) Furtak, T. E.; Reyes, J. *Surf. Sci.* **1980**, *93*, 351-382.
(6) Otto, A. *Appl. Surf. Sci.* **1980**, *6*, 309-355.
(7) Seki, H. *J. Electron. Spectrosc. Relat. Phenom.* **1986**, *39*, 289-310.
(8) Pemberton, J. E.; Buck, R. P. *Anal. Chem.* **1981**, *53*, 2263-2267.
(9) Tran, C. D. *Anal. Chem.* **1984**, *56*, 824-826.
(10) Vo-Dinh, T.; Hiromoto, M. Y. K.; Begun, G. M.; Moody, R. L. *Anal. Chem.* **1984**, *56*, 1667-1670.
(11) Vo-Dinh, T.; Meier, M.; Wokaun, A. *Anal. Chim. Acta*, in press.
(12) Meier, M.; Wokaun, A.; Vo-Dinh, T. *J. Phys. Chem.* **1985**, *89*, 1843-1846.
(13) Enlow, P. D.; Buncick, M.; Warmack, R. J.; Vo-Dinh, T. *Anal. Chem.* **1986**, *58*, 1119-1123.
(14) Jennings, C.; Aroca, R.; Hor, A.-M.; Loutfy, R. O. *Anal. Chem.* **1984**, *56*, 2033-2035.
(15) Gautner, E.; Steinert, D.; Reinhardt, J. *Anal. Chem.* **1985**, *57*, 1658-1662.
(16) Sheng, R.-S.; Zhu, L.; Morris, M. D. *Anal. Chem.* **1986**, *58*, 1116-1119.
(17) Creighton, J. A.; Blatchford, C. G.; Albrecht, M. G. *J. Chem. Soc., Faraday Trans. 2*, **1979**, *75*, 790-798.
(18) Koglin, E.; Séquaris, J. M.; Valenta, P. *J. Mol. Struct.* **1980**, *60*, 421-425.
(19) Ervin, K. M.; Koglin, E.; Séquaris, J. M.; Valenta, P.; Nürmberg, H. W. *J. Electroanal. Chem. Interfacial Electrochem.* **1980**, *114*, 179-194.
(20) Koglin, E.; Séquaris, J. M.; Valenta, P. *J. Mol. Struct.* **1982**, *79*, 185-189.
(21) Otto, C.; van den Tureel, T. J. J.; de Mul, F. F. M.; Greve, J. *J. Raman Spectrosc.* **1986**, *17*, 289-298.
(22) Koglin, E.; Séquaris, J. M.; Valenta, P. In *Surface Studies with Lasers*; Aussenegg, F. R., Leitner, A., Lippitsch, M. E., Eds.; Springer-Verlag: New York, 1983.
(23) Koglin, E.; Séquaris, J. M.; Fritz, J. C.; Valenta, P. *J. Mol. Struct.* **1984**, *114*, 219-223.
(24) Séquaris, J. M.; Koglin, E. *Fresenius' Z. Anal. Chem.* **1985**, *321*, 758-759.
(25) Tsuboi, M.; Takahashi, S.; Harada, I. In *Physiochemical Properties of Nucleic Acids*; Duchesne, J., Ed.; Academic: New York, 1973.
(26) Lord, R. C.; Thomas, G. J., Jr. *Spectrochim. Acta, Part A* **1967**, *23A*, 2551-2591.
(27) Dollish, F. R.; Fateley, W. G.; Bentley, F. F. *Characteristic Frequencies of Organic Compounds*; Wiley-Interscience: New York, 1974.
(28) Suh, J. S.; Di Lella, D. P.; Moskovits, M. *J. Phys. Chem.* **1983**, *87*, 1540-1544.
(29) O'Neal, J. S.; Sloan, K. B.; Schulman, S. G. *J. Pharm. Biomed. Anal.* **1986**, *4*, 103-106.
(30) Clarke, E. G. C. *Isolation and Identification of Drugs*; The Pharmaceutical Press: London, 1969.
(31) *The Sadler Standard Spectra*; Sadler Research Laboratories: Philadelphia, PA; Raman Number 2583.
(32) Lippitsch, M. E. *Chem. Phys.* **1980**, *74*, 125-127.
(33) Lee, P. C.; Meisel, D. *Chem. Phys. Lett.* **1983**, *99*, 262-265.
(34) Siimian, O.; Bumm, L. A.; Callaghan, R.; Blatchford, C. G.; Kerker, M. *J. Phys. Chem.* **1983**, *87*, 1014-1023.
(35) Heard, S. M.; Grieser, F.; Barraclough, C. G. *Chem. Phys. Lett.* **1983**, *95*, 154-158.
(36) Heard, S. M.; Grieser, F.; Barraclough, C. G. *J. Phys. Chem.* **1985**, *89*, 389-392.
(37) Laserna, J. J.; Torres, E. L.; Winefordner, J. D. *Anal. Chim. Acta*, in press.

RECEIVED for review December 29, 1986. Accepted March 5, 1987. This research supported by NIH-GM-11373-23.

Simultaneous Laser-Based Refractive Index and Absorbance Determinations within Micrometer Diameter Capillary Tubes

Darryl J. Bornhop[1] and Norman J. Dovichi*

Department of Chemistry, University of Alberta, Edmonton, Alberta T6G 2G2, Canada

A high-sensitivity, small-volume refractive index detector has been reported, which is based upon the diffraction of a probe laser beam by a capillary tube. High-sensitivity thermooptical absorbance measurements may simultaneously be made with this detector if a second, modulated pump laser beam is focused into the capillary. The modulated component of the probe beam intensity is related to the sample absorbance whereas the unmodulated component is related to refractive index. In this capillary refractive index and absorbance detector, a 1-mW helium–neon probe laser and a 2-mW helium–cadmium pump laser are employed to generate refractive index detection limits of 4×10^{-6} ΔRI and absorbance detection limits of 6.3×10^{-6}, both measured across a 50-μm-diameter cuvette. Similar results were obtained for 100- and 500-μm-diameter capillaries. The dead volume of the system, 50 pL for the 50-μm capillary, is limited by the tube radius; 6 million amaranth molecules are present within the detector volume at the absorbance detection limit. Linearity in both refractive index change and absorbance extends for at least 3 orders of magnitude.

[1] Present address: Lee Scientific, 4426 South Century Dr., Salt Lake City, UT 84123.

The problem of analytical measurements within small-volume, cylindrical samples is of particular importance in capillary separation techniques. Both open tubular capillary liquid chromatography and electrophoresis require low dead volume detectors with good detection limits to preserve separation efficiency (*1*, *2*). A good concentration detection limit, better than 10^{-4} M, is required because dilute analyte must be analyzed to prevent column overload. Low dead volume, less than 10^{-9} L, is required to minimize peak spread. The combination of good concentration detection limit with small dead volume produces heroic requirements for mass detection; femtomole or better detection limits are required for the capillary separation methods.

Lasers are convenient light sources for optical analysis within capillary tubes. Laser beams with good spatial coherence may be focused to small spots with no loss of power. For example, laser-induced fluorescence has been applied to conventional capillary tubes with excellent detection limits for chromatographic detection (*3*, *4*). Also, the sheath flow cuvette has been combined with laser-induced fluorescence to produce excellent detection limits within micrometer diameter sample streams (*5*, *6*), approaching single molecule detection in favorable cases (*7*, *8*). Laser-based light scatter measurements within the sheath flow cuvette have been ap-

0003-2700/87/0359-1632$01.50/0 © 1987 American Chemical Society

plied to size analysis of nanometer diameter particles within picoliter probe volumes (*9–13*), including capillary hydrodynamic chromatographic detection (*13*). Photothermal refraction, based upon the crossed-beam thermal lens, uses laser excitation to measure very weak absorbance within micrometer square-bore tubes to produce excellent mass detection limits for neat samples (*14*) and capillary liquid chromatography (*15, 16*). Lastly, a simple, rugged laser-based refractive index detector has been developed for measurement of refractive index changes on the order of 5×10^{-7} within micrometer diameter tubes (*17, 18*).

In the determination of the refractive index of solutions contained within capillaries, a laser beam is focused into the cylindrical tube. Interaction of the laser beam and the capillary produces a fan of scattered light in the plane perpendicular to the capillary tube axis (*3*). The distribution of scattered light is complex, consisting of many light and dark fringes (*19, 20*). Although the fringe pattern may be described by conventional light scattering theory, evaluation of the theory is impractical for tubes much larger than the wavelength of light. Instead, the fringes are treated phenomenologically. The position of some of these fringes is observed to change with the refractive index of the solution. A small area photodiode is located at the border of a fringe; a change in the position of the fringe results in a change in intensity monitored by the photodiode.

This capillary refractive index detector has been demonstrated for nanoliter, neat samples. Detection limits of 6×10^{-7} ΔRI were obtained within a 500-μm-diameter cuvette (*17*). The capillary refractive index detector has also demonstrated detection of nanogram quantities of sugars separated with a 250 μm diameter packed chromatographic column and a 100 μm diameter detector cuvette (*18*). As in other refractive index detectors, the primary noise source in these measurements appears to be associated with temperature fluctuations. Since the refractive index of most liquids changes by several parts per ten thousand with a one degree temperature change, detection limits of 10^{-6} ΔRI correspond to temperature fluctuations of a few millidegrees.

The variation in refractive index with temperature of most solvents suggests that the capillary-refractive index detector may be applied for thermooptical absorbance measurements (*2, 22*). In thermooptical techniques, absorbance of a pump laser beam, followed by nonradiative relaxation of the excited states, produces a temperature rise within the sample that is proportional to both absorbance and pump laser intensity. Since the refractive index of the solvent changes with temperature, the heated region can act as an optical element to perturb the propagation properties of a probe beam. In this paper, a capillary thermooptical absorbance measurement is described in which a modulated pump laser beam is tightly focused at right angles to the sample capillary and to the probe laser beam. Absorbance of the pump beam produces a periodic temperature rise and refractive index change within the sample, which periodically deflects the probe beam. Lock-in detection of the modulated component of the probe beam intensity is used to measure absorbance within the capillary tube. The unmodulated component of the signal remains proportional to refractive index.

The capillary absorbance measurement is quite similar to two thermooptical techniques: photothermal refraction, based upon the crossed-beam thermal lens (*23–28*), and photothermal deflection, based upon a crossed-beam thermal prism (*29, 30*). In photothermal refraction, a cylindrically symmetric heated region is produced by absorbance of a pump laser beam. This heated region acts to defocus the probe beam out of the plane containing the pump and probe beams. Photothermal deflection acts similarly to deflect the probe beam

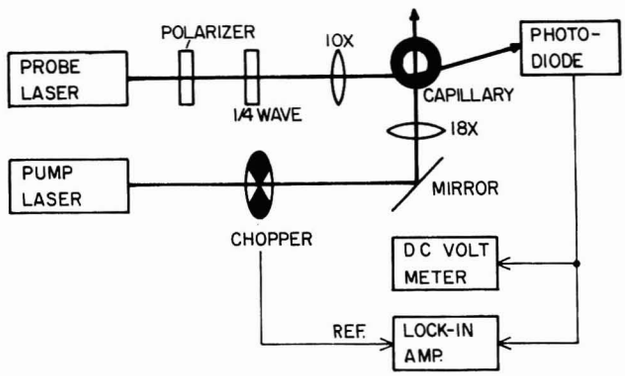

Figure 1. Experimental diagram. The probe laser is a 1-mW, polarized helium–neon laser. The probe beam passes through a polarizer and $^1/_4$ wave plate, used to minimize retroreflections. The beam is focused with a 10× microscope objective into the capillary tube. Upon traversing the capillary, the probe beam propagates to a 1-mm^2 photodiode. The pump laser is a 2.8-mW, linearly polarized helium–cadmium laser, operating at 442 nm. The pump beam is modulated in a symmetric square wave with a chopper, reflected from a mirror, and focused into the capillary with a 18× microscope objective. The output of the photodiode is conditioned with a current-to-voltage converter and sent to both a $4^1/_2$ digit dc voltmeter and a vector-sum lock-in amplifier. The reference signal for the lock-in amplifier is generated within the chopper head.

out of the plane containing the two beams. Defocusing or deflection of the probe beam is detected by measuring a change in the probe beam center intensity or position. Since the pump of probe beams only interact in their intersection region, very small samples may be probed with tightly focused laser beams. However, the analytical signal is obtained by monitoring the probe beam intensity so that the optical quality of the probe beam must be preserved through the optical train. Flat optical windows are required to preserve the probe beam quality. For chromatographic detection, small cross-section, square bore capillary tubes are glued to the end of the column. The use of flat windows is a definite annoyance since these square tubes are fragile, have mediocre optical quality, and are tedious to align perpendicularly to the beam axes.

The capillary thermooptical absorbance measurement appears to differ from both photothermal refraction and deflection. The photothermal techniques produce an optical element, which acts to defocus or deflect the probe beam *out* of the plane containing the pump and probe beams. Instead, the capillary thermooptical absorbance measurement produces a shift of the probe beam *in* the plane containing the two beams. This shift occurs because the refractive index of the solvent at the cylindrical wall changes with the temperature, which changes the deflection angle of the probe beam.

The modulated component of the probe beam intensity measured by the photodiode is related to sample absorbance whereas the dc or unmodulated component is related to the refractive index of the sample. Simultaneous measurement of absorbance and refractive index within micrometer diameter tubes should prove useful in chromatographic detection since both selective (absorbance) and universal (refractive index) information is produced.

EXPERIMENTAL SECTION

Apparatus. A block diagram of the simultaneous refractive index and absorbance detector is shown in Figure 1. A helium–neon laser produces a linearly polarized, 1-mW probe beam with a wavelength of 632.8 nm. The beam passes through a polarizing filter and a quarter-wave retardation plate. The quarter-wave plate is rotated to extinguish light retroreflected from other optical components. A 10×, 16 mm focal length microscope objective is used to focus the probe beam into the capillary tube. After traversing the capillary tube, the beam propagates about 20 cm to a 1-mm^2 silicon photodiode. The output of the photodiode is

conditioned by a current-to-voltage converter with a 1-MΩ feedback resistor in parallel with a 47-pF capacitor. The dc component of the signal is displayed upon a $4^1/_2$ digit voltmeter. The mean and standard deviation are estimated from 15 data points recorded at 1-s intervals.

A helium–cadmium laser produces a linearly polarized, 2-mW pump laser beam with a wavelength of 442 nm. A mechanical chopper modulates the pump beam in a square wave, typically at 12.5 Hz. This beam is focused with a 18×, 10 mm focal length microscope objective into the capillary tube at right angles to both the tube and the probe laser beam.

The interaction of the pump laser beam with the sample results in a refractive index change within the sample. This refractive index change produces a deflection of the probe beam profile and a change in the probe beam intensity which is synchronized with the pump beam modulation functon. The modulated component of the probe beam intensity is measured by using a vector-sum lock-in amplifier with a 3-s time constant. A reference signal for the lock-in amplifier is generated within the chopper head. The mean and standard deviation of the lock-in signal are estimated from a set of 15 points recorded at 5-s intervals.

Alignment. A significant effort was taken to minimize vibration of optical components. For example, the optical components are held with massive fixtures to a well damped optical table. The optical components for the probe beam are fixed in space and not held with translation stages. A three-axes translation stage holds the pump beam lens to provide complete freedom in the location of the pump beam waist, a two-axes stage is used to move the sample cuvette in the plane formed by the two laser beams, and a one-axis stage moves the detector across the probe beam profile.

The interaction of the probe beam and the fluid-filled capillary tube produces a complicated beam profile, consisting of a set of diffraction fringes. One set of fringes undergoes translation upon change in solvent composition, apparently by an amount proportional to the change in the refractive index of the solvent. A 1-mm^2 photodiode detects the fringe movement. The photodiode is located near the center of a fringe; movement of the fringe produces a corresponding change in the photodiode signal. As a general rule of thumb, the photodiode is first located in the most intense portion of the probe beam profile. Then the photodiode is translated perpendicularly to the laser beam axis and away from the unperturbed beam path a distance such that the photodiode intensity is approximately 0.37 ($1/e$) times the maximum intensity. This position of the photodiode results in both good sensitivity and reasonable linearity. Higher sensitivity is produced if the photodiode is located near the most intense portion of the beam profile; however, linearity suffers at that position. It may be necessary to translate slightly the capillary tube perpendicularly to the probe beam axis and iterate the detector alignment to generate good refractive index sensitivity and linearity.

Large thermooptical signals are observed for a number of positions of the photodiode across the probe beam profile. The position of the photodiode which generates good sensitivity and linearity for refractive index measurements also produces good sensitivity and linearity for the thermooptical capillary absorbance measurement.

Chemicals. All chemicals are reagent grade or better. Methanol is used as the solvent. Refractive index standards are 0%, 0.2%, 0.4%, 0.6%, 0.8%, and 1.0% (v/v) glycerol in methanol. A stock absorbance standard 2.2×10^{-4} M amaranth dye is prepared in methanol. A number of dilutions are prepared to construct the absorbance calibration curve. For this dye, ϵ(442 nm) = 6000 L M^{-1} cm^{-1}.

RESULTS AND DISCUSSION

A calibration curve was constructed for refractive index measurements by using glycerol solutions in methanol within 50-, 100-, and 500-μm-diameter capillary tubes. The results are summarized in Table I. The refractive index calibration curves were linear, $r > 0.997$, over at least a factor of 500 in refractive index change from the detection limit, about 2.5×10^{-6} ΔRI, to the highest concentration sample analyzed, ΔRI = 1.2×10^{-3}. Although no decrease in linearity was observed for the highest concentration sample investigated, nonlinear behavior is expected at higher concentrations; the fringe maximum had shifted near the photodetector at the highest concentration sample investigated. Smaller cuvettes produced slightly poorer refractive index detection limits, presumably because of greater temperature drift within the low heat capacity tubing.

Table I. Limits of Detection for Absorbance and Refractive Index

cuvette diameter, μm	refractive index detection limit,[a] ΔRI	absorbance detection limit[a]	absorbance per unit length at detection limit, cm^{-1}
50	4×10^{-6}	6×10^{-6}	1.2×10^{-3}
100	3×10^{-6}	9×10^{-6}	9.0×10^{-4}
500	3×10^{-6}	6×10^{-5}	1.2×10^{-3}

[a] Detection limits are two standard deviations larger than the noise in the background signal.

Detection limits of ΔRI = 6×10^{-7} were reported for our earlier refractive index measurements, obtained within a 500-μm-diameter Pyrex tube and aqueous samples (*17*). The present refractive index detection limits are a factor of 5 poorer. However, the current results are obtained with methanol solutions. Since the change in refractive index with temperature is also a factor of 5 greater for methanol than water, the refractive index detection limits probably are a result of greater sensitivity to temperature change for methanol compared with water. It appears that the low heat capacity of a thin capillary tube results in significant sensitivity to environmental temperature fluctuations. To produce better refractive index detection limits, it will be necessary to regulate the temperature of the capillary tube.

Methanol was chosen as the solvent because it produces greater sensitivity than water for thermooptical absorbance measurements. Absorbance calibration curves were obtained for the three capillary tubes and also are summarized in Table I. The calibration curves were all linear, $r > 0.9998$, over more than 3 orders of magnitude. For the 50-μm cuvette, linearity extended from the detection limit, $A = 6 \times 10^{-6}$, to the highest concentration sample studied, $A = 0.01$. Slightly poorer detection limits were obtained for the other cuvettes. No deviation from linearity was observed for any of the samples studied.

It is interesting that the concentration detection limits produced by the capillary thermooptical absorbance measurements were virtually identical for the three cuvettes, 2×10^{-7} M, and independent of path length. The slope of the calibration curves, about 4×10^2 V/M, was relatively consistent for each cuvette. A constant sensitivity, independent of path length, suggests that the instrument is not measuring absorbance but rather the absorptivity–concentration product in units of cm^{-1}. It appears that the signal is generated in a localized region within the cuvette, probably at the portion of the cuvette nearest the entrance of the pump beam. Noise also is independent of cuvette diameter and appears to be associated with probe beam intensity fluctuations. This independence of detection limit upon path length is very exciting; if the independence holds for smaller diameter capillary tubes, high-sensitivity absorbance measurements may be made for open-tubular capillary liquid chromatography.

A finite time will be required to reach thermal equilibrium in the thermooptical absorbance measurement. To characterize the time constant for thermal equilibrium, the lock-in signal was measured as a function of modulation frequency and is presented in Figure 2 in the form of a Bode plot. The signal amplitude demonstrated a relatively modest change with frequency below about 120 Hz. At the highest frequencies

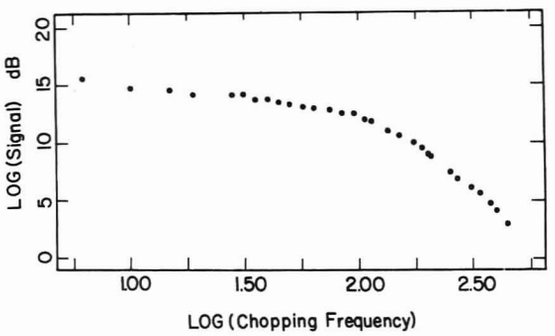

Figure 2. Chopping frequency dependence. The logarithm of the amplitude of the lock-in amplifier signal, in dB, is plotted against the logarithm of the chopping frequency in Hz. A 20 dB/decade roll-off in signal is observed for high chopping frequency, whereas a small change in signal is observed at low chopping frequency.

probed, the signal approached a 20 dB decrease in amplitude per decade increase in modulation frequency. The shape of this curve is similar to that observed for other thermooptical absorbance measurements (*23*, *24*, *31*) with a time constant on the order of 0.2 ms. This time constant is about a factor of 10 faster than that observed for the crossed-beam thermal lens with the same focusing lens and the same pump laser (*24*). One possible source of the short time constant is enhanced heat flow at the capillary wall. A short time constant is of value since very fast phenomena may be studied without degradation due to instrumental artifacts.

Several alignment constraints were qualitatively investigated for the thermooptical capillary absorbance measurement. As expected, the signal was highest when the pump laser beam waist was centered in the cuvette. Since a tightly focused pump beam also minimizes the system volume, all measurements reported in this manuscript were obtained with the pump waist located in the cuvette. The offset of the pump and probe beam axes turns out to be quite critical. Small changes in alignment of the axes, on the order of 20-μm, produces a significant change in absorbance signal. This alignment constraint probably reflects the very small beam spot-sizes produced by the short focal length microscope objectives used in the experiment. The sample cuvette was located at a number of positions before, at, and after the probe beam waist. No systematic difference in absorbance or refractive index sensitivity was noted at these positions. To minimize system volume, all measurements were obtained with the probe beam waist also located in the cuvette.

The definition of detector volume for crossed-beam instruments is somewhat arbitrary. For example, the intersection volume of the pump and probe beams in this instrument is quite small, slightly less than a picoliter. Instead, we use a much more conservative definition of the detection volume as a cylinder whose radius and height are given by the capillary radius. In a chromatographic application, it is difficult to imagine an eluted peak with smaller volume. For the 50-μm-diameter tube, the detector volume was about 50 pL. At the detection limit of 2×10^{-7} M, only 10^{-17} mol or 6 million analyte molecules were present within the detector volume. Of course, a significantly smaller amount of analyte was present within the small intersection volume of the laser beams. It is amusing to extrapolate these detection limits to smaller capillary tubes, higher pump laser power, and more strongly absorbing analyte. Assuming signal linearity with regard to pump laser power and sample absorptivity and independence with regard to capillary diameter, then detection of tens of analyte molecules will be possible with a 100-mW pump laser, 5-μm-diameter capillary tube, and analyte with molar absorptivity of 10^5 L M^{-1} cm^{-1}.

Two other laser-based detectors have been employed for measurement of refractive index and absorbance (*32*, *33*). In the first case, the sensitivity of refractive index to temperature change is used to construct a thermooptical absorbance measurement. A very sensitive Fabry–Perot interferometer is used to measure the refractive index of the analyte. A second pump laser beam is introduced along the probe beam path; absorbance of the pump laser beam produces a temperature rise and refractive index shift. Absorbance detection limit of 2×10^{-6} and refractive index detection limits of 1.5×10^{-8} were obtained over a 10-cm path with a 60-mW pump laser. Linearity extended for 2 orders of magnitude in absorbance and the detector volume about 200 μL. A second combination absorbance–refractive index detector has been reported which utilizes reflection near the critical angle to produce absorbance detection limits of 2.1×10^{-4} and refractive index detection limits of 2×10^{-7} within a 1-μL probe volume. A high-frequency acoustooptic modulator and lock-in amplifier were employed to reduce laser intensity noise. Absorbance was measured by sample transmission and could not be distinguished from refractive index changes.

Absorbance detection limits for the capillary instrument are similar to those of the Fabry–Perot interferometer and 2 orders of magnitude superior to those of the internal reflection instrument. Refractive index detection limits reported for the interferometer and the critical angle detector are 2 and 1 order of magnitude superior, respectively, to our results. It appears the large heat capacity of the interferometer and the prisms used in the critical angle instrument generate much lower sensitivity to temperature fluctuations than the micrometer capillary tube used in our instrument. Of course, the sample volume utilized in the capillary detector is over 4 orders of magnitude smaller than the critical angle reflection instrument and 6 orders of magnitude smaller than those of the interferometer.

Very low power, relatively inexpensive, and reliable lasers were employed to measure simultaneously absorbance and refractive index within micrometer diameter capillary tubes. The optical and electronic system, minus the optical table, could be duplicated for about US $5000. The combination of relative low cost, high reliability, small volume, and excellent detection limits for both absorbance and refractive index should prove attractive for a number of applications in capillary separation techniques.

LITERATURE CITED

(1) Novotny, M. *Anal. Chem.* **1981**, *53*, 1294A–1308A.
(2) Jorgenson, J. W.; Lukacs, K. D. *Science* **1983**, *222*, 266–272.
(3) Folestad, S.; Johnson, L.; Josefsson, B.; Galle, B. *Anal. Chem.* **1982**, *54*, 925–929.
(4) Gluckman, J.; Shelly, D.; Novotny, M. *J. Chromatogr.* **1984**, *317*, 443–453.
(5) Hershberger, L. W.; Callis, J. B.; Christian, G. D. *Anal. Chem.* **1979**, *51*, 1444–1446.
(6) Kelly, T. A.; Christian, G. D. *Anal. Chem.* **1981**, *53*, 2110–2114.
(7) Dovichi, N. J.; Martin, J. C.; Jett, J. H.; Keller, R. A. *Science*, **1983**, *219*, 845–847.
(8) Dovichi, N. J.; Martin, J. C.; Jett, J. H.; Trkula, M.; Keller, R. A. *Anal. Chem.* **1984**, *56*, 348–354.
(9) Zarrin, F.; Dovichi, N. J. *Anal. Chem.* **1987**, *59*, 846–850.
(10) Zarrin, F.; Risfelt, J. A.; Dovichi, N. J. *Anal. Chem.* **1987**, *59*, 850–854.
(11) Zarrin, F.; Bornhop, D. J.; Dovichi, N. J. *Anal. Chem.* **1987**, *59*, 854–860.
(12) Zarrin, F.; Dovichi, N. J. *Anal. Chem.* **1985**, *57*, 2690–2692.
(13) Zarrin, F.; Dovichi, N. J. *Anal. Chem.* **1985**, *57*, 1826–1829.
(14) Nolan, T. G.; Dovichi, N. J. *IEEE Circuits Devices Mag.* **1986**, *2*, 54–56.
(15) Nolan, T. G.; Bornhop, D. J.; Dovichi, N. J. *J. Chromatogr.* **1987**, *384*, 189–195.
(16) Nolan, T. G.; Dovichi, N. J., submitted for publication in *Anal. Chem.*
(17) Bornhop, D. J.; Dovichi, N. J. *Anal. Chem.* **1986**, *58*, 504–505.
(18) Bornhop, D. J.; Nolan, T. G.; Dovichi, N. J. *J. Chromatogr.* **1987**, *384*, 181–187.
(19) Kerker, M.; Matijević, E. *J. Opt. Soc. Am.* **1961**, *51*, 506–508.
(20) Watkins, L. S. *J. Opt. Soc. Am.* **1974**, *64*, 767–771.
(21) Harris, J. M.; Dovichi, N. J. *Anal. Chem.* **1980**, *52*, 695A–706A.
(22) Dovichi, N. J. *CRC Crit. Rev. Anal. Chem.*, in press.

(23) Dovichi, N. J.; Nolan, T. G.; Weimer, W. A. *Anal. Chem.* **1984**, *56*, 1700-1704.
(24) Nolan, T. G.; Weimer, W. A.; Dovichi, N. J. *Anal. Chem.* **1984**, *56*, 1704-1707.
(25) Weimer, W. A.; Dovichi, N. J. *J. Appl. Phys.* **1986**, *59*, 225-230.
(26) Weimer, W. A.; Dovichi, N. J. *Appl. Opt.* **1985**, *24*, 2981-2986.
(27) Weimer, W. A.; Dovichi, N. J. *Appl. Spectrosc.* **1985**, *39*, 1009-1013.
(28) Burgi, D. S.; Nolan, T. G.; Risefelt, J. A.; Dovichi, N. J. *Opt. Eng.* **1984**, *23*, 756-758.
(29) Jackson, W. B.; Amer, N. M.; Boccara, A. C.; Fournier, D. *Appl. Opt.* **1981**, *20*, 1333-1344.
(30) Wetsel, G. C.; Stotts, S. A. *Appl. Phys. Lett.* **1983**, *42*, 931-933.
(31) Dovichi, N. J.; Harris, J. M. *Proc. SPIE-Int. Soc. Opt. Eng.* **1981**, *288*, 372-375.
(32) Woodruff, S. D.; Yeung, E. S. *Anal. Chem.* **1982**, *54*, 1174-1178.
(33) Wilson, S. A.; Yeung, E. S. *Anal. Chem.* **1985**, *57*, 2611-2614.

RECEIVED for review December 23, 1986. Accepted March 2, 1987. This work was funded by the Natural Sciences and Engineering Research Council of Canada.

Fluorescence Emission as a Probe To Investigate Electrochemical Polymerization of 9-Vinylanthracene

Prashant V. Kamat

Radiation Laboratory, University of Notre Dame, Notre Dame, Indiana 46556

The cationic polymerization of 9-vinylanthracene can be initiated at a transparent SnO_2 electrode with the application of anodic potentials ($E > 1.1$ V vs. saturated sodium chloride calomel electrode) in acetonitrile solutions. The excimer emission (emission maximum ~500 nm) of poly(9-vinylanthracene) which is distinguishable from the monomer fluorescence emission (emission maxima 410, 430 nm) has been used to probe the electrochemical polymerization process directly. The in situ spectroelectrochemical technique, which would be useful in obtaining kinetic and mechanistic information of the electropolymerization process, is described.

In recent years, much attention has been drawn to the development and characterization of conducting polymers (*1-4*). Many aromatic heterocyclic molecules, upon electrochemical oxidation, lead to the formation of an electrically conducting organic polymer film at the electrode surface (*1*). Recently we reported (*5*) electrochemical polymerization of 1-vinylpyrene at a conducting SnO_2 electrode achieved with the application of anodic potentials. Such polymers with aryl molecules as pendent groups often exhibit excimer emission which is distinctively different from the monomer fluorescence emission. It is of interest to see whether one could utilize this photophysical property to probe the polymerization process directly. The purpose of this study is to demonstrate the feasibility of an in situ spectroelectrochemical technique in monitoring the electropolymerization process by using fluorescence emission as a probe. As shown earlier (*6-10*), such a technique could be useful for electrochemists to study the electrode surface as well as the transients and products generated in an electrochemical reaction.

EXPERIMENTAL SECTION

Materials. 9-Vinylanthracene (Aldrich), acetonitrile (Aldrich, gold label), and tetrabutylammonium perchlorate, TBAP (Alfa), were used as supplied. SnO_2 electrodes were cut from an antimony-doped NESA glass obtained from PPG industries and were cleaned as described earlier (*11*).

Instrumentation. Electrochemical and spectroelectrochemical measurements were done with a Princeton Applied Research (PAR) Model 173 potentiostat/galvanostat, a PAR Model 175 universal programmer, and a Kipp and Zonnen X-Y recorder. Experiments were performed in a standard three-compartment cell with a Pt wire as a counter electrode (CE) and a saturated sodium chloride calomel electrode (SSCE) as a reference electrode (RE). The potentiostat had a provision to compensate for the *iR* drop and this was employed during the electrochemical measurements. For spectroelectrochemical measurements a poly(tetrafluoroethylene) block was machined to accommodate a 0.5 cm × 4 cm SnO_2 plate (WE), a Pt wire (CE), and an Ag wire (RE) and was inserted into the 1 × 1 × 4.5 cm cuvette (Figure 1). The distance between the SnO_2 and the front wall of the cuvette, which was about 0.5 mm, allowed a thin layer of the sample. The whole assembly could then be inserted into the sample chamber of the fluorometer such that the excitation beam was at 45° to the SnO_2 electrode. In principle this spectroelectrochemical cell was similar to a previously described OTTLE—optically transparent thin layer electrochemical—cell (*9, 10*). Fluorescence measurements were carried out in the front face geometry. A SLM single photon counting fluorescence spectrometer was used to monitor the fluorescence emission.

RESULTS AND DISCUSSION

Electropolymerization of 9-Vinylanthracene. Cyclic voltammograms observed under anodic scans are shown in Figure 2. At potentials around 1.1 V (vs. SSCE) 9-vinylanthracene exhibited an irreversible oxidation and led to a curve crossing in the reverse scan. Successive anodic scans led to the decrease in the peak current and simultaneous growth of the polymer film at the electrode surface. This behavior was similar to the electrochemical polymerization of 1-vinylpyrene and is induced by the radical cation of 9-vinylanthracene formed during electrochemical oxidation The

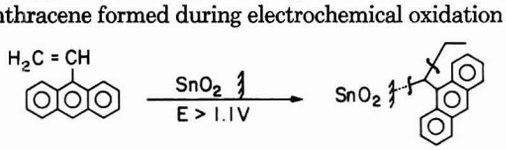

polymer is insoluble in acetonitrile but soluble in solvents such as THF or CH_2Cl_2.

Absorption and Emission Characteristics. The excitation and emission spectra of 9-vinylanthracene in CH_3CN and poly(9-vinylanthracene) film coated on the SnO_2 electrode are shown in Figure 3. (The polymer film coated SnO_2 plate was carefully washed with CH_3CN to remove any traces of the monomer.) The monomer exhibits absorption maxima at 350, 368, and 388 nm and emission maxima at 420 and 428 nm. The polymer film has absorption maxima at 358, 376, and 396 nm which is red-shifted compared to its monomer

0003-2700/87/0359-1636$01.50/0 © 1987 American Chemical Society

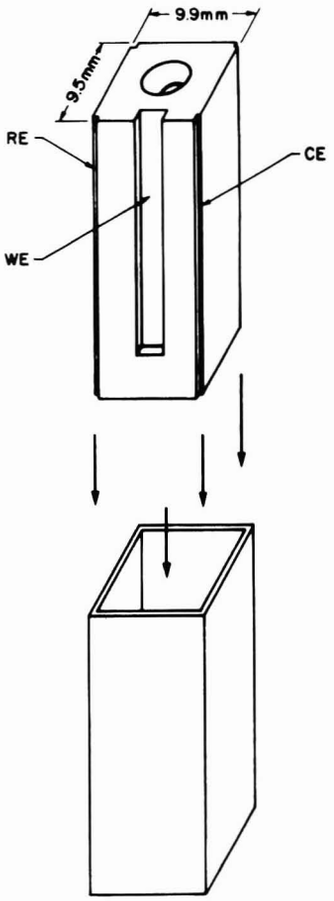

Figure 1. Design of the cell used in spectroelectrochemical measurements.

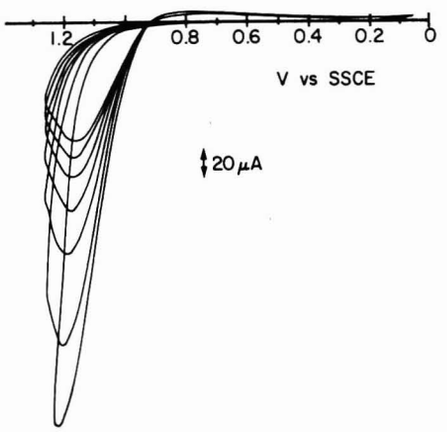

Figure 2. Cyclic voltammograms of 0.1 M 9-vinylanthracene in acetonitrile which exhibit electropolymerization at the SnO_2 electrode during repetitive scans (scan rate, 50 mV/s; electrolyte, 0.1 M TBAP).

absorption maxima. The emission of poly(9-vinylanthracene) is broad with a maximum around 500 nm and is distinctively different from the monomer emission. Such an emission which is commonly observed with many anthracene polymers is attributed to the formation of the excimers (*14*, *15*). Two anthracene units attached to the C–C chain can partially overlap to induce an excimer emission in such polymers. Since the emission bands of the monomer and the polymer are well separated from each other (e.g., at 520 nm the fluorescence emission is dominated only by the polymer), it should be possible to probe the polymerization process directly by monitoring the fluorescence emission.

Spectroelectrochemistry To Probe the Electropolymerization Process. It has been demonstrated earlier (*8–13*) that spectroelectrochemistry can be useful in investigating the

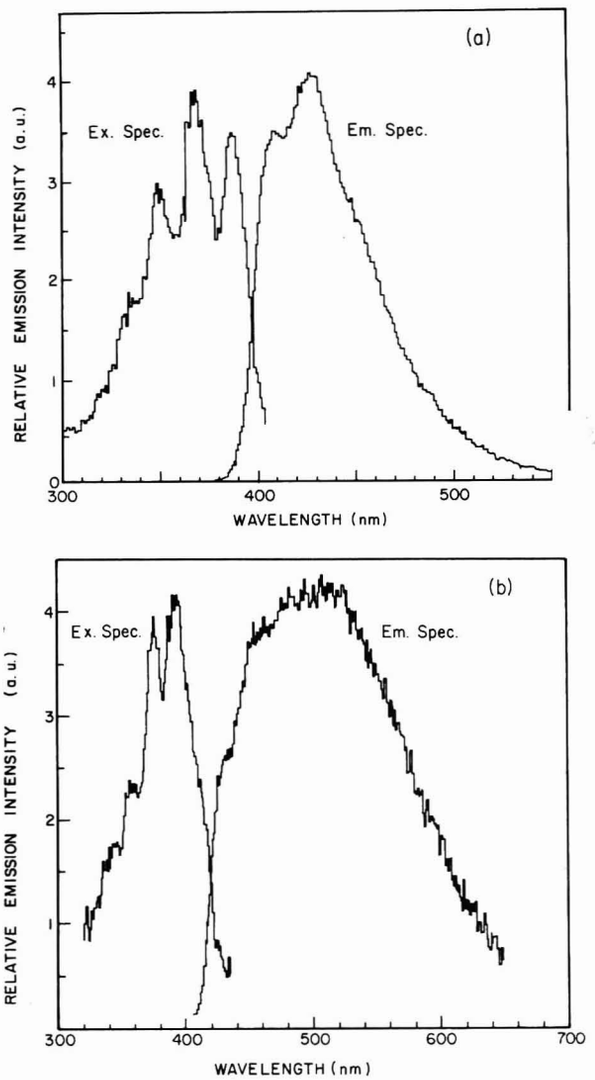

Figure 3. Excitation and emission spectra of (a) 9-vinylanthracene in acetonitrile and (b) poly(9-vinylanthracene) film formed at the SnO_2 electrode.

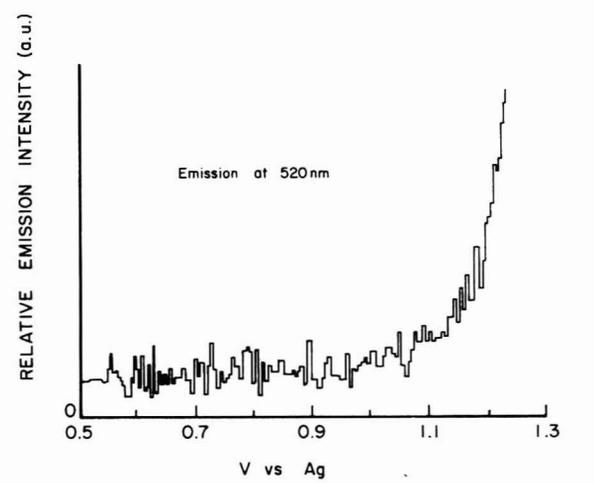

Figure 4. Fluorescence emission monitored at 520 nm during anodic cycling (WE, SnO_2; electrolyte, 0.2 M 9-vinylanthracene, 0.1 M TBAP; scan rate, 10 mV/s).

events that follow the electrochemical oxidation or reduction step. We have employed a similar approach to monitor the electrochemical polymerization of 9-vinylanthracene. The effect of anodic cycling on the fluorescence emission at 520 nm is shown in Figure 4. During the anodic scan, a sudden increase in the emission at 520 nm was observed as the potential was increased beyond 1.0 V. Such an increase in the

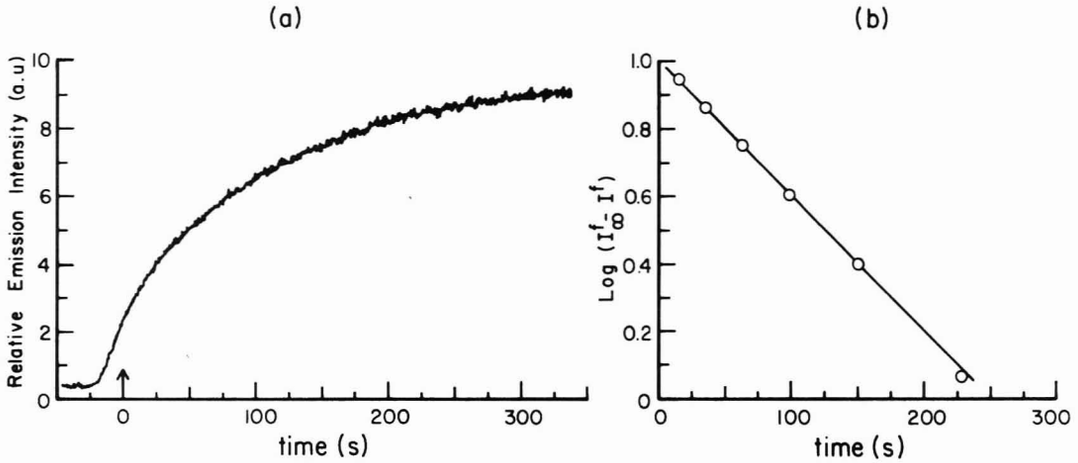

Figure 5. (a) Increase in the relative emission intensity at 520 nm after the application of an anodic potential of 1.1 V and passage of 1.2 × 10^{-2} C through the circuit. The growth in the emission was monitored after disconnecting the applied potential at t = 0 s (WE, SnO_2; electrolyte, 0.2 M 9-vinylanthracene, 0.1 M TBAP in acetonitrile at 295 K). (b) Plot of log ($I_\infty^f - I^f$) vs. time representing the pseudo-first-order fit of the fluorescence emission growth.

fluorescence emission at 520 nm represents the formation of poly(9-vinylanthracene) at the SnO_2 electrode. When observed separately, the emission at 420 nm was found to decrease during the anodic scan in a similar way which indicated the depletion of the monomer during the electropolymerization process.

The potential at which the sudden increase in the excimer emission at 520 nm (or decrease in the monomer fluorescence emission at 420 nm) could be seen matched the oxidation of 9-vinylanthracene observed in the cyclic voltammogram.

Kinetics of Polymerization. Electrochemical oxidation of the vinylaryl compound leads to the formation of its radical cation which is capable of initiating the polymerization process. The mechanism of the polymerization process can be described by the steps

initiation

$$M \xrightarrow{-e^-} P_1 \qquad (1)$$

propagation

$$P_n + M \rightarrow P_{n+1} \qquad n = 1, 2, \ldots \qquad (2)$$

where M is a monomer and P_n and P_{n+1} are growing radical-cations having n and (n + 1) monomeric units linked together covalently. The application of anodic potential results in the generation of P_1 at the electrode (reaction 1). Subsequent chemical reaction of electrogenerated species (reaction 2) can be monitored optically to investigate the kinetics of polymerization.

If the mechanism described by reactions 1 and 2 is true, one would expect these radical cations to continue to propagate and add on monomeric molecules until all the monomer is depleted. Indeed, when the applied potential (~1.1 V) at the SnO_2 electrode was disconnected, the fluorescence emission at 520 nm continued to increase until the monomer is exhausted. A typical growth in the excimer emission observed with the electrochemical initiation is shown in Figure 5a. (t = 0 represents the time at which the applied potential was disconnected.) The observed exponential growth in the excimer emission represented the propagation of the polymer chain to add on monomeric units. This experimental trace can be treated with pseudo-first-order kinetics as represented in Figure 5b. The plot of log ($I_\infty^f - I^f$) vs. t, where I_∞^f, the fluorescence intensity at infinite time, and I^f, the fluorescence intensity at any given time t, was a straight line and gave a value of 0.004 s^{-1} as the apparent pseudo-first-order rate constant for the chain propagation reaction. The concentration of the monomer was 0.2 M (30 μmol in 0.15 mL) and the concentration of the initiation, which was controlled by monitoring the charge passed through the circuit, was 1.2 × 10^{-7} mol.

The feasibility of an in situ spectroelectrochemical technique to investigate the electropolymerization process has been demonstrated in this paper. Further details regarding the kinetics and the mechanistic features of the electrochemical polymerization of 9-vinylanthracene will be published elsewhere (*16*).

ACKNOWLEDGMENT

Helpful discussions with Santosh K. Gupta, Department of Chemical Engineering, are greatly appreciated.

Registry No. SnO_2, 18282-10-5; 9-vinylanthracene, 2444-68-0; poly(9-vinylanthracene), 29659-51-6.

LITERATURE CITED

(1) Waltman, R. J.; Bargon, J. *Can. J. Chem.* **1986**, *64*, 76.
(2) Frommer, J. E. *Acc. Chem. Res.* **1986**, *19*, 2, and references cited therein.
(3) Waltman, R. J.; Diaz, A. F.; Bargon, J. *J. Electrochem. Soc.* **1984**, *131*, 740.
(4) Kamat, P. V.; Basheer, R. A. *Chem. Phys. Lett.* **1984**, *103*, 503.
(5) Kamat, P. V.; Basheer, R. A.; Fox, M. A. *Macromolecules* **1985**, *18*, 1366.
(6) Murray, R. W.; Heinemann, W. R.; O'Dorn, G. W. *Anal. Chem.* **1967**, *39*, 1666.
(7) Kuwana, T.; Winograd, N. In *Electroanalytical Chemistry*; Bard, A. J., Ed.; Marcel Dekker: New York, 1974; Vol. 7, p 1.
(8) Kuwana, T.; Heineman, W. R. *Acc. Chem. Res.* **1976**, *9*, 241, and references cited therein.
(9) Heineman, W. R. *Anal Chem.* **1978**, *50*, 390A, and references cited therein.
(10) De Angelis, J. P.; Heineman, W. R. *J. Chem. Educ.* **1976**, *53*, 594.
(11) Kamat, P. V.; Fox, M. A.; Fatiadi, A. J. *J. Am. Chem. Soc.* **1984**, *106*, 1191.
(12) Albertson, D. E.; Blount, H. N.; Hawkridge, R. M. *Anal. Chem.* **1979**, *51*, 556.
(13) Blubaugh, E. A.; Yacynych, A. M.; Heineman, W. R. *Anal. Chem.* **1979**, *51*, 561.
(14) Hargreaves, J. S.; Webber S. E. *Macromolecules* **1984**, *17*, 235.
(15) Semerak, S. N.; Frank, W. C. *Adv. Polym. Sci.* **1983**, *54*, 31.
(16) Kamat, P. V.; Gupta, S. K., submitted for publication in *J. Electroanal. Chem.*

RECEIVED for review October 16, 1986. Accepted March 19, 1987. The research described herein was supported by the Office of Basic Energy Sciences of the Department of Energy. This is Document No. NDRL-2914 from the Notre Dame Radiation Laboratory.

Error Modeling and Confidence Interval Estimation for Inductively Coupled Plasma Calibration Curves

Robert L. Watters, Jr.*

National Bureau of Standards, Center for Analytical Chemistry, Gaithersburg, Maryland 20899

Raymond J. Carroll

University of North Carolina at Chapel Hill, Chapel Hill, North Carolina 27514

Clifford H. Spiegelman

National Bureau of Standards, Center for Applied Mathematics, Gaithersburg, Maryland 20899

A simple linear calibration function can be used over a wide concentration range for the inductively coupled plasma (ICP) spectrometer due to its linear response. The random errors over wide concentration ranges are not constant, and constant variance regression should not be used to estimate the calibration function. Weighted regression techniques are appropriate if the proper weights can be obtained. Use of the calibration curve to estimate the concentration of one or more unknown samples is straightforward, but confidence interval estimation for multiple use of the calibration curve is less obvious. We describe a method for modeling the error along the ICP calibration curve and using the estimated parameters from the fitted model to calculate weights for the calibration curve fit. Multiple and single-use confidence interval estimates are obtained and results along the calibration curve are compared.

A widely used method for determining inorganic elements in aqueous samples is the inductively coupled plasma (ICP) spectrometric technique (*1–3*). One of the principal advantages of the ICP technique is its wide range of linear response to analyte concentration. This feature, together with relative freedom from interelement interferences, often allows the analyst to determine a given element in a variety of sample matrices with only infrequent recalibration of the instrument. Although the variability of the calibration process is sometimes assumed to be negligible compared to sample measurement variability, it is desirable to establish procedures whereby this assumption may be conveniently tested. If calibration is indeed a significant contributor to the overall variation of the measurement process, this source of variation should be estimated and included in the overall uncertainty statement.

The calibration curve for ICP spectrometry is an example where weighted regression should be used because the measurements may exhibit nonconstant variance (heteroscedasticity). In general, if the calibrated region includes the widest range of concentration for which straight-line response is assured, nonuniform precision of measurement is evident. Agterdenbos (*4*) approached the problem of "ICP type" calibration curves by dividing the range of calibration into segments that exhibit either constant standard deviation or constant relative standard deviation characteristics. Maessen and Balke (*5*) also compared the effects of treating ICP calibration curves as combinations of linear and logarithmic segments. The usefulness of simple weighted linear regression was mentioned, but not considered. It was stated by these authors that no suitable method exists for obtaining the confidence interval for an unknown analyte concentration calculated from a weighted linear regression.

More recently, Bubert and Klockenkamper (*6*) have considered the effects of heteroscedasticity in ICP and X-ray fluorescence (XRF) calibration curves. They outline a scheme for using established tests for the normality of the distribution of the measured values as well as the homogeneity of variance. An algorithm for evaluating the sources of variance was used, and a weighted linear regression was carried out. Confidence limits for the concentration of an analyzed sample can be calculated by using their approach. Schwartz (*7*) and Oppenheimer et al. (*8*) have given methods for weighted regression of calibration curves with nonuniform variance. Confidence intervals for a single determination of an unknown are given using propagation of error in the case of Schwartz (*7*). Although the main focus was to treat weighted calibration curve estimation of detection limits, single-use intervals can also be obtained by adapting the approach described by Oppenheimer et al. (*8*) to higher concentration levels. A multiple-use procedure has been presented by Garden et al. (*9*) that often results in intervals wider than those developed by the methods described in this paper. Garden et al. acknowledge the conservative nature of their interval estimates, which allows for some nonrandom error that often occurs in spectrometric measurement. We prefer to restrict our estimation of confidence intervals to include random error only. Assessment of systematic errors should be carried out separately, using techniques specifically designed for this task.

We describe here a simple method for characterizing the variance along an ICP calibration curve due to the principal sources of noise in this specific technique. Our approach is philosophically similar to that of Garden et al. (*9*) except that we use calibration data only as a starting point to model the error along the calibration curve. Our method involves standard regression techniques and can be incorporated into routine analytical schemes due to its simplicity. A flow chart of the procedures is presented in Figure 1. We model both the standard deviation and the variance of instrument noise as a function of sample concentration over the range of straight-line response. We use a quadratic model of concentration as suggested by Oppenheimer et al. (*8*) rather than a quadratic model of intensity as used by Bubert and Klockenkamper (*6*) and Schwartz (*7*). We choose to model the error in terms of concentration rather than intensity, since we are dealing with a specific technique whose linear response is well documented. A particular feature of our approach is that each iteration of the noise model fit is itself a weighted fit using estimates from the previous iteration. This procedure differs from the unweighted modeling used by Oppenheimer et al. (*8*). The final set of fitted standard deviations or variances is then used for the weighted regression of the

0003-2700/87/0359-1639$01.50/0 © 1987 American Chemical Society

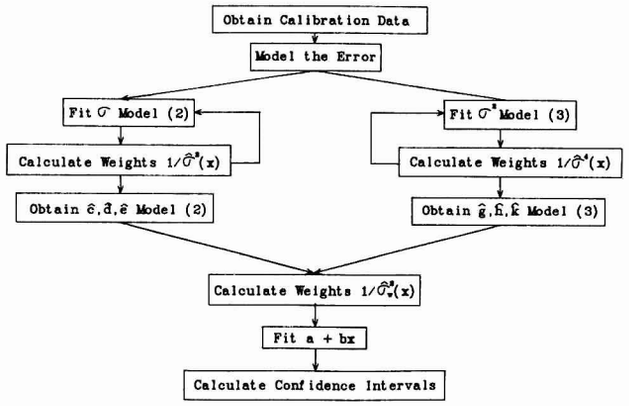

Figure 1. Flow chart of procedures for modeling ICP calibration error, weighted linear regression of the calibration function, and estimation of confidence intervals for an unknown sample measurement.

straight-line calibration curve. Confidence limits for concentrations obtained by using the calibration curve are calculated in a straightforward manner.

ALGORITHM

The method we use for characterizing the ICP calibration curve assumes the model

$$Y_{ij} = a + bx_i + \text{error}_{ij} \quad (1)$$

where Y_{ij} is the measured intensity for $i = 1, 2, ..., I$ calibration standards of concentration x_i, and $j = 1, 2, ..., J \geq 2$ instrumental replicates. The calibration function is $a + bx$, and the random errors have mean 0 and variance $\sigma^2(x_i)$. The errors are independent and normally distributed. The model for the standard deviation is

$$\sigma(x) = c + dx + ex^2 \quad (2)$$

The estimate of standard deviation s_i at each calibration point, x_i, is calculated by using the replicate measurements of each standard solution. These s_i's are then fitted according to model (2) by unweighted least squares to obtain predicted standard deviations, $\hat{\sigma}(x_i)$. We now iterate the fit by using weights, $1/\hat{\sigma}^2(x_i)$, to obtain a new set of predicted standard deviations. Each iteration uses weights calculated from the predicted values of the previous step. The procedure stops when successive predicted values agree to within 0.1% relative.

Alternately, we also model variance in a similar manner. The model is

$$\sigma^2(x) = g + hx + kx^2 \quad (3)$$

and the s_i^2's are fitted according to model (3). The iteration is performed as before except that the variance fit is now weighted by $1/\hat{\sigma}^4(x_i)$. Predicted variances are used to obtain standard deviations at each x_i.

There exists a spectrochemical basis for certain aspects of models (2) and (3). Constant noise sources such as detection electronics account for the concentration-independent term in either model. Shot noise expressed as a variance is proportional to intensity, or in this case the concentration x, which corresponds to the coefficient h in model (3). Source flicker noise corresponds to the second term in model (2) or the third in model (3). A similar partition of noise sources is mentioned in ref 6.

The final set of predicted standard deviations, $\hat{\sigma}_w(x_i)$ obtained from either (2) or (3) is used to calculate weights $1/\hat{\sigma}^2_w(x_i)$ for the least-squares fit of the calibration function, $a + bx$. The results of this fit include an estimate for the intercept, $\hat{a}$, the slope, $\hat{b}$, the residual standard deviation $\hat{\sigma}$, and the standard error for the predicted mean at each x, $\hat{\sigma}_{f(x)}$

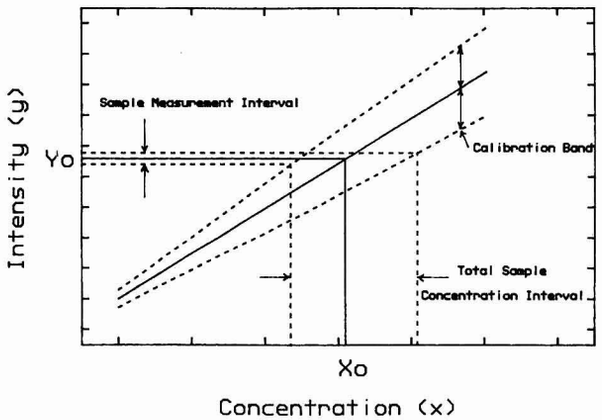

Figure 2. Calibration curve, confidence bands, and construction of the confidence interval for the measurement of an unknown sample concentration for the constant variance case.

at concentration x. We assign degrees of freedom, γ for $\hat{\sigma}_{f(x)}$ by

$$\gamma = I - 2$$

The estimated calibration function is then

$$f(x) = \hat{a} + \hat{b}x$$

To obtain a concentration value for an unknown sample, we can solve $Y_0 = \hat{a} + \hat{b}x_0$, the mean measured analyte intensity, for x_0; i.e., we invert the calibration function. To obtain an approximate confidence interval for the sample concentration, we combine the confidence interval about the mean sample intensity with the confidence band about the estimated calibration function. The interval is constructed with probability $1 - \alpha$, and the band is constructed with probability $1 - \delta$.

Let $t_\gamma(1 - \alpha/2)$ be the $1 - \alpha/2$ percentile from a t distribution with γ degrees of freedom and $F_{2,\gamma}(1 - \delta)$ be the $1 - \delta$ percentile of an F distribution with 2 and γ degrees of freedom. The confidence interval for an unknown sample concentration is obtained by measuring its intensity, Y_0, and finding all x's that satisfy the following inequalities:

$$f(x) - t_\gamma(1 - \alpha/2)\hat{\sigma}_w(x)\hat{\sigma} - (2F_{2,\gamma}(1 - \delta))^{1/2}\hat{\sigma}_{f(x)} \leq Y_0 \leq f(x) + t_\gamma(1 - \alpha/2)\hat{\sigma}_w(x)\hat{\sigma} + (2F_{2,\gamma}(1 - \delta))^{1/2}\hat{\sigma}_{f(x)} \quad (4)$$

where $t_\gamma(1 - \alpha/2)\hat{\sigma}_w(x)\hat{\sigma}$ is the half-width of the confidence interval about Y and $(2F_{2,\gamma}(1 - \delta))^{1/2}\hat{\sigma}_{f(x)}$ is the half-width of the confidence band at x about $f(x)$. Typically, equal values for α and δ are chosen. The derivation of (4) for the homoscedastic case is given in ref 10, and the resulting confidence band applies to multiple use of the calibration curve. We allow here for the inclusion of weights as determined by the error modeling. The inequalities for calibration followed by a single use (*8*, *11*) of the curve reduce to

$$f(x) - t_\gamma(1 - \alpha/2)\{\{\hat{\sigma}_w(x)\hat{\sigma}\}^2 + \{\hat{\sigma}_{f(x)}\}^2\}^{1/2} \leq Y_0 \leq f(x) + t_\gamma(1 - \alpha/2)\{\{\hat{\sigma}_w(x)\hat{\sigma}\}^2 + \{\hat{\sigma}_{f(x)}\}^2\}^{1/2} \quad (5)$$

The relationships of the calibration function, confidence interval, and confidence band for the homoscedastic case ($\hat{\sigma}_w(x)$ = constant) are depicted in Figure 2. The construction of the confidence interval for an unknown sample concentration from replicate measurements of emission intensity is readily discernible from the figure. However, the heteroscedastic case is not so easily represented. We choose to represent the combination of the confidence interval with the confidence band as a widened band whose upper bound, $U(x)$, is the right-hand side of the inequalities (4), and the lower bound, $L(x)$, is the left-hand side. The resulting band is plotted in

Table I. ICP Data for Ni at 231.604 nm Using 10 Replicates, $1/\hat{\sigma}^2_w(x)$, Weighting of Model (2), and $1/\hat{\sigma}^2_w(x)$ Weighting of the Calibration Function[a]

concn, μg/μL	intensity (counts)	s_i (obsd)	s (10 reps)	s (4 reps)	SI	CB	total
0.00	11.33	8.54	7.88	6.97	17.95	10.54	28.48
0.0101	16.60	7.88	7.98	7.03	18.17	10.49	28.66
0.0251	37.92	9.06	8.12	7.12	18.50	10.43	28.93
0.0503	57.00	8.46	8.36	7.28	19.05	10.33	29.39
0.101	149.88	6.13	8.84	7.58	20.14	10.19	30.34
0.251	369.24	11.57	10.25	8.50	23.34	10.13	33.47
0.503	763.36	11.94	12.48	10.02	28.42	11.20	39.62
2.51	3688.46	26.24	25.42	22.25	57.89	37.85	95.74
5.03	7431.08	29.12	29.30	37.55	66.74	76.67	143.40

[a] Values at each concentration are listed for observed standard deviation, s_i (obsd); predicted standard deviation for 10 replicates, S (10 reps), and 4 replicates, s (4 reps); sample measurement interval, SI; calibration uncertainty bandwidth, CB; and total uncertainty band, total.

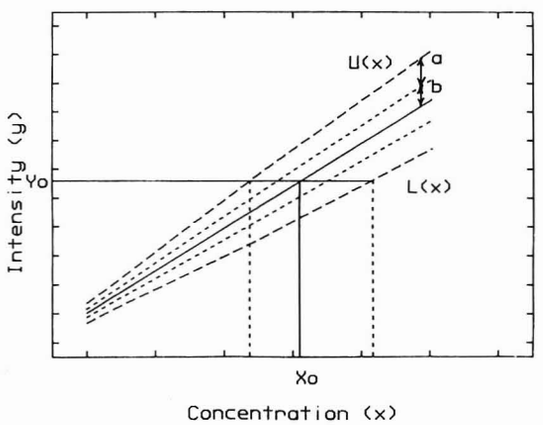

Figure 3. Construction of the sample measurement interval band (a) and the calibration confidence band (b) for the heteroscedastic linear calibration function. The total confidence band is comprised of the upper bound, $U(x)$, and the lower bound, $L(x)$, so that the confidence interval for an unknown sample measurement is defined by the intersection of Y_0 with $U(x)$ and $L(x)$.

Figure 3. The confidence interval for an unknown sample concentration is then simply determined by the intersection of Y_0 with $U(x)$ and $L(x)$. This approach requires that the slope be positive and sufficiently large to ensure that Y_0 crosses the bounds, $U(x)$ and $L(x)$, only once. In most applications of ICP spectrometry, these conditions are fulfilled if analytically useful spectral emission lines are chosen. Other types of calibration curves with negative slope can be treated by using simple modifications to (4) and (5). The location of the minimum calibration bandwidth is dependent on the particular set of concentration standards used. The dilution scheme described in the following section results in the appearance of the bands in Figures 2 and 3.

We examine the effects of calibration in various ICP analysis schemes in the following example.

EXPERIMENTAL SECTION

The measurements were performed on a sequential ICP spectrometer system with a spectral band-pass of 0.007 nm. The normal ICP spectrometer experimental parameters and operating conditions were used. Various spectral lines were used in this study, but we present the data for Ni at 231.604 nm as being representative of the characteristics of most ICP spectral lines normally used for analysis. The spectral background at 231.625 nm was measured and subtracted from the peak intensity for each instrumental integration.

A total of ten standard solutions were prepared by using volumetric pipets and flasks. However, each aliquot and final dilution volume was weighed so that the calculated concentrations of the calibration standards were based on the gravimetric data. The concentrations of the standards ranged from 0 to 5.03 μg/mL, with a reagent blank used as the zero standard. Vials containing these 10 solutions were placed in the autosampler of the spectrometer and the run sequence was programmed. The order of standard solution introduction was randomized, and adequate rinsing for the widest concentration range was accommodated. In this case, the run sequence included a rinse of 45 s in 1% nitric acid in distilled water followed by a washout of 30 s with the next solution to be measured. The first 15 s of this washout period take place with a solution uptake rate of 8 mL/min. The sample peristaltic pump returns to the normal rate of 1 mL/min 15 s before measurements begin. Spectral intensities are measured by electronic integration of the photomultiplier current for 0.25 s.

RESULTS AND DISCUSSION

Ten replicate integrations of each solution were recorded, and the average net intensity value, Y_i, and standard deviation, s_i, for each were calculated. The first analysis of the data included all ten replicates at each of the 10 standard concentrations. Since the ICP is often used in laboratories where the sample analysis rate is high, instrumental replicates in such situations may be limited to as few as four. We therefore examined this case by repeating the fit using only the first four replicates from each set of 10. At this point the data were examined to test the assumption of measurement independence and outliers. The occurrence of outliers and nonrandom variability caused by the performance characteristics of ICP nebulizers has been previously described (*12*), and this issue has also been addressed by Garden et al. (*9*). Extensive experience with ICP results for Ni in our laboratory indicated that the set of replicate integrations at 1.01 μg/mL was not representative of normal ICP instrument behavior.

This set of 10 replicates has a calculated standard deviation of 15.1, which is the expected level of variability for this concentration level. However, if the ninth integration is excluded, this statistic is 6.2. These data represent a period of measurement wherein the ICP sample delivery and signal detection systems were atypically stable. When only the first four data points are used, the estimated standard deviation (5.5) severely underestimates typical variability at this concentration. Successive integrations over short periods of time often show some degree of drift. However, the interdependence of successive integrations at 1.01 μg/mL and the existence of the outlier (ninth integration) indicate that the data at this concentration cannot be used to estimate ICP variability. Accordingly, we analyzed the remaining data excluding the entire data set at this concentration. The data are listed in Table I.

The fit of the estimated standard deviation, $\hat{\sigma}(x)$, for both the 10 and 4 replicate cases according to model (2) yields the parameter estimates listed in Table II. Results for unweighted, weighted by $1/s^2_i$, and weighted by $1/\hat{\sigma}^2_w(x)$ are given in the table. The largest differences in parameter estimates are observed between the unweighted case and either of the two weighted fits. Even these differences are relatively small and have little effect on the remainder of the analysis.

Table II. Coefficient and Standard Error (SE) Estimates for Fit of Model (2) Using Nine Standard Concentrations

	10 replicates		4 replicates	
coefficient	estimate	SE	estimate	SE
unweighted				
$\hat{c}$	7.78	0.56	6.80	1.29
$\hat{a}$	10.28	1.17	7.25	2.67
$\hat{e}$	−1.20	0.24	−0.26	0.55
weighted by $1/s^2_i$				
$\hat{c}$	7.88	0.56	7.00	1.42
$\hat{a}$	9.66	2.63	5.84	6.82
$\hat{e}$	−1.07	0.58	0.046	1.62
weighted by $1/\hat{\sigma}^2_w(x)$				
$\hat{c}$	7.88	0.56	6.97	1.41
$\hat{a}$	9.69	2.59	6.07	6.56
$\hat{e}$	−1.08	0.57	0.0025	1.60

Table III. Coefficient and Standard Error (SE) Estimates for Fit of Model (3) Using Nine Standard Concentrations

	10 replicates		4 replicates	
coefficient	estimate	SE	estimate	SE
unweighted				
$\hat{g}$	45.6	15.1	51.0	20.3
$\hat{h}$	332.6	31.2	135.5	41.8
$\hat{k}$	−34.2	6.42	23.9	8.6
weighted by $1/s^4_i$				
$\hat{g}$	71.6	22.8	65.1	23.0
$\hat{h}$	−46.6	254.6	5.1	189.8
$\hat{k}$	62.8	62.2	57.2	62.9
weighted by $1/\hat{\sigma}^4_w(x)$				
$\hat{g}$	60.6	22.9	60.6	22.9
$\hat{h}$	42.7	148.7	42.7	148.7
$\hat{k}$	50.4	56.7	50.4	56.7

The fit of variance, however, is significantly affected by weighting. The fit of estimated variance, $\hat{\sigma}^2(x)$, according to model (3) results in the parameter estimates listed in Table III for unweighted, weighted by $1/s^4_i$, and weighted by $1/\hat{\sigma}^4(x)$ fitting. The method of weighting has a significant effect on the parameter estimates. The weights, $1/\hat{\sigma}^2_w(x)$, for the fit of s using model (2) range over 1 order of magnitude. However, the weights, $1/\hat{\sigma}^4_w(x)$, for the variance fit of model (3) range over 2 orders of magnitude. Although the high concentration points are important for estimating this fit in the quadratic region, they have extremely low weighting. Therefore, the weighted fitting procedure has difficulty distinguishing between a linear and a quadratic model. Thus, the estimates of the linear and quadratic terms will be determined with large uncertainties, although the fit of either (2) or (3) may be quite adequate.

For limited sets of ICP calibration data, the iterative fitting procedure with $1/\hat{\sigma}^2(x)$ weighting of model (2) or with $1/\hat{\sigma}^4(x)$ weighting of model (3) is preferred, since it appears to be generally applicable and reliable. The iteratively weighted fitting procedure for $\sigma^2(x)$ using model (3) yields a set of predicted standard deviations quite similar to the set obtained by fitting $\sigma(x)$ with model (2). Therefore, we will further examine the fit of model (2) using parameter values from the $1/\hat{\sigma}^2_w(x)$-weighted case in Table II.

The adequacy of the fit for the 10-replicate case is evident in Table I, where the observed standard deviations and predicted standard deviations are listed for each of the nine concentrations. The largest difference is at 0.101 μg/mL, where the observed standard deviation value is approximately 70% of the predicted value. This deviation is well within expected instrumental variability at the count level indicated in the table. The predicted standard deviations for the 4-replicate case are also listed in Table I, and the exhibit reasonable agreement with the 10-replicate estimates. The only

Table IV. Effects of Weighting Method on the Calibration Curve Fit, $a + bx$

		10 replicates		4 replicates	
case	coefficient	estimate	SE	estimate	SE
unweighted	a	0.62	5.61	2.87	4.21
	b	1476.04	2.98	1477.69	2.24
weighted by $1/s^2_i$	a	0.95	3.95	−0.89	3.71
	b	1476.66	6.11	1481.12	9.01
weighted by $1/\hat{\sigma}^2_w(x)$	a	0.94	4.13	1.52	3.69
	b	1476.30	6.16	1480.38	7.00

significant difference between the two data sets lies in the standard error of the parameter estimates listed in Table II. It is expected that 10 replicates are more reliable for estimating the fit than 4. This is especially true when problems of interdependence of data arise, as mentioned with regard to the data for the standard at 1.01 μg/mL.

We now examine the fit of the calibration function. A comparison of fitting effects on the calibration curve is presented in Table IV. Weights equal to 1.00, $1/s^2_i$, and $1/\hat{\sigma}^2_w(x)$ are compared. In this case, the $1/s^2_i$ weights are derived directly from the standard deviation of the calibration data at each concentration (Table I). The $1/\sigma^2_w$ weights are calculated from the final set of predicted standard deviations using the fit of model (2) for the σ^2 case. The coefficient and standard error estimates for the 10-replicate data are quite similar regardless of whether $1/s^2_i$ or $1/\hat{\sigma}^2_w(x)$ weights are used. The unweighted case (weights = 1.00) yields slightly different (and erroneous) values for the standard errors. Of course, uncertainty interval estimates for an unknown sample concentration should not be calculated for the unweighted case since homoscedasticity would have to be assumed. Data in Table I indicate that no single value for the standard deviation is suitable over the range of calibration.

Using only four replicates causes a small change in the slope and a relatively larger change in the intercept, especially for the $1/s^2_i$-weighting case. However, the standard errors for these estimates are large enough to minimize the significance of these differences. In practical applications where the chief concern is trace analysis near the intercept, a more limited range of calibration is appropriate and the standard error of the intercept is likely to be smaller. In terms of the standard error of the estimated coefficients, the four-replicate data represent a minor deterioration in the variability of the fit, except for the unweighted case.

Although the spectral background near a number of ICP spectral lines for a variety of elements may exhibit more complex structure, the background near the 231.604-nm line of Ni is quite flat. Therefore, net intensity measurements for Ni could be fitted to a zero-intercept calibration model, as is indicated by the intercept estimates and their standard errors listed in Table IV.

Multiple-use confidence interval estimation was carried out using $\alpha = 0.10$. The components of inequalities (4) were evaluated for the 10-replicate case and are listed in Table I. It is evident that the uncertainty interval for the unknown sample measurement and the calibration uncertainty band contribute almost equally to the total uncertainty. Ignoring either source of variability will result in a significant underestimation of the random error in a sample analysis.

Comparisons of final multiple-use confidence intervals obtained for the concentration of an unknown sample are presented in Figures 4 and 5. The average value for the last four integrations at 0.101 μg/mL and at 5.03 μg/mL was used as the mean intensity for each of two unknown sample measurements. Multiple-use confidence intervals were calculated for 10- and 4-replicate calibration and for weighting with

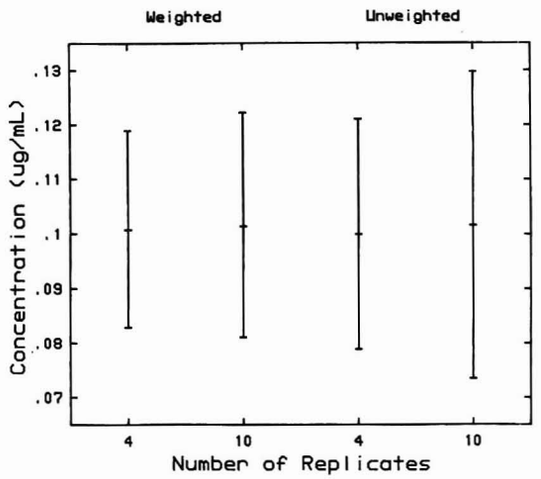

Figure 4. Multiple-use confidence bands for the measurement of an unknown sample with a true concentration of 0.101 μg/mL. Confidence bands are constructed for calibration using 4- and 10-replicate integrations and with and without weighting of the calibration function.

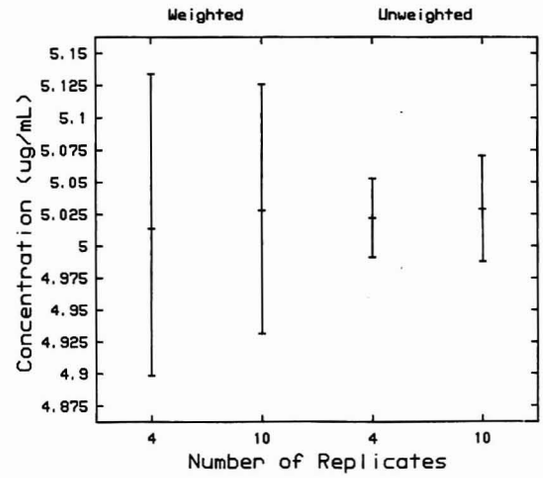

Figure 5. Multiple-use confidence bands for the measurement of an unknown sample with a true concentration of 5.03 μg/mL. Confidence bands are constructed for calibration using 4- and 10-replicate integrations and with and without weighting of the calibration function.

$1/\hat{\sigma}^2_w(x)$ and 1.00 as weights at each x_i. Figure 4 depicts data at the low end of the calibration curve where the true concentration of the unknown is 0.1006 μg/mL. At this end of the calibration curve, each multiple-use interval is 41% wider than its corresponding single-use interval. When intervals for 10- and 4-replicate cases are compared, it is useful to consider which elements in the inequalities (4) differ. Different parameter estimates for model (2) lead to different sets of predicted standard deviations. These are used for the weighted calibration curve fit, so that the $f(x)$ term in (4) is affected, as is the standard deviation of the fit, $\hat{\sigma}$. The predicted standard deviation at the unknown concentration, $\hat{\sigma}_w(x_i)$, is also obtained from the fit of model (2), so that this term will also be affected. For the data plotted in Figure 4, the predicted value for $\hat{\sigma}_w(x_i)$ for four replicates was less than that for 10-replicate calibration. Again, this phenomenon is due to short-term stability of four replicate integrations that leads to lower estimates of variability. This underscores the need for caution when sample throughput demands force a reduction in the number of instrumental replicates taken.

An important difference in interval width exists between the weighted and unweighted cases. In the latter case, the value of $\hat{\sigma}_w(x_i)$ is 1.0, and at the low end of the calibration curve, $\hat{\sigma}$ is appreciably larger for the unweighted fit than for the weighted fit. The product, $\hat{\sigma}_w(x_i)\hat{\sigma}$, is therefore slightly larger for the unweighted case. This causes a small overestimation of confidence interval widths at the low end of the calibration curve.

Multiple-use intervals for the high end of the calibration curve are depicted in Figure 5, where the true value of the unknown concentration is 5.03 μg/mL. In this case, the predicted value for $\hat{\sigma}_w(x_i)$ for four replicates is greater than that for 10, causing the 4-replicate intervals to be wider than the corresponding 10-replicate intervals. At this end of the calibration curve, however, the interval widths for fitting with weights 1.0 significantly underestimate the true interval widths as estimated by the weighted cases. The larger variance at the high end of the calibration curve, as estimated by $\hat{\sigma}_w(x_i)$, accounts for this difference. At this end of the calibration curve, each multiple-use interval is approximately 63% wider than its corresponding single-use interval.

In summary, estimation of the error along the calibration curve is important for weighted regression. Error modeling is more stable than using the standard deviations of the calibration standard measurements themselves. The iterative weighted fitted procedure is applicable to standard deviation modeling and is the preferred approach in variance modeling. Clearly, if heteroscedasticity is ignored, confidence intervals will be too narrow at the high end and too wide at the low end of the ICP calibration curve. The magnitude of these effects will depend on the particular dilution scheme used to make the calibration standard solutions. Estimates of both single and multiple-use confidence intervals differ significantly. Therefore, care should be taken in applying these procedures to a particular analysis scheme.

ACKNOWLEDGMENT

Helpful suggestions were provided by K. Eberhardt and L. Currie, for which the authors are grateful.

LITERATURE CITED

(1) Fassel, V. A.; Kniseley, R. N. *Anal. Chem.* **1974**, *46*, 1110A–1120A.
(2) Greenfield, S.; McGeachin, H. McD.; Smith, P. B. *Talanta* **1976**, *23*, 1–14.
(3) Fassel, V. A. *Science* **1978**, *202*, 183–191.
(4) Agterdenbos, J. *Anal. Chim. Acta* **1979**, *108*, 315–323.
(5) Maessen, F. J. M. J.; Balke, J. *Spectrochim. Acta, Part B* **1982**, *37B*, 37–42.
(6) Bubert, H.; Klockenkamper, R. *Fresenius' Z. Anal. Chem.* **1983**, *316*, 186–193.
(7) Schwartz, L. M. *Anal. Chem.* **1979**, *51*, 723–727.
(8) Oppenheimer, L.; Capizzi, T.; Weppeiman, R.; Mehta, H. *Anal. Chem.* **1983**, *55*, 638–643.
(9) Garden, J. S.; Mitchell, D. G.; Mills, W. N. *Anal. Chem.* **1980**, *52*, 2310–2315.
(10) Carroll, R. J.; Sacks, J.; Spiegelman, C. H., submitted for publication in *Technometrics*.
(11) Seber, G. A. F. *Linear Regression Analysis*; Wiley: New York, 1977.
(12) Watters, R. L., Jr.; Norris, J. A. *Proceedings of the 17th Eastern Analytical Symposium*; Franklin Institute Press: New York, 1977; pp 65–81.

RECEIVED for review November 3, 1986. Resubmitted March 2, 1987. Accepted March 23, 1987. The authors gratefully acknowledge support for this work from the Office of Naval Research, Grant NR-042544, and from the Air Force for support of R.J.C., Grant AFSOR-F-49620-85-C-0114.

External Heavy-Atom Effect in Room-Temperature Phosphorescence

Georg W. Suter,* Alan J. Kallir, and Urs P. Wild

Physical Chemistry Laboratory, Swiss Federal Institute of Technology, ETH-Zentrum, CH-8092 Zurich, Switzerland

Tuan Vo-Dinh

Advanced Monitoring Development Group, Health and Safety Research Division, Oak Ridge National Laboratory, Oak Ridge, Tennessee 37831-6101

The effect of external heavy-atom perturbers on the room-temperature phosphorescence (RTP) spectrum of dibenzo-[*f*,*h*]quinoxaline (DBQ) adsorbed on Whatman 4 filter paper is reported. The totally symmetric vibrational bands are predominantly enhanced, leading to a spectral change in vibrational structure. Inhomogeneity effects of molecule–perturber interactions are investigated by time-resolved phosphorimetry and lifetime measurements.

Room-temperature phosphorescence (RTP) is a sensitive and simple analytical method to characterize molecules adsorbed on solid substrates (*1*). Originally observed from compounds adsorbed onto solids (*2*, *3*), the RTP phenomenon has been further developed for chemical analysis of organic species in solid substrates (*4–7*) as well as liquid media (*8*, *9*). In particular, it has been successfully applied to the detection of polyaromatic hydrocarbons (PAHs) and N-heterocycles in environmental samples (*10–13*). Filter paper is the most widely used substrate for RTP, since it is inexpensive and commercially available. The corresponding sample preparation is also simple and rapid: only 2–5 μl of the sample solution is required for a typical assay. The solution is spotted on the paper, and after thorough drying in a stream of hot air or under an IR lamp, the sample is ready for measurement in a spectrometer equipped with a standard phosphoroscope (*1*).

In previous works, we have investigated photophysical aspects related to the interactions of molecules with the substrate: the guest–host interaction (electron-phonon coupling) on a filter paper substrate was studied by measuring laser-induced phosphorescence line narrowing (*14*). Hydrogen-bonding interactions were investigated by using two-dimensional total luminescence spectroscopy (*15*). In this work we investigate the external heavy-atom effect in RTP and study experimental factors that could affect analytical applications.

The sensitivity of RTP may be drastically increased by the external heavy-atom effect (*16–19*) and limits of detection in the picogram range have been achieved. The filter paper may be impregnated with a heavy-atom solution prior to spotting the analyte solution or the two solutions may be spotted simultaneously. The heavy-atom enhancement factors depend not only on the concentration but also on the particular properties of the heavy atoms used: high enhancement factors have been found with Tl^+ and Pb^{2+} for PAHs and with I^- and Hg^{2+} for N-heterocycles (*13*). Apart from the overal phosphorescence intensity enhancement, other effects such as spectral shifts and changes in the spectral intensity profiles, due to external heavy-atom perturbers, should also be considered in the interpretation of RTP spectra. Short and long RTP decaying components of several indoles on ion-exchange paper substrates have been previously reported (*20*). In a recent work (*13*) it was demonstrated, that RTP spectra of N-heterocycles are red-shifted—compared to the spectrum obtained with no heavy-atom perturbers—when using $HgCl_2$ as the heavy atom salt. No such shift was observed when using a mixture of thallous and lead acetate. However, the spectral intensity profiles were reported to remain essentially unchanged.

It has been reported from low-temperature experiments that the external heavy atoms could affect the spectral structure of phosphorescence (*21*). A typical example of this effect is the drastic increase of the 0–0 band in the phosphorescence spectra of coronene and triphenylene, which has also been observed on filter paper at room temperature (*1*). This effect is based on the dominant quantum mechanical coupling mechanism responsible for the phosphorescence enhancement, namely, a second-order mixing of the perturber's singlet states with the lowest triplet state T_1 of the chromophore being analyzed. Since this coupling involves no vibronic term, the bands belonging to totally symmetric modes of the chromophore are enhanced selectively by the external heavy atoms (*22*). External heavy atoms, therefore, are expected to change the phosphorescence spectral structure whenever both nontotally and totally symmetric vibronic bands of comparable intensity are present.

The low-temperature phosphorescence spectra of *p*-diazines all contain prominent (nontotally symmetric) out-of-plane modes (*23*, *24*). In this work we study the external heavy-atom effect in RTP by using dibenzo[*f*,*h*]quinoxaline (DBQ) as the model compound; this molecule is ideally suited for such an investigation because its phosphorescence spectrum exhibits vibronic modes that could provide information on the heavy-atom interactions. Compared to DBQ, negligible changes in the spectra of benzoquinoxaline, benzo[*a*]-phenazine, and dibenzo[*a*,*c*]phenazine adsorbed on Whatman 4 filter paper have been observed. Comparative studies were conducted to study spectra obtained from samples treated with thallous acetate as the heavy-atom perturber and sodium acetate. Time-resolved phosphorescence spectra and lifetime measurements were performed for DBQ adsorbed on filter paper substrates. A general discussion on how these results could affect analytical applications is given.

EXPERIMENTAL SECTION

Instrumentation and Procedure. The sample preparation was the same as that described previously (*14*, *15*). In brief, the paper samples were prepared by spotting 5 μL of the sample solution together with an equal amount of either 1 M thallous or sodium acetate. Spots with a diameter of ~10 mm were obtained in this manner. The samples were subsequently dried either under an infrared lamp (5 min) or in a stream of hot air (1 min). The measurements were carried out on a computer-

0003-2700/87/0359-1644$01.50/0 © 1987 American Chemical Society

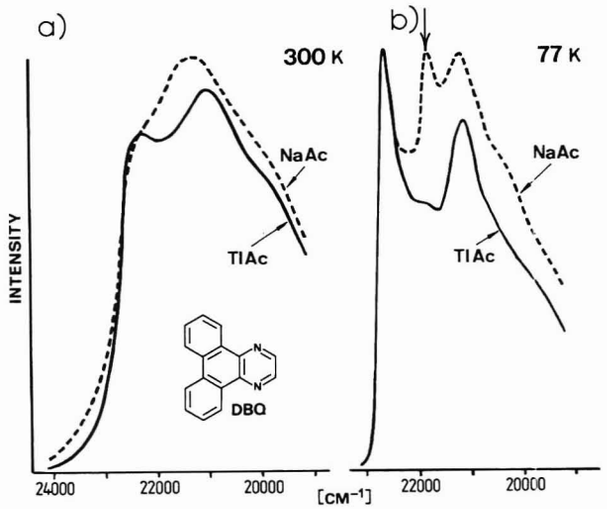

Figure 1. (a) Room-temperature phosphorescence spectra of DBQ on Whatman 4 filter paper impregnated with thallous acetate (solid curve) and sodium acetate (dashed curve). (b) Phosphorescence spectra of the same samples at 77 K. (The background signal has been subtracted. Note, all spectra are normalized at 23 600 cm^{-1}.)

controlled high-resolution (spectral bandwidth 1.5 nm) luminescence spectrometer and on a Spex Fluorolog with spectral resolutions of 20 nm in excitation and 5 nm in emission. Both spectrometers were equipped with phosphoroscopes operated at a minimum frequency of 100 Hz. The phosphorescence decay curves and the time-resolved spectra were recorded as follows: After steady-state conditions were reached, the excitation light was cut off and the photomultiplier pulses were accumulated in a recently developed multichannel scaler, interfaced to a PDP 11/23 computer (*25*).

Materials and Reagents. A mixture of ethanol/water 1:1 was used as a solvent for all components, and the sample concentration in solution was 10^{-3} M. All solvents and reagents used are commercially available (Fluka). DBQ was generously provided by J. Sepiol, Academy of Sciences, Poland.

RESULTS AND DISCUSSION

Figure 1a shows the RTP spectra of DBQ adsorbed on filter paper impregnated with thallous acetate (solid curve: with heavy atom) and sodium acetate (dashed curve). Sodium acetate was used in order to provide an environment similar to that obtained with thallous acetate. For comparison purposes, the intensity scales of the two spectra were adjusted such that the intensities of the 0–0 bands are similar. Whereas no significant spectra shift of the 0–0 band was apparent, the RTP spectra of DBQ with and without external heavy atom are visibly different (Figure 1a). The emission maximum of the RTP spectrum is located at 21 300 cm^{-1} for DBQ with sodium acetate and at 21 000 cm^{-1} with the heavy perturber (thallous acetate). Although the effect is not dramatic, the difference in the intensity distribution of the two RTP spectra is reproducible. The apparent spectral differences in maximum peaks could be due to either real spectral shifts of vibronic bands or the selective appearance of additional vibronic components.

In order to get more conclusive results on spectral assignments, phosphorescence measurements of the same samples were conducted at 77 K. The low-temperature phosphorescence (LTP) spectra shown in Figure 1b clearly demonstrate that the apparent spectral profiles and shift mentioned previously are due to the different intensity ratios between the 0–0 band and a prominent vibronic band with a frequency at ~860 cm^{-1} (indicated by an arrow in Figure 1b). Note that the intensity scales of the two spectra in Figure 1b are also adjusted such that the 0–0 bands have identical intensities. These intensity scale adjustments were necessary since the external heavy-atom effect induces a significant increase in the RTP and LTP spectra. The relative enhancement factors for these spectra are given in Table I. In order to get a better understanding of the effect of external heavy atoms on the RTP spectra, it is useful to discuss the nature of the main vibronic peaks involved in Figure 1. The spectral position of the 0–0 band appears unchanged with the use of heavy-atom perturber

Table I. The Approximate Relative Enhancement Factors for DBQ (for the 860-cm^{-1} Vibronic Band) as a Function of Temperature with Thallous and Sodium Acetate

	intensity[a]	
temp, K	Tl	Na
300	6	1
77	350	40

[a] The intensities were normalized such that the band at 860 cm^{-1} of DBQ measured with sodium acetate treated paper has an intensity value of 1.

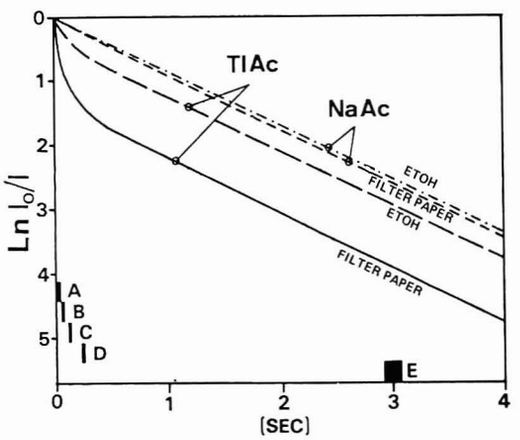

Figure 2. Phosphorescence decays of DBQ at 77 K in ethanol/water containing 1 M of thallous acetate or sodium acetate, and from paper samples obtained by spotting the same solutions on Whatman 4 filter paper.

(Figure 1b). The significant feature revealed in the LTP spectra is the appearance of the vibronic band at 860 cm^{-1} with sodium acetate substrate (arrow on dashed curve, Figure 1b). This vibronic coupling between $n\pi^*$ and $\pi\pi^*$ states of polycyclic azines and has been investigated in previous studies (*24*, *25*). The phosphorescent state of DBQ is of $\pi\pi^*$ (c_{2v} symmetry) and polarized perpendicularly to the molecular plane. The 860-cm^{-1} band is a nontotally symmetric out-of-plane vibronic mode (b_2 symmetry) involving a folding of the DBQ molecule along the N–N axis. In the absence of heavy-atom perturber, this type of nontotally symmetric vibration is known to be important in inducing phosphorescence emissions through vibronic coupling. When the heavy-atom perturber is used (solid curve, Figure 1b), the 860 cm^{-1} is masked by the prominence of the band at 1350–1450 cm^{-1}. This band was assigned to two vibrational modes at 1330 and 1420 cm^{-1}, which represent in-plane hydrogen rocking and ring-stretching modes (*24*). The results provided by the LTP spectra with and without heavy atom therefore, confirm the spectral changes observed in the RTP spectra and provide a better insight into the external heavy-atom effect in RTP. Heavy-atom perturbation modifies the RTP spectral structure; the effect is related to the selective enhancement of bands belonging to totally symmetric vibrations and, therefore, should be observable whenever a phosphorescence spectrum contains both totally and nontotally symmetric vibrations with comparable intensity. The limited resolution achievable at room temperature often prevents a detailed discussion of the nature and changes in the vibronic structure.

Time-resolved phosphorimetry is an analytical technique with great potential for improving the specificity of RTP. This analytical tool, however, has not yet been extensively exploited in RTP. It is essential to investigate in detail the behavior of spectra under time-resolved conditions in order to avoid potential spectroscopic artifacts and to optimize experimental conditions. In a previous study, it was demonstrated that the phosphorescence decays of chromophores adsorbed onto solid substrates such as filter paper are not represented by a single exponential, as in solutions (*15*). Figure 2 shows a logarithmic plot of the phosphorescence decay of DBQ at 77 K in ethanol/water (v/v, 1/1) and on Whatman 4 filter paper with the addition of 1 M sodium

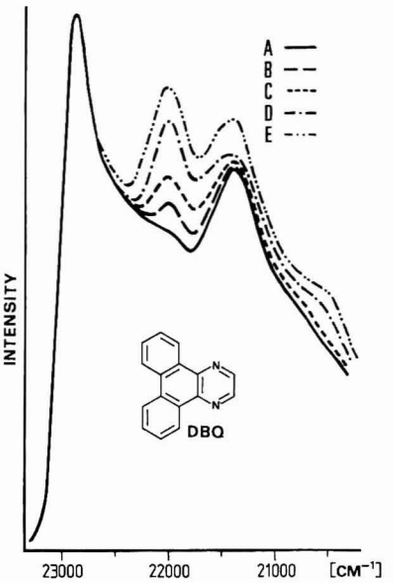

Figure 3. Time-resolved phosphorescence spectra of DBQ on Whatman 4 filter paper treated with thallous acetate.

or thallous acetate. The time windows A–E referring to the time-resolved spectra of Figure 3 are also indicated. The lifetime of DBQ in ethanol at 77 K is 1.29 s (*15*). With thallium the decay shortens and clearly deviates from a single exponential function. This effect is much more pronounced on the paper substrate than in solution, which is readily understood since the phosphorescence lifetime of a given chromophore decreases with decreasing distance from the perturbing heavy atom and increasing concentration of neighboring heavy atom (*21*, *27*). The overall phosphorescence decay of a heavy-atom sample may, therefore, be understood as the superposition of many exponential decays originating from chromophores with different lifetimes, i.e., different interactions with the heavy atoms. A mathematical analysis of such complex multiexponential decays is, however, rather complicated and inconclusive (*28*). It is interesting to note that the asymptotic behavior of the overall decay for long time periods is the same with thallium and sodium, which reflects the presence of a small amount of DBQ molecules on the thallium sample with no or very weak coupling to heavy atoms (*21*, *27*).

The phosphorescence decays of the samples with heavy atoms were found to be wavelength dependent, thus revealing that different parts of the spectra exhibited different lifetimes. In order to investigate this effect, we measured, time-resolved phosphorescence spectra using different time windows following the excitation cut off (window A, 0–31 ms; B, 31–62 ms; C, 93–124 ms; D, 217–248 ms; E, 2914–3100 ms). Figure 3 depicts the spectra from a filter paper sample of DBQ with thallium measured with the time windows A–E. These spectra are normalized to equal the amplitude at 22 800 cm^{-1}. These results show that the long-lived spectra (obtained with time window E) are similar to the spectra in absence of the heavy-atom perturber; i.e., they show more intense nontotally symmetric vibronic bands than the steady-state spectrum of the thallous sample. In particular, the relative intensity of the 860-cm^{-1} vibrational band increases drastically. This feature underscores again the relationship between external heavy-atom perturbation, phosphorescence lifetime, and spectral structure.

CONCLUSION

The results obtained in this study are of importance not only to researchers involved in the fundamental investigation of the RTP process but also to analytical chemists dealing with practical applications of the RTP technique. The external heavy-atom effect is an important tool for improving the sensitivity of RTP. Knowledge of subtle but visible spectral changes induced by the heavy-atom effect would lead to improved spectral assignments and more accurate identification of individual components in complex mixtures. The results obtained with time-resolved measurements are also of analytical interest. The data demonstrate that the inhomogeneity in molecule–perturber interactions could lead to substantial differences in the phosphorescence spectra of one single chemical species. Knowledge of this effect is helpful in avoiding possible misinterpretation of RTP spectra in time-resolved phosphorescence measurements.

LITERATURE CITED

(1) Vo-Dinh, T. *Room Temperature Phosphorimetry for Chemical Analysis*; Wiley: New York, 1984.
(2) Roth, M. *J. Chromatogr.* **1967**, *30*, 276.
(3) Schulman, E. M.; Walling, C. *J. Phys. Chem.* **1972**, *178*, 53.
(4) Vo-Dinh, T.; Winefordner, J. D. *Appl. Spectrosc. Rev.* **1977**, *13*, 261.
(5) Parker, R. T.; Freedlander, R. S.; Dunlap, R. B. *Anal. Chim. Acta* **1980**, *119*, 189.
(6) Parker, R. T.; Freedlander, R. S.; Dunlap, R. B. *Anal. Chim. Acta* **1980**, *120*, 1.
(7) Hurtubise, H. J. *Solid Surface Luminescence Analysis*; Marcel Dekker: New York, 1981.
(8) Donkerbrock, J. J.; Goo'jer, C.; Velthorst, N. H.; Frei, R. W. *Talanta* **1981**, *28*, 717.
(9) Cline Love, L. J.; Skrilec, M.; Habarta, J. G. *Anal. Chem.* **1980**, *52*, 754.
(10) Vo-Dinh, T.; Gammage, R. B. *Anal. Chem.* **1978**, *50*, 2054.
(11) Vo-Dinh, T.; Hooyman, J. R. *Anal. Chem.* **1979**, *51*, 1915.
(12) Vo-Dinh, T.; Gammage, R. B.; Martinez, P. R. *Anal. Chim. Acta* **1980**, *118*, 313.
(13) Abbott, D. W.; Vo-Dinh, T. *Anal. Chem.* **1985**, *57*, 41.
(14) Vo-Dinh, T.; Suter, G. W.; Kallir, A. J.; Wild, U. P. *J. Phys. Chem.* **1985**, *89*, 3025.
(15) Suter, G. W.; Kallir, A. J.; Wild, U. P.; Vo-Dinh, T. *J. Phys. Chem.* **1986**, *90*, 4941.
(16) White, W.; Seybold, P. G. *J. Phys. Chem.* **1977**, *81*, 2035.
(17) Vo-Dinh, T.; LueYen, E.; Winefordner, J. D. *Anal. Chem.* **1976**, *48*, 1186.
(18) Jakovljevic, I. M. *Anal. Chem.* **1977**, *49*, 2048.
(19) LueYen, Bower E.; Winefordner, J. D. *Anal. Chim. Acta* **1978**, *102*, 1.
(20) Aaron, J. J.; Andino, M.; Winefordner, J. D. *Anal. Chim. Acta* **1984**, *160*, 171.
(21) Najbar, J.; Radakiewicz-Nowak, J.; Chodkowska, A. *J. Lumin.* **1978**, *17*, 449.
(22) Giachino, G. G.; Kearns, D. R. *J. Chem. Phys.* **1970**, *53*, 3886.
(23) Suter, G. W.; Wild, U. P.; Brenner, K.; Ruziewicz, Z. *J. Chem. Phys.* **1985**, *98*, 455.
(24) Lim, E. C.; Li, I. R.; Li, Y. H. *J. Chem. Phys.* **1969**, *50*, 4925.
(25) Tschaggelar, R.; Forrer, J.; Kallir, A. J.; Wild, U. P., to be submitted for publication.
(26) Brenner, K.; Ruziewicz, Z. *J. Lumin.* **1977**, *15*, 235.
(27) Najbar, J.; Birks, J. B.; Hamilton, T. D. S. *Chem. Phys.* **1977**, *23*, 281.
(28) Knight, A. E. W.; Selinger, B. K. *Aust. J. Chem.* **1973**, *26*, 1.

RECEIVED for review October 27, 1986. Accepted March 20, 1987. Financial support from the Swiss National Science Foundation is gratefully acknowledged. T.V.D. acknowledges the U.S. Department of Energy, Office of Health and Environmental Research (Contract DE-ACO5-840R21400 with Martin Marietta Energy Systems, Inc.) for support in the preparation of this paper.

Direct Experimental Evidence for in Situ Graphite and Palladium Selenide Formations with Improvement on the Sensitivity of Selenium in Graphite Furnace Atomic Absorption Spectrometry

Janet E. Teague-Nishimura and Takeshi Tominaga

Department of Chemistry, Faculty of Science, University of Tokyo, Hongo, Bunkyo-ku, Tokyo 113, Japan

Tsutomu Katsura

Environmental Safety Center, Waseda University, Okubo, Shinjuku-ku, Tokyo 160, Japan

Kazuko Matsumoto*

Department of Chemistry, School of Science and Engineering, Waseda University, Shinjuku-ku, Tokyo 160, Japan

The potential of albumin to be converted into graphite on the surface of a pyrolitically coated graphite tube during the determination of selenium by graphite furnace atomic absorption spectrometry has been discovered. Utilizing this "new graphite surface" formed in situ, along with palladium as a Se retainer, has considerably improved the selenium sensitivity. Electron-probe microanalysis has revealed for the first time that Se and Pd exist on the surface of the graphite tube in a 1:1 mole ratio and that no free selenium was seen. Application to freeze-dried human serum was successfully made. The detection limit was 0.017 ppm.

The addition of "matrix modifiers" to produce a more accurate determination of volatile elements in graphite furnace atomic absorption spectrometry is not novel (*1–10*). However, if one was to make a quick survey of some of these papers, it soon becomes evident that very little experimental evidence is presented to try and explain the true mechanism behind "the matrix modification method of enhancement". Several reports (*1*, *5*, *7*, *10*) favoring the addition of nickel claim the formation of a high boiling selenide. Ihnat (*10*) remarked that reduction by nickel oxide of SeO_2, formed by decomposition of selenite or selenate, to a less volatile form is another possibility. As an example of a different modifier Henn (*11*) utilized molybdenum and put forward that the formation of a high molecular weight heteropoly molybdate anion is successful at isolating the selenium. The work presented in this paper was undertaken with the hope of being able to throw light on the mechanism for one of these matrix modifiers, i.e., Pd.

From some of the papers published (*11–14*) on the atomization mechanism in a graphite furnace, it is known that the carbon surface of the graphite tube plays an important role in the atomization process of the analyte. Indeed, one of the models often quoted (*11*, *12*, *15*) is the reduction of the metal oxide by the carbon surface of the graphite tube. Botha et al. (*15*) reported that on the addition of ascorbic acid to solutions containing gallium, the gallium sensitivity could be improved by a factor of 2. In this sense the carbon which is assumed to be formed on pyrolysis of the ascorbic acid during the heating stages in the furnace has a reductive effect, allowing the gallium to be put into a more easily atomization form.

There are many other papers (*16–18*) reporting a similar carbon effect. Recently L'vov (*19*, *20*) has coined the phrase "carbothermal reactions" for those reactions in which carbon plays a reductive role. We too, are reporting an improvement on the sensitivity of selenium in graphite furnace atomic absorption spectrometry by a carbon-surface phenomenon. That is, the selenium signal is improved by the addition of albumin which, under the conditions used, is believed to be converted into graphite. This "in situ" formation of graphite along with the use of palladium as a Se retainer has allowed us to measure selenium concentrations with much higher sensitivity. However, unlike the above, selenium not being a refractory forming element simple reaction of the metal oxide with the carbon surface is improbable. The phenomenon we describe in this paper is thought to be the first of its kind to be reported.

In 1983 Verlinden et al. (*21*) presented a detailed review on the determination of Se by AAS. In the area of biological investigations many workers have preferred to separate the Se from its organic matrix only to find difficulties reoccurring with the inorganic matrix into which the Se is extracted. Saeed et al. (*7*) have shown interferences from phosphates and iron on Se signals to occur at wavelengths below 220 nm, leading to overcompensation by deuterium arc background correction systems. Carnrick et al. (*22*) claim however that, with the use of a Zeeman background correction system, this problem can be avoided. Nevertheless, there are several reports to date (*5*, *6*, *8*) claiming the successful direct determination of Se by graphite furnace AAS in serum and other biological fluids. Each of these works employs a metal to ensure the retention of Se in the furnace. Again, this is another interesting area of conflict, with Ni generally coming out tops. Ping et al. (*3*) reported contrary to other authors (*5*, *6*) that Pd could produce better sensitivities for Se when present in an organic matrix. They reported that albumin severly decreased the Se sensitivity but upon addition of Pd the sensitivity was restored to that of a simple inorganic Se(IV) solution. Our studies showed that palladium produced a 30% improvement on the sensitivity of a simple Se(IV) solution. However, a somewhat unexpected result appeared when albumin (0.1%) was added to the Se(IV) (0.05 μg/mL) solution containing Pd at 100 μg/mL. Unlike Ping et al. who reported on the negative effect of albumin, it was discovered that under a carefully constructed set of conditions a doubling of the selenium signal was possible in the presence of albumin provided palladium was contained in the solution as a Se retainer. Investigation by scanning electron microscopy (SEM) has revealed, that albumin appears to be converted into graphite. Further detailed studies by electron-probe microanalysis have enabled us to report for the first time that Pd and Se exist in the ashing stage together in a 1:1 mole ratio.

EXPERIMENTAL SECTION

Apparatus. A Hitachi H-180-50 atomic absorption spectrometer equipped with a Hitachi GA-3 graphite furnace and deuterium background corrector was used. All measurements when necessary were checked against possible molecular absorption by using only a deuterium lamp. All measurements were

0003-2700/87/0359-1647$01.50/0 © 1987 American Chemical Society

made with pyrolitically coated tubes, Hitachi No. 180-7403. A Drummond microdispenser (Drummond Scientific USA) was used to deliver 10-μL aliquots of the sample.

Scanning electron microscope (SEM) micrographs were obtained with a Hitachi S570 scanning electron microscope equipped with a Horiba X-ray microanalyzer EMAX-2200. In the dark region below the pictures, the following information is displayed from left to right: SEM number, accelerating voltage in kilovolts, magnification, and scale of picture. The EMAX-2200 was equipped with a Si(Li) detector. Diffraction patterns were obtained with a Hitachi HU-11D transmission electron microscope.

Instrument Setting. The 196.0-nm line with a spectral bandwidth of 1.3 nm was used for all measurements. The line source was a selenium hollow cathode lamp operated at 7.5 mA. The dry, ash, atomize, and clean steps of the Model GF-3 were experimentally optimized, and the furnace was automatically taken through its steps. The purge gas flow (argon gas 1.0 L/min) was interrupted during the atomization stage. Optimized furnace conditions were as follows: dry, 30–80 °C 30 s, 80–120 °C 60 s; ash, 300–400 °C 50 s, 400–600 °C 60 s, 600–1000 °C 60 s; atomize, 2400–2400 °C 6 s.

Reagents and Standard Solutions. A Se(IV) standard was prepared by dissolving 1 g of selenium metal in 7 mL of nitric acid and 7 mL of water on heating then diluting to 1 L giving a 1000 μg/mL solution. The Pd, Pt, Cu, Al, and Ni solutions (1000 μg/mL) as the chloride were purchased from Koisei Chemical Co. Bovine albumin was purchased from Kokusan Chemical Co.

Freeze-dried human serum NIES 4 (*23*) was kindly supplied by K. Okamoto, National Institute for Environmental Studies, Tsukuba, Ibaraki, Japan. Reconstitution of the sample was carried out according to the instructions sent by the supplier. However in order to obtain a clear solution, further 5-fold dilution was necessary.

RESULTS AND DISCUSSION

Selenium being a volatile element has been one of the more difficult elements to be determined by atomic absorption spectrometry. Determination of Se in biological fluids such as whole blood, serum, and seminal fluids, where the Se is known to associate with proteins (*24*, *25*), poses problems from not only interference of molecular species formed during the determination but also the loss of volatile Se compounds. Dimethyl selenide and diethyl selenide have very low melting points of 58 °C and 135 °C, respectively. Also formation of smoke and carbon particles causes blocking of the light path through the graphite tube (*10*). However if some or all of the above could be avoided, the usefulness of the graphite furnace in the determination of Se will be improved.

Optimization of the furnace conditions is as follows: dry, 30–150 °C 40 s; ash, 150–400 °C 60 s; atomize, 2400 °C 6 s on a 0.05 μg/mL Se(IV) solution. When Pd was added to the above solution, the ashing temperature was increased to 150–1200 °C. In Figure 1 these conditions were used in the measurement of signals A, B, and C. However when we applied the same set of conditions to a Se and Pd solution containing albumin (0.1%), the results were disappointing. Unlike Ping et al. (*3*) who found that on addition of Pd the signal from a Se–albumin solution equalized that of a Se solution, we found that the Se–Pd–albumin solution gave poorer sensitivities than the Se solution under the same conditions. On closer inspection it was found that selenium was being lost in the drying stage. On reoptimization of the furnace conditions we realized that we were able to at least double the selenium sensitivity in the presence of both palladium and albumin. The realization of these findings is shown in Figure 1. These reoptimized conditions are shown in the Experimental Section, under instrument settings. From Figure 1D–F, it can be seen that as the period of the drying stage was gradually increased the selenium signal also increased with a corresponding decrease in the loss of Se in the drying stage. The peaks marked with an asterisk in Figure 1 correspond to this loss in the drying stage, these peaks

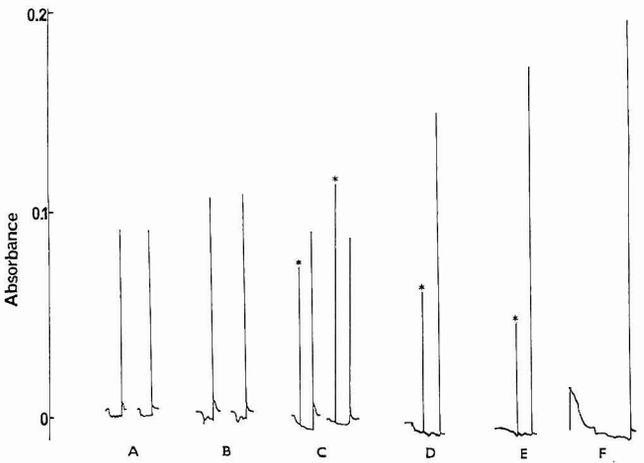

Figure 1. Realization of albumin/graphite enhancement effect on the Se signal: (A, C, D, E, F) Se 0.05 μg/mL, Pd 100 μg/mL, albumin 0.1%; (B) Se 0.05 μg/mL, Pd 100 μg/mL. A, B, and C show two measurements of each solution. D, E, and F show single measurements of each solution. Peaks marked with an asterisk show Se loss. Sample volume was 10 μL.

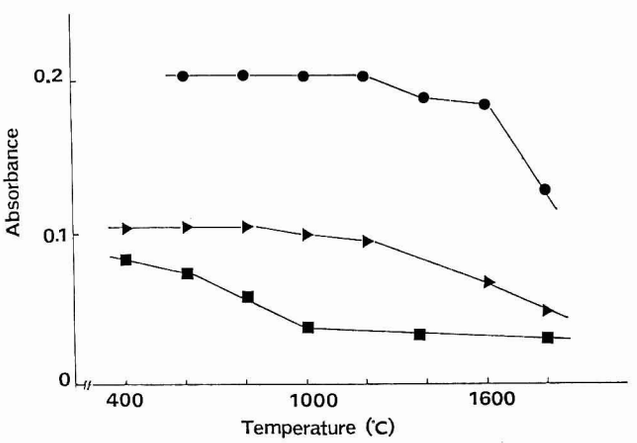

Figure 2. Effect of ashing temperature on selenium sensitivity: ●, 0.05 μg/mL Se + 100 μg/mL Pd + 0.1% albumin; ▲, 0.05 μg/mL Se + 100 μmg/mL Pd; ■, 0.05 μg/mL Se. Sample volume was 10 μL.

appeared at temperatures around 130 °C. It can be clearly seen from peak F of Figure 1 that when the early peak has been completely diminished, the selenium signal is approximately doubled compared to when albumin is not present, i.e., peak B in Figure 1.

Effect of Ashing Temperature on the Se Signal. In graphite furnace atomic absorption spectrometry selection of the appropriate ashing temperature is particulary important when a volatile analyte occurs in an organic matrix. For most elements, as the ashing temperature is raised the sensitivity is decreased. Figure 2 shows that with the addition of Pd the Se sensitivity in the presence of albumin (0.1%) is stable until 1200 °C which is similar to that of the middle curve (Se–Pd only). Selenium present in the furnace alone shows loss of sensitivity after the ashing temperatures reaches 400 °C. Therefore it can be confidently stated that palladium successfully retains selenium in the graphite furnace.

Background absorptions for both palladium and albumin were scrupulously checked. Figure 2 also shows that albumin enhances the sensitivity two times (upper curve) compared to the signal obtained with Se–Pd only (middle curve). We began to question ourselves as to the cause of this improvement in the selenium signal. If during the heating stage the albumin is rendering "new graphite", the surface being presented to the Se species may be different from that if albumin was not present. It therefore appears that this "new graphite surface" is better able to physically adsorb the sel-

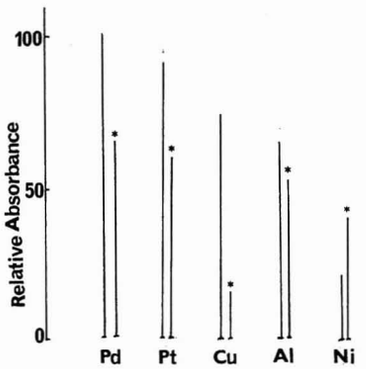

Figure 3. Comparison of the effects of Pd, Pt, Cu, Al, and Ni on Se sensitivity. Each solution contains 0.05 μg/mL Se and 0.1% albumin. The metals are present as their chlorides at 100 μg/mL. The peaks marked with an asterisk contain no albumin.

enium species. Thus with successful retainment of Se by Pd and a "new graphite surface" in the furnace tube, higher sensitivity is obtainable for the determination of Se by graphite furnace atomic absorption spectrometry (GF-AAS).

Effect of Palladium Amount. Julshamn et al. (25) reported that the amount of modifier has a significant effect on the enhancement factor. It was found in this study that after addition of 40 μg/mL of Pd the Se signal remained unchanged. However additions of Pd higher than 150 μg/mL caused the albumin in the matrix to precipitate. Addition of buffers could not prevent the precipitation.

Effect of Albumin Amount. Studies were undertaken to examine the effect of the increase in albumin concentration on the selenium sensitivity. Results showed that as little as 0.01% albumin improves the Se signal. However, when concentrations exceed the 1.5% level, severe background absorptions were seen. At 3% molecular absorptions were seen in the drying and ashing stages. If albumin was, through conversion to graphite, giving this enhancement on the Se signal, then a carbon substitute for albumin should give similar results. Active carbon at 0.1% and 1.0% replaced albumin and in the Se(IV) solution along with the presence of Pd was taken through the heating cycle. In both cases the signals were 30% higher than in the albumin case. However, due to the fact that active carbon is insoluble, the reproducibility of the signal was poor. As another example poly(vinyl alcohol) was added to a similar Pd/Se solution; examination by SEM again showed graphite formation. It therefore appears that any low volatile organic compound, if convertible into graphite, leads to improvement in the Se sensitivity in GF-AAS. Therefore it seems that albumin, like active carbon and poly(vinyl alcohol), is converted by pyrolysis to graphite in the furnace. From time to time a Se/Pd solution only was injected into the furnace after a previous injection of a Se/Pd/albumin solution. However, no enhancement effect was seen. It therefore appears that a "new graphite surface" is required for each measurement.

Enhancement Effect of Palladium, Platinum, Aluminum, Copper, and Nickel Addition in the Determination of Selenium in 0.1% Albumin Solution. The retainment abilities of several other metals were subsequently investigated. The results are shown in Figure 3. All metals were added as their chloride (100 μ/mL). Except for Ni all elements showed an improvement over the absorption reported in the absence of albumin marked by an asterisk.

Electron Microscopy Studies. In order to get direct experimental evidence to support the albumin/graphite theory, electron microscopy studies were carried out. If the formation of graphite was occurring, its presence should be able to be revealed by this technique. Initially three tubes were analyzed: JET 1, no pretreatment; JET 2, 50 injections of a Se 0.05 μg/mL + Pd 100 μg/mL + albumin (0.1%) (10 μL); JET 3, 50 injections of a Se 0.05 μg/mL + Pd 100 μg/mL + active carbon (0.1%) (10 μL). All tubes were taken through the furnace cycle after each injection, no cleaning stage was carried out. The tubes were cut with a diamond cutter and washed with acetone prior to examination by SEM. Photographs taken of the scanning electron micrographs are shown in Figure 4. The typical layer structure of graphite can be clearly seen. Although the buildup of the graphite did vary along the length of the tube surface, estimation of buildup depth is possible by use of the scale at the bottom of the SEM micrograph. As an example; the tube injected with active carbon gave 39 μm of graphite JET 3, while the tube injected with albumin gave 27.4 μm of graphite JET 2. These SEMs were taken in the region directly below the injection port hole of the graphite tube. Figure 4 shows vertical sections of the three tubes, JET 1, JET 2, and JET 3. However, these SEMs only allow us to see information on depth of the surface being presented to the atomizing species. Figure 5 shows SEMs taken from above, the surface appearances are clearly different. The graphite formed from the albumin has a much more lumpier appearance compared to the graphite found on the original tube.

Energy dispersive spectroscopy (EDS) results show that when Pd and Se have been injected into a graphite tube without albumin, the Se amount decreased substantially (<10%) compared to the Pd amount which remained virtually

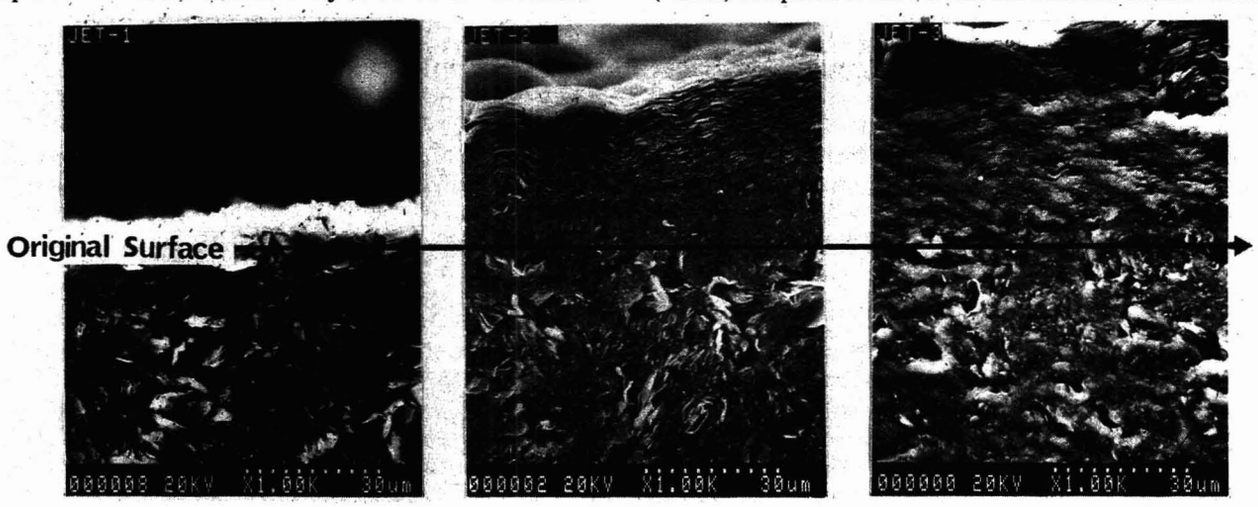

Figure 4. SEM photographs of vertical sections of pyrocoated graphite tubes: JET 1, no pretreatment; JET 2, 50 injections of a 0.05 μg/mL Se + 100 μg/mL Pd + 0.1% albumin solution, sample volume 10 μL; JET 3, 50 injections of a 0.05 μg/mL Se + 100 μg/mL Pd + 0.1% active carbon solution, sample volume 10 μL.

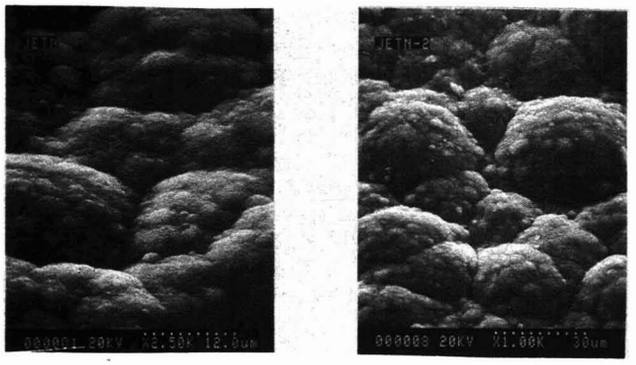

Figure 5. Surface morphology of graphite tubes: JETN, no pretreatment; JETN-2, albumin 0.1%, 20 injections of 10 μL volume.

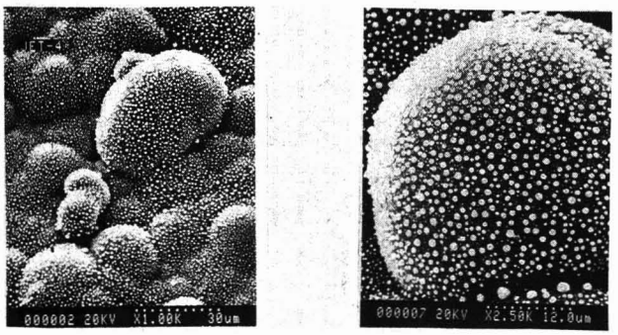

Figure 6. Surface morphology of JET 4: JET 4, 20 injections of a 200 μg/mL Se + 100 μg/mL Pd + 0.1% albumin solution. Sample volume 10 μL.

unchanged. This result shows that graphite formation along with Pd addition is necessary for the effective retainment of Se in the graphite furnace. As this scanning electron microscope is equipped with a X-ray microanalyzer, thus having the same capabilities as an electron probe microanalyzer, semiquantitative measurements were done. It was thought that if the situation in JET 2 was repeated but instead of taking the tube through the complete heating cycle of the furnace, it was stopped at the ashing stage, i.e., to 1000 °C, it would allow pyrolysis of the albumin in the matrix and also ensure the retainment of the Se/Pd species inside the graphite tube. Therefore we would be able to get direct experimental information on the Se/Pd species existing inside the graphite tube furnace. Again as in Figure 4 the layer-like structure of graphite was clearly seen although not so profuse as in JET 2. This however may be due to the lower temperature and the reduced number of injections for JET 4 in comparison with JET 2. Figure 6 shows the surface morphology of JET 4. The photograph on the right-hand side is the magnified part of JET 4's surface; the spherical object is carbon and the white "pools" or speckles are the Se/Pd species. The solid-state detector was then set to detect one particular characteristic line of the element, in this case the Se or Pd Lα line was used and the output is linked to the cathode ray oscilloscope (CRO). As the electron beam is scanned in a raster over the surface of the tube, an image is formed which represents the distribution of that element; this technique is referred to as mapping. Figure 7 shows the mapping scans for Se and Pd. By superimposition of these two scans it was found that for every Se point a corresponding Pd point existed; i.e., Se and Pd can be said to be physically associated with each other on the surface of the graphite tube. Excess Pd was also seen, existing most probably as the metal. Energy dispersive spectra taken for one of the speckles in Figure 6 were used to obtain semiquantitative data on the Pd/Se species. From all the energy dispersive measurements taken for many speckles, the molar ratio of the Pd:Se compound existing on the graphite tube surface was always estimated to be 1:1. These values were

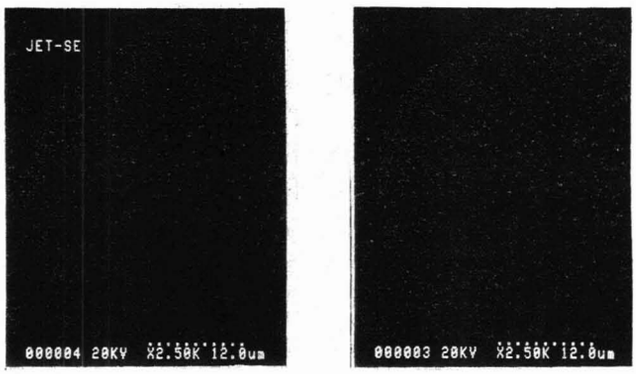

Figure 7. Mapping scans of JET 4: left, Se; right, Pd.

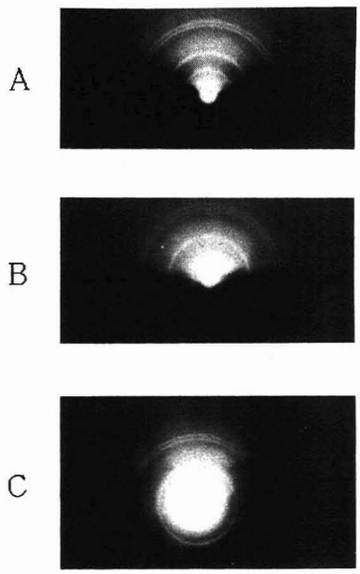

Figure 8. Diffraction patterns of graphite tubes: (A) no pretreatment; (B) active carbon 0.1%, 20 injections of 10 μL; (C) albumin 0.1%, 20 injections of 10 μL.

obtained by using integrated area-count rates after background correction with adjustments for detector efficiency (*26*).

Although Figure 4 shows the typical lamellar structure of graphite, characterization and verification studies were carried out by transmittance electron microscopy (TEM). Since TEM only allows the analysis of ultrathin specimens (<10 μm), we could discriminate between any "new" graphite formed and existing graphite from the tube itself. Initially a powder sample was taken from a graphite tube (no pretreatment) by scratching the surface, which was submitted for powder X-ray diffraction analysis. The confirmation that the tube was graphite was done by comparing the results from the above analysis to the standard values in the ASTM. Three tubes were analyzed by TEM; their diffraction patterns are shown in Figure 8. Comparison of the diffraction patterns confirms the formation of graphite from albumin and active carbon.

Application to Human Freeze-Dried Serum. Since we had been able to measure selenium in an organic matrix without problems of molecular interference, direct measurement of Se in human serum was undertaken. Usually the determination of selenium in biological samples requires longer drying and ashing times than those necessary for optimizing simple Se(IV) solutions. This, Welz et al. (*9*) reported, caused loss of Se(IV), which poses problems when Se(IV) is used as a reference for biological Se; as it would lead to results that are too high in the case of Se(−II) compared to Se(IV). However, since we did not encounter the above problem both in a simple inorganic Se(IV) solution and in the presence of an albumin matrix, provided palladium had been added. The

Table I. Selenium in Freeze-Dried Human Serum (Standard Reference Material NIES 4)[a]

method	amt added, μg/mL	amt found, μg/mL	% recovery
standard addition	0	0.12 ± 0.02	
Se/Pd/albumin calibration curve	0	0.15 ± 0.02	
	0.15	0.15 ± 0.02	100
Se/Pd calibration curve	0	0.13 ± 0.02	
	0.15	0.15 ± 0.02	97

[a] Accepted mean 0.14 (±0.1) μg/mL, ref 23.

determination of Se in the serum (standard reference material NIES 4) was carried out by the standard addition method. The value found was compared to those obtained from a Se/Pd/albumin and Se/Pd calibration curves. The results in Table I show good agreement with each other and the accepted mean.

CONCLUSION

Two recent papers (*27*, *28*) have reported on the usefulness of Pd as a modifier in graphite furnace atomic absorption spectrometry. However they did not give any experimental evidence to explain how Pd retains and improves analyte sensitivities. The results presented in this paper give insight into a possible mechanism for the improvement of Se sensitivities when present in an organic matrix along with the addition of Pd as a Se retainer.

Electron microscopy studies show that Pd and Se are physically associated with each other in a 1:1 mole ratio at 1000 °C on the surface of the graphite tube. Furthermore, since EDS results show that every Pd and Se speckle exists in a 1:1 mole ratio, it can be said that Pd and Se exist as an alloy.

Registry No. Se, 7782-49-2; Pd, 7440-05-3; Pd:Se 1:1, 12137-76-7; graphite, 7782-42-5.

LITERATURE CITED

(1) Ediger, R. D. *At. Absorpt. Newsl.* **1974**, *14*, 127–30.
(2) Kirkbright, G. F.; Hisao-Chan, S.; Snook, R. D. *At. Spectrosc.* **1980**, *1*, 85–88.
(3) Ping, L.; Wei-Lei; Matsumoto, K.; Fuwa, K. *Anal. Sci.* **1985**, *1*, 257–261.
(4) Henn, E. L. *Anal. Chem.* **1975**, *47*, 428–432.
(5) Saeed, K.; Thomassen, Y. *Anal. Chim. Acta* **1979**, *110*, 285–289.
(6) Tada, Y.; Yonemoto, T.; Iwasa, A.; Nakazawa, K. *Bunseki Kagaku* **1980**, *29*, 248–252.
(7) Saeed, K.; Thomassen, Y. *Anal. Chim. Acta* **1981**, *130*, 281–287.
(8) Ito, N.; Funato, Y.; Iwanaga, Y. *Shimadzu Hyoron* **1983**, *40*, 207–210.
(9) Welz, B.; Schlemmer, G.; Voellkopf, U. *Spectrochim. Acta, Part B* **1984**, *39B*, 501–510.
(10) Ihnat. M. *Anal. Chim. Acta* **1976**, *82*, 293–309.
(11) Cambell, W. C.; Ottaway, J. M. *Talanta* **1974**, *21*, 837–844.
(12) Sturgeon, R. E.; Chakrabarti, C. L.; Langford, C. H. *Anal. Chem.* **1976**, *48*, 1792–1807.
(13) Smets, B. *Spectrochim. Acta, Part B* **1980**, *35B*, 33–42.
(14) Chung, C. H. *Anal. Chem.* **1984**, *58*, 2714–2720.
(15) Vasile Botha, P.; Fazakas, J. *Anal. Chim. Acta* **1984**, *162*, 413–417.
(16) Wendl, B.; Schlemmer, G.; Voellkopf, U. *Spectrochim. Acta, Part B* **1985**, *40B*, 527–531.
(17) Wendl, W.; Mueller-Vogt, G. *GIT Fachz. Lab.* **1984**, *28*, 271–272, 275–276. *Chem. Abstr.* **1984**, *100*, 220703.
(18) Wendl, W.; Mueller-Vogt, G. *Spectrochim. Acta, Part B* **1984**, *39B*, 237–242.
(19) L'vov, B. V. *Zh. Anal. Khim.* **1985**, *39*, 153–160. *Chem. Abstr.* **1985**, *102*, 142307.
(20) L'vov, B. V.; Yatsenko, L. F. *Zh. Anal. Khim.* **1984**, *39*, 1773–1780. *Chem. Abstr.* **1985**, *102*, 55137.
(21) Verlinden, H.; Deelstra, H.; Adrianssens, E. *Talanta* **1981**, *28*, 637–646.
(22) Carnrick, G. R.; Manning, D. C.; Slavin, W. *Analyst (London)* **1983**, *108*, 1297–1312.
(23) NIES (National Institute for Environmental Studies, Tsukuba, Japan) publication. Freeze-dried human serum, interlaboratory study; June 1983.
(24) Burk, R. F. *Biochim. Biophys. Acta* **1974**, *372*, 255–265.
(25) Julshamn, K.; Ringdal, O.; Slinning, K. E.; Braekkan, O. R. *Spectrochim. Acta, Part B* **1982**, *37B*, 473.
(26) X-ray micro analyzer Data Manual, Horiba Ltd.: Kyoto, Japan, 1986.
(27) Schlemmer, G.; Welz, B. *Spectrochim. Acta, Part B* **1986**, *41B*, 1157–1165.
(28) Beach, L. Paper 501, 13th Annual FACSS Meeting. St. Louis, MO, Sept 28–Oct 3, 1986.

RECEIVED for review November 3, 1986. Accepted March 24, 1987.

High-Performance Tandem Mass Spectrometry: Calibration and Performance of Linked Scans of a Four-Sector Instrument

Kimio Sato, Tohru Asada, Morio Ishihara, Fumio Kunihiro, Yoshihiro Kammei, and Eiji Kubota

JEOL, Ltd., Nakagami Akishima, Tokyo 197, Japan

Catherine E. Costello, Stephen A. Martin,[1] Hubert A. Scoble,[2] and Klaus Biemann*

Department of Chemistry, Massachusetts Institute of Technology, Cambridge, Massachusetts 02139

Procedures are described for the calibration of a four-sector tandem mass spectrometer for experiments in which the second mass analyzer is scanned at constant B_2/E_2 ratio. Hardware and software have been developed to control the fields in such a manner that any nonuniformity in the magnet scan is compensated. Mixtures of standards have been prepared that provide reference masses for calibration in the positive and negative modes. In either mode, the method is simple and only one calibration curve is required for any precursor ion up to mass 3500. Transmission is maximized even for product ions of very low mass and mass assignment accuracy of better than 0.3 u is achieved over the entire range. The performance is demonstrated with a peptide in the positive ion mode and a glycolipid in the negative mode.

The measurement of the mass of product ions derived from a specific precursor generated by electron ionization (EI) has been used for many years, chiefly to study mass spectrometric fragmentation processes or to confirm the presence of a certain compound in a mixture. However, the paucity of fragment ions and the corresponding lack of structural information of spectra produced by the various "soft" ionization techniques, such as chemical ionization (CI), field ionization or desorption (FI, FD), and most recently, fast atom bombardment ionization (FAB) or secondary ionization with a liquid matrix (liquid SIMS) have made it necessary to generate structurally significant fragment ions from the molecular species produced originally in the soft ionization process. These fragment ions form either spontaneously (microseconds after the molecular ion has been generated) in the course of so-called metastable decompositions or are formed in a separate step, generally by collision induced decomposition (CID) when passing the precursor ion beam through a region filled with a gas such as helium (*1*). In a double focusing magnetic deflection mass spectrometer, the product ions can be mass separated by scanning the electric field (E) alone (*2*) or together with the magnetic field (B) (*3-5*). The electric field of the electrostatic sector must be scanned to transmit ions of different kinetic energy, because each product ion carries only that fraction of the kinetic energy of the fully accelerated precursor, which corresponds to the retained mass fraction:

$$E_2 = E_1 m_2/m_1 \quad (1)$$

where E_2 is the kinetic energy of m_2 and E_1 is the kinetic energy of the precursor ion m_1 for the reaction $m_1^+ \rightarrow m_2^+ + m_3^0$.

To record the m/z values of all product ions produced by decomposition of a precursor ion, the fields of E and B of a double focusing mass spectrometer of the Nier-Johnson geometry in which E precedes B are scanned in such a way as to keep the B/E ratio constant. This is referred to as a "linked scan at constant B/E". It is characterized by poor precursor ion resolution and good product ion resolution (*4*) and is sometimes subject to artifacts (*6*). Beynon and Cooks (*2*) introduced true tandem mass spectrometry by reversing the Nier-Johnson geometry, using the magnetic field as a single focusing mass spectrometer (MS-1) to mass select the precursor ion and then recording the product ions formed in the field-free region between the magnetic and electric field by scanning the latter, which functions as the second mass spectrometer (MS-2). The m/z values of the product ions can be determined from E_2 (eq 1). This approach provides good precursor ion resolution (within the limits of a single magnetic sector mass spectrometer) but rather poor product ion resolution (R = 50-200). The transfer of some kinetic energy to the neutral atom (*7, 8*) also causes an error to lower mass in the mass assignment of the product ions, and there is still the possibility of the appearance of artifact peaks (*9*).

Improvements can be made by adding an additional electric or magnetic field, thus converting either MS-1 or MS-2 to a double focusing mass spectrometer. The *EBE* configuration of the Kratos MS50 triple analyzer and the *BEB* configuration of the three-sector ZAB (VG Analytical) are examples (*10*). The former has high resolution in MS-1 (*EB*) but still has poor resolution in MS-2 because it is only an electric field, just as in the reverse Nier-Johnson geometry mentioned above. On the other hand, the $B_1E_1B_2$ configuration can be used as double focusing MS-1 (*BE*) and a single focusing magnetic mass spectrometer as MS-2. The resolution in the latter is about 200-500. Conversely, one can use B_1 as a single focusing MS-1 of low resolution and transmission and E_1B_2 as a double focusing MS-2 (*11*).

For magnetic tandem mass spectrometers a configuration consisting of two double focusing mass spectrometers, i.e., a total of four sectors (two electric and two magnetic fields) represents the most favorable arrangement, by combining the potential for good resolution with good transmission in both MS-1 and MS-2. It also assures correct mass assignment for the product ions, which is difficult in a three sector instrument of the $E_1B_1E_2$ configuration because of the loss of kinetic energy during the collision process. This can amount to as much as 50 eV for a 10 000 eV ion (*8*) and can lead to an error of up to 0.5% in mass if the mass assignment is made by measuring the E_2 potential necessary to pass the beam through a resolving slit centered after E_2. The double focusing principle of the Nier-Johnson geometry compensates for this energy spread (*12*) because the lower energy beam traverses the electric sector at a larger deflection angle, exiting somewhat off-axis, and enters the magnetic field (B_2) at a point and angle that brings the lower energy ions into focus at the same point as those of the original energy. Therefore, the mass assignment for the ions passing through the slit located at the focal point after B_2 is correct, even though a small fraction of kinetic energy was lost in the collision process.

It may be noted that Futrell et al. combined two double focusing mass spectrometers in the mid 1960s (*13*), but the

[1] On leave of absence from the Department of Cell and Molecular Pharmacology and Experimental Therapeutics, Medical University of South Carolina, Charleston, SC.

[2] Present address: Genetics Institute, 87 CambridgePark Dr., Cambridge, MA 02140.

0003-2700/87/0359-1652$01.50/0 © 1987 American Chemical Society

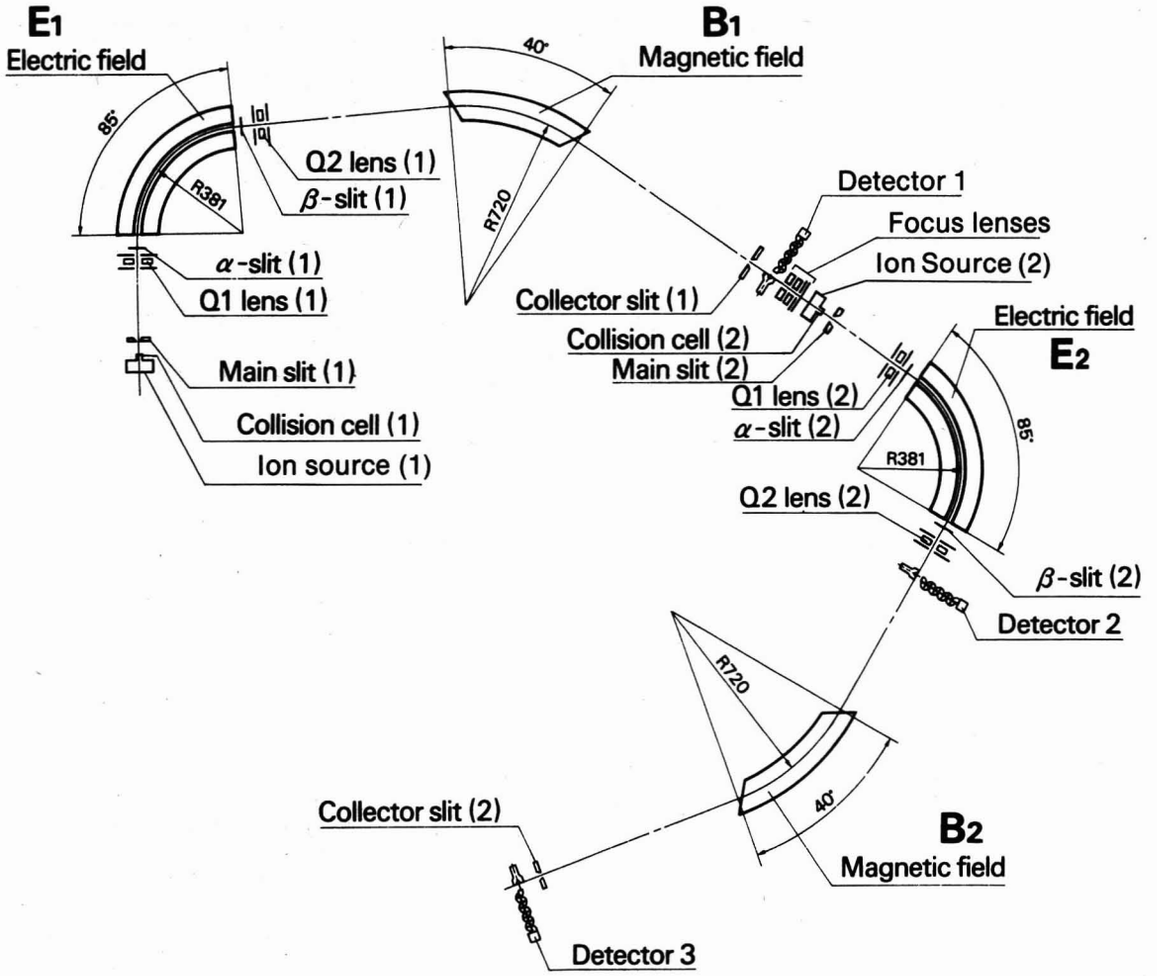

Figure 1. Ion optics of the JEOL HX110/HX110 tandem mass spectrometer.

first four-sector instrument applicable to organic compounds of higher mass was constructed in McLafferty's laboratory (*14*). It consists of two double focusing mass spectrometers of normal Nier–Johnson geometry where MS-1 is a modified Hitachi RMH-2 with a mass range of 10 000 at 10 kV and MS-2 is further modified by the incorporation of a magnet of inhomogeneous field. While this instrument for various reasons did not achieve the expected resolution at high mass (F. W. McLafferty, personal communication), it provided an opportunity to carry out detailed studies of collision processes by virtue of the long (60 cm) field-free region between MS-1 and MS-2. Useful product ion spectra of large molecules (M_r < 2000) were obtained when operating the instrument in the three sector mode ($E_1B_1E_2$) (*15*).

The first commercial four–sector instrument was the VG ZAB-4F consisting of two ZAB-HF double focusing mass spectrometers (mass range 3000 at 8 kV) of the *BE* configuration, assembled tail-to-tail, forming a $B_1E_1E_2B_2$ instrument with the main collision cell between E_1 and E_2, i.e., operating both MS-1 and MS-2 in the double focusing mode (*16*). This instrument is now located at the NIEHS, Research Triangle Park, NC. A high mass version, incorporating two ZAB-SE spectrometers (mass range 12 000 at 10 kV) was installed in the summer of 1986, at SmithKline Beckman, Philadelphia, PA (*17*). Both McLafferty's design and the ZAB-4F are of the S configuration, which makes for a very long instrument.

This report describes another four-sector tandem mass spectrometer, which has been in use in the Mass Spectrometry Facility at MIT since September 1985. It consists of two identical JEOL HX110 double focusing mass spectrometers (*18*) of normal Nier–Johnson geometry (*EB*), modified for third order correction by Matsuda (*19*). They are assembled head-to-tail ($E_1B_1E_2B_2$) in the C configuration, i.e., the ion beam generated by MS-1, after passing through the collision interface, turns back toward MS-1 (Figure 1). Thus, the ion source of MS-1 and the detector of MS-2 are only 225 cm apart in this relatively compact instrument where all points along the ion path are easily accessible to the operator. Both MS-1 and MS-2 have a mass range of 14 500 at 10 kV accelerating voltage.

In the work at MIT, which is concerned with the determination of the structure of relatively large, complex organic compounds of biological interest, particularly polypeptides derived from proteins, it is important to generate mass spectra that are rich in structurally significant product ions, but devoid of artifacts, multiplets, and excessive fragment ions due to the FAB matrix, and allow the analysis of components in mixtures. This requires an instrument of high mass range and good resolution for the precursor ions in MS-1 as well as for the product ions in MS-2. We have found that reliable and simple mass assignment of the product ions and their detection with high sensitivity over the entire mass range, from the precursor to the smallest structurally significant fragment ion, is of utmost importance in the interpretation of the CID spectrum of a compound of unknown structure (*20*).

This prerequisite necessitates high accuracy and reliability of the calibration of the linked scan of MS-2. Furthermore, since the compounds to be analyzed often occur in mixtures and may have quite different molecular weights, the calibration and measurement procedure must be easily and quickly applicable to a wide mass range because, in the determination of the structure of polypeptides, proteins, and other biopolymers, the availability of sample is usually limited; any time delay between measurements of the various com-

ponents of the mixture must, therefore, be kept at a minimum.

A detailed procedure for calibrating a four-sector tandem mass spectrometer, the VG ZAB-4F, has been reported recently (*21*). It is based on the measurement of the known product ion spectrum, recorded during a linked scan at constant B/E of MS-2 of a "standard" precursor ion (P_s) selected by setting the magnetic field of MS-1 to the appropriate value. Scan time to mass conversion for the linked scan is achieved by the data system as in normal mass spectra and the resulting conversion table is then used to determine the mass scale of a product ion spectrum derived from an unknown precursor ion (P_u). It is stated to be essential that the magnetic field, B_1, which selects P_s must be the same that selects P_u and accelerating voltage switching (using the peak matching circuit) is employed to achieve this, if—as is usually the case—$P_s \neq P_u$. The mass assignments for the product ions derived from P_u must then be corrected by the apparent peak matching ratio, P_s/P_u. As a consequence, this procedure does not allow for a single calibration to be applicable to precursor ions differing widely in mass, as P_u must be reasonably close to P_s because the accelerating voltage ratio should not deviate too much from unity. From a practical point of view, this method has major disadvantages: not only is it cumbersome, but one also has to calibrate the product ion scan function separately for each different precursor ion, unless their m/z values are quite close. Unfortunately, this is rarely the case. For example, the molecular weights of peptides generated chemically or enzymatically from even a single protein differ widely and almost each one would require separate calibration. This is virtually impossible if these peptides occur as a mixture in the same sample, which is often the situation even after partial separation of the complex digest by HPLC.

We have developed a much simpler calibration procedure for the JEOL HX110/HX110 tandem mass spectrometer of the $E_1B_1E_2B_2$ configuration. A scan time/mass calibration table covering a wide mass range is generated for MS-2, by ionizing a suitable calibrant in a second ion source located in the interface between MS-1 and MS-2 and scanning B_2 while E_2 is kept constant. This data set, which represents the normal mass spectrum of the calibrant in MS-2, is then used by the JEOL DA5000 data system for any selected precursor mass to calculate the linked scan functions for E_2 and B_2, keeping their ratio constant. A simple second ion source has now also been added to the four-sector VG ZAB-SE tandem mass spectrometer (*22*).

If the ratio of the magnetic field strength, B, to electric field strength, E, were not kept exactly constant, the ion transmission would decrease and the mass assignments would become inaccurate. While an electric field can be linearly scanned with a high degree of accuracy, a magnetic field is difficult to scan linearly, even with Hall probe controlled circuitry. Since the B/E ratio must remain constant, the inherent nonlinearity in effective magnetic field strength must be corrected (linearized) (*23*, *24*), or conversely, the electric field voltage must be adjusted to track the nonlinearity of the magnetic field scan (*25*). The results that are described below were obtained in the magnetic field linearization mode, which is achieved under complete software control by the data system rather than separate microprocessors as described in ref *24*. This involves prior calibration of the magnetic field strength and construction of a correction table, which is then used to compensate for nonlinearity throughout the calibrated region. In such a manner, the proper B/E ratio can be maintained accurately over a wide mass range, ensuring both good transmission and mass assignments even at low mass where the mass of the product ions (and, therefore, their kinetic energy) may be as low as 0.1–0.02 times that of the precursor ion. The calibration also holds for precursor ions covering a wide mass range (we have applied it to precursor ions ranging from m/z 58 to over 3000 (*20*)).

EXPERIMENTAL SECTION

Description of the Tandem Mass Spectrometer. The ion optics of the JEOL HX110 (Figure 1) are those described by Matsuda (*19*) incorporating quadrupole lenses before and after the electric sector to limit the Z-axis dispersion in the region of the magnetic field. Thus, a narrow magnet gap (permitting high field strength) can be tolerated and the total transmission is increased. Both MS-1 and MS-2 have a mass range of 14 500 at 10 kV accelerating voltage. The interface located between the collector slit of MS-1 and entrance slit of MS-2 is about 35-cm long and contains an off-axis electron multiplier (detector 1) as well as a lens system to focus the beam on the collision cell that is part of and beyond ion source 2. This ion source is identical to the EI/CI/FAB source of MS-1 (except that the CI portion is eliminated) and primarily serves to calibrate MS-2. Calibrants can be introduced via a vacuum lock, either with a solids probe (for EI) or on a FAB target. This ion source also contains an independent FAB gun with power supplies. Alternatively, a separate collision cell can replace the ion source after it has served its purpose of MS-2 calibration, which holds for at least a few days. The stand-alone collision cell can be electrically floated (up to 9.9 kV above ground) and allows for changing cell inserts via the vacuum lock to vary collision conditions.

In contrast to MS-1, MS-2 has an additional off-axis electron multiplier (detector 2) after E_2 to allow recording of energy spectra, mass analyzed ion kinetic energy spectroscopy (MIKES), in the $E_1B_1E_2$ mode. In the E_2B_2 experiment, more highly resolved spectra of the product ions generated by CID in the collision cell (or by unimolecular decomposition in the entire field-free region between MS-1 and MS-2) are recorded by detector 3, after passing through B_2. All electron multipliers have 16 stages and are equipped with ±20-kV postaccelerating electrodes.

Materials. All alkali halides were purchased from Aldrich Chemical Co. (Milwaukee, WI). Lithium and rubidium iodide were 99.9% pure, and sodium, potassium and cesium iodide were gold label, 99.999%. Triethanolamine (TEA) was obtained from Mallinckrodt (Science Products Div., Paris, KY). Glycerol was MCB ACS reagent grade and was redistilled before use.

Physalaemin (I) was purchased from Bachem (Torrance, CA), checked for purity by reversed-phase HPLC, and used as such. *N*-α-Hydroxystearoyl dihydrogalactosylcerebroside (II) was isolated from parasitic helminths and was kindly provided by B. N. Singh.

Calibration of MS-2 for Linked Scans at Constant B/E. *Calibration in the Positive Mode.* For positive ion calibration an aqueous solution of LiI (1.5 F), NaI (4.5 F), KI (0.01 F), RbI (0.01 F), and CsI (1.0 F) is prepared and mixed 5:1 (v/v) with acetonitrile (which improves the surface distribution of NaI). About 0.4 μL of this solution is applied to the FAB probe, evaporated to dryness, and inserted into ion source 2. The relative abundance of the CsI cluster, m/z 912, and NaI cluster, m/z 922, provides an indication of the surface distribution of the various alkali halides. A ratio of no more than 4:1 for 912/922 cluster is an indication that all ions used for calibration will have sufficient abundance. This is usually achieved by depositing only a thin layer of the salt mixture. The instrument is scanned in the normal two-sector mode and position data are acquired from m/z 0 to 3550 in 3.85 min with secondary electron multiplier voltage of −1 kV and postacceleration of −18 kV. The ions used for calibration are listed in Table I.

Measurement of a CID Spectrum in the Positive Mode. Physalaemin, pGlu-Ala-Asp-Pro-Asn-Lys-Phe-Tyr-Gly-Leu-Met-NH_2 (I), M_r = 1264.59, was dissolved in glycerol and 30% acetic acid (3:1) and 1 nmol in 0.5 μL of matrix was deposited on a stainless steel probe tip and placed in the ion source of MS-1 where it was bombarded with a beam of xenon atoms from a JEOL neutral atom gun (6 keV, 2 A cathode current, 10 mA emission). The precursor ion was then selected with sufficient resolution to transmit only the ^{12}C $(M + H)^+$ ion beam, 1265.6, into the collision region. Helium was introduced into the collision region at a pressure that attenuated the precursor ion to 10–30% of its original abundance measured at detector 3 before and after admission of helium. In this experiment, the resolution of MS-2

Table I. Mass Assignment for Positive Ion B/E Calibration

m/z	elemental composition	m/z	elemental composition
1.0078	H	1072.2490	Na_7I_6
6.0151	^6Li	1172.1451	Cs_5I_4
7.0160	^7Li	1222.1430	Na_8I_7
14.0320	$^7Li_2$	1322.0393	$NaCs_5I_5$
22.9898	Na	1372.0370	Na_9I_8
38.9637	^{39}K	1431.9550	Cs_6I_5
45.9797	Na_2	1521.9320	$Na_{10}I_9$
62.9613	HNaK	1581.8492	$NaCs_6I_6$
84.9118	^{85}Rb	1671.8261	$Na_{11}I_{10}$
132.9054	Cs	1691.7649	Cs_7I_6
172.8839	Na_2I	1821.7202	$Na_{12}I_{11}$
188.8579	KNaI	1841.6591	$NaCs_7I_7$
265.8109	Cs_2	1951.5748	Cs_8I_7
282.7996	NaCsI	1971.6143	$Na_{13}I_{12}$
322.7781	Na_3I_2	2101.4690	$NaCs_8I_8$
392.7153	Cs_2I	221.3847	Cs_9I_8
432.6938	$CsNa_2I_2$	2361.2789	$NaCs_9I_9$
472.6723	Na_4I_3	2471.1946	$Cs_{10}I_9$
542.6094	$NaCs_2I_2$	2621.0888	$NaCs_{10}I_{10}$
582.5880	$CsNa_3I_3$	2731.0045	$Cs_{11}I_{10}$
622.5665	Na_3I_4	2880.8987	$NaCs_{11}I_{11}$
652.5253	Cs_3I_2	2990.8144	$Cs_{12}I_{11}$
722.4607	Na_6I_5	3140.7086	$NaCs_{12}I_{12}$
802.4194	$NaCs_3I_3$	3250.6244	$Cs_{13}I_{12}$
912.3352	Cs_4I_3	3400.5185	$NaCs_{13}I_{13}$
922.3549	Na_6I_5	3510.4343	$Cs_{14}I_{13}$
1062.2294	$NaCs_4I_4$		

was 1:1000, the secondary electron multiplier −1.7 kV and −18 kV postacceleration. The product ion spectrum was scanned from m/z 30 to beyond the precursor ion of m/z 1265.6 in 2.25 min with 100 Hz filtering.

Calibration in the Negative Mode. In the negative ion mode, MS-2 is calibrated with a 2:1 mixture (v/v) of a solution of CsI in water (260 mg/mL) and glycerol. (The addition of glycerol is necessary to generate a sufficient number of negative ions at very low mass.) The spectrum obtained is time-dependent, as the glycerol cluster ions first dominate, but with time the CsI cluster ions become more abundant. The spectrum observed after 1–2 min is used for calibration. The proper time for the scan can be determined by monitoring the region of the m/z 1426 CsI cluster ion. When other ions in this mass region are less than 10% of the abundance of m/z 1426, the resulting scan has a useful distribution of the calibration peaks from m/z 1 to 3500 (Table II). The mass range m/z 0–10 is recorded with an electron multiplier voltage of +2.0 kV; m/z 10–50, voltage +1.3 kV; m/z 50–2000, voltage +1.0 kV; m/z 2000–3500, voltage +1.3 kV. Postacceleration voltage is kept at +18.5 kV throughout the entire mass range. The resolution is set to 1:1000 and the mass range from m/z 0 to 3600 is scanned in 4 min, 10 s.

Measurement of a CID Spectrum in the Negative Mode. The cerebroside II was dissolved in 2:1 chloroform/methanol (1.4 μg/μL). To this solution was added an equal volume of triethanolamine and 0.3 μL of this mixture was used for the negative ion measurements. The resolution in both MS-1 and MS-2 was 1:1000. The He pressure in the collision cell was such as to reduce the $(M - H)^-$ ion signal to 50%. The secondary electron multiplier voltage was +2.0 kV and the postacceleration was +18.2 kV. The mass range m/z 10–760 was scanned in 1 min, 45 s with 100 Hz filtering, and five consecutive scans were summed.

RESULTS AND DISCUSSION

In principle, generation of a linked scan calibration table involves scanning the magnetic field as in a traditional two-sector-type experiment (i.e., E field constant) while using a suitable calibrant (e.g., alkali halides). From this scan one can relate magnetic field scan voltage to magnetic field intensity and generate a curve as shown (exaggerated) by line a in Figure 2. Furthermore, after proper calibration of this scan, the effective magnetic field strength can be converted to an m/z scale. Using this curve, the DA5000 software

Table II. Mass Assignments in the FAB(−) Calibration Table for CsI in Glycerol

m/z	elemental composition	m/z	elemental composition
1.0078	H	442.8967	$C_6H_{15}O_6CsI$
12.0000	C	478.7617	$C_3H_8O_3CsI_2$
13.0078	CH	513.6189	CsI_3
15.9949	O	578.6695	$C_3H_7OCs_2I_2$
17.0027	OH	610.6593	$C_3H_7O_3Cs_2I_2$
25.0078	C_2H	646.5243	Cs_2I_3
41.0391	C_3H_5	738.5473	$C_3H_8O_3Cs_2I_3$
59.0497	C_3H_7O	870.4692	$C_3H_7O_3Cs_3I_3$
71.0133	$C_3H_3O_2$	906.3342	Cs_3I_4
91.0395	$C_3H_7O_3$	1166.1441	Cs_4I_5
126.9045	I	1425.9540	Cs_5I_6
151.0606	$C_5H_{11}O_5$	1685.7639	Cs_6I_7
183.0869	$C_6H_{15}O_6$	1945.5739	Cs_7I_8
218.9518	$C_3H_8O_3I$	2205.3838	Cs_8I_9
253.8090	I_2	2465.1937	Cs_9I_{10}
259.8064	CsI	2725.0036	$Cs_{10}I_{11}$
318.8596	C_3H_7OCsI	2984.8135	$Cs_{11}I_{12}$
350.8494	$C_3H_7O_3CsI$	3244.6234	$Cs_{12}I_{13}$
386.7144	CsI_2	3504.4333	$Cs_{13}I_{14}$

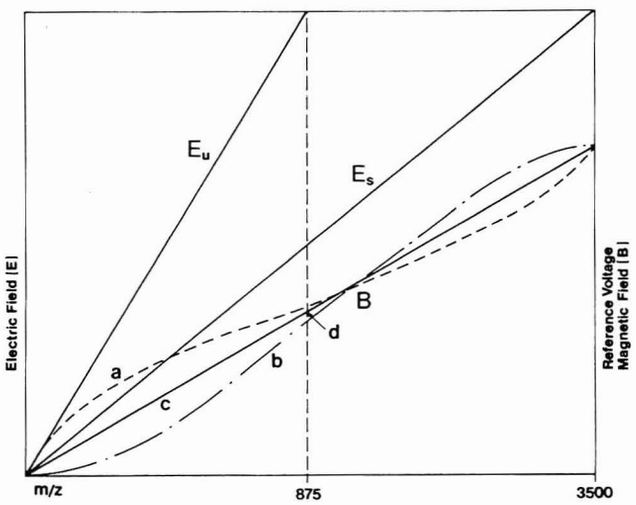

Figure 2. Schematic diagram (not to scale) of the linearization of the magnetic field (B): (a) uncorrected field vs. time; (b) correction to reference voltage; (c) final linearized magnetic field. Example shows B and E_s for standard representing a calibration mixture up to mass 3500 (see Table I). For an unknown (e.g., precursor m/z 875) the magnetic field is scanned along c to the value (point d) where m/z 875 is in focus when the electric sector voltage (E_u) reaches the full value.

calculates the proper offset voltages (line b in Figure 2) such that when these voltages are applied over the entire scanning range, the magnetic field is effectively linearized over this range (line c in Figure 2). The potential of the electric sector (E_2) scans from 0 to its full value along line E_s while the magnetic field (B_2) scans from 0 to the value appropriate to focus on the precursor ion (P_s) of the standard calibrant. For the measurement of the product ion spectrum of the unknown, the linearized magnetic field is scanned to the proper value (d) to bring P_u into focus while the electric sector is scanned along line E_u from 0 to its full value (see Figure 2). In the example the mass range is calibrated to m/z 3500 (P_s) and the CID spectrum of an unknown, P_u, of m/z 875 is determined, requiring scanning the magnetic field to half the value reached in the calibration.

Figure 3 illustrates the hardware and software interrelation involved in execution of the linked scan at constant B/E function. In normal operation, DAC1 controls the magnetic field scanning voltage and DAC2 controls the electric sector voltage. In linked scan operation, the DA5000 scans DAC1 and DAC2 simultaneously and DAC3 sends the appropriate

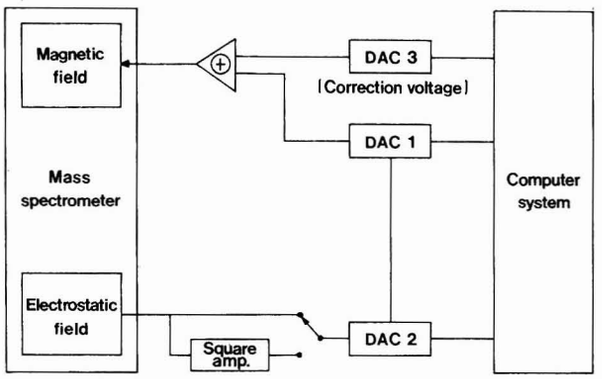

Figure 3. Schematic diagram of the DA5000 control circuits for the electric and magnetic field scans.

offset voltage to the ADD amplifier.

The operator specifies the m/z value of the precursor ion and where the scan should start and end (usually 10–20 u beyond the precursor). The scan is then initiated from low mass to high mass at the operator-specified scan rate. The correction voltages calculated ensure that the B/E ratio can be maintained highly constant over a wide range regardless of precursor ion mass.

Since such a linked scan at constant B/E from low to high mass begins at very low magnetic field, proportionally more calibration points are required in this region and more evenly spaced at higher mass. For this reason, a mixture of alkali halides (see the Experimental Section and Table I) is used, rather than CsI alone.

The position intensity data acquired during a calibration scan are then displayed by the JEOL DA5000 and the first three standard masses assigned manually. The resulting calibration file, which contains mass, position, and intensity information, may be used for normal as well as linked scans at constant B/E of any sample with molecular weight less than the upper limit of the calibration table. The integrity of the calibration table is checked by ionizing a standard compound in ion source 1 and scanning MS-2 in the linked scan at constant B/E mode. The mass assignments of the product ions and the relative abundance of the ions of lowest mass and, therefore, lowest energy, which are most affected by slight variations in the magnetic fields, are an indication of good calibration. We use the tetradecapeptide renin substrate as such a standard because it is inexpensive, its $(M + H)^+$ ion of m/z 1758.9 falls in the middle of our practical B/E mass range and provides an excellent distribution of well-characterized product ions from m/z 70 to the precursor. If the mass assignments are not well within ±0.3 u, a correction can be made by slightly offsetting the magnetic field.

The product ion spectrum is acquired as raw data with individual scans being transferred to the host computer upon completion of the scan. The acquisition processor of the HX110 has a storage capacity of 128K data points (4 bytes each) and these are used to record and display the ion current profile data. After the acquisition is complete, the peak profile data may be processed, including the summation of several individual scans and calculation of mass values with the peak detection software. (It should be noted that we have found these profile data to represent the most useful display of the MS/MS data, although other options, such as bar graphs, are available.) Since the profile data is stored on disk, it may be processed more than once with different peak detection parameters, varying thresholds and resolution parameters, etc.

The undecapeptide physalaemin (I), M_r = 1264.6, was chosen as an example to allow comparison with the data reported in the literature (*21*). The CID spectrum (Figure 4) combined with the data in Table III demonstrates the performance of the linked scan function. Although the mass calibration data used covered the range from m/z 1 to 3510, the mass assignments (Table III) for a compound of a molecular weight less than half of the maximum of the mass range are just as good, if not better than those achieved for the same compound in the previous work (*21*) where the P_u/P_s ratio was close to unity (1265.60/1222.14). More important is the appearance of the product ion spectrum. Although the spectrum of physalaemin shown in the earlier work agrees quite well with Figure 4 from the precursor, m/z 1265.59 (M

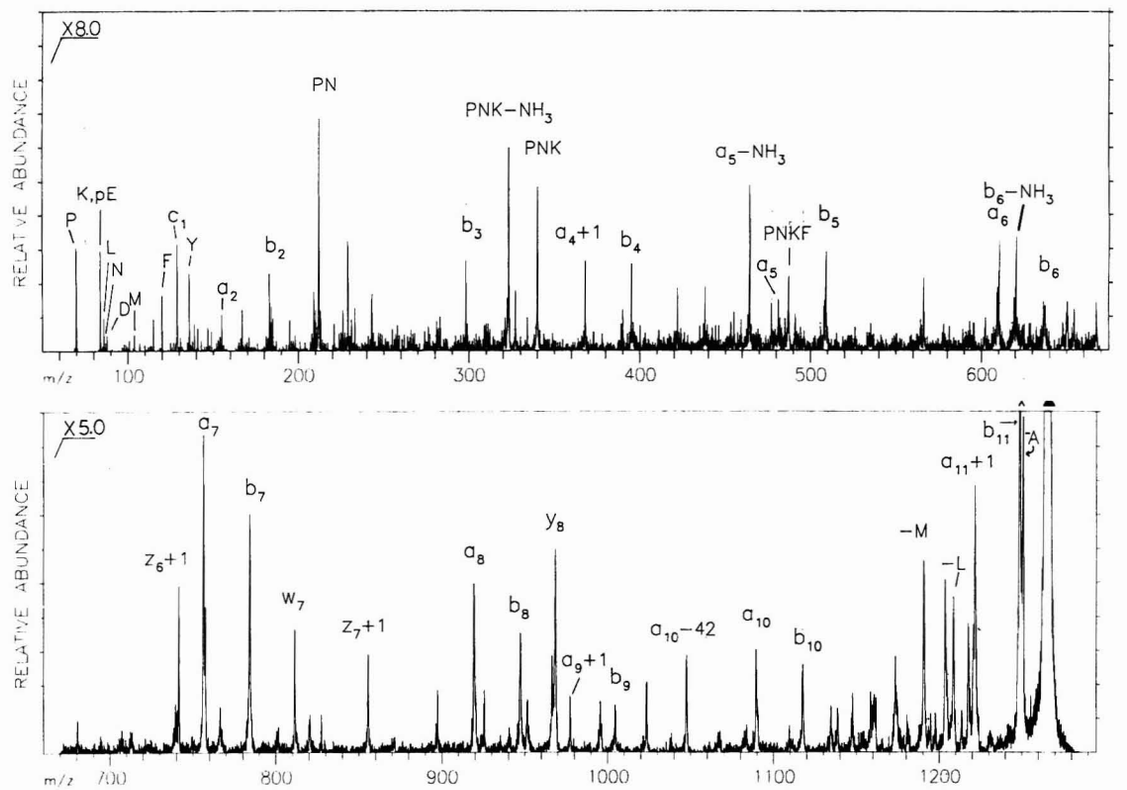

Figure 4. FAB(+) CID MS/MS spectrum of physalaemin (I) $(M + H)^+$, m/z 1265.6. For an explanation of labeling, see Table III.

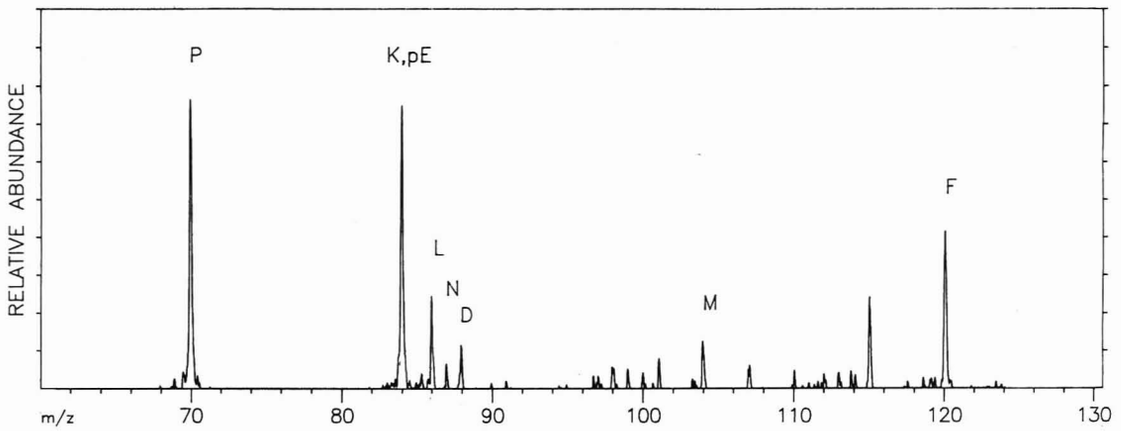

Figure 5. Low-mass region (m/z 60–130) in the FAB(+) CID MS/MS spectrum of physalaemin (I) $(M + H)^+$, m/z 1265.6.

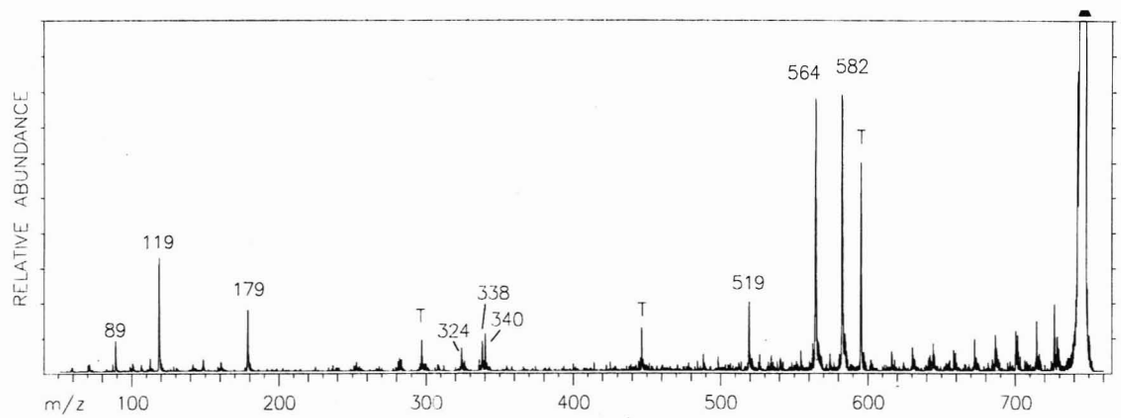

Figure 6. FAB(–) CID MS/MS spectrum of *N*-α-hydroxystearoyl dihydrogalactocerebroside (II) $(M - H)^-$, m/z 744.6. Peaks labeled T are from triethanolamine.

$+ H)^+$ down to m/z 750 (about 60% of the mass of the precursor ion), the abundant fragment ions apparent in Figure 4 in the region of m/z 750 down to 70 are absent in the spectrum reported by Boyd et al. (*21*), with the exception of two small peaks at m/z 620 and 340.

In our experience with the interpretation of a large number of CID spectra of peptides of known or unknown amino acid sequence (*20*, *26*), the lower portion of the mass spectrum is extremely important because ions in the region of m/z 50–200 represent either immonium ions, $(H_2N{=}CHR)^+$, indicative of the amino acids present in the peptide or are ions that reveal the first and last one or two amino acids. This range is expanded in Figure 5, which demonstrates that not only mass accuracy (Table III) but also resolution is well maintained. These fragment ions have a mass as low as 0.1–0.05 times that of the precursor ion and, therefore, correspondingly low kinetic energy (e.g., 553 eV m/z 70 from a 10 keV precursor of m/z 1265.6).

CID MS/MS spectra of peptides have been described elsewhere. The assignments made in Table III are consistent with these observations (*26*). The accuracy of the mass assignments is at least as good as ±0.3 u over the entire mass range. Table III reports the values obtained for the particular scan shown in Figures 4 and 5 as well as the mass values calculated for the fragment ions shown. Also listed is the standard deviation and mean value of six measurements of the spectrum of the same compound obtained on different days. Clearly, they are sufficiently accurate to reliably assign all sequence specific ions in this spectrum.

From the data reported here, it is also evident that it is not necessary to decelerate the precursor ion prior to collision and reaccelerate the ions before entering MS-2 to assure that product ions of low mass are efficiently transmitted through MS-2, in contrast to what has been suggested previously (*16*).

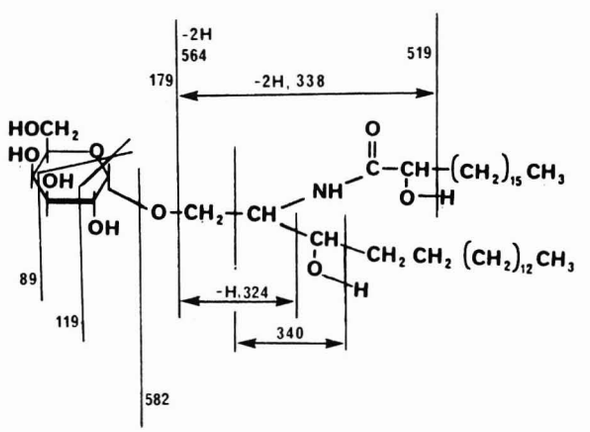

Figure 7. Assignments of product ions observed in the FAB(–) CID MS/MS spectrum of *N*-α-hydroxystearoyl dihydrogalactocerebroside (II) $(M + H)^-$, m/z 744.6.

The good transmission of fragment ions of low mass, which have not only low kinetic energies but also a relatively wide angular spread, is due (a) to the accurate linked scan function set up by the data system which keeps the B/E ratio very constant even at low values of B_2 and (b) to the z-axis focusing effect of the quadrupole lens located after E_2, which helps to compensate for the angular spread.

Similar performance is observed in the negative ion mode. In this case, the calibration ranges from m/z 1.0 (H^-) to m/z 3504.4, $I(Cs_{13}I_{13})^-$ (Table II). Figure 6 shows the collision spectrum obtained for the $(M - H)^-$ ion of *N*-α-hydroxystearoyl dihydrogalactosylcerebroside (II), m/z 744.60 (calcd), with triethanolamine as the matrix. Table IV lists the observed masses and the calculated values for the assigned compositions. Fragmentation pathways (Figure 7) indicated

Table III. Mass Assignment and Error Analysis of Fragment Ions Observed in the MS/MS Mass Spectra of Physalaemin (I)

ion type[a]	m/z obsd[b]	Δ[b]	mean[c]	$N = 6$ std dev[c]	Δ[c]
P	69.84	−0.22	69.86	0.11	−0.20
K	83.88	−0.19	83.89	0.10	−0.18
L	85.89	−0.20	85.95	0.11	−0.14
F	119.97	−0.11	119.95	0.11	−0.13
Y	135.99	−0.08	135.96	0.09	−0.11
a_2	155.02	−0.06	154.99	0.09	−0.09
b_2	183.00	−0.08	182.98	0.09	−0.10
PN	212.05	−0.05	212.04	0.10	−0.06
b_3	298.04	−0.06	298.00	0.06	−0.10
PNK − NH_3	323.23	+0.07	323.18	0.07	+0.01
PNK	340.16	−0.04	340.15	0.07	−0.05
$a_4 + 1$	368.22	+0.05	368.11	0.08	−0.06
b_4	395.23	+0.07	395.14	0.07	−0.02
$a_5 - NH_3$	464.30	+0.13	464.17	0.10	0.00
a_5	481.33	+0.13	481.24	0.13	+0.04
b_5	509.11	−0.09	509.16	0.05	−0.04
a_6	609.55	+0.25	609.37	0.11	+0.07
$b_6 - NH_3$	620.33	+0.07	620.34	0.09	+0.08
b_6	637.57	+0.28	637.43	0.10	+0.14
a_7	756.42	+0.05	756.45	0.12	+0.08
b_7	784.33	−0.03	784.40	0.05	+0.04
a_8	919.43	0.00	919.49	0.09	+0.06
b_8	947.52	+0.09	947.48	0.14	+0.05
$a_9 + 1$	977.55	+0.09	977.48	0.05	+0.02
b_9	1004.46	+0.01	1004.41	0.08	−0.04
$a_{10} - 42$[d]	1047.69	+0.20	1047.57	0.12	+0.08
a_{10}	1089.53	−0.01	1089.63	0.11	+0.09
b_{10}	1117.83	+0.30	1117.57	0.14	+0.04
$a_{11} + 1$	1221.63	+0.05	1221.68	0.12	+0.10
b_{11}	1248.72	+0.15	1248.63	0.10	+0.06

[a] Structures of ions: a_n = $H(HNC(R)HCO)_xNH{=}C(R_{x+1})H$, b_n = $H(HNC(R)HCO)_xNHC(R_{x+1})HCO^+$. Interchain immonium ions of the type $H_2N{=}C(R)H$ and interchain fragments of the type $H_2N(C(R)HCONH)_xC(R)HCO^+$ and labeled with the single letter codes of the amino acids. This nomenclature is a slight variation of that proposed by Roepstorff, P., Fohlman, J. *Biomed. Mass Spectrom.* **1984**, *11*, 601. [b] In the spectrum shown in Figure 4. [c] Six spectra taken at different times. SD = standard deviations. [d] Due to presence of leucine (Martin, S. A.; Biemann, K. 34 Annual Conference on Mass Spectrometry and Allied Topics, Cincinnati, OH, 1986; pp 854–855).

for II are based on comparisons of its CID spectrum with those of related compounds and with FAB(−) spectra as obtained in our laboratory (*27*) or as reported in the literature (*28–30*). Peaks in the high mass region are formed by loss of methyl or water. A series of peaks arises by loss of saturated hydrocarbons, starting with methane. Cleavages along the hydrocarbon backbone remote from the site of charge localization in the FAB(−) CID spectra of long-chain fatty acids has been discussed by Tomer et al. (*28*), although they report loss of alkanes with CH_4 as the smallest entity, whereas loss of CH_3 and C_2H_5 are also observed here. Fragments that arise by loss of the sugar moiety occur in the FAB(−) mass spectra of all the glycosphingolipids reported by Hemling et al. (*29*). These authors have designated the fragment shown here as m/z 324 as x and m/z 340 as y. The y ion has a second possible structure similar to m/z 324 but with cleavage on the other side of the glucoside oxygen bond. Cleavage of the sugar ring to produce m/z 179, 119, 89, and 87 has been described by Barber et al. as a characteristic process in negative ion mass spectra obtained by neutral beam bombardment of a dry film of a simple monosaccharide cast on a copper target (*30*).

By coincidence, a cluster ion of TEA $(TEA_5 - H)^-$, m/z 744.52 (calcd), occurs at the same nominal mass as the cerebroside $(M - H)^-$, and its product ions also appear in the CID spectrum at m/z 595, 446 and 297. Because the compositions of the TEA clusters are unambiguous, their mass assignments, also listed in Table IV, provide further confirmation of the accuracy of the method described.

Table IV. Assignments for Peaks in the FAB(−) CID MS/MS Spectrum of II in TEA

m/z obsd	m/z calcd	Δ	assignment
87.04	87.01	+0.03	$C_3H_3O_3$
89.10	89.02	+0.08	$C_3H_5O_3$
118.67	119.03	−0.36	$C_4H_7O_4$
178.79	179.06	−0.27	$C_6H_{11}O_6$
297.08	297.20	−0.12	$TEA_2 - H$
324.18	324.30	−0.12	$C_{20}H_{38}NO_2$
338.23	338.27	−0.04	$C_{20}H_{36}NO_3$
340.26	340.29	−0.03	$C_{20}H_{38}N_3$
446.43	446.31	+0.12	$TEA_3 - H$
519.37	519.34	+0.03	$C_{26}H_{49}NO_9$
564.61	564.54	+0.07	$C_{36}H_{70}NO_3$
582.46	582.55	−0.09	$C_{36}H_{72}NO_4$
595.35	595.41	−0.06	$TEA_4 - H$
616.42	616.44	−0.02	$(M - H) - C_9H_{20}$
630.29	630.46	−0.17	$(M - H) - C_8H_{18}$
644.42	644.47	−0.05	$(M - H) - C_7H_{16}$
658.39	658.49	−0.10	$(M - H) - C_6H_{14}$
672.58	672.51	+0.07	$(M - H) - C_5H_{12}$
686.45	686.52	−0.07	$(M - H) - C_4H_{10}$
700.46	700.54	−0.08	$(M - H) - C_3H_8$
714.54	714.55	−0.01	$(M - H) - C_2H_6$
715.75	715.57	+0.18	$(M - H) - C_2H_5$
726.51	726.59	−0.08	$(M - H) - H_2O$
728.65	728.57	+0.08	$(M - H) - CH_4$
729.51	729.58	−0.07	$(M - H) - CH_3$
	744.52		$TEA_5 - H$
744.60[a]	744.60		M − H

[a] Precursor.

CONCLUSION

A calibration spectrum covering the range from m/z 1 (H^+) to m/z 3510.4 $(Cs(CsI)_{13}^+)$ or from m/z 1 (H^-) to 3504.4 $(I(CsI)_{13}^-)$ can be used to generate a product ion spectrum of any precursor ion within this mass range. The method described here is simple, reliable, and allows the recording of

CID spectra of precursor ions of a wide mass range with a single set of calibration data and results in mass assignments within ±0.3 u or better, sufficient for the reliable interpretation of the product ion spectra of compounds ranging in molecular weight to at least 3000 mass units.

Registry No. I, 2507-24-6; II, 107982-40-1.

LITERATURE CITED

(1) McLafferty, F. W.; Bente, P. F., III; Kornfeld, R. T.; Sai, S.-C.; Howe, I. *J. Am. Chem. Soc.* **1973**, *95*, 2120–2129.
(2) Beynon, J. H.; Cooks, R. G. *Res./Dev.* **1971**, *22*, 26.
(3) Boyd, R. K.; Beynon, J. H. *Org. Mass Spectrom.* **1977**, *12*, 163–165.
(4) Millington, D. S.; Smith, J. A. *Org. Mass Spectrom.* **1977**, *12*, 264–265.
(5) Bruins, A. P.; Jennings, K. R.; Evans, S. *Int. J. Mass Spectrom. Ion Phys.* **1978**, *26*, 395–404.
(6) Morgan, R. P.; Porter, C. J.; Beynon, J. H. *Org. Mass Spectrom.* **1977**, *12*, 735–738.
(7) Neumann, G. M.; Derrick, P. J. *Org. Mass Spectrom.* **1984**, *19*, 165–170.
(8) Bricker, D. L.; Russell, D. H. *J. Am. Chem. Soc.* **1986**, *108*, 6174–6179.
(9) Ast, T.; Bozorgzadeh, M. H.; Wiebers, J. L.; Beynon, J. H.; Brenton, A. G. *Org. Mass Spectrom.* **1979**, *14*, 313–318.
(10) Gross, M. L.; Russell, D. H. in *Tandem Mass Spectrometry*; McLafferty, F. W., Ed.; Wiley: New York, 1983; pp 255–270.
(11) Gilliam, J. M.; Occolowitz, J. Presented at the 31st Annual Conference on Mass Spectrometry and Allied Topics, Boston, MA, 1983; p 193.
(12) Johnson, E. G.; Nier, A. O. *Phys. Rev.* **1953**, *91*, 10–17.
(13) Futrell, J. H.; Miller, C. D. *Rev. Sci. Instrum.* **1966**, *37*, 1521–1526.
(14) Todd, P. J.; McGilvery, D. C.; Baldwin, M. A.; McLafferty, F. W. In *Tandem Mass Spectrometry*; McLafferty, F. W., Ed.; Wiley: New York, 1983; pp 271–286.
(15) Amster, I. J.; Baldwin, M. A.; Cheng, M. T.; Proctor, C. J.; McLafferty, F. W. *J. Am. Chem. Soc.* **1983**, *105*, 1654–1655.
(16) Hass, J. R.; Green, B. N.; Bateman, R. H.; Bott, P. A. Presented at the 32nd Annual Conference on Mass Spectrometry and Allied Topics, San Antonio, TX, 1984; pp 380–381.
(17) Carr, S. A.; Roberts, G. D.; Hemling, M. E.; Killmer, L. B.; Johnson, W.; Mentzer, M. Presented at the 34th Annual Conference on Mass Spectrometry and Allied Topics, Cincinnnati, OH, 1986; pp 630–631.
(18) Kammei, Y.; Itagaki, Y.; Kubota, E.; Kunihiro, H.; Ishihara, M. Presented at the 33rd Annual Conference on Mass Spectrometry and Allied Topics, San Diego, CA, 1985; p 855.
(19) Matsuda, H.; Matsuo, T.; Fujita, Y.; Wollnik, H. *Mass Spectrom. (Japan)* **1976**, *24*, 19.
(20) Biemann, K.; Martin, S. A.; Scoble, H. A.; Johnson, R. S.; Papayannopoulos, I. A.; Biller, J. E.; Costello, C. E. In *Mass Spectrometry in the Analysis of Large Molecules*; McNeal, C. J., Ed.; Wiley: Chichester, England, 1986; pp 131–149.
(21) Boyd, R. K.; Bott, P. A.; Harvan, D. J.; Hass, J. R. *Int. J. Mass Spectrom. Ion Proc.* **1986**, *69*, 251–263.
(22) Carr, S. A., personal communication.
(23) Matsuo, T.; Matsuda, H.; Katakuse, I.; Shimonishi, Y.; Maruyama, Y.; Higuchi, T.; Kubota, E. *Anal. Chem.* **1981**, *53*, 416–421.
(24) Friedli, F. *Org. Mass Spectrom.* **1984**, *19*, 183–189.
(25) Haddon, W. F. *Anal. Chem.* **1979**, *51*, 983–988.
(26) Biemann, K. In *The Proceedings of the Sixth International Conference on Methods in Protein Sequence Analysis*; Walsh, K. A., Ed.; Humana: Clifton, NJ, 1986; in press.
(27) Costello, C. E.; Singh, B. N.; Domon, B., M.I.T., 1986, unpublished work.
(28) Tomer, K. B.; Crow, F. W.; Gross, M. L. *J. Am. Chem. Soc.* **1983**, *105*, 5487–5488.
(29) Hemling, M. E.; Yu, R. K.; Sedgwick, R. D.; Rinehart, K. L. *Biochemistry* **1984**, *23*, 5706–5713.
(30) Barber, M.; Bordoli, R. S.; Sedgwick, R. D.; Vickerman, J. C. *J. Chem. Soc., Faraday Trans. 1* **1982**, *78*, 1291–1296.

RECEIVED for review December 18, 1986. Accepted March 12, 1987. This work was supported by the National Institutes of Health, Division of Research Resources (Grant RR00317).

Analysis of Molecular Orientational Order in Solid Samples by Nuclear Magnetic Resonance: Application to Lignin and Cellulose in Wood

Galen R. Hatfield, Maziar Sardashti, and Gary E. Maciel*

Department of Chemistry, Colorado State University, Fort Collins, Colorado 80523

A two-dimensional Fourier transform solid-state nuclear magnetic resonance experiment designed to yield anisotropy information can be used to probe molecular orientational order of specific components in a complex, inhomogeneous (e.g., biological) solid. This technique is applied to wood in order to determine the extent of macroscopic orientation and ordering of lignin and cellulose. Model systems are also considered to demonstrate the ability of this technique to probe orientational order. Results for *Eucalyptus polyanthemus* wood reveal that there is no net molecular orientational order of lignin or cellulose over a *macroscopic* volume of about 0.9 cm^3.

Molecular orientational order is an important physical property in many areas of science, including biological membranes, surface chemistry, and oriented polymers. In many cases, the physical properties (and possibly chemical behavior) of these systems are dominated by the degree of molecular orientational order present. In order to understand, use, and modify these chemical systems, it is important to have a detailed knowledge of the type and extent of order present. To date, most methods for readily determining orientational order can be applied only to relatively simple homogeneous samples or else have required substantial experimental limitations. For example, in highly ordered and chemically homogeneous systems, techniques that rely on X-ray or neutron diffraction may be useful. However, with samples that are chemically inhomogeneous and/or with small degrees of molecular orientational order, the diffraction patterns are poorly defined and orientational information is difficult, if not impossible, to obtain. For less ordered systems, ^2H NMR has proven to be an excellent technique for extracting orientational information, based on the anisotropic nature of the nuclear electric quadrupole interaction (*1*). However, this method requires isotopic labeling, which presents a severe experimental limitation, especially if the system of interest is a natural biopolymer. We report here a two-dimensional Fourier transform (2-D FT) NMR experiment that readily permits analysis of molecular orientational order at the molecular level in *both* homogeneous and complex inhomogeneous solids.

During the past few years the scope of NMR applications has been broadened from liquid samples to include a range of solid samples that represent a wide variety of chemical systems, from polymers and resins to molecules adsorbed on catalytically active surfaces (*2*). The chemical shift observed in an NMR experiment is the spectroscopic parameter used most often for the elucidation of molecular structure. This

0003-2700/87/0359-1659$01.50/0 © 1987 American Chemical Society

parameter depends upon two factors. These are (1) the disposition of the nuclear spin with respect to its electronic environment (i.e., the chemical structural environment of the nucleus) and (2) the orientation of the structural environment of the nucleus with respect to the applied external magnetic field, B_0. In a typical liquid-state NMR experiment, this orientation dependence is averaged out by the tumbling (Brownian) motion of molecules in a liquid, yielding a sharply defined "isotropic chemical shift" average. However, in the solid state, motion is far more restricted, and the chemical shift anisotropy (CSA) gives rise to broad CSA powder patterns. These patterns contain valuable information on the orientation dependence of the chemical shift, but they can constitute serious line-broadening effects in the spectra of complex samples. If one wishes to obtain high-resolution spectra in such cases, say for ^{13}C, the sample is usually rotated rapidly at the so-called "magic-angle" (54.7°) to average out this orientation dependence (*3*). The result of either magic-angle spinning (MAS) of a solid or natural Brownian motion for a liquid is one or more sharp resonance lines characteristic of the isotropic chemical shifts, which reflect the chemical environments of the nuclei under study. However, in such experiments information on the orientation dependence of the chemical shift is lost.

For relatively simple systems, CSA patterns containing orientational information can be obtained on static samples or from the spinning sideband patterns in a MAS experiment (*3*). However, for complex organic systems such as wood, the CSA patterns from many ^{13}C nuclei in a wide variety of structural environments are hopelessly overlapped in the spectrum of a static sample, and the spinning sideband patterns in a slow-spinning MAS experiment are usually obscured by overlaps, preventing information on either the chemical structures orientation from being readily discerned.

An experiment recently developed in this laboratory (*4*) permits the observation of both isotropic chemical shift information and CSA patterns associated with each of the isotropic chemical shifts. In this 2-D FT NMR experiment, the angle between the direction of B_0 and the spinning axis of the sample is flipped between 54.7° and another angle (typically 90°) during a time between the evolution and detection periods of the experiment. It can be shown (*5*) that, for sample spinning at 90°, the CSA is manifested as an anisotropy pattern that is reversed along the frequency scale and collapsed to half the width of the static (nonspinning) case, but the "shape" of the CSA pattern is the same as for the static experiment. After the evolution period, the sample-spinning axis is flipped to 54.7°, where the chemical shift manifests itself as its isotropic average for detection. Details of this experiment have been described elsewhere (*4*, *6*) and will not be repeated here.

In order to determine the ability of this technique to probe molecular orientational order in a complex, inhomogeneous solid, a series of experiments were carried out on *Eucalyptus polyanthemus* wood. Wood is an excellent choice for studying order in a complex, inhomogeneous solid. The molecular architecture of wood and the organization of the cell wall itself have been the subject of intense study (*7*). Despite substantial strides, many crucial questions remain to be answered. Wood consists of a wide variety of constituents, including lignin, cellulose, hemicelluloses, tannins, and so forth. In this paper we will directly address the molecular orientational order of the two major constituents in wood, lignin and cellulose. Lignin has been generally considered to be somewhat "gluelike" in nature and randomly dispersed around oriented cellulosic fibers (*8*). Compared to cellulose, which is homogeneous at the level of primary polymer structure, lignin is much more heterogeneous, having a variety of different bonding patterns and therefore an inhomogeneous primary structure. A recent study gave evidence suggesting that lignin in woody tissue "is more highly organized at the molecular level than had heretofore been recognized" and proposed "that the orientation of the phenyl ring is most often preferentially in the plane of the cell wall" (*9*). To address this type of issue, we have applied the above-mentioned 2-D FT NMR experiment designed to yield anisotropy information (*4*) to examine the molecular orientation of lignin and cellulose in whole wood. In solid-state NMR the sample is studied in its "natural" and unaltered solid state. The solid-state 2-D FT CSA approach of the present study provides information on anisotropy patterns associated with each distinct isotropic chemical shift. Thus, one can probe the orientation of each atomic site or moiety in a macromolecular system and detect the presence of molecular orientational order. We report here definitive physical proof that these components are largely unoriented, in a *macroscopic* sense, in unaltered, whole wood.

EXPERIMENTAL SECTION

All spectra shown in this paper were accumulated at a ^{13}C resonance frequency of 25.3 MHz on a home-built spectrometer using a Nalorac 89-mm magnet and a Nicolet 1180/293B data-system/pulse-programmer. ^{13}C magnetization was generated by means of cross polarization (CP) from proton spins (*10*). ^{13}C CP/MAS (*11*, *12*) spectra of *Eucalyptus polyanthemus* wood were obtained with a CP contact time of 2 ms and a repetition time of 1 s. ^{13}C CP/MAS spectra of homovanillic alcohol were obtained with a contact time of 5 ms and a repetition time of 1 s. Both the cellulose and sucrose spectra were obtained at a contact time of 2 ms, with repetition times of 2 and 5 s, respectively. For the 2-D spectra, the t_1 period was incremented in steps of 83 μs. In all cases, samples were spun at 2.4 kHz.

RESULTS AND DISCUSSION

It is possible to obtain precise information on the orientations of molecules under study from a mathematical analysis of an observed chemical shift pattern (*13*). In the limit of a single crystal, with only one molecular orientation per unit cell, the chemical shift or CSA pattern consists of only discrete sharp lines, each reflecting a specific "chemical environment" and a specific orientation. In the limit of a completely disordered powder or a completely amorphous solid, the CSA pattern consists of an infinite number of resonance lines representing an infinite number of orientations. This infinite set of resonance peaks overlap to form a broad CSA pattern, reflecting a specific "chemical environment" and the statistical probabilities of the various orientations. Thus, a highly ordered system gives rise to sharp, discrete resonance lines, while a random system results in a broad, so-called "powder pattern". It is this difference which serves as the basis for studying the orientation of lignin and cellulose in wood through the use of this 2-D FT NMR experiment.

The strategy used in this study was to compare ^{13}C CSA patterns of cellulose and lignin resonances obtained when sample spinners were loaded in the following four ways: (1) with the wood grain collinear with the spinner axis, (2) with the direction of the grain oriented at an angle of 45° with respect to the spinner axis, (3) with the wood grain perpendicular to the spinner axis, and (4) with powdered wood. If a wood component is highly ordered, the corresponding CSA patterns should be markedly different for each of the four samples. If, on the other hand, the component (e.g., lignin) is randomly oriented, the CSA patterns corresponding to a specific isotropic chemical shift should be the same for each sample and will appear no different from the CSA pattern obtained for powdered wood.

The oriented wood samples used in this study were intact wood plugs removed from a naturally dried section of a fallen *Eucalyptus polyanthemus* tree, taken from the sapwood region located just beneath the inner bark. The plugs were

Figure 1. ^{13}C CP/MAS NMR spectra: (A) sucrose, showing with arrows the peaks at 73 and 106 ppm used for the 2-D FT experiments; (B) cellulose powder (Whatman CC31), showing with arrows the peaks at 73 and 106 ppm used for the 2-D FT experiments; (C) *Eucalyptus polyanthemus* wood used in this study, showing with arrows the lignin peak at 152 pm and the cellulose peaks at 106 and 73 ppm used for the 2-D FT experiments; (D) homovanillic alcohol, showing with an arrow the 149 ppm peak used for the 2-D FT experiments.

roughly 1.8 cm in length and 0.8 cm in diameter and thus probe molecular orientational order over a 0.9 cm^3 volume. The powdered wood sample was prepared by collecting sawdust taken from the same region of sapwood and grinding it in a ball mill. Care was taken to ensure that the milling was not so extensive as to destroy the molecular structural integrity of wood components. ^{13}C CP/MAS spectra were taken (not shown) in order to ensure that the lignin and cellulose contributions to the spectra remain unaltered by ball milling.

Shown in Figure 1C is the normal ^{13}C CP/MAS NMR spectrum of the wood used in this study. Lignin in *Eucalyptus polyanthemus*, a hardwood, is a heterogeneous mixture of polymers consisting of syringylpropane (I) and guaiacylpropane (II) repeat units (*14*), as well as significant quantities

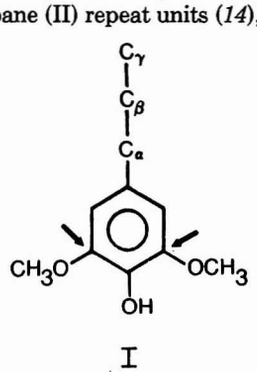

I

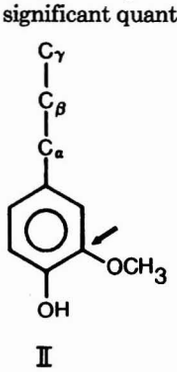

II

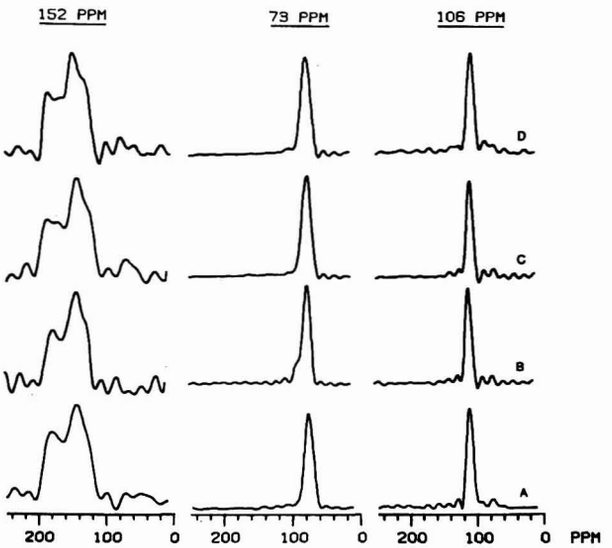

Figure 2. ^{13}C 2-D FT CSA patterns for the specified chemical shifts in the spectrum of *Eucalyptus polyanthemus* wood: (A) grain collinear; (B) 45°; (C) perpendicular to the spinning axis; (D) powdered wood.

of *p*-hydroxyphenylpropane moieties. Among the aromatic carbons in these structures are those with methoxy groups attached. These carbons have been shown (*15*) to give rise to ^{13}C resonances at 152–154 ppm and this position is marked in structures I–III by an arrow.

The ^{13}C CSA patterns corresponding to these carbons in the oriented and powdered wood samples, as given by the 2-D FT experiment (*4*), are shown in Figure 2. It is immediately obvious that the CSA patterns for the samples in which the wood grain was oriented with respect to the spinner axis are virtually identical with that of the powdered wood. This clearly proves that lignin can *not* be highly ordered or oriented in whole wood over a 0.9 cm^3 macroscopic volume, and a "preferred" in-plane orientation for the aromatic rings over the macroscopic volume of the sample can be ruled out. Slight differences between the patterns are almost certainly within signal-to-noise limits and should be neglected. Even in the case of a partially ordered system, the CSA patterns would differ markedly and this is demonstrated below. We believe that this represents the first concrete physical proof that demonstrates lignin to be orientationally disordered with respect to a macroscopic sample of whole wood.

In order to illustrate the ability of this 2-D FT NMR technique to detect orientation and order, a set of experiments was carried out on homovanillic alcohol (III). Note that the

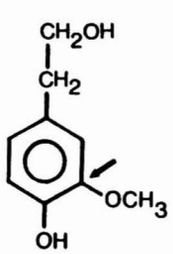

III

aromatic moiety in this model compound closely resembles that of a guaiacylpropane unit (II). More significantly, it contains a methoxy-substituted aromatic carbon in a local environment that is essentially identical with those found in lignin. The ^{13}C CP/MAS spectrum of this compound is given in Figure 1D. The resonance at 149 ppm corresponds to this methoxy-substituted aromatic carbon, and CSA patterns obtained by the 2-D FT experiment were taken from this isotropic chemical shift. The CSA pattern corresponding to

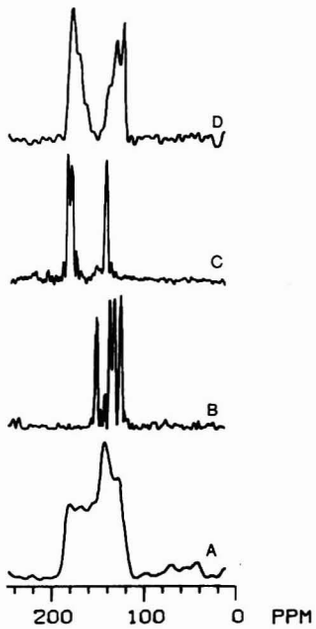

Figure 3. ^{13}C CSA patterns obtained for the 149 ppm isotropic chemical shift for homovanillic alcohol: (A) powdered sample; (B) single crystal at one orientation relative to the spinning axis; (C) the same single crystal at another orientation relative to the spinning axis; (D) collection of crystalline intergrowths (see text).

this peak for powdered homovanillic alcohol is given in Figure 3A. The similarity of this pattern to the CSA patterns obtained for the wood samples (Figure 2) reinforces our judgement regarding the suitability of this compound as a model for a methoxy-substituted aromatic carbon of the type found in lignin. Also, the similarity of the CSA pattern of *powdered* homovanillic alcohol with those obtained for wood again demonstrates that the molecular orientation of lignin is macroscopically random in these wood samples.

Attempts to grow a single crystal of homovanillic alcohol suitably large enough for the 2-D FT experiment, although ultimately successful, proved to be difficult at first. Figure 3D shows the CSA pattern obtained for a large sample comprised of a collection of crystalline intergrowths. Note that even for this partly oriented system, the CSA pattern is substantially different from that of the random powder case. Figure 3B,C shows that CSA pattern obtained for a single crystal of homovanillic alcohol at two different orientations in the spinner. As expected for a highly ordered system, the CSA patterns contain only sharp lines and are different for the two orientations. X-ray diffraction analysis revealed the presence of four molecules per unit cell, each with a significantly different orientation. These give rise to the four ^{13}C NMR lines shown in Figure 3B. Figure 3C also contains four lines, two of which overlap, and Figure 3D appears to have four broad contributing components, which reflect the limited order present. In addition, Figure 3D demonstrates by analogy that, if the aromatic rings of lignin were preferentially oriented in the plane of the cell wall (or in any other plane), dramatic differences in the CSA patterns would be expected among the wood plots of Figure 2. As this is not the case, we can confidently conclude that lignin is not preferentially oriented in any way over the dimensions observed in this experiment.

It should be noted that the "dips" seen at about 160 ppm in the 2-D FT CSA powder patterns for the 152 ppm resonances in Figure 2 and the 149 ppm resonance in Figure 3A have been assigned to cross-polarization dynamics. Variable contact-time experiments (data not shown) on an isolated lignin sample showed similar dips in the 2-D FT CSA powder patterns obtained with a CP contact time of 2 ms. The nature of these distortions changes with contact time.

Having determined from these experiments that the molecular orientation of lignin is random and exhibits no preferred macroscopic orientation throughout whole wood, we sought to employ this 2-D FT NMR technique to probe order in the cellulose in wood. Cellulose has long been known to be well organized within the cell ultrastructure (*8*). Shown in Figure 1B is the ^{13}C CP/MAS spectrum of cellulose powder (Whatman CC31). The ^{13}C CP/MAS NMR spectrum of cellulose has been extensively studied (*16–19*) and the details of its spectrum will not be repeated here. The sharp intense peak at 73 ppm, indicated with an arrow, is largely responsible for the intensity at 73 ppm in the spectrum of *Eucalyptus polyanthemus*, shown in Figure 1C. From this isotropic chemical shift, CSA patterns for cellulose in *wood* were generated by the 2-D FT NMR technique. These patterns are given in Figure 2. It is immediately obvious that these patterns are very similar, suggesting that cellulose, like lignin, is largely disordered in a macroscopic sense in wood. Slight differences in line width and line shape for the 73 ppm cellulose patterns in Figure 2 may reflect a slight degree of gross molecular order, but such differences are too small to be highly significant at the present level of experimental error.

The peak at 73 ppm has been previously assigned to carbons 2, 3, and 5 of cellulose (*16–19*). In order to ensure that the CSA patterns from these three different carbons were not overlapping in such a way as to obscure the CSA pattern of interest, we also generated patterns from ^{13}C resonance corresponding to the isotropic shift at 106 ppm. This resonance has been assigned to carbon 1 of cellulose. These patterns are also given in Figure 2. Like those patterns obtained at 73 ppm, these are all very similar to each other and actually show less deviation from each other than those shown in Figure 2 for the 73 ppm resonance. This reinforces the result that cellulose is largely disordered in a macroscopic sense in wood. At first glance, this seems disturbing in light of the unquestionable gross order present for cellulose in wood (*8*). However, there are several possible reasons for this result, which are discussed later in this paper.

To demonstrate how order at the molecular level would affect the CSA patterns of cellulose, we carried out a similar set of experiments on sucrose. Sucrose consists of one glucose-type unit and one fructose-type unit, the former of which contains carbons essentially identical in local molecular environment with those found in cellulose. For sucrose, like cellulose, we again chose the resonances at 73 and 106 ppm from which to generate the ^{13}C CSA patterns. These resonances are marked with arrows in the ^{13}C CP/MAS spectrum of sucrose shown in Figure 1A. Figure 4 gives the CSA patterns for powdered (A) and single-crystal (B, C) sucrose taken from the isotropic shifts at 73 and 106 ppm. Note that the powder patterns (A) are relatively broad and very similar to those for cellulose in wood (Figure 2). However, a single crystal of sucrose, which is highly ordered at the molecular level, results in sharp lines, and the effect of an oriented sample is seen by comparing corresponding parts B and C of Figure 4. Note the large differences in the 73 ppm line shapes between parts B and C of Figure 4. These differences may reflect the number of different carbons attributed to the peak at 73 ppm, as discussed above. While the 106 ppm line shapes in Figure 4 are very similar, note that the resonance positions differ by about 10 ppm. These two illustrations demonstrate that if cellulose in wood were, in fact, highly oriented at the molecular level over the macroscopic volume of our experiments, we would expect to see large differences between the cellulose patterns given for wood in Figure 2.

Relevant to this study is an examination of the CSA behavior of a regenerated cellulose sample that was believed to be highly oriented at the molecular level. Results of this

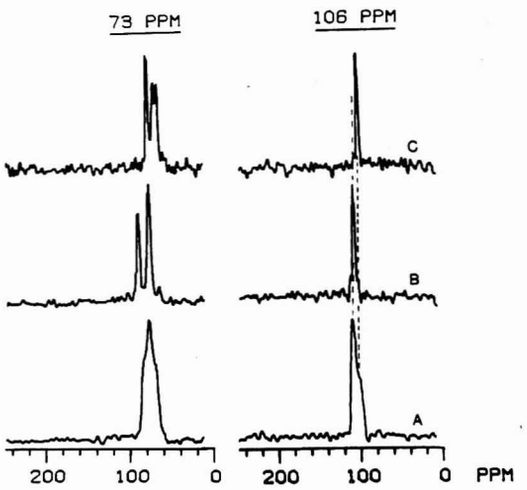

Figure 4. ^{13}C 2-D FT CSA patterns for two specified chemical shifts in the spectrum of sucrose: (A) powdered sample; (B) single crystal at one orientation relative to the spinning axis; (C) the same single crystal at another orientation relative to the spinning axis.

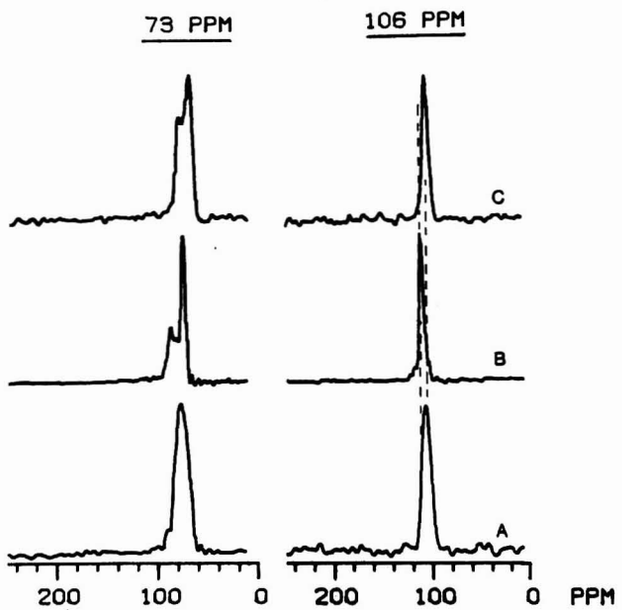

Figure 5. ^{13}C 2-D FT CSA patterns for two specified chemical shifts in the spectrum of cellulose: (A) powdered cellulose (Whatman CC31); (B) cellulose fibers oriented collinear with respect to the spinning axis; (C) cellulose fibers oriented perpendicular to the spinning axis.

examination are summarized in Figure 5, which give the patterns obtained in the 2-D FT CSA experiment. Long strands of the regenerated cellulose sample were cut and placed into the spinner collinear with the spinning axis (Figure 5B) and perpendicular to the spinning axis (Figure 5C). For comparison, Figure 5A shows the CSA patterns corresponding to the isotropic shifts of 73 and 106 ppm, for powdered cellulose (Whatman CC31). Note in Figure 5 the general decrease in the width of the 73 ppm peak in spectrum B relative to that in spectrum A and the significant changes in line shape observed upon sample rotation. Similar changes in line width are also observed for the 106 ppm peak in Figure 5 and a roughly 10 ppm shift occurs when the sample is rotated, as seen in parts B and C of Figure 5. These samples are clearly much more oriented over the macroscopic volume of these experiments than is the cellulose found in wood.

Within the cell wall ultrastructure there exist several subdivisions, each different from the next both in chemical composition and in orientation of the structural (i.e., cellulose) elements (*8*). Models for this cell wall organization have been developed and summarized elsewhere (*7*, *8*, *19–21*) and will not be repeated in detail here. However, it is pertinent to point out that the cell wall is typically divided into the following subdivisions: the primary (P), or outermost wall; the secondary wall, usually divided into two regions (S1 and S2); and the tertiary (T), or innermost wall. Between the individual cells there is a thin layer called the middle lamella (ML), which "glues" the cells together to form the tissue (*8*). From electron microscopy studies (*23*), considerable detail is known about the orientation of cellulose in each of these subdivisions. The ML is in principle free of cellulose. In the primary wall (P), the cellulose fibrils are arranged in thin, crossing oblique layers. The orientation here is very gross in nature, with the outermost region of P containing less order than the inner region. In S1, the orientation of the fibrils is somewhat more ordered, running nearly perpendicular to the cylindrical axis of the cell wall, while the fibrils in S2 are more ordered and run nearly parallel with the cylindrical axis of the cell wall. In T, the cellulose is less ordered than for S1, but with the same type of fibril orientation. Thus, in a gross sense, cellulose is very ordered in wood at a *microscopic* level (*23*).

The 2-D FT CSA NMR technique employed in this study addresses the issue of *molecular* orientation, as manifested over the entire *macroscopic* size of the sample, in the present case 0.9 cm^3. This technique does *not* provide information on the degree of molecular orientational order over a much smaller volume, say a few to several molecular volumes. Thus, it may be possible, or even likely, that lignin or cellulose macromolecules are highly ordered with respect to some preferred orientation over linear dimensions of, say, 100 Å in or near a specific fibril. And, in some other 10^6-$Å^3$ (volume) region in another part of the sample the same kind of molecular orientational order may exist, yet if the orientational characteristics for each of these 10^6-$Å^3$ regions are not highly correlated (mutually oriented in some preferred manner) among the different regions, then evidence for macroscopic molecular orientational order, as summed over a 0.9-cm^3 sample in the specific 2-D FT NMR experiments reported here, will not be manifested in the results. Hence, it may be true that a high degree of molecular orientational order exists for cellulose and lignin within each subdivision of the cell wall ultrastructure; but if that is the case, then the results reported here show that the microscopic orientational characteristics of the various subdivisions must be sufficiently randomized over a 0.9 cm^3 sample to yield a zero degree of molecular orientational order in the macroscopic NMR experiment. This situation would be analogous to the case of randomly oriented crystallites in a powder, in which the highly ordered structure within each crystallite is "averaged" by the random orientation of the crystallites with respect to each other.

The present 2-D FT NMR technique at its current level of natural-abundance sensitivity is not capable of examining the possible (likely?) existence of molecular orientational order over the individual ultrastructure components in *Eucalyptus polyanthemus* wood. A major improvement in the signal-to-noise ratio of the NMR experiment would permit one to examine the macroscopic molecular orientational order over a much smaller sample size than the 0.9 cm^3 of the present study. One way of working toward this goal is to enrich the ^{13}C concentration in the wood sample by employing ^{13}C-enriched CO_2 for the growing of the wood. Such experiments have been initiated.

CONCLUSIONS

The results of this paper demonstrate how the 2-D FT CSA technique allows one to study molecular orientational order of the various molecular components in a complex, inhomogeneous sample. The technique was applied to *Eucalyptus polyanthemus* wood, where it was determined that no net

molecular orientational order of lignin in cellulose exists over a macroscopic volume of about 0.9 cm^3. Work is currently under way to enable one to quantitate the type and degree of order present in similar systems.

ACKNOWLEDGMENT

The authors thank Joseph Reibenspies for the crystallographic work and Cyril Heitner, Pulp and Paper Research Institute of Canada, for providing the oriented cellulose samples.

Registry No. Lignin, 9005-53-2; cellulose, 9004-34-6; sucrose, 57-50-1; homovanillic alcohol, 2380-78-1.

LITERATURE CITED

(1) Hentschel, R.; Sillescu, H.; Spiess, H. W. *Polymer* **1981**, *22*, 1516.
(2) Maciel, G. E. *Science* **1984**, *226*, 282.
(3) Herzfeld, J.; Berger, A. E. *J. Chem. Phys.* **1980**, *73*, 602.
(4) Bax, A.; Szeverenyi, N. M.; Maciel, G. E. *J. Magn. Reson.* **1983**, *55*, 494.
(5) Mehring, M. *High Resolution NMR in Solids*; Springer: New York, 1983.
(6) Maciel, G. E.; Szeverenyi, N. M.; Sardashti, M. *J. Magn. Reson.* **1985**, *64*, 365.
(7) Preston, R. D. *The Molecular Architecture of Plant Cell Walls*; Wiley: New York, 1952.
(8) Fengel, D.; Wegener, G. *Wood: Chemistry, Ultrastructure, Reactions*; de Gruyter: Berlin, 1984.
(9) Atalla, R. H.; Agarwal, U. P. *Science* **1985**, *227*, 636.
(10) Pines, A.; Gibby, M. G.; Waugh, J. S. *J. Chem. Phys.* **1973**, *59*, 569.
(11) Schaefer, J.; Stejskal, E. O. *J. Am. Chem. Soc.* **1976**, *98*, 1031.
(12) Schaefer, J.; Stejskal, E. O. *Topics in Carbon-13 NMR Spectroscopy*; Levy, G. C., Ed.; Wiley: New York, 1979.
(13) Veeman, W. S. *Prog. Nucl. Magn. Reson. Spectrosc.* **1984**, *16*, 193.
(14) Browning, B. L. *The Chemistry of Wood*: Robert E. Krieger Publishing Co.: New York, 1975.
(15) Hatfield, G. R.; Maciel, G. E.; Erbatur, O.; Erbatur, G. *Anal. Chem.* **1987**, *59*, 172.
(16) Vanderhart, D. L.; Atalla, R. H. *Macromolecules* **1984**, *17*, 1465.
(17) Atalla, R. H.; Vanderhart, D. L. *Science* **1984**, *223*, 283.
(18) Dudley, R. L. *J. Am. Chem. Soc.* **1983**, *105*, 2469.
(19) Maciel, G. E.; Kolodziejski, W. L.; Bertran, M. S.; Dale, B. E. *Macromolecules* **1982**, *15*, 686.
(20) Cote, W. A. *Cellular Ultrastructure of Woody Plants*: Syracuse University Press: Syracuse, NY, 1965.
(21) Frey-Wyssling, A. *The Plant Cell Wall*; Borntraeger: Berlin, 1976.
(22) Kollmann, F. F. P., Cote, W. A. *Principles of Wood Science an Technology*; Springer-Verlag: New York, 1968; Vol. 1.
(23) Cote, W. A. *Wood Ultrastructure*; University of Washington Press: Seattle, WA, 1967.

RECEIVED for review December 8, 1986. Accepted March 3, 1987. The authors gratefully acknowledge partial support of this research by a grant from the Colorado State University Experimental Station. The Nicolet R3m/E diffractometer and computer system at Colorado State University were purchased with funds provided by NSF Grant CHE-8103011.

Use of the Microwave-Induced Nitrogen Discharge at Atmospheric Pressure as an Ion Source for Elemental Mass Spectrometry

Daniel A. Wilson,[1] George H. Vickers, and Gary M. Hieftje*

Department of Chemistry, Indiana University, Bloomington, Indiana 47405

A microwave-induced nitrogen discharge at atmospheric pressure (MINDAP) is used as the ion source for elemental mass spectrometry (MS) and compared to the use of the inductively coupled plasma (ICP). Optimization studies are presented to illustrate the dependence of signals on various instrumental parameters. Detection limits determined for five elements range from 3 to 22 ng/mL, somewhat higher than those determined with an ICP and the same mass spectrometer system. The background mass spectrum from the MINDAP is dominated by NO^+; oxide and hydroxide ion ratios are higher than for ICP-MS. The linear dynamic range is similar to that in ICP-MS, but interferences caused by concomitant elements are much worse in MINDAP-MS.

Since the introduction of inductively coupled plasma mass spectrometry (ICP-MS) (*1*), the technique has shown a great deal of potential for elemental analysis. Recent reviews (*2*, *3*) have described the advantages of ICP-MS, including a relatively simple mass-spectral background, the ability to perform isotope-ratio determinations, and sub-nanogram-per-milliliter detection limits for many elements.

[1] Present address: Alcoa Technical Center, Bldg C, Alcoa Center, PA 15069.

Although the ICP has been proven to be an attractive ion source for elemental mass spectrometry, it is important to investigate other types of plasmas as ion sources to assess whether further improvement in analytical characteristics is possible. Possible improvements that are desired include better sensitivity, greater freedom from interferences, ease of analytical use, lower operating and instrumental costs, and better precision. One type of discharge which has been used as an ion source is a microwave-induced plasma (MIP). In fact, the earliest work reported using continuum plasma sampling, the type most commonly used in ICP-MS at present, employed an argon MIP (*4*). This early work was later carried further and compared with ICP-MS (*5*). Detection limits in MIP-MS were about an order of magnitude lower than those from ICP-MS. However, matrix interferences were much more severe in the MIP than in the ICP, with the ICP being reported as matrix-free (*5*). More recent papers (*6*, *7*) on ICP-MS have revealed that matrix interferences are observed in that method also.

Work with a microwave plasma as the ion source for mass spectrometry continues (*8*). These recent studies coupled both argon and helium MIP ion sources with a mass spectrometer adapted from a commercial gas chromatograph–mass spectrometer system.

An alternative and attractive plasma which has been used for atomic emission studies is the microwave-induced nitrogen discharge at atmospheric pressure (MINDAP) (*9*, *10*). This

0003-2700/87/0359-1664$01.50/0 © 1987 American Chemical Society

plasma is similar to argon and helium MIPs but is supported in nitrogen (at a relatively high flow rate compared to many MIPs) and at forward powers of 200–250 W. Atomic emission detection limits for the MINDAP were comparable to those obtained for the ICP or argon MIP. In general, atomic emission lines provided better sensitivity than ion lines and for most elements were significantly more sensitive than those from atom lines in the ICP; ion lines, however, were much less sensitive than in the ICP. Ionization and vaporization interferences were noted in the MINDAP but could be eliminated by the use of Cs as an ionization suppressant (for an ionization interference) or a releasing agent such as EDTA to suppress refractory-complex formation (to eliminate a vaporization interference).

One of the most interesting features of the MINDAP from the standpoint of mass-spectral sampling is its generation of a long flamelike plume which extends several centimeters beyond the cavity and the torch. This tail flame permits sampling of gases and ions directly from a fairly hot portion of the plasma and thus provides less opportunity for ion recombination with ambient gases.

Results obtained by sampling ions from the MINDAP and separating them in a quadrupole mass spectrometer are presented. Analytical characteristics that were assessed include mass-spectral background, precision, detection limits, the degree of formation of oxide and hydroxide ions, and interference effects. The linear working range is more than 4 orders of magnitude and detection limits range from 3 to 22 ng/mL for five elements. Interferences are a much more important problem in MINDAP-MS than in ICP-MS.

EXPERIMENTAL SECTION

Instrument. *Plasma System.* The plasma instrumentation used here is similar to that described previously (*9*, *10*). The power supply for the microwave plasma (Model 420, Micro-Now Instrument Co., Chicago, IL) operates at 2450 MHz, with a maximum power level of 500 W. Tuning stubs (Model DS109, Weinschel Engineering) were used to match the impedance of the plasma and cavity to that of the generator. The resonant structure which is used for coupling the power into the plasma is a modified Beenakker-type TM_{010} cavity (*11*). This cavity has a depth (thickness) of 1 cm and is not cooled.

The torch used with the MINDAP, based on the ICP-torch design, consists of two concentric quartz tubes. The central tube has an inner diameter of 1 mm and an outer diameter of 2 mm and extends approximately halfway into the Beenakker cavity. The portion of the torch in the cavity is used as a secondary tuning device (*9*). The outer tube has a 4-mm i.d. and a 6-mm o.d. and extends slightly past the end of the cavity. The central gas flow is approximately 300 mL/min while the outer gas flow is about 3 L/min. The gas flow into the outer tube is introduced from a side arm oriented tangentially to the tube and produces a gas-flow pattern similar to that in the ICP. Sample aerosol is introduced through the central tube of the torch and into the center of the plasma, which is in turn suspended in the middle of the torch by the tangential plasma gas flow. The tail flame of the plasma extends about 4 cm beyond the end of the cavity and can be unsymmetrical if the quartz tubes are not concentric.

Even if the tail flame is not symmetrical, however, samples introduced into the plasma are observed both visually and mass spectrometrically to be concentrated in a small radial region of the discharge. Mass-spectral signals drop off by 90% within 0.25 mm of the optimum sampling position. This sampling position must be optimized each time the plasma is ignited; after a warmup period of approximately 30 min, the sample location within the plasma is stable. The plasma is then moved beneath the sampling orifice until the maximum analyte signal is obtained. Once the optimal position is determined, the same sampling location can be used continuously, until or unless the plasma has to be reignited.

Sample-Introduction System. Because the central gas flow is relatively low in a stable MINDAP, a glass-frit nebulizer of the type described by Layman and Lichte (*12*) was used in this study. This nebulizer is reported to produce a high efficiency and small droplet-size distribution even at low nebulizing gas flows.

The MINDAP is able to be sustained stably when aqueous aerosols are introduced into it. For the work performed here, however, a desolvation system was used to minimize the amount of water introduced into the plasma and to increase the stability of the plasma (*9*). The desolvation apparatus consists of a glass tube, 20 cm long by 2 cm diameter, wrapped with heating tape and followed by a 14 cm long condenser with a spiral condensing tube. The temperature of the heated tube was maintained at 120 °C by a Variac connected to the heating tape. The cooling water to the condenser was held at 5 °C by use of a recirculating cooler (Model CFT-33, Neslab, Newington, NH). This unit also provided cooling water for the mass spectrometer sampling-orifice plate and for the turbomolecular pumps.

Vacuum System and Mass Spectrometer. The vacuum system and mass spectrometer are the same as those used previously for ICP-MS (*13*). The two-stage interface between the atmospheric-pressure plasma and the low-pressure mass-spectrometer region is similar to that used in commercial ICP-MS systems. Beyond this interface, ions are directed by ion lenses into the third region of the vacuum system, in which the quadrupole mass spectrometer (Model QMG 511, Balzers, Hudson, NH) is located. The discrete-dynode secondary electron multiplier used for detection of the ions is located off-axis from the mass spectrometer and is used in the ion-counting mode for this work.

Procedures. *Plasma Background Scans.* Distilled, deionized water was used as the blank for mass-spectral scans of the plasma background. Plasma conditions were optimized for detection of an analyte (barium) before the scans were begun. The resolution of the mass spectrometer was increased slightly over the unit-mass setting routinely used for single-ion monitoring in order to provide better separation of adjacent mass peaks. The resolution setting on the QMG 511 was 52 for the scans compared to 46 usually used for single-ion monitoring studies. Scans were taken at the rate of 30 s/Da.

Detection Limits. Detection limits were determined from signal-to-noise (S/N) ratios obtained for solutions over a concentration range within 1–2 orders of magnitude of the detection limit. For this purpose, S/N is defined as the background-corrected signal divided by the standard deviation of the background noise, here approximated by one-fifth of the peak-to-peak noise on the blank trace (*14*). Linear regression was used to obtain an equation for S/N vs. concentration, from which the detection limit was obtained at $S/N = 3$.

Examination of Ionization Effects. For determination of the effect of atomic ionization potential on elemental signals, 1×10^{-3} M of each element was introduced into the plasma, by means of a simple flow-injection system. Elements were chosen to provide a fairly wide range of ionization potentials. For each element, the plasma and mass spectrometer were optimized for analyte signal on its most abundant isotope. Distilled deionized water was then used as the flow-injection mobile phase while at least five replicate injections of the sample were made through a four-way valve with an 85-μL injection loop. Signals for the injections were a factor of about 3 lower than for continuous sample introduction, and relative standard deviations for the groups of injections were in the range 3–9%. Signals obtained for each element were corrected for the isotopic abundance of the isotope used, but no correction was made for mass bias. The mass bias curve for this instrument, published elsewhere (*15*), is fairly flat in the middle of the mass range, so elements from about 50 to 150 Da were used for the comparison.

Oxide/Atomic Ion Ratios. To measure oxide/singly charged ion ratios, the instrument was first optimized for determination of the major isotope of the singly charged analyte ion. Signals were determined for that isotope, adjacent lesser-abundance isotopes, and the oxide and hydroxide of the most abundant isotope. From these signals and literature values of the natural abundances, it was possible to calculate oxide and hydroxide ratios corrected for interferences by oxides and hydroxides of the other isotopes.

Interferences. The analyte species used for interference studies was calcium. Sodium, lead, and uranium at molar concentration ratios of 1000:1 Ca were studied for the effects of an easily ionized element and of a heavy concomitant element. The vaporization

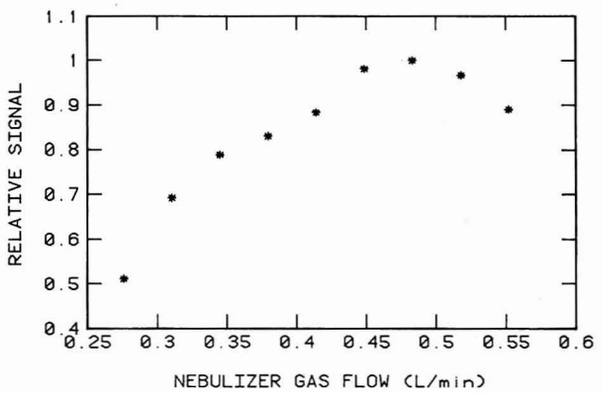

Figure 1. Effect of nebulizer gas flow on Ba^+ signal: applied rf power, 220 W; extraction voltage, −6 V; bias voltage, 2 V. All other conditions are listed in Table I.

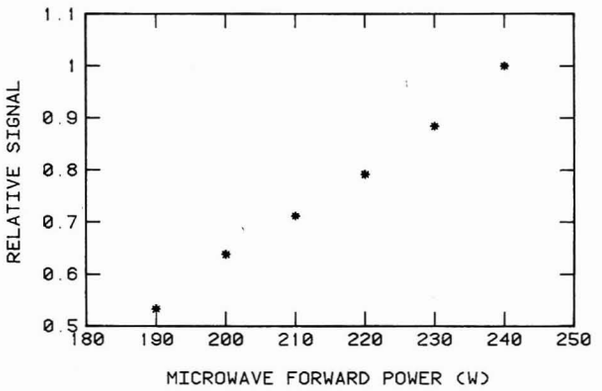

Figure 2. Effect of microwave foward power on Ba^+ signal: nebulizer flow, 0.48 L/min; extraction voltage, −6 V; bias voltage, 2 V. All other conditions are given in Table I.

interference of phosphate on calcium was studied at a 5:1 molar ratio. The solutions of elements being used as interferents were checked on the instrument for the presence of calcium, which was not found at levels which would be significant in this study.

Because fairly high concentrations of interferents were present, the flow-injection system was used in order to minimize washout time and solids deposition on the mass-spectrometer sampling orifice. The instrument was optimized for determination of calcium at 40 Da before the interferent solutions were run. Each injection of an interferent-containing solution was bracketed by two injections of a solution containing only calcium. The ratio of the signal for the interferent solution to the average of the calcium signals was calculated and four such replicates were averaged. This procedure corrects for instrumental drift.

RESULTS AND DISCUSSION

Instrument Optimization. Studies were performed to determine the sensitivity of the instrument to four operating parameters: central (nebulizer) gas flow, forward plasma power, and two ion-lens potentials, termed extraction voltage and bias voltage. Other parameters such as sampling height, outer gas flow, and other ion-optic potentials were held constant. Sampling height was found not to have a large effect on the determined signal over a small distance range and changes in the nebulizer-gas flow could recover signal losses caused by height adjustments. Similar effects have been reported for ICP-MS (*16*). Outer gas flow cannot be altered a great deal in the MINDAP without causing the plasma to become asymmetric and producing damage to the torch; over the small permissible range of outer flows, ion signals are influenced only slightly. Small changes in ion-lens potentials (other than the bias or extraction voltages) were found also to have little effect on signal levels.

Figure 1 shows the effect of nebulizer gas flow on the signal from a 5 μg/mL solution of barium. A convenient region where small changes in gas flow do not greatly affect the signal extends from about 0.45 to 0.52 L/min. The highest flow rate explored, 0.55 L/min, produced a 10% decrease in signal below the peak at 0.48 L/min; at higher flow rates, the plasma became unstable and contacted the walls of the torch. The exact position of the optimum nebulizer flow rate varies with each plasma ignition and needs to be optimized somewhat for each element. However, the shape of the curve is consistent regardless of the exact position of the peak.

The shape of the optimization curve for the MINDAP nebulizer gas is less sharply peaked than that seen in ICP-MS, both on the present instrument (*17*, *18*) and on a commercial system (*16*). This difference is probably due in large part to the fact that the efficiency of the glass-frit nebulizer is not as sensitive to gas flow as is the concentric pneumatic nebulizer often used for ICP-MS. In ICP-MS, the nebulizer gas flow can strongly affect both the nebulizer and the sampling conditions, possibly necessitating a compromise value for the flow.

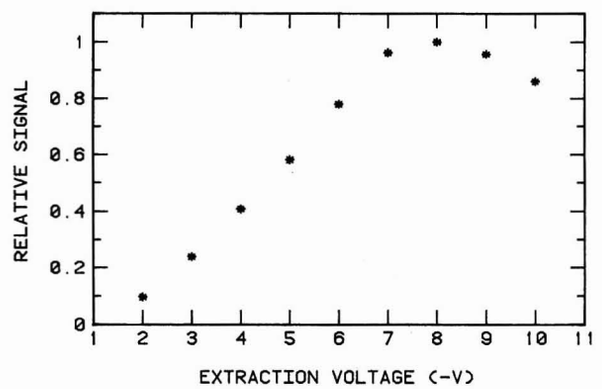

Figure 3. Effect of mass-spectrometer extraction voltage on Ba^+ signal: nebulizer flow, 0.48 L/min; power, 220 W; bias voltage, 2 V. All other conditions are listed in Table I.

A fairly linear increase in signal with microwave power is seen in Figure 2, indicating that it would be desirable to employ as high a power as possible. However, at the highest power levels shown in Figure 2, the signal became noisy because of generator instabilities; power changes monitored on the forward power meter of the generator were then approximately ±10 W. A second limitation is that the resonant cavity, tuning stubs, and microwave-coupling cable can become quite warm at applied power levels above about 220 W. Although the cavity and tuning stubs could be cooled, that approach is somewhat inconvenient and has not been taken with the current system. The power level was therefore limited to 220 W for the work reported below.

The "extraction voltage" represents the potential applied to a ring ion optic located behind the skimmer in the second chamber (10^{-3} torr) of the vacuum system. It is used to extract ions from the gases entering the vacuum chamber and to focus them through a 1-mm orifice into the third chamber (10^{-6} torr) of the vacuum system. The effect of changes in this voltage on the measured Ba^+ ion signal is shown in Figure 3. The shape of this curve is similar to that observed with an ICP as the ion source, although the optimum voltage is substantially lower here (by at least 10 V). The reason for the lower optimal extraction voltage is unclear at this time but might be related to ion energies. The signal in MINDAP-MS is slightly more sensitive to small changes in the extraction voltage, because of the lower potentials involved; similar percentage changes in the potential cause approximately the same signal variation, however.

On the present plasma-source mass spectrometer system, the bias voltage is used to match the potential of the mass spectrometer system to that imparted to the ions by the plasma; the mass spectrometer voltages all float on top of the bias potential. For optimal and representative sampling of

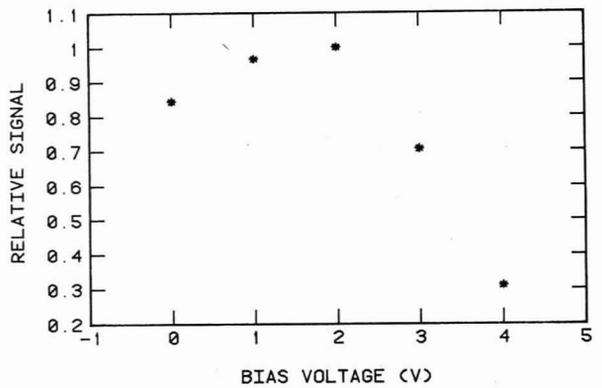

Figure 4. Effect of mass-spectrometer bias voltage on Ba^+ signal: negulizer flow, 0.48 L/min; power, 220 W; extraction voltage, −6 V. All other conditions are listed in Table I.

Table I. Operating Conditions Used for MINDAP-MS

forward microwave power	220 W
reflected microwave power	<10 W
outer gas flow	3 L/min
central (nebulizer) gas flow[a]	200–400 mL/min
sample uptake rate	0.8 mL/min
sampling height above top of cavity	5 mm
bias voltage[a]	0–3 V
extraction voltage[a]	−5 to −8 V

[a] Values optimized independently for each element.

Table II. Background Ions Observed in MINDAP-MS

mass	tentative ID	mass	tentative ID
1	H^+	31	NOH^+
14	N^+	32	O_2^+
16	O^+	40	Ar^+
17	OH^+	42	N_3^+?
18	H_2O^+	45	N_2OH^+?
19	H_3O^+	56	N_4^+?
23	Na^+	58	N_3O^+?
28	N_2^+	60	$N_2O_2^+$?
29	N_2H^+		
30	NO^+		

ions from any plasma, the extraction orifice that leads directly to the mass spectrometer should be adjusted as closely as possible to the plasma potential. In the Balzers PAM 150 plasma-sampling monitor, on which the new system is based, this capability is provided by having the entire orifice/ion optical/mass spectrometer system float on top of an adjustable "bias potential". The utility of this approach will be addressed more fully in a future communication. In ICP-MS, the optimized bias potential is approximately 20 V, in agreement with ion potentials determined on systems with the load coil grounded near the end (*19*). Figure 4 shows the influence of bias voltage on Ba^+ signals from the MINDAP. For all elements, the optimal bias potential here is much lower than in ICP-MS, and lies between 1 and 2 V. This difference would indicate that the microwave plasma has a much lower potential than does the ICP, probably because of the way the power is coupled into the plasma, the lower power levels that are employed, and the higher frequencies involved. The shape of the bias-voltage optimization curve is, however, similar to that found in ICP-MS (*18*).

From the above studies and curves such as those in Figures 1–4, operating conditions were determined for the MINDAP-MS instrument (Table I). Those conditions listed with ranges were optimized daily and for each element studied. Importantly, compromise operating conditions can be chosen that would reduce sensitivity not more than 10% for any element.

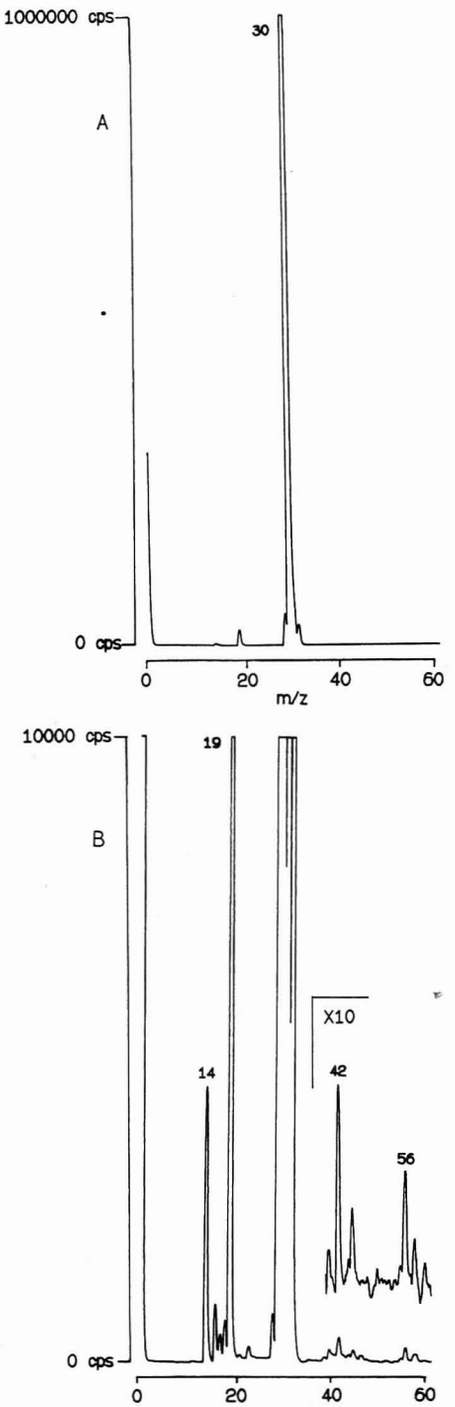

Figure 5. Background spectra for MINDAP-MS. Sample is distilled deionized water. (A) Full scale = 10^6 counts/s. (B) Full scale = 10^4 counts/s; insert is 10 times more sensitive. Conditions are as listed in Table I, optimized for barium.

Background Studies. Background count rates at masses where there is no ion present are about 5–15 counts/s in MINDAP-MS, somewhat lower than the background noted in ICP-MS (*18*). This difference is believed to be due to the relative absence of high-energy photons that reach the detector; such photon noise from either the plasma or a discharge in the vacuum system constitutes the dominant base-line background in the ICP (*13*).

Figure 5 shows a mass spectrum obtained when distilled deionized water was introduced into the MINDAP at three different detection sensitivities. By far the largest background-ion signal in the plasma is from NO^+ at 30 Da, which is about 100 times the magnitude of the next most concentrated ion (N_2H^+ at 29 Da). Other observed ions and their

Table III. Detection Limits Measured in MINDAP-MS

element	isotope	ionization energy, eV	detection limit, ng/mL
barium	138	5.21	11
cobalt	59	7.86	10
calcium	40	6.11	22
cadmium	114	8.99	18
strontium	88	5.69	3

tentative assignments are listed in Table II. No background ions were observed above 60 Da.

Most of the ions observed are from gas species present in the plasma, introduced as water, or entrained into the MINDAP. The high concentration of NO^+ is interesting. This ion has been observed in boundary-layer sampling of argon ICPs (*1*) and in previous work involving argon MIPs (*4*), so it is not particularly surprising to observe it from a nitrogen plasma. The source of the oxygen that is responsible for this large signal is unclear at this time, however. Our first assumption, that the oxygen was entrained into the plasma from the surrounding atmosphere, was checked by shielding the plasma with a quartz "bonnet". A short piece of 2.5-cm-diameter quartz tubing was placed on the Beenakker cavity, with about 2 mm separating the top of this tube and the plate containing the sampling orifice. This modification caused no discernible reduction in the signal at 30 Da; flushing the space between the orifice and the cavity with nitrogen or argon also produced no change. Turning off the peristaltic pump to stop the introduction of water into the nebulizer did not reduce the peak either. It is possible that there is enough oxygen impurity in the dry nitrogen supply to cause the NO^+ signal; alternatively, the methods used to shield the plasma from entrainment of oxygen might not have been effective or enough water was introduced from the still-wet spray chamber to yield oxygen measured in the stable NO^+ signal. Further attempts to eliminate or minimize this background signal are warranted.

Except for NO^+, the background ions in MINDAP-MS are lower in magnitude than those in ICP-MS. They also do not extend as high into the mass range, so a larger background-free region is available than in ICP-MS.

Precision. The short-term precision obtained for analyte signals on the MINDAP-MS system was about 5% relative standard deviation, somewhat better than that observed on the same instrument in the ICP-MS configuration. Much of the improvement in precision is probably due to the glass-frit nebulizer, which is more stable than the concentric pneumatic nebulizer ordinarily employed with an ICP.

Long-term drift on the instrument was similar to that observed in ICP-MS, about 10–15% over a 2-h period.

Detection Limits. Detection limits for five elements in MINDAP-MS are listed in Table III. These values are slightly (less than an order of magnitude) higher than those previously determined for ICP-MS on the same mass-spectrometer system (*13*). The two higher detection limits can be explained in part. For calcium, there is a small background peak at 40 Da (cf. Figure 5) which limits somewhat the detectability. This isotope of calcium is not used in ICP-MS because of the large $^{40}Ar^+$ signal. For cadmium, the most abundant isotope is present at only 28.86%, so its detection limit is understandably poorer than those of elements with higher-abundance principal isotopes.

Improvements in the instrumental system, including the use of higher and more stable plasma power levels, would be expected to produce detection limits similar to those determined on the ICP-MS system. At present, the sensitivity for MINDAP-MS is about 10^4 counts/(s ppm) for most elements, a factor of approximately 10 lower than that observed on this system for ICP-MS (*18*).

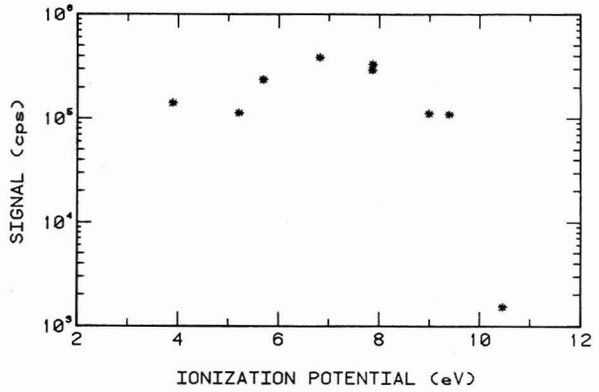

Figure 6. Response of 10^{-3} M solutions of various elements as a function of ionization potential. Values are corrected for isotopic abundance. Conditions are as listed in Table I, optimized for each element.

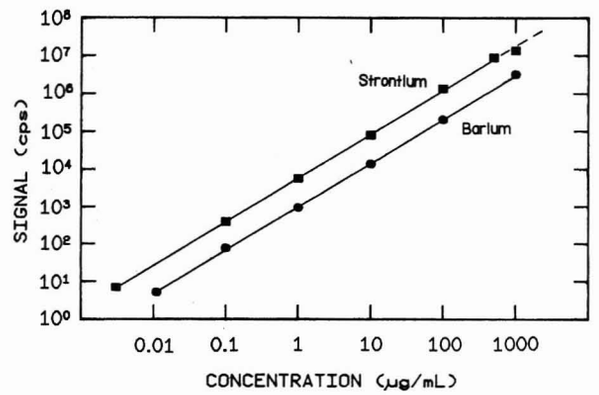

Figure 7. Analytical curves determined for strontium and barium. Lowest point on the curves is the detection limit for that element. Conditions are listed in Table I, optimized for each element.

One reason for the lower sensitivity of MINDAP-MS might be the high concentration of NO^+ that it produces. Previous work with an argon MIP as an ion source (*4*, *5*) showed decreased sensitivity for elements with ionization potentials close to or greater than that of NO^+ (9.27 eV). To gauge the effect of charge exchange with this abundant background ion in MINDAP-MS, signals for 10^{-3} M solutions of various elements were plotted vs. the respective ionization potential (see Figure 6). Although there is obviously some scatter in the data for elements with low ionization potentials, there is no significant drop in signal for elements below 9 eV. Both Cd (8.991 eV) and Zn (9.391 eV) are at the lower end of the sensitivity range observed for the other elements, but the signal for I (10.454 eV) is far below that of the other elements.

A similar drop in sensitivity was observed between Pb (7.415) and Au (9.22 eV). However, these points are not plotted on Figure 6 because they are both at the high end of the mass range where significant mass bias exists in our mass spectrometer (*15*). No correction for mass bias was applied here because it cannot be assured that the mass bias would be the same for both the ICP and MINDAP ion sources.

Analytical Curves. Analytical curves for strontium and barium are plotted in Figure 7. The linear portion of each curve extends from the detection limit to between 500 and 1000 μg/mL, although there is a slight roll-off above that level.

On the log–log plots shown in Figure 7, the slope for the lines drawn is 1.18, indicating that there is a larger increase in signal than there is in concentration. The reason for this larger-than-expected increase is unclear at this time. log–log calibration plots with slopes up to 1.5 have been reported for atomic emission from a microwave-induced plasma (*20*).

The linear range on the MINDAP-MS system appears to extend somewhat further toward high concentrations than has

Table IV. Oxide and Hydroxide Ratios in MINDAP-MS

element	MO^+/M^+	MOH^+/M^+
barium	0.48	4.4
strontium	0.062	0.73
cerium	150	0.60
molybdenum	0.076	0.094
zirconium	20	0.030
uranium	150	0.25

Table V. Interferences Observed in MINDAP-MS

sample	relative signal	% RSD
Ca	1.00	20.98
1 Ca:1000 Na	2.02	12.58
1 Ca:1000 Pb	1.92	19.90
1 Ca:1000 U	1.31	32.19
1 Ca:5 PO_4	0.212	37.94

been observed in ICP-MS (*13*). The difference in the location of the roll-off is probably determined by the absolute count rates, which have been observed to be a factor of approximately 10 lower from the MINDAP than from the ICP.

Oxide and Hydroxide Levels. The oxide and hydroxide ratios determined for six different elements are listed in Table IV. For Ce and U there is more oxide present than analyte; zirconium also produces a high oxide ratio. The other three elements in Table IV have oxide ratios below 1%. Three elements, Ba, Sr, and Mo, have larger hydroxide ion ratios than oxide, with barium being quite significant at more than 4%.

The oxide and hydroxide levels observed in MINDAP-MS are substantially higher than those in ICP-MS, which are well below 1% for all elements (0.26% for CeO^+/Ce^+, for example) (*15*). The larger ratios here are believed to be due partly to the lower temperature of the MINDAP than the ICP; oxides formed during the desolvation and vaporization process are not completely decomposed. Also, there is probably more air entrained into the MINDAP and into the sampling orifice because of the small size of the plasma and the low plasma-gas flow rates. This situation possibly leads to formation of oxides and hydroxides during the sampling process. Use of the quartz bonnet, however, did not significantly change the oxide and hydroxide ratios observed for barium. Finally, there is no evidence of a discharge in the vacuum chamber as there is in the ICP-MS system (*15*), so that oxides would not be dissociated by the additional discharge.

Doubly charged ions have not been observed for barium, which has the lowest second ionization potential for all elements. This observation is further evidence for the absence of an orifice discharge; some doubly charged ion formation would be expected from the discharge. The doubly charged ion ratio for barium measured in ICP-MS is greater than 10% (*15*).

Interferences. Interferences observed in MINDAP-MS are listed in Table V. Sodium and lead present at 1000:1 molar excess cause the signal from calcium to nearly double, whereas uranium causes a smaller increase. Phosphate, as would be expected from the common vaporization interference observed in flames and in the MINDAP before (*10*), causes a decrease of about 80% in the calcium signal when it is present at a 5:1 molar ratio to calcium. The large relative standard deviations (RSD) observed in all of the data are due to the relatively low Ca signal at a concentration of 5×10^{-6} M and to the presence of relatively high concentrations of interferents. These high concentrations possibly cause nebulizer instabilities. Also, the RSD shown for the calcium signal was taken over a period of several hours and indicates the drift present in the instrument. Signals for each interferent injection were ratioed to the adjacent calcium signals to correct partially for signal drift.

The reason for the increases caused by concomitant elements is unclear. A similar interference of sodium on Ca was observed in the MINDAP by emission, particularly when the sample was introduced into the center of the plasma instead of into the outer gas flow (*21*). One possibility is that a high concentration of any element with a reasonably low ionization potential greatly increases the electron number density in the MINDAP. These added electrons then alter the ionizing characteristics of the plasma by changing energy coupling or modifying the efficiency of electron impact.

CONCLUSIONS

The MINDAP provides a promising alternative to the ICP as an ion source for elemental mass spectrometry. Detection limits are currently somewhat worse with the MINDAP, but further work might make the two sources comparable. The background from the MINDAP is somewhat more simple, although the high concentration of NO^+ ions in the plasma might limit sensitivity for elements with high ionization energies. Precision is somewhat better with the MINDAP but is at least in part nebulizer-dependent. Oxide and hydroxide interferences are larger with the MINDAP, although doubly charged ions are not present. Interferences are significantly worse with the MINDAP ion source than with the ICP, but the same interferences are observed with atomic-emission studies with the MINDAP and can be eliminated through use of releasing agents or ionization suppressants.

One major advantage of the MINDAP is its simplicity and low cost. Although such economy might be dwarfed by the cost of a mass spectrometer, the MINDAP offers a simpler, more compact system that requires less frequent changing of gas supplies, a smaller, lower-power-consumption generator, and a resonant cavity/tuning-stub arrangement which is much smaller than a torch housing/impedance-matching box combination such as used in ICP-MS.

Some of the major areas in which improvement could be made in the MINDAP-MS system include minimization of NO^+ in the background spectrum and changes to the plasma itself. The decrease in background at 30 Da that would result from a reduction of NO^+ would be accompanied by an increase in N^+ signals. However, the N^+ peaks do not exhibit significant spectral interferences. In addition, lowering of NO^+ in the MINDAP would likely yield an increase in ionization of elements with ionization potentials above that of NO (9.27 eV). In turn, sensitivity for those elements would be improved.

Improvements in the MINDAP system should increase the utility of the MINDAP-MS combination. One desirable change is stabilization of the microwave generator at higher power levels. Also useful might be cooling of the resonant cavity and tuning stubs to minimize heat buildup, so higher foward-power levels can be employed.

ACKNOWLEDGMENT

The authors wish to thank the Perkin-Elmer Corporation for providing the plasma-sampling mass-spectrometer system used in this study and to Karl Höfler for most of its design.

LITERATURE CITED

(1) Houk, R. S.; Fassel, V. A.; Flesch, G. D.; Svec, H. J.; Gray, A. L.; Taylor, C. E. *Anal. Chem.* **1980**, *52*, 2283.
(2) Douglas, D. J.; Houk, R. S. *Prog. Anal. Atom. Spectrosc.* **1985**, *8*, 1.
(3) Houk, R. S. *Anal. Chem.* **1986**, *58*, 97A.
(4) Douglas, D. J.; French, J. B. *Anal. Chem.* **1981**, *53*, 37.
(5) Douglas, D. J.; Quan, E. S. K.; Smith, R. G. *Spectrochim. Acta, Part B* **1983**, *38B*, 39.
(6) Olivares, J. A.; Houk, R. S. *Anal. Chem.* **1986**, *58*, 20.
(7) Gregoire, D. C. Presented at the Federation of Analytical Chemistry and Spectroscopy Societies Meeting, St. Louis, MO, Sept 1986; paper 192.
(8) Satzger, R. D.; Fricke, F. L.; Caruso, J. A.; Brown, P. G. Presented at the Federation of Analytical Chemistry and Spectroscopy Societies

Meeting, St. Louis, MO, Sept 1986; paper 195.
(9) Deutsch, R. D.; Hieftje, G. M. *Appl. Spectrosc.* **1985**, *39*, 214.
(10) Deutsch, R. D.; Keilsohn, J. P.; Hieftje, G. M. *Appl. Spectrosc.* **1985**, *39*, 531.
(11) Beenakker, C. I. M. *Spectrochim. Acta, Part B* **1976**, *31B*, 483.
(12) Layman, L. R.; Lichte, F. E. *Anal. Chem.* **1982**, *54*, 638.
(13) Wilson, D. A.; Vickers, G. H.; Hieftje, G. M.; Zander, A. T. *Spectrochim. Acta, Part B* **1987**, *42B*, 29.
(14) Hieftje, G. M. *Anal. Chem.* **1972**, *44*(6), 81A.
(15) Wilson, D. A.; Vickers, G. H.; Hieftje, G. M., submitted for publication in *J. Anal. Atom. Spectrosc.*
(16) Horlick, G.; Tan, S. H.; Vaughan, M. A.; Rose, C. A. *Spectrochim. Acta, Part B* **1985**, *40B*, 1555.
(17) Vickers, G. H.; Wilson, D. A.; Hieftje, G. M.; Zander, A. T. Presented at the 34th Annual Conference on Mass Spectrometry and Allied Topics, Cincinnati, OH, June 1986; paper MPD6.
(18) Wilson, D. A. Ph.D. Dissertation, Indiana University, 1987.
(19) Douglas, D. J.; French, J. B. *Spectrochim. Acta, Part B* **1986**, *41B*, 197.
(20) Matousek, J. P.; Orr, B. J.; Selby, M. *Talanta* **1986**, *33*, 875.
(21) Wilson, D. A.; Hieftje, G. M. Presented at the Pittsburgh Conference on Analytical Chemistry and Applied Spectroscopy, New Orleans, LA, Feb 1985; paper 1167.

RECEIVED for review January 5, 1987. Accepted March 3, 1987. Supported in part by the National Science Foundation through Grant CHE 83-20053, the Office of Naval Research, The Upjohn Company, and American Cyanamid.

Collision-Activated Dissociation of Negative Ions in an Ion Trap Mass Spectrometer

Scott A. McLuckey* and Gary L. Glish

Analytical Chemistry Division, Oak Ridge National Laboratory, Oak Ridge, Tennessee 37831

Paul E. Kelley

Finnigan-MAT Corporation, 355 River Oaks Parkway, San Jose, California 95134

Polyatomic anions derived from several dinitrotoluene isomers, 2,4,6-trinitrotoluene, and 1,3,5-trinitro-1,3,5-triazacyclohexane have been formed by use of negative ion chemical ionization and trapped in an ion trap mass spectrometer. Mass spectrometry/mass spectrometry daughter ion spectra were obtained for most of these ions. In most cases, the parent anions were converted very efficiently to daughter ions (>10%), but for the $(M - H^{\cdot})^{-}$ ions the efficiencies were relatively low. Conversion efficiencies were observed to differ by as much as 2 orders of magnitude between anions. The major cause for these differences is attributable to differences in the propensity for collisional electron detachment vs. that for collision-activated dissociation.

The performance characteristics of the ion trap or three-dimensional quadrupole (*1–4*) have been dramatically improved in recent years with the development of the mass selective instability mode of mass analysis and the use of a light background gas (usually helium) at a pressure of ≈1 mtorr (*4*, *5*). It has been found that collisions with the background gas tend to reduce large amplitude motions of the ions in the ion trap (*6*, *7*). The net effect of the background gas is to concentrate the ions in the center of the trap, thereby enhancing mass resolution and sensitivity. These developments have resulted in the recent commercial introduction of an ion trap as a detector for gas chromatography (*8*) and has generated interest in other possible uses of the ion trap as an analytical tool. Recently, for example, it has been demonstrated that two or more stages of mass spectrometry can be performed in a single ion trap (*9*) making available the technique of mass spectrometry/mass spectrometry (MS/MS) (*10*, *11*). Most analytical applications of MS/MS use the technique of collision-activated dissociation (CAD) between stages of mass analysis in order to identify a mass-selected ion. CAD of positive ions has been demonstrated in an ion trap (*9*, *12*) where an ac voltage (the frequency of which is tuned to excite only one m/z ratio) with an amplitude of a few hundred millivolts is applied to the end caps of the trap for a few tens of milliseconds. CAD can then result from collisions between the translationally excited ions and the background gas. The two major objectives of this study were to form polyatomic *anions* in an ion trap and to determine the facility with which these ions undergo CAD using the conditions under which the ion trap is currently being operated for MS/MS.

Although the widespread use of negative ions in analytical mass spectrometry is relatively recent, the high sensitivity and specificity obtained for the analysis of some compounds in the negative ion mode relative to the positive ion mode has been amply demonstrated (*13*). In an ion trap both positive and negative ions can be trapped simultaneously under conditions in which both ion polarities are formed (*14*). With trapping times on the order of tens to hundreds of milliseconds, it is conceivable that positive ion–negative ion recombination could reduce sensitivity for a compound ionized in an ion trap. The only negative ions reported to have been trapped in a three-dimensional quadrupole are I^- (*15*) and Cl^- (*14*). These ions were formed by photodissociation of thallium iodide and 50-eV electron impact of dichloromethane, respectively. It has recently been demonstrated that positive ion chemical ionization could be readily performed in an ion trap using an appropriate pulse sequence (*16*, *17*). We therefore chose to investigate the possibility of using negative ion chemical ionization (NICI) in an ion trap with molecules known to form very stable negative ions. We studied *p*-dinitrobenzene, 2,4-dinitrotoluene (DNT), 2,6-dinitrotoluene, 3,4-dinitrotoluene, 2,4,6-trinitrotoluene (TNT), and 1,3,5-trinitro-1,3,5-triazacyclohexane (RDX). As a further test of the applicability of the ion trap to the study of negative ions we also studied the CAD of anions derived from these compounds.

EXPERIMENTAL SECTION

All experiments were carried out with a Finnigan-MAT ITMS research ion trap (shown schematically in Figure 1) equipped with a DeTech Model 300 conversion dynode/electron multiplier detector (*18*). Helium was used as a background gas at a pressure of ≈1 mtorr. Samples were admitted via a solids probe and for most chemical ionization experiments water was admitted into the vacuum system to a pressure of $\approx 2 \times 10^{-5}$ torr through a separate valve. NICI MS/MS spectra were obtained by using

0003-2700/87/0359-1670$01.50/0 © 1987 American Chemical Society

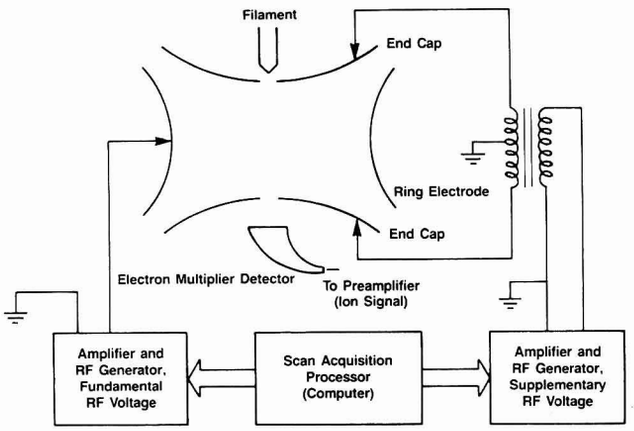

Figure 1. Schematic diagram of the Finnigan-MAT ITMS research ion trap configured for MS/MS operation.

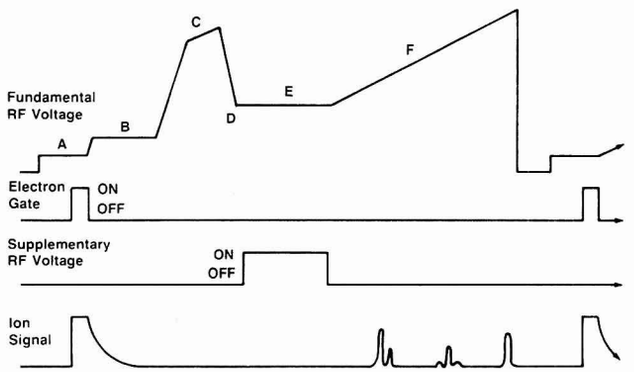

Figure 2. Pulse sequence employed for MS/MS analysis (daughter ion scan) of ions formed via chemical ionization in the ion trap: (A) ionize and store CI reagent ions; (B) CI reagent ions react with neutral sample molecules and form sample ions; (C) select parent (remove all m/z below parent m/z); (D) select mass range for daughter spectrum; (E) CAD parent and store daughters; (F) scan resultant mass spectrum.

the following pulse sequence (*16*) (shown in Figure 2): electrons from a filament above one of the end caps were gated into the trap through a hole in the end cap for ≈13 ms. The rf voltage applied to the ring electrode was adjusted to a suitably low level (≈100 V p-p) such that during this period the relatively low mass reagent ions were stored efficiently. Next, the electrons were gated off and a 100-ms reaction period followed where the rf voltage applied to the ring electrode of the trap was set (≈160 V p-p) to trap both reagent ions and any higher mass ions which may be produced via ion/molecule reactions. MS/MS data were then acquired following NICI by scanning the rf voltage up to the parent ion of interest (thereby eliminating all m/z values lower than that of the parent ion) and returning the voltage to a low m/z cutoff of ≈40 and applying an ac voltage of ≈200 mV to the end caps at a frequency corresponding to the frequency of motion of the parent ion in the direction between the end caps (*9*) (thereby translationally exciting the parent ion in the direction between the end caps) for a period of ≈10 ms. Following this reaction period, the rf voltage was then quickly scanned up at a rate of 5.5×10^3 Da/s. As the rf voltage is increased, progressively higher masses lose their stable trajectories in the direction between the end caps. A hole is situated in the end cap opposite the filament where ions can pass out of the trap and be drawn into the conversion dynode or multiplier. NICI mass spectra were obtained by using the same scan function with the elimination of those steps only required for MS/MS. Between 10 and 20 scans were accumulated and averaged. For the detection of negative ions a conversion dynode voltage of +5 kV was used with −2 kV applied to the front of the multiplier.

In this method only the ions of m/z less than that of the parent are eliminated from the trap prior to the ac excitation voltage applied to the end caps. Only the parent ion of interest, however, is translationally excited so that the ions which are observed at lower mass come primarily from the ion of interest. (Though not employed here, a newer technique has been developed to allow for the selection of only one nominal m/z value (*16*).) Under the conditions used here ions undergo multiple collisions with the background gas. The energy of the collisions depends upon the amplitude of the rf voltage applied to the ring electrode, the amplitude of the ac voltage applied to the end caps, and the duration of the applied ac voltage. The effects of these parameters on the MS/MS spectra obtained with an ion trap have been discussed (*19*).

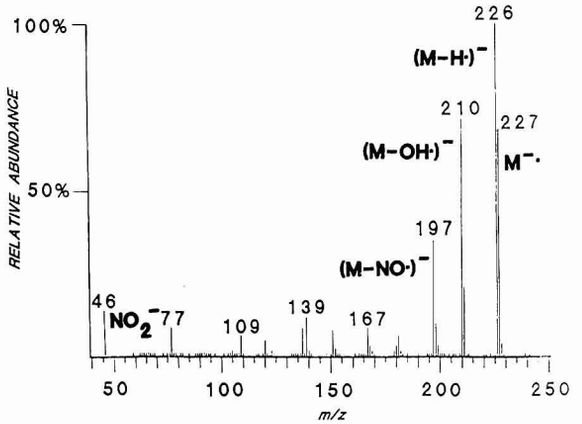

Figure 3. NICI mass spectrum of TNT.

Table I. Negative Ion H_2O Chemical Ionization Mass Spectra of Three Dinitrotoluene (DNT) Isomers Listing All Ions >5% of the Base Peak

		% base peak		
m/z	ion	2,4-DNT	3,4-DNT	2,6-DNT
182	$M^{\bullet -}$	27	27	46
181	$(M - H^{\bullet})^-$	100	32	32
165	$(M - OH^{\bullet})^-$	28		7
152	$(M - NO^{\bullet})^-$	50	100	100
137		9		5
122	$(M - 2NO^{\bullet})^-$			11
46	NO_2^-	26	27	26

RESULTS AND DISCUSSION

NICI Mass Spectra. Negative reagent ions OH^- and $O^{\bullet -}$ were readily formed under the conditions described above with $(OH^-)/(O^{-\bullet}) \approx 3$ and with no other reagent ions greater than 5% of the intensity of OH^-. Figure 3 shows the mass spectrum observed for TNT obtained with water as the reagent gas. The base peak in the spectrum (m/z 226) corresponds to $(M - H^{\bullet})^-$ formed primarily by proton abstraction by OH^-. The gas phase acidity of water is 16.9 eV and that of TNT is 14.2 eV (*20*). A relatively intense peak is also observed at m/z 227 indicating that the molecular anion is also formed. Electron transfer from the reagent ions and electron capture can both give this ion. The electron affinities of $OH^{\bullet}$ and O are 1.8 and 1.5 eV, respectively. The electron affinity of TNT has not been measured but is expected to be a few tenths of an electronvolt less than the 2.6-eV electron affinity of trinitrobenzene. When the water inlet was closed the total ion abundance observed decreased to roughly half of that observed in Figure 3 and the abundance of $(M - H^{\bullet})^-$ decreased relative to most of the other ions in the spectrum including $M^{\bullet -}$. The intense ions at m/z 210, 197, 181, 167, 151, and 139 can be attributed to fragmentations of $M^{\bullet -}$ (see below).

Table I lists the relative abundances of the major ions in the mass spectra of 2,4-DNT, 3,4-DNT, and 2,6-DNT. The isomers are readily distinguishable based on the relative abundances of $M^{\bullet -}$, $(M - H^{\bullet})^-$, $(M - OH^{\bullet})^-$, and $(M - NO^{\bullet})^-$. The 2,4-DNT isomer is most clearly distinguishable from the other two isomers in that $(M - H^{\bullet})^-$ is the base peak in the mass spectrum. Also, $(M - OH^{\bullet})^-$ and $(M - NO^{\bullet})^-$ are more

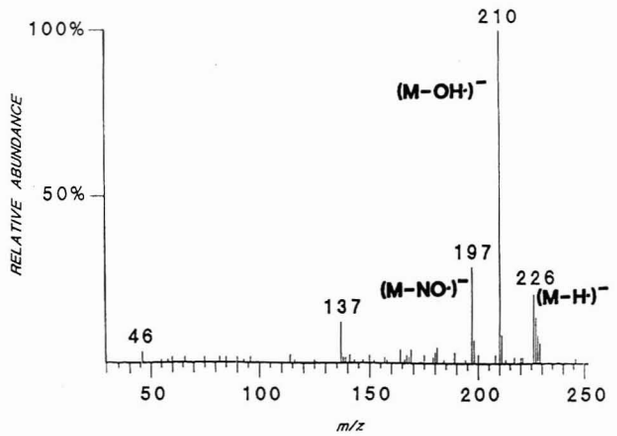

Figure 4. MS/MS daughter ion scan of the molecular anion of TNT.

intense than $M^{\bullet-}$. For the 3,4 and 2,6 isomers the $(M - NO^{\bullet})^-$ ions are most abundant but differences are observed in the relative abundances of the respective $M^{\bullet-}$ and $(M - H^{\bullet})^-$ ions and a $(M - OH^{\bullet})^-$ ion is essentially absent for the 3,4 isomer. The $(M - OH^{\bullet})^-$ ion is due to an ortho effect and is observed for some anions with a ring substituent containing labile protons ortho to a nitro group (*21*).

The NICI mass spectrum of RDX (molecular weight 222 amu) was acquired. As has been observed elsewhere with negative chemical ionization (*22*, *23*) of RDX, a peak at m/z 268 is observed corresponding to $(M + NO_2)^-$. No ions near to the molecular weight are apparent. By far the base peak in the spectrum corresponds to NO_2^- with significant peaks at m/z 176, 129, and 102 corresponding to $(M - NO_2)^-$, $(M - HNO_2, NO_2)^-$, and $(CH_2NCH_2NNO_2)^-$, respectively.

NICI MS/MS Spectra. MS/MS spectra were obtained for most of the ions listed in the mass spectra discussed above. In the present mode of operation for obtaining MS/MS data using an ion trap, ions are subjected to many low-energy collisions (*12*) prior to the second mass analysis step. In many respects the CAD experiment in the ion trap is similar to that in a triple quadrupole instrument where electronvolt energy collisions occur in a rf-only central quadrupole. A major difference, however, which could cause significant differences in the appearance of MS/MS spectra obtained by using the ion trap and a beam-type instrument, for example, is that sample still present as background in the trap allows for the possibility of charge transfer from a daughter ion to a sample molecule. This cannot occur in beam-type instruments since ionization, mass analysis stages, and collisional excitation are physically separated.

A mechanism that competes with CAD for negative ions is electron detachment. Electron detachment is particularly important for anions with neutral counterparts with low electron affinities. The compounds studied here, however, have high electron affinities (e.g., the electron affinity of 2,4-DNT is ≈1.4 eV (*20*)) which minimizes electron detachment but may tend to enhance the possibility of electron transfer from a daughter ion to a parent molecule.

For most of the anions studied here CAD was observed to occur with relatively high efficiency; i.e., the number of parent ions observed prior to excitation could be largely accounted for by the number of daughter ions detected. For example, Figure 4 shows the MS/MS spectrum of the molecular anion of TNT. The major high mass daughter ions observed have also been reported from a beam-type MS/MS instrument (*23*) and correspond to losses of $H^{\bullet}$ (m/z 226), $OH^{\bullet}$ (m/z 210), $NO^{\bullet}$ (m/z 197), and $NO_2^{\bullet}$ (m/z 181). (Note that ions at m/z 228 and m/z 229 were also present in the NICI mass spectrum and were not removed prior to excitation of m/z 227. The absolute abundances of the ions at m/z 228 and m/z 229 were unaffected by the MS/MS experiment.) The total number of counts observed for the daughter ions in this spectrum is roughly 75% of the number of counts measured for the TNT anion prior to excitation (≈80% of the initial parent ion signal can be accounted for when residual parent ions are also included). This indicates, assuming that the efficiency of detection does not vary greatly with mass over the range of 40–230 Da, that the parent ions primarily undergo CAD upon translational excitation (as opposed to other ion loss mechanisms such as electron detachment, scattering, etc.), and that the daughter ions are trapped with high efficiency. Similar high efficiencies, where efficiency is defined as (total daughter ion signal)/(parent ion signal before CAD) × 100, have been observed for positive ion MS/MS in the ion trap (*9*). Efficiencies greater than 20% were also observed for the CAD of the $(M - OH^{\bullet})^-$ and $(M - NO^{\bullet})^-$ anions. Under the same conditions, however, less than 1% of the $(M - H^{\bullet})^-$ ion signal in the mass spectrum appeared as daughter ions in the MS/MS experiment with m/z 226 as the parent ion despite the fact that the parent ion signal was attenuated to 20% of its initial value. Similar observations were also noted for the other nitroaromatic anions; viz., high efficiencies were noted for the $M^{\bullet-}$ ions whereas efficiencies for the $(M - H^{\bullet})^-$ anions were somewhat lower. An effort was made to increase the efficiency by increasing the amplitude of the ac voltage applied to the end caps and increasing the low mass cutoff of the MS/MS experiment. With an increase of the low mass cutoff, the frequency of motion of the parent ion in the direction between the end caps is increased which has been shown for positive ions to increase the amount of energy which is deposited into the ion (*19*). This was ineffective, however, in increasing the efficiency for the $(M - H^{\bullet})^-$ ions.

Table II. Relative Daughter Ion Abundances Observed in the Ion Trap MS/MS Spectra of the Major High Mass Ions in the Negative Chemical Ionization Mass Spectrum of RDX[a]

268^- $(M + NO_2)^-$ (15%)		176^- $(M - NO_2)^-$ (95%)		129^- $(M - HNO_2, NO_2)^-$ (58%)		102^- $(CH_2NCH_2N-NO_2)^-$ (8%)	
m/z	% base	m/z	% base	m/z	% base	m/z	% base
46	100	102	100	85	100	58	31
				58	17	46	100
				46	61		

[a] Parent ion to daughter ion conversion efficiencies are listed parenthetically.

Figure 5 compares the MS/MS spectra of the molecular anions of 2,4-DNT, 2,6-DNT, and 3,4-DNT. These isomeric ions are readily distinguishable by MS/MS just as they are by the negative chemical ionization mass spectra. The 2,4-DNT anion, for example, shows an abundant $OH^{\bullet}$ loss whereas the 2,6-DNT anion shows relatively less and the 3,4 isomer shows essentially none. The MS/MS efficiencies for these ions under these conditions were measured to be from 50 to 70%. The efficiencies observed for the $(M - H^{\bullet})^-$ ions, however, were 15–25%.

Table II summarizes the MS/MS spectra of the major high mass ions observed in the negative ion mass spectrum of RDX using water as the reagent gas and gives the percentage of parent ions converted to detected daughter ions. Wide variation is observed in the efficiency with which the different parent ions are converted to daughter ions, reminiscent of the difference in CAD efficiencies observed for the $M^{\bullet-}$ and $(M - H^{\bullet})^-$ anions of the nitroaromatics. The anion at m/z 176, for example, which corresponds to $(M - NO_2^{\bullet}, CH_2NNO_2)^-$, readily fragments to give virtually only the anion at m/z 102 (95% efficiency). However, this ion, $(CH_2NCH_2NNO_2)^-$, does

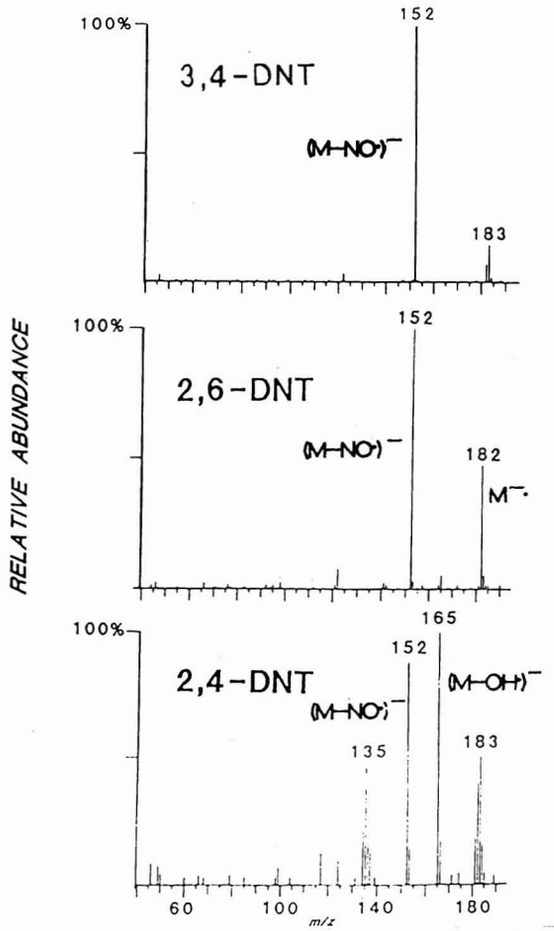

Figure 5. MS/MS daughter ion spectra of the molecular anions of (a) 3,4-DNT, (b) 2,6-DNT, and (c) 2,4-DNT.

not produce daughter ions as readily under the same conditions (8% efficiency).

Another noteworthy observation is that the MS/MS data obtained by using the ion trap are very similar to the corresponding data reported for high collision energy MS/MS (*23*) in some cases but are markedly different in others. For example, the MS/MS data for the $(M - NO_2, CH_2NNO_2)^-$ anion (m/z 176) is identical for the ion trap and for MS/MS data acquired with a reverse geometry sector mass spectrometer; viz., only one daughter ion, $(CH_2NCH_2NNO_2)^-$, (m/z 102), is observed. On the other hand, the high collision energy data for the m/z 102 anion shows peaks at m/z 86 ($CH_2NCH_2NNO^-$, 31%), m/z 74 ($CH_2NNO_2^-$, 95%), m/z 60 (NNO_2^- or $CH_2NO_2^-$, 34%), m/z 54 (CH_2NCN^-, 12%), and 46 (NO_2^-, 100%), whereas on the ion trap the only daughter ion other than NO_2^- is observed at m/z 58 (possibly CH_2NNO^-). An ion at m/z 58 also appears in the ion trap MS/MS experiment for the anion at m/z 129 but does not appear in the sector instrument data. The base peak in the ion trap for the m/z 129 anion is observed at m/z 85, probably resulting from the loss of N_2O, whereas this ion is not a major ion in the sector instrument results. The reason(s) for these differences cannot be determined from these results and merit further study.

There are several major differences in important aspects of the two experiments including conditions of ion formation, collision energies, numbers of collisions, time scales of the experiments, and chemical environments after the first mass analysis step. Any of these could at least in part account for the differences observed between the ion trap and sector mass spectrometer data. It seems likely, however, that the relatively reactive chemical environment in the ion trap after mass selection will have a major influence on the appearance of some MS/MS spectra. The importance of this situation will be clearer as more experience is gained with the ion trap as an instrument for MS/MS.

A significant observation in these studies is the relatively wide variation with parent ion in the efficiency of conversion to daughter ions in the MS/MS experiment. Efficiencies recorded here were seen to vary by as much as 2 orders of magnitude (the anion at m/z 176 from RDX was converted to the daughter ion at m/z 102 at an efficiency of 95% whereas an efficiency of <1% was observed for $(M - H^\bullet)^-$ from TNT). A number of loss mechanisms can be operative in the ion trap for negatively charged parent ions including: (1) CAD; (2) electron transfer to another molecule in the ion trap; (3) ion/molecule reaction involving atom transfer(s); (4) double electron detachment (charge inversion) to form positive ions; (5) single electron detachment; (6) scattering out of the trap; (7) ion/ion reaction resulting in the formation of neutral products.

Charged products are formed and should be observable in the trap for the first four mechanisms. Differences in CAD cross sections can only account for the observed efficiencies if their magnitudes relative to other loss mechanisms vary substantially. The parent ion signal is readily depleted under these experimental conditions even for ions which give low efficiencies for daughter ion production indicating that, in these cases, some parent ion loss process other than CAD predominates. Major products following the first stage of mass analysis clearly resulting from ion/molecule reactions or from charge transfer were not observed over a mass range of several hundred atomic mass units which encompassed the range in which CAD products were expected to appear. Charge inversion is generally not observed in triple quadrupole instruments and has not as yet been reported to occur in an ion trap under the conditions used here.

The final three loss processes do not give detectable charged products (free electrons are not trapped under the experimental conditions) so that they result in a net decrease in the number of ions in the trap. The most likely cause for the rather large differences in MS/MS efficiencies is differences in the extent to which parent ions are lost via electron detachment relative to CAD. Cross sections for collisional electron detachment from anions can be greater than 10^{-15} cm^2 (*24*), of the same order or greater than those for CAD under these conditions, and can therefore be expected to compete with CAD. Indeed, this has been observed for some anions in other types of MS/MS spectrometers such as triple quadrupole instruments (*25*) and reverse geometry sector mass spectrometers (*26*). Scattering of ions out of the trap cannot explain the large differences in the efficiencies for daughter ion production. A 75% efficiency for $M^{\bullet-}$ from TNT vs. <1% for $(M - H^\bullet)^-$ cannot easily be rationalized based on differences in the propensity for scattering. Neither can the reaction between positive ions and negative ions account for the results. Ion/ion recombinations are characterized by large rate constants (*27*) (generally (1–5) × 10^{-7} cm^3/(molecule s)) due to the coulombic attraction between opposite charges. However, even assuming rather large ion number densities of 10^5 ions/cm^3 following mass selection and a rate constant of 5 × 10^{-7} cm^3/(molecule s) cannot account for the loss of ≈80% of the ions in the MS/MS experiment for $(M - H^\bullet)^-$ from TNT. With a resulting reaction rate of ≈5 × 10^3/(cm^3 s) and a reaction time of 10 ms, only 50 ions (0.05%) are lost.

CONCLUSIONS

It has been demonstrated that polyatomic negative ions can be readily formed from sample molecules with high electron affinities in an ion trap using chemical ionization. The ion trap, with its attractive features of small size, simplicity, and relatively low cost, should therefore be applicable to many of

the problems for which it has been shown that negative ions are most suitable. For most of the negative ions studied, MS/MS spectra were readily obtainable with high conversion (>10%) of parent ions to daughter ions. In some cases, however, the parent ion to daughter ion conversion efficiency was observed to be relatively low. This can be interpreted as being due to collisional electron detachment competing effectively with CAD.

Registry No. 2,4-DNT, 121-14-2; 2,6-DNT, 606-20-2; 3,4-DNT, 610-39-9; TNT, 118-96-7; RDX, 121-82-4; *p*-dinitrobenzene, 100-25-4.

LITERATURE CITED

(1) Dawson, P. H. *Quadrupole Mass Spectrometry*; Dawson, P. H., Ed.; Elsevier: Amsterdam, 1976; Chapter 11.
(2) Todd, J. F. J.; Lawson, G.; Bonner, R. F. *Quadrupole Mass Spectrometry*; Dawson, P. H., Ed.; Elsevier: Amsterdam, 1976; Chapter 8.
(3) Todd, J. F. J.; Lawson, G. *International Review of Science Physical Chemistry, Series 2: Mass Spectrometry*; Maccoll, A., Ed.; Butterworth: London, 1975; Vol. 5, p 289.
(4) Stafford, G. C.; Kelley, P. E.; Stephens, D. R. U.S. Patent 4 540 884, 1985.
(5) Stafford, G. C.; Kelley, P. E.; Syka, J. E. P.; Reynolds, W. E.; Todd, J. F. J. *Int. J. Mass Spectrom. Ion Proc.* **1984**, *60*, 85.
(6) Fulford, J. E.; Hoa, D.-N.; Hughes, R. J.; March, R. E.; Bonner, R. F.; Wong, G. J. *J. Vac. Technol.* **1980**, *17*, 4.
(7) Kelley, P. E.; Stafford, G. C.; Fies, W. J.; Syka, J. E. P.; McIver, R. T.; Hunter, R. L.; Todd, J. F. J.; Bexon, J. J. Proceedings of the 32nd Annual Conference on Mass Spectrometry and Allied Topics, San Antonio, TX, 1984; p 505.
(8) Stafford, G. C.; Kelley, P. E.; Bradford, D. C. *Am. Lab.* (*Fairfield, Conn.*) **1983**, *15*(6), 51.
(9) Kelley, P. E.; Stafford, G. C.; Syka, J. E. P.; Reynolds, W. E.; Louris, J. N.; Amy, J. W.; Todd, J. F. J. Proceedings of the 33rd Annual Conference on Mass Spectrometry and Allied Topics, San Diego, CA, 1985; p 707.
(10) Cooks, R. G.; Glish, G. L. *Chem. Eng. News* **1981**, *59*(48), 40.
(11) *Tandem Mass Spectrometry*; McLafferty, F. W., Ed.; Wiley: New York, 1983.
(12) Louris, J.; Brodbelt, J.; Cooks, R. G.; Syka, J.; Stafford, G. Proceedings of the 34th Annual Conference on Mass Spectrometry and Allied Topics, Cincinnati, OH, 1986; p 685.
(13) Bowie, J. H. *Mass Spectrom. Rev.* **1984**, *3*, 161.
(14) Mather, R. E.; Todd, J. F. J. *Anal. Chem.* **1980**, *33*, 159.
(15) Schermann, J.-P.; Major, F. G. NASA Rep. X-524-71-343; Goddard Space Flight Center, Greenbelt, MD, 1971.
(16) Kelley, P. E.; Syka, J. E. P.; Ceja, P. C.; Stafford, G. C.; Louris, J. N.; Grutzmacher, H. F.; Kuck, D.; Todd, J. F. J. Proceedings of the 34th Annual Conference on Mass Spectrometry and Allied Topics, Cincinnati, OH, 1986; p 963.
(17) Kelley, P. E.; Stafford, G. C.; Syka, J. E. P.; Reynolds, W. E.; Louris, J. N.; Todd, J. F. J. *Adv. Mass Spectrom.* **1985**, *10B*, 869.
(18) Stafford, G. C.; Reeher, J.; Smith, R.; Story, M. S. In *Dynamic Mass Spectrometry*; Price, D., Todd, J. F. J., Eds.; 1978; Vol. 5, Chapter 4, p 55.
(19) Louris, J. N.; Cooks, R. G. Syka, J. E. P.; Kelley, P. E.; Stafford, G. C.; Todd, J. F. J., submitted for publication in *Anal. Chem.*
(20) Bartmess, J. E., *J. Phys. Chem. Ref. Data*, in press.
(21) McLuckey, S. A.; Glish, G. L. *Org. Mass Spectrom.*, in press.
(22) Yinon, J. *J. Forensic Sci.* **1980**, *25*, 401.
(23) McLuckey, S. A.; Glish, G. L.; Carter, J. A. *J. Forensic Sci.* **1985**, *30*, 773.
(24) Christophorou, L. G. *Atomic and Molecular Radiation Physics*; Wiley-Interscience: New York, 1971; pp 539–544.
(25) Dawson, P. H.; Sun, W.-F. *Int. J. Mass Spectrom. Ion Processes* **1984**, *61*, 123.
(26) Zakett, D.; Shaddock, V. M.; Cooks, R. G. *Anal. Chem.* **1979**, *51*, 1849.
(27) Kaufman, F. *Chemical Reactions in Electrical Discharges: Advances in Chemistry Series 80*; Gould, R. F., Ed.; American Chemical Society: Washington, DC, 1969, p 29.

RECEIVED for review November 24, 1986. Accepted March 16, 1987. S.A.M. and G.L.G. acknowledge support from the U.S. DOE Office of Basic Energy Sciences, under Contract DE ACO5-840R21400 with Martin Marietta Energy Systems, Inc.

Stable Isotope Dilution Thermospray Liquid Chromatography/Mass Spectrometry Method for Determination of Sugars and Sugar Alcohols in Humans

Nora V. Esteban, Daniel J. Liberato,[1] James B. Sidbury,[2] and Alfred L. Yergey*

Laboratory of Theoretical and Physical Biology, National Institute of Child Health, National Institutes of Health, Building 6, Room 136, Bethesda, Maryland 20892

The development of a thermospray high-performance liquid chromatography/mass spectrometry method for the determination of carbohydrates and sugar alcohols is reported. The simultaneous separation and identification of mono- and disaccharides as well as sugar alcohols has a detection limit of about 50 pmol of material on column. Isotope dilution mass spectrometry (IDMS) allows determinations of glucose at low isotopic enrichments (0.1–1%) and sorbitol at ~1:1 labeled/unlabeled ratio, in small serum or amniotic fluid samples (200 μL), respectively. Application of the IDMS method to the determination of sorbitol concentration in amniotic fluid and in a child with glycogen storage disease type I confirmed the validity of this technique for clinical investigation.

There is considerable demand in biochemical research for a specific, sensitive, and general analytical method for the identification of mono- and disaccharides and related sugar alcohols. While chromatographic and specific enzyme methods are commonplace for many such analyses, a chromatographic inlet coupled with a mass spectrometer, in combination with isotopically labeled internal standards, is widely accepted as the analytical methodology that will permit the determination of these materials in biological matrices at good to excellent sensitivities and precisions. In addition to the identification and measurement of these materials at low levels however, the investigation of production rates using stable isotopic tracers is an area particularly suited to chromatographic/mass spectrometric instrumentation. Stable isotope tracer methodology offers important advantages over radiotracer techniques since both substrate content and isotope enrichment can be measured at the same time, the same individual can be studied repeatedly, several stable isotope tracers can be

[1] Present address: Hoffman–La Roche, Department of Drug Metabolism, Nutley, NJ 07110.
[2] Human Genetics Branch, National Institute of Child Health, National Institutes of Health, Bethesda, MD 20892.

This article not subject to U.S. Copyright. Published 1987 by the American Chemical Society

used simultaneously, metabolic pathways can be followed, and studies in pregnant women and children can be undertaken (*1*).

Gas chromatography/mass spectrometry (GC/MS) has been shown to be an important tool for analysis of carbohydrates and polyols (2–8), but the technique requires derivatization of the samples before analysis. A liquid chromatography/mass spectrometry (LC/MS) combination offers the potential to be the instrumental approach of choice for these materials since it should permit identification of all the substances in this class without the need for prior derivatization while retaining the advantages of a chromatographic inlet for quantification. In most biological systems to which such analysis might be applied, the materials are sufficiently abundant so that ultimate sensitivity is generally not an issue, but rather the accuracy and reproducibility of the measurements. In principle, LC/MS should be no different than GC/MS with regard to precision and accuracy and should function with little or no sacrifice in sensitivity. Under such circumstances, the simplification in sample preparation inherent in LC/MS would become a significant advantage.

This paper reports the development of a general method for the separation, identification, and quantification of mono- and disaccharides and related sugar alcohols using thermospray LC/MS. The paper also reports the use of this methodology for the measurement of glucose production rate in children by use of isotope dilution mass spectrometry as well as the quantification of sorbitol in human amniotic fluid.

EXPERIMENTAL SECTION

Materials. D-[$^{13}C_6$]Glucose (98.8 atom % ^{13}C) and D-[1-^{13}C]sorbitol (99.3 atom % ^{13}C) were obtained from Merck Sharpe & Dohme of Canada, and purity was confirmed by LC/MS. Ammonium acetate was purchased from J. T. Baker (Phillipsburg, NJ). HPLC grade water was obtained from Hydroservices (Rockville, MD). Other materials were purchased from various sources: methyl alcohol (Burdick & Jackson Laboratories, Inc., Muskegon, MA); ion exchange resins AG 50W-X8 and AG 1-X8 (Bio Rad Laboratories, Richmond, CA); Sep-PAK C18 cartridges (Waters Associated, Milford, MA); and carbohydrates (Sigma, St. Louis, MO).

Analysis of Samples. *Serum and Amniotic Fluid Samples.* The infusion study was approved by the Human Clinical Research Subpanel of the National Institute of Child Health (NICHD) and a written informed consent was obtained after the procedure was fully explained. Vials of amniotic fluid were provided by the George Washington University Medical Center, Washington, DC. For glucose analysis 2–3 mL of heparinized blood was obtained and immediately centrifuged at each sampling time. For sorbitol determinations 1 mL of frozen amniotic fluid was required. Aliquots of 200 μL of plasma or amniotic fluid were deproteinized with methanol, and the supernatant was removed after centrifugation. After sequential anion (AG 1-X8) and cation (AG 50W-X8) exchange chromatography, all samples were passed through a Sep-PAK C18 cartridge, filtered (0.45 μm), dried under a stream of argon at 40 °C, and reconstituted to 100 μL with water.

Liquid Chromatography/Mass Spectrometry. Solvents were filtered (0.45 μm) and degassed prior to carrying out LC studies. The glucose separation was done with a Beckman μ-Spherogel Carbohydrate Column (Beckman Instruments, Inc., Berkeley, CA) using an LKB 2150 HPLC pump (LKB, Bromma, Sweden) to deliver pure water at a flow rate of 0.5 mL min^{-1}. Column temperature was maintained at 90 °C by a dual zone column temperature control system (Systec, Inc., Minneapolis, MN). A second LKB 2150 HPLC pump (LKB, Bromma, Sweden) was used for postcolumn addition of 0.2 M ammonium acetate (*9*) to give a total flow rate of 1 mL min^{-1}. Both pumps were coupled through a T connector (Scientific Systems, Inc., State College, PA) to a slightly modified Finnigan quadrupole mass spectrometer using a thermospray interface (Vestec, Houston, TX), as described previously (*10*). The solvent is pumped through the electrically heated interface forming a supersonic jet. Ions are formed by direct desorption and/or ion/molecule reactions.

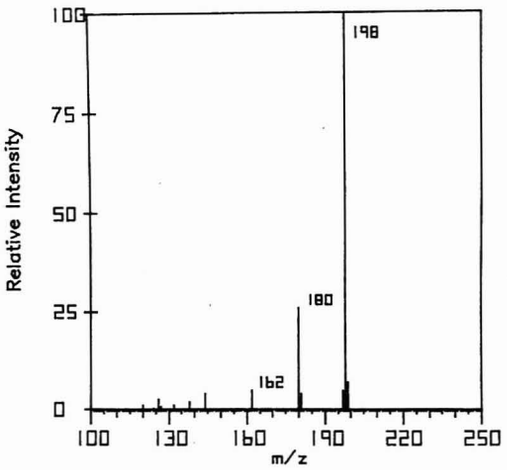

Figure 1. Thermospray HPLC mass spectra of glucose (20 μg).

Table I. Mass Spectra Obtained by Thermospray LC/MS

		% rel intensity m/z			
compound	mol wt	$(M + NH_4)^+$	$(M + H)^+$	$(M + NH_4 - H_2O)^+$	$(M + NH_4 - 2H_2O)^+$
ribose	150	100	3	18	3
xylitol	152	100	13	7	
galactose	180	100	2	7	5
glucose	180	100	3	20	5
fructose	180	100	2	21	11
mannose	180	100	3	10	5
inositol	180	100	1	2	2
sorbitol	182	100	52	20	2
galactitol	182	100	32	39	2
mannitol	182	100	22	3	4
trehalose	342	100	10	7	9

The mass spectrometer conditions were optimized for the ammoniated molecule being studied. For glucose at m/z 198 these typically were as follows: source, 230 °C; vaporizer, 210 °C; and down jet, 230 °C. The scan functions of the mass spectrometer were controlled and data analyzed by a Teknivent Data System (Teknivent, St. Louis, MO). For glucose the ions monitored were m/z 198 and m/z 204, corresponding to the $(M + 18)^+$ ions in the mass spectrum of glucose and [U-^{13}C]glucose, respectively. The ions at m/z 200 and 201 were monitored for sorbitol. A mixture of 0.02 M ammonium acetate, 0.9 μM tetrabutylammonium iodide, 0.09 μM benzyltriphenylphosphonium chloride, and 0.027 μM hexadecylpyridinium chloride was used for mass calibration of the data system.

RESULTS AND DISCUSSION

Figure 1 shows the mass spectrum from standard glucose, on column, obtained by thermospray mass spectrometry in 0.1 M ammonium acetate. The spectrum is characterized by abundant $(M + 18)^+$ ions at m/z 198, assigned to the ammoniated molecule, accompanied by small fragments, $(M + NH_4 - 18)^+$, $(M + NH_4 - 36)^+$, $(M + NH_4 - 54)^+$, and $(M + NH_4 - 72)^+$ ions, which can be accounted for by the loss of one, two, three, and four molecules of water from the ammoniated molecule. The ratios of intensities of the ions at m/z 181 and m/z 180 were higher than the ratio expected from the calculated natural abundance of $(M + 1)/(M + 0)$ and from the observed ratio m/z 199:m/z 198, indicating that protonation of the intact molecule also probably occurs, making this ion unsatisfactory for isotope dilution measurements. Successive losses of one, two, and three molecules of water from the protonated molecule were also observed at m/z 163, m/z 145, and m/z 127, respectively.

The spectra obtained from several other carbohydrates by LC/MS are summarized in Table I. Mass spectra are characterized by abundant $(M + 18)^+$ ions and small fragment

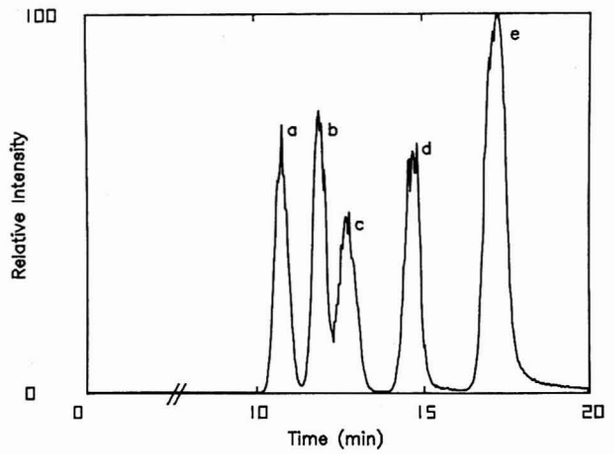

Figure 2. HPLC/MS total ion current chromatogram of five carbohydrates: glucose (a); galactose (b); fructose (c) (10 μg); mannitol (d); sorbitol (e) (5 μg).

ions $(M + 18 - nH_2O)^+$ and are similar to those observed by ammonia chemical ionization (*11*). Sample amounts in the range of 1–10 nmol were sufficient to obtain reproducible spectra when scanning at rates on the order of 100 Da/s over the full spectral range (m/z 120 to 220).

After LC/MS conditions were optimized, increased fragmentation was observed when amounts less than 0.1 nmol of material were injected on column. Increased fragmentation is also obtained by either increasing or decreasing the source temperature. The detection limit for standard glucose on direct injection, i.e., no column, when monitoring $(M + 18)^+$ ions by specific ion monitoring (1 s/cycle) was 50 pmol. Similar sensitivities were observed for sorbitol as well as other monosaccharides.

LC conditions used for the analysis of glucose or sorbitol by combined LC/MS were chosen to give separation of glucose from other carbohydrates normally present in a human sample matrix while maintaining relatively sharp peaks and short retention times. The separation and detection by LC/MS of a standard mixture of glucose, galactose, fructose (10 μg), mannitol, and sorbitol (5 μg) using pure water at 0.5 mL/min on a Beckman μ-Spherogel Carbohydrate Column with postcolumn addition of 0.2 M ammonium acetate at 0.5 mL/min are shown in Figure 2.

Isotope Dilution MS Method. The assay of glucose by the IDMS method was carried out by using [U-^{13}C]glucose (98.8 atom % ^{13}C) as internal standard and monitoring ions at mass 198 and 204, corresponding to the (M + 18) ions of unlabeled and labeled material, respectively. To determine the validity of the procedure, standard solutions were prepared in which the concentration of unlabeled glucose was constant but the percentage of [U-^{13}C]glucose varied. Standard curves were obtained by plotting relative peak area abundances between the m/z 204 and the m/z 198 ions vs. the expected ratio in the range of ratios 0.001:1 to 0.01:1. For the low isotopic enrichments required by the tracer work, ions at m/z 204 were collected through a 0–100 mV full scale amplifier vs. the 0–10 V full scale amplifier normally used. Thus, a 1:100 $(m + 6)/(m + 0)$ ratio will appear as a 1:1 ratio, thereby improving the accuracy and precision of a measured ratio. Amplifier calibration was done by applying a fixed voltage to both amplifiers simultaneously and was accounted for in plotting the data. Under these conditions, linearity was observed between 0.1% and 1% of [U-^{13}C]glucose for 10 μg of unlabeled material with a regression line $y = 0.9288x + 0.0803$, standard error of the estimate of 0.0489. Same day and interassay precision for a labeled/unlabeled glucose ratio of 1:100 was 7% (n = 7) and 8.3% (n = 15, six consecutive days). These precisions compare quite favorably with ±5% relative standard deviation published for a study of glucose production rate that employed a GC/MS analysis using the cyclic butylboronate 6-acetate derivative (*3*), but were not as good as the high precisions (<2% relative standard deviation), reported for the determination of glucose turnover in vivo by Bier (*6*). Since natural abundance of [U-^{13}C]glucose is a negligible quantity, accuracy of this method could only be estimated by comparison with ratio expected from carefully prepared, weighed mixtures of labeled and unlabeled material that was then serially diluted. Nevertheless, determinations at 1:1 and 1:100 ratios differed from the expected ratio by less than 2% and 5%, respectively.

While the reproducibility of individual measurements is relatively large, it is of the same order as the variation observed in clinical studies of glucose production rates (GPR). An example of this is obtained from one patient participating in our studies of GPR in type I glycogen storage disease. The patient was infused continuously for 6 h with the [U-^{13}C]-glucose tracer at 20 μg/(kg/min) and for 3 h with natural glucose at 4.5 mg/(kg/min) followed by a 3-h infusion at 1.1 mg/(kg/min) with natural glucose. Six blood samples were drawn, three each during the "steady state" portions of the natural glucose infusions, i.e., when the ratio of tracer to natural glucose reached a plateau. The first three samples were taken at 2, 2.5 (*1*), and 3 h and the second three at 5, 5.5, and 6 h after the start of the study. The measurements of the isotope ratio of the first three samples were 0.00448 ± 0.00036 (8%), mean ± standard deviation, and of the second three samples were 0.01010 ± 0.00093 (9.2%). As can be seen, the mean of isotope ratio measurements, taken where the infusions reach a plateau in an experiment for which the method was developed, exhibit as much variation as the isotope ratios of the standards. The GPRs calculated from these ratios are consistent with clinical expectations of the study and reflect the ability of the method to make useful measurements.

The IDMS method for the analysis of sorbitol was carried out by using [1-^{13}C]sorbitol (99.3 atom % ^{13}C). Standard curves constructed in the range of ratios labeled/unlabeled material 0.2:1 to 8:1 showed a regression line $y = 0.9376x - 0.037$, standard error of the estimate of 0.0258, with an intraday and interday relative standard deviation (RSD) of 2.76% and 2.99%, respectively, at 1:1 labeled to unlabeled ratio. When concentration of sorbitol was determined by adding six different amounts of [1-^{13}C]sorbitol as internal standard to six aliquots of the same amniotic fluid sample to cover the range of ratios 0.2:1 to 4:1 labeled to unlabeled material, the RSD of the mean value obtained was 4.15%. Sorbitol concentration measured in 10 normal amniotic fluid samples by HPLC/MS (17 to 22 weeks of gestation = 30.71 ± 7.15 mg/L), using [1-^{13}C]sorbitol as internal standard showed good agreement with previous published work using GC/MS (*12*). We observed a significant decrease of sorbitol concentration in amniotic fluid along gestation.

CONCLUSIONS

The combination of chromatographic separation and mass spectrometry provides the basis for highly specific analysis. Various IDMS procedures using GC/MS have been employed in the quantitative analysis of carbohydrates (*5*, *7*). Although inductively coupled plasma (ICP) has been used for glucose detection in aqueous solutions (*13*) and the moving belt approach to LC/MS is capable of handling carbohydrates and can give molecular information (*11*), these methods present sensitivity problems, and as yet no on-line quantitative LC/MS studies have been reported for carbohydrates. The method described in this paper offers an alternate approach that is both sensitive and specific. With thermospray LC/MS, the sugar components of interest from biological samples were

separated and analyzed after a simple sample cleanup and without requiring derivatization. Mass spectra of monosaccharides yield molecular weight information with little fragmentation. IDMS, using [U-^{13}C]glucose as internal standard, shows linearity even at very low isotopic enrichment (0.1% to 1%). The accuracy of this method was determined on standard mixtures at low percentage of [U-^{13}C]glucose rather than 50% (1:1 ratio) since the accuracy is lower with the smaller percentage enrichment. When used on biological samples (e.g., glucose from human serum), this method shows the same degree of sensitivity and accuracy. The data given show that combined LC/MS can be successfully applied to quantitative analysis of glucose or sorbitol in small biological samples. Since the use of stable isotopes is a general accepted procedure for the measurement of daily glucose production and utilization, and it is considered superior to radioisotopes in accuracy, specificity, and patient safety (*14*), this analytical method, using D-[$^{13}C_6$]glucose is likely to prove useful in kinetic studies where good precision, sensitivity, and specificity are required. We are currently applying this method in our laboratory to determine production rates in type I GSD patients with no glucose-6-phosphatase enzyme activity, as determined by liver biopsy, and to further elucidate mechanisms by which these patients can produce glucose. Future studies will be performed in patients with other metabolic disorders.

Registry No. D-Glucose, 50-99-7; D-sorbitol, 50-70-4.

LITERATURE CITED

(1) Matthews, D. E.; Bier, D. M. *Annu. Rev. Nutr.* **1983**, *3*, 309.
(2) Bier, D. M.; Arnold, K. J.; Sherman, W. R.; Holland, W. H.; Holmes, W. F.; Kipnis, D. M. *Diabetes* **1977**, *26*, 1005.
(3) Dan, P.; Clemons, P. M.; Sperling, M. I.; Gelfand, M. J.; Chen, I. W.; Sperling, M. A.; Norman, E. J. *Anal. Lett.* **1983**, *16*(B9), 655.
(4) Tserng, K.; Kalhan, S. C. *Am. J. Physiol.* **1983**, *245*, E476.
(5) White, E.; Welch, M. J.; Sun, T.; Sniegoski, L. T.; Schaffer, R.; Hertz, H. S.; Cohen, A. *Biomed. Mass. Spectrom.* **1982**, *9*, 395.
(6) Bier, D. M.; Sherman, W. R.; Holland, W. H.; Kipnis, D. M. In Proceedings of the First International Conference for Stable Isotopes in Chemistry, Biology and Medicine, May 1973, USAEC Conf-730525, p 397.
(7) Pelletier, O.; Cadieux, S. *Biomed. Mass Spectrom.* **1983**, *10*, 130.
(8) Roboz, J.; Kappatos, D. C.; Greaves, J.; Holland, J. B. *Clin. Chem. (Winston-Salem, N.C.)* **1984**, *30*, 1611.
(9) Voyksner, R. D.; Bursey, J. T.; Pellizzari, E. D. *Anal. Chem.* **1984**, *56*, 1507.
(10) Blakley, C. R.; Vestal, M. L. *Anal. Chem.* **1983**, *55*, 750.
(11) Games, D. E.; McDowal, M. A.; Levsen, K.; Schafer, K. H.; Dobberstein, P.; Gower, J. L. *Biomed. Mass Spectrom.* **1984**, *11*(2), 87.
(12) Jakobs, C.; Warner, T. G.; Sweetman, L.; Nyhan, W. L. *Pediatr. Res.* **1984**, *18*, 714.
(13) Houk, R. S.; Fassel, V. A.; Svee, J. *Org. Mass Spectrom.* **1982**, *17*, 240.
(14) Bier, D. M. *Nutr. Rev.* **1982**, *40*(5), 129.

RECEIVED for review August 8, 1986. Accepted March 13, 1987.

Instrumentation, Applications, and Energy Deposition in Quadrupole Ion-Trap Tandem Mass Spectrometry

John N. Louris and R. Graham Cooks*

Department of Chemistry, Purdue University, West Lafayette, Indiana 47907

John E. P. Syka, Paul E. Kelley, and George C. Stafford, Jr.

Finnigan MAT, 355 River Oaks Parkway, San Jose, California 95134

John F. J. Todd

Chemical Laboratory, University of Kent, Canterbury, Kent, CT 27NH, U.K.

The use of an ion-trap mass spectrometer to generate daughter spectra of selected parent ions is shown. Ions are created within the trap by electron impact, undesired ions are ejected from the trap, and the selected parent ion undergoes collisionally activated dissociation (CAD). The CAD efficiency can be greatly increased by applying a small supplementary ac voltage of appropriate frequency. The energy transferred to the selected ion, which depends upon the radio frequency voltage applied to the trap as well as the supplementary ac voltage and frequency, is explored with the molecular ions of tetraethylsilane, *n*-butylbenzene, and nitrobenzene. Extraordinarily high CAD efficiency (~100%) is readily achieved although the internal energy deposited is small (≤2 eV) under these conditions. Under conditions that yield greater average internal energy deposition, dissociation efficiencies are smaller and activated ions with a wide range of internal energies are generated. Scan modes, which allow daughter spectra to be recorded for the products of ion/molecule reactions and for fragment ions generated in a previous collision (sequential daughter MS/MS/MS), are also illustrated.

Mass spectrometers that allow two stages of mass analysis (MS/MS instruments) have found application in qualitative analysis, quantitative analysis, and mechanistic studies (*1*). They are used to study such gas-phase ion reactions as collisionally activated dissociation (CAD) and photodissociation (*2*), as well as electron-transfer reactions (*3*, *4*), and ion/molecule reactions (*5*). Spectrometers capable of MS/MS experiments are of two types: those in which the stages of mass analysis are performed in different mass analyzers, and spectrometers in which the several stages of mass analysis are performed in a single mass analyzer. Multiple quadrupole, multiple sector, and hybrid sector/quadrupole instruments are of the first type, while ion cyclotron resonance (ICR) instruments were, until recently, the only MS/MS instruments that used a single mass analyzer for the sequential stages of mass analysis.

The quadrupole ion trap has been used for the trapping and mass analysis of ions since the early work of Fischer (*6*, *7*). The ion trap is now widely used for applications ranging from mass spectrometry to optical spectroscopy of trapped atomic and molecular ions (*8*, *9*). The device consists of a chamber formed between metal surfaces in the shape of a hyperboloid of one sheet (the ring electrode) and a hyperboloid of two sheets (the two end-cap electrodes, Figure 1). Ions are created within the chamber by electron impact from an electron beam admitted through a small aperture in one of the surfaces. Radio frequency (rf) voltages (and sometimes direct current voltage offsets) are applied between the ring electrode and

0003-2700/87/0359-1677$01.50/0 © 1987 American Chemical Society

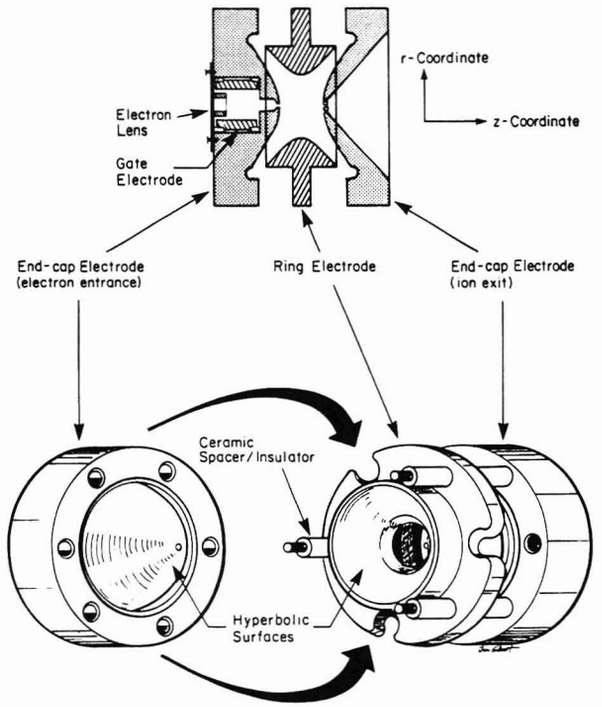

Figure 1. Ion-trap electrodes. An rf field is established between the ring electrode and the two end-cap electrodes. The assembled structure is shown in cross section.

the two end-cap electrodes establishing a quadrupole electric field. This field is uncoupled in the three directions so that ion motion can be considered independently in each direction; the force acting upon an ion increases with the displacement of the ion from the center of the field but the direction of the force depends on the instantaneous voltage applied to the ring electrode. A restoring force along one coordinate (such as the distance, r, from the ion trap's axis of radial symmetry) will exist concurrently with a repelling force along another coordinate (such as the distance, z, along the ion trap's axis), and if the field were static the ions would eventually strike an electrode. However, in an rf field the force along each coordinate alternates direction so that a stable trajectory may be possible in which the ions do not strike a surface. In practice, ions of appropriate mass-to-charge ratios may be trapped within the device for periods of many seconds.

Various methods of mass analysis of the trapped ions have been available since the invention of the ion trap, but the usefulness of the device as a mass spectrometer has recently been greatly increased by a new method of operation, the mass-selective instability mode (*8*). In this method, a radio frequency voltage (without a direct current component) is applied to the ring electrode, while the two end-cap electrodes are held at ground potential. All ions whose mass-to-charge ratio exceeds a minimum cut-off value (which is linearly proportional to the magnitude of the radio frequency voltage) are trapped. To record a mass spectrum, the radio frequency voltage is increased with time so that ions of successively greater mass-to-charge ratios develop unstable trajectories, are ejected through perforations in an end-cap, and are detected with an electron multiplier. The resolution attained with this mode of operation is greatly enhanced by the presence of about a millitorr of helium, presumably because this buffer gas damps the otherwise stable ion trajectories to the center of the trap.

In the mass-selective instability mode, all ions of less than a given mass-to-charge ratio may be excluded from the trap by raising the radio frequency voltage to the appropriate level. For example, if a single compound is introduced into the trap, the molecular ion and its isotopic variants may be trapped.

Table I. Typical Operating Parameters

trap size	r_0 = 1.0 cm
rf frequency	1.1 MHz
rf voltage	0.15–15 kV (pp)
ac frequency	50–550 kHz
ac voltage	10 mV to 15 V (pp)
ionization gate time	1 ms
interval P, figure 4	5 ms
interval D, figure 4	1–50 ms
interval S, figure 4	180 μs/Da
He pressure	1×10^{-3} torr
analyte pressure	$(2–4) \times 10^{-7}$ torr

If the ring voltage is then reduced so ions of lower mass-to-charge ratio may be trapped, any fragment ions produced after the drop in voltage will accumulate in the trap and may be observed by a second scan of the ring electrode voltage to higher values. Thus, if a molecular ion is selected to be trapped, a spectrum can be obtained of the fragment ions it produces over time. This paper discusses the use of a quadrupole ion trap for such MS/MS experiments. Special attention is given to the methodology for CAD within the ion trap and to the internal energy deposited in the ion selected for dissociation.

INSTRUMENTATION AND EXPERIMENTAL SECTION

The ion-trap mass spectrometer used in this study was constructed from components of a Finnigan MAT model 700 ion-trap detector (ITD). The trap was removed from the commercially supplied vacuum manifold and modified to permit installation on an optical rail in a large, rectangular vacuum manifold (Figure 2). Also, ceramic insulators were added to permit the electrical isolation of both end-caps. The upper surface of the manifold is formed by glass plates (sealed with Viton seals), which allow ready access to the system. The manifold is evacuated by using a turbomolecular pump (170 L/s, Balzers) backed by a mechanical pump. Base pressure is 2×10^{-7} torr. Sample is introduced via a direct insertion probe or via a precision leak valve. Helium buffer gas is introduced by using a separate leak valve.

Ionization is effected by electron impact, occurring within the trap, obtained by using the gated electron beam technique employed in the commercial ITD. Ion detection is by a channel electron multiplier (Detech), which is external to the trap and placed near small perforations in an end-cap.

A single-board microcomputer is used to control timing sequences in the instrument, including the scanning of the rf voltage, the application of the supplementary ac voltage, and the gating of the electron beam and the electron multiplier voltage. The supplementary ac voltage is provided by a single-board frequency synthesizer (SCI-TEK), which is also interfaced to the single-board computer. The single-board computer is also used to acquire and transmit data to the main data system, which is based on an IBM XT. Figure 3 shows a block diagram of the ion trap electronics.

Typical operating voltage sequences are shown in Figure 4. Typical voltage levels and frequencies, as well as other typical operating parameters, are gathered in Table I. A number of these parameters were varied and the results of such changes form part of the present paper.

RESULTS AND DISCUSSIONS

Comparison with Other MS/MS Spectrometers. The quadrupole ion trap confines ions by using an electric field while an ICR spectrometer confines ions with a combination of magnetic and electric fields. Both devices may be operated in a variety of ways, but in a typical mode of operation for both, a mass spectrum is acquired by pulsing an electron beam into the chamber and trapping all ions formed by electron impact; the contents of the trap are then subjected to mass analyses. For the ICR spectrometer, mass analysis is often performed by exciting the ions with a radio frequency pulse, observing the resulting current induced in plates of the cell

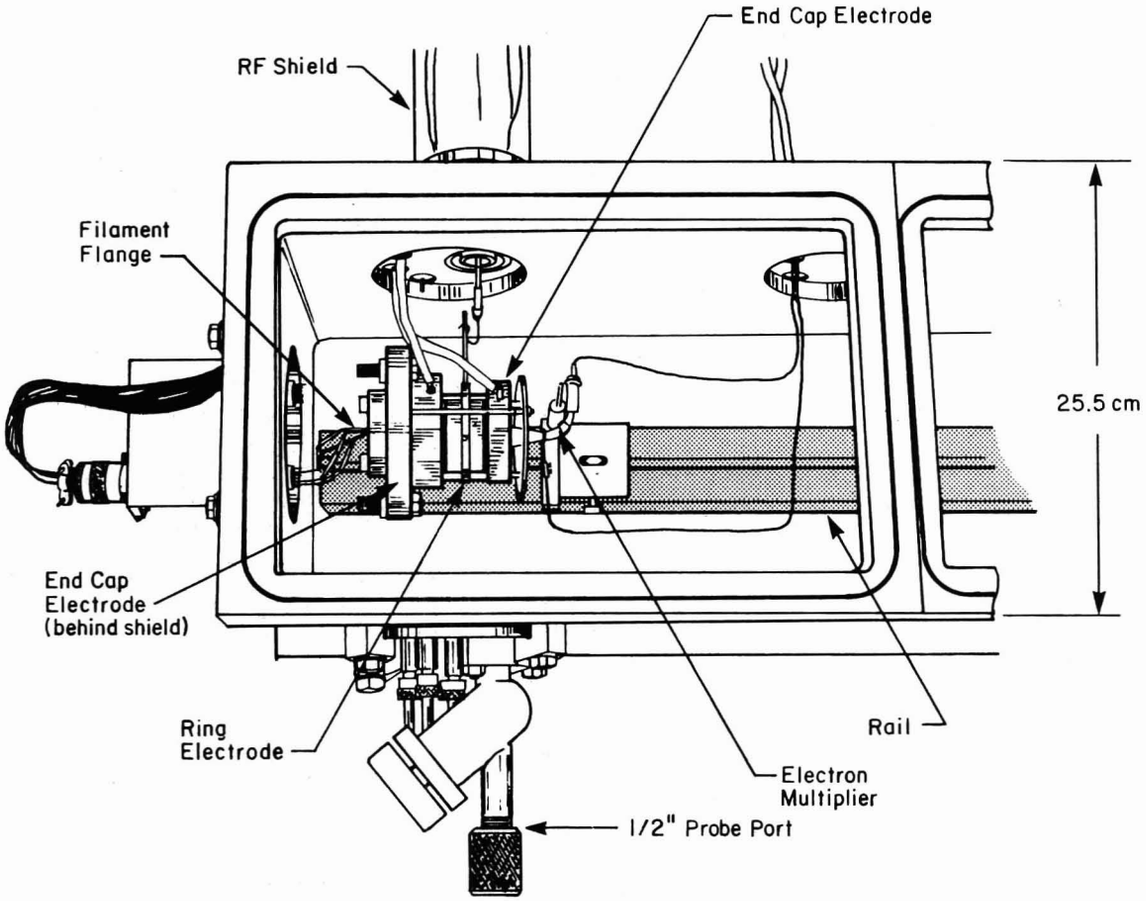

Figure 2. Ion trap mounted on an ion optical rail in a vacuum manifold which allows easy access to components.

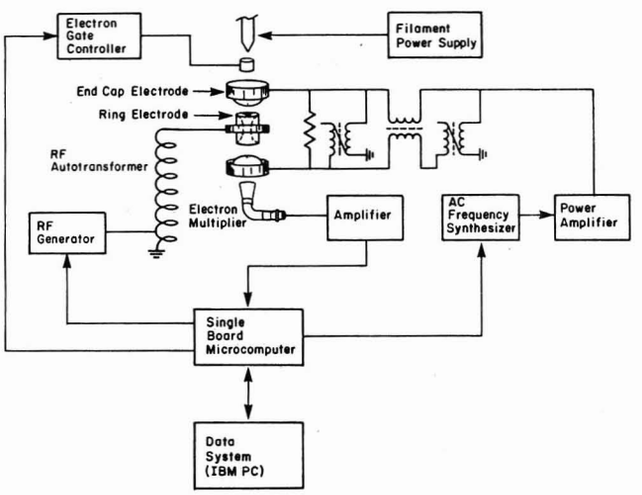

Figure 3. Ion-trap control system including the supplementary ac supply needed for MS/MS experiments.

by the motion of the ions, and recovering the spectrum of frequencies present (and thus the mass spectrum) via the Fourier transform (*10–12*). In the quadrupole ion trap, mass analysis is performed by sequentially ejecting ions from the trap and detecting them with an electron multiplier. In both types of spectrometers, the mass analysis step may be modified or replaced by a step that removes unwanted ions from the trap and allows only those ions of a narrow mass range to remain trapped. These ions may then be allowed to undergo some reaction such as CAD in which collision with a gas induces fragmentation, and the products of this reaction may be subjected to mass analysis to yield a daughter MS/MS spectrum.

In comparison, MS/MS spectrometers in which the stages of mass analysis are performed in different mass analyzers must convey the ions from one mass analyzer to the next. While both classes of MS/MS spectrometers are capable of producing daughter spectra, there are important differences in the other types of MS/MS scan modes that are possible. For example, FT-ICR and quadrupole ion-trap spectrometers can, in principle, perform any number of sequential steps of reaction and ion isolation (MS^n). Spectrometers that use separate mass analyzers are limited by the number of stages of mass analysis that are present in the instrument. However, such spectrometers are capable of two important experiments, the parent scan and the neutral loss scan (*13*), that are not directly accessible in the ICR or quadrupole ion trap spectrometer.

Ion Motion in the Quadrupole Ion Trap. The theory of ion motion within conventional quadrupoles and within quadrupole ion traps was presented by Paul and co-workers in their early papers describing the devices (*6*, *7*, *14*). Later authors have also presented this theory (*15*, *16*). Essentially, it is possible to generate a parametrized stability diagram (Figure 5) that characterizes the solutions to the derived equations of motion. The coordinates of this stability diagram are parameters a_z and q_z such that $a_z = -8zU/mr_0^2\Omega^2$ and $q_z = -4zV/mr_0^2\Omega^2$, where U is the direct current voltage, V is the radio frequency peak voltage level, r_0 is the radius of the trap, Ω is the angular frequency of the radio frequency voltage, m is the mass of the ion, and z is the charge of the ion.

The most important characteristic of the trajectory is whether it is stable or unstable; if the a_z, q_z, pair falls within the region indicated (Figure 5), the trajectory can be stable (although an unfavorable initial velocity and position may produce an amplitude so large that the ion strikes an electrode). Outside the region indicated, the trajectory is unstable regardless of the initial velocity and position. Another important characteristic of the trajectory is the component frequencies in the axial and radial directions. The parameters

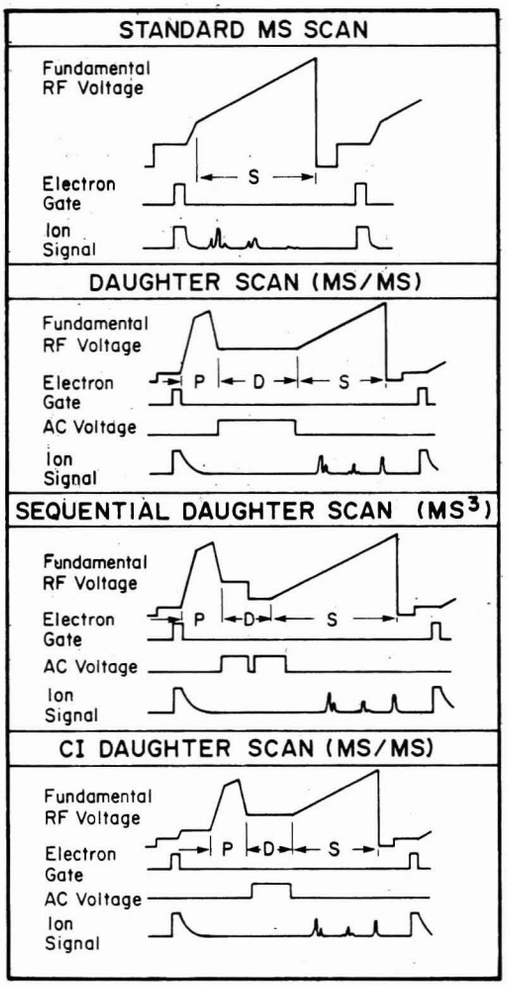

Figure 4. Ion-trap scan programs used to obtain the types of spectra indicated. The selection of the parent ion occurs in the interval P, daughters are generated during the period D, and the mass analysis scan is indicated as S.

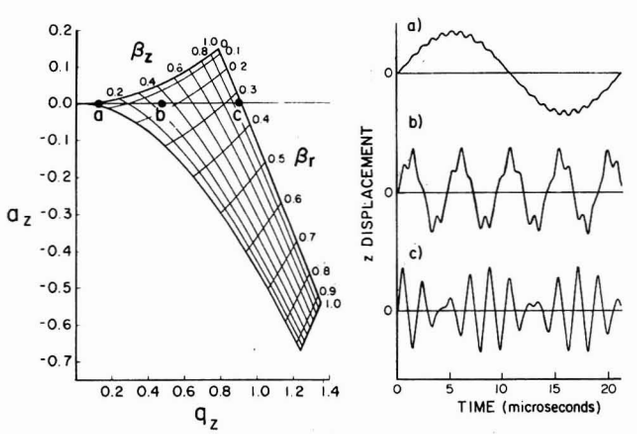

Figure 5. Stability diagram (left) and calculated trajectories (right) of three ions trapped using no dc offset (i.e. $a_z = 0$) and the same ring electrode voltage. The displacement from the center along the axis of the trap (z-coordinate, Figure 1) is plotted vs. time: (a) m/z 502, $q_z = 0.123$, $\beta_z = 0.087$; (b) m/z 119, $q_z = 0.519$, $\beta_z = 0.390$; (c) m/z 69, $q_z = 0.895$, $\beta_z = 0.892$.

β_z and β_r, which indicate these frequencies, are obtained from a_z and q_z by calculation (*16*) or from the stability diagram. The component frequencies for each direction are given by $f_s = (s + \beta/2)\Omega$, where $s = 0, \pm1, \pm2, \ldots$ The relative contribution of each frequency component may also be calculated.

Representative trajectories for trapped ions of different mass (under fixed conditions and with no dc voltage) are shown in Figure 5. In particular, the axial components of the trajectories for ions of m/z 502, 119, and 69 are shown for the case where the rf voltage is adjusted to bring m/z 68 to the boundary between stability and instability. The q_z parameter is then easily calculated for any other m/z value by using the known q_z value (0.908) for the boundary of the stability region where $q_z/0.908 = (m/z)/68$. Since β_z may be determined once q_z is known, the frequency components of the trajectory are also readily determined. Examination of the trajectories of Figure 5 shows that the fundamental frequency ($s = 0$) makes the most important contribution to the frequency spectrum; at low values of β_z the contribution of the higher order frequencies ($s > 0$) is relatively slight but their importance increases with β_z. Most importantly, at larger m/z values, q_z is lower, β_z is lower, and the ions move more slowly.

An important consequence for MS/MS experiments of this dependence of β_z (and thus the fundamental frequency) on the q_z value is the measure of control it permits over the average energy deposited in a collision of an ion and a neutral compound. At higher q_z values collisions are more energetic, provided the amplitudes of the oscillations are the same. However, more energetic collisions are achieved at the expense of the mass range of the fragment ions that can be trapped for subsequent mass analysis. In the example of Figure 5, while m/z 502 has a low q_z value, all fragment ions of m/z greater than 68 can be trapped. If the q_z value of m/z 502 is increased (by increasing V) so that the ion trajectory resembles Figure 5b, more energetic collisions are possible but only ions of m/z greater than 287 can be trapped. Fragments of lower m/z will be lost from the trap.

Another way of increasing the energy deposition is to increase the amplitude of the trajectories. This can be achieved by applying between the end-cap electrodes a small sinusoidal voltage that is of the same frequency as the axial component of motion of the parent ion. This supplementary voltage excites the parent ion to a larger trajectory. To avoid confusion with the radio frequency voltage on the ring electrode, this supplementary voltage will be referred to as the ac voltage. The frequency, amplitude, and duration of the ac voltage can all be shown to affect the nature of the MS/MS spectrum. Several conference proceedings have shown examples of these MS/MS capabilities (*17–19*).

Fischer (*6*, *7*) used a small ac voltage applied across the end-caps of an ion trap for the resonance detection of ions. Similarly, Paul et al. (*14*), applied a small ac voltage across opposing electrodes of a quadrupole mass filter to selectively remove ions by resonance ejection. In both cases, the perturbation produced in the field within the quadrupole device was treated theoretically by assuming a superimposed homogeneous field. Fischer pointed out that this approximation leads to some simple generalizations about the effect of the supplementary ac voltage on the ion trajectories (*7*):

(a) Resonance occurs if the frequency of the ac voltage coincides with any of the frequencies $(s + \beta/2)\Omega$.

(b) During resonance, the average amplitude of the trajectory increases linearly with time.

(c) As the amplitude increases, all frequency components increase equally, not just the frequency component that coincides with the ac frequency.

(d) The rate of increase in amplitude is proportional to the relative contribution of the frequency component that coincides with the ac frequency.

In addition, the rate of increase in the amplitude is proportional to the ac voltage and inversely proportional to the mass-to-charge ratio of the ion.

While the simple theory only treats the case of an isolated ion, the general, qualitative results are nevertheless useful in understanding the effect of the ac voltage on ion trajectories under the actual experimental conditions in which a high

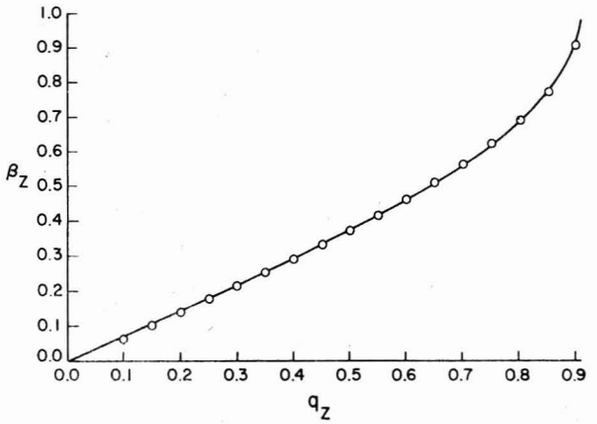

Figure 6. Comparison of theoretical (line) and experimental (circles) values for the stability parameter β_z as a function of q_z, which is proportional to the main rf voltage. Data are for the molecular ion of chrysene in the presence of a millitorr of helium.

pressure (1 mtorr) of helium is present. For example, the fundamental frequency may be determined experimentally at a particular rf voltage by determining the ac frequency (β_z) at which particular ions are ejected from the trap when using the lowest possible ac voltage. Figure 6 compares a typical set of such determinations (circles) with theoretical values (smooth curve); within the region of q_z values which are most useful for MS/MS work (0.2–0.8), the experimentally determined fundamental frequencies agree (within experimental error) with the theoretical values. Significant deviations do appear at the lower q_z values, however. Similarly, the nonfundamental frequencies may be determined and are found to agree well with the theoretical values. Larger voltages must be used to achieve the same ejection time with these higher frequencies, as expected.

Effects of Experimental Parameters on MS/MS Spectra. The presence of helium does have some important consequences. Figure 7 shows daughter spectra of the molecular ion of nitrobenzene recorded in the presence and the absence of helium. The results are surprising. First, the addition of helium has a small but favorable effect in improving the resolution, but it actually causes a decrease in the abundance of the daughter ion of m/z 93 (compare scans a and b in Figure 7). This decrease may in part be due to collisional deexcitation of internally excited molecular ions which would otherwise undergo unimolecular dissociation. Alternatively, the helium may tend to damp the trajectory of the parent ion without inducing fragmentation, so that the mean velocity of the parent ion decreases so much that all collisions (with helium and with nonionized nitrobenzene) are ineffective at producing fragments.

The molecular ions can be given increased kinetic energy by excitation from a supplementary ac source. In the absence of helium gas (Figure 7c) this broadens the peak associated with the parent ion without leading to significant fragmentation. However, in the presence of helium, collisionally activated dissociation occurs and the daughter spectrum (Figure 7d) shows characteristic fragments at m/z 93 and 65. The parent ion is completely removed, the isotopic peak at m/z 124 forming the remaining high-mass signal. These results are typical of those for other systems, and one concludes that, in the presence of helium, the use of a supplementary ac voltage (in resonance with the motion of a mass-selected ion) is an effective means of obtaining MS/MS spectra. Note that two separate means are used to select the parent ion. First, the parent ion is selected by scanning the ring electrode (rf) voltage so as to empty the trap of lower mass ions and, second, the parent ion is brought into resonance by using the supplementary ac voltage.

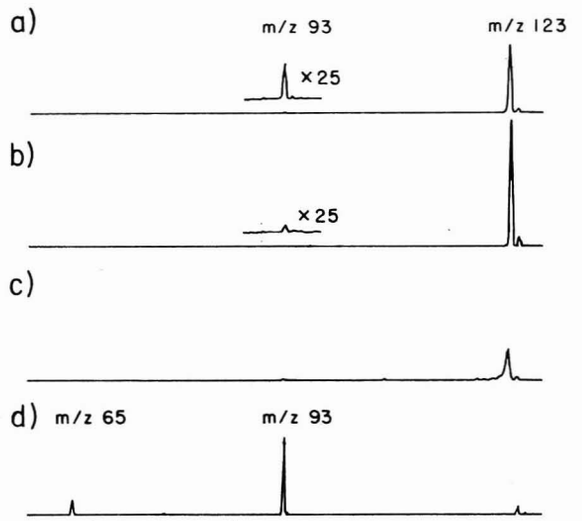

Figure 7. MS/MS daughter spectra of ionized nitrobenzene (m/z 123) (a) without helium and without application of the supplementary ac voltage, (b) with helium and without the ac voltage, (c) without helium and with the ac voltage, and (d) with helium and with the ac voltage.

The preceding observations, including the considerations regarding ion motion in the trap, lead to some simple guidelines about the manipulation of the daughter (MS/MS) spectrum through the choice of the scan parameters. Firstly, the q_z value (at which the parent ion is trapped) influences the collision energy by determining the frequency of the ion motion. The voltage of the ac excitation signal also influences the collision energy by affecting the rate of increase in the amplitude of the parent ion trajectory which affects the mean velocity of the ions. The interaction between these two effects is complex. Secondly, as Fischer showed (*7*), excitation at a resonant frequency other than the fundamental frequency will require a larger voltage to achieve the same rate of increase in the amplitude of the trajectory, but the relative contribution of each frequency component will be the same as if the fundamental frequency were excited. Lastly, before the ac voltage is applied, the parent ions are in trajectories of low amplitude; by selecting a low ac voltage the average velocity of ions can be made to increase so gradually that low-energy dissociations are promoted.

The efficiency of CAD in the ion trap is frequently quite high as is illustrated in Figure 7. Following previous practice (*11*) with MS/MS instruments with separate mass analyzers, the overall CAD efficiency is defined as the sum of the fragment ion abundances measured after mass analysis divided by the abundance of the mass-analyzed parent ion prior to dissociation. Since all spectra in Figure 7 are recorded by using the same detector sensitivities, it is clear that the total fragment ion abundance is approximately equal to the parent ion abundance and that the CAD efficiency approaches 100%.

Energy Deposition. *n*-Butylbenzene was ionized by electron impact and its CAD in the ion trap was examined to obtain information on the internal energy deposited in the parent ion (m/z 134). The ratio of the daughter ions of m/z 91 and 92 has been used repeatedly to gauge internal energy deposition in experiments ranging from photodissociation (*20*, *21*) through collisional activation (*22*, *23*) and charge exchange (*24*).

By the use of a q_z value of 0.36 as shown in Table II, ionized *n*-butylbenzene is dissociated, giving m/z 91 and 92 in the ratio 1:2. Since the ions examined in this study do not show significant ion dissociation in the absence of excitation, this ratio can be used directly to estimate that most molecular ions, after excitation, have internal energies between 1 and 2 eV (the activation energies for the two dissociations are 1.1 and 1.7 eV, respectively (*21*)). A value for the average internal energy

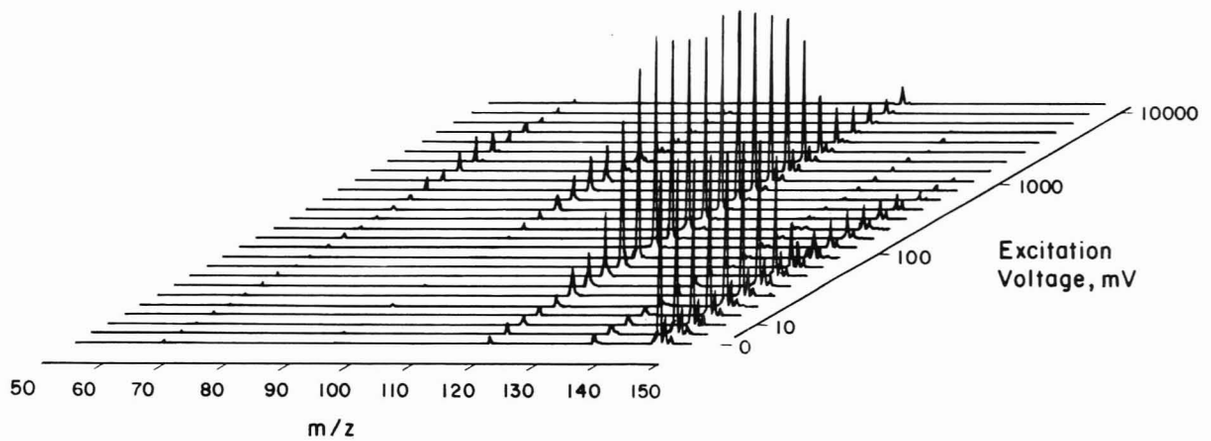

Figure 8. MS/MS daughter spectra of ionized tetraethylsilane. The scan program of Figure 4b was used with all parameters being constant except that each spectrum was acquired with a different excitation ac voltage.

Table II. Ratios of [91⁺]/[92⁺] from the Dissociation of the Molecular Ion of Butylbenzene

ac voltage, V	q_z	β_z	[91⁺]/[92⁺]
2.7	0.36	0.26	0.069
3.8	0.36	0.26	0.50
1.6	0.60	0.46	0.36
2.5	0.60	0.46	1.7
14.4	0.60	0.46	4.2

of the activated ions of about 2 eV also is consistent with ratios of these fragment ion abundances published for charge exchange (*24*).

The [91⁺]/[92⁺] ratio may be varied over a wide range by varying the ac voltage and frequency β_z (by working at different q_z values). The parent ion could be efficiently converted into 92⁺ at the lower q_z value, with very little 91⁺ being produced. At the higher q_z value, the production of 91⁺ could be promoted. As the ac voltage was increased, a ratio of [91⁺]/[92⁺] larger than 4:1 could be produced, but the absolute intensity of the two daughter ions decreased as an increasing fraction of the ions were rapidly ejected from the trap; under these conditions the parent may simply be ejected before daughters are produced, or the daughter ions may be created with initial conditions of velocity and position that prohibit trapping. This behavior of MS/MS in the trap appears to be general: a fragment ion associated with a low-energy process may be produced in excellent yield; fragment ions associated with higher energy processes may also be produced, but often at the expense of the efficiency of the production of detectable fragments. Note that the ratio of [91⁺]/[92⁺] of 4.2:1 approaches the highest value (7:1) recorded for CAD (*22–24*); based on charge exchange (*24*) and calculation (*20*) such ratios correspond to internal energies of the excited *n*-butylbenzene molecular ions in excess of 5 eV. However, since most of the ions are ejected from the trap when such high ratios are observed, it cannot be concluded that this is the average internal energy of the excited ions.

A rough measure of the *distribution* of internal energies associated with a population of internally excited ions can be obtained when one knows the activation energy for each fragmentation reaction and records the fragment ion abundances. In the simple case where a linear sequence of reactions is available to the selected ion, the abundance of each fragment ion represents the probability that the excited parent ion has an internal energy sufficient to access its activation energy but insufficient to cause more extensive dissociation. By considering the series of fragment ions, the energy distribution of the initially excited ion population is approximated. Evidence has been given (*25*) that this is a useful method of characterizing distributions of internal energy and of following the effects of experimental conditions on them.

The fragmentation of the tetraethylsilane molecular ion was chosen to study the effect of the operating parameters on internal energy deposition. Its main fragmentation pathway consists of the following reaction sequence of known activation energies (ϵ_0) (*17*, *18*).

$$[Si(C_2H_5)_4]^{\cdot+} \xrightarrow{\epsilon_0 = 0.5\ eV} [Si(C_2H_5)_3]^+ \xrightarrow{\epsilon_0 = 2\ eV}$$

m/z 144 *m/z* 115

$$[HSi(C_2H_5)_2]^+ \xrightarrow{\epsilon_0 = 3.5\ eV} [H_2Si(C_2H_5)]^+$$

m/z 87 *m/z* 59

A study of the effect on the CAD process of varying the excitation voltage while all other parameters remain constant is shown in Figure 8. When no ac voltage is applied, only a small amount of fragmentation occurs, as already noted. At an ac voltage of 100 mV the parent tetraethylsilane ion is efficiently converted into m/z 115. At higher voltages, fragments corresponding to more energetic processes appear. Also, unit mass specificity for the excitation of the parent ion is achieved at the lower voltages, but not at the higher voltages. At the highest voltages used the number of ions detected is rather small, probably because of the rapid ejection of ions from the trap.

These data indicate that the distribution of internal energies associated with the excited molecular ions, which lead to detectable fragments, broadens as the ac voltage increases. Low-energy processes still occur but those of higher energy accompany them. For example, the fragment ions of m/z 115, 87, and 59, which are significant products at 1000 mV of excitation, require internal energies of 0.5, 2.0, and 3.5 eV, respectively.

Figure 9 shows the effect on the same daughter spectrum, of varying q_z while keeping the other parameters constant. Changes in q_z are made by varying the rf voltage while maintaining a constant ac excitation voltage. At very low q_z, the parent ion is ejected from the trap without producing fragments. At somewhat larger q_z values, only the m/z 115 fragment is produced. The fragments corresponding to more energetic processes begin to appear at a q_z value of about 0.2. Note that the q_z value of the parent ion determines the minimum mass of the daughter ion that can be trapped. As q_z is increased, the energy deposition increases, but the mass range is diminished so that m/z 87 and 59 appear at intermediate q_z values but are not recorded at high q_z values.

The extent of conversion of parent ions to fragment ions is also dependent upon the duration of the excitation. For example, at an ac voltage of 50 mV, the dissociation of the parent ion required an excitation time of 10 ms (Figure 10), but with an ac voltage of 160 mV, the reaction was complete in about 2.1 ms. In both experiments, the parent ion is

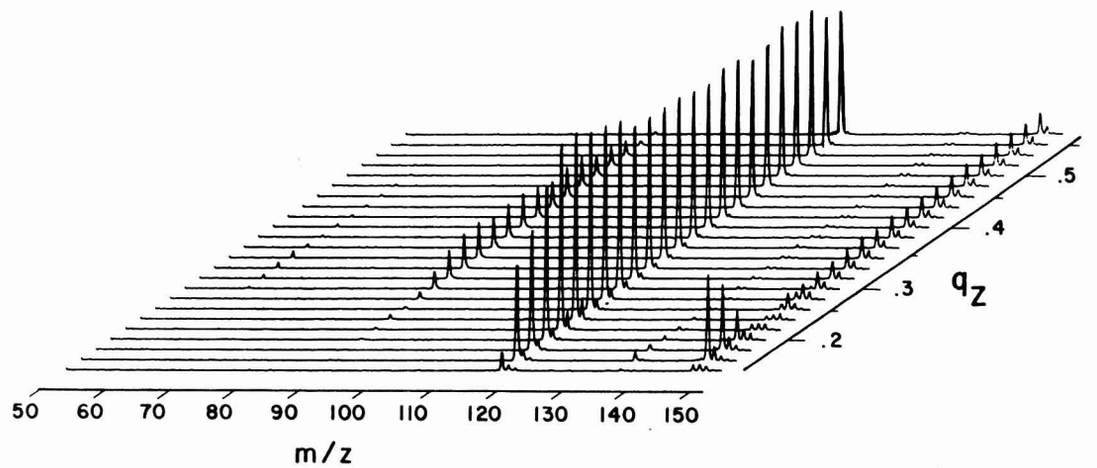

Figure 9. MS/MS daughter spectra of ionized tetraethylsilane. The scan program of Figure 4b was used with all parameters being constant except that each spectrum was acquired at a different q_z value. The ac voltage was 500 mV (pp) for all spectra.

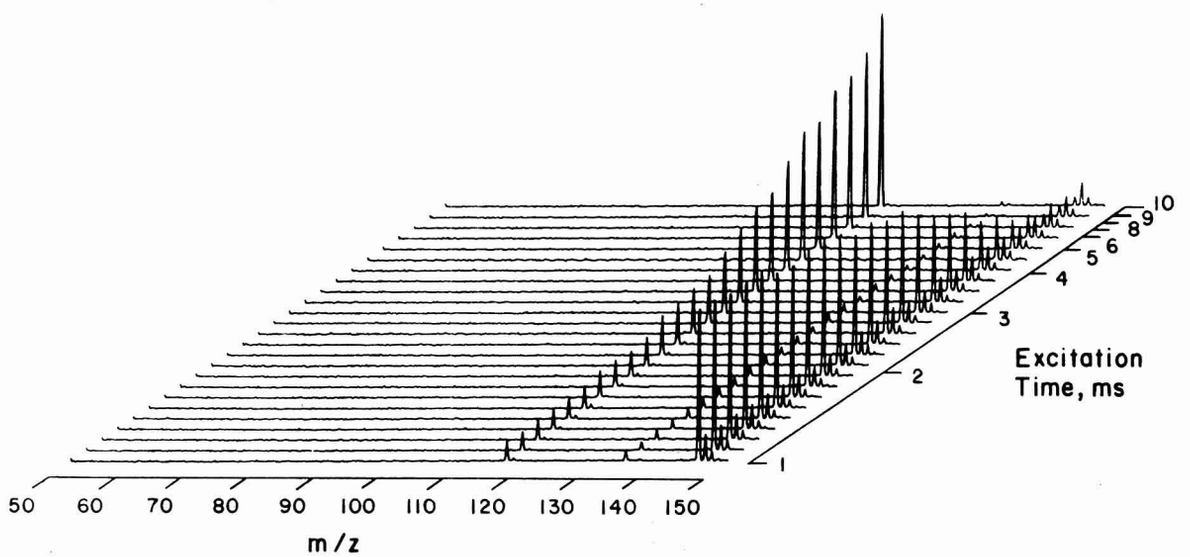

Figure 10. Time course of the decomposition of the molecular ion of tetraethylsilane. The scan program of Figure 4b was used with all parameters being constant except that each spectrum was acquired with a different duration of the application of the ac excitation voltage. The ac voltage is 50 mV (pp).

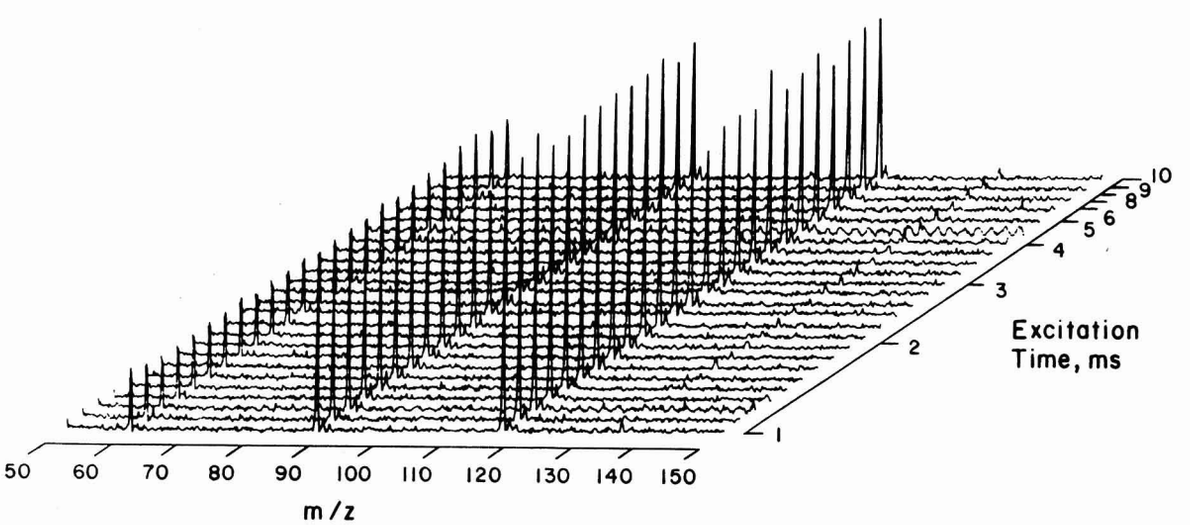

Figure 11. Time course of the decomposition of the molecular ion of tetraethylsilane. The conditions are the same as for Figure 10, except that an ac voltage of 5000 mV (pp) was used. The vertical scale for this plot is increased over that used for Figure 10 because of the diminished peak height due to the ejection of ions from the trap (cf. Figure 8).

converted quantitatively into fragments. At an ac voltage of 5000 mV, all parent ions disappeared within 1 ms (Figure 11), but the CAD process was no longer 100% efficient.

The daughter spectrum of tetraethylsilane molecular ion is dominated by the molecular ion and the dissociation products m/z 115, 87, and 59. However, even in this simple system ion/molecule reactions occur and their products appear in the daughter spectrum, almost always in very low abundance. Noteworthy among the products of these reactions is m/z 133, formally due to addition of water to triethyl-

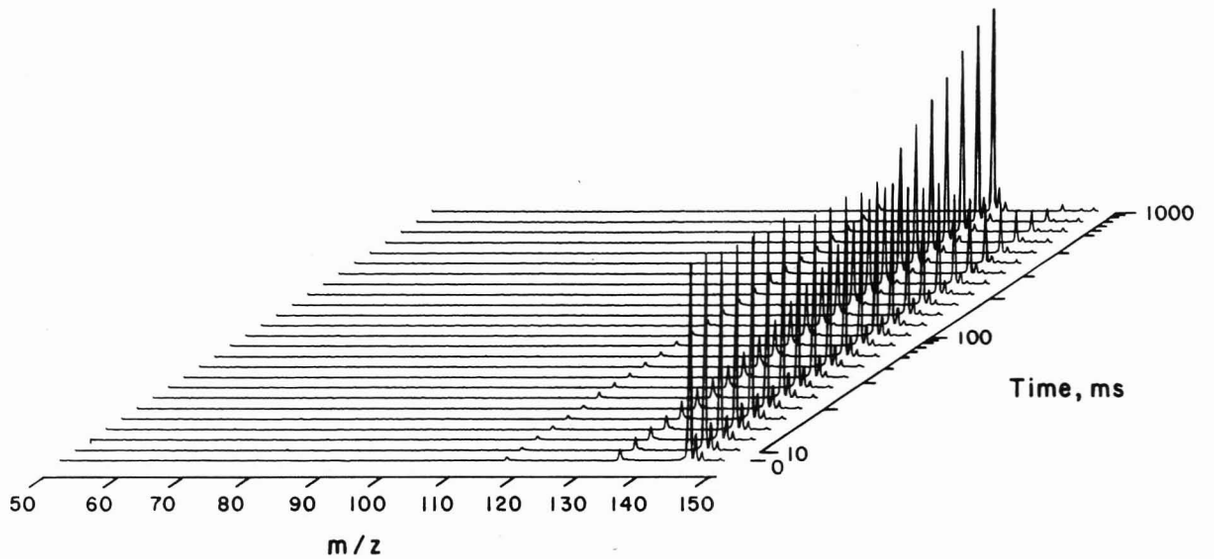

Figure 12. Reaction of the molecular ion of tetraethylsilane with adventitous water. The scan program shown in Figure 4b was used, except that no excitation voltage was used.

siliconium ion, m/z 115. This ion appears in the spectra presented above, in which the effects of experimental variables upon the dissociation of tetraethylsilane are examined. In the absence of a supplementary excitation voltage, little dissociation occurs and the ion/molecule reactions can be studied in detail (Figure 12). As the delay time between ion selection and product ion analysis is increased, products due to ion/molecule reactions increase in abundance. After a 1-s delay, the entire initial ion current has been quantitatively converted into m/z 133 product ions. Obviously, the presence of appropriate neutral reagent gases allows ion/molecule reactions to be efficiently promoted and studied in the ion trap by using MS/MS scan techniques.

Other Modes of Operation. While the emphasis of this study is on the energization and subsequent dissociation of ions trapped in a three-dimensional quadrupole field, additional experiments become possible with the microprocessor-controlled ac generator. The ion trap could be cleared of undesired ions by sweeping the frequency of the ac generator through the approximate range. Alternatively dc voltage offsets may be used for this purpose. In particular, the use of a dc offset during the ionization period has proven to be useful when the desired parent ion is present as a small proportion of the total number of ions.

Successive ions may be dissociated (MS^n) by changing the frequency of the excitation voltage during the experiment or by changing the ring rf voltage so that first a parent ion and then its daughter ion are brought into resonance at the same frequency (Figure 4c). In the experiment shown the daughter ions are not isolated so ions may be present in the sequential daughter spectrum that are not due to two steps of CAD. To demonstrate the selective daughter scan capability, protonated dimethylmorpholinophosphoramidate (m/z 196) was generated under conditions that promote ion/molecule reactions (vide supra). This ion was either dissociated under CAD conditions to yield m/z 152 as the major fragment or else the scan program of Figure 4c was used to further fragment m/z 152, yielding a sequential daughter spectrum. This simple procedure demonstrates the feasibility of successive steps of MS/MS, but a more complex experiment that could isolate each product would be more desirable.

Applications. The use of chemical ionization in conjunction with the mass selective instability mode of operation has recently been described (*26*, *27*). Reagent gas is introduced at a low pressure. Then time is allowed for the formation of reagent gas ions, and for those ions to react with neutral analyte; the MS/MS part of the experiment is then performed as usual. Figure 13 compares an ion-trap CI mass spectrum of amphetamine with a CIMS/MS daughter spectrum of protonated amphetamine (mz 136) obtained by using the scan program of Figure 4d. Note that the degree of fragmentation of the protonated molecule can be controlled by the time of application and amplitude of the supplementary ac voltage.

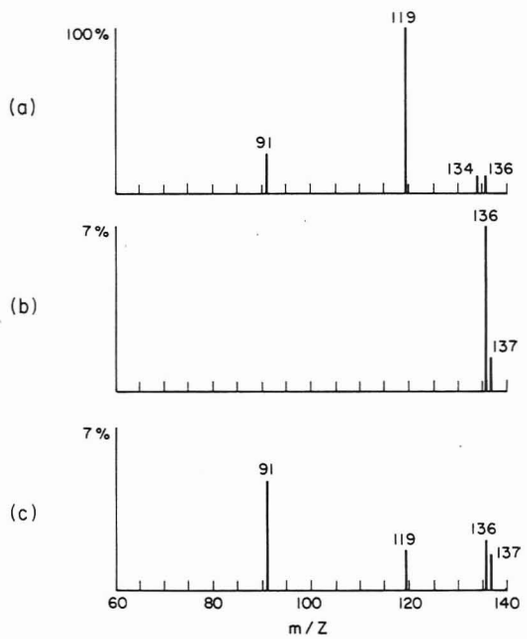

Figure 13. CIMS/MS of amphetamine (a) CI scan without MS/MS, (b) the scan program of Figure 4d, but without an excitation ac voltage, and (c) the scan program of Figure 4d, but with an ac voltage to excite m/z 136.

Photodissociation can also be performed in conjunction with the mass selective instability mode of ion-trap operation. The scan program of Figure 4b was used except that the ac voltage was not used; instead light from a pulsed Nd:YAG laser was admitted into the ion trap during the excitation period (*28*). In favorable cases complete conversion of the parent ion into fragment ions was achieved.

CONCLUSIONS

The most important observation made in this study is that very efficient CAD may be achieved in an ion trap. The scanning procedure developed here provides a practical me-

thod of producing MS/MS spectra. These spectra show a strong dependence on the scan parameters used (and by implication, the energy deposition) so that care must be exercised in choosing and maintaining particular instrumental parameters. This is a consequence of the complex ion motion in the trap and hence the distribution of velocities in the ion population. The possibility of studying ion/molecule reactions adds further information and complexity. However, ion trap MS/MS spectra can be made highly reproducible, and the three principal factors that determine the appearance of these spectra, q_z, supplementary ac voltage, and ac voltage duration are readily controlled.

LITERATURE CITED

(1) *Tandem Mass Spectrometry*; McLafferty, F. W., Ed.; Wiley: New York, 1983.
(2) Harris, R. M.; Beynon, J. H. In *Gas Phase Ion Chemistry*; Bowers, M. T., Ed.; Academic: New York, 1984; Vol. 3, Chapter 19, pp 100–127.
(3) Kenttämaa, H. I.; Wood, K.; Busch, K. L.; Cooks, R. G. *Org. Mass Spectrom.* **1983**, *18*, 561–567.
(4) Beynon, J. H.; Caprioli, R. M.; Baitinger, W. E.; Amy, J. W. *Org. Mass Spectrom.* **1970**, *3*, 455.
(5) Kinter, M. T.; Bursey, M. M. *J. Am. Chem. Soc.* **1986**, *108*, 1797.
(6) Fischer, E. *Z. Phys.* **1959**, *156*, 1–26.
(7) Fischer, E. Doctoral Dissertation, University of Bonn, 1958.
(8) Stafford, G. C., Jr.; Kelley, P. E.; Syka, J. E. P.; Reynolds, W. E.; Todd, J. F. J. *Int. J. Mass Spectrom. Ion Processes* **1984**, *60*, 85–98.
(9) Wineland, D. J.; Itano, W. M. *Adv. At. Mol. Phys.* **1983**, *19*, 135.
(10) Comisarow, M. B.; Marshall, A. G. *Chem. Phys. Lett.* **1974**, *25*, 282–283.
(11) Wanczek, K. P. *Int. J. Mass Spectrom. Ion Processes* **1984**, *60*, 11–60.
(12) Lande, D. A., Jr.; Johlman, C. L.; Brown, R. S.; Weil, D. A.; Wilkins, C. L. *Mass Spectrom. Rev.* **1986**, *5*, 107–166.
(13) Yost, R. A.; Enke, C. G. *Anal. Chem.* **1979**, *51*, 1251A–1264A.
(14) Paul, W.; Reinhard, H. P.; von Zahn, V. *Z. Phys.* **1958**, *152*, 143–182.
(15) Lawson, G.; Todd, J. F. J.; Bonner, R. F. *Dyn. Mass Spectrom.* **1976**, *4*, 39–81.
(16) Dawson, P. H. *Quadrupole Mass Spectrometry*; Elsevier: New York, 1976; Chapters 2–3.
(17) Kelly, P. E.; Stafford, G. C., Jr.; Syka, J. E. P.; Reynolds, W. E.; Louris, J. N.; Amy, J. W.; Todd, J. F. J. 33rd Annual Conference of Mass Spectrometry and Allied Topics, San Diego, CA, 1985; p 707.
(18) Louris, J. N.; Brodbelt, J.; Cooks, R. G.; Stafford, G. C., Jr.; Syka, J. E. P. 34th Annual Conference of Mass Spectrometry and Allied Topics, Cincinnati, OH, 1986; p 685.
(19) Kelley, P. E.; Syka, J. E. P.; Ceja, P. C.; Stafford, G. C., Jr.; Louris, J. N.; Grutzmacher, H. F.; Kuck, D.; Todd, J. F. J. 34th Annual Conference of Mass Spectrometry and Allied Topics, Cincinnati, OH, 1986; p 963.
(20) Griffiths, I. W.; Harris, F. M.; Mukhtar, E. S.; Beynon, J. H. *Int. J. Mass Spectrom. Ion Phys.* **1981**, *41*, 83.
(21) Chen, J. H.; Hayes, J. D.; Dunbar, R. C. *J. Phys. Chem.* **1984**, *88*, 4759–4764.
(22) McLuckey, S. A.; Sallans, L.; Cody, R. B.; Burnier, R. C.; Verma, S.; Freiser, B. S.; Cooks, R. G. *Int. J. Mass Spectrom. Ion Phys.* **1982**, *44*, 215.
(23) McLuckey, S. A.; Ouwerkerk, C. E. D.; Boerboom, A. J. H.; Kistemaker, P. G. *Int. J. Mass Spectrom. Ion Phys.* **1984**, *59*, 85.
(24) Nacson, S.; Harrison, A. G. *Int. J. Mass Spectrom. Ion Processes* **1985**, *63*, 325.
(25) Wysocki, V. H.; Kenttämaa, H. I.; Cooks, R. G. *Int. J. Mass Spectrom. Ion Processes* in press.
(26) Kelley, P. E.; Stafford, G. C.; Syka, J. E. P.; Reynolds, W. E.; Louris, J. N.; Todd, J. F. J. *Adv. Mass Spectrom.* **1985**, *10*, 869–870.
(27) Brodbelt, J. S.; Louris, J. N.; Cooks, R. G. *Anal. Chem.*, in press.
(28) Louris, J. N.; Brodbelt, J. S.; Cooks, R. G. *Int. J. Mass Spectrom. Ion Processes*, in press.

RECEIVED for review December 23, 1986. Accepted March 19, 1987. This work was supported by the National Science Foundation CHE 84-08728.

Focused, Rasterable, High-Energy Neutral Molecular Beam Probe for Secondary Ion Mass Spectrometry

Anthony D. Appelhans, James E. Delmore,* and David A. Dahl

Idaho National Engineering Laboratory, EG&G Idaho, P.O. Box 1625, Idaho Falls, Idaho 83415

Beams of focused (~0.5 mm diameter at 2.5 m), rasterable, 3–17 keV neutral SF_6 molecules produced via autoneutralization from the corresponding anion have been demonstrated to be effective for producing secondary ions from electrically insulating specimens (e.g., Mylar, Teflon) without sample charging problems. Secondary ion currents measured with the quadrupole were ~10^{-14} A (10^5 counts/s equivalent) for major peaks when using a picoampere (neutral equivalent) level primary beam which was more than adequate to characterize the specimens. No contaminating effects from S or F were seen in the spectra. The results demonstrate the feasibility of using the autoneutralizing SF_6 fast neutral source for a variety of static secondary ion mass spectrometry applications that require electrically neutral primary particles focused into a near-parallel small diameter beam (over distances of 18 cm to several meters). Applications could include the analysis of polymers, ceramics, and biospecimens or the generation of ions inside the magnetically confined cell of an Fourier transform ion cyclotron resonance mass spectrometer.

Secondary ion mass spectrometry (SIMS) and fast atom bombardment mass spectrometry (FABMS) have found many distinct areas of application in recent years (*1*). A variety of ion and neutral atom sources have been developed for these applications, ranging from micrometer-dimensioned ion beams capable of imaging to a variety of schemes for producing broad, unfocused beams of neutral atoms. However, one area that has seen little development is that of focused (as opposed to collimated), rasterable neutral atom/molecule beams.

There are several areas of applicability for such a primary beam probe. The principal application of static SIMS/FABMS has been the study of large, fragile molecules most of which are electrically nonconducting. A focused, rasterable, small diameter (millimeters and less) neutral primary beam capable of producing easily measurable secondary ions at low (nondamaging) fluence would simplify analysis of small areas (interfaces, boundary regions) on polymers, ceramics, and biological specimens. Extending this to spatial analysis/imaging requires a microfocused neutral beam that can be rastered over the sample. This type of imaging has recently been demonstrated by Eccles et al. (*2*), although using an approach substantially different from the one taken in this study.

In addition to the obvious applications of a focused neutral beam for SIMS there is another area where such a beam has significant potential application: sputtering of secondary ions from samples in the magnetically confined ion cell of Fourier transform ion cyclotron resonance (FTICR) mass spectrometers. The magnetic and electric fields of the FTICR cells make it difficult to inject a beam of charged particles into the

0003-2700/87/0359-1685$01.50/0 © 1987 American Chemical Society

ion trapping region. Although methods employing tandem quadrupole ion beam transmission systems have been used experimentally (*3*) to generate secondary ions in an ICR cell, it necessitates a complex apparatus and is plagued by sample charging problems (*4*) inherent to using ions as the primary sputtering beam. Current commercial FAB sources do not have sufficiently fine focusing for such applications and the high gas load imposed by charge-exchange neutralization cells (*2*) is unacceptable for the high vacuum requirements of FTICR. A pulsed, rasterable, near-parallel focused beam of high-energy neutral particles, unaffected by magnetic and electric fields and generated in a differentially pumped primary source at a relatively low source pressure ($\sim 10^{-6}$ torr), should prove an ideal probe for producing secondary ions in FTICR systems.

To produce such a beam, we have applied a unique neutralization mechanism: autoneutralization, the spontaneous ejection of an electron from an anion leaving a neutral molecule (*5*, *6*). The specific ion being used is the sulfur hexafluoride anion, a significant fraction of which autoneutralizes in 2–20 μs. Sulfur hexafluoride has a unique combination of properties: a very high electron capture cross section, which greatly simplifies the production of the gas phase anion, and a relatively low electron affinity (~1 eV), which expedites the detachment of electrons from the gas phase anions that are in certain excited quantum states. Earlier studies in our laboratory (*6*) have shown that there are several autoneutralizing excited states, corresponding to different excited quantum states, and that about 35–40% of the ions undergo the second step of the following sequence:

$$SF_6 + e^- \rightarrow SF_6^{-*} \xrightarrow{k} SF_6 + e^- \qquad (1)$$

where $1/k$, the mean lifetime, is 10–20 μs. This makes it possible to focus and accelerate the SF_6^- ions prior to autoneutralization and still achieve adequate neutralization within a reasonable length flight tube (~18 cm) to yield a usable neutral beam. The composite lifetime is well suited to accelerating the anions to energies ranging from 3 keV up to 25 keV (or more). Recent unpublished results from this laboratory have shown that the energy state distribution can be shifted toward the shorter lived states (~2 μs) by heating the gas, thus improving neutralization efficiency. The mass of the ejected electron is of the order of 10^{-4} that of the ion, thus there is little translational energy transferred to the molecule during neutralization. This permits the molecules to maintain focus as neutralization occurs.

There are both advantages and disadvantages to the autoneutralization approach. The advantages are the following: (1) the particles can be accelerated to much higher energies (eV/amu) than practical in conventional FAB sources with minimum loss of neutralization efficiency; (2) the autoneutralization mechanism does not defocus the beam; (3) the gas load on the sample chamber from the primary ion source is small (primary source pressure $\sim 10^{-6}$ torr); (4) high neutralization efficiency (~15% within an 18-cm and ~40% within a 200-cm drift tube at 16 kV acceleration). The disadvantages are the following: (1) the requirement of completing all focusing either in or just after the acceleration lens (it is not possible to refocus the beam just prior to the sample as is often done with ion beams); (2) the length of the drift tube (neutralization region).

Prior to the experiments reported here the performance of the seven-atom SF_6 molecule (vs. an atom) for the production of secondary ions was not known; thus it was unclear as to whether the large size of the primary particle would be an advantage or a disadvantage. Geometric coupling between the primary beam molecules and the surface molecules could conceivably play a role in desorbing secondary ions.

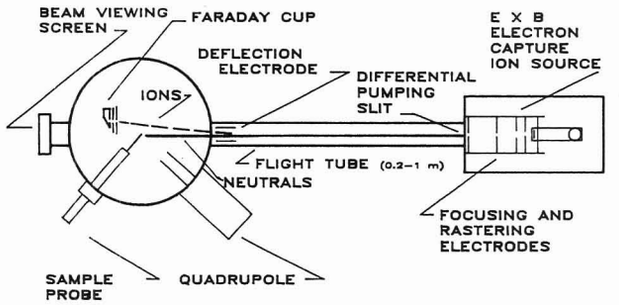

Figure 1. Schematic diagram of the SF_6 neutral beam prototype. The flight tube length is oversized to permit special experiments to be performed.

The question of the performance of the seven-atom molecule in sputtering ions from specimens is the most important issue to resolve prior to committing to a major effort to develop this technology into an analytical tool. Previous work (*7*) has shown that the energy and momentum of the primary particles affect the secondary ion sputtering efficiency. It also seems reasonable to expect that energy density (instantaneous energy deposited per unit surface area of the sample) would also play a role, particularly for sputtering large molecular ions. The kinetic energy of the SF_6 molecule is distributed among the seven atoms and the SF_6 molecule is large (geometrically) compared to an atom. The SF_6 molecule would need to be accelerated to a higher velocity than an atom to obtain an equivalent energy density on the sample matrix, however the energy density would be produced over a larger area compared to the atom. A typical SIMS or FAB source operates at about 5 kV, resulting in an energy of ~122 eV/amu for Ar (typical) atoms. Thus a voltage of ~18 kV would be necessary to obtain an equivalent energy/amu for SF_6.

Thus, with the previous demonstration (*5*, *6*) that the autoneutralization mechanism can be applied to produce a focused, small-diameter neutral beam that can be transported over meter distances, the objectives of the studies reported here were to (1) demonstrate the efficiency of fast (3–17 keV) neutral SF_6 molecules for desorbing secondary ions from a variety of nonconducting polymer surfaces and (2) do this without the use of any external surface charge neutralization. The results demonstrate the feasibility of developing this technique for the applications discussed.

EXPERIMENTAL SECTION

The experimental system consists of an ion source with a focusing and accelerating lens, a 2.5-m flight tube (longer than necessary for most applications), a multichannel plate array detector (MPAD) and viewing screen for beam display, a Faraday cup, sample introduction system, and a secondary ion quadrupole mass spectrometer. SF_6^- ions are produced in the source, and focused and accelerated prior to entering the flight tube through a differential pumping slit. Within the flight tube autoneutralization occurs producing the neutral beam. Those ions that have not neutralized by the end of the flight tube are electrostatically deflected away from the sample and into the Faraday cup, permitting dynamic monitoring of the beam stability. Both the source housing and sample/detector housing are pumped with 170 L/s turbomolecular pumps. Figure 1 shows a schematic diagram of the system.

The electron capture cross section of SF_6 is dependent upon the electron energy, requiring <0.1-eV electrons for efficient capture. To provide a large number of electrons at these low energies, an $E \times B$ electron capture ion source has been developed (*8*). The magnetic field traps the electrons emitted from a hot (Re) filament and forces them into a cycloidal path in which there are energy minimums that permit capture by the SF_6 molecules. Two different accelerating and focusing lenses were used to produce the primary beam. One version, an adaptation of an existing mass spectrometer lens, produced a ribbon beam, focused and rasterable in the y direction and mechanically collimated in

the z direction. The other lens was designed by using the SIMION electrostatic lens modeling program (*9*) as modified by Dahl (*10*). This lens produced a cylindrically focused near-parallel beam of ~0.5 mm diameter (at 2.5 m from the source) with a divergence angle of ~0.01°, rasterable in the y and z directions. The beam profiles were measured with the MPAD. Analysis of these lenses using SIMION indicated an ion residence time in the lenses of ~2–3 μs (depending upon acceleration voltage).

The effective (neutral) beam current was determined by measuring the relative ratio of the neutrals to ions with the MPAD (*5*) in its linear range with a photometer. The MPAD was operated with the front plane at ground to avoid preferential acceleration of the ions and it was assumed that the ions and neutrals had equal gains in the MPAD. The absolute intensity of the ion component was measured with a Faraday cup assembly consisting of a grounded front aperture followed by a secondary electron shield at −60 V followed by a molybdenum cup. It was found during the initial design and testing of the assembly that the secondary electron shield was critical for making repeatable and stable measurements. The apertures permitted the entire beam to enter into the cup, while preventing loss of secondary electrons. The cup current was measured with an electrometer that was calibrated against a standard current source. The reliability of the beam current measurement was considered to be highly significant since (1) the efficiency of the SF_6 molecule for sputtering secondary ions is of major importance for determining the areas for application of this source, and (2) this study shows that the SF_6 beam produces good SIMS spectra at primary beam fluxes 2 or more orders of magnitude lower than those reported elsewhere.

Slow neutrals (ions that autoneutralize in the acceleration field of the lens) were removed from the beam by maintaining a deflection voltage on the lens exit raster plates sufficient to separate the full energy beam from any slow neutrals. The neutralization efficiency ranged from 30% to 40% for a 2-m neutralization path, depending upon the acceleration voltage (time spent in the lens and flight tube). The flight tube could easily be reduced to 18 cm or less (as shown later) and still provide adequate neutralization efficiency (~15%). The beam purity was confirmed by mass-separating the ion beam with a small magnetic field and observing the separated beam images on the MPAD, as well as by characterizing the SF_6 gas on a magnetic-sector mass spectrometer.

The sample chamber includes the MPAD, Faraday cup, a direct insertion sample probe with x, y, z and rotational adjustment, and the secondary ion quadrupole mass spectrometer with ion extraction lens. The neutral beam strikes the sample at an angle of 30° (from normal to the sample surface) and the ion extraction lens is normal to the sample surface. The secondary ion extraction lens was designed by using the SIMION code (*9*, *10*). The lens uses an immersion design, which produces an electrostatic field that envelopes the sample. The immersion field acts both to focus the secondary (positive) ions into the lens aperture and to repel secondary electrons back onto the sample. All samples were analyzed without any active (e.g., electron flood, conductive grid, etc.) sample neutralization. The secondary ion quadrupole mass spectrometer was operated with a channeltron multiplier (gain ~ 3×10^6) in the analog mode that was calibrated against an integral Faraday cup. The amplifier of the quadrupole was calibrated against a standard current source. Primary neutral beam currents (amp-equivalent) were 1–10 pA and the quadrupole signals were 10^{-15} to 10^{-14} A. The primary beam was focused to 1–3 mm in diameter for ease of use, although it was operable at 0.5 mm. The source housing pressure was 2×10^{-6} or lower resulting in sample housing pressures in the 10^{-7} torr range.

RESULTS AND DISCUSSION

The SF_6 neutral beam has been used to sputter secondary ions from bulk samples of electrically nonconducting polymers that historically have been difficult to analyze with charged particle beams. These studies were conducted to explore and demonstrate some of the potential capabilities of the fast SF_6 neutral beam, not to study particular characteristics of the samples themselves. As such the discussion will focus on the performance of the beam as a surface probe.

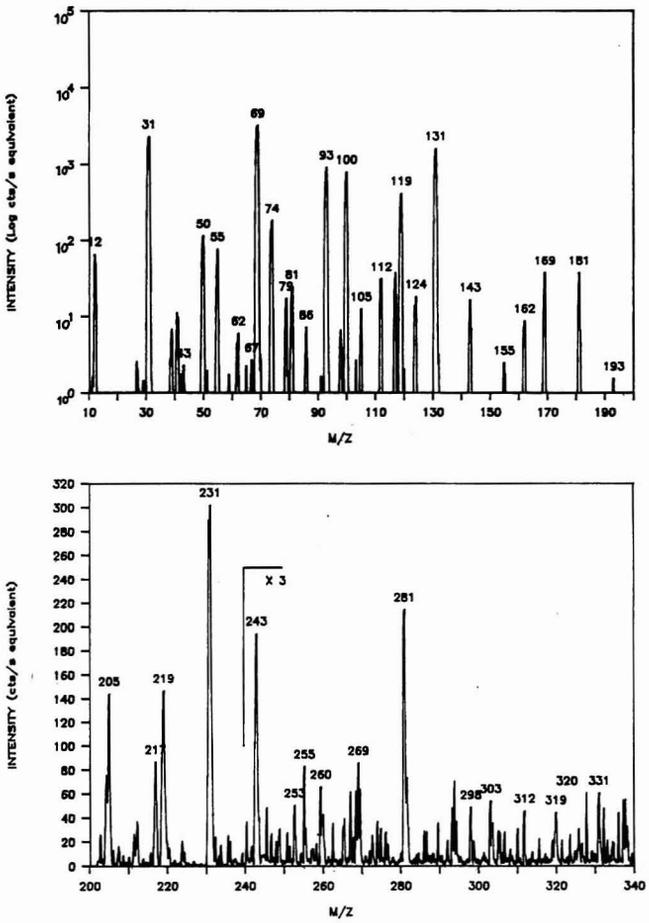

Figure 2. Secondary ion mass spectrum of a sample of bulk Teflon (PTFE) produced with a 17-keV SF_6 neutral beam at 3×10^{-11} A equivalent/cm^2: 10 scans at 3.4 min/scan, 0.02 cm^2 beam. No active sample charge neutralization mechanism was used.

Secondary ion spectra of bulk samples (~1 cm square by 0.5–2 mm thick) of Teflon (poly(tetrafluoroethylene)), Mylar (poly(ethylene terephthalate)), Acrylic (poly(methyl methacrylate)), a thin film (~10 Å) of polyphosphazene (poly[bis(trifluoroethoxy)phosphazene]) polymer on quartz, and KCl on Al foil have been measured under a variety of beam conditions. The polymer materials were mounted on the sample probe with an adhesive and the sample surface would "float" if charge accumulated. The Al was attached with a small pin and the probe was kept at ground potential. Measurements of the secondary ion spectra were made with a pure neutral SF_6 primary beam and with a combined ion-plus-neutral beam (ion deflection electrodes off). The results are presented in terms of counts per second (cts/s), converted from secondary ion current (cts/s = amps/(1.6×10^{-19})), to facilitate comparison with the literature.

Figure 2 shows typical spectra for bulk Teflon using the neutral SF_6 beam focused to a ~1.5 mm spot at 17 keV with a primary beam current of 3×10^{-11} A equivalent/cm^2 time averaged over 34 min (10 scans). Note that the 10–200 amu range is plotted on a log scale (to ease display of the lower intensity peaks), while the 200–350 amu range is plotted linearly. The relatively long scan time is due primarily to the quadrupole data system, which is limited to ~1 amu/s maximum scan rate. The many peaks in the spectra correspond to fragments of the Teflon polymer; Table I lists the fragment corresponding to each of the labeled peaks. Spectra were also acquired at a primary beam energy of 3 keV, as shown in Figure 3, using the lens that produced a 1-mm ribbon beam (to permit focusing at the low voltage) at a total neutral equivalent current of ~5 pA. Both the 17- and the 3-keV spectra are readily interpretable with major peaks well above

Table I. Mass Peaks of PTFE Polymer and Associated Fragments

m/z	fragment	m/z	fragment
12	C	162	C_4F_6
31	CF	169	C_6F_7
43	C_2F	181	C_4F_7
50	CF_2	193	C_5F_7
55	C_3F	205	C_6F_7
62	C_2F_2	217	C_7F_7
67	C_4F	219	C_4F_9
69	CF_3	231	C_5F_9
74	C_3F_3	243	C_6F_9
79	C_5F	255	C_7F_9
81	C_2F_3	260	C_9F_8
86	C_4F_2	267	C_8F_9
93	C_3F_3	269	C_5F_{11}
100	C_2F_4	281	C_6F_{11}
105	C_4F_3	293	C_7F_{11}
112	C_3F_4	298	C_9F_{10}
117	C_5F_3	303	$C_{11}F_9$
119	C_2F_5	310	$C_{10}F_{10}$
124	C_4F_4	312	C_7F_{12}
131	C_3F_5	319	C_6F_{13}
143	C_4F_5	320	$C_{14}F_8$
155	C_5F_5	331	C_7F_{13}

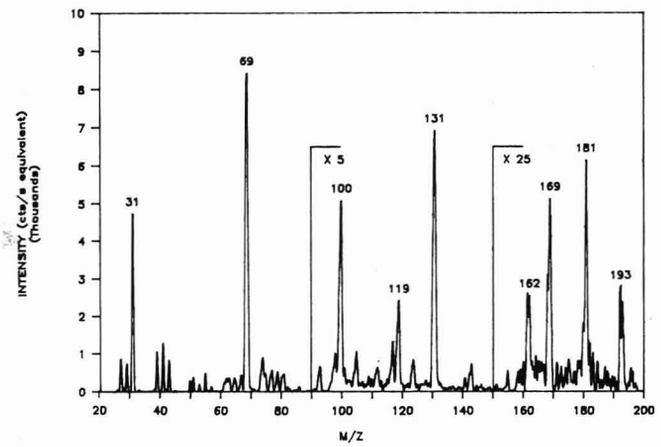

Figure 3. Secondary ion mass spectrum of bulk Teflon produced with a 3-keV neutral beam, ~1 pA neutral equivalent current.

the noise level, demonstrating that the large SF_6 molecule can produce adequate secondary ions for measurement. The dose levels ($\sim 1.5 \times 10^{12}$ molecules/cm^2 or $\sim 1.0 \times 10^{11}$ atoms/cm^2) are well within what is nominally considered the static SIMS nondamage range while providing easily measurable secondary ion signals (10^{-14} A or 6×10^4 counts/s).

It was observed during the measurements of Teflon that the higher energy primary beam appeared to produce a higher intensity of high mass fragments relative to lower mass fragments. To explore this phenomenon a series of measurements were made at primary beam energies ranging from 6 to 17 keV and the relative intensity of the 131 amu fragment to the 31 amu fragment was compared. The measurements were made both by peak stepping and by acquiring full spectra. The primary beam conditions (flux and spot size) were kept as constant as possible (flux varied by ~30% from one voltage setting to the next) and the secondary ion extractor lens focusing was held constant as the primary beam energy was varied. Two different sets of extractor lens settings were used to determine if the extractor lens focusing had a significant effect on the observation. One set was based on the optimum voltage settings for maximum signal intensity and the other set on acceptable yet substantially different voltages. Figure 4 displays the results of these measurements, showing

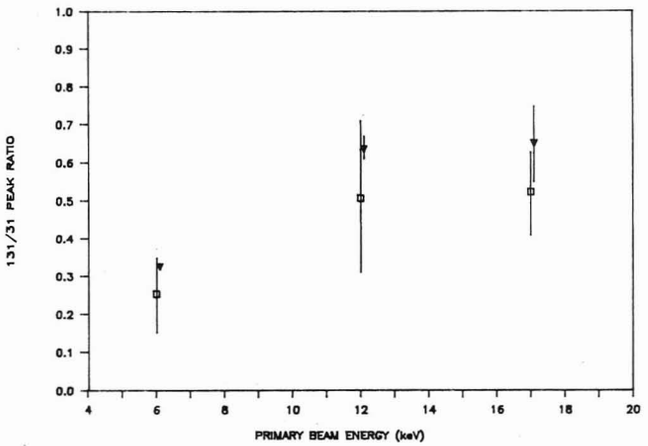

Figure 4. Ratio of high (131) to low (31) Teflon mass peaks as a function of primary beam energy for two different secondary ion extraction lens settings (boxes, optimum settings; triangles, alternate settings). Error bars show the standard variance of the average.

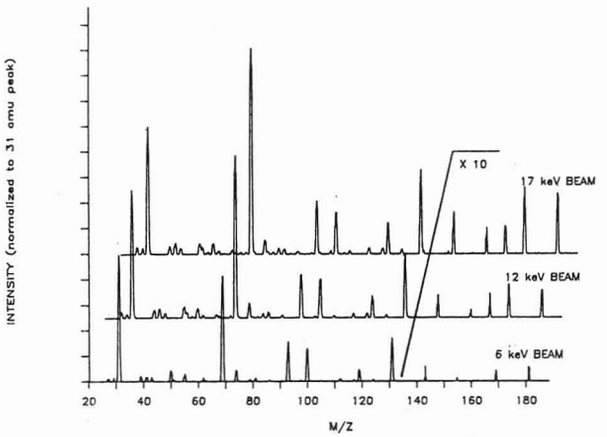

Figure 5. Teflon spectra for 6-, 12-, and 17-keV primary beam energies. Each spectra is internally normalized to the 31 amu peak and offset to ease comparison of the individual peak heights. Three scans were taken per spectrum at 3.4 min/scan.

that as the primary beam energy is increased the ratio of the higher mass to lower mass peaks increases. This implies either that more higher mass fragments are being produced by the higher energy beam or that the energy distribution of the secondary ions is changing with primary beam energy in such a way that more high mass fragments are being focused into the quadrupole at higher primary beam energy. The experimental evidence does not support the latter hypothesis since the trend is relatively insensitive to the extractor lens focusing conditions (the 131/31 ratio increases by a factor of 2 as primary beam energy goes from 6 to 12 keV, independent of extractor lens settings). This trend is evident for all of the major peaks of the Teflon spectra. Figure 5 displays three Teflon spectra, each taken under identical extractor lens settings on the same sample with a primary beam that varied only in energy (again the flux varied by ~25% from one spectra to the next, although in repeated runs at a variety of beam fluxes this degree of variation had no measurable effect on the results). The spectra are offset to permit easy comparison of peak height and the peaks within each spectra have been normalized to the 31 amu peak intensity. Spectra that were acquied from virgin (no previous dose) samples showed the same trend as those acquired on a "used" sample (one exposed to the beam at a variety of primary beam energies). Thus it does not appear that sample damage (none was expected at the low fluences used) was a contributing factor. We conclude that for the Teflon (PTFE) polymer an increase in the SF_6 primary beam energy from low (~6 keV) to high (~12

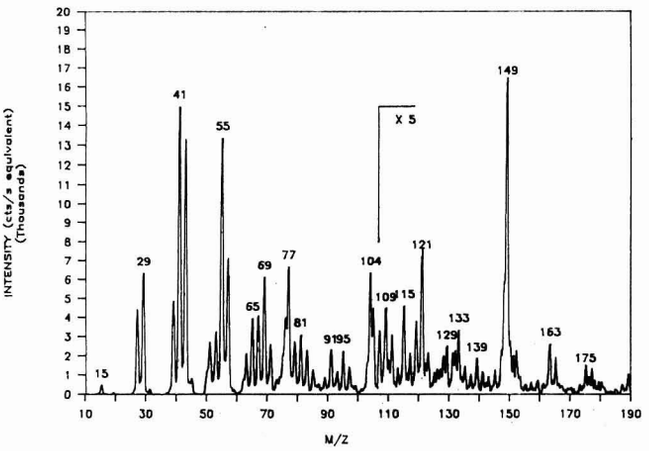

Figure 6. Secondary ion mass spectrum of bulk Mylar sheet: 17-keV primary neutral SF_6; 6×10^{-11} A equivalent/cm^2; 10 scans at 3.4 min/scan; 0.02 cm^2 beam.

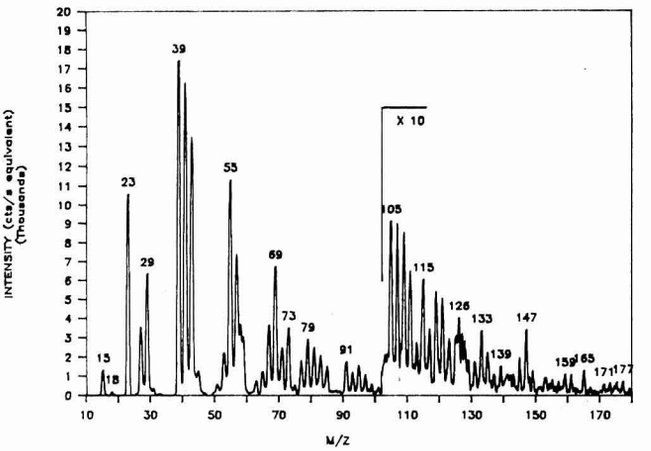

Figure 7. Secondary ion mass spectrum of bulk Acrylic sheet: 17-keV primary neutral SF_6; 5×10^{-11} A equivalent/cm^2; 10 scans at 3.4 min/scan; 0.02 cm^2 beam.

keV) results in increased production of higher mass fragments by a factor of ~2. In later studies we plan to pursue this further (higher primary beam energies) to see if the effect is saturating (as implied in Figure 4), if it occurs with an atomic primary beam, and if it occurs in other polymers of more complex monomers.

Although Teflon is an insulator and previous SIMS measurements (*11*) have empolyed some type of sample surface charge neutralization (e.g., electron flood guns or conductive grids), there are other polymers that are generally considered more difficult to measure with SIMS, such as Mylar. In addition it cannot be determined from the Teflon spectra whether the fluorine in the SF_6 beam is enhancing secondary ion production since the polymer itself is a fluorocarbon. Thus bulk samples of Mylar and Acrylic (both fluorine free, highly insulating polymers) were studied to determine whether the SF_6 beam produced adequate secondary ions from these materials and if any unexpected results were present in their SIMS spectra due to the SF_6. Figure 6 shows the Mylar spectra produced with a 17-keV primary neutral SF_6 beam at a flux of 6×10^{-11} A equivalent/cm^2 under the same scanning conditions as previously described for the Teflon spectra of Figure 2. The only change necessary to acquire the Mylar spectrum was to slightly refocus the extractor lens. The spectrum agrees qualitatively with previously published spectra (*12*), showing no obvious influence of the SF_6 components on the spectra. Again these data were acquired without any active sample surface charge neutralization. Figure 7 shows the SIMS spectrum of Acrylic taken under the same conditions, again with minor changes to the extractor lens focusing to maximize signal. The results agree qualitatively with published spectra (*12*) and there is no evidence of contamination by the SF_6 beam components.

On comparison of the results of Figures 5–7 and Figure 3 (low primary beam energy) with previously published data (*11–16*), it appears that the SF_6 beam is doing an excellent job of producing secondary ions at very low primary beam fluxes. Typical primary beam currents employed in the previous studies (*11–16*) with atomic ion beams were 10^{-9} A/cm^2 or higher, and the secondary ion yields, defined as the ratio of major secondary ion peak intensity (ions per second) to the primary beam intensity (ions or neutrals per second), were in the 10^{-7} to 10^{-6} range. The primary beam intensities employed in this study were ~10^{-11} A equivalent/cm^2 and the secondary ion yields were in the 10^{-3} range for the major peaks. The SF_6 beam appears to produce 3 to 4 orders of magnitude more intense secondary ion yields than equivalent-energy atomic (charged or neutral) beams. This comparison is hampered somewhat by the differences in experimental apparatus and procedures applied by the various groups, and we plan to directly compare the performance of an atomic beam with the SF_6 beam in our apparatus in the future. However, the current evidence strongly suggests that the SF_6 beam, although composed of seven-atom molecules with lower per-atom-momenta than commonly used atomic (Ar, Xe) beams, is unexpectedly efficient at sputtering secondary ions from these polymer surfaces.

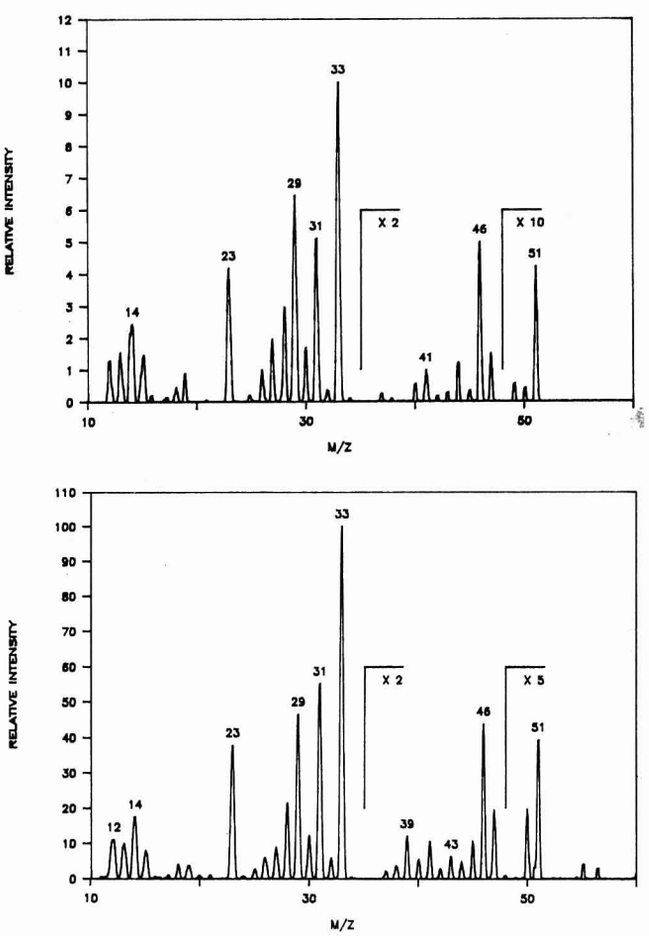

Figure 8. Secondary ion mass spectra of a 10-Å film of poly[bis(trifluoroethoxy)phosphazene] on a quartz substrate produced with a 4-keV (top) and 16-keV (bottom) SF_6 neutral beam, picoampere (neutral-equivalent) current over a ~0.1 cm^2 sample area for 5 min/spectra.

To assess the capability of the SF_6 beam for producing spectra from very thin films at nondamaging flux levels, secondary ion spectra of a ~10-Å poly[bis(trifluoroethoxy)-

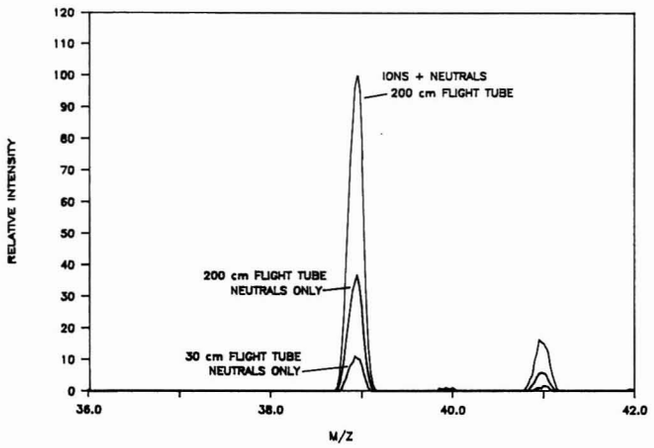

Figure 9. Secondary ion mass spectra of KCl on Al substrate showing the relative intensity of the 39 amu K peak for three different primary beam compositions.

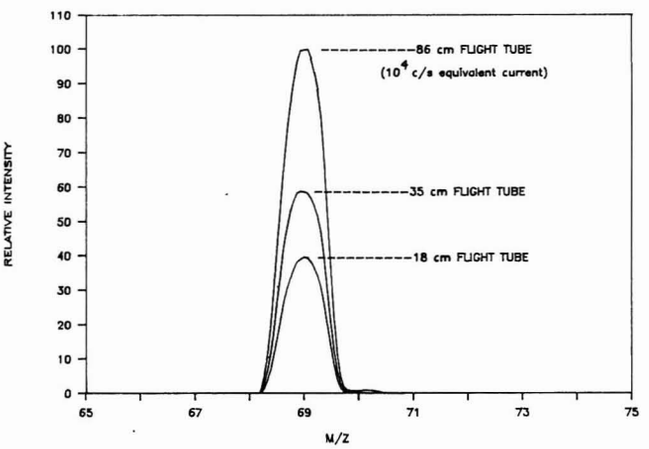

Figure 10. Relative intensity of the 69 amu Teflon peak for three different flight tube lengths (17 keV primary at 5×10^{-11} A equivalent/cm^2).

phosphazene] polymer film dip cast onto a 1 mm thick quartz disk were acquired at low and high primary beam energies. Figure 8 shows the spectra for 4- and 16-keV primary beams, at a neutral flux of $\sim 10^{-11}$ A equivalent/cm^2. The spectra are essentially the same (except for the signal intensity, which was a factor of ~ 10 lower for the lower energy beam) and showed no sign of degradation after repeated measurement (hours of exposure to the beam).

The Al sample consisted of a square of bulk Al foil on which KCl had been deposited by evaporation of a water-based solution. This sample was used to confirm the relative primary beam intensities (ion and neutral) and illustrate the effect of flight tube length (degree of neutralization) on the secondary ion signal. The spectra, shown in Figure 9, were taken at 4 keV and $\sim 3 \times 10^{-11}$ A/cm^2 under the following conditions: ion-plus-neutral primary beam with a 200-cm neutralization flight path, pure neutral beam with a 200-cm neutralization path, and pure neutral beam with a 30-cm neutralization path. All spectra were taken under identical system conditions (no refocusing etc.). The peak heights increased as the neutralization path increased, due to the increased neutral intensity, and again when the ions were added to the beam. The difference between the 200 cm flight tube neutral-only and ion-plus-neutral peaks is proportional to the relative intensity of the ion and neutral beams as measured with the photometer on the MPAD, i.e., about a 2:1 ratio. This supports the assumption that ions and neutrals of the same species have equivalent sensitivity in the MPAD and thus the method used for computing absolute neutral flux. The effect of flight tube length is also illustrated in Figure 10 where the peak intensity as a function of flight tube length is shown for the 69 amu Teflon peak with a 17-keV, 3 pA/cm^2 neutral beam. Even with an 18-cm neutralization distance, acceptable spectra were obtained. The Teflon spectra were taken in the analog mode with the quadrupole amplifier operating in mid-range (10^4 counts/s equivalent current for major peaks), again demonstrating that abundant secondary ions are being produced, even with a short neutralization path and (Figure 3) at relatively low (3 keV) energy.

In all cases for the polymers the secondary ion extraction lens required minor retuning to maximize signal when changing from one sample type to another. It was also noted that when an ion-plus-neutral beam was used on the Teflon samples, a major retuning of the extraction lens was necessary to get maximum signal. For the Acrylic and Mylar the secondary ion signals were unstable when the ions were included in the beam. Since this was not observed on the KCl/Al sample (a good conductor), it is suspected that these focusing changes are most likely due to a buildup in surface charge, possibly due to loss of secondary electrons when the pure neutral beam is employed, and to the charge from the anions when the ion-plus-neutral beam is employed.

The results show that even at low energy (20 eV/amu at 3 keV, equivalent to an 800-V Ar atom beam) and fluence (10^{-11} A equivalent/cm^2), the SF_6 neutral beam produces excellent secondary ion signals (10^4–10^5 counts/s) from insulating samples without any active sample neutralization. A reasonable length neutralization distance (~ 18 cm) is sufficient to achieve adequate neutral beam intensity, making it straightforward to add the source to existing systems with only minor modifications (if a suitable vacuum port is available). The source imposes low gas loads on the sample chamber and is simple to operate. Secondary ion signals for all samples were very stable with time (hours), the spectra were readily interpretable and agreed with previously published data based on atomic noble gas beams, and there was no indication of contamination or alteration of the spectra by the SF_6 beam components.

REMARKS AND CONCLUSIONS

The results of these experiments indicate that the focused SF_6 fast neutral molecular beam will perform quite well as a surface probe for insulating materials at zero-damage primary beam fluences. However, a focused, small-diameter (0.5 mm), high-energy neutral particle beam also has a variety of potential applications in the areas of FABMS and FTICR mass spectrometry. The focusing potential of the SF_6 neutral beam coupled with its relatively large mass and capability for high-energy operation makes it a very promising prospect for analysis of biological specimens, bulk or thin film polymers, ceramics, and the interfaces of combinations of these types of materials. The success of FABMS in producing spectra of fragile, high mass molecules is thought to be primarily due to the liquid matrix, rather than the use of the neutral beam (*17*), although the neutral atom beam does reduce sample charging problems. The generally agreed upon explanation is that the liquid matrix permits the sample of interest to move to the surface as it is depleted by sputtering; thus the signals can be maintained long enough to perform a measurement. It has been suggested (*18*) that by using dynamic emmitance matching of the secondary ion extraction lens with a rastered primary beam, bulk sample depletion and/or damage could be minimized and thus measurement sensitivity extended for solid-matrix samples. This may make it possible to perform measurements without the liquid matrix, since sample damage/depletion could be restricted to a small area and the beam rastered over the sample to increase measurement time. This concept, if used with a neutral beam, would require that the neutral beam be both focusable and rasterable. The SF_6

neutral beam meets these requirements (focusing is now at ~0.5 mm and improved lens designs are being developed) and thus would be an ideal candidate for such an application, particularly since the secondary ion yield appears to be 3 to 4 orders of magnitude higher than for atomic beams.

The maximum neutral flux produced with the source to date has been about 100 pA equivalent. This flux level is expected to increase as new ion source designs are developed and as the understanding of the autoneutralization mechanism evolves. Thus although the present source is limited to static SIMS flux levels, it is anticipated that higher fluxes will be possible. The maximum beam energy attained has been 25 keV, limited by the source housing feedthroughs. However we see no obvious constraints to preclude increasing this to 100 keV or higher levels. Since ion velocity (time to autoneutralize) goes up as the square root of the energy, a 100-keV beam would adequately neutralize in a 2-m flight tube. This would permit the sample analysis region and detectors to be well removed from the high-voltage source while providing a focused beam of neutral primary particles.

Another very promising application of the focused neutral beam is in Fourier transform ion cyclotron resonance mass spectrometry (FTICR) (*19–22*). The magnetic fields employed in FTICR and the high vacuum requirements place severe constraints on the types of ion introduction techniques applicable. Use of a focused ion beam for producing secondary ions in the FTICR cell, though experimentally possible (*3*, *4*), is difficult due to the defocusing and deflecting forces of the magnetic field and the resultant complexity and expense of overcoming these. Use of conventional FAB sources in FTICR has been hampered by their historically poor focusing capabilities and generally high gas loads. The autoneutralized, focused molecular beam overcomes these constraints. It is focusable down to submillimeter, near parallel beam diameters, maintains this focusing over long ranges (meters) which will permit the beam to be injected into the ICR cell, is not affected by electrostatic or magnetic fields (once neutralized), imposes a low gas load on the sample chamber, is an efficient secondary ion sputterer, and is simple and inexpensive to build and operate.

In summary, the autoneutralization mechanism provides a means for producing a high-energy, focused, rasterable neutral molecular beam that maintains focusing over a long range. The SF_6 molecule has been shown to be very efficient for producing secondary ions from conducting and nonconducting materials and thus can be used as a primary beam for static SIMS. The controllable and long-range focusing capability should allow the source to be applied to techniques such as FTICR where the beam must penetrate electrostatic or magnetic fields and low gas loads are required. We are currently designing a source to operate on a double focusing magnetic mass spectrometer and plan to install and test the source on an FTICR.

LITERATURE CITED

(1) *Desorption Mass Spectrometry, Are SIMS and FAB the Same?*; Lyon, P. A., ACS Symposium Series 291; American Chemical Society: Washington, DC 1985.
(2) Eccles, A. J.; van den Berg, J. A.; Brown, A.; Vickerman, J. C. *J. Vac. Sci. Technol. A* **1986**, *4*(4), 1888–1892.
(3) Shabanowitz, J.; Hunt, D. F.; Castro, M.; Russel, D. H. Proceedings of the 34th American Society of Mass Spectrometry Conference, Cincinnati, 1986; p 945.
(4) Amster, I. J., Loo, J. A.; Furlong, J.; Wang, B. H.; Williams, E. R.; McLafferty, F. W. Proceedings of the 34th American Society of Mass Spectrometry Conference, Cincinnati, 1986, p 947.
(5) Delmore, J. E.; Appelhans, A. D. *Int. J. Mass Spectrom. Ion Processes* **1986**, *68*, 327–336.
(6) Delmore, J. E.; Appelhans, A. D. *J. Chem. Phys.* **1986**, *84*, 6238–6246.
(7) Briggs, D.; Hearn, M. J. *Int. J. Mass Spectrom. Ion Processes* **1985**, *67*, 47–56.
(8) Delmore, J. E. *Intl. J. Mass Spectrom. Ion Processes* **1983**, *51*, 191–205.
(9) McGlivery, D. C. Ph.D. Dissertation, LaTrobe University, 1978.
(10) Dahl, D. A.; Delmore, J. E. Proceedings of the 34th American Society of Mass Spectrometry Conference, Cincinnati, 1986; p 304.
(11) Briggs, D.; Wootton, A. B. *SIA, Surf. Interface Anal.* **1982**, *4*, 109–115.
(12) Briggs, D. *SIA, Surf. Interface Anal.* **1982**, *4*, 151–155.
(13) Colton, R. J. *Nucl. Instrum. Methods Phys. Res.* **1983**, *218*, 276–286.
(14) Briggs, D.; Hearn, M. J.; Ratner, B. D. *SIA, Surf. Interface Anal.* **1984**, *6*, 184–192.
(15) Brown, A.; van den Berg, J. A.; Vickerman, J. C. *Spectrochim. Acta, Part B* **1985**, *40B*, 871–877.
(16) Wittmaack, K. *Nucl. Instrum. Methods Phys. Res., Sect. B* **1984**, *2*, 674–678.
(17) Perel, J. In *Desorption Mass Spectrometry*; ACS Symposium Series 291; American Chemical Society: Washington, DC, 1985; Chapter 8.
(18) Magee, C. W. In *Desorption Mass Spectrometry*, ACS Symposium Series 291; American Chemical Society: Washington, DC 1985; Chapter 6.
(19) Laude, D. A., Jr.; Johlman, C. L.; Brown, R. S.; Weil, D. A.; Wilkins, C. L. *Mass Spectrometry Rev.* **1986**, *5*(2), 107–166.
(20) Russel, D. H. *Mass Spectrom. Rev.* **1986**, *5*(2), 167–190.
(21) De Pauw, E. *Mass Spectrom. Rev.* **1986**, *5*, 191–212.
(22) Marshall, A. G. *Accounts Chem. Res.* **1985**, *18*, 316–322.

RECEIVED for review August 25, 1986. Accepted March 23, 1987. Work supported by the U.S. Department of Energy INEL internal research funds and by the Office of Health and Environmental Research, Office of Energy Research, DOE, under Contract 4AA901.

Effect of Sample-Charge Volume on the Sensitivity of Chromatographic Analysis

Michal Roth* and Josef Novák[1]

Institute of Analytical Chemistry, Czechoslovak Academy of Sciences, 61142 Brno, Czechoslovakia

A simple model for the dependence of the sensitivity of chromatographic determination of the mass of analyte on the sample-charge volume is suggested and discussed. The model applies to the situation in which the mass of analyte introduced into the column is constant and independent of the sample-charge volume, i.e., the concentration (mass/volume) of the analyte in the sample is inversely proportional to the sample-charge volume. The model makes it possible to quantify the gain in the sensitivity of the analyte-mass determination brought about by concentrating the sample. Two limiting column-inlet analyte-concentration profiles are considered, viz., rectangular and exponential-decay concentration profiles. The theoretical results compare favorably with the outcome of a simple experimental test of the model.

In trace analysis by column chromatography, it is essential to assess the effects of the individual experimental parameters on the sensitivity of chromatographic analysis (*1–3*). One of these parameters is the volume of the sample charge. In analytical practice, especially if trace amounts of analytes are to be determined, it is often necessary to apply a sample-enrichment technique prior to the chromatographic run proper. The sample-enrichment (i.e., concentrating) step may ideally be viewed as a reduction of the sample-charge volume while maintaining a constant mass of the analyte in the sample. Although the sample-enrichment techniques are applied routinely, little attention seems to be paid to quantitative evaluation of the resulting improvement in the sensitivity of analysis. In other words, if the sample is concentrated n times, what will be the corresponding increase in the sensitivity of analysis?

In the present paper, a general model for the dependence of the sensitivity of analyte-mass determination on the volume of the sample charge is described and tested. The aim is to develop a model that can readily be applied with minimum computation involved. Any theoretical model is necessarily idealized; the validity of the present model is qualified by the following conditions:

(i) Along the entire path of zone migration in the column, the zone-maximum analyte concentration is within the Henry-law region.

(ii) The zone-maximum analyte concentration in the mobile phase at the column outlet is within the region of dynamic linearity of the detector response.

(iii) The intracolumn and extracolumn zone-spreading factors operate independently of each other.

(iv) The nonzero volume of the sample charge is the only cause of the extracolumn zone spreading.

(v) The peak distortion due to the fact that a record is provided of analyte concentration as a function of time at the column outlet rather than that of analyte concentration as a function of position in the column at a given time is negligible.

(vi) The peak distortion due to nonzero time constants of the detection and signal-recording system is negligible.

Provided that the states of aggregation of the sample and the mobile phase are the same (gas–gas, liquid–liquid, or fluid–fluid), the treatment described below applies to any type of column chromatography.

SENSITIVITY OF ANALYTE-MASS DETERMINATION

The sensitivity of chromatographic determination of the mass of analyte, i.e., the efficiency with which the chromatographic column–detector system responds to the mass of analyte introduced into the column, can be expressed as the peak-maximum response per unit mass of analyte. The sensitivity criterion so defined is given by the product of the sensitivity of detection toward a given analyte i and the zone-maximum analyte concentration per unit mass of the analyte in the mobile phase at the column outlet

$$\varphi_{mi} = \mathrm{d}R_i^*/\mathrm{d}m_i = (\mathrm{d}R_i^*/\mathrm{d}q_i^*)(\mathrm{d}q_i^*/\mathrm{d}m_i) = \varphi_{qi}(\mathrm{d}q_i^*/\mathrm{d}m_i) \quad (1)$$

where m_i is the mass of analyte within the zone, q_i^* is the maximum concentration of the analyte in the column effluent, and R_i^* is the detector response corresponding to q_i^*.

Provided that the maximum concentration of analyte i in the column effluent is within the range of dynamic linearity of the detector response (cf. assumption ii above), the sensitivity of detection toward analyte i (φ_{qi}) is constant, so that the sensitivity of analyte-mass determination, φ_{mi}, is directly proportional to the differential quotient ($\mathrm{d}q_i^*/\mathrm{d}m_i$). In the development of the model, it is therefore sufficient to consider the relationship between the sample-charge volume and the quotient ($\mathrm{d}q_i^*/\mathrm{d}m_i$).

COLUMN-OUTLET ANALYTE-CONCENTRATION PROFILE

There are several ways to express the dependence of the column-outlet analyte concentration on time and/or volume of the mobile phase passed through the column. If the column-outlet concentration profile results from combined actions of several mutually independent effects, it is expedient (*4*) to use the Laplace transform or the convolution integral. The convolution integral, especially the exponentially modified Gaussian function, has often been applied to the study of the effects on the peak shape of the extracolumn zone-broadening factors (*5–16*).

Under the above conditions (i–vi), a hypothetical zero-volume injection of a mass m_i of analyte i into the column results in a Gaussian column-outlet concentration profile of analyte i, $q_{i,c}(V)$. If the mass m_i of analyte i enters the column within an inlet chromatographic zone with a concentration profile $q_{i,e}(V)$, the resulting column-outlet concentration profile of the analyte, $q_{i,ap}(V)$, is given by the convolution integral

$$q_{i,ap}(V) = (1/m_i)\int_0^\infty q_{i,e}(V')q_{i,c}(V - V')\,\mathrm{d}V' \quad (2)$$

where V is the volume of the mobile phase passed through the column, and V' is a dummy variable of integration. The

[1] Deceased April 6, 1986.

0003-2700/87/0359-1692$01.50/0 © 1987 American Chemical Society

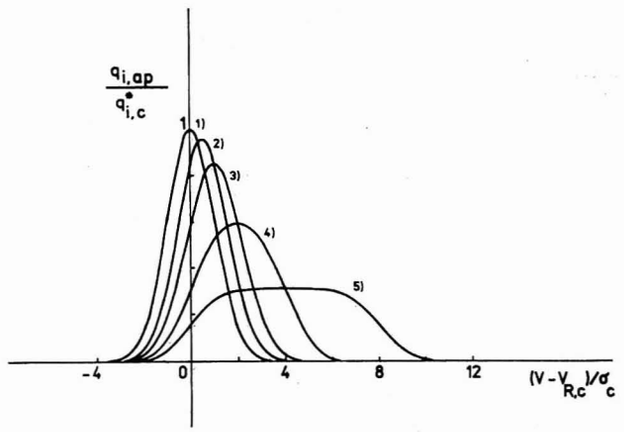

Figure 1. Dependence of the shape of concentration profile $q_{i,ap}(V)$ (eq 6) on the reduced volume of the sample charge at constant values of m_i and σ_c: (1) $a = 0$, (2) $a = 1$, (3) $a = 2$, (4) $a = 4$, (5) $a = 8$.

value $V = 0$ corresponds to the start of introducing the sample into the column. Since both $q_{i,c}(V)$ and $q_{i,e}(V)$ include the mass m_i of the analyte (see below), the preintegral factor $1/m_i$ is required in eq 2.

Provided the intracolumn and extracolumn zone-broadening factors operate independently of each other, the variances of the three concentration profiles are related by

$$\sigma^2[q_{i,ap}] = \sigma^2[q_{i,c}] + \sigma^2[q_{i,e}] = \sigma_c^2 + \sigma^2[q_{i,e}] \qquad (3)$$

In the following part of the theoretical section, relationships are derived between the sensitivity of analyte-mass determination and the sample-charge volume for rectangular and exponential-decay column-inlet concentration profiles. These two particular column-inlet profiles were chosen because, from a practical viewpoint, they represent the best and worst possible alternatives of the sample introduction into the column, respectively. For each of the two profiles, the maximum concentration of the analyte in the column effluent is derived, and the corresponding sensitivity of the analyte-mass determination is expressed as a fraction of that pertaining to a hypothetical zero-volume injection of the sample. All the retention volumes mentioned below refer to the elution of the *maximum* concentration of the analyte in the chromatographic zone.

DEVELOPMENT OF THE MODEL

Rectangular Column-Inlet Concentration Profile. If the sample containing a mass m_i of analyte i enters the column by plug flow from a nonmixed sample loop of a volume v, the column-inlet concentration profile of the analyte is given by

$$\begin{aligned} q_{i,e}(V) &= m_i/v \qquad \text{for } 0 < V < v \\ &= 0 \qquad \text{otherwise} \end{aligned} \qquad (4)$$

In the case of gas chromatography, the volume v should refer to the selected reference values of temperature and pressure. The Gaussian concentration profile is described as

$$q_{i,c}(V) = m_i/(\sigma_c(2\pi)^{1/2}) \exp\{-(V - V_{R,c})^2/2\sigma_c^2\} \qquad (5)$$

where $V_{R,c}$ is the retention volume of analyte i resulting from a hypothetical zero-volume injection of the sample. By combination of eq 2, 4, and 5, the column-outlet concentration profile of analyte i can be written as

$$q_{i,ap}(V) = m_i/v\{Q[(V - V_{R,c} - v)/\sigma_c] - Q[(V - V_{R,c})/\sigma_c]\} \qquad (6)$$

where $Q(u)$ is the area under the normalized normal distribution curve between u and ∞

$$Q(u) = 1/(2\pi)^{1/2} \int_u^\infty \exp\{-y^2/2\}\, dy$$

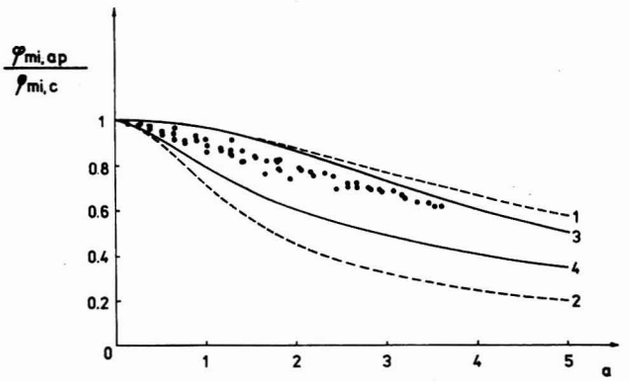

Figure 2. Dependence of the sensitivity of analyte-mass determination on the reduced volume of the sample charge: (curve 1) rectangular inlet profile, Gaussian outlet profile; (curve 2) exponential-decay inlet profile, Gaussian outlet profile; (curve 3) rectangular inlet profile, convoluted outlet profile; (curve 4) exponential-decay inlet profile, convoluted outlet profile. Data points show the results of the experimental test of the model.

Figure 1 shows the shapes of column-outlet concentration profiles (eq 6) corresponding to elution of a constant mass m_i of analyte i contained in different sample-charge volumes. All calculations in this paper were performed with hand-held calculators and a polynomial approximation for $Q(u)$ (*17*).

To proceed further, it is necessary to express the maximum concentration of the analyte in the elution zone, i.e., when $V = V_{R,ap}$. The retention volume $V_{R,ap}$ is given by (*18*, *19*)

$$V_{R,ap} = V_{R,c} + v/2 \qquad (7)$$

so that the maximum concentration of analyte i in the column effluent is

$$q_{i,ap}^* = q_{i,ap}(V_{R,ap}) = m_i/v\{1 - 2Q[v/(2\sigma_c)]\} \qquad (8)$$

Finally, combining eq 1, 5, and 8 yields

$$\varphi_{mi,ap}/\varphi_{mi,c} = q_{i,ap}^*/q_{i,c}^* = (2\pi)^{1/2}/a\{1 - 2Q(a/2)\} \qquad (9)$$

where $a = v/\sigma_c$ is the reduced volume of the sample charge, $\varphi_{mi,c}$ is the sensitivity of the analyte-mass determination corresponding to a hypothetical zero-volume injection of a mass m_i of analyte i, and $\varphi_{mi,ap}$ is the sensitivity corresponding to plug flow of a sample containing the mass m_i of the analyte into the column from a nonmixed sample loop of volume v. It is apparent from eq 9 that the sensitivity ratio $\varphi_{mi,ap}/\varphi_{mi,c}$ depends on the reduced volume of the sample charge only (see curve 3 in Figure 2).

The sensitivity ratio can also easily be calculated on a simplifying assumption that, regardless of the sample-charge volume, the column-outlet concentration profile of the analyte remains Gaussian throughout, with a variance given by eq 3. In such a case

$$\varphi_{mi,ap}/\varphi_{mi,c} = 1/(1 + pa^2)^{1/2} \qquad (10)$$

where $p = 1/12$ for the rectangular column-inlet concentration profile. The result of this simplified treatment is shown by the dashed curve 1 in Figure 2.

Exponential-Decay Column-Inlet Concentration Profile. If the sample containing a mass m_i of analyte i enters the column from an ideal mixing chamber of a volume v, the column-inlet concentration profile of the analyte is given by

$$\begin{aligned} q_{i,e}(V) &= m_i/v \exp\{-V/v\} \qquad \text{for } V > 0 \\ &= 0 \qquad \text{otherwise} \end{aligned} \qquad (11)$$

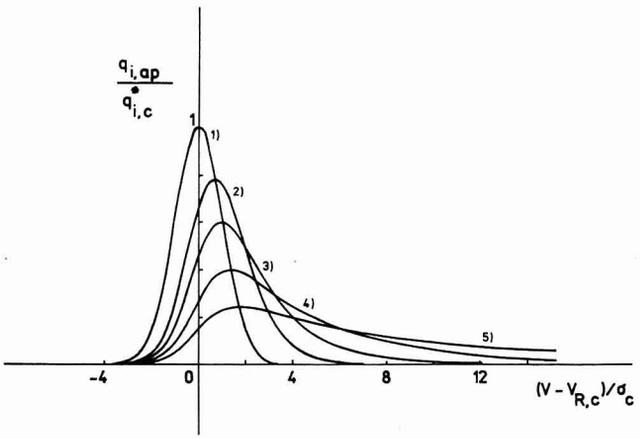

Figure 3. Dependence of the shape of concentration profile $q_{i,ap}(V)$ (eq 12) on the reduced volume of the sample charge at constant values of m_i and σ_c: (1) $a = 0$, (2) $a = 1$, (3) $a = 2$, (4) $a = 4$, (5) $a = 8$.

Substitution into eq 2 from eq 5 and 11 yields after rearrangement (*20*)

$$q_{i,ap}(V) = m_i/(v\pi^{1/2}) \exp\{-\sigma_c^2/2v^2\} \exp\{-\sigma_c Z 2^{1/2}/v\} \times \int_{-\infty}^{Z} \exp\{-y^2\}\, dy$$
$$= m_i/v \exp\{-\sigma_c^2/2v^2\} \exp\{-\sigma_c Z 2^{1/2}/v\}[1 - Q(Z2^{1/2})] \quad (12)$$

where

$$Z = 1/2^{1/2}[(V - V_{R,c})/\sigma_c - 1/a]$$

In Figure 3, the shapes are shown of the column-outlet concentration profiles (eq 12) corresponding to elution of a constant mass m_i of the analyte contained in different sample-charge volumes.

Similarly as with the rectangular column-inlet concentration profile, it is necessary now to express the maximum concentration of the analyte in the mobile phase at the column outlet. For the exponential-decay inlet profile, however, there is no parallel to eq 7 since the relationship between $V_{R,ap}$ and $V_{R,c}$ cannot be expressed analytically. In order to calculate $V_{R,ap}$ and $q_{i,ap}$*, Barber and Carr (*10*) fitted a second-order Gram polynomial to the points near the apex of the concentration profile. In the present paper, a different route is followed; setting the d/dV derivative of eq 12 equal to zero, it can be shown that, in the concentration maximum

$$1/a \int_{-\infty}^{Z^*} \exp\{-y^2\}\, dy = 1/2^{1/2} \exp\{-Z^{*2}\} \quad (13)$$

where

$$Z^* = 1/2^{1/2}(Y - 1/a),\ Y = (V_{R,ap} - V_{R,c})/\sigma_c$$

Since

$$\int_{-\infty}^{Z^*} \exp\{-y^2\}\, dy = \pi^{1/2}[1 - Q(Z^* 2^{1/2})] \quad (14)$$

the reduced concentration-maximum shift, Y, can easily be calculated from eq 13 for any value of the reduced sample-charge volume, a, using the Newton–Raphson iteration method and a proper numerical technique for calculating $Q(u)$. Substitution for the integral in eq 12 from eq 13 gives

$$q_{i,ap}^* = q_{i,ap}(V_{R,ap}) = m_i/(\sigma_c(2\pi)^{1/2}) \exp\{-Y^2/2\} \quad (15)$$

Combining eq 1, 5, and 15 yields finally

$$\varphi_{mi,ap}/\varphi_{mi,c} = \exp\{-Y^2/2\} \quad (16)$$

The dependence of the sensitivity ratio $\varphi_{mi,ap}/\varphi_{mi,c}$ on the reduced volume of the sample charge is shown graphically by curve 4 in Figure 2. Curve 2 in Figure 2 shows the result of a simplified calculation based upon the assumption that the column-outlet concentration profile remains Gaussian throughout, regardless of the volume of the sample charge. Curve 2 in Figure 2 is described by eq 10 with $p = 1$.

EXPERIMENTAL SECTION

Apparatus. A simple experimental test of the above model was carried out with a CHROM 5 gas chromatograph (Laboratory apparatus, Prague, Czechoslovakia) equipped with a flame ionization detector and modified to increase the precision of the measurement of retention data. Provided the mass flow rate of the carrier gas is kept constant and the analyte concentration in the carrier gas is very low, the response of the flame ionization detector is directly proportional to the analyte concentration in the column effluent. A glass column 2.5 m × 3 mm i.d. was packed with 5% (w/w) poly(dimethylsiloxane) DC 200 (Packard-Becker B.V., Delft, The Netherlands) coated on Chromosorb G AW 30/60 (Carlo Erba, Milan, Italy). The column temperature was kept at 30 °C by means of a water jacket through which the water from an external thermostat (type U15C, VEB MLW Prüfgeräte-Werk, Medingen, GDR) was circulated. The volumetric flow rate of the nitrogen carrier gas was 5.3 cm^3/min (25 °C, 0.97 bar); it was monitored continuously by a precolumn differential capillary flowmeter. The column inlet pressure was not higher than 0.09 bar above the barometric pressure. *n*-Pentane (p.a. grade, VEB Laborchemie, Apolda, GDR) was employed as a testing substance.

Procedure. It is impossible to determine the standard deviation σ_c exactly. Therefore, an approximation was obtained from repeated injections of 50-μL samples of *n*-pentane vapor using a gas-tight syringe (type 1001, Hamilton, Bonaduz, Switzerland). The peaks obtained were nearly symmetric. The standard deviations were calculated from chart records assuming the peak shape was Gaussian. Twenty-two injections yielded the value $\sigma_c = (0.795 \pm 0.019)$ cm^3 at 25 °C and 0.97 bar. Therefore, a 50-μL sample corresponded to $a = 0.06$.

When the dependence of the peak height on the volume of the sample charge was tested, the injections were made from a hypodermic syringe with a stainless steel plunger. This particular type of syringe was employed in order to avoid the "memory effect" exhibited by the Teflon-coated plungers of gas-tight syringes; with pentane vapor, the effect is appreciable. A 50-μL sample of pentane vapor was diluted with air to yield the volume required. Before an injection, the sample was allowed to equilibrate in the syringe for a few minutes. The maximum volume of the sample charge was 2.8 cm^3 ($a = 3.6$). Although a glass syringe with a metallic plunger was employed, it was impossible to maintain a constant mass of pentane in the sample throughout the procedure. Therefore, the peak areas were evaluated by use of a CI 100 computing integrator (Laboratory apparatus, Prague, Czechoslovakia), and the peak heights were normalized to a unit peak area.

The results of the test are represented by the points in Figure 2. As can be expected, all experimental points fall into the region between the curves 3 and 4. When the volume of the sample charge is increased, the experimental points converge toward the curve derived for a rectangular column-inlet concentration profile. At the same time, however, the peaks showed increasing amounts of tailing. This apparent contradiction results from the fact that a syringe was employed to introduce the samples into the column and that the instrument was operated at a constant flow rate of the carrier gas. In such a case, an increased volume of the sample charge is bound to cause an increased pressure surge on injection. Therefore, when the volume of the sample charge is increased, the effective value gradually becomes smaller than the apparent one.

RESULTS AND DISCUSSION

The model has been derived showing the dependence of the sensitivity of analyte-mass determination on the volume of the sample charge for two limiting column-inlet concentration profiles of the analyte. The word "limiting" means that the two column-inlet profiles represent the best and worst possible cases of the sample introduction into the column. Since the final eq 9 and 16 are written in terms of dimensionless (reduced) quantities, they apply generally to any column chro-

matography system as long as the qualifying conditions (see introductory section) are satisfied. In other words, in any system of column chromatography and for any volume of the sample charge, the sensitivity of analyte-mass determination should range between the "extreme" values given by eq 9 and 16 (or by curves 3 and 4 in Figure 2). Although the reducing parameters σ_c and $\varphi_{mi,c}$ cannot be determined exactly, fair approximations to these may be obtained from a chromatogram of the smallest possible sample charge. Once the volume σ_c is known, the increase in the sensitivity of analyte-mass determination on concentrating the sample may readily be calculated. To do so, eq 9 or eq 13 and 16 are applied to the volumes of charges of the concentrated and original samples, respectively. Naturally, the volumes are concerned containing the same amounts of analyte. For the model to be applicable directly, the state of aggregation of both concentrated and original samples should be the same as that of the mobile phase. The increase required is then given by the ratio of the two results. The choice between the two column-inlet profiles depends upon the performance characteristics of the particular sample-introduction device employed. In principle, relationships analogous to eq 9 and 16 may be derived for any other column-inlet concentration profile. It may be shown that for large values of a, the sensitivity ratio $\varphi_{mi,ap}/\varphi_{mi,c}$ is nearly equal to $(2\pi)^{1/2}/a$ regardless of the column-inlet concentration profile. The use of eq 9, 13, and 16 may be managed even with a programmable pocket calculator.

Finally, a brief evaluation should be given of the relative significance of qualifying conditions (i–vi) (see introductory section). Obviously, the most severe limitations to the practical applicability of the model are those imposed by conditions iv and vi. The adherence of the behavior of a real instrument to the model described improves on decreasing the dead volume of the chromatographic system and on decreasing the time constants of the detection and registration system. For very slightly retained compounds and/or for very quick analyses, condition v may impose significant restriction to the applicability of the model.

LITERATURE CITED

(1) Kalmanovskii, V. I.; Zhukhovitskii, A. A. *J. Chromatogr.* **1965**, *18*, 243–252.
(2) Karger, B. L.; Martin, M.; Guiochon, G. *Anal. Chem.* **1974**, *46*, 1640–1647.
(3) Guiochon, G.; Colin, H. "Analytical Techniques in Environmental Chemistry"; *Proceedings of the 2nd International Congress, Barcelona, Spain, November 1981*; Albaiges, J., Ed.; Pergamon: Oxford–New York–Sydney, 1981; pp 169–176.
(4) Sternberg, J. C. *Advances in Chromatography*; Giddings, J. C., Keller, R. A., Eds.; Marcel Dekker: New York, 1966; Vol. 2, pp 205–270.
(5) McWilliam, I. G.; Bolton, H. C. *Anal. Chem.* **1969**, *41*, 1755–1762.
(6) Gladney, H. M.; Dowden, B. F.; Swalen, J. D. *Anal. Chem.* **1969**, *41*, 883–888.
(7) Anderson, A. H.; Gibb, T. C.; Littlewood, A. B. *J. Chromatogr. Sci.* **1970**, *8*, 640–646.
(8) Grushka, E. *Anal. Chem.* **1972**, *44*, 1733–1738.
(9) Pauls, R. E.; Rogers, L. B. *Anal. Chem.* **1977**, *49*, 625–628.
(10) Barber, W. E.; Carr, P. W. *Anal. Chem.* **1981**, *53*, 1939–1942.
(11) Foley, J. P.; Dorsey, J. G. *Anal. Chem.* **1983**, *55*, 730–737.
(12) Foley, J. P.; Dorsey, J. G. *J. Chromatogr. Sci.* **1984**, *22*, 40–46.
(13) Anderson, D. J.; Walters, R. R. *J. Chromatogr. Sci.* **1984**, *22*, 353–359.
(14) Delley, R. *Chromatographia* **1984**, *18*, 374–382.
(15) Hanggi, D.; Carr, P. W. *Anal. Chem.* **1985**, *57*, 2395–2397.
(16) Delley, R. *Anal. Chem.* **1986**, *58*, 2344–2346.
(17) *Handbook of Mathematical Functions*; Abramowitz, M., Stegun, I. A., Eds.; National Bureau of Standards: Washington, DC, 1964; Applied Mathematics Series No. 55, p 932.
(18) van Deemter, J. J.; Zuiderweg, F. J.; Klinkenberg, A. *Chem. Eng. Sci.* **1956**, *5*, 271–289.
(19) Porter, P. E.; Deal, C. H.; Stross, F. H. *J. Am. Chem. Soc.* **1956**, *78*, 2999–3006.
(20) Gradshtein, I. S.; Ryzhik, I. M. *Tablitsy Integralov, Summ, Ryadov i Proizvedenii* (*Tables of Integrals, Summations, Series, and Products*), 4th ed.; Fizmatgiz: Moscow, 1962; p 321, formula 3.322.

RECEIVED for review October 10, 1986. Accepted March 3, 1987.

Identification of Mutagenic Methylbenz[*a*]anthracene and Methylchrysene Isomers in Natural Samples by Liquid Chromatography and Shpol'skii Spectrometry

Philippe Garrigues,*[1] Marie-Pierre Marniesse,[1] Stephen A. Wise,[2] Jacqueline Bellocq,[1] and Marc Ewald[1]

Groupe d'Océanographie Physico-chimique, LA 348 CNRS, Université de Bordeaux I, 33405 Talence Cedex, France, and Organic Analytical Research Division, National Bureau of Standards, Gaithersburg, Maryland 20899

Chromatographic extracts of natural samples (rock and air particulate matter) have been examined by high-resolution Shpol'skii spectrometry (HRS) at 15 K in *n*-alkane polycrystalline frozen solutions for the identification of the 12 methylbenz[*a*]anthracenes (MBA) and the six methylchrysenes (MC). This is the first report on the unambiguous identification of each MBA isomer in real samples which will provide a better understanding of carcinogenic potency and further quantification of these compounds in tetraaromatic fractions.

Polycyclic aromatic hydrocarbons (PAH) and their alkylated derivatives are well recognized as ubiquitous contaminants of the environment. The major analytical problem in the determination of PAH in complex natural mixtures is the separation and the identification of individual components in the presence of the numerous other isomeric parent and alkyl-substituted PAH. Since the biological activity of aromatic compounds is isomer specific, the identification of each compound in an alkylated aromatic series is a vital part of understanding the carcinogenic activity of PAH mixtures.

Methylbenz[*a*]anthracenes (MBA) and methylchrysenes (MC) are among the most biologically active alkylated aromatic series found in man's environment (Figure 1) (*1–6*). There are 12 possible isomers in the MBA series which vary significantly with respect to carcinogenicity (Figure 1). 7-MBA has been recognized as the most tumorigenic compound, followed by 6-, 8-, and 12-MBA, which are of equal carcinogenicity, while 9- and 11-MBA are the next most carcinogenic compounds. The low tumorigenicity of the 1-, 2-, 3-, and 4-MBA has been generally cited in support of the bay region

[1] Université de Bordeaux.
[2] National Bureau of Standards.

0003-2700/87/0359-1695$01.50/0 © 1987 American Chemical Society

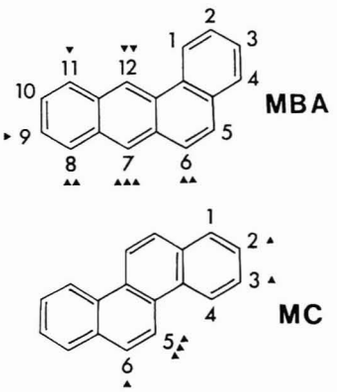

Figure 1. Relative carcinogenic activity of methylbenz[*a*]anthracene (MBA) and methylchrysene (MC) isomers on a scale of zero to ▲▲▲.

theory of PAH carcinogenesis (*7–11*). In the methylchrysene series, 5-MC is one of the most carcinogenic compounds while 2-, 3-, 4-, and 6-MC are moderately active (*1, 12*). However, identification of methyl tetraaromatic compounds is particularly difficult because of their similar behavior in chromatographic techniques (liquid or capillary gas chromatography) (*13, 14*). Capillary gas chromatography on conventional nonpolar phases (e.g., SE-54) and liquid chromatography are unsuccessful in the separation of all MBA and MC isomers (*12, 13*). Recent reports on liquid crystalline stationary phases in capillary gas chromatography demonstrated improved separation of these isomers (*15*); however, several isomers were still unresolved. Whereas the identification of MC isomers in natural extracts has been realized (*12, 14, 16*) only one tentative identification of MBA isomers was reported previously by ^{1}H NMR (*3, 14*).

One way to overcome the limitation of classical analytical techniques in the differentiation of isomeric compounds is to use high-resolution spectrometry (HRS) in *n*-alkane matrices (Shpol'skii effect) which has been shown to be adequate for solving such problems (*16–18*). This technique takes advantage of the sharpening of the fluorescence emission spectra when aromatics are incorporated into an appropriate *n*-alkane matrix at low temperature (*19*). During the past decade, Shpol'skii spectrometry has attracted the attention of analytical chemists considering the numerous publications recently reviewed (*20*).

In this paper, we report the low-temperature emission properties of MBA and their identification in rock and air particulate samples which also contained MC. Such studies will lead to the quantification of individual MBA and MC isomers, which is of particular interest in environmental chemistry and organic geochemistry (*21*).

EXPERIMENTAL SECTION

Chemicals and Samples. The MBA were purchased from the chemical repository of the National Cancer Institute (Bethesda, MD). The purity of each MBA was reported as greater than 96%. The six MC were purchased from the Community Bureau of Reference (BCR, Commission of the European Community, Brussels, Belgium). The purity of each MC was certified to be greater than 99.6%.

All the solvents (spectroscopic grade from Fluka and Merck) used for HPLC fractionation and Shpol'skii analysis were purified by distillation and then dried and kept over molecular sieves. Residual fluorescence emission of solvents was verified by room-temperature spectrofluorometry.

The sedimentary rock sample came from a well in an Indonesian petroleum field (*21*) and was provided by J. L. Oudin (TOTAL-CFP, Pessac, France). The tetraaromatic fractions from a Philadelphia, PA, air particulate sample and from a Washington, DC, air particulate sample (Standard Reference Material, SRM 1649, Urban Dust/Organics) were obtained according to the analytical procedure reported previously (*22, 23*).

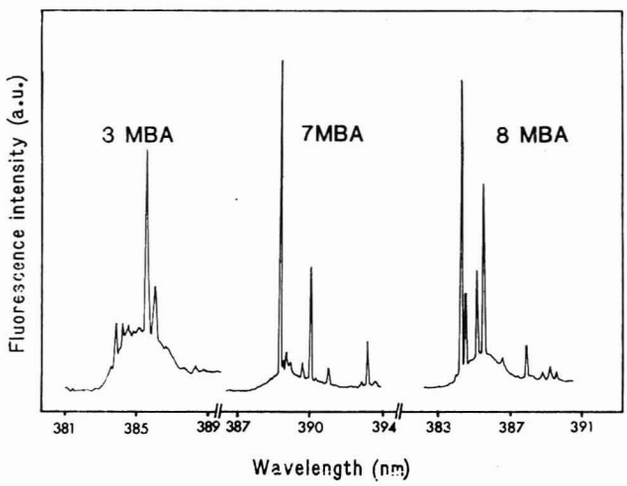

Figure 2. Fluorescence emission spectra of some individual reference MBA in *n*-octane at 15 K ($c = 10^{-6}$ M). Excitation was at 294 nm. Note the important diffuse base for the 3-MBA.

Isolation of Monomethyl Tetraaromatic Isomers. The fractionation procedure of aromatics, proposed by Wise et al. (*24*) has been modified and used as applied previously to the isolation of alkylated PAH (*16, 18, 21*). Briefly, the first normal-phase high-performance liquid chromatography (HPLC) step on an aminosilane column separates the aromatics into ring classes. A two-step reversed-phase LC fractionation procedure then utilizes the differences in selectivity between monomeric and polymeric C_{18} columns to isolate fractions suitable for HRS analysis. The separation on a monomeric reversed-phase C_{18} allows the collection of the methyl tetraaromatic fraction. This fraction is then separated on a polymeric reversed-phase C_{18} column which has high selectivity for the separation of PAH isomers (Supelcosil, type LC-PAH) (*13, 18, 25, 26*). A mixture of 70% acetonitrile in water was used as the mobile phase to yield fractions of one to four methyl tetraaromatic isomers that were amenable to identification by HRS.

High Resolution Shpol'skii Spectrometry (HRS). Low-temperature luminescence experiments were performed with a homemade spectrofluorometer described previously (*16*). Fused silica tubes containing the solutions were attached to the cold head of a closed cycle cryogenerator (CTI, Cryodyne 21 SC) operating at 15 K. Excitation was provided by a xenon lamp (450 W). Emission spectra were recorded and stored on a hard disk of a microcomputer (IBM/XT). Processing of the spectra gives emission peak wavelengths with a precision of 0.1 nm.

RESULTS AND DISCUSSION

Low-Temperature Spectrofluorometry of MBA Reference Compounds. Some previous studies have already reported the Shpol'skii emission spectra of some MBA isomers (*27–30*). The site multiplet structure for the 0–0 transition of the 12 MBA in *n*-octane at 15 K covers a spectral region of about 10 nm (Table I and Figure 2). Each compound exhibits sharp fluorescence emission spectra with a multiplet structure containing up to four quasi-line emission peaks arising from several different orientations of the MBA guest molecules in the frozen *n*-octane host (*29, 31*). The maximum long-wavelength displacement relative to the emission peak of the parent compound (benz[*a*]anthracene, BA) is observed when the methyl group is introduced at position 7 or 12, whereas 1-, 2-, 3-, 4-, 5-, 6-, 10-, and 11-methyl derivatives exhibited a shift of about 2–3.5 nm. The 9-MBA exhibits a slight short-wavelength displacement while the 8-MBA gives rise to a quasi-line structure in the same spectral area as the BA. All these observations are in good agreement with previous studies (*27, 28*).

When the low-temperature fluorescence emission spectra on the complete series of the 12 MBA are obtained, some interesting observations can be made. Some isomers (1-, 2-,

Table I. Characteristic Shpol'skii Fluorescence Emission Peaks of MBA and MC Isomers in *n*-Octane at $T = 15$ K[a]

compound	fluorescence emission peak, nm	Δλ, nm
benz[*a*]anthracene (BA)	384.0 (+++), 384.3 (+++)	
1-MBA	386.7 (+++), 387.0	2.7; 2.4
2-MBA	386.7 (+++), 387.0 (+++), 387.9 (+)	2.7; 2.4
3-MBA	385.3 (+++), 385.8 (+++)	1.3; 1.0
4-MBA	386.2 (+++), 388.5 (+++), 387.3 (+++)	2.2; 2.9
5-MBA	387.6 (+++), 387.9 (+), 388.1 (++), 388.5 (+)	3.6; 3.3
6-MBA	385.0 (++), 386.3 (++), 386.5 (+++), 386.8 (+)	2.5; 2.2
7-MBA	389.2 (+++), 390.9 (+)	5.2; 4.9
8-MBA	384.1 (+++), 384.3 (++), 385.0 (++), 385.4 (++)	0.1; 0.2
9-MBA	383.1 (+), 384.0 (+++), 384.5 (+)	−0.9; −1.2
10-MBA	386.1 (+), 387.0 (+++), 387.1 (++), 387.4 (+)	2.1; 1.8
11-MBA	384.3 (+), 385.6 (+++), 385.9 (++), 386.7 (++)	1.6; 1.3
12-MBA	390.6 (+++), 390.8 (+++), 391.4 (++), 392.1 (+)	6.6; 6.3
chrysene (C)	360.5 (+++), 361.1 (+++), 362.2 (++)	
1-MC	361.3 (++), 361.9 (++), 362.2 (++), 362.5 (+++)	0.8; 0.2
2-MC	361.2 (+++), 361.5 (+++)	0.7; 0.1
3-MC	362.0 (+++), 362.2 (++), 362.6 (++), 363.1 (+)	1.5; 0.9
4-MC	365.4 (+++), 366.0 (+), 366.9 (++)	4.9; 4.0
5-MC	367.2 (+++), 367.6 (++), 367.9 (+)	6.7; 5.8
6-MC	362.6 (+), 363.3 (+++), 364.6 (++)	1.9; 1.3

[a] Excitation at 294 nm for MBA and at 274 nm for MC. Δλ represents the peak shifts (in nm) of the major fluorescence peak of each methylated derivatives relative to the two major fluorescence peaks of the respective parent compound. Intensity scale is from zero to +++.

3-, 10-, and 12-MBA) exhibit quasi-linear emission peaks that emerge from a broad diffuse base (Figure 2) which could be attributed to a strong interaction between aromatic molecules and the *n*-octane chains. Such interaction could be due to the position of the methyl group which leads to a nonplanar character for some MBA molecules (*32*), e.g., the sterically hindered MBA with substituents in position 1 and 12. The presence of this diffuse base is also observed for MBA molecules for which the substituted carbon is bonded to carbon atoms not engaged in ring structure (2-, 3-, and 10-MBA). On the contrary, very nearly planar structures such as 4- and 11-MBA (*32*) do not exhibit such a diffuse base.

As shown in Table I, the multiplets of the MBA are subject to spectral interferences in the emission region of the 0–0 transition. Particularly 1- and 2-MBA exhibit major emission at the same wavelengths. However, as presented in Figure 3, the most carcinogenic compounds (6-, 7-, 8-, and 12-MBA) are easily identified in the synthetic mixture of the 12 isomers. The other MBA isomers could be identified tentitatively by two different analytical approaches: (a) by using selective excitation with a laser (*29*) or (b) by HRS analysis of fractions collected with a highly selective reversed-phase column (*18*). This second approach has been developed for the identification of MBA and MC as described in this paper.

Analysis of MBA and MC in Natural Extracts. Specific emission and excitation wavelengths of tetraaromatic parent compounds are listed in Table II. Despite numerous tetracyclic alkylaromatic derivatives, the selectivity of spectrofluorometry allows the observation of each series (chrysene, benz[*a*]anthracene, triphenylene, naphthacene, benzo[*c*]phenanthrene) without interferences between each other (Table I and II) (*33*). Methyltriphenylenes have also been observed as minor components of this fraction: indeed triphenylene exhibits fluorescence emission in *n*-octane at about 350 nm (*30*) and fluorescence emission peaks corresponding to possible methyltriphenylenes have been observed at about 355 nm; but without reference standards a true identification was not possible. Naphthacene (linear) and benzo[*c*]phenanthrene (sterically hindered) derivatives have not been detected and are most likely minor contributors according to

Table II. Characteristic Room-Temperature Fluorescence Properties of Tetraaromatic Parent Compound (*31*, *33*)[a]

tetraaromatic compounds	max emission wavelengths, nm	max absorption wavelengths, nm	structure	possible methyl derivatives
benz[*a*]anthracene	*385*, 405, 430	222, 268.5, 278, 299	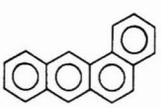	12
chrysene	*361*, 380, 402	218, 259, *269*	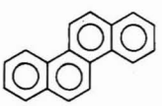	6
triphenylene	*355*, 362, 373	284, 273, *258*, 249		2
naphthacene	482.5, *513*, 551	294, *275*, 265	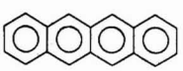	3
benzo[*c*]phenanthrene	broad band centered at 400	218.5, 222, 272, *283*	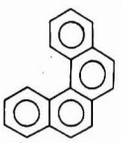	6

[a] The most intense band is italicized.

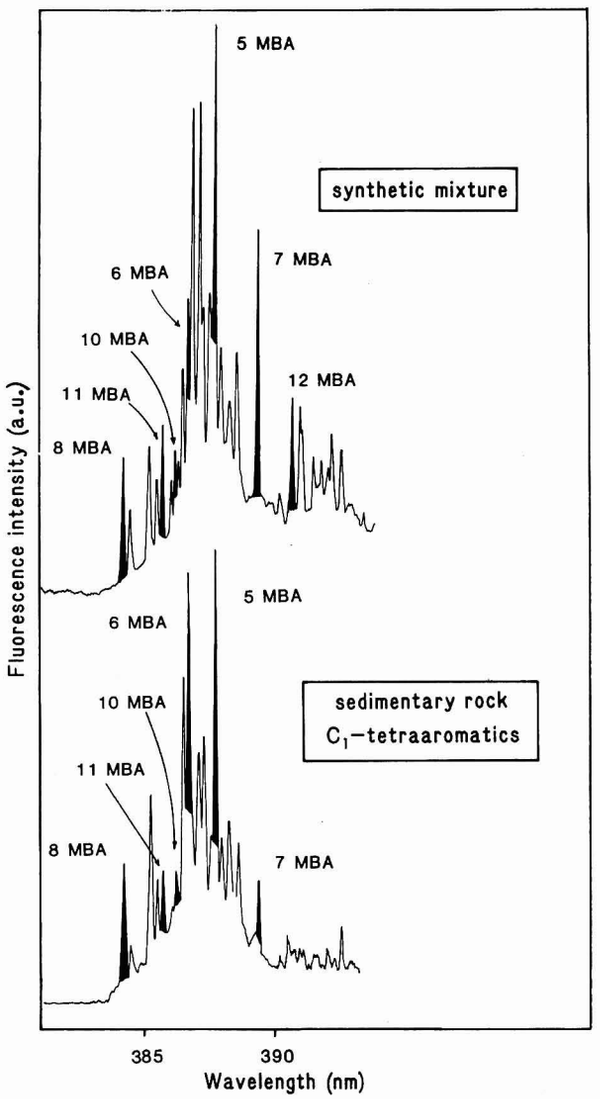

Figure 3. Fluorescence emission spectra of MBA isomers (excitation at 294 nm): (a) in an equimolar synthetic mixture of the 12 MBA (each at $c = 10^{-7}$ M); (b) in a C_1 tetraaromatic rock extract. Note the lack of 12-MBA and the presence of the very carcinogenic 7-MBA.

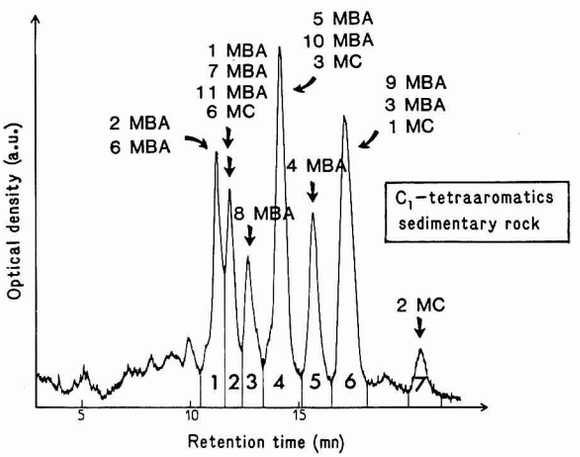

Figure 4. Reversed-phase LC analysis of C_1 tetraaromatic fraction from a sedimentary rock. Absorption detection was centered at 288 nm. Compounds are identified on the basis of HRS spectra of reference compounds. Note the lack of 12-MBA.

the predominance of angular over linear annelated and sterically hindered structures (*34*). Therefore, the distribution of monomethyl tetraaromatics is dominated by the methylbenz[*a*]anthracenes and methylchrysenes.

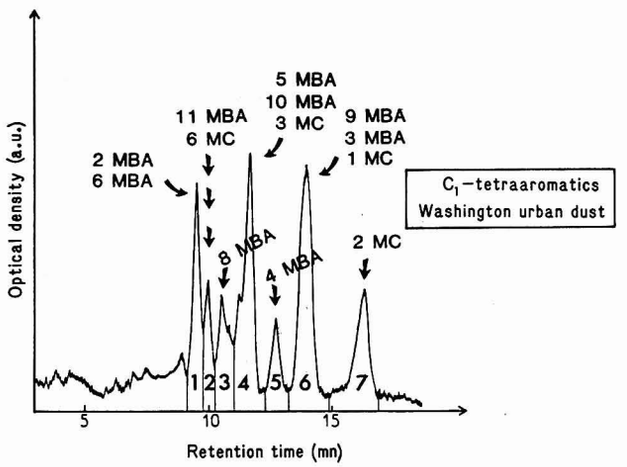

Figure 5. Reversed-phase LC analysis of C_1 tetraaromatic fraction from Washington urban dust (SRM 1649). Absorption detection was centered at 288 nm. Compounds have been identified on the basis of HRS spectra of reference compounds. Note the lack of 1-, 7-, and 12-MBA.

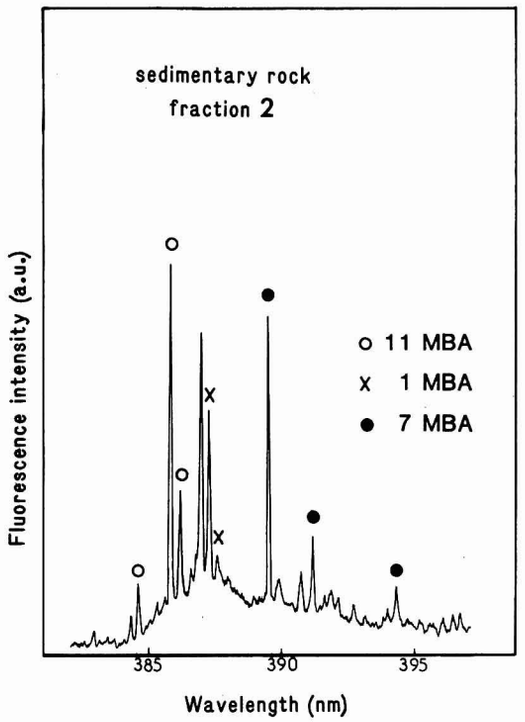

Figure 6. Fluorescence spectra of some MBA in subfraction 2 of C_1 tetraaromatic fraction from the sedimentary rock. Excitation was at 294 nm.

The total C_1 tetraaromatic fraction of the sedimentary rock which was isolated by reversed-phase LC on the monomeric C_{18} column was analyzed by HRS for MBA determination. Despite MBA emission interferences, HRS allows a partial identification of selected MBA isomers (Figure 3). In particular, it is possible to observe the lack of 12-MBA and the presence of 7-MBA in the C_1 tetraaromatic rock extract which are two of the most carcinogenic compounds of the series.

The C_1 tetraaromatic fractions from the sedimentary rock and air particulate samples were submitted to an HPLC step on the highly selective polymeric C_{18} column (Figures 4 and 5). As indicated by Wise et al. (*13*) and in Table III, only part of the methyl tetraaromatic isomers could be cleanly separated from each other. The identification of MBA and MC isomers in HPLC subfractions is demonstrated in Figures 6–8. Indeed, despite the use of an observation centered at an absorption of 288 nm that favors MBA detection, MC

Table III. LC Retention Index (log *I*, ref 13) of MBA and MC and Their Identification in Natural Sample Fractions (See Figures 4 and 5)

compound	retention index (log *I*)	sedimentary rock	Washington urban dust	Philadelphia air particulate matter
2-MBA	4.09	fraction 1	fraction 1	fraction 1
12-MBA	4.10			
6-MBA	4.10	fraction 1	fraction 1	fraction 1
11-MBA	4.13	fraction 2	fraction 2	fraction 2
1-MBA	4.14	fraction 2		
5-MC	4.14			
6-MC	4.14	fraction 2	fraction 2	fraction 2
7-MBA	4.14	fraction 2		
4-MC	4.18			
8-MBA	4.19	fraction 3	fraction 3	fraction 3
10-MBA	4.24	fraction 4	fraction 4	fraction 4
5-MBA	4.88	fraction 4	fraction 4	fraction 4
3-MC	4.29	fraction 4	fraction 4	fraction 4
4-MBA	4.33	fraction 5	fraction 5	fraction 5
3-MBA	4.39	fraction 6	fraction 6	fraction 6
9-MBA	4.39	fraction 6	fraction 6	fraction 6
1-MC	4.43	fraction 6	fraction 6	fraction 6
2-MC	4.52	fraction 7	fraction 7	fraction 7

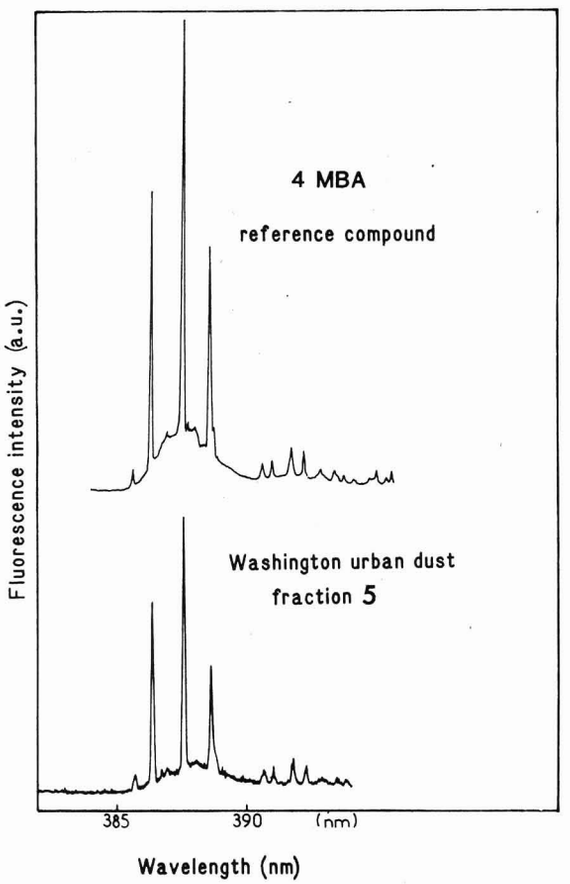

Figure 7. Fluorescence spectra of 4-MBA in *n*-octane at $T = 15$ K (excitation at 294 nm): (a) reference compound ($c = 10^{-6}$ M); (b) Washington urban dust subfraction.

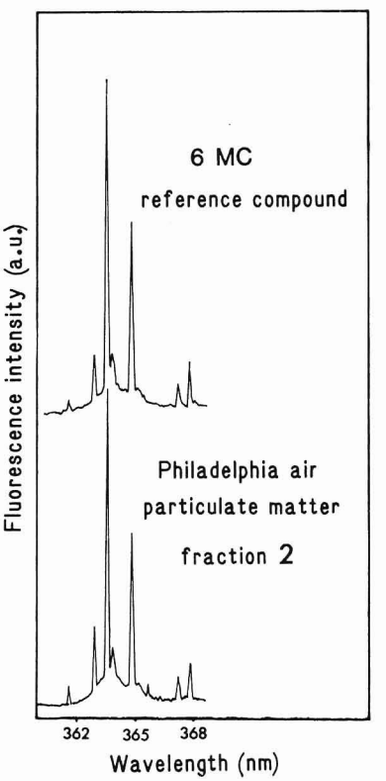

Figure 8. Fluorescence spectra of 6-MC in *n*-octane at $T = 15$ K (excitation at 274 nm): (a) reference compound ($c = 10^{-6}$ M); (b) subfraction from Philadelphia air particulate matter. Note the lack of the highly carcinogenic 5-MC which would be eluted with 6-MC, if present.

isomers contribute to the HPLC fingerprint (see Figures 4 and 5 where peak 7 is due only to 2-MC).

The 11 MBA and four MC presented in Table III could be identified by comparison of their HRS emission spectra with that of the respective standard spectra. Both a coincidence in the position of the quasi-lines and also a good agreement in the relative intensities of the quasi-lines provide a definitive identification of each compound (Figures 7 and 8). 12-MBA is absent from the three natural extracts. Steric hindrance could be responsible for the lack of 12-MBA as well for the lack of 4- and 5-MC, which has been previously mentioned (*21*). 1- and 7-MBA have been specifically identified in the rock extract but where not found in the air particulate extracts. These two compounds are presumably less stable than the other isomers. Methyl shift reactions could occur at higher temperatures in aerosol formation than in the sedimentary matter and would favor the formation of more stable methyl isomers. The absence of 7- and 12-MBA in the atmospheric particulate samples is in good agreement with the only previously reported determination of these compounds in air particulate matter (*3*).

These studies on the methylbenz[*a*]anthracene and methylchrysene series demonstrate the capability of HRS coupled with HPLC separations for the differentiation of very closely

related compounds such as MBA and MC. Positive identification of the 12 MBA isomers has not been reported previously due to the chromatographic interferences of MBA from each other or from other methyltetraaromatic isomers.

This work is only the first step toward a better understanding of MC and MBA behavior in environmental samples. Further developments will lead to the relative quantification of these methyl-PAH in various natural samples to give a real evaluation of biological activity of PAH fractions.

ACKNOWLEDGMENT

We thank J. Joussot-Dubien for his continuous interest and support. Thanks are due to J. L. Oudin (CFP-TOTAL) for providing sedimentary rock samples and to J. Lewtas (U.S. EPA) for providing the Philadelphia air particulate sample. The authors also wish to thank R. De Sury and N. Chedozeau for technical assistance with the analytical work.

Registry No. 1-MBA, 2498-77-3; 2-MBA, 2498-76-2; 3-MBA, 2498-75-1; 4-MBA, 316-49-4; 5-MBA, 2319-96-2; 6-MBA, 316-14-3; 7-MBA, 2541-69-7; 8-MBA, 2381-31-9; 9-MBA, 2381-16-0; 10-MBA, 2381-15-9; 11-MBA, 6111-78-0; 12-MBA, 2422-79-9; 1-MC, 3351-28-8; 2-MC, 3351-32-4; 3-MC, 3351-31-3; 4-MC, 3351-30-2; 5-MC, 3697-24-3; 6-MC, 1705-85-7.

LITERATURE CITED

(1) Hoffman, D.; Schmeltz, I.; Hecht, S. S.; Wynder, E. L. *Polycyclic Hydrocarbons and Cancer*; Gelboin, H. V., P.O.P.T.'s O, Eds.; Academic: New York, 1978; Vol I, pp 85–117.
(2) Thomas, R. S.; Lao, R. C.; Wang, D. T.; Robinson, D.; Sakuma, T. *Carcinogenesis Vol. 3: Polycyclic Aromatic Hydrocarbons*; Jones, P. W., Freudenthal, R. I., Eds.; Raven Press: New York, 1978; pp 9–19.
(3) Bartle, K. D.; Lee, M. L.; Novotny, M. *Analyst (London)* **1977**, *102*, 731–738.
(4) Carruthers, W.; Stewart, H. N. M.; Watkins, D. A. M. *Nature (London)* **1967**, *213*, 691–692.
(5) Grimmer, G.; Jacob, J.; Naujack, K. W.; Dettbarn, G. *Fresenius' Z. Anal. Chem.* **1981**, *309*, 13–19.
(6) Lee, M. L.; Novotny, M.; Bartle, K. D. *Anal. Chem.* **1976**, *48*, 1566–1572.
(7) Morgan, D. D.; Warshawsky, D.; Atkinson, T. *Photochem. Photobiol.* **1977**, *25*, 31–38.
(8) Snook, M. E.; Severson, R. F.; Higman, H. C.; Arrendale, R. F.; Chortyk, O. T. *Polycyclic Aromatic Hydrocarbons*; Jones, P. W., Leber, P., Eds.; Ann Arbor Science Publishers: Ann Arbor, MI, 1979; pp 231–260.
(9) Smith, I. A.; Seybold, P. G. *Int. J. Quantum Chem., Quantum Biol. Symp.* **1978**, *No. 5*, 311–320.
(10) Wislocki, P. G.; Florentini, K. M.; Fu, P. P.; Yang, S. K.; Lu, A. Y. H. *Carcinogenesis* **1982**, *3*, 215–217.
(11) Newman, M. S. *Carcinogenesis Vol. I, Polycyclic Aromatic Hydrocarbons: Chemistry, Metabolism and Carcinogenesis*; Raven Press: New York, 1976; pp 203–207.
(12) Hecht, S. S.; Bondinell, W. E.; Hoffman, D. *J. Natl. Cancer Inst. (U. S.)* **1974**, *52*, 1121–1133.
(13) Wise, S. A.; Bonnett, W. J.; Guenther, F. R.; May, W. E. *J. Chromatogr. Sci.* **1981**, *19*, 457–465.
(14) Lee, M. L.; Novotny, M.; Bartle, K. D. *Analytical Chemistry of Polycyclic Aromatic Compounds*; Academic: London, 1981; pp 353.
(15) Bradshaw, J. S.; Schregenberger, C.; Chang, K. H.-C.; Markides, K. E.; Lee, M. L. *J. Chromatogr.* **1986**, *358*, 95–106.
(16) Garrigues, P.; Ewald, M. *Anal. Chem.* **1983**, *55*, 2155–2159.
(17) Garrigues, P.; Bourgeois, G.; Veyres, A.; Rima, J.; Lamotte, M.; Ewald, M. *Anal. Chem.* **1985**, *57*, 1068–1070.
(18) Radke, M.; Willsch, H.; Garrigues, P.; De Sury, R.; Ewald, M. *Chromatographia* **1984**, *19*, 355–361.
(19) Shpol'skii, E. V.; Bolotnikova, T. N. *Pure Appl. Chem.* **1974**, *37*, 183–195.
(20) De Lima, C. G. *CRC Crit. Rev. Anal. Chem.* **1985**, *16*, 177–222.
(21) Garrigues, P.; De Sury, R.; Angelin, M. L.; Ewald, M.; Oudin, J. L.; Connan, J. *Org. Geochem.* **1984**, *6*, 829–837.
(22) Wise, S. A.; Benner, B. A.; Chesler, S. N.; Hilpert, L. R.; Vogt, C. R.; May, W. E. *Anal. Chem.* **1986**, *58*, 3067–3077.
(23) Wise, S. A.; Chesler, S. N.; Hilpert, L. R.; May, W. E.; Rebbert, R. E.; Vogt, C. R.; Nishioka, M. G.; Austin, A.; Lewtas, J. *Environ. Int.* **1985**, *11*, 147–160.
(24) Wise, S. A.; Chesler, S. N.; Hertz, H. S.; Hilpert, L. R.; May, W. E. *Anal. Chem.* **1977**, *49*, 2306–2310.
(25) Sander, L. C.; Wise, S. A. *Anal. Chem.* **1984**, *56*, 504–510.
(26) Wise, S. A.; Sander, L. C. *HRC CC, J. High Resolut. Chromatogr. Chromatogr. Commun.* **1985**, *8*, 248–255.
(27) Fenina, N. A. *Opt. Spectrosc. (Engl. Transl.)* **1966**, *20*, 768–772.
(28) Fenina, N. A. *J. Appl. Spectrosc. (Engl. Transl.)* **1967**, *6*, 216–219.
(29) Yang, Y.; D'Silva, A. P.; Fassel, V. A. *Anal. Chem.* **1981**, *53*, 894–899.
(30) Garrigues, P.; De Sury, R., unpublished results, Laboratoire de Chimie Physique A, Université de Bordeaux I, France.
(31) Garrigues, P.; Ewald, M. *Spectral Atlas of Polycyclic Aromatic Compounds*; Karcher, W., Fordham, R. J., Dubois, J. J., Glaude, P. G. J. M., Ligthart, J. A. M., Eds.; Reidel: Dordrecht, 1985.
(32) Briant, C. E.; Jones, D. W.; Shaw, J. D. *J. Mol. Struct.* **1985**, *130*, 167–176.
(33) Berlman, I. In *Handbook of Fluorescence Spectra of Aromatic Molecules*; Academic: New York, 1971.
(34) Blumer, M. *Sci. Am.* **1976**, *234*, 34–45.

RECEIVED for review November 20, 1986. Accepted March 2, 1987. Certain commercial equipment, instruments, or materials are identified in this report to specify adequately the experimental procedure. Such identification does not imply recommendation or endorsement by the National Bureau of Standards, nor does it imply that the materials or equipment identified are necessarily the best available for the purpose.

Sampling of Airborne Polycyclic Aromatic Hydrocarbons

Rein Otson*

Environmental Health Directorate, Health and Welfare Canada, Room B-19, E.H.C., Tunney's Pasture, Ottawa, Ontario, Canada K1A 0L2

John M. Leach and Lambert T. K. Chung

B.C. Research, 3650 Wesbrook Mall, Vancouver, British Columbia, Canada V6S 2L2

Limitations of NIOSH sampling method P and CAM 183 were defined for airborne standard mixtures of polycyclic aromatic hydrocarbons (PAH) generated as vapors in a flow-through apparatus. The PAH fell into three categories: those that were too volatile to be collected by the NIOSH filtration method at normal ambient temperatures and were best sampled with Tenax or XAD-2 sorbent (i.e., indane, naphthalene, biphenyl, acenaphthene, fluorene, 9,10-dihydrophenanthrene, phenanthrene, and anthracene); those that were quantitatively collected by filters, even after a brief airborne residence time (i.e., benz[*a*]anthracene, chrysene, benzo[*a*]pyrene, dibenz[*a*,*h*]anthracene, and benzo[*ghi*]perylene); and those that partitioned between filter and sorbent (i.e., fluoranthene and pyrene). A combination glass fiber/silver membrane filter backed by two sorbent tubes in series gave overall mean recoveries of 94–96% for the 15 PAH studied at total concentrations of, nominally, 0.2 and 0.02 mg/m^3. Individual PAH concentrations were 0.03–0.05 and 0.003–0.005 mg/m^3, respectively.

A recent study of emissions to the workplace from bench-scale coal liquefaction units (*1*) indicated that concentrations of total polycyclic aromatic hydrocarbons (PAH) were usually less than 0.1 mg/m^3 and levels of individual PAH rarely exceeded 0.001 mg/m^3. However, there was concern that use of NIOSH sampling procedure P & CAM 183 (*2*), which employs glass fiber and silver membrane filters, may have resulted in low recoveries of PAH. Several studies have shown that recovery of airborne PAH containing two to four rings is inefficient when conventional filter capture techniques are used. Collection of the more volatile compounds is incomplete, and fractions of those that are initially retained by the filters subsequently vaporize. Ratios of particulate and vapor-phase PAH in automobile emissions (*3–5*) and urban air (*6–8*) have been recorded, but none of these studies included method validation with known concentrations of standard compounds.

NIOSH procedures for determining recovery efficiencies of organic compounds involve injection of a solution containing the contaminant of interest onto the collection medium. A more realistic method is to use dynamic, flow-through calibration with atmosheres containing known concentrations of the compounds of interest. In this way overall collection and recovery efficiencies can be determined taking into account factors such as humidity, temperature, sampling time and air flow rate, contact with aerial oxygen, and exposure to light, which are believed to affect recoveries of PAH. One study (*9*) has used a flow-through vapor generation system to determine the collection and recovery efficiency of four vapor-phase PAH on Amberlite XAD-2 resin. However, there was no attempt to generate a known, constant concentration of vapor, and filters were not used to determine vapor:particulate phase ratios for standard mixtures of PAH.

Recently, an apparatus was designed and used to determine the effectiveness of filters and sorbents for collection of airborne aromatic amines (*10*). This apparatus was also used to measure the effectiveness of NIOSH filter method P & CAM 183 for collecting 15 airborne PAH and to determine recoveries on back-up tubes containing polymeric sorbents (Tenax or XAD-2) of PAH that were not retained by the NIOSH glass fiber/silver membrane filter combination. The concentration of total PAH in air was adjusted as closely as practical to the American Conference of Governmental Industrial Hygienists (*11*) threshold limit value (TLV) of 0.2 mg/m^3 (1 × TLV) for coal tar pitch volatiles and to 0.02 mg/m^3 (0.1 × TLV). Airborne particulates affect the partitioning of PAH between vapor and solid phases by providing nuclei for condensation and surfaces for adsorption. In some experiments a chamber was used to provide a known contact time for vapors with particulate-containing laboratory air.

EXPERIMENTAL SECTION

Materials. PAH were obtained from the following sources (specified purity in parentheses): naphthalene (95%), biphenyl (95%), fluorene (95%), phenanthrene (95%), anthracene (95%), fluoranthene (90%), pyrene (95%), and chrysene (95%) were from MicroTek, Baton Rouge, LA; indane (95%), benz[*a*]anthracene (99%), benzo[*a*]pyrene (99%), dibenz[*a*,*h*]anthracene (99%), and benzo[*ghi*]perylene (99%) were supplied by Ultra Scientific, Hope, RI; acenaphthene (purity not specified) was from K & K Laboratories, Inc., Plainview, NY; and 9,10-dihydrophenanthrene (97%) was from Aldrich Chemicals, Milwaukee, WI.

PAH were tested in three groups with similar volatilities (Table I). Standard solutions of the PAH groups were prepared by dissolving the compounds in diethyl ether (glass distilled, BDH Limited) to give concentrations of 0.64 and 0.064 mg/mL of each group 1 PAH, 1.0 and 0.1 mg/mL of each group 2 PAH, and 0.4 and 0.04 mg/mL of each group PAH. Inadvertently, the concentration of acenaphthene was twice that for each of the other group 1 PAH. Calibration solutions (group 1, 16 and 1.6 μg/mL; group 2, 25 and 2.5 μg/mL; group 3, 20 and 2 μg/mL) containing *n*-tridecane internal standard (30 μg/mL for 1 × TLV and 4 μg/mL for 0.1 × TLV tests) were prepared from the appropriate standard solutions. Solutions were stored in the dark at −10 °C and warmed to room temperature before use.

Glass tubes containing 100 mg front and 50 mg backup sections of Tenax or 150 and 75 mg sections of XAD-2 resin were obtained from SKC, Inc. Glass fiber and silver membrane filters (37 mm diameter) from SKC, Inc., and filter support pads (37 mm) from Millipore Corp. were Soxhlet extracted with cyclohexane (*10*).

Gas Chromatography. Gas chromatography (GC) analyses were generally done as previously reported (*10*). The GC oven temperature was adjusted to suit each PAH group and concentration. Typically, the oven temperature was held at 100 °C during injection and was then immediately raised at a rate of 8 °C/min for at least 14 min. The injector split ratios were 1:50 and 1:10 for experiments at 1 × TLV and 0.1 × TLV, respectively.

Vaporization and Sampling Tests. Vaporization and collection of PAH were generally done as previously described for aromatic amines (*10*). Laboratory air was normally 22 °C and at 45–60% relative humidity (RH). Standard solutions of group 1 or group 2 PAH (25–50 μL) were injected into the quartz capillary tube of a Hewlett-Packard Model 18580A pyroprobe. The pyroprobe temperature was programmed to vaporize PAH into a stream of high-purity nitrogen (120 mL/min) at a steady rate over 3 to 4 h. Nitrogen flow rate and temperatures required were

0003-2700/87/0359-1701$01.50/0 Published 1987 by the American Chemical Society

Table I. Polycyclic Aromatic Hydrocarbons and Some Properties

compound	bp, °C (760 mmHg)[a]	RRT[b]	EVC,[c] μg/m³
Group 1			
IND indane	178	0.40	
NAP naphthalene	218	0.71	5.4×10^5
BIP biphenyl	255	1.24	
ACE acenaphthene	279	1.54	1.8×10^4
FLU fluorene	294	1.82	5.4×10^3
DHP 9,10-dihydrophenanthrene		2.11	
Group 2			
PHE phenanthrene	338	2.64	1.2×10^3
ANT anthracene	340	2.67	6.0×10^2
FLA fluoranthene	383	3.53	1.0×10^2
PYR pyrene	393	3.69	4.9×10
			7.4×10[e]
Group 3			
BaA benz[*a*]anthracene	435	4.61	2.6, 1.1[e]
CHR chrysene	441	4.64	
BaP benzo[*a*]pyrene	496	5.60	0.85×10^{-1}[e]
DBA dibenz[*a,h*]anthracene	270[d]	6.37	
BPE benzo[*ghi*]perylene	278[d]	6.50	0.16×10^{-2}[e]

[a] *Handbook of Polycyclic Aromatic Hydrocarbons*; Bjorseth, A., Ed.; Marcel Dekker: New York, 1983; p 709. [b] Relative to *n*-tridecane. [c] Equilibrium vapor concentration at 25 °C calculated from vapor pressures in ref 18. [d] Melting point. [e] EVC from ref 17.

Table II. PAH Extraction Recoveries[a] (%) with Cyclohexane

compound	amt added, μg	% recovery Tenax	XAD-2	filters
indane	1.6	95.9		
	8	103.0	95.2	
	16	89.6	90.5	
naphthalene	1.6	98.4		
	8	86.8	94.2	
	16	85.2	87.0	
biphenyl	1.6	97.7		
	8	86.8	89.5	
	16	83.9	84.1	
acenaphthene	3.2	98.8		
	16	85.7	85.0	
	32	81.9	80.0	
fluorene	1.6	99.6		
	8	86.5	84.1	
	16	81.8	80.4	
9,10-dihydro-phenanthrene	1.6	98.5		
	8	90.6	89.9	
	16	84.6	84.1	
phenanthrene	2.5	91.5		
	8	88.0	81.9	
	25	90.2		99.5 (93.1)[b]
anthracene	2.5	93.1		
	8	89.2	82.7	
	25	91.5		101.0 (93.6)[b]
fluoranthene	2.5	86.5		
	25	86.5		103.0 (94.0)[b]
pyrene	2.5	85.9		
	25	87.3		102.0 (92.9)[b]
benz[*a*]anthracene	2			94.3
	20			97.5
chrysene	2			97.3
	20			92.0
benzo[a]pyrene	2			94.8
	20			98.8
dibenz[a,h]anthracene	2			103.7
	20			98.5
benzo[*ghi*]perylene	2			101.8
	20			99.3

[a] Averages for triplicate determinations. [b] Values in parentheses are for benzene extraction.

determined in prior tests involving analyses of PAH residues in the pyroprobe tube after 1, 2, 3, and 4 h. The pyroprobe outlet was connected by a Swagelok adapter (3.2 to 6.4 mm) to one of two types of mixing units. In one mixing unit, which gave an airborne time of ca. 0.5 s between generation and collection, PAH vapors and air were mixed in a T- or Y-shaped unit made from glass tubing (10 cm × 6.4 mm i.d.) encased in an electrical heating mantle to minimize condensation of PAH. A second apparatus (*10*) consisted of a glass vortex mixer and 2-L residence chamber wrapped with heating tape and gave a mean airborne time of ca. 37 s, based on smoke tests. In experiments with the least volatile PAH (group 3), the pyroprobe and mixing unit were replaced by a straight length of glass tubing (90 mm × 5 mm i.d., I piece) wrapped with heating tape. Group 3 PAH were vaporized directly from the tubing into an air stream. Each mixing unit was attached directly to the inlet of a 37-mm closed-face cassette containing a glass fiber filter, backed by a silver membrane filter and support pad. Normally, a sorbent tube containing Tenax followed by a tube containing XAD-2 resin was coupled in series to the outlet of the cassette. The combined flow rate for nitrogen and air through the sampling train was ca. 2 L/min (*10*). For 0.1 × TLV concentration, laboratory air was purified by passage through ca. 50 cm^3 Tenax in a glass tube (*10*).

Extraction. Extraction of sorbents, filters, and support pads and preparation of the extracts for analysis were done by using cyclohexane instead of 2-propanol as previously described for aromatic amines (*10*). The vaporization and mixing apparatus components were also rinsed with cyclohexane, and the extracts were concentrated by evaporation prior to analysis. Appropriate amounts of *n*-tridecane internal standard were added to all extracts. In most cases, GC analysis was completed the same day as PAH vaporization and collection.

Extraction recoveries were determined in triplicate (*10*). Aliquots of PAH standard solutions (25 μL for group 2, 50 μL for group 3) were injected onto the filters and support pad in a 50-mL beaker and the ether was allowed to evaporate for 1 min before extraction. Group 1 or 2 PAH solution (25 μL) was also injected onto Tenax or XAD-2 resin in the front sections of sorbent tubes. The tubes were capped immediately and stored at 2 °C for 16 to 24 h, then the resin sections were extracted separately, as was done for the sampling runs. Tests for contamination were done periodically by analysis of solvents and rinses and extracts from the pyroprobe assembly, filters, support pads, and sorbents in blank determinations using only nitrogen and laboratory air.

The concentration and size of suspended particulate matter in laboratory air used to dilute PAH vapors were measured with a calibrated Berkeley Telonics QCM particle size classifier. Sampling periods were 3 to 4 h at an air flow of 250 mL/min through the instrument.

RESULTS AND DISCUSSION

Boiling points, relative retention times, and equilibrium vapor concentrations (EVC) for the 15 PAH are listed in Table I. The nominal GC quantitation limits were 1 ng injected for each PAH. For calibration solutions containing individual PAH at nominally 2 and 20 μg/mL and with quantitation based on the internal standard GC response, results from all injections were within ±5% of the calibrated concentration value. Group 3 compounds at 2 μg/mL were the exceptions in that the analytical precision sometimes ranged to ±10%.

Since the use of benzene can pose a health hazard and cyclohexane gave somewhat better recoveries in initial tests (Table II), the latter solvent was used for all extractions. Mean extraction efficiencies for group 1 and 2 PAH from Tenax with cyclohexane ranged from 82 to 103% (Table II). Best recoveries were obtained at loadings corresponding to 0.1 × TLV concentrations (overall mean recovery of 94.6%). For XAD-2, extraction efficiencies for group 1 and 2 PAH ranged from 80 to 95% at loadings corresponding to 1 × TLV concentrations. Since they were not found on the corresponding col-

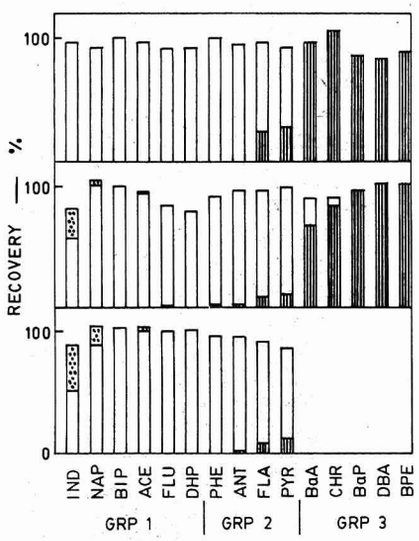

Figure 1. Mean recoveries of PAH (see Table I) from filters (striped), Tenax (clear), and XAD-2 (dotted): top, 0.1 × TLV, 0.5 s; middle, 1 × TLV, 0.5 s; bottom, 1 × TLV, 37 s.

lection media during sampling tests, extraction efficiencies for group 3 PAH on Tenax and XAD-2 and group 1 PAH on filters were not determined. Mean extraction efficiencies of group 2 PAH from filters ranged from 99 to 103% at a loading corresponding to 1 × TLV. For group 3 PAH on filters, mean extraction efficiencies were 92–99% and 94–104%, respectively, at 1 × TLV and 0.1 × TLV loadings. The precision of each triplicate extraction efficiency determination was better than 7% relative standard deviation.

Blank determinations on the complete experimental system using different types of mixing apparatus, and on the various components separately, showed no contamination from laboratory air, from PAH residues on the equipment, or from filters, sorbents, or solvents under the conditions used for experiments at 1 × TLV. At the higher sensitivity required for experiments at 0.1 × TLV, it was necessary to use Tenax sorbent to remove trace contaminants from the laboratory air used for dilution and to provide clean blanks. Impurities from XAD-2 resin, as received, interfered with analyses at 0.1 × TLV, and it was necessary to extract the resin with cyclohexane and diethyl ether prior to use.

Calculated average total (i.e., sum of individual PAH) concentrations of airborne PAH during 3–4.5 h of sampling ranged from 0.16 to 0.27 mg/m^3 in experiments targeted at 1 × TLV concentration (0.2 mg/m^3); 70% of the runs averaged 0.18–0.22 mg/m^3. For experiments at ca. 0.1 × TLV, mean total PAH concentrations were 0.017–0.021 mg/m^3. The volume of air sampled was usually 0.45–0.55 m^3. Particulate concentrations in laboratory air used to dilute the PAH vapors ranged from 1.3 to 14.4 μg/m^3. The principal size fractions had mass median diameters of 0.1–0.4 and 2.1–9.0 μm.

The most volatile PAH (group 1) were not retained by the filters but were collected by backup sorbent resins (Figure 1). At 1 × TLV concentration (0.2 mg/m^3 total PAH) a second sorbent tube (containing XAD-2) was necessary for complete recovery of indane, naphthalene, and acenaphthene (Figure 1), but biphenyl, fluorene, and 9,10-dihydrophenanthrene were retained by the first tube. A second tube containing XAD-2 instead of Tenax was used in the attempt to obtain some information on the breakthrough characteristics and potential use of XAD-2 as an alternative sorbent. Group 1 PAH were not retained by the filters even with a mean airborne residence time of 37 s (Figure 1). The filter surface temperature was approximately 22 °C. Overall recoveries tended to decrease with decreasing volatility of group 1 PAH at 1 × TLV concentration (Figure 1). At 0.1 × TLV (0.02 mg/m^3 total PAH) there was also no detectable retention of group 1 compounds by the filters and support pad (Figure 1). More than 90% was recovered from the initial Tenax tube. However, 25–50% of the indane was in the back section of the tube.

PAH in group 2 were partly retained on the filters and support pad but mostly in the front section of the first sorbent tube (Figure 1). In experiments at 1 × TLV, 0.5-s airborne time, mean retention by the filters was 1.5% for phenanthrene and anthracene and approximately 8% for fluoranthene and pyrene. However, results were variable, with recoveries by the filters and support pad ranging from 0 to 6% for phenanthrene and anthracene, and 0 to 25% for fluoranthene and pyrene. The filter surface temperature was approximately 25 °C as a result of heat applied to the mixing apparatus to minimize condensation on the walls. With a mean airborne residence time of 37 s, the proportion of group 2 PAH collected on the filters increased with decreasing volatility, from 0.7% for phenanthrene to approximately 16% for pyrene. The filter surface temperature was 22 °C. At 0.1 × TLV, all the detectable phenanthrene and anthracene was collected by the first tube front section; none was present on the filters and support pad (Figure 1). Higher portions of fluoranthene (mean 26%, range 11–34%) and pyrene (mean 28%, range 11–42%) were retained by the filters and pad than at 1 × TLV.

The least volatile group of PAH condensed in the outlet of the normal apparatus used for generation of airborne PAH and therefore were vaporized from a heated glass tube directly into a stream of dilution air. Group 3 PAH (Figure 1) were collected entirely on the filters at 1 × TLV and 0.1 × TLV concentrations even after an airborne residence time of only 0.5 s. The filter surface temperature was 40 °C as a consequence of the 160–180 °C apparatus temperature needed to prevent condensation of the compounds.

Overall recoveries of 15 PAH on filters and sorbents, corrected for extraction efficiencies, averaged 94.4% (range 79.5–105.0%) at 1 × TLV concentration, 0.5-s airborne time (Table III). At 0.1 × TLV concentration under the same conditions, mean recovery of individual PAH was 92.4% (range 82.5–105.3%; Table III). When the mean airborne time was ca. 37 s, recoveries of group 1 and 2 PAH averaged 97.6% (86.5–105.7%) at 1 × TLV concentration (Table III). Sampling limitations of the NIOSH filtration method P & CAM 183 were thus defined for airborne PAH generated in a flow-through apparatus. The PAH fell into three categories: those that were too volatile to be collected by filters at normal ambient temperatures and were best sampled with a sorbent (i.e., indane, naphthalene, biphenyl, acenaphthene, fluorene, 9,10-dihydrophenanthrene, phenanthrene, and anthracene); those that were quantitatively collected by filters even after a brief airborne residence time (i.e., benz[*a*]anthracene, chrysene, benzo[*a*]pyrene, dibenz[*a,j*]anthracene, and benzo[*ghi*]perylene); and those that partitioned between filter and sorbent (i.e., fluoranthene and pyrene). Similar distributions of particulate:vapor-phase PAH have been reported in the sampling of emissions from automobiles (*5*, *12*), from coke ovens (*9*, *13*), in urban air (*6*, *8*) and in office air (*14*).

The airborne PAH generation system used in this study provided a means to calibrate and standardize collection efficiencies of vapor phase and condensable PAH on a combination glass fiber/silver membrane filter backed by sorbent tubes. Recoveries of 82–105% were obtained from airborne concentrations of 0.003–0.005 mg/m^3 individual PAH—total PAH concentration 0.02 mg/m^3 (0.1 × TLV)—at a sampling air flow rate of 2 L/min over 3–4.5 h. Similar recoveries were obtained at 10 times these concentrations, i.e., at the TLV.

Compounds with intermediate volatility, such as fluoranthene and pyrene, were sensitive to sampling conditions and gave a lower distribution precision between filter and sorbent

Table III. Mean Recoveries of PAH

PAH	1 × TLV, 37 s[a]			1 × TLV, 0.5 s[a]			0.1 × TLV, 0.5 s[a]		
	no. of tests	recovery, %	RSD, %	no. of tests	recovery, %	RSD, %	no. of tests	recovery, %	RSD, %
indane	3	89.4	3.1	4	82.7	6.7	3	96.1	4.8
naphthalene	3	105.7	3.8	4	105.0	7.2	3	91.9	3.0
biphenyl	3	103.5	7.6	4	100.0	5.2	3	100.6	1.6
acenaphthene	3	105.0	4.9	4	97.2	8.5	3	97.5	1.1
fluorene	3	100.2	8.3	4	84.9	7.8	3	91.3	4.5
9,10-dihydrophenanthrene	3	101.1	8.6	4	79.5	4.4	3	92.1	4.9
phenanthrene	3	96.5	6.7	4	91.2	2.8	4	100.0	1.4
anthracene	3	96.1	6.1	4	97.1	4.7	4	95.5	2.5
fluoranthene	3	92.4	5.2	4	97.3	4.8	4	96.4	5.4
pyrene	3	86.5	7.0	4	99.1	3.8	4	91.0	6.3
benz[*a*]anthracene		na[b]	na	4	90.6	7.0	3	96.2	5.7
chrysene		na	na	4	91.2	5.2	3	105.3	7.8
benzo[*a*]pyrene		na	na	4	96.6	4.0	3	86.8	4.0
dibenz[*a,h*]anthracene		na	na	4	102.1	2.2	3	82.5	7.4
benzo[*ghi*]perylene		na	na	4	101.8	2.8	3	88.3	2.1

[a] Airborne time. [b] na, not analyzed.

than other compounds with greater or less volatility. However, there were no evident relationships between collection patterns and sampling conditions over the relatively narrow range of temperature and humidity prevailing during the tests. Minor differences in the ratios of polynuclear aromatic hydrocarbons on filters and sorbents in other studies (*5, 6, 8–12*) are probably attributable to differences in sampling and environmental conditions. Careful control and recording of sampling variables are necessary to ensure consistency in interpretation of airborne PAH measurements.

A detailed examination (*16*) of sorbent breakthrough characteristics by use of chromatographic principles was not attempted partly due to the small number and nonuniform length and composition of the sorbent sections in the two types of tubes. However, the results showed that, under the test conditions, a single tube containing Tenax was sufficient for quantitative collection of the PAH in groups 2 and 3, as well as biphenyl, fluorene, and 9,10-dihydrophenanthrene in group 1. In fact, more than 85% of the amounts of each of these PAH collected on Tenax was found in the 100 mg front section. A significant percentage of indane (27% at 0.1 × TLV, 42% at 1 × TLV) and naphthalene (11% at 1 × TLV), and some acenaphthene (4% at 1 × TLV), was found in the backup tube containing XAD-2. Only 50% of the indane was retained on the Tenax front section in tests with group 1 PAH at 0.1 and 1 × TLV. The Tenax front section retained 70% naphthalene and 78% acenaphthene in tests at 1 × TLV. It was estimated that an air sample volume of ca. 0.3 m^3 would allow quantitative collection of indane, naphthalene, and acenaphthene in a single tube containing Tenax.

The maximum amount of total PAH found in Tenax front sections was 54 μg. This amount was determined in several tests where there was breakthrough of at least one group 1 or 2 PAH and is similar to the Tenax load capacity for aromatic amines (70 μg) determined under similar conditions (*10*). Indane and naphthalene were found in the 50-mg back section of the backup tube containing XAD-2 in a few of the tests where up to 8 μg of total PAH was found on the 100-mg front section. On the basis of these results, Tenax appeared to be at least as effective as XAD-2 resin for collection of PAH vapors, in contrast to observations in other reports (*13*).

The physical state of airborne PAH and factors such air flow rate (blow off effect), temperature, and humidity will influence their collection by particulate filters (*7, 17*). An estimate of the distribution of a PAH between vapor and particulate phases can be obtained from its equilibrium vapor concentration (EVC). The EVC will only represent the maximum losses possible during collection of airborne PAH on filters since kinetic and adsorption effects also influence collection efficiency (*17, 18*). In addition, different methods for determining vapor pressure and EVC can give values that are quite different (*16, 17, 19*). Table I lists some EVC values for comparison with total airborne concentrations and collection results for PAH in this study. The EVC exceeded the maximum airborne concentration of individual group 1 PAH in tests at 0.1 × TLV (3 μg/m^3) and 1 × TLV (34 μg/m^3) and no significant amounts of these compounds were found on the filters. Conversely, EVC values for group 3 PAH in tests at 0.1 × TLV (3.8 μg/m^3) and 1 × TLV (54 μg/m^3) were less than the maximum individual PAH concentrations and no significant amounts of these compounds were found in the sorbent. Group 2 PAH had EVC values near or greater than the individual PAH concentration and were found chiefly in the sorbent in tests at 0.1 × TLV (4.8 μg/m^3) and 1 × TLV (50 μg/m^3). These results confirmed that the EVC calculated from the vapor pressure of a compound could be used to estimate its collection by NIOSH method P & CAM 183 under the test conditions. However, the distribution between filters and sorbent in these tests does not necessarily correspond to the ratio of vapor to particulate PAH in the air stream (*16*).

The amount of airborne particulate material can also influence the proportions of material collected on filters and sorbent. Effects of suspended particulate matter could not be assessed because of very low concentrations of particulate in the laboratory air used for dilution. Even a 74-fold increase in airborne residence time did not measurably alter the collection pattern of PAH, possibly because of the low levels of aerosol present. The 37-s contact time was based on the calculated residence period for vapors in workplace air near the B.C. Research continuous coal liquefaction unit (*1*). Retention of material from the vapor phase by filters was probably due to condensation or adsorption on the filter surface rather than filtration of particulate. The least volatile group of hydrocarbons was collected entirely on the filters in spite of an airborne time of only 0.5 s and a filter surface temperature of 40 °C. There was no indication that significant degradation of PAH had occurred on the filters, although this has been cited as a problem in other studies (*13, 19*).

ACKNOWLEDGMENT

Helpful comments on the manuscript by D. T. Williams and F. M. Benoit are gratefully acknowledged.

Registry No. Tenax, 24938-68-9; XAD-2, 9060-05-3; Ag, 7440-22-4; indane, 496-11-7; naphthalene, 91-20-3; biphenyl, 92-52-4; acenaphthene, 83-32-9; fluorene, 86-73-7; 9,10-dihydrophenanthrene, 776-35-2; phenanthrene, 85-01-8; anthracene,

120-12-7; fluoranthene, 206-44-0; pyrene, 129-00-0; benz[a]anthracene, 56-55-3; chrysene, 218-01-9; benzo[a]pyrene, 50-32-8; dibenz[a,h]anthracene, 50-70-3; benzo[ghi]perylene, 191-24-2.

LITERATURE CITED

(1) Otson, R.; Armstrong, V.; Leach, J. M. *Am. Ind. Hyg. Assoc. J.*, in press.
(2) *Manual of Analytical Methods*, 2nd ed.; Publication No. 77-157A; DHEW (NIOSH): Cincinnati, OH, 1977; Vol. 1.
(3) Stenberg, U.; Alsberg, T.; Westerholm, R. *EHP, Environ. Health Perspect.* **1983**, *47*, 43–51.
(4) Stenberg, U.; Alsberg, T.; Westerholm, R. *EHP, Environ. Health Perspect.* **1983**, *47*, 53–63.
(5) Scheutzle, D. *EHP, Environ. Health Perspect.* **1983**, *47*, 65–80.
(6) Cautreels, W.; Van Cauwenberghe, K. *Atoms. Environ.* **1978**, *12*, 1133–1141.
(7) Yamasaki, H.; Kuwata, K.; Miyamoto, H. *Environ. Sci. Technol.* **1982**, *16*, 189–194.
(8) Thrane, K. E.; Mikalsen, A. *Atoms. Environ.* **1981**, *15*, 909–918.
(9) Andersson, K.; Levin, J.-O.; Nilsson, C.-A. *Chemosphere* **1983**, *12*, 197–207.
(10) Otson, R.; Leach, J. M.; Chung, L. T. K. *Anal. Chem.* **1987**, *59*, 58–62.
(11) *TLVs Threshold Limit Values for Chemical Substances and Physical Agents in the Work Environment and Biological Exposure Indeces with Intended Changes for 1984-85*; American Conference of Governmental Industrial Hygienists: Cincinnati, OH, 1984.
(12) Lee, F. S.-C.; Prater, T. J.; Ferris, F. In *Polynuclear Aromatic Hydrocarbons*; Jones, P. W., Leber, P., Eds.; Ann Arbor Science Publishers: Ann Arbor, MI, 1979; pp 83–110.
(13) Jones, P. W. *VDI-Ber.* **1980**, *No. 358*, 23–38.
(14) Otson, R.; Hung, I.-F. *Polynuclear Aromatic Hydrocarbons: Mechanism, Methods and Metabolism*; Cooke, M., Dennis, A. J., Eds.; Battelle Press: Columbus, OH, 1984; pp 999–1012.
(15) You, F.; Bidleman, T. F. *Environ. Sci. Technol.* **1984**, *18*, 330–333.
(16) Bidleman, T. F.; Billings, W. N.; Foreman, W. T. *Environ. Sci. Technol.* **1986**, *20*, 1038–1043.
(17) Pupp, C.; Lao, R. C.; Murray, J. J.; Pottie, R. F. *Atmos. Environ.* **1974**, *8*, 915–925.
(18) Sonnefeld, W. J.; Zoller, W. H.; May, W. E. *Anal. Chem.* **1983**, *55*, 275–280.
(19) Spitzer, T.; Dannecker, W. *Anal. Chem.* **1983**, *55*, 2226–2228.

RECEIVED for review November 5, 1986. Accepted March 4, 1987. This work was supported by the Canadian Interdepartmental Panel on Energy Research and Development.

Extraction and Recovery of Polycyclic Aromatic Hydrocarbons from Environmental Solids Using Supercritical Fluids

Steven B. Hawthorne* and David J. Miller

University of North Dakota Energy Research Center, Grand Forks, North Dakota 58202

The use of supercritical fluids for the extraction and recovery of polycyclic aromatic hydrocarbons (PAH) from environmental solids has been developed and tested by using urban dust, fly ash, and river sediment. Supercritical N_2O with 5% methanol modifier gave the best recoveries of PAH from all three samples when compared to supercritical CO_2 with 5% methanol, N_2O, CO_2, and ethane. Quantitative recovery of PAH from National Bureau of Standards SRM 1649 (urban dust) and of deuteriated PAH spikes (phenanthrene-d_{10}, pyrene-d_{10}, and perylene-d_{12}) from the river sediment was obtained with supercritical fluid extractions in as little as 30 min. In most cases, 30–60 min extractions of the river sediment and fly ash with supercritical N_2O/5% methanol gave better recovery of the deuteriated PAH spikes than the recoveries obtained by using 4 h of sonication or 8 h of Soxhlet extraction with either benzene or methylene chloride. Supercritical fluid extractions yield good PAH recoveries, require only small amounts of sample, minimize analyte concentration steps, and are simple and rapid to perform.

The extraction and recovery of organic species from environmental solids are critical and often the limiting steps in analysis schemes used to identify and quantitate organic pollutants. Extractions of polycyclic aromatic hydrocarbons (PAH) from solid samples such as airborne particulates, soil, and fly ash are usually performed with liquid solvents either in a Soxhlet apparatus or with sonication, although variations such as extraction with liquid CO_2 have been described (*1*). These traditional liquid solvent extraction methods generally take several hours to perform, require relatively large volumes of ultrapure solvent (often making subsequent concentration steps necessary), and may yield incomplete recovery and/or degradation of sample species (*2–5*).

Besides their strong solvating ability, supercritical fluids have several characteristics that may make them useful for the rapid and quantitative extraction and recovery of organic pollutants from environmental solids. The solvent strength of a supercritical fluid is directly related to its density as can be described by the empirical correlation $\delta = 1.25P_c^{1/2}(\rho_g/\rho_l)$ where δ is the Hildebrand solubility parameter, P_c is the critical pressure of the fluid, ρ_g is the density of supercritical fluid, and ρ_l is the density of the fluid in its liquid state (*6*). Thus, the solvating ability of a particular supercritical fluid toward a particular species can easily be modified by changing the extraction pressure (and, to a lesser extent, the temperature). Supercritical fluids with widely varying polarities are available (i.e., pentane, CO_2, and ammonia have Hildebrand solubility parameters at liquid densities of 7.0, 10.6, and 13.2 $(cal/cm^3)^{1/2}$, respectively), and the polarity of a supercritical fluid can also be controlled by the addition of solvent modifiers. The low viscosities and high solute diffusivities of supercritical fluids should yield good mass transfer during extraction. Supercritical fluids that have low critical temperatures (e.g., CO_2, nitrous oxide, and ethane have critical temperatures of 31, 36.5, and 32 °C, respectively) can be used to avoid decomposition of thermally labile compounds. Finally, many supercritical solvents are gases at room temperature which should simplify analyte concentration steps and help reduce the loss of volatile sample species.

Recent studies have demonstrated analytical uses for supercritical fluid extractions including the extraction of diesel fuel components from silica gel and marine sediments (*7*), the coupled supercritical fluid extraction/supercritical fluid analysis of caffeine from coffee beans (*8*), the silica column fractionation of oil residuals (*9*) and of polycyclic aromatic hydrocarbons (PAH) (*10*), and the direct mass spectrometric analysis of supercritical fluid extraction products (*7, 11*). The ability of supercritical CO_2 extractions to yield quantitative extraction and recovery of PAH from diesel exhaust partic-

0003-2700/87/0359-1705$01.50/0 © 1987 American Chemical Society

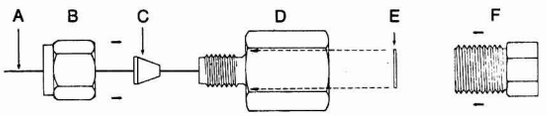

Figure 1. Supercritical fluid extraction cell. The components of the cell are (A) 10 cm × 20–30 μm i.d. fused silica capillary outlet restrictor, (B) $^1/_{16}$ in. nut, (C) 15/85 graphite/polyimide (Supeltex M-2A) ferrule, (D) $^1/_{16}$ in. NPT × $^1/_{16}$ in. tubing union, (E) $^1/_4$ in. × 10 μm stainless steel frit, and (F) $^1/_{16}$ in. low dead volume union. All fittings were stainless steel "Parker" brand.

ulates and from urban dust has also recently been reported (*12–14*). The purpose of the present study is to investigate and develop the use of supercritical fluid extractions to extract and recover PAH from three different environmental solids including fly ash, river sediment, and urban dust. Five different supercritical solvent systems including ethane, CO_2, nitrous oxide (N_2O), CO_2 with methanol modifier, and nitrous oxide with methanol modifier were tested for their ability to extract PAH from each of the three samples. A comparison between supercritical fluid extraction and the more traditional liquid solvent extraction methods, sonication and extraction using a Soxhlet apparatus, is also reported.

EXPERIMENTAL SECTION

Sample Description. The urban dust sample (SRM 1649) was purchased from the National Bureau of Standards (Washington, DC). The fly ash sample was an ESP hopper ash (no. 3401.9) supplied by the DOE Fossil Fuels Research Materials Facility (Oak Ridge National Laboratory, Oak Ridge, TN). River sediment was collected near the banks of the Red River in Grand Forks, ND. The sediment was allowed to air-dry and sieved through a screen having 0.6-mm holes to remove debris before use. Both the fly ash and river sediment were spiked with 2 μg/g each of phenanthrene-d_{10}, pyrene-d_{10}, and perylene-d_{12} by suspending 2-g samples in 10 mL of methylene chloride and adding the appropriate amount of the deuteriated spikes. The samples were stirred occasionally and the solvent was allowed to evaporate overnight.

Methods. All of the supercritical fluid extractions were performed with an SFT Model 250-TMP supercritical fluid pumping system (Lee Scientific, Inc.). Five percent by volume methanol modified CO_2 and N_2O were prepared by pipetting 12.5 mL of methanol (Baker "Resi-Analyzed") directly into the 250-mL syringe pump (held at 15 °C) and then filling the entire pump volume with liquid CO_2 (or N_2O). The extraction cell was constructed with "Parker" brand 316 stainless steel fittings as shown in Figure 1 and had an internal volume of approximately 0.2 mL. (**Caution**: Care must be taken to ensure that fittings used to construct extraction cells are capable of withstanding the required extraction pressures. Since N_2O is a strong oxidant, extractions involving large amounts of easily oxidized material, particularly at elevated temperatures, may represent an explosion hazard and should be avoided. As an added precaution for this study, a pressure relief valve set to vent at 400 atm was installed at the top of the pump so that both the pump and extraction cells could be rapidly vented.) Supercritical pressures were maintained inside the extraction cell by using 10-cm lengths of capillary fused silica tubing (Polymicro Technologies, Phoenix, AZ) for outlet restrictors. Flow rate through the extraction cell was controlled by using tubing with internal diameters ranging from 20 to 30 μm. No cross-contamination between samples has been observed when the same restrictor is used for multiple extractions. However, since restrictors grow fragile after several uses, a new restrictor was used for each extraction in this study. (This poses no limitation since the capillary tubing is very inexpensive and a new restrictor is made by simply cutting off a new piece of the tubing.) Temperature was maintained by inserting the extraction cell into a thermostated tube heater.

Extractions were performed on 20-mg samples of the urban dust that had been weighed into the extraction cell. Sample size was approximately 50 mg for the fly ash and the river sediment. The extracted species were collected by inserting the end of the outlet restrictor into a 19 × 65 mm glass vial containing approximately 2 mL of methylene chloride (Baker "Resi-Analyzed") and 0.5 μg of 4,4′-dichlorobiphenyl as an internal standard. Because of the cooling effect caused by the rapid expansion of the supercritical fluid as it exited the restrictor capillary, no significant evaporation of the methylene chloride occurred during the extraction. After sample collection the solvent was evaporated under nitrogen to approximately 100 μL.

Analysis of the extracts was performed with a Hewlett-Packard Model 5985B GC/MS using selected ion monitoring (SIM). Separations were achieved with on-column injections into a 60 m × 0.25 mm i.d. (0.25 μm film thickness) DB-5 chromatographic column (J&W Scientific, Inc.). Standards for the quantitation of the PAH extracted from the urban dust were prepared from National Bureau of Standards SRM 1647, which contains certified concentrations of various PAH species in acetonitrile. Quantitation of the deuteriated PAH extracted from the fly ash and river sediment was based on gravimetrically prepared solutions of the pure deuteriated compounds. The concentration of each PAH and deuteriated PAH fell within a three-point calibration curve. Each standard and sample vial contained 0.5 μg of 4,4′-dichlorobiphenyl as an internal standard. During SIM analysis the molecular ion of each PAH, the deuteriated PAH species, and the 4,4′-dichlorobiphenyl was monitored in groups of two ions with a dwell time of 50 ms for each ion.

Soxhlet extractions of 1-g samples of fly ash and river sediment were performed with a micro-Soxhlet apparatus with 50 mL of either benzene or methylene chloride. Solvent cycle time was approximately 15 min. One-half-gram samples were also extracted with 10 mL of both solvents using sonication at 100 W. After extraction, the 4,4′-dichlorobiphenyl internal standard was added to each extract, the solvents were evaporated to near dryness, and the extracts were analyzed as described above.

RESULTS AND DISCUSSION

A comparison of the extraction efficiencies obtained by using the five different supercritical fluids (ethane, CO_2, N_2O, CO_2 with 5% methanol by volume, and N_2O with 5% methanol) is shown in Figure 2. The extraction conditions used were purposely chosen to yield less than quantitative recovery of the PAH so that comparisons between the different solvent systems could be made. Each sample was extracted in triplicate for 30 min with each supercritical solvent at 300 atm. A 20 μm i.d. restrictor outlet was used to maintain supercritical pressures in the extraction cell resulting in approximately 10 mL of solvent (measured in the liquid state at the pump) being used for each extraction. Extraction temperatures were 45 °C for the pure solvents and 65 °C for the solvents modified with methanol. Recoveries of the PAH from the urban dust were based on the certified values for each individual PAH. Recoveries of the deuteriated PAH from the fly ash and river sediment were based on 2 μg/g spikes as described above. The resultant extraction efficiencies showed good reproducibility as indicated on Figure 2 by the error bars representing one standard deviation unit (1σ) for triplicate extractions of each sample with each solvent.

Supercritical ethane and supercritical CO_2 gave the poorest recovery of PAH from each of the three samples, while the recovery with N_2O was moderately higher (Figure 2), as might be expected based on reports that N_2O is a stronger eluant than CO_2 (*15*, *16*). The similarity of extraction efficiencies obtained with ethane and CO_2 might be explained based on the similar solubilities reported for PAH in supercritical ethane and CO_2 (*17*). The addition of the methanol modifier yielded much better extraction efficiencies with both CO_2 and N_2O. Supercritical N_2O/5% methanol extraction gave the best extraction efficiency for each of the three sample matrices.

Figure 2 also demonstrates that higher molecular weight PAH are extracted at lower efficiency than lower molecular weight PAH from the same sample matrix. This result is consistent with the decrease in solubility of PAH with increasing molecular weight reported for supercritical CO_2 and supercritical ethane (*17*). The extraction efficiency of PAH from the fly ash sample was much lower than from the urban

Table I. Recovery of PAH from Urban Dust (SRM 1649) Using Supercritical Nitrous Oxide/5% Methanol Extraction

PAH (mol wt)	concentration, μg/g		
	certified value[a]	30-min extraction[b]	60-min extraction[b]
fluoranthene (202)	7.1 ± 0.5	7.4 ± 0.4	8.0 ± 0.6
benz[*a*]anthracene (228)	2.6 ± 0.3	2.5 ± 0.3	2.9 ± 0.5
benzo[*a*]pyrene (252)	2.9 ± 0.5	2.9 ± 0.2	3.2 ± 0.3
benzo[*ghi*]perylene (276)	4.5 ± 1.1	3.2 ± 0.3	4.4 ± 0.3
indeno[1,2,3-*cd*]pyrene (276)	3.3 ± 0.5	2.3 ± 0.2	3.1 ± 0.2

[a] PAH concentrations on the urban dust sample (Standard Reference Material 1649) are given as certified by the National Bureau of Standards. [b] PAH concentrations and standard deviations (1σ) are based on triplicate extractions of 20-mg samples.

dust and the river sediment as might be expected since quantitative revovery of PAH from fly ash has been reported to be extremely difficult to achieve using extractions with liquid solvents (*4*, *5*).

On the basis of the results just discussed, additional extractions of each sample were performed in order to determine the ability of supercritical N_2O/5% methanol extractions to yield quantitative recovery of PAH. The extraction pressure was raised to 350 atm, and higher solvent flow rates were achieved by using an outlet restrictor capillary with a larger internal diameter (25 μm). Under these conditions, approximately 20 mL of solvent was used for a 30-min extraction. Each sample was extracted in triplicate and the PAH concentrations were determined as described above. Table I shows the quantities of PAH extracted from the urban dust sample (SRM 1649) using supercritical N_2O/5% methanol compared with the values certified by the National Bureau of Standards. PAH recoveries obtained from triplicate supercritical fluid extractions showed good reproducibility with relative standard deviations generally <10%. The 30-min supercritical fluid extraction gave good agreement with the certified values for fluoranthene, benz[*a*]anthracene, and benzo[*a*]pyrene, but the values for benzo[*ghi*]perylene, and indeno[1,2,3-*cd*]pyrene were low. Good agreement with certified values was achieved for these two species when the sample was extracted for 60 min. The 60-min supercritical fluid extraction also yielded slightly higher values for fluoranthene, benz[*a*]anthracene, and benzo[*a*]pyrene than the certified values. Since the certified values are based on 48-h extractions (both methylene chloride and 1:1 benzene/methanol were used by NBS as solvents) in a Soxhlet apparatus, the higher values obtained from the 60-min supercritical fluid extraction may be a result of slightly increased extraction efficiency.

The recoveries of the deuteriated PAH spikes from river sediment and fly ash using supercritical N_2O/5% methanol are shown in Table II. Triplicate extractions were performed at 350 atm with a 25 μm i.d. outlet restrictor. The recovery of the deuteriated phenanthrene, pyrene, and perylene from the river sediment was essentially quantitative with both 30- and 60-min extractions. The extraction efficiencies from the fly ash were much lower, particularly for the perylene-d_{12} even when the extraction was performed for 60 min. The relatively poor recoveries from fly ash are not surprising since the quantitative extraction of PAH from fly ash is notoriously dificult (*4*, *5*). Two attempts were made to improve the efficiency of the supercritical fluid extraction step. First, the concentration of the methanol modifier in the N_2O was raised to 10% by volume (and the extraction temperature was raised to 70 °C to maintain supercritical conditions), but no significant increase in PAH recoveries resulted. A second attempt to improve the PAH recoveries from fly ash was made by increasing the internal diameter of the outlet restrictor to 30 μm and extracting the fly ash for 60 min. Approximately 70 mL of N_2O/5% methanol was used for each extraction. These conditions yielded recoveries ranging from a low of 44% for perylene-d_{12} to 102% for phenanthrene-d_{10} (Table II). The use of restrictors with internal diameters larger than 30 μm was impractical because the resulting flow rates were too high for the pumping system to maintain. The investigation of different solvent systems and improvements in cell design should allow better recoveries to be obtained.

Table II. Recovery of PAH from River Sediment and Fly Ash Using Supercritical Nitrous Oxide/5% Methanol Extraction

PAH (mol wt)	% recovery[a]		
	25-μm restrictor		30-μm restrictor
	30 min	60 min	60 min
River Sediment			
phenanthrene-d_{10} (188)	102 ± 4	103 ± 7	
pyrene-d_{10} (212)	95 ± 2	101 ± 8	
perylene-d_{12} (264)	92 ± 10	97 ± 6	
Fly Ash			
phenanthrene-d_{10} (188)	72 ± 5	89 ± 8	102 ± 6
pyrene-d_{10} (212)	48 ± 8	67 ± 4	74 ± 8
perylene-d_{12} (264)	19 ± 5	28 ± 5	44 ± 9

[a] Recoveries and standard deviations (1σ) are based on triplicate extractions of 50-mg samples performed as described in the text.

Table III. Recovery of PAH from River Sediment and Fly Ash Using Sonication and Soxhlet Extraction with Methylene Chloride and Benzene

	% recovery[a]		
	phenanthrene-d_{10}	pyrene-d_{10}	perylene-d_{12}
Methylene Chloride			
Soxhlet (8 h)			
fly ash	60 ± 1	71 ± 1	77 ± 6
sediment	98 ± 3	96 ± 3	86 ± 6
sonication (4 h)			
fly ash	30 ± 1	33 ± 1	23 ± 1
sediment	79 ± 5	77 ± 5	61 ± 6
Benzene			
Soxhlet (8 h)			
fly ash	34 ± 3	58 ± 3	69 ± 6
sediment	28 ± 3	31 ± 2	36 ± 5
sonication (4 h)			
fly ash	35 ± 2	52 ± 9	43 ± 2
sediment	42 ± 2	40 ± 1	29 ± 1

[a] Recoveries and standard deviations (1σ) are based on triplicate determinations using selected ion monitoring GC/MS as described in the text.

Two traditional liquid solvent extraction methods, sonication and extraction using a Soxhlet apparatus, were used to extract the river sediment and fly ash samples so that PAH recoveries using these methods could be compared to those obtained by using supercritical N_2O/5% methanol. Extractions were performed with two commonly used solvents, benzene and methylene chloride. The results of these liquid

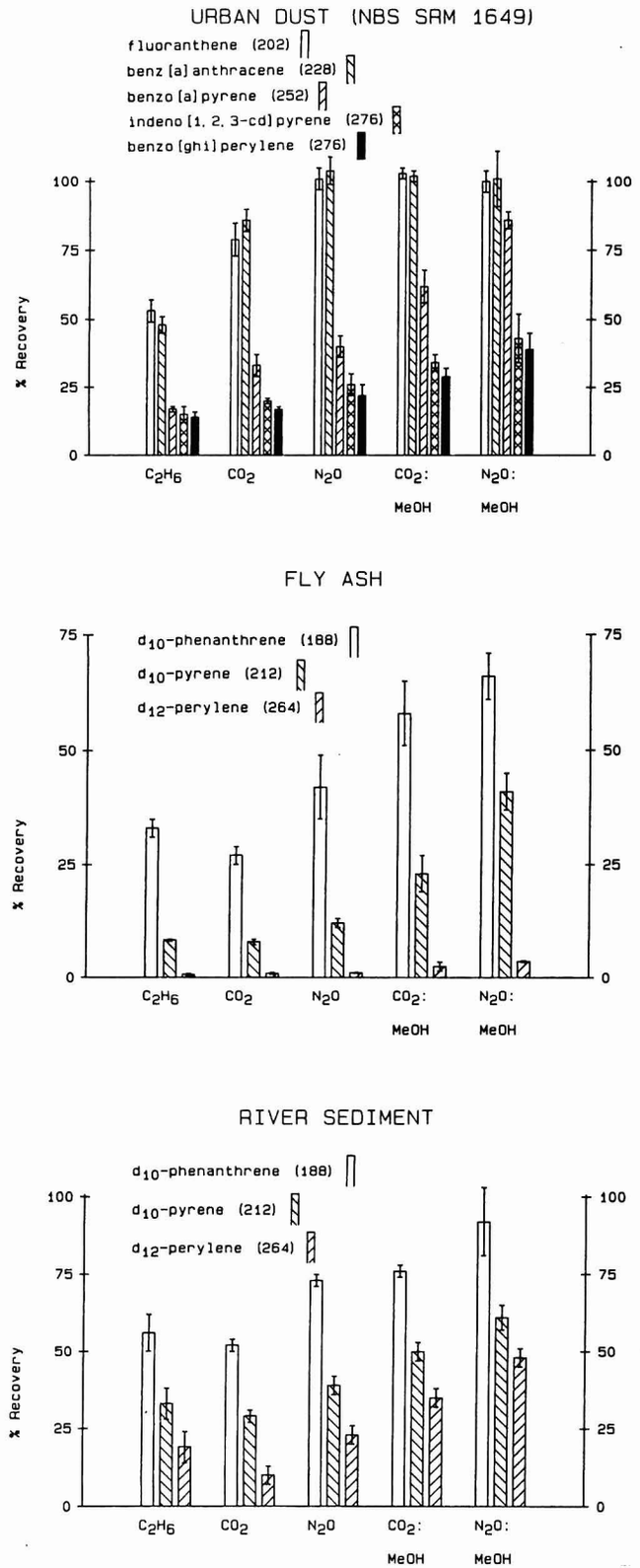

Figure 2. Comparison of PAH extraction efficiencies obtained from urban dust (National Bureau of Standards SRM 1649), fly ash, and river sediment using five different supercritical fluids: ethane, CO_2, N_2O, CO_2 with 5% methanol modifier, and N_2O with 5% methanol modifier. Error bars represent one standard deviation unit for triplicate extractions of each sample with each solvent. Extraction and analysis conditions are given in the text.

solvent extractions are shown in Table III. With benzene as the solvent, neither 4 h of sonication nor 8 h of Soxhlet extraction yielded quantitative recovery (i.e., >90%) of any of the deuteriated PAH from the fly ash or the river sediment. Soxhlet extraction with methylene chloride gave the best PAH recovery from both samples, yielding quantitative recovery of phenanthrene-d_{10} and pyrene-d_{10} from the river sediment. None of the deuteriated PAH were quantitatively recovered from the fly ash using liquid solvents.

A comparison of the data presented in Tables II and III shows that, in most cases, 30–60-min extractions of fly ash and river sediment using supercritical N_2O/5% methanol yielded better recoveries of the deuteriated PAH than those obtained from 4 h of sonication or 8 h of Soxhlet extraction using either benzene or methylene chloride. Liquid solvent extractions yielded better recovery than the supercritical fluid extractions (i.e., 60 min using a 30 μm i.d. restrictor) only for Soxhlet extractions of the perylene-d_{12} from the fly ash sample.

CONCLUSIONS

The results of this study demonstrate that the use of supercritical fluids for the extraction and recovery of PAH from environmental solids may have several advantages over traditional extraction methods using liquid solvents. In most cases, supercritical fluid extractions gave better recovery of PAH than sonication or Soxhlet extraction, and the supercritical fluid extractions required an order-of-magnitude less time to complete. A single analyst can easily extract 10 to 15 samples in 1 day, and the method is well-suited to small samples sizes (thus reducing the collection time required for samples such as atmospheric particulates). In contrast to liquid extraction methods no large volumes of ultrapure solvents are required, and concentration steps are minimized. The further development and optimization of extraction conditions including cell design, pressure and temperature effects, and investigations into the use of different supercritical fluids and polarity modifiers should result in methodology suited for the analytical extraction of PAH and other organic pollutants from a variety of environmental samples.

ACKNOWLEDGMENT

The authors thank R. Wallace Harvey (Oak Ridge National Laboratory) for providing the fly ash sample.

Registry No. Fluoranthene, 206-44-0; benz[*a*]anthracene, 56-55-3; benzo[*a*]pyrene, 50-32-8; benzo[*ghi*]perylene, 191-24-2; indeno[1,2,3-*cd*]pyrene, 193-39-5; phenanthrene-d_{10}, 1517-22-2; pyrene-d_{10}, 1718-52-1; perylene-d_{12}, 1520-96-3.

LITERATURE CITED

(1) Jennings, W. J. *HRC CC, J. High Resolut. Chromatogr. Commun.* **1979**, *2*, 221–224.
(2) Lee, M. L.; Novotny, M. V.; Bartle, K. D. *Analytical* Chemistry *of Polycyclic Aromatic Compounds*; Academic: New York, 1981; pp 78–116.
(3) Fowlie, P. J. A.; Bulman, T. L. *Anal. Chem.* **1986**, *58*, 721–723.
(4) Griest, W. H.; Yeatts, L. B., Jr.; Caton, J. E. *Anal. Chem.* **1980**, *52*, 199–201.
(5) Junk, G. A.; Richard, J. J. *Anal. Chem.* **1986**, *58*, 962–965.
(6) Giddings, J. C.; Myers, M. N.; McLaren, L.; Keller, R. A. *Science* **1968**, *162*, 67–69.
(7) Smith, R. D.; Udseth, H. R.; Hazlett, R. N. *Fuel* **1985**, *64*, 810–815.
(8) Sugiyama, K.; Saito, M.; Hondo, T.; Senda, M. *J. Chromatogr.* **1985**, *332*, 107–116.
(9) Lundanes, E.; Greibrokk, T. *J. Chromatogr.* **1985**, *349*, 439–446.
(10) Campbell, R. M.; Lee, M. L. *Anal. Chem.* **1986**, *58*, 2247–2251.
(11) Smith, R. D.; Udseth, H. R. *Sep. Sci. Technol.* **1983**, *18*, 245–252.
(12) Schantz, M. M.; Chesler, S. N. *J. Chromatogr.* **1986**, *363*, 397–401.
(13) Locke, D. C.; Martin, J. L.; Scott, J. C.; Wang, J. S. *Abstracts of Papers*, 191st National Meeting of the American Chemical Society, New York, NY; American Chemical Society: Washington, DC, 1986; ANYL 125.
(14) Hawthorne, S. B.; Miller, D. J. *J. Chromatogr. Sci.* **1986**, *24*, 228–264.
(15) Wright, B. W.; Kalinoski, H. T.; Smith, R. D. *Anal. Chem.* **1985**, *57*, 258–264.
(16) Lauer, H. H.; McManigill, D.; Board, R. D. *Anal. Chem.* **1983**, *55*, 1370–1375.
(17) Johnston, K. P.; Ziger, D. H.; Eckert, C. A. *Ind. Eng. Chem. Fundam.* **1982**, *21*, 191–197.

RECEIVED for review December 8, 1986. Accepted March 9, 1987. The financial support of the U.S. Environmental Protection Agency, Office of Exploratory Research (Grant No. R-812229-01-0) is gratefully acknowledged.

Simultaneous Determination of Linear Alkylbenzenesulfonates, Alkylphenol Polyethoxylates, and Nonylphenol by High-Performance Liquid Chromatography

Antonio Marcomini[1] and Walter Giger*

Swiss Federal Institute for Water Resources and Water Pollution Control (EAWAG), CH-8600 Dübendorf, Switzerland

Linear 4-alkylbenzenesulfonates (LAS), 4-alkylphenol polyethoxylates (APEO) (i.e., 4-octylphenol polyethoxylates (OPEO) and 4-nonylphenol polyethoxylates (NPEO)), and 4-nonylphenol (NP) are simultaneously determined by reversed-phase high-performance liquid chromatography (HPLC) using octylsilica columns and water/acetonitrile gradient elution. LAS are separated according to their alkyl chain lengths and coelution of NPEO and NP is observed in contrast to the separation of OPEO and NPEO. The determination of oligomer distributions of APEO and quantitation of NP, NP1EO, and NP2EO require additional information attainable by normal-phase HPLC. Recoveries of 85–100% were found for LAS, APEO, and NP isolated by Soxhlet extraction under basic conditions from laundry detergent powders, sewage sludges, sludge-amended soils, and river sediments. Relative standard deviations for all analytes in the different matrices did not exceed 6%. Detection limits with UV fluorescence detection are 95 ng for NP, 80 ng for LAS, and 65 ng for NPEO with respect to injected amounts.

Linear alkylbenzenesulfonates (LAS) and alkylphenol polyethoxylates (APEO) are very widely used synthetic anionic and nonionic surfactants, respectively. In particular, LAS are major surfactants in laundry detergents, whereas APEO are important surfactants in institutional and industrial surface cleaners (*1*, *2*). Linear alkylbenzenesulfonates are synthesized by Friedel–Crafts alkylation of benzene followed by sulfonation of the aromatic ring (predominantly at the para position). The technical LAS products are mixtures containing homologues with alkyl chain lengths usually varying from 10 to 14 carbon atoms (Figure 1). The phenyl group may be attached to the alkyl chain at any carbon atom except at the end position (so-called phenyl positional isomers). The alkylphenolic nonionic surfactants are manufactured from highly branched 4-nonyl- and 4-octylphenols by reaction with different amounts of ethylene oxide leading to mixtures of oligomers with varying lengths of the polyethoxy chain. The most utilized APEO have nonyl alkyl chains (NPEO, Figure 1) and are complex mixtures of isomers with differently branched alkyl substituents (*3*).

LAS and APEO are of environmental concern because of their high abundance in municipal wastewaters (*4*, *5*). NPEO is biotransformed during wastewater and sewage treatment partially forming more persistent and more toxic metabolites with only one (NP1EO) or two (NP2EO) ethoxy units as well as NP (*6*). Linear alkylbenzenesulfonates have been detected worldwide in many different environmental compartments (*7*, *8*). Unaltered LAS accumulate in the range of 0.3–1.2% of the total dry matter in sewage sludges (*9*).

Colorimetric analytical procedures based on complex formation with dye cations (*10*, *11*), followed by photometric detection, are routinely used to measure levels of anionic surfactants in various environmental samples (*12–14*). However, the need to obtain information on specific surfactants, as well as on individual homologues and phenyl positional isomers of LAS, prompted the application of gas chromatography (*15*) or gas chromatography/mass spectrometry (GC/MS) (*16*). For these two techniques, the surfactant molecules had to be transformed by desulfonation to yield alkylbenzenes (*8*) or by derivatization to sulfonyl chlorides (*16*) or sulfonate esters (*17*). The determination of LAS without any derivatization has also been carried out by reversed-phase HPLC (*18–23*).

APEO were also largely determined in environmental samples by nonspecific methods (*24–26*) that measure total contents of nonionic surfactants. These methods fail to differentiate between APEO and linear alcohol polyethoxylates which are also widely used nonionic surfactants. Methods capable of specific determination of APEO employ GC/MS using chemical ionization (*27*) or both reversed- and normal-phase HPLC (*5*, *28–30*).

We present here the first report on procedures for the simultaneous determination of the aromatic surfactants of the LAS and APEO types by using reversed-phase HPLC. In addition, the important refractory metabolite NP can also be measured, if corroborated by normal-phase HPLC analysis.

EXPERIMENTAL SECTION

Reagents and Materials. The two commercial surfactants Marlon A and Marlophen 810 were supplied by Chemische Werke Hüls AG, Marl, Federal Republic of Germany. Marlon A is a C_{10}–C_{13} LAS mixture and Marlophen 810 contains NPEO oligomers with an average of 11 and a range of 1–18 ethoxy units. Imbentin-N/7A, a mixture of 4-nonylphenol mono-, di-, and triethoxylates, was received from W. Kolb AG, Hedingen, Switzerland. Synperonic OP10 was obtained from Imperial Chemical Industries, Petrochemical Division, Middlesbrough, U.K. The latter is an octylphenol-based product with an average of 10 and a range of 2–15 ethoxy units. Sodium dodecyl sulfate (SDS) was purchased from BDH, Poole, U.K., and recrystallized in ethanol/water. 1-Octylbenzenesulfonate and 1-nonylbenzenesulfonate (1-C_8- and 1-C_9-LAS) were synthesized by direct sulfonation at 70 °C of *n*-octylbenzene and *n*-nonylbenzene (Fluka AG, Buchs, Switzerland; ref 31). The reaction products were recrystallized in water/ethanol. 3-Tetradecylbenzenesulfonate (3-C_{14}-LAS) and 3-pentadecylbenzenesulfonate (3-C_{15}-LAS), supplied by Unilever, Port Sunlight, U.K., were used without further purification. Technical 4-nonylphenol was employed as received from Fluka. Sodium chloride, sodium perchlorate, and sodium hydroxide were all analytical grade from Merck, Darmstadt, FRG, and were used without further purification. The cellulose thimbles (22 × 80 mm) were purchased from Schleicher and Schüll, Dassel, FRG and were Soxhlet extracted with methanol for 2 h before use. All solvents were HPLC grade (Mallinkrodt, St. Louis, MO) and the water for HPLC elution was "carbon free" grade (Mallinkrodt).

Samples, Extraction, and Sample Preparation. Laundry detergent powders were obtained from commercial sources in Switzerland. Sewage sludges were collected in the treatment plants of Altenrhein and Zürich-Glatt. The sludges were conserved by the immediate addition of 1% (v/v) of formaldehyde (37%, analytical grade, Merck). After vigorous shaking, aliquots of 500 mL were dried at 60 °C and the resulting solids finely ground. When not immediately dried, the sewage sludges were stored in

[1] On leave from the University of Venice, Department of Environmental Sciences, I-30123 Venice, Italy.

0003-2700/87/0359-1709$01.50/0 © 1987 American Chemical Society

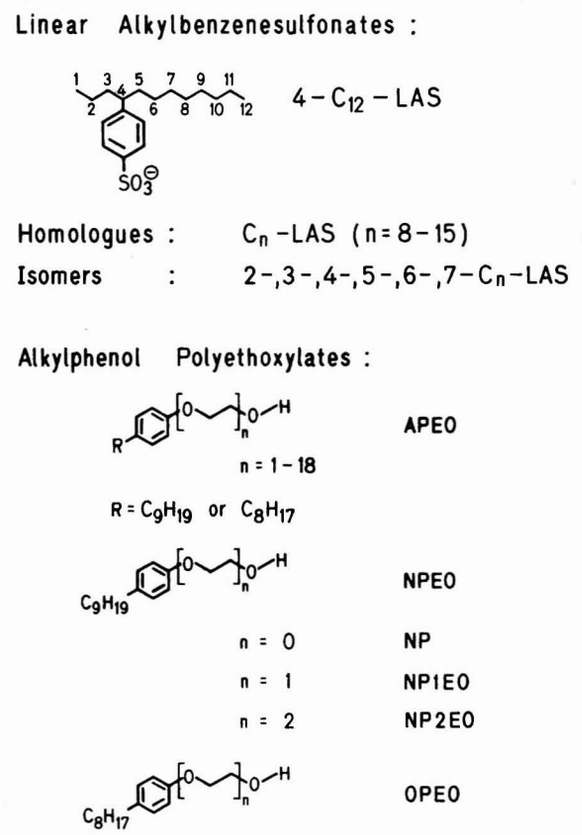

Figure 1. Constitutions and acronyms of linear alkylbenzenesulfonates, alkylphenol polyethoxylates, and alkylphenols: LAS, mixture of homologues and phenyl positional isomers; APEO, 2-[(4-alkylphenyl)-poly(oxyethylene)oxy]ethanol; NPEO, 2-[(4-nonylphenyl)poly(oxyethylene)oxy]ethanol; NP2EO, 2-[2-(4-nonylphenyloxyethylene)oxy]-ethanol; NP1EO, 2-(4-nonylphenoxy)ethanol; NP, complex mixture of isomers with differently branched nonyl substituents; OPEO, 2-[4-(1,1,3,3-tetramethylbutyl)phenyl)poly(oxyethylene)oxy]ethanol.

the dark at 4 °C. Sludge-amended soil samples were obtained from the Swiss Federal Research Station for Agricultural Chemistry and Hygiene of the Environment at Liebefeld, dried at 60 °C overnight, and then pulverized. Sediment samples from the surface (0–3 cm) and from a deeper layer (9–12 cm) of a bottom core of the Rhine River at Village Neuf (6 km downstream from Basle) were obtained as dried powders. Sediment dating was based on measurement of ^{137}Cs (*32*).

Typically, 500 mg of detergent powder, 2 g of dried sewage sludge, and 20 g of dried soil or sediment were transferred into a preextracted paper thimble. Amounts of the internal standards 1-C_8- and 3-C_{15}-LAS, according to those used in the standard solutions (see below), and solid NaOH (20% (w/w)) were added and allowed to equilibrate for 15 min. The thimbles were covered with preextracted cotton in order to prevent removal of fine powder from the thimble into the extracting solvent. The samples were extracted in a Soxhlet apparatus with 80 mL of methanol for 30 min for detergents, 4 h for sludges, and 12 h for soils and sediments. The extracts were evaporated to 20 mL (detergents and sludges) or 5 mL (soils and sediments) and then diluted to 50 mL (detergent and sludges) or 20 mL (soils and sediments) with water containing 5×10^{-2} M SDS and acetone in such a way that a final composition of methanol (MeOH), water (H_2O), and acetone of 1:1:2 was attained. The mixtures were finally centrifuged and aliquots of 20–80 μL were injected into the reversed-phase HPLC columns. The addition of SDS prevented adsorption losses of the analytes in the chromatographic system (*20*). The MeOH/H_2O/acetone mixture was centrifuged in order to precipitate the fine suspended material (formed after addition of water) and to get a clear solution which could be injected without filtration. Portions (200–500 μL) of these mixtures, as well as, separately, aliquots of NP, NP1EO, and NP2EO standard solution in MeOH/H_2O (1:1) (NP, 0.1 μg; NP1EO, 0.17 μg; NP2EO, 0.02 μg), were diluted in a narrow neck volumetric flask to about 20 mL with doubly distilled water to which solution 500 mg of NaCl and 1 mL of *n*-hexane were added. The resulting suspensions were centrifuged for 15 min and 20–50-μL aliquots of the *n*-hexane phase were injected into the normal-phase HPLC column.

In order to obtain the oligomeric distribution of APEO by normal-phase HPLC, 1 g of detergent powder was extracted by stirring or Soxhlet with 100 mL of *n*-hexane, a solvent which is perfectly compatible with the applied mobile phase. A sample of raw sludge was extracted in a continuous steam-distillation/solvent extraction apparatus as described elsewhere (*30*), in order to compare the recovery of NP, NP1EO, and NP2EO from the steam-distillation and the Soxhlet extraction.

High-Performance Liquid Chromatography (HPLC). The HPLC system consisted of a Perkin-Elmer Series 4 solvent delivery system equipped with a Rheodyne syringe loading sample injector (Model 7125). Detection was performed either by the spectrophotometers Kontron SFM22 and Perkin-Elmer LS3 or by the UV–vis absorption detector Kratos Spectroflow 773 UV-VIS. Prepacked bonded-phase octylsilica, octadecylsilica, and aminosilica columns were supplied by Knauer, Berlin, FRG.

In the reversed-phase mode the following gradient elution programs were used. When the irregularly shaped 10-μm LiChrosorb RP8 octylsilica column (100 mm × 4 mm i.d.) equipped with a 30 mm × 4 mm i.d. precolumn of the same packing material was employed, first 6.5 min of 5% 2-propanol (IP), 40% H_2O, 55% acetonitrile/H_2O (ACN/H_2O, 45/55) + 0.02 M $NaClO_4$ were applied, followed by a 0.4 convex elution gradient for 10 min leading to 5% IP, 80% ACN/H_2O (45/55) + 0.02 M $NaClO_4$, 15% ACN. An 8-min linear gradient reestablished initial conditions. The HPLC was operated with the column at ambient temperature and a flow rate of 1.2 mL min^{-1}. With the spherically shaped 3-μm ODS II octadecylsilica column (250 mm × 4 mm i.d.), 4 min of 3% IP, 12% H2O, 85% ACN/H_2O (45/55) + 0.02 M $NaClO_4$ were followed by a 0.3 convex gradient elution of 23 min leading to 25% ACN and 75% ACN/H_2O (45/55) + 0.02 M $NaClO_4$. An 8-min linear gradient was used to return to the starting eluent composition. The flow rate was 0.8 mL min^{-1}, and the column was held at ambient temperature. The composition of the mobile phase in the reversed-phase mode yielded a neutral pH (7.2).

In normal-phase HPLC, an aminosilica 3-μm column (Hypersil APS, 100 mm × 4 mm i.d.) was employed according to Ahel and Giger (*5*). For determination of NP, NP1EO, and NP2EO, an isocratic elution with an *n*-hexane/2-propanol mixture (H/IP, 98.5/1.5) was used at a flow rate of 1.5 mL min^{-1}, whereas for the determination of the APEO in laundry detergents, 2 min of 100% H/IP (98/2) was followed by a 25-min linear elution gradient leading to 50% H/IP (98/2) and 50% H/IP (98/2), at a flow rate of 1.5 mL min^{-1}. A 5-min linear gradient restored the initial conditions.

UV fluorescence detection was achieved at an excitation wavelength of 225 nm (Kontron SFM 22, slit width 10 nm, flow cell volume 30 μL) or 230 nm (Perkin-Elmer LS3, slit width 10 nm, flow cell volume 15 μL) and an emission wavelength of 295 nm. Reversed-phase HPLC with UV fluorescence detection or with UV absorption detection at 225 nm was used; the work in the normal-phase separations was carried out with absorption detection at 277 nm. In order to obtain the relative molar absorptivities of NPEO with one and two polyethoxy units at the mentioned fluorescence conditions, the commercial product Imbentin-N/7A was preparatively chromatographed by normal-phase HPLC (*5*). Aliquots of the collected oligomers were weighed by a Cahn microbalance, gently evaporated, and then made up to 1 mL with MeOH/H_2O (1/1) before injection into HPLC with an octylsilica column.

Quantitation. Two sets of calibration curves were routinely used in the reversed-phase mode, depending on the samples analyzed. For commercial laundry detergents and sludges, standard solutions were prepared by dissolving in a mixture of MeOH/H_2O (1/1) with SDS (5×10^{-3} M), 0.040–0.400 mg/mL LAS, 0.020–0.500 mg/mL of Marlophen 810 or Synperonic OP10, or 0.010–0.500 mg/mL NP. Since Marlon A contains only C_{10}–C_{13} chain length LAS (whereas in detergent formulations C_9- and C_{14}-LAS were also found), additional standards of 1-C_9-LAS (0.005–0.060 mg/mL) and 3-C_{14}-LAS (0.006–0.110 mg/mL) were prepared. 1-C_8-LAS (0.07 mg/mL) and 3-C_{15}-LAS (0.09 mg/mLe), which were used as recovery standards and as internal quantitation

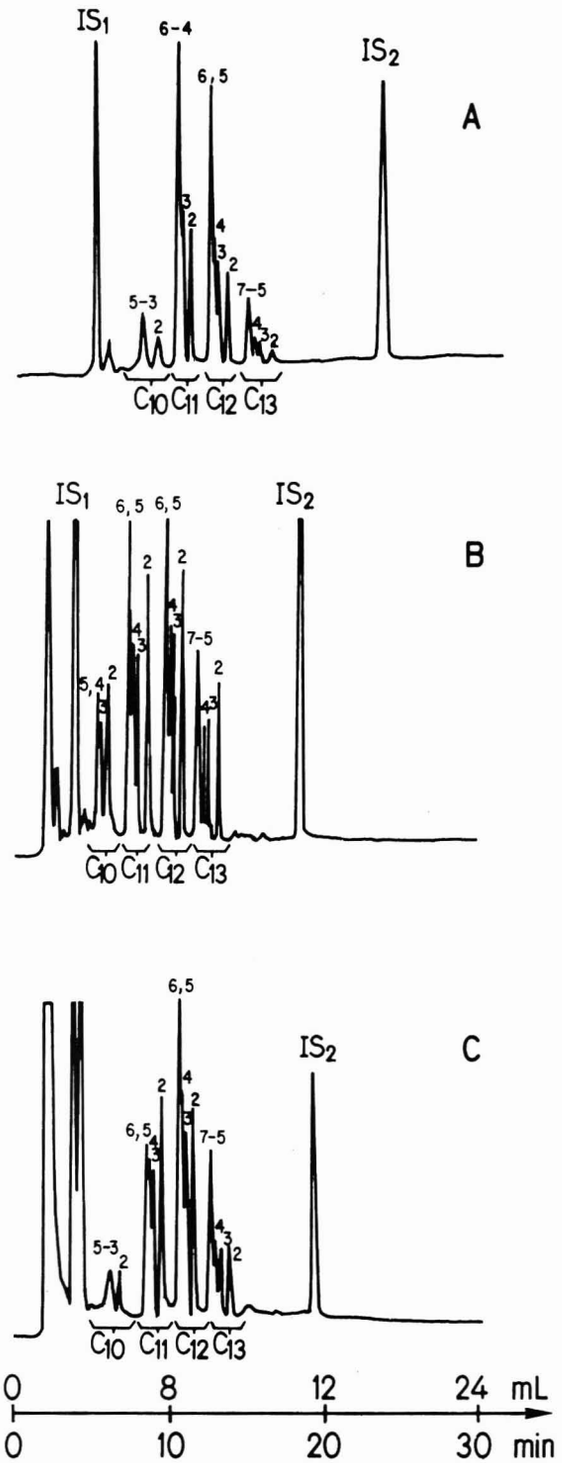

Figure 2. Reversed-phase high-performance liquid chromatograms of Marlon A (A), a laundry detergent (B), and a digested sludge extract (C): HPLC column, Spherisorb ODS II, 3 μm; detection, UV absorption; C_{10}, C_{11}, C_{12}, and C_{13}, LAS homologues. The numbers above the LAS peaks indicate the position of the phenyl group on the alkyl chain; IS_1, 1-octylbenzenesulfonate; IS_2, 3-pentadecylbenzenesulfonate.

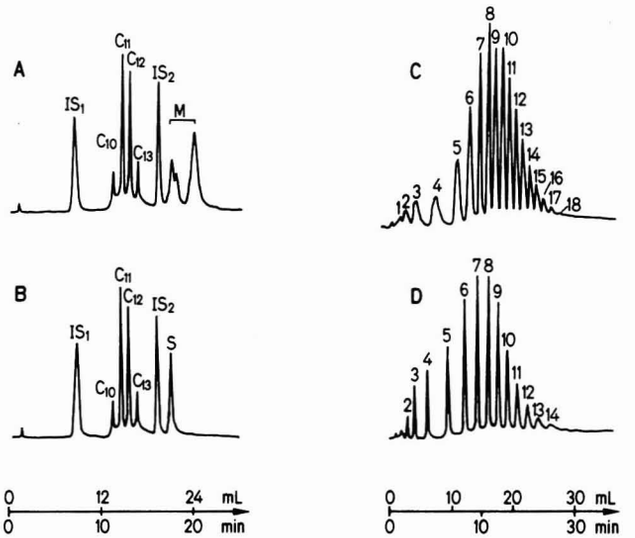

Figure 3. Reversed-phase (A, B) and normal-phase (C, D) high-performance liquid chromatograms of mixtures of technical surfactants: (A) Marlon A and Marlophen 810, (B) Marlon A and Synperonic OP1O, (C) Marlophen 810, (D) Synperonic OP10; HPLC columns, 100 mm × 4 mm i.d., LiChrosorb RP8, 10 μm for A and B; 100 mm × 4 mm i.d., Hypersil APS, 3 μm for C and D; Detection, UV fluorescence (A, B), UV absorption (C, D). Key: M, Marlophen 810; S, Synperonic OP1O; C_{10}, C_{11}, C_{12}, C_{13}, IS_1, and IS_2 as in Figure 2. Peak numbers in C and D refer to numbers of ethoxy groups.

standards, were added to each standard solution. Internal calibration curves were calculated for each LAS homologue, as well as for Marlophen 810, Synperonic OP10, and nonylphenol. Following this procedure, recovery was automatically being corrected. For the analysis of sludge-amended soils and sediments, standard solutions with concentrations 1 order of magnitude lower than the previous ones were used. Marlophen 810 (0.015–7.5 mg/mL), Synperonic OP10 (0.010–0.550 mg/mL), nonylphenol (0.005–0.200 mg/mL), and Imbentin-N/7A (0.008–0.28 mg/mL) mixture were also separately dissolved in *n*-hexane/2-propanol (80/20) in order to obtain external calibration curves for normal-phase HPLC analyses. The curves were calculated for each APEO oligomer as well as for NP.

RESULTS AND DISCUSSION

HPLC Separation. Nakae and co-workers (*21*) obtained an excellent HPLC separation of the many LAS components (homologues and isomers) by using an octadecylsilica column at 40 °C with isocratic elution using an aqueous acetonitrile solution containing 0.1 M sodium perchlorate. However both the application of internal standards with alkyl chain lengths of 8 and 15 carbon atoms and the determination of LAS in complex sample matrices such as sewage sludges and sediments make it necessary to apply gradient elution. Good results were achieved by increasing the initial water content of the reported eluent mixture (*21*) followed by elevated acetonitrile percentages for the elution of the more retained compounds. Figure 2 shows the chromatograms of a commercial LAS surfactant, an extract of a granular laundry detergent, and a sewage sludge. Three-micrometer octadecylsilica columns at room temperature and absorption detection at 225 nm were used. In addition to the LAS peaks, a broad peak, not shown in the figure, was detected around a retention volume of 34 mL. It was suspected that the latter peak could be assigned to APEO which are the most important aromatic surfactants other than LAS in laundry detergents and which are biotransformed during wastewater and sludge treatment to form more biorefractory intermediates with one and two ethoxy units as well as the not ethoxylated product NP (*7*). We collected a fraction corresponding to the broad peak and subsequently performed an extraction using *n*-hexane. The collected fraction was then identified as APEO in laundry detergents and as NP, NP1EO, and NP2EO in the sewage sludge extracts by normal-phase HPLC employing an aminosilica column with elution conditions reported by Ahel and Giger (*30*).

The octadecylsilica column was not satisfactory for the simultaneous and routine determinations of LAS, APEO, and NP because of the long analysis time and the band broadening of the APEO/NP peak. The chromatograms of Figure 3A,B were obtained by employing a 10-μm octylsilica column in combination with a higher initial water content of the eluent

Table I. Extraction Yields of LAS and APEO from Commercial Laundry Detergent Powders

		% yield, stirring			% yield, Soxhlet extraction	
solvent	extraction time, min	LAS	APEO	extraction time, min	LAS	APEO
methanol	60	43	95			
	180	101	101	40	100	102
methanol + NaOH	60	102	101	30	101	103
ethanol	60	71	95			
	180	101	102	30	102	101
ethanol + NaOH	60	101	100	20	100	101
n-hexane	12		94			
	24		100	30		100

Table II. Precision and Recovery of the Determination of LAS, NPEO, NP, NP1EO, and NP2EO in Detergents and Environmental Samples

	relative standard deviation,[a] %									% recovery[b]	
	LAS										
sample	C_9	C_{10}	C_{11}	C_{12}	C_{13}	NPEO	NP	NP1EO	NP2EO	LAS	NP
laundry detergent	1.0	1.5	1.1	0.7	2.0	1.7				100	100
digested sewage sludge	–	4.1	2.5	1.8	2.1	–	3.1	2.8	3.6	95	99
sludge-amended soil	–	–	5.2	3.2	3.4	–	5.3	4.9	5.6	85	93
surface river sediment	–	–	5.6	4.6	4.3	–	4.8	4.9	5.2	91	94

[a] Triplicate determinations. –, not determinable. [b] After addition of LAS and NP in amounts of the same order of magnitude as those previously determined for each sample. The recovery was calculated by subtracting the previous values from the amounts measured in the spiked samples.

mixture and a successively sharper and higher increase of the acetonitrile content, in the presence of 0.02 M $NaClO_4$ and 5% 2-propanol. The technical surfactants Marlon A, Marlophen 810, and Synperonic OP10 were used as standard materials containing LAS, NPEO and OPEO, respectively. Linear alkylbenzenesulfonates were separated according to their alkyl chain length; the phenyl isomers with the same alkyl chain length coeluted. The NPEO compounds of Marlophen 810 eluted under two peaks (see Figure 3A), which were tentatively attributed to two groups of alkyl isomers with differently branched nonyl side chains (*28*). Coelution was observed for the OPEO oligomers of Synperonic OP10 (peak S in Figure 3B). The minor NPEO peak had the same retention volume as the OPEO peak, which would preclude separate determination of NPEO and OPEO in reversed-phase HPLC. Nonylphenol eluted with same retention volume as NPEO. This suggests that the difference of the length of the ethoxy chains does not influence the partition of APEO between the mobile and stationary phases under the chromatographic conditions employed here. Figure 3C,D shows the oligomeric distributions of Marlophen 810 and Synperonic OP10 in the normal-phase mode.

Extraction and Recovery. Both LAS and APEO can be quickly and completely extracted from laundry detergent powders either by vigorous stirring of an ethanolic or methanolic suspension or by Soxhlet extraction with the same solvents. When only APEO are to be determined by injection into normal-phase HPLC, 20 min of stirring in *n*-hexane is sufficient to completely extract APEO. Table I gives the extraction yields obtained for LAS and APEO from a granular laundry detergent by different extraction procedures. The yields of the internal standards 1-C_8-LAS and 3-C_{15}-LAS added before the extraction were the same as those of LAS mixture contained in the detergent. The same yields were obtained by attributing 100% recovery to the extracted amounts which did not increase any more with longer extraction times. Both ethanol and methanol extract APEO more quickly than LAS. Moreover, in some detergents the basic properties of the extracts improved the chromatographic separation of the LAS homologues. In normal-phase HPLC the APEO yield which did not increase any more with longer extraction times was taken as 100%.

Four hours of Soxhlet extraction with methanol is sufficient to almost completely extract the LAS contained in sludges but only extract around 50% of the NP, NP1EO, and NP2EO. The recoveries from sludge shown in Table II were achieved after the addition of solid NaOH (20% (w/w)) to the dried sludge powder before the extraction. Since NP, NP1EO, and NP2EO coeluted in reversed-phase HPLC, determination of individual compounds was possible only by normal-phase HPLC (*30*). Therefore, 200–500-μL aliquots of the MeOH/H_2O/acetone mixture of raw sludge, diluted with water, was centrifuged after addition of NaCl and 1 mL of *n*-hexane. Aliquots of a saturated solution of NP, NP1EO, and NP2EO were processed in the same way. Moreover, the same raw sludge previously Soxhlet extracted was also extracted in a continuous steam-distillation apparatus. Steam distillation extraction provided recoveries of 95–98% for NP, NP1EO, and NP2EO (*30*). The latter chemicals contained in the aliquots of the standard solution were efficiently recovered (95–100%) into the *n*-hexane layer as was evident from comparison of the added and found concentrations. A further evaluation of the enrichment efficiency was carried out by comparing the results obtained from steam distillation and from Soxhlet extractions (Table III). The values of NP, NP1EO, and NP2EO found by the two extraction methods were very similar indicating an exhaustive transfer of the analytes into *n*-hexane.

Sample Preparation. In order to achieve the high recoveries reported in Table II, the solvent composition of the samples must be adjusted before injection onto the reversed-phase column. The injection of the methanol solution from Soxhlet extraction gave poor HPLC results for LAS, i.e., broad and distorted peaks. It is suspected that intramolecular interactions of LAS in pure methanol interfere with the chromatographic performance. For detergent powders better

Table III. Normal-Phase (A, B) and Combined Normal- and Reversed-Phase (C) HPLC Determinations of NP, NP1EO, and NP2EO in Raw Sewage Sludge Using Steam-Distillation/Solvent Extraction (A) and Soxhlet Extraction (B, C)

	concentration,[a] mg/kg dry weight		
	NP	NP1EO	NP2EO
A	0.47 ± 0.02	0.69 ± 0.1	0.04 ± 0.01
B	0.48 ± 0.02	0.70 ± 0.1	0.05 ± 0.01
C	0.46 ± 0.02	0.66 ± 0.1	0.04 ± 0.01

[a] Arithmetic means and standard deviations of triplicate determinations.

results were obtained when methanol extracts were partially evaporated and diluted with at least 30% water containing 2×10^{-2} M SDS. When the same solvent composition was used for the sludge extracts, chromatographic separations were satisfactory, but considerably lower amounts of higher chain length LAS, as well as NP, NP1EO, and NP2EO, were recovered. The use of two internal standards braketing the elution volume of the LAS helped to clarify this point. It was observed that the methanol/water mixture led to a recovery of the first internal standard between 75 and 90% and to a recovery of the second internal standard between 40 and 70% (in the case of sludges). Even lower recoveries were found for soils and sediments. The low recovery was not due to incomplete extraction from the matrices but to interactions between the emulsified material formed by the addition of water to the methanol extract. When the mixture included acetone (methanol/water/acetone, 1/1/2), the extent of emulsification decreased and the recoveries of both internal standards were 85–95% as NP, NP1EO, and NP2EO.

Detection and Quantitation. Absorption maxima of LAS and APEO mixtures such as Marlophen 810, Synperonic OP10, and NP in the solvent mixtures used for reversed-phase are at 225 nm with similar molar absorptivities. Additionally, APEO and NP also display an absorption maximum approximately 5 times less intense around 280 nm, the wavelength usually exploited for HPLC detection (*28–30*). The emission of UV fluorescence for LAS is at 270–320 nm, that of APEO and NP is at 280–350 nm. The fluorescence maxima are as follows: LAS, 295 nm; OPEO, 302 nm; NPEO and NP, 306 nm. Because LAS elute under as many peaks as the number of homologues, unlike the elution of single peaks of OPEO, NPEO, and NP, the conditions best suited for the detection of LAS were used in reversed phase, i.e., 225 nm as excitation wavelength and 295 nm as emission wavelength in fluorescence and 225 nm in absorption. In the normal-phase mode APEO and NP were detected by absorption at 277 nm.

Since LAS with alkyl chain lengths greater than or equal to six have the same molar absorptivity (*33*), peak area ratios of LAS correspond to molar ratios of the LAS components. Thus, the average molecular weight of LAS mixtures can easily be calculated. Quantitation of LAS was carried out in the fluorescence detection mode by using the internal standards 1-C_8-LAS and 3-C_{15}-LAS. The calibration curves used for each homologue were all linear (r = 0.9982–0.9991) in the concentration range 0.004–0.400 mg/mL of total LAS. In the normal-phase mode, the APEO oligomers and NP were quantitated through calibration curves (r = 0.9974–0.9995) of Synperonic OP10, Marlophen 810, and Imbentin-N/7A. The summed APEO oligomers as well as NP were also quantified in reversed-phase HPLC with the internal standards 1-C_8-LAS and 3-C_{15}-LAS. The calibration curves were linear (r = 0.9988–0.9994) in the concentration range 0.001–0.500 mg/mL. Since the molar extinction coefficients for APEO are independent of the ethoxylate chain length (*34*) (extinction coefficient for NP1EO to NP16EO at 230 nm was between 8.9 and 10.6×10^3), the quantitation in reversed-phase HPLC based on the total areas of the APEO standards implies the availability of standards with APEO oligomeric distributions similar to those of the examined environmental samples.

Due to the coelution of NP, NP1EO, and NP2EO in reversed-phase HPLC, their individual quantitation in the reversed-phase mode needed the knowledge of NP, NP1EO, and NP2EO percentages and of their molar absorptivities. For this purpose, the fraction of eluent corresponding to their peak or aliquots of the Soxhlet extract were diluted with water, NaCl and *n*-hexane were added, and the mixture was centrifuged. The *n*-hexane extract was analyzed in normal-phase HPLC, and from the knowledge of the response factors (*30*), the percentages of NP, NP1EO, and NP2EO were calculated. After collection by preparative HPLC from the standard Imbentin-N/7A, NP1EO and NP2EO displayed in the reversed-phase solvents mixture molar absorptivities 1.5 times higher than NP. Table III shows that the concentrations of NP, NP1EO, and NP2EO determined by the combined normal- and reversed-phase HPLC are in quite good agreement with those obtained in the normal-phase mode.

Accuracy, Precision, and Sensitivity. Recovery and reproducibility of the described determination method for different samples are reported in Table II. Compared to commercial detergents and sewage sludges, the recoveries of LAS in sludge-amended soils and river sediments were lower with almost two times higher relative standard deviations. Fluorescence detection at 230/295 nm after separation on an octylsilica column gave detection limits (S/N = 5) for APEO and LAS mixtures and NP of 95, 80, and 65 ng injected, respectively. When laundry detergents and sewage sludges were analyzed by reversed-phase HPLC, it was possible to employ either fluorescence or absorption detection. For sludge-amended soils and sediments only detection by fluorescence provided the necessary selectivity to reliably quantify LAS. However, NP, NP1EO, and NP2EO in sludge-amended soils and sediments could not be accurately measured by reversed-phase HPLC, even by using fluorescence, because of interferences in the resulting chromatograms. The detection in normal-phase HPLC was made by absorption at 277 nm, since the response factors of APEO and NP were already available from the literature (*5*). However, for sediments and soils, fluorescence detection at 225/306 nm or absorption at 225 nm is recommended for their higher sensitivity.

Applications. The described analytical method was used to determine LAS, APEO, and NP in laundry detergents, sewage sludges, sludge-amended soils, and river sediments. Typical results obtained by reversed-phase HPLC on a 10-μm octylsilica column are presented in Figure 4. The high concentration of hydroxy ions of the Soxhlet extracts caused a shift toward lower retention volumes of LAS, APEO, NP, and particularly of the first internal LAS standard (1-octylbenzenesulfonate). The same shift was displayed by standard solutions containing the similar hydroxy ion concentrations. Many analyses of extracts of detergents and sludges did not deteriorate the HPLC column when careful maintenance was performed, such as cleaning of the precolumn filters, replacement of the precolumns, and regeneration of the column after approximately 60 runs.

The LAS analysis on the 10-μm octylsilica column provides only the homologues distributions, compared with the 3-μm octadecylsilica column by which both homologues and partial phenyl positional isomer distributions can be obtained. Substantial variability of the LAS phenyl positional isomers distributions was found in granular laundary detergents (*35*), whereas phenyl positional isomers distributions were observed to be remarkably constant in sludges. Therefore, the 10-μm

Table IV. LAS, OPEO, NPEO, NP, NP1EO, and N2EO Concentrations in Granular Laundry Detergents and Environmental Samples

	LAS	OPEO	NPEO
laundry detergent[a]	8.6		3.9
laundry detergent[a]	2.4	2.7	0.2

	LAS	NP	NP1EO	NP2EO
digested sewage sludge[b,c]	7.3	1.2	0.22	0.03
sludge amended soil[d,e]	15.0	1.6	0.40	0.07
river sediment[d,f]	5.6	0.9	0.80	0.70

[a] Values are percent w/w. [b] Values are g/kg dry weight. [c] Grab sample from the treatment plant of Altenrhein, Switzerland. [d] Values are mg/kg dry weight (ppm). [e] Grab sample from the Swiss Federal Research Station for Agricultural Chemistry and Environmental Hygiene at Liebefeld. [f] Surficial sediment (0–3 cm) from the River Rhine at Village Neuf (6 km downstream of Basle).

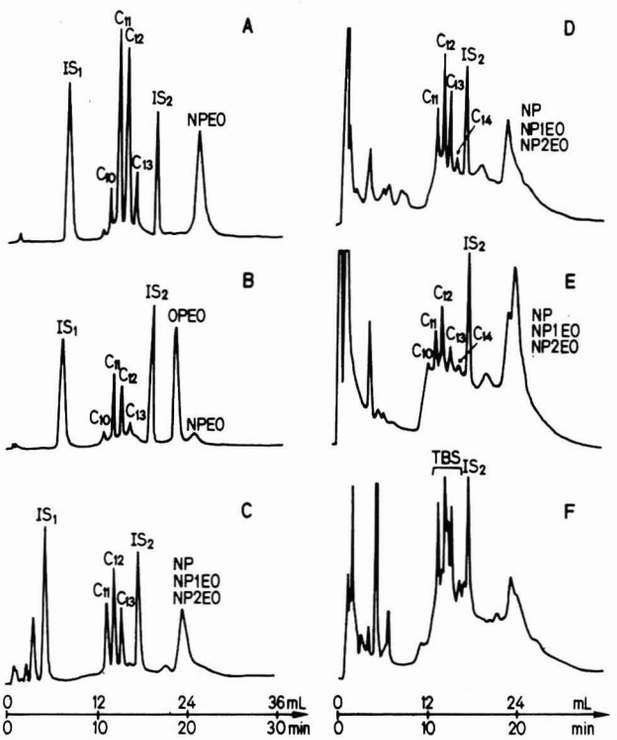

Figure 4. Reversed-phase high-performance liquid chromatograms of two commercial laundry detergents containing LAS and APEO (A, B), and digested sludge (C), a sludge-amended soil (D), and surficial (E) and deep (F) sections of a river sediment core: HPLC conditions as described for Figure 3; NP, NP1EO, NP2EO, NPEO, OPEO as in Figure 1; TBS, tetrapropylenebenzenesulfonate; C_{10}, C_{11}, C_{12}, C_{13}, C_{14}, IS_1, IS_2 as for Figure 2.

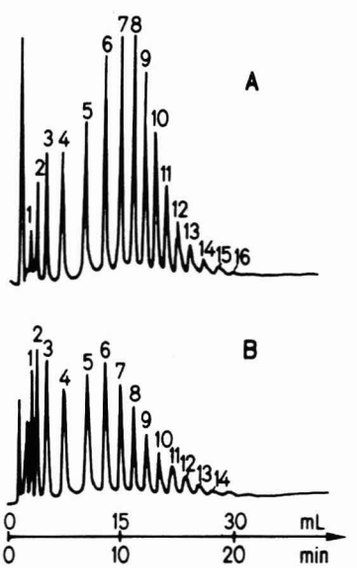

Figure 5. Normal-phase high-performance liquid chromatograms of commercial laundry detergents containing NPEO (A) and OPEO (B), respectively. HPLC conditions are described in Figure 3. Peak numbers refer to the numbers of ethoxy units.

octylsilica column is particularly well suited for routine analyses of LAS, and the octadecylsilica column may be used as an ancillary technique when insights into phenyl isomer distributions are needed.

As shown in Figure 4, the LAS homologue distributions vary remarkably between extracts from detergents, sewage sludges, sludge-amended soils, and sediments. The higher homologues are more abundant in sludges, soils, and sediments. This is of ecotoxicological significance since an increase in the length of alkyl chain has been associated with an increase in the toxicity toward various aquatic species (*36*). The chromatograms E and F of Figure 4 reflect the alkylbenzenesulfonate mixtures found on the surface (0–3 cm) and in a deeper layer (9–12 cm, corresponding to the years 1965–1970) of a dated river sediment core (*32*). The oligomer distribution in the surface sample is typical for the LAS, whereas in the deeper layer the tetrapropylene-derived branched alkylbenzenesulfonates (TBS) appear (*21*). The latter surfactants were of environmental concern because they caused foaming in sewage treatment plants and receiving waters. The quantitative determination of TBS would be possible by using the methods discussed here and a TBS standard. However, it would not be feasible to analyze for LAS and TBS occurring in the same sample because of insufficient chromatographic separation efficiency.

Figure 5 displays typical chromatograms obtained by normal-phase HPLC of two granular laundry detergents, one containing NPEO and the other OPEO. In the reversed-phase mode (Figure 4A,B) no split of the NPEO oligomers contained in the granular powder detergents (*35*) was observed. From the comparison of the chromatograms of Figure 3C and Figure 5A, it appears that the peaks of Marlophen 810, which was used as an NPEO standard mixture, are broader than those of NPEO recorded from the granular detergents. Broadening of the peaks in normal-phase HPLC and splitting into two peaks in reversed-phase HPLC were observed only in Marlophen 810. Therefore, separate determinations of OPEO and NPEO by reversed-phase HPLC were possible.

The majority of the commercial powder detergents we examined were found to contain NPEO with up to 17 ethoxy units (*35*). The results from quantitation of APEO in the reversed- and normal-phase HPLC agreed within ±8% suggesting that Marlophen 810 and Synperonic OP10 are good standards for determining APEO in granular laundry detergents by reversed-phase HPLC.

Table IV presents the concentrations of LAS, APEO, and NP typically found in environmental samples. The environmental occurrence of these contaminants in sewage sludge, amended soils, and sediments depends on the rate of appli-

cation of sludge to the land and on the rate of degradation in the soil. Similarly, the distance of the river sediments from a sewage treatment plant outflow and microbial transformation in the sediments determine the residual LAS levels in sediments. An investigation into the occurrence and fate of LAS, NP, and the NPEO during sewage treatment and after sludge application to land is currently being carried out in our institute using the methods presented in this paper.

CONCLUSIONS

The presented analytical procedure employing reversed-phase HPLC is particularly suited for routine analyses of large numbers of samples because of its detection selectivity, simplicity, and short analysis time. Quantitation of individual APEO oligomers and NP requires additional information attainable by normal-phase HPLC. Therefore the combined use of reversed- and normal-phase HPLC provides detailed information on the concentrations and structural identities of LAS, APEO, and NP in a broad range of solid matrices including commercial detergents, sludges, soils, and aquatic sediments.

ACKNOWLEDGMENT

We are grateful to M. Ahel, P. Brunner, J. McEvoy, and C. Schaffner for helpful discussions. We thank Unilever, Port Sunlight, U.K., for supplying LAS standard compounds, H. Bolliger for drafting the figures, and E. Heyerdahl for helping to prepare the manuscript.

Registry No. NPEO, 9016-45-9; NP, 104-40-5; OPEO, 26636-32-8; SDS, 151-21-3; 1-C_8-LAS, 17012-98-5; 1-C_9-LAS, 47019-68-1; 3-C_{14}-LAS, 65186-01-8; 3-C_{15}-LAS, 107514-80-7; Marlon A, 25155-30-0.

LITERATURE CITED

(1) Layman, P. L. *Chem. Eng. News* **1984**, (Jan 23), 17–49.
(2) Layman, P. L. *Chem. Eng. News* **1986**, (Jan 20), 21–42.
(3) Kunkel, E. *Tenside Deterg.* **1980**, *14*, 247–249.
(4) Osburn, Q. W. *J. Am. Oil Chem. Soc.* **1986**, *63*, 257–263.
(5) Ahel, M.; Giger, W. *Anal. Chem.* **1985**, *57*, 2584–2590.
(6) Giger, W.; Brunner, P.; Schaffner, C. *Science* **1984**, *225*, 623–625.
(7) Waters, J.; Garrigan, J. T. *Water Res.* **1983**, *17*, 1549–1562.
(8) Kikuchi, M.; Tokai, A.; Hoshida, T. *Water Res.* **1986**, *20*, 643–650.
(9) McEvoy, J.; Giger, W. *Environ. Sci. Technol.* **1986**, *20*, 376–383.
(10) Abott, D. C. *Analyst (London)* **1962**, *87*, 286–293.
(11) Waters, J. *Vom Wasser* **1976**, *47*, 131–140.
(12) Greenberg, A. E.; Connors, J. J.; Jenkins, D. In *Standard Methods for the Examination of Water and Wastewater*, 16th ed.; American Public Health Association: Washington, DC, 1985; Section 512A.
(13) Ambe, Y. *Environ. Sci. Technol.* **1973**, *6*, 542–545.
(14) Swisher, R. D. *Surfactant Biodegradation*; 2nd ed., Marcel Dekker: New York, 1987.
(15) Llenado, R. A.; Neubecker, T. A. *Anal. Chem.* **1983**, *55*, 93R–102R.
(16) Non-nami, H.; Hamia, T. *J. Chromatogr.* **1978**, *161*, 205–212.
(17) Kirkland, J. J. *Anal. Chem.* **1960**, *32*, 1389–1393.
(18) Gloor, R.; Johnson, E. L. *J. Chromatogr. Sci.* **1977**, *15*, 413–423.
(19) Taylor, P. W.; Nickless, G. *J. Chromatogr.* **1979**, *178*, 259–269.
(20) Nakae, A.; Tsuij, K.; Yamuanaka, M. *Anal. Chem.* **1980**, *52*, 2275–2277.
(21) Nakae, A.; Tsuij, K.; Yamuanaka, M. *Anal. Chem.* **1981**, *53*, 1818–1821.
(22) Saito, T.; Migashi, K.; Hagiwara, K. *Z. Anal. Chem.* **1982**, *313*, 21–23.
(23) Linder, D. E.; Allen, M. C. *J. Am. Oil Chem. Soc.* **1982**, *59*, 152–155.
(24) Wickbold, R. *Tenside Deterg.* **1972**, *9*, 173–177.
(25) Favretto, L.; Stancher, B.; Tunis, F. *Analyst (London)* **1980**, *105*, 833–840.
(26) Crisp, P. T.; Eckert, J. M.; Gibson, N. A.; Webster, I. J. *Anal. Chim. Acta* **1981**, *123*, 355–357.
(27) Stephanou, E. *Int. J. Environ. Anal. Chem.* **1985**, *27*, 41–54.
(28) Garti, N.; Kaufman, V. R.; Aserin, A. *Sep. Purif. Methods* **1983**, *12*, 49–116.
(29) Kudoh, M.; Ozawa, H.; Fudano, S.; Tsuij, K. *J. Chromatogr.* **1984**, *287*, 337–344.
(30) Ahel, M.; Giger, W. *Anal. Chem.* **1985**, *57*, 1577–1583.
(31) Paquette, R. G.; Lingafelter, E. C.; Tartar, H. V. *J. Am. Chem. Soc.* **1943**, *65*, 686–692.
(32) Sturm, M., EAWAG, Dübendorf, private communication, 1986.
(33) Weber, W. J.; Morris, J. C.; Stumm, W. *Anal. Chem.* **1962**, *34*, 1844–1845.
(34) Rothman, A. M. *J. Chromatogr.* **1982**, *253*, 283–288.
(35) Marcomini, A.; Filipuzzi, F.; Giger, W., submitted for publication in *Chemosphere*.
(36) Kimmerle, R. A.; Swisher, R. D. *Water Res.* **1977**, *2*, 31–37.

RECEIVED for review September 18, 1986. Accepted March 9, 1987. This project was partly funded by the Swiss National Science Foundation (Nationales Forschungsprogramm 7D, research project on "Organic Contaminants in Sewage Sludges"). Additional support was obtained from the project COST 641 "Organic Micropollutants in the Aquatic Environment" in the framework of the European Cooperation for Scientific and Technical Research.

Determination of Water by Liquid Chromatography Using Conductometric Detection

Timothy S. Stevens*[1] and Karen M. Chritz

The Dow Chemical Company, U.S.A., Michigan Division Analytical Laboratories, 574 Building, Midland, Michigan 48667

Hamish Small

4176 Oxford Drive, Leland, Michigan 49654

Most determinations for water are easily made by a Karl Fischer titration but interferences are known including oxidizing agents, unsaturated compounds, and thio compounds. Gas chromatography (GC) can be both rapid and sensitive but some components of a sample can elute slowly or decompose on-column and interfere. This contribution describes the determination of water by liquid chromatography with a conductivity detector. The inclusion of an acid in the eluent significantly improved sensitivity of detection, which was limited at about 2.5 ppm. At the 20% water level, precision of determination was 0.22%. Examples are shown for the determination of water in samples that interfered with GC and/or Karl Fischer methods.

Most determinations for water are easily made by a Karl Fischer titration. However, interferences are known including oxidizing agents, unsaturated compounds, and thio compounds (*1*). Thermal conductivity detection gas chromatography (GC) is probably the second most used method, often resulting in a water peak that elutes rapidly, e.g., 1–2 min, and with good sensitivity, e.g., 1 ppm (*2*). However, with GC the other components of a sample can take much longer to elute than water and can even decompose on-column and interfere with the analysis.

We were faced with the need to determine water in commercial formulations of dibromonitrilopropionamide (DBNPA), an antimicrobial product of The Dow Chemical Co. DBNPA is an oxidizing agent and reacts with iodide to yield iodine and thus interferes with the Karl Fischer method. DBNPA is thermally labile and decomposed on-column in a GC. The products of the decomposition (believed to include HBr) corroded and eventually severed the filaments of the GC detector.

We thus considered high-performance liquid chromatography (HPLC). Blasius et al. determined water by using a cyclic polyether column with a refractive index (RI) detector but water and other nonionic components eluted without retention (*3*). Fehrman et al. determined water by gel permeation chromatography using a RI detector. Toluene was used as the eluent which significantly improved separation of water from other low molecular weight interfering components (*4*). However, the DBNPA formulation was not miscible in toluene, and water itself has a limited solubility in toluene. Bjorkquist et al. reacted phenyl isocyanate with water to form *N,N'*-diphenylurea (*NN'*-DPU), with a total reaction time of about $^1/_2$ h, and then analyzed the *NN'*-DPU by reverse-phase HPLC (*5*). We wanted a simpler and faster procedure than this. Roof et al. used an anion-exchange column with a "density detector" to determine water in a fluorination process stream in about 12 min, but with relatively poor column efficiency, i.e., about 30 effective theoretical plates (*6*).

This contribution describes the use of an HPLC system for the determination of water by using an electrical conductivity detector. Considering the extensive use of direct conductometric determination of water (*7*) it is surprising that HPLC/conductivity has not been previously described. Examples are shown for the determination of water in samples that would otherwise frustrate or complicate water determination by the frequently used GC and/or Karl Fischer methods. Generally, water is the last peak to elute in the chromatogram and analytical time is less than 5 min with detection limits of about 2.5 ppm.

Columns filled with ion-exchange resin were selected due to the known affinity of such resins for water (*8*). Nevertheless other chromatographic packings were also evaluated.

EXPERIMENTAL SECTION

The chromatographic system included an LDC Constametric III pump, a Rheodyne 7120 injection valve, a Chromatronix CM1-A conductivity meter with MCC-75 flow cell, and a Sargent SRG-1 recorder.

The chromatographic columns used included a Whatman Partisil 10-ODS, 10-ODS-3, 10-SAX, and 10-SCX as well as a Du Pont Zorbax SIL, all 4.6 × 250 mm, and a Hamilton PRP-1 column, 4.6 × 150 mm. The glass column was an LDC Cheminert LC-9-MA-13, 9-mm inside diameter (i.d.) packed with Bio-Rad AG-1X2 anion-exchange resin, 200–400 mesh, or Bio-Rad Aminex 50WX4, cation exchange resin, 20–30 μm, by slurry packing with eluent.

Solvents used included Fischer HPLC grade methanol and acetonitrile. The acids used included Baker Analyzed concentrated sulfuric acid (96%) and hydrochloric acid (37%). The *p*-toluenesulfonic acid was obtained from Eastman Chemicals. The inorganic salts used were Baker Analyzed grade sodium chloride and lithium bromide. Water was determined in samples of carbon tetrachloride, toluene, and in eluent by using a Metrohm Model 652-KF coulimetric Karl Fischer analyzer and all water results reported herein are in units of micrograms of water per milliliter of sample (ppm) or in grams of water per 100 mL of sample (%). The following chromatographic conditions were used to generate Figures 1–7.

Figure 1: eluent, 0.0024 M NaCl in methanol at 2 mL/min; column, 9 × 54 mm, Aminex 50WX4, Na^+ ion form, 20–30 μm; injection, 10 μL loop; detection, 7.5 μs cm^{-1} per 10 mV; recorder, 10 mV span, normal polarity.

Figure 2: eluent, 0.0024 M NaCl in methanol at 1 mL/min; column, Partisil-10-ODS-3, Zorbax-SIL, or Partisil-10-SCX; injection, 10 μL loop; detection, 7.5 μs cm^{-1} per 10 mV; recorder, 10 mV span, reversed polarity.

Figure 3: eluent, 0.0015 M *p*-toluenesulfonic acid (PTSA) in methanol, or 0.0012 M HCl in methanol, or 0.0012 M H_2SO_4 in methanol, at 1.5 mL/min; column, 9 × 21 mm, Aminex 50WX4, H^+ ion form, 20–30 μm; injection, 30 μL loop; detection, 30 μs cm^{-1} per 10 mV; recorder, 10 mV span, reversed polarity.

[1] Present affiliation: Dow Patent Department, 1776 Bldg., Midland, MI.

0003-2700/87/0359-1716$01.50/0 © 1987 American Chemical Society

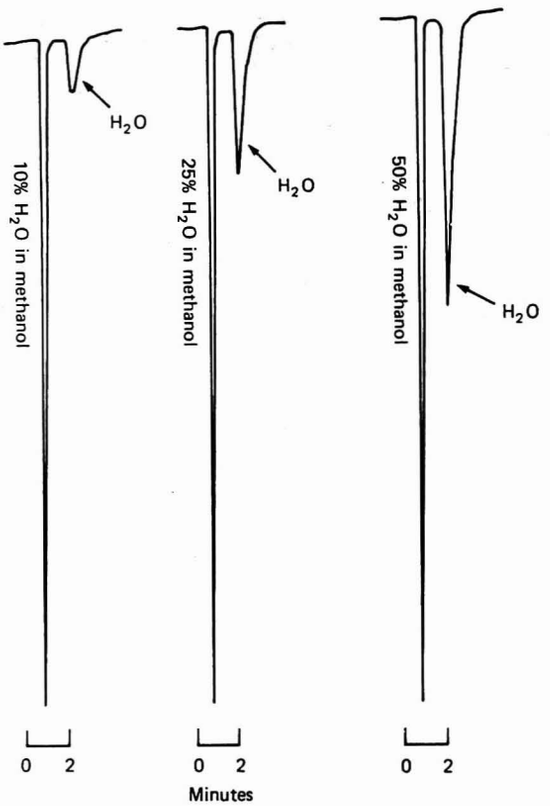

Figure 1. HPLC determination of water with NaCl in the eluent.

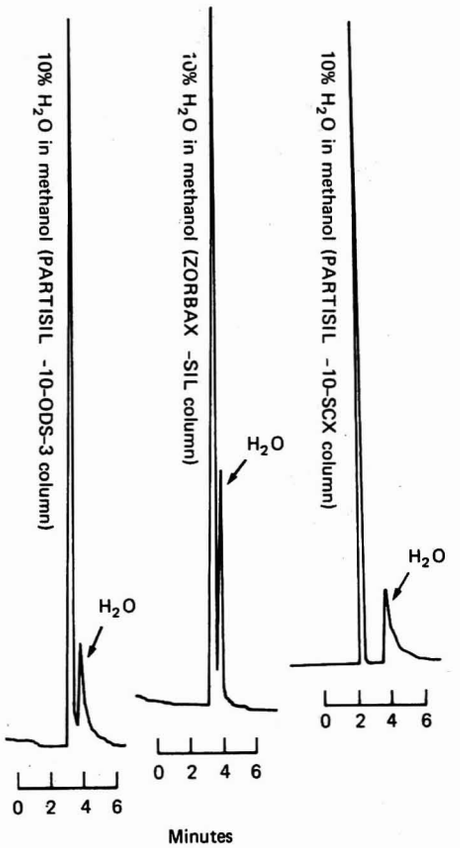

Figure 2. HPLC determination of water using microparticulate normal-phase, reverse-phase, and ion-exchange columns with NaCl in the eluent.

Figure 4: eluent, 0.0012 M H_2SO_4 in methanol at 1.5 mL/min; column, 9 × 21 mm Aminex 50WX4, H^+ ion form, 20–30 μm; injection, 1 μL; detection, 60 μs cm^{-1} per 10 mV; recorder, 8 mV span, reversed polarity.

Figures 5 and 6: eluent, 0.0012 M H_2SO_4 in methanol at 1.5 mL/min; column, 9 × 21 mm Aminex 50WX4, H^+ ion form, 20–30 μm; injection, 50 μL loop; detection 7.5 μs cm^{-1} per 10 mV; recorder, 10 mV span, reversed polarity.

Figure 7: eluent, 0.0012 M H_2SO_4 in methanol at 1.5 mL/min; column, 9 × 18 mm Aminex 50WX4, H^+ ion form, 20–30 μm; injection, 100 μL loop; detection, Wescan model ICM conductivity detector, range 1, 10 mV output; recorder, 2 mV span, reversed polarity.

RESULTS AND DISCUSSION

Eluents Containing Salt. It was concluded that the addition of an electrolyte to a nonaqueous eluent would increase the conductivity of the water peak as it passed through the detector from the column. Thus, we began our work with eluents containing NaCl. Instead of positive peaks, negative peaks (dips) were seen as shown in Figure 1.

Two dips were seen in the chromatogram for each injection. The one at about 0.8 min was explained as the void volume upset resulting from the lack of NaCl in the injected sample. The one at about 2.1 min was explained as the water "peak", and its size was proportional to the amount of water in the injected standard. Doubling the amount of NaCl in the eluent doubled the water "peak" height and also doubled the background conductivity of the eluent from about 250 μs cm^{-1} to about 500 μs cm^{-1}. As expected, the base line noise increased with background conductivity, and the limit of detection observed with either eluent was about 0.1% water (in a standard) with a 500-μL injection. The use of LiBr in the eluent instead of NaCl resulted in similar system performance. When the eluent contained no added salt, only a small response was seen for the same injections shown in Figure 1. Reversing the recorder polarity resulted in upscale "peaks" and this became standard operating procedure.

Other Columns. The conventional microparticulate HPLC columns listed in the Experimental Section were also tested and with the exception of the Hamilton PRP-1 column, all yielded a retained water peak whose height was proportional to the amount of water injected in a standard. However, the water peak in each case was little retained (k' less than 1) and tailed. For example, Figure 2 shows the performance for the Du Pont Zorbax SIL column, the Whatman Partisil ODS-3 column, and the Whatman Partisil SCX column.

With the Hamilton PRP-1 column, the water peak coeluted with the void volume upset. The best performing microparticulate column, the Partisil 10-25-SCX, was judged to perform poorer than the one filled with Aminex 50WX4. The retention mechanism with the use of the columns packed with ion-exchange resin is probably liquid/liquid partition given the known affinity of ion-exchange resins for water (*8*). It is more difficult to explain the retention mechanism with the use of the columns packed with silica based microparticulate normal- and reverse-phase packings but it may well be a size exclusion chromatography mechanism.

Eluent Containing Acid. In dilute aqueous solution a strong acid has about 5 times the specific conductivity of an equal concentration of the salt of the acid formed by neutralization with a strong base. The use of HCl, H_2SO_4, or *p*-toluenesulfonic acid (PTSA) in an eluent of methanol on a 9 × 21 mm column of H^+ ion form Aminex 50WX4 resulted in significantly improved performance. With the NaCl containing eluent of Figure 1, a 50-μL injection of 1% H_2O in methanol resulted in a water peak 0.11 μs cm^{-1} tall. Use of any of the above acids (also of a concentration sufficient to give an eluent background conductivity of about 250 μs cm^{-1}) resulted in a water peak about 18 μs cm^{-1} tall (see Figure 3), an increase in sensitivity of about 160-fold!

Explanation of the Negative Water Peak. It was originally expected that the water peak would be positive with the use of conductivity detection and an eluent of methanol containing an electrolyte, i.e., an increase in conductivity with

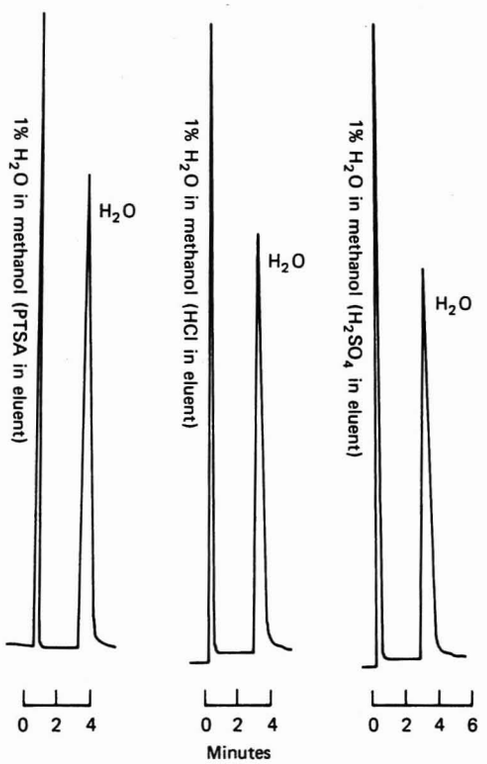

Figure 3. HPLC determination of water with various acids in the eluent.

Table I. Measured Conductivity of Methanol–Water Mixtures Containing 0.0012 M Sulfuric Acid

eluent	ppm H_2O	conductivity,[a] μs cm^{-1}
1	200	252
2	1 200	228
3	2 200	212
4	4 200	191
5	8 200	170
6	16 000	156
7	31 000	146
8	61 000	140
9	113 000	144
10	203 000	167
11	340 000	238

[a] Measured with the Chromatronix CM1-A detector and MCC-75 cell at a flow rate of 1.5 mL/min.

the addition of water. However, when the conductivity of methanol/water mixtures containing a constant concentration of H_2SO_4 (0.0012 M) was measured, the data in Table I resulted.

The data in Table I indicate that only above about 6% water does the conductivity increase with increasing water content. The data in Table I parallel the work of Jones et al. who found a minimum in the conductivity of hydrochloric acid in mixtures of methanol and water at about 10% water (*9*). Jones et al. also found a minimum in the conductivity of many salts in mixtures of methanol and water, e.g., at about 35% water for KI and at about 50% water for $LiNO_3$ (*10*). Thus, the negative peaks observed in this work and the greater sensitivity of the determination of water with the use of an acid added to the eluent relative to the use of a salt added to the eluent are both consistent with the data of Jones et al.

The data in Table I suggest that there is a possibility that a calibration curve could show the same response for two different sample water concentrations. However, dilution of the injected sample in the eluent through the system prevented this, i.e., an injection of 100% water resulted in less than 6% water at the detector as long as the injection size

Figure 4. HPLC determination of water in a formulation of DBNPA.

Figure 5. HPLC determination of water in Telone-II soil fumigant.

was less than about 25 μL. The data in Table I also show that the calibration curves of this procedure are not linear. However, the calibration curves are essentially linear to about 1000 ppm of water at the detector.

Effect of Water in the Eluent. A "vacancy chromatography" (*11*) water peak appeared in the chromatogram at the retention time for water when the eluent contained water and a relatively dry sample was injected. As expected, the magnitude of the vacancy peak was proportional to the concentration of water in the eluent. Best results were obtained when the eluent contained little water, i.e., about 100 ppm water or less.

Other Examples. Figure 4 shows a chromatogram for the injection of a 20% DBNPA formulation in a water/glycol based formulation. This formulation was injected 10 times and a statistical evaluation of the data indicated an average water content of 20.1% with a standard deviation of 0.22%.

During the development of the HPLC procedure for the determination of water in DBNPA formulations a headspace gas chromatographic (HSGC) procedure was successfully developed that eliminated the need to inject the formulation directly into the GC. A comparative study of the HSGC and HPLC results for nine DBNPA formulation samples showed a difference of from 0% to 15% relative with an average bias of 7% relative. This was considered to be a good agreement

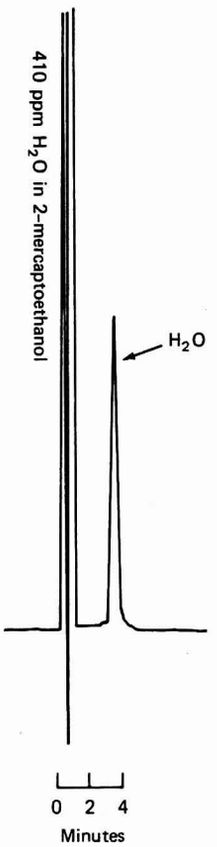

Figure 6. HPLC determination of water in 2-mercaptoethanol.

between the methods. The HPLC procedure was preferred as being less complicated and faster.

Figure 5 shows a chromatogram for an injection of Telone-II soil fumigant (isomers of dichloropropene, a product of The Dow Chemical Co.). As is generally the case, water was the last peak to elute in the chromatogram and the level of water estimated in the sample was 67 ppm. A GC analysis of the same sample estimated a water level of 71 ppm. In the GC analysis, the water elutes at about 2 min followed by dichloropropene peaks for the next 45 min (*12*). Thus, the HPLC procedure was faster overall. Water cannot be determined in Telone-II soil fumigant by the Karl Fischer method since iodine adds across the double bonds of the dichloropropenes.

Figure 6 shows a chromatogram for an injection of 2-mercaptoethanol. Water cannot be determined in many thio compounds by the Karl Fischer method (*1*).

Interferences. As a rule, water elutes as the last peak in the chromatogram well resolved from the other components of a sample. However, dimethyl sulfoxide (Me_2SO) eluted just before water and seriously interfered. It is clear that the procedure could be used to determine Me_2SO and perhaps other compounds in favorable matrixes. Samples containing hydroxide ion would interfere when the eluent contains an acid. Samples containing ketones or aldehydes interfere due to their reaction with methanol to form ketals and acetals with the resultant liberation of water just as when a Karl Fischer reagent contains methanol (*1*). A possible solution to this problem, as with the Karl Fischer method, is to replace the methanol with another nonreactive solvent.

Acetonitrile in the Eluent. Water eluted later ($k' = 58$) and with poor efficiency ($N = 144$) when using an eluent of 0.0012 M H_2SO_4 in acetonitrile at 1.5 mL/min and a 9 × 16 mm Aminex 50WX4 column. However, unlike the use of methanol in the eluent the water peak was positive. A 50-μL injection of a 1% water standard resulted in a water peak that was 2.4 $\mu s\ cm^{-1}$ tall on a background conductivity of 7.2 $\mu s\ cm^{-1}$. A comparison of the peak area (in units of $\mu s\ cm^{-1}\ mL$) for the water peaks in Figure 3 and the water peak obtained by using the acetonitrile-based eluent indicated that both had about the same area (10 vs. 9, respectively). Since the background conductivity obtained when using the acetonitrile based eluent was 36 times lower, it was concluded that a system using an acetonitrile-based eluent with a more efficient and less retentive column might result in rapid analyses, improved detection limits, and reduced interferences. Of the columns listed in the Experimental Section the only one that even came close to meeting this potential was one filled with AG-1X2, but poor peak efficiency ($N = 16$) severely limited practical usefulness and sensitivity. The poor efficiency obtained with the acetonitrile-based eluent is explained by slow mass transfer in the stationary phase due to the limited swelling of the ion-exchange resins in acetonitrile. Further work, perhaps with smaller diameter resin or with partially sulfonated or aminated ion-exchange resins that may swell more in acetonitrile, is planned. In addition, size exclusion chromatography columns of appropriate pore size could prove to be useful with this technique since they have already been used with refractive index detection (*4*).

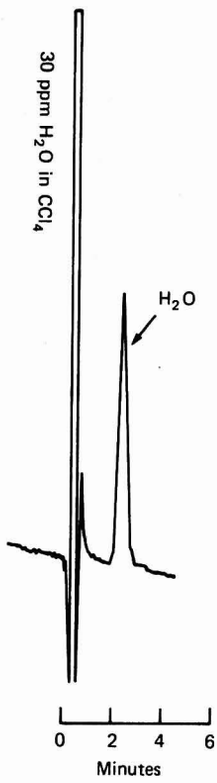

Figure 7. HPLC determination of water using a low noise detector.

Refractive Index Detection. An Altex Model 156 RI detector was evaluated on the basis of a signal to noise comparison. It was estimated that the detection limit with this RI detector was about 10–50 times poorer than with the conductivity detector.

Detection Limits. The relatively high background conductivity (and its associated noise level) of this method, upon which the water peak or dip is seen, is a major limitation of detection limits. This situation is analogous to "single column ion chromatography" (*13*) where the commercially available conductivity detectors are especially designed to work at relatively high background conductivity with minimum noise. One such detector is the Wescan Model ICM conductivity detector, which places the column and conductivity cell in a temperature-controlled enclosure. Figure 7 shows the performance of a system using the Wescan Model ICM detector. The data in Figure 7 indicate that at a signal to noise ratio

of 2.5 to 1 the detection limit for water would be about 2.5 ppm.

ACKNOWLEDGMENT

Richard Solomon of our laboratory developed the headspace GC method and used it for the comparative determinations of water in formulations of DBNPA. Danial Martin of our laboratory performed the comparative GC determination of water in Telone-II soil fumigant.

Registry No. DBNPA, 10222-01-2; H_2O, 7732-18-5; Telone-II, 542-75-6; 2-mercaptoethanol, 60-24-2.

LITERATURE CITED

(1) Mitchell, J., Jr.; Smith, D. M. *Aquametry, Part III*; Wiley-Interscience: New York, 1980.
(2) Mitchell, J., Jr.; Smith, D. M. *Aquametry, Part I*; Wiley-Interscience: New York, 1977.
(3) Blasius, E.; Janzen, K. P.; Adrian, W.; Klein, W.; Klotz, H.; Luxenburger, H.; Mernke, E.; Nguyen, V. B.; Nguyen-Tien, T.; Rausch, R.; Stokemer, V.; Toussaint, A. *Talanta* **1980**, *27*, 127.
(4) Fehrman, V.; Schnabel, W.; *Fresenius' Z. Anal. Chem.* **1974**, *269*(2) 116.
(5) Bjorkquist, B.; Toivoner, H. *J. Chromatogr.* **1979**, *178*, 271.
(6) Roof, L. B. U.S. Patent 3 935 097, 1976.
(7) Smith, D. M.; Mitchell, J., Jr.; *Aquametry, Part II*; Wiley-Interscience: New York, 1984.
(8) Helfferich, F. *Ion Exchange*; McGraw-Hill: London, 1962; p 104.
(9) Jones, H. C.; Carroll, C. G. *Am. Chem. J.* **1904**, *32*, 521–583.
(10) Jones, H. C.; Lindsay, C. F. *Am. Chem. J.* **1902**, *28*, 329–370.
(11) Snyder, L. R.; Kirkland, J. J. *Introduction To Modern Liquid Chromatography*, 2nd ed.; Wiley: New York, 1979; p 812.
(12) Analytical Method ML-AM-81-45, available from the Methods Editor, The Dow Chemical Company, Michigan Division, Analytical Laboratories, 574 Building, Midland, Michigan 48667.
(13) Gjerde, D. T.; Schmuckler, G.; Fritz, J. *J. Chromatogr.* **1980**, *187*, 230.

RECEIVED for review July 21, 1986. Resubmitted February 17, 1987. Accepted March 16, 1987. A United States Patent Application has been filed covering the subject of this contribution.

Estrogen Conjugates in Late-Pregnancy Fluids: Extraction and Group Separation by a Graphitized Carbon Black Cartridge and Quantification by High-Performance Liquid Chromatography

Franca Andreolini,[1] Claudio Borra,[1] Federica Caccamo, Antonio Di Corcia,* and Roberto Samperi

Dipartimento di Chimica, Università "La Sapienza" di Roma, Piazza Aldo Moro, 00185 Roma, Italy

A stepwise elution system was elaborated for the fractionation in classes of conjugation of estrogens in pregnancy body fluid samples by exploiting the presence of charged active centers on the surface of graphitized carbon black (Carbopack). After biological samples were percolated through an experimental Carbopack cartridge, five classes of estrogens were eluted in the following order: unconjugated, A-ring glucuronides, D-ring glucoronides, monosulfates, double conjugates. After solvent elimination, each class of conjugation was subfractionated and quantified by ion-pair high-performance liquid chromatography. The major advantages of this procedure over those based upon ion exchangers are that minimum sample manipulation is required, it permits analysis of double conjugates, and the time of analysis is drastically reduced. Recoveries of all compounds of interest ranged between 90% and 98%. The levels of estrogens and their conjugates in late pregnancy urine, serum, and amniotic fluid samples were measured.

It is known that only a fraction of the steroid hormones are present in biological materials as unconjugated forms, the major part of them being conjugated with sulfuric and glucuronic acids. Although steroid conjugates do not possess a direct biological activity, they can act as precursor hormone reservoirs able to be converted to either unconjugated precursor steroids or physiologically active steroids (*1*, *2*). Moreover, the level of each conjugate in biological materials is controlled by complex metabolic and transport mechanisms, which may be altered by pathological disturbances. For these reasons, a more complete understanding of the relationship of steroids with diseases may be achieved from the knowledge of the levels of these conjugates in normal and abnormal status. The recent trend in clinical chemistry is that of devising analytical systems for measuring one selected intact steroid conjugate (*3–5*) or all the conjugated forms of a single steroid (*6–9*) or the conjugation profile of one class of steroids.

Group separation of urinary steroid conjugates has been performed by anion exchangers (*10–12*). After fractionation, steroids are deconjugated, derivatized, and analyzed by capillary gas chromatography. With this procedure and the use of the chromatograph coupled to a mass spectrometer, impressive results have been obtained as to the determination in pregnancy urine of the conjugate profile not only of the three main estrogens but also of their metabolites (*13*). Although various modifications have been tried in order to simplify and increase the speed of all steps, this methodology is time-consuming, prone to errors due to excessive manipulation of the sample, and thus unsuitable for routine analysis. In addition, the procedure cited above does not permit determination of double conjugates and it has not been employed for body fluids other than urine.

The elution and separation of synthetic mixtures of intact estrogen conjugates have been successfully performed by ion-pair "high-performance" liquid chromatography (IP-HPLC) (*14*, *15*). By the use of this technique, we succeeded recently in determining the conjugation profile of estriol in various body fluids of pregnancy (*9*). The purification of the biological specimens was accomplished by solid-phase extraction with Vulcan (Carbopack B), a well-known example of graphitized carbon black (GCB), which has been extensively used for isolating analytes of clinical interest from biological materials (*16–18*).

Interestingly, during the experiments we made in order to find the most effective eluant phase for simultaneous de-

[1] Present address: Department of Chemistry, Indiana University, Bloomington, IN 47405.

0003-2700/87/0359-1720$01.50/0 © 1987 American Chemical Society

sorption of estriol and its ionogenic, conjugated forms, we observed that these latter compounds were so strongly adsorbed that no simple solvent system was able to desorb them. Although Vulcan is known to behave as a natural reversed phase, this material was supposed by us to contain on its surface particular chemical groups able to bind anions via electrostatic forces.

The purpose of this work has been that of evaluating the ability of Vulcan in fractionating steroids according to their classes of conjugation in order to develop more convenient HPLC methods for the measurement of the three main estrogens and their major conjugates in fluids of the late human pregnancy, such as urine, serum, and amniotic fluid.

EXPERIMENTAL SECTION

Chemicals and Solvents. Chloroform was of analytical grade and was used after redistillation in a glass system. The other solvents were of HPLC grade and were used as supplied. Tetrapropylammonium bromide (TPABr) and tetramethylammonium hydroxide (TMAOH) 2.2 mol/L in methanol were from Fluka AG (Buchs, Switzerland). When necessary (see later), TPABr was converted to its chloride form by percolating water containing TPABr 20 mmol/L through a column filled with a strong anionic exchanger in the chloride form.

The solvent mixtures utilized for the purification and fractionation of the estrogen and their conjugates with the Carbopack cartridge were as follows: (A) 100 mmol/L of formic acid in methanol; (B) chloroform/methanol (60/40, by volume); (C) 250 mmol/L of formic acid in chloroform/methanol (27/73, by volume); (D) 250 mmol/L of formic acid in chloroform/methanol (60/40, by volume); (E) 5 mmol/L of TMAOH in chloroform/methanol (10/90, by volume); (F) 0.5 mmol/L of TMAOH in chloroform/methanol (80/20, by volume); (G) 5 mmol/L of TMAOH in chloroform/methanol (80/20, by volume).

The following authenthic steroids were purchased from Sigma Chemical Co. (St. Louis, MO): androsterone (A), androsterone sulfate (A-S), estriol (E_3), estradiol (E_2), estrone (E_1), estriol 3-glucuronide (E_3-3-G), estradiol 3-glucuronide (E_2-3-G), estrone 3-glucuronide (E_1-G), estriol 16-α-glucuronide (E_3-16-G), estradiol 17-β-glucuronide (E_2-17-G), estriol 3-sulfate (E_3-3-S), estradiol 3-sulfate (E_2-3-S), estrone 3-sulfate (E_1-S), estradiol 3-sulfate 17-β-glucuronide (E_2-3-S-17-G). Estriol 3-sulfate 16-α-glucuronide (E_3-3-S-16-G), commercially unavailable, was prepared (*19*) and purified (*9*) as reported elsewhere.

Preparation of the Carbopack Cartridge. The Carbopack cartridge is an experimental kit developed and kindly supplied by Supelco (Bellefonte, PA). The cartridge consists of a 6-cm × 1-cm-id cylindrical polypropylene tube, which is one-sixth full of 250 mg of GCB with a particle size range between 125 and 20 μm. Polyethylene frits are located above and below the adsorbent bed to hold the minute particles in place and keep the chromatographic column intact. The cartridge fits directly into the vacuum manifold. Vacuum was obtained with a water pump, taking no care to ensure a low and costant flow-rate of the samples percolating through the cartridge. Before use, the cartridge was washed by passing through it, sequentially: 3 mL of chloroform, 2 mL of methanol, and 2 mL of water.

Procedure with Serum and Amniotic Fluid Samples. One milliliter of pregnancy serum or amniotic fluid was deproteinized with 5 mL of methanol at 0 °C followed by centrifugation at 2000*g* for 3 min. For amniotic fluid samples, the supernate was applied directly to the Vulcan column. On the contrary, to remove phospholipids, which interfere with the analysis, the methanolic extract of serum samples was diluted with 0.5 mL of water and passed through a C_{18} chemically bonded silica column (Sep-PAK, Waters Associates) followed by 4 mL of methanol/water (80/20, by volume). The entire effluent was collected and percolated through the Vulcan column. After this, we passed sequentially through the column: (1) 10 mL of solvent A, discarded; (2) 5 mL of methanol, discarded; (3) 3 mL of solvent B, collected (It contains unconjugated estrogens.); (4) 3 mL of methanol, discarded; (5) 5 mL of solvent C, collected (It contains estrogens A-ring glucuronides.); (6) 5 mL of solvent D, collected (It contains estrogen D-ring glucuronides.); (7) 2 mL of methanol, discarded; (8) 5 mL of solvent E, discarded; (9) 2 mL of methanol, discarded; (10) 5 mL of solvent F, collected (It contains estrogen sulfates.) (11) 5 mL of solvent G, collected (It contains double conjugated estrogens.).

With Urine Samples. One milliliter of pregnancy urine was diluted with 9 mL of water and passed through the Carbopack cartridge. After it was washed with 5 mL of water followed by 10 mL of solvent A, the scheme described above was followed starting from step 5, as unconjugated estrogens are virtually absent in urine (*7*).

Whatever the body fluid analysed and the fraction of estrogens collected, solvents were removed by evaporation in a water bath at 60 °C under a stream of nitrogen. Before heating, the solution containing double conjugates was suitably neutralized, in order to avoid partial decomposition. The residue was reconstituted in 50 μL of the HPLC mobile phase (starting composition) and injected into the HPLC apparatus.

HPLC. Liquid chromatography was carried out with Varian, Model 5000 having a Rheodyne Model 7125 injector with a 40-μL loop and equipped with both UV (Varian, Model 2050) and fluorometric (Perkin Elmer, Model 650-10s) detectors, in series. A 4.6-mm × 25-cm column filled with 5-μm particle size, C_{18} reversed-phase packing and a guard column containing "Pelliguard", both from Supelco, were used. Solvent A was a phosphate buffer (5 mM, pH 3.2) containing TPABr, 20 mmol/L; solvent B was acetonitrile/methanol (60/40, by volume). The flow rate was 1.5 mL/min. Chromatographic conditions are reported in detail in Results and Discussion.

The concentrations of estrogens and their conjugates in standard and patient samples were calculated by comparing peak heights produced by the analytes in the sample with those of reference standards. These were prepared for chromatography by mixing appropriate volumes of working standard solutions and, after solvent removal, by reconstituting the residue with 50 μL of the HPLC mobile phase.

RESULTS AND DISCUSSION

As mentioned above, attempts to desorb anionic compounds, such as estrogen conjugates, from the Vulcan surface by washing it extensively with various, neutral solvent mixtures at high elution strength failed. This effect can be explained by assuming that the GCB surface is contaminated by certain, positively charged chemical impurities which may be a burnt-off residue left over from the heating at 2700–3000 °C of carbon black. Recently, we had experimental evidence (*20*) for the existence of chromene-like structures included in the surface framework of GCB. This oxygen complex in the presence of oxygen and water can be rearranged to form a structure similar to benzpyran and benzpyrylium salts according to:

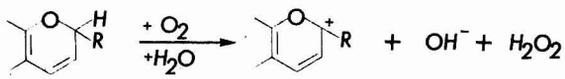

The surface density of this oxygen complex was assessed by determining the maximum amount of an ionogenic compound, such as E_3-3-S, that can be chemically adsorbed on a given amount of Vulcan. After slow percolation through 250 mg of the GCB column of aqueous solutions containing different concentrations of E_3-3-S, chloroform/methanol (60/40, by volume) was passed through to remove the steroid physically adsorbed. Then, the fraction of E_3-3-S still remaining adsorbed via electrostatic forces was recovered by using chloroform/methanol basified with TMAOH and quantified by HPLC. From the data obtained, which are shown in Figure 1, by assigning to Vulcan a surface area of 100 m^2/g (*22*), we calculated a surface density of chromene groups equal to 54 $nmol/m^2$. It is interesting to note that this value is in fair agreement with those obtained by measuring both the amount of H_2O_2 (*20*) and OH^- (*21*) liberated on suspending Vulcan in water, thus substantiating the hypothesis made on the nature of the oxygen complexes present on the GCB surface.

The peculiarity of GCB of acting as an anion exchanger as well as a nonspecific adsorbent is well illustrated in Figure

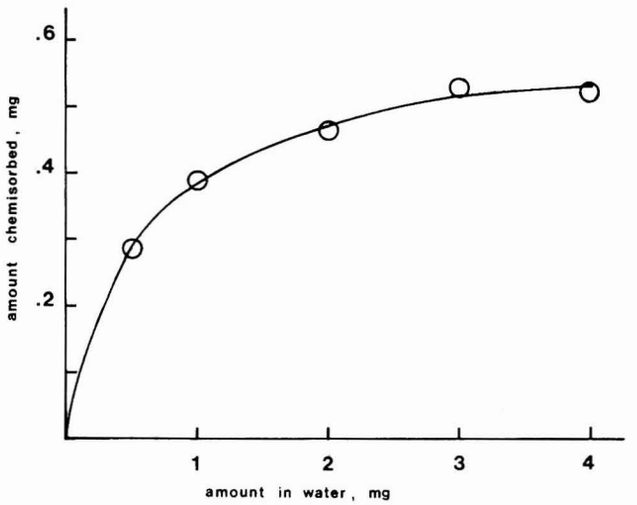

Figure 1. Plot of the amount of E_3-3-S chemisorbed on 250 mg of GCB vs. the amount of estrogen dissolved in water.

2, where the separation of some, selected steroids representative of each type of steroid both unconjugated and conjugated is shown. In this experiment, steroids were adsorbed onto the GCB surface from water. Moreover, the initial sequence of percolation of the eluants was modified with respect to that followed in practice in order to avoid the coelution of androsterone and its glucuronide.

In accordance with the behavior shown by a commonly used anion exchanger (*22*), the acidification of a suitable, organic solvent mixture caused complete desorption of the steroid glucuronides, while the more acidic sulfates and sulfoglucuronides still remained adsorbed onto the GCB surface. These compounds were effectively removed from the adsorbent by adding a basic agent to a chloroform/methanol mixture. Moreover, by properly adjusting the base concentration, the complete separation of sulfates from double conjugated steroids was achieved.

Because of the double nature of GCB, this material offers the advantage over conventional ion exchangers in that extraction of both charged and uncharged analytes from a complex matrix, their fractionation, and purification can be made with a single analytical step, provided that a careful choice of washings and eluants is done. As an example, complete separation of androsterone and its conjugates from the corresponding estrogen forms was achieved by properly selecting the composition of the eluants. This effect is due to the particular affinity that the flat surface of GCB has for the aromatic ring of estrogens, which results in lower mobility of these compounds with respect to androsterone. It is noteworthy that this selectivity is not remarkably decreased even when glucuronide or sulfate groups are attached to the steroid moiety.

The retardation of D-ring glucuronides with respect to A-ring glucuronides, which results in complete separation of E_2-3-G from E_2-16-G, is probably due to the presence of the free phenolic group in the latter compound, which is able to interact with certain active centers of the GCB surface. This hypothesis is supported by the anomalously high breakthrough volume measured for phenol when adsorbed from water on Vulcan (*23*). However, the subfractionation of estrogen glucuronides was not complete as E_1-G and E_3-16-G were partially coeluted. Increasing the column efficiency by doubling the weight of the adsorbent remarkably reduced this carryover from 15% to 4% (Figure 3). This modification should be adopted if the Carbopack cartridge is introduced in an analytical scheme involving a hydrolysis step of estrogens after group separation. In this case, especially when pregnancy urine samples are analyzed, the noncomplete subfractionation of glucuronides results in a double error, that is understimation of E_3-16-G and a fairly large overstimation of E_3-3-G, as the concentration of the former compound in pregnancy urine is much higher than that of the latter one. A correct assessment of the level of urinary E_3-3-G can be of aid in the management of some pathological disturbances of pregnancy, such as preeclampsia (*7*).

On the other hand, the increase of the column size of the adsorbent decreases the speed of analysis, as for each class of conjugation a proportionally larger volume of eluant has to be collected and eliminated by evaporation. Since the analytical scheme elaborated by us is based upon direct determination of intact conjugates, we chosed to maintain the column size of Vulcan as small as possible in order to develop a method that could be readily applied for routine use.

The effect of the flow rate at which the biological samples and the solvent systems were percolated through the Vulcan column on the recovery and class separation of steroids was evaluated by varying it from 0.5 mL/min, which is the flow rate usually employed with conventional ion exchangers, to 6 mL/min, which is the maximum flow rate possible with the

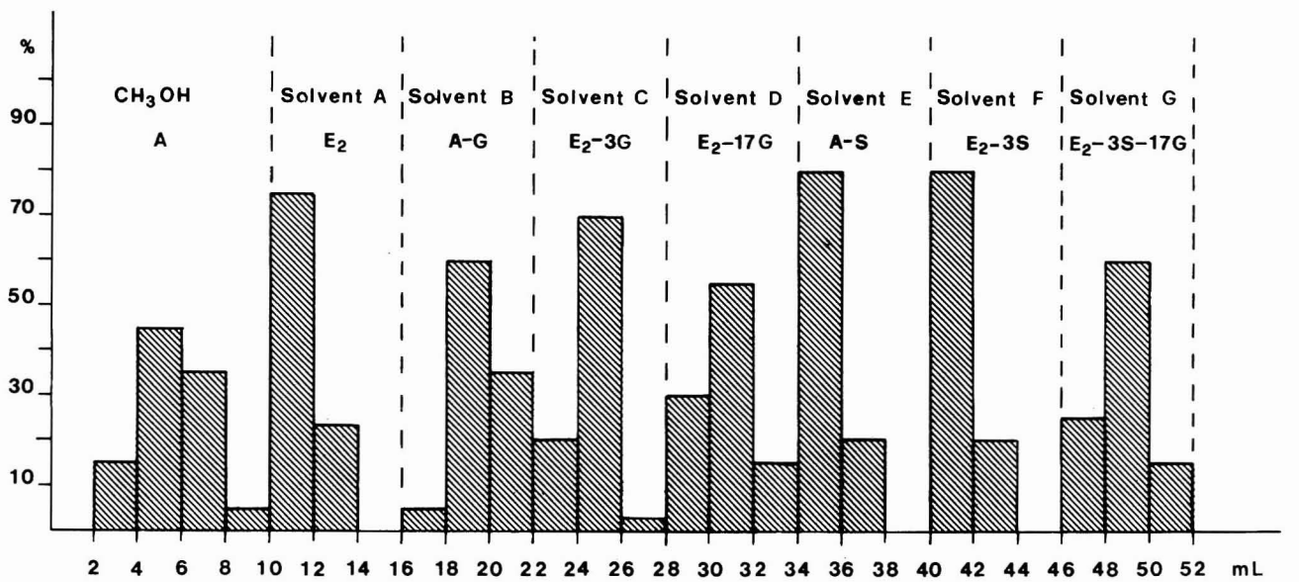

Figure 2. The group separation of some steroids and their conjugates by the Carbopack cartridge. See the Experimental Section for the abbreviations used.

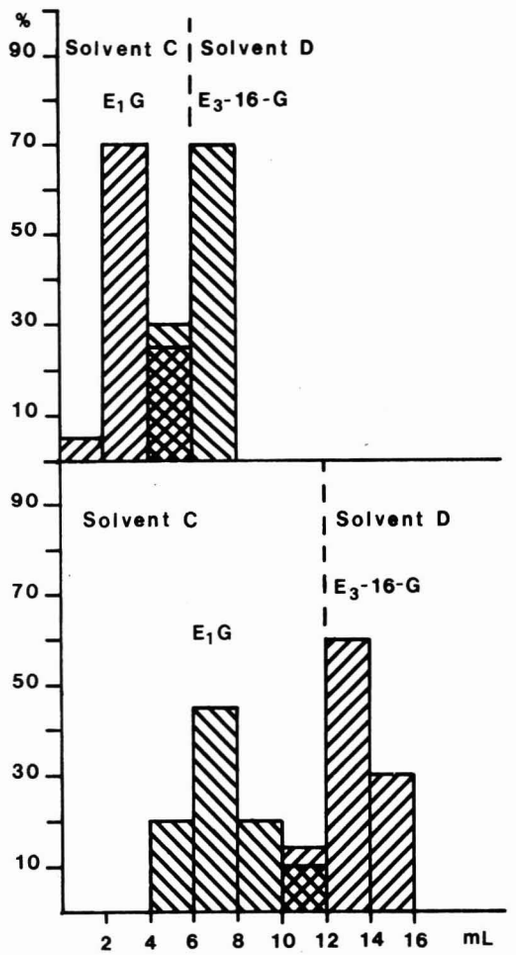

Figure 3. The rate of coelution of E_1-G and E_3-16-G by varying the amount of Vulcan filling the cartridge: upper, 250 mg; lower, 500 mg.

apparatus used. No significant variation was observed in terms of recovery and group fractionation of estrogens in the range of flow rate investigated. From a practical point of view, this means that what can be done in about 6 h by an anion exchanger (*12*) is accomplished in about 20 min by a Carbopack cartridge. At present, extremely large analysis times for measuring the conjugation profile of steroids is one of the major obstacles to the convertibility of research methodologies to routine clinical assays.

The influence of the nature and amount of the biological fluid applied to the GCB column on the recovery and group separation of steroids was assessed by processing increasing amounts of pooled pregnancy urine, serum, and amniotic fluid, respectively.

Increasing the urine volume had the effect of progressively increasing the mobility of conjugates with the result that E_3-3-G and E_2-3-G, which are the earliest eluted estrogen conjugates, are partially lost in the methanol effluent. Recoveries and group separation of the other conjugates were unaffected by passing from 1 to 4 mL of urine. Probably, the partial loss of the two glucuronides in the methanol washing can be due to partial formation of ion pairs with organic cations present in the urine, which increases their mobility. For the sake of rapidity and simplicity, no attempt was made to eliminate this effect by adopting a preliminary passage of the urine samples through a cation exchanger, as the limit of detection of the method was sufficiently low to determine estrogen conjugates present in only 1 mL of late pregnancy urine.

In experiments with serum, when the methanolic extract was directly passed through the Vulcan column, a severe carryover between A-ring and D-ring glucuronides occurred.

Table I. Optimized Chromatographic Conditions for Subfractionation and Quantification of Estrogens

class of conjugation		solvent B, % start	solvent B, % end	time, min	wavelength, nm fluorometer		wavelength, nm UV
unconjugated	U[a]						
	S[b]	38	38		282[c]	308[d]	215
A-ring glucuronides	U	20	40[e]	35	275	304	280
	S	38	38				215
D-ring glucuronides	U	20	60	40	282	308	
	S	38	38				
sulfates	U	20	50	30	275	304	280
	S	38	38				215
sulfoglucuronides	U	20	60	40	275	304	
	S	38	38				

[a] U = urine. [b] S = serum. [c] Excitation wavelength. [d] Emission wavelength. [e] To purge the column, the percentage was then increased to 60% in 5 min.

This may be explained by the fact that phospholipids, which are abundant in serum, are coextracted with steroids by methanol and partially saturate both specific and nonspecific adsorptive sites of the GCB surface. By use of a method elaborated by Andersson and Sjövall (*24*) and slightly modified by us, the isolation of steroids from phospholipids was achieved by passing the methanolic extract suitably diluted with some water through a C_{18}-substituted silica column. Under the experimental conditions used, phospholipids were almost completely blocked by the modified silica cartridge while steroids passed unretained through it and were collected directly on the Carbopack cartridge.

For amniotic fluid samples, the step mentioned above could be omitted since the relatively low amount of phospholipids usually present in amniotic fluid did not affect the group separation of steroids.

In Table I are reported chromatographic conditions that, depending upon the particular fraction injected, were optimized in terms of detectability, accuracy, and elution time. On analyzing amniotic fluid, we followed the same chromatographic conditions as those for serum.

Contrary to E_3 and E_2, E_1 and its two derivatives are about 30 times less fluorescent. To detect them, we coupled a UV detector to a fluorometer. With respect to 280 nm, estrogens possess a much higher UV adsorption at 215 nm. This effect was exploited for determining small amounts of estrone and its derivatives, as those present in pregnancy serum. At 215 nm, however, the detector was saturated because of the presence of TPABr added to the mobile phase for ion-pair HPLC. This difficulty was eliminated by replacing the bromide ion, as described in the Experiment Section, with a less UV absorbing ion, such as chloride. Nevertheless, gradient elution at 215 nm was precluded as it caused too large a base-line drift. Figure 4 shows some typical chromatograms.

For each body fluid considered, analytical recoveries were evaluated by supplementing pooled pregnancy biological specimens with known amounts of the estrogens and their conjugates and reassaying. In all cases, mean recoveries ranged between 90% and 98%.

Under the experimental conditions used, the limits of sensitivity (signal to noise ratio = 3) for all the compounds of interest were calculated and are reported in Table II.

The precision of the method and a rough assessment of the normal levels of estrogens and their conjugates present in late pregnancy body fluids were performed by pooling biological samples, respectively, from 9, 6, and 4 urines, sera and amniotic fluids of apparently healthy women in their third trimester of pregnancy. Each one of the three resulting pools

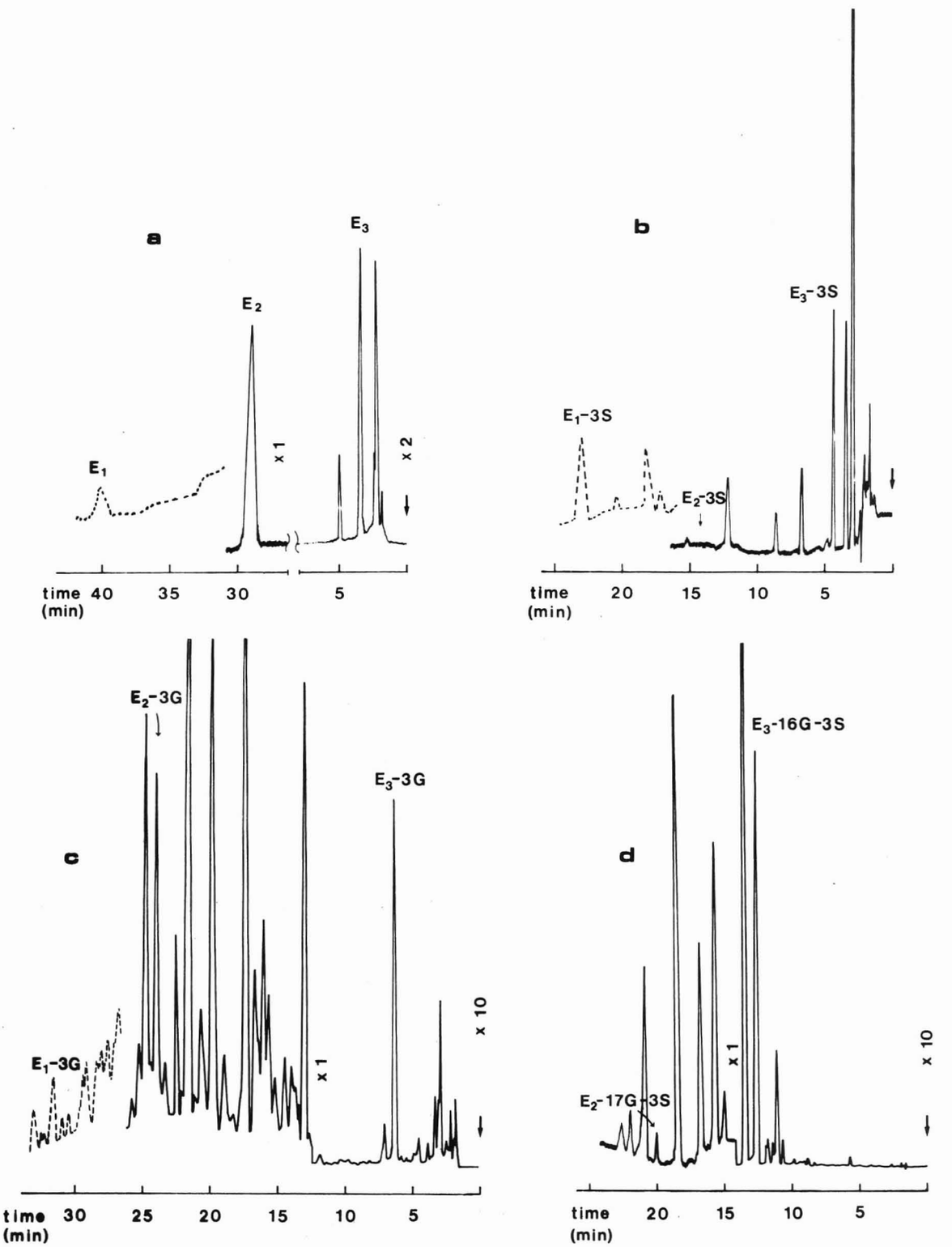

Figure 4. Some, selected chromatograms of purified specimens from pregnant women: a, unconjugated estrogens in serum; b, estrogen sulfates in amniotic fluid; c, estrogen A-ring glucuronides in urine; d, mixed conjugates in urine. Dotted line = UV signal; full line = fluorometry signal.

was divided in five aliquots and assayed. Results are shown in Table III.

As to the levels of the urinary glucuronides and sulfates, our results agree fairly well with those found by combining ion-exchange columns and capillary gas chromatography (*12*), except for E_1-G and E_1-S. Contrary to the previous finding, we observed that estrone is excreted in pregnancy urines preferentially as sulfate instead of as glucuronide. The excreted amount of E_3-3-S-16-G as measured by us is in accordance with that determined by an indirect RIA procedure (*7*). For E_2-3-S-17-G, no comparison was possible because no data are reported in the literature. With respect to the estrogen concentrations in pregnancy serum, good agreement was found between our results and those obtained by various RIA procedures concerning E_3 and its four conjugates (*25*), E_1 and E_1-S (*26*), and unconjugated E_2 (*27*). On the contrary, we measured serum concentrations of E_2-3-S and E_3-3-S-16-G, which were much lower than those monitored by two different, direct RIA procedures (*5*, *28*). Overestimations by these methods may be due to the fact that antisera insufficiently specific were used in assays that did not involve any purification step. Only very few attempts were made in the past

Table II. Limit of Sensitivity of the Method for Estrogens in Various Body Fluids

estrogen	urine, ng/24 h	serum,[a] ng/mL
E_3		0.5
E_2		1.5
E_1		3.5
E_3-3-G	6.0	2.0
E_2-3-G	4.0	1.5
E_1-G	12.0	1.0
E_3-16-G	4.0	1.0
E_2-17-G	3.5	1.5
E_3-3-S	4.0	2.0
E_2-3-S	9.5	6.0
E_1-S	25.0	4.0
E_3-S-16-G	5.5	4.0
E_2-3-S-17-G	10.0	7.0

[a] The limiting values for amniotic fluid are equal to those for serum.

Table III. Precision of the Method and the Mean Content of Estrogens in Pregnancy Urine (n = 9), Serum (n = 6), and Amniotic Fluid (n = 4)

compound	urine, mean[a] ± SD	serum, mean[b] ± SD	amniotic fluid, mean[b] ± SD
E_3		11.5 ± 0.49	15.7 ± 0.64
E_2		12.0 ± 0.53	*c*
E_1		4.4 ± 0.38	*d*
E_3-3-G	4.61 ± 0.157	47.1 ± 1.55	10.1 ± 0.48
E_2-3-G	0.166 ± 0.0109	*d*	*c*
E_1-G		1.0 ± 0.12	*d*
E_3-16-G	14.8 ± 0.38	43.7 ± 1.44	145.0 ± 3.92
E_2-17-G	0.101 ± 0.0070	*c*	*c*
E_3-3-S	1.03 ± 0.037	19.8 ± 0.77	18.7 ± 0.71
E_2-3-S	0.055 ± 0.0042	*d*	*c*
E_1-S		63.0 ± 1.97	11.1 ± 0.50
E_3-3-S-16-G	1.21 ± 0.046	41.0 ± 2.27	70.7 ± 3.65
E_2-3-S-17-G	0.019 ± 0.002	*c*	*c*

[a] mg/24 h of the free estrogen. [b] ng/mL of the free estrogen. [c] Not detected. [d] Traces.

to determine the pattern of conjugation of estrogens in amniotic liquid and all of these were limited to profiling E_3 and its metabolites. For these compounds, our data compared well with those reported elsewhere (*6*).

ACKNOWLEDGMENT

We thank E. Raponi for the synthesis of E_3-3-S-16-G, A. Pachì for useful discussions and for supplying us with amniotic fluid specimens, and G. Carfagnini for skillful assistance.

Registry No. A, 53-41-8; E_1, 53-16-7; E_2, 50-28-2; E_3, 50-27-1; A-G, 1852-43-3; A-S, 2479-86-9; E_1-G, 2479-90-5; E_1-S, 481-97-0; E_3-3-G, 2479-91-6; E_2-3-S, 481-96-9; E_2-3-G, 15270-30-1; E_2-17-G, 1806-98-0; E_3-3-S, 481-95-8; E_3-16-G, 1852-50-2; E_2-3-S-17-G, 26923-03-5; E_3-3-S-16-G, 4661-65-8.

LITERATURE CITED

(1) Unnérus, H. A. *Acta Endocrinol. (Copenhagen) Suppl.* **1979**, *91*, 226.
(2) Adessi, G. L.; Nhuan, T. Q.; Vingler, P. *J. Steroid Biochem.* **1982**, *16*, 107–116.
(3) Adlercreutz, H.; Lehtinen, T.; Tikkanen, M. *J. Steroid Biochem.* **1975**, *7*, 105–107.
(4) Stanczyk, F. Z.; Miyakawa, I.; Goebelsmann, U. *Am. J. Obstet. Gynecol.* **1980**, *137*, 443–450.
(5) Nambara, T.; Niwa, T.; Shimada, K. *Clin. Chim. Acta* **1985**, *149*, 275–280.
(6) Young, B. K.; Jirku, H.; Slyper, A. J.; Levitz, M.; Kelly, W. G.; Yaverbaum, S. *J. Clin. Endocrinol. Metab.* **1974**, *39*, 842–849.
(7) Alexander, S.; Stavric, V.; Smuk, M. *J. Clin. Endocrinol. Metab.* **1979**, *49*, 588–593.
(8) Young, B. K.; Jirku, H.; Kadner, S.; Levitz, M. *Am. J. Obstet. Gynecol.* **1976**, *126*, 38–41.
(9) Andreolini, F.; Borra, C.; Caccamo, F.; Di Corcia, A.; Samperi, R. *Clin. Chem. (Winston-Salem, N.C.)* **1985**, *31*, 1698–1702.
(10) Jäme, O.; Vikho, R.; Sjövall, J.; Sjövall, K. *Clin. Chim. Acta* **1969**, *23*, 405–411.
(11) Setchell, K. D. R.; Almé, B.; Axelson, M.; Sjövall, J. *J. Steroid. Biochem.* **1976**, *7*, 615–629.
(12) Axelson, M.; Sahlberg, B. L.; Sjövall, J. *J. Chromatogr.* **1981**, *224*, 355–370.
(13) Fotsis, T.; Adlercreutz, H.; Järvenpaa, P.; Setchell, K. D. R.; Axelson, M.; Sjövall, J. *J. Steroid Biochem.* **1981**, *14*, 457–463.
(14) Van der Wal, S. J.; Huber, J. F. K. *J. Chromatogr.* **1978**, *149*, 431–453.
(15) Shimada, K.; Kaji, M.; Xie, F.; Nambara, T. *J. Liq. Chromatogr.* **1982**, *5*, 1763–1770.
(16) Andreolini, F.; Di Corcia, A.; Laganà, A.; Samperi, R. *Clin. Chem. (Winston-Salem, N.C.)* **1983**, *29*, 2076–2078.
(17) Andreolini, F.; Borra, C.; Di Corcia, A.; Laganà, A.; Samperi, R. *Clin. Chem. (Winston-Salem, N.C.)* **1984**, *30*, 742–744.
(18) Andreolini, F.; Borra, C.; Di Corcia, A.; Raponi, G. M. *J. Chromatogr.* **1985**, *337*, 379–383.
(19) Levitz, M.; Katz, J.; Twonbly, G. H. *Steroids* **1965**, *6*, 553–559.
(20) Campanella, L.; Di Corcia, A.; Samperi, R.; Gambacorta, A. *Mater. Chem.* **1982**, *7*, 429–438.
(21) Di Corcia, A.; Samperi, R.; Sebastiani, E.; Severini, C. *Anal. Chem.* **1980**, *52*, 1345–1350.
(22) Fotsis, T.; Järvenpaa, P.; Adlercreutz, H. *J. Steroid Biochem.* **1980**, *12*, 503–510.
(23) Borra, C.; Di Corcia, A.; Marchetti, M.; Samperi, R. *Anal. Chem.* **1986**, *58*, 2048–2052.
(24) Andersson, S. H. G.; Sjövall, J. *Anal. Biochem.* **1983**, *134*, 309–312.
(25) Levitz, M.; Kadner, S.; Young, B. K. *J. Steroid Biochem.* **1984**, *20*, 971–974.
(26) Nambara, T.; Ohkubo, T.; Shimada, K. *Clin. Chim. Acta* **1982**, *119*, 81–87.
(27) Adlercreutz, H.; Tikkanen, M. J.; Hunneman, D. H. *J. Steroid Biochem.* **1974**, *5*, 211–217.
(28) Tanaka, T.; Suguro, N.; Kubodera, A. *Clin. Chem. (Winston-Salem, N.C.)* **1985**, *31*, 1846–1848.

RECEIVED for review November 10, 1986. Accepted February 11, 1987. We are grateful to the Ministero della Pubblica Istruzione for economic support of this work.

Temperature Dependence of the Electron Spin Resonance Spectra of a Coal-Derived Vacuum Distillation Residue and Components

Salvatore M. Castellano,[1] William P. Chisholm,[2] Richard F. Sprecher,* and Herbert L. Retcofsky

Division of Coal Science, Pittsburgh Energy Technology Center, Pittsburgh, Pennsylvania 15236

Measurements of the intensities of the electron spin resonance (ESR) absorptions, in the $g \sim 2$ region of the spectrum, of the title materials were performed over a wide range of temperatures. Linear correlations of the measured intensities vs. the reciprocal of the absolute temperature were obtained. The regression lines have intercepts which are larger than the standard deviations of the measurements. This study shows that the intercepts arise from systematic errors in the measurements that introduce curvature into the plots. Two converging lines of research were followed: (a) a theoretical study of the effect of systematic errors on the outcome of ESR intensity measurements; and (b) repeated sets of measurements on two major fractions of the title materials. A complete analysis of all data shows conclusively that the materials of both fractions obey the Curie law exactly and that any observed deviation from this behavior lies within the range of systematic errors predicted by the theoretical study.

Interest in the nature of the paramagnetic centers that give rise to electron spin resonance (ESR) absorptions near $g = 2$ in coal and coal-derived products continues to be strong. Because of the location of the ESR signal, it is generally thought that the unpaired spins reside on organic moieties whose precise structures are still completely unknown. Although this hypothesis remains the most plausible, one cannot exclude that some contribution to the total intensity of the rather broad and unstructured signal observed in this region of the spectrum may also arise from inorganic paramagnetic species.

In their work in this area, Retcofsky et al. (*1*, *2*) showed that there is an inverse relationship between the intensity of the ESR signal and the temperature. From this they inferred that the system of spins responsible for the ESR absorption was in a doublet ground state. This inference led to the conclusion that organic free radicals were the main source of the observed ESR absorption. Recent electron spin echo measurements provide supporting evidence that the coal radical spin multiplicity is doublet, $S = 1/2$ (*3*).

Retcofsky et al. (*1*, *2*) found excellent linear correlations between the intensities of the ESR signals and the reciprocal of the absolute temperature. This is the prerequisite condition for the validity of the Curie law. The same law requires that the correlation lines pass through the origin. This is a much more stringent requirement because, in effect, one needs to extrapolate the experimental data from a finite range of temperature to $T = \infty$ (or alternatively to $1/T = 0$). Since the great majority of experimental data pass the first test but fail the second, Retcofsky et al. (*2*) referred to them as data exhibiting "Curie law-type behavior". A mistaken interpretation of the significance of the intercepts can lead to erroneous conclusions (*4*).

The hypothesis that the paramagnetic centers of coal and coal-derived products may be located in electron donor–acceptor complexes was put forward in an early paper of Elofson and Schultz (*5*). The same hypothesis was later reproposed by Schwanger and Yen (*6*). In both cases, experimental evidence in support of the proposed hypothesis was insufficient. The idea that such charge-transfer complexes may make a major contribution to the ESR signal of coal products can be dismissed at once, since in that case the temperature dependence of the absorption intensities should show a trend considerably different from that observed experimentally (*7*). The case in which only minor contributions are expected must be dealt with in more detail.

Experimental data may be fit to a regression line of the form

$$Y = A + BX \tag{1}$$

where

$$Y = I \quad \text{...relative ESR intensity} \tag{2}$$

$$X = 1/T \quad \text{...reciprocal absolute temperature}$$

$$A \text{ and } B \quad \text{...constants}$$

If a good fit can be found, then the data satisfy the inverse linear relationship between I and T demanded by the Curie law

$$I = C/T \tag{3}$$

At low enough temperature ($\hbar\omega \gg kT$), this approximation is expected to break down. However, the lowest temperature used in this study is still far above that necessary to satisfy the requirement that $\hbar\omega$ be much less than kT (*8*).

In practice, all regression lines will have intercepts (A) at the origin. In some cases, the values of A will lie outside the range of stochastic errors. Attempts to interpret the values of those intercepts in physical terms are speculative and dangerous. A more reasonable approach is to try to find an explanation in terms of systematic errors that may affect the measurements. A large number of possible sources of systematic errors can be readily listed. This treatment assumes that only three types of systematic errors occur during the measurements. Clearly several sources may contribute to the same type of error.

EXPERIMENTAL SECTION

A Varian Associates Model E112 spectrometer equipped with a field frequency lock, a Model E102 microwave bridge, and a Model E232 dual sample cavity was used in this study. The magnetic field strength and the field scan were calibrated with peroxylaminedisulfonate (PADS) in aqueous sodium carbonate solution before every run. A g value of 2.005 50 for the PADS

[1] Present address: Instituto di Chimica Fisica, Università di Parma, Via Massimo D'Azeglio 85, 53100 Parma, Italy.

[2] Present address: US DOE-METC JO3, Collins Ferry Rd., Morgantown, WV 26507-0880.

0003-2700/87/0359-1726$01.50/0 © 1987 American Chemical Society

Table I. Temperature Dependence of the ESR Signal Intensity for the Distillation Residue and Four Components

		ESR intensity/10^{15} [a]					
T/K	$(1/T)/10^{-3}$ K^{-1}	run 1	run 2	run 3	run 4	run 5	average
325.5	3.075				3114 (48)	923 (14)	
300.2	3.332	1387 (18)	4422 (33)	92 (6)	3380 (34)	1009 (23)	1683
275.2	3.634	1508 (20)	4817 (56)	37 (4)	3762 (25)	1117 (16)	1869
248.7	4.022	1660 (26)	5198 (79)	26(4)	4268 (34)	1231 (14)	2084
225.2	4.441	1857 (14)	5561 (31)	27 (4)	4775 (50)	1373 (19)	2310
202.2	4.947	2091 (31)	6131 (49)	34 (4)	5411 (63)	1540 (19)	2601
179.7	5.566	2431 (28)	6844 (34)	33(6)	6212 (64)	1770 (32)	2969
164.7	6.073	2710 (29)	7689 (95)				*b*
$A/10^{15}$		−260.3	583.8	42	−767.3	−114.0	−208.4
$B/10^{18}$ K		483.1	1142.4		1250.8	336.4	571.2
r^2		0.9960	0.9918		0.9997	0.9992	*c*

[a] Parentheses indicate standard deviation of a group of five consecutive measurements. [b] Calculated as weight-average of Runs 2, 3, 4, and 5. [c] Calculated as weight-average of the parameters of Runs 2, 3, 4, and 5.

Table II. Temperature Dependence of the ESR Signal Intensity for the Acid Fraction, the Base Fraction, and Mixtures of the Two Fractions

		ESR intensity/10^{15} [a]				
T/K	$(1/T)/10^{-3}$ K^{-1}	run 6	run 7	run 8	run 9	average[b]
310.7	3.218	4297 (34)	1244 (16)	2362 (26)	1068 (23)	2632.9
282.4	3.542	4771 (82)	1346 (20)	2601 (55)	1112 (12)	2904.6
253.6	3.943	5270 (87)	1501 (25)	2924 (27)	1202 (11)	3216.0
225.5	4.435	5902 (54)	1674 (26)	3359 (67)	1326 (14)	3597.9
197.2	5.072	6623 (86)	1893 (15)	3720 (59)	1495 (23)	4045.1
179.9	5.558	7300 (67)		4025 (81)	1634 (14)	
168.5	5.935	7711 (82)	2176 (40)	4341 (54)	1738 (20)	4694.8
149.3	6.697	8479 (97)	2424 (55)	4797 (48)	1947 (18)	5179.0
137.0	7.301	9331 (109)	2704 (61)	5188 (48)	2108 (31)	5718.0
d		15324 (304)	4507 (57)			
$A/10^{15}$		476.6	114.0	200.4	188.0	279.3[c]
$B/10^{18}$ K		1211.6	350.0	689.5	261.2	742.0[c]
r_2		0.9988	0.9985	0.9973	0.9974	

[a] Parentheses indicate standard deviation of group of five consecutive measurements. [b] Calculated as weight-average of runs 6 and 7. [c] Calculated as weight-average of the parameters of runs 6 and 7. [d] Probe with liquid N_2 Dewar. Data are not included in the correlations.

was assumed for the field calibration, and the hyperfine splitting was taken to be 1.3 mT for the scan calibration. The microwave frequency was measured with an EiP Model 350D high-frequency counter. The signal from a sample of diphenylpicrylhydrazyl (DPPH) was used as an intensity reference and to check the field stability during experiments. No significant drift of the field was noted during any of the measurements. Before every series of measurements, the integrated intensity of the reference signal was calibrated against the integrated intensity of the signal from a standard sample of DPPH in silica, which contained 6.31×10^{-6} mol of DPPH/g of silica. The reference sample was shielded by a Dewar insert and maintained at 20 °C by a steady flow of nitrogen gas. Microwave power incident on the sample was never greater than 0.5 mW. All samples were contained in 4 mm diameter quartz tubes and were evacuated and sealed.

The ESR spectra were measured and the data were reduced with a Nicolet Model 1180 data system and programs developed in this laboratory. Intensities are reported for 1 g of sample relative to a hypothetical standard that would contain one unpaired electron per gram of standard and would be maintained at 20 °C.

Altogether 11 sets of ESR measurements (runs 1 through 11) were made in the course of this study. They are reported in Tables I, II, and III. The sample was produced from an Illinois No. 6 coal at the Catlettsburg, KY, H-coal Pilot Plant while operating in the synfuel mode (*9*). A blend of "light" and "heavy" oil products (1:1.5) was distilled by Chevron into narrow-boiling range samples. The start–400 °F distillate and the 850 °F+ vacuum still bottoms were also obtained.

The bottoms fraction was separated into an acid fraction (29.2% yield), a base fraction (30.6% yield), an aromatic fraction (32.3% yield), and an insoluble fraction (7.9% yield) by a published procedure (*10*). All ESR samples were prepared from stock materials generated by one separation.

Runs 1 and 5 were made with ESR samples left over from a previous exploratory study. Unfortunately, an attempt to extend the upper end of the range of temperatures under study caused the melting of the materials in the ESR tubes, thus preventing their use for further intensity measurements. When an analysis of the early results suggested the need for new measurements (runs 6 through 11) to further probe some interpretative hypothesis, new samples had to be prepared from the original stock materials. Since the available amounts of the latter were rather limited, the material of several samples had to be used, after a given run was over, for the preparation of other samples. The following list establishes the relationship between the entries of Tables I, II, and III, and the materials to which they refer: run 1, H-coal bottoms (first sample from stock); run 2, insolubles (first sample from stock); run 3, aromatics (first sample from stock); run 4, bases (first sample from stock); run 5, acids (first sample from stock); run 6, bases (second sample from stock); run 7, acids (second sample from stock); run 8, mechanical mixture of bases (45.9%) and acids (54.1%) (prepared from samples 6 and 7); run 9, reprecipitated mixtures of bases (45.9%) and acids (54.1%) (prepared from sample 8); run 10, bases (third sample from stock); run 11, reprecipitated bases (prepared from sample 10).

The mechanical mixture of the bases and acids fractions was prepared by mixing the two fractions in a mortar and using the pestle to establish intimate contact between the two materials. For the reprecipitated samples, CH_2Cl_2 solutions were allowed to stand under nitrogen atmosphere for several hours. Afterward, the evaporation of the solvent, and the drying of the materials were carried out in a vacuum line. All operations were executed with weight losses amounting to only a few percent of the ma-

Table III. Effect of Reprecipitation of the Base Fraction on the Temperature Dependence of the ESR Signal Intensity

		ESR intensity/10^{15}	
T/K	$(1/T)/10^{-3}$ K^{-1}	run 10	run 11
310.7	3.218	4412 (73)	2068 (43)
282.4	3.542	4859 (51)	2205 (41)
253.6	3.943	5451 (92)	2446 (12)
225.5	4.435	6129 (88)	2759 (35)
197.2	5.072	7071 (116)	3112 (32)
179.9	5.558	7743 (138)	3373 (46)
168.5	5.935	8321 (120)	3663 (66)
149.3	6.697	9391 (99)	4085 (62)
137.0	7.301	10019 (120)	4488 (69)
$A/10^{15}$		-71.8	111.5
$B/10^{18}$ K		1401.3	595.0
r^2		0.9989	0.9989

terials.

The lower scale of the temperature control unit was calibrated twice. The first time, a digital thermometer was used. The second calibration was made later on, between runs 5 and 6, when the control unit malfunctioned and had to be repaired. After repairs, both a digital thermometer and a thermocouple (copper–constantan) were used. A comparison of the earlier and later calibrations indicated that changes had occurred during repair. The older calibration was therefore used only for the readings of runs 1 through 5. The comparison between the calibrations made with the digital thermometer and the thermocouple showed only minor differences. Since it was thought that the calibration obtained by the use of the thermocouple and a Fluke Model 893A differential voltmeter was the more reliable, the latter calibration was used for all other runs.

Tabulating of the Data, Correlations, and Errors. Each entry of Table I represents the average of at least five consecutive measurements. Seven to ten measurements were used for the entries of Tables II and III. The numbers in parentheses give the corresponding standard deviations. Considering that each computer output (measurement) represents, by itself, the average result over three scans of the resonance signal, it is safe to assume that the average value of the observed relative standard deviations (σ_{av} = 2–3%) gives a good measure of the stability of the instrument and of the reproducibility of the results, for given instrumental calibrations and settings. According to this criterion, the data of run 3 are the least precise. This and the fact that the recorded values are at the threshold of the sensitivity of the instrument make that set of data less reliable. The data of all other runs were fitted with regression lines of the form of eq 1. The coefficients A and B are given at the bottom of each column in Tables I, II, and III, as is the coefficient of determination (r^2).

RESULTS

The systematic error ΔT surely occurs in the measurements of the temperature. Its sources may be the erroneous calibration of the dial of the temperature control unit, the shifts in the scale of the same unit, the failure to reach thermal equilibrium at the sample, and the changes in the calibration of the temperature scale caused by variations in the gas flow and microwave power.

For computing the ESR intensity, the computer utilizes experimental information provided by the operator of the spectrometer, including the weight and the length of the sample, and some instrumental parameters. If any piece of information is incorrect, the constant C appearing in the Curie law will be affected by a systematic error, ΔC.

The effect of ΔT and ΔC on the measurement of I can be obtained immediately from the Curie law, assuming T and C to be independent variables. It is convenient to rewrite eq 3 in a new notation

$$I^* = C/T^* \tag{4}$$

where T^* is the true temperature of the sample and I^* is the ESR intensity demanded by the Curie law. We define now

$$\Delta T = T - T^* \tag{5}$$

$$\delta I = I_0 - I^* \tag{6}$$

In eq 5, T is the temperature at which one assumes the experiment is being performed; I_0 is the ESR intensity that is expected from measurements affected solely by the errors ΔT and ΔC. By differentiation of eq 4, one obtains

$$\delta I^* = I^*\left(-\frac{\Delta T}{T^*} + \frac{\Delta C}{C}\right) \tag{7}$$

Combining eq 6 and 7 yields

$$I_0 = I^* + \delta I = \frac{C}{T^*}\left(1 - \frac{\Delta T}{T^*} + \frac{\Delta C}{C}\right)$$

Equation 8 is not convenient for current use, since in general T^* is unknown. However, by the use of eq 5, followed by series expansion, one obtains

$$I_0 = \frac{C}{T}\left[1 - \left(\frac{\Delta T}{T}\right)^2 - 2\left(\frac{\Delta T}{T}\right)^3 - 3\left(\frac{\Delta T}{T}\right)^4 - \dots\right] + \frac{\Delta C}{T}\left[1 + \left(\frac{\Delta T}{T}\right) + \left(\frac{\Delta T}{T}\right)^2 + \left(\frac{\Delta T}{T}\right)^3 + \left(\frac{\Delta T}{T}\right)^4 + \dots\right] \tag{9}$$

Keeping only terms up to the second order in the errors yields

$$I_0 = \frac{C}{T} + \frac{\Delta C}{T} + \frac{\Delta C \Delta T}{T^2} - \frac{C(\Delta T)^2}{T^3} \tag{10}$$

The interesting feature of eq 10 is the presence of quadratic terms. The magnitudes of these terms are relatively small and so is the local curvature that they introduce in the plots of I_0 vs. I/T. The local curvature is surely smoothed out by the stochastic errors that are always present in the measurements, and it generally goes undetected. This is evidenced by the excellence of the linear correlations that one obtains. The integral effect of the curvature, however, remains and manifests itself in correlation lines that do not pass through the origin.

A third independent systematic error ΔI may also affect the measurement of the intensities. Its origin lies both in the heterogeneous nature of the samples studied and in the numerical algorithms and computational procedures needed to integrate the raw signal (derivative of the absorption peak) obtained from the spectrometer.

Adding ΔI to I_0 in eq 10, we obtain

$$I = I_0 + \Delta I = \Delta I + \frac{C}{T} + \frac{\Delta C}{T} + \frac{\Delta C \Delta T}{T^2} - \frac{C(\Delta T)^2}{T^3} \tag{11}$$

and remembering $X = 1/T$

$$I = \Delta I + (C + \Delta C)X + \Delta C \Delta T X^2 - C(\Delta T)^2 X^3 \tag{12}$$

This equation seems to be a formal extension of eq 1, suited for the polynomial fitting of the experimental data. This, however, is not the case. First, ΔI and ΔT are assumed to be functions of the temperature, and therefore of X, and cannot be treated as constants. Second, there is no need for new correlative expressions to fit the data; eq 1 does that exceedingly well. The reason for developing eq 12 is to find the physical meaning of the parameters A and B obtained from the experimental data through the use of eq 1.

To achieve this goal, we first need to find the derivative of I with respect to X. We introduce the simplified notation

$$\frac{d\Delta I}{dT} = \dot{\Delta} I \quad \text{and} \quad \frac{d\Delta T}{dT} = \dot{\Delta} T \tag{13}$$

After tedious algebraic manipulations, we obtain

$$\frac{dI}{dX} = [C + \Delta C(1 - \dot{\Delta}T)] - \frac{\dot{\Delta}I}{X^2} + 2\Delta T(\Delta C + C\dot{\Delta}T)X - 3C(\Delta T)^2X^2 \quad (14)$$

Assume now that a set of measurements are carried out at different temperatures (constituting a run) using the same sample, the same equipment, and of course the same initial instrumental calibration and computer input information. The relationship between the measured intensities (I) and the reciprocal absolute temperature (X) will be that given by eq 12. However, with the measurements of our run, we will cover only a limited portion of the curve described by eq 12. If T_1 and T_2 are called the highest and the lowest temperatures of the experiments, all experimental points will cover the interval X_1, X_2, ($X_1 < X_2$). The middle point of this

$$\mathbf{X} = \frac{1}{2}(X_1 + X_2) = \frac{1}{2}\frac{T_1 + T_2}{T_1T_2} \quad (15)$$

and the corresponding intensity from eq 12 is

$$\mathbf{I} = \Delta\mathbf{I} + (C + \Delta C)\mathbf{X} + \Delta C\Delta\mathbf{T}\mathbf{X}^2 - C(\Delta\mathbf{T})^2\mathbf{X}^3 \quad (16)$$

In eq 16, and in successive formulas, a boldface variable indicates a value calculated at **X**.

If the least-squares algorithm is now used to fit the data with eq 1, the slope of the correlation line will be equal to the slope of the tangent line of eq 12 at **X**

$$B = (\mathbf{dI/dX}) \text{ v } [C + \Delta C(1 - \dot{\Delta}\mathbf{T})] - \dot{\Delta}\mathbf{I}/\mathbf{X}^2 + 2\Delta\mathbf{T}(\Delta C + C\dot{\Delta}\mathbf{T})X - 3C(\Delta\mathbf{T})^2\mathbf{X}^2 \quad (17)$$

Since the correlation line with slope B passes through the point (**X**, **I**), or nearby, its intercept A at the origin will be

$$A = \mathbf{I} - B\mathbf{X} = \Delta\mathbf{I} + \dot{\Delta}\mathbf{I}/\mathbf{X} + \Delta C\dot{\Delta}\mathbf{T}\mathbf{X} - \Delta\mathbf{T}(\Delta C + 2C\dot{\Delta}\mathbf{T})\mathbf{X}^2 + 2C(\Delta\mathbf{T})^2\mathbf{X}^3 \quad (18)$$

Equations 17 and 18 give the sought-for relationships between the constants of eq 1 and the error parameters and their gradients.

Error Estimates. It is worthwhile to analyze these equations and eq 12 and 16 with the aid of some rough estimates of the various terms. Of course, no estimates of $\Delta\mathbf{I}$ and $\dot{\Delta}\mathbf{I}$ can be given, since the values of these terms may include contributions from materials that do not follow the Curie law. Computational errors, which are impossible to predict, also contribute to these terms.

For these experiments, a reasonable choice of representative parameters for the calculation of all other terms appearing in eq 16, 17, and 18 is

$$\mathbf{X} = 5 \times 10^{-3}\ \mathrm{K}^{-1} \quad (19)$$

$$C = 1.4 \times 10^{21}\ \mathrm{K}$$

$$\Delta C = 2.0 \times 10^{20}\ \mathrm{K}$$

$$\Delta\mathbf{T} = 5\ \mathrm{K}$$

$$\dot{\Delta}\mathbf{T} = 5 \times 10^{-2}$$

The first three values were chosen on the basis of a comparison between run 10 and runs 4 and 6; the last two values were chosen on the basis of an educated guess. Through eq 19, we obtain

a. $\Delta C\mathbf{X} = 1.0 \times 10^{18}$

b. $\Delta C\dot{\Delta}\mathbf{T}\mathbf{X} = 5.0 \times 10^{16}$

c. $\Delta C\Delta\mathbf{T}\mathbf{X}^2 = 2.5 \times 10^{16}$

d. $C\Delta\mathbf{T}\dot{\Delta}\mathbf{T}\mathbf{X}^2 = 8.8 \times 10^{15}$

e. $C(\Delta\mathbf{T})^2\mathbf{X}^3 = 4.4 \times 10^{15}$

f. $\Delta C\dot{\Delta}\mathbf{T} = 1.0 \times 10^{19}$ K

g. $C\Delta\mathbf{T}\dot{\Delta}\mathbf{T}\mathbf{X} = 1.8 \times 10^{18}$ K

h. $\Delta C\Delta\mathbf{T}\mathbf{X} = 5.0 \times 10^{18}$ K

i. $C(\Delta\mathbf{T})^2\mathbf{X}^2 = 9.0 \times 10^{17}$ K

Considering first eq 16, the proper corrective terms are 20.a, 20.c, and 20.e. By far the largest error in the intensity measurements is provided by 20.a; its contribution may have either sign. This term, however, does not introduce "apparent" deviation from the Curie law, since the proportionality between I and $1/T$ remains unaltered.

The higher order terms 20.c and 20.e introduce curvature in the plots of I versus $1/T$. The contribution of 20.e is always negative. The contribution of 20.c may have either sign, depending on the relative signs of ΔC and ΔT. However, even in the case in which the two terms are additive, their total effect

$$-20.c - 20.e = -29 \times 10^{15} \quad (21)$$

is of the same order of magnitude as σ_{av}. It follows that the curvature of the plots is contained in the noise background owing to random errors.

Other larger contributions to the errors of intensity measurements arise from the $\Delta\mathbf{I}$ term. However, barring unexpected large variations of $\dot{\Delta}\mathbf{I}$ with X, the contributions of the latter terms are, at most, linear in X, so that the use of eq 1 for correlative purposes remains fully justified.

Examination of eq 14, 15, and 17 shows that the sources of error in the determination of B are ΔC, 20.f, 20.g, 20.h, and 20.i. Again, and by far, the largest contribution is that of ΔC. Taking into account the numerical coefficients accompanying each of the other terms in the above equations, one notices that the contributions of 20.f and 20.h and those of 20.g and 20.i are roughly equal in magnitude. The total contribution of the four terms will depend on the actual signs of ΔC, $\Delta\mathbf{T}$, and $\dot{\Delta}\mathbf{T}$. Nothing can be said about the sign of ΔC; however, for experiments carried out below room temperature, it is most likely that $\Delta\mathbf{T}$ is negative and $\dot{\Delta}\mathbf{T}$ is positive. Heat leakage and microwave heating of the sample tend to bring the sample to a temperature higher than that indicated by the control unit dial ($\Delta\mathbf{T} < 0$). The magnitude of this effect should grow larger at lower experimental temperatures ($\dot{\Delta}\mathbf{T} > 0$). With this assumption, the total contribution of 20.f, 20.g, 20.h, and 20.i to the error in B becomes

$$\Delta C > 0: \quad -f - 2g - 2h - 3i = 2.6 \times 10^{19}\ \mathrm{K} \quad (22)$$

$$\Delta C = 0: \quad -2g - 3i = -6.3 \times 10^{18}\ \mathrm{K}$$

$$\Delta C < 0: \quad f - 2g + 2h - 3i = 1.5 \times 10^{19}\ \mathrm{K}$$

Note that always when $\Delta C \neq 0$, the quadratic terms tend to reduce the error produced by the linear term. The correlation parameter B is not affected by $\Delta\mathbf{I}$ directly, but only by its gradient $\dot{\Delta}\mathbf{I}$, which in general cannot have large values. All the above considerations lead to the conclusion that the errors incurred in the experimental determination of C are, in general, smaller than those affecting the measurements of the intensities.

Proceeding with the analysis of eq 18 while keeping the same assumptions about the signs of $\Delta\mathbf{T}$ and $\dot{\Delta}\mathbf{T}$ in the above paragraph, one finds that the total contribution of the terms 20.b, 20.c, 20.d, and 20.e amounts to

Table IV. Comparison of Replicate Determinations of Slopes and Intercepts for Acid and Base Fractions

run	$A/10^{15}$	$B/10^{18}$ K
5	−114.0	336.4
7	114.0	350.0
av	0.0	343.2
4	−767.3	1250.8
6	476.6	1211.6
10	−71.8	1401.3
av	−120.8	1287.9

$$\Delta C > 0: \quad b + c - 2d + 2e = 6.6 \times 10^{16} \qquad (23)$$

$$\Delta C = 0: \quad -2d + 2e = -8.8 \times 10^{15}$$

$$\Delta C < 0: \quad -b - c - 2d + 2e = -8.4 \times 10^{16}$$

First notice that even in the unlikely instance that $\Delta\mathbf{I} = \dot{\Delta}\mathbf{I} = 0$, an intercept will always occur at the origin, even when $\Delta C = 0$. This is due to the higher order terms in eq 13, which introduce a curvature in the I vs. $1/T$ plots. Even though locally undetectable, it is nevertheless the effect of this curvature that bars the correlation lines from passing through the origin. The signs of the intercepts (eq 3) are those expected on the basis of physical intuition.

Next, observe that by far the largest contribution to A comes from the first-order term $\Delta\mathbf{I}$. All things considered, one soon realizes that the A coefficient plays the role of a sink for the cumulative effects of all systematic errors in the measurements. Although it is true that evidence for the possible presence of paramagnetic species that do not obey the Curie law may be hidden within the data, it is unreasonable to attempt the extraction of this kind of information from the value of A without independent experimental evidence.

DISCUSSION

The general conclusions drawn from the above theoretical error analyses are confirmed by the data reported in Tables I, II, and III. Of course, one should not expect numerical agreement between the estimates in eq 21, 22, and 23 and those calculated from the experimental data, but simply the verification of predicted trends.

Runs 5 and 7 and runs 4, 6, and 10 provide the results of the sets of replicate independent measurements on different samples of the same materials: the acids fraction in the case of the first set; the bases fraction in the case of the second set. To our knowledge, no such comparison of experimental data has ever been presented in reported ESR studies of coal and/or of coal-derived materials.

Notice, in Table IV, runs 5 and 7, that the value of A is negative in one case and positive in the other. This indicates very clearly that the $\Delta\mathbf{I}$ term entering eq 18, whatever its actual values for the two runs may be, cannot contain contributions that are due to the presence of spurious paramagnetic species. Actually one can see that the values of $\Delta\mathbf{T}$ must be small in either case. If, in fact, the true value of C is about the same as the average value of B, then ΔC must be negative for run 5 and positive for run 7. Since the signs for A for the two cases agree with those predicted by eq 23 for the contributions of the second-order terms to eq 19, it follows that $\Delta\mathbf{I}$ contributions cannot be much larger than the latter.

We see that for runs 4, 6, and 10 (Table IV), the signs of A alternate, thus proving beyond reasonable doubt that no spurious paramagnetic substances are present in the base fractions. The large values of A obtained for two of the runs in this set of measurements indicate that the $\Delta\mathbf{I}$ contributions in these cases must be rather large. This is at odds with the findings from the previous set. However, if one considers that the ESR intensities of the base fraction are 3 to 4 times larger than those of the acid fractions, it should not be surprising to discover that the additive contributions of integration and/or of computational systematic errors of the two sets are also of the same relative size.

The average values of B in Table IV represent the best experimental estimates of the Curie constant C for the acid and base fractions. An independent check of these values can be made through the intensity measurements reported in Table II, runs 6 and 7, which were obtained by using a special probe whereby the samples could be kept in a Dewar jacket filled with liquid nitrogen. The results of these measurements were never used in the correlations of other data. From eq 1 and the average B values in Table IV, the temperatures of the samples corresponding to the above intensities are 76.3 K for acids and 84.4 K for the bases. Because the boiling point of liquid nitrogen is 77.4 K, the results for the bases are more in line with expectation. In any case, this independent test of the results confirms that the materials of both fractions obey the Curie law as closely as it is possible to verify experimentally. The values of C given in Table IV are believed to be within ±7% of the true values.

The mechanical mixtures and reprecipitated samples were prepared in an attempt to unravel the sources of the ESR signal in a coal-derived fuel. As can be seen by comparison of run 9 with run 8 and the weight average of runs 6 and 7 (see Table II), mechanical handling of the sample produced small systematic differences in the radical content of the sample. As shown by the data from run 9 (see Table II), reprecipitation from methylene chloride produced gross changes in the sample. Table III shows further evidence for gross changes on reprecipitation of a single fraction. The conclusion that the free radicals in these samples were altered by handling and solvent exposure is inescapable.

The extent to which the nature of the radicals in the sample was altered during the separation procedure is not known with certainty. The weight averages in Table I show that the changes are small relative to the changes produced by methylene chloride and documented in Table III. Nonetheless, differences are detectable and suggest that further investigation may be worthwhile. The smaller value of the Curie law constant for the original sample as compared to the weight average of the separated fractions indicates that some free radicals were produced by the separation process, perhaps by dissociation of compounds present in the original sample or by oxidation of the sample during handling.

This study shows that the intercepts in plots of I vs. $1/T$ arise from systematic errors in the measurements that introduce curvature into the plots. The effects of the curvature over the experimentally accessible range of temperatures are hidden by the stochastic errors in the measurements, so that excellent linear fits of the data are always possible. It is the integral effects of the curvature that are responsible for the nonzero intercepts at the origins of the plots.

LITERATURE CITED

(1) Retcofsky, H. L.; Thompson, G. P.; Hough, M.; Friedel, R. A. *ACS Symp. Ser.* **1978**, *No. 71*, 142.
(2) Retcofsky, H. L.; Hough, M. R.; Maguire, M. M.; Clarkson, R. B. *Adv. Chem. Ser.* **1981**, *No. 192*.
(3) Doetschman, D. C.; Mustafi, D. *Fuel* **1986**, *62*, 684.
(4) Duber, S.; Wieckowski, A. B. *Fuel* **1984**, *63*, 1474.
(5) Elofson, R. M.; Schulz, K. F. *Prepr. Pap.—Am. Chem. Soc., Div. Fuel Chem.* **1967**, *11*, 513.
(6) Schwanger, I.; Yen, T. F. *Prepr. Pap.—Am. Chem. Soc., Div. Fuel Chem.* **1976**, *24*, 199.
(7) Bijl, D.; Kaimer, H.; Rose-Innes, A. C. *J. Chem. Phys.* **1959**, *30*, 765.

(8) Poole, C. P., Jr. *Electron Spin Resonance, a Comprehensive Treatise on Experimental Techniques*; Wiley-Interscience: New York, 1983; p 410.
(9) Sullivan, R. F. "Refining and Upgrading of Synfuels from Coal and Oil Shales of Advanced Catalytic Processes"; Monthly Report for Feb 1983; U.S. DOE Contract No. DE-AC22-76ET10532.
(10) Schiller, J. E.; Mathiason, D. R. *Anal. Chem.* **1977**, *49*, 1225–1228.

RECEIVED for review August 25, 1986. Accepted Novemeber 3, 1986. Reference to brand names is to facilitate understanding and is not meant to imply endorsement by the U.S. Department of Energy. S.M.C. acknowledges support from the faculty research program administered by Oak Ridge Associated Universities for the U.S. Department of Energy. W.P.C. acknowledges support from the USDOE postgraduate research training program administered by Oak Ridge Associated Universities for the U.S. Department of Energy.

CORRESPONDENCE

Enantioselective Binding of 2,2,2-Trifluoro-1-(9-anthryl)ethanol on a Chiral Stationary Phase: A Theoretical Study

Sir: During the past 15 years a large variety of chiral stationary phases have appeared in the literature (*1*). To better understand how chiral stationary phases interact with optical analytes, we have initiated a computational approach aimed at enlightening our views of the mechanism by which chiral surfaces enantioselectively bind optical isomers.

The objective of our work is to provide a computational protocol for analysis of optical analytes on chiral stationary phases used in chromatography. We employ molecular orbital theory, molecular mechanics, and computer graphics as our tools. In this communication we report our preliminary results concerning the mode of binding of 2,2,2-trifluoro-1-(9-anthryl)ethanol, **2**, to the commercially available CSP, **1**. This is a particularly well-studied system for which there exists a chiral recognition model (*2*).

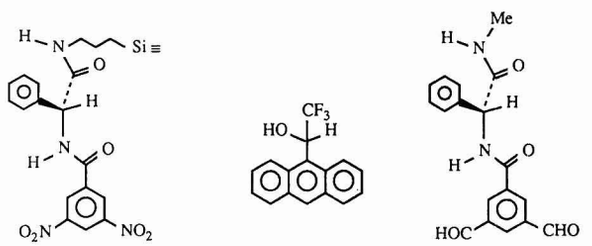

1 2 3

We introduce here new methodology and software needed in separation science to understand, from first principles, how analytes interact with organic stationary phases. We conclude with an alternative chiral recognition model to one which currently exists.

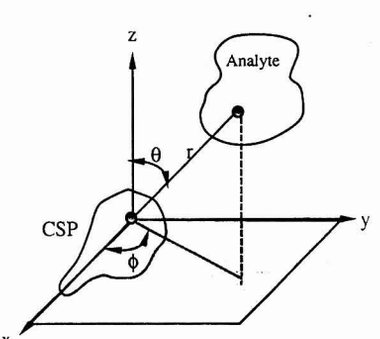

Figure 1. Position of analyte with respect to the chiral stationary phase represented by spherical coordinates (r, θ, ϕ).

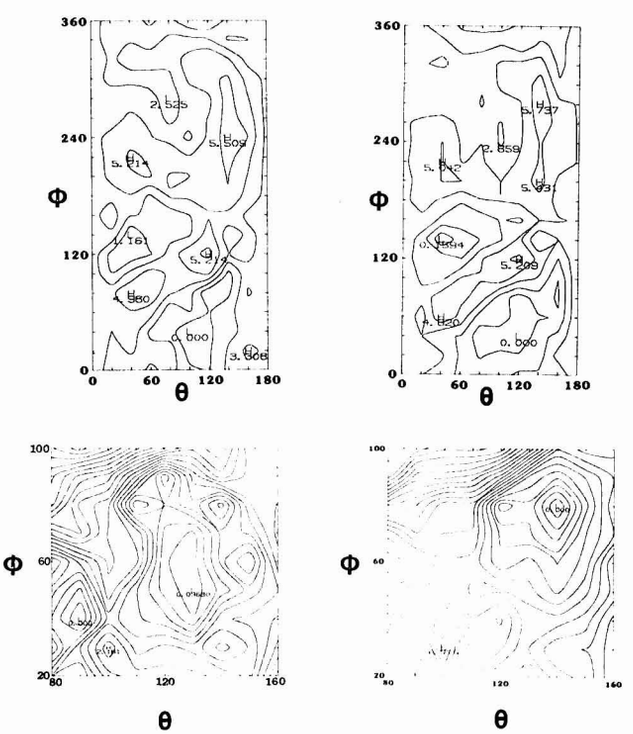

Figure 2. Intermolecular energy (kcal mol^{-1}) for *RR* and *RS* diastereomeric complexes: top left, *RR*; top right, *RS*. Contour lines are spaced every 1.0 kcal mol^{-1}. H = high point, L = low point. Global minima are artificially set = zero. The top contours were constructed from 190 grid points with 816 unique orientations at each grid point (155 040 total samples). Bottom left shows expansion of the minimum energy region from the *RR* plot directly above it. Contours are spaced every 0.25 kcal mol^{-1}. The surface was created from 81 grid points with 3465 unique orientations at each grid point (280 665 total orientations). Bottom right shows expansion of the minimum energy region from the *RS* plot directly above it. Contours are spaced every 0.25 kcal mol^{-1}. Definitions of spherical coordinates θ and ϕ are in the text.

EXPERIMENTAL SECTION

Our approach first involves a conformational analysis of the stationary phase. If the phase is to act as a template with which analyte is to bind, one must know what forms are energetically allowed and which are forbidden. This has already been accomplished by using empirical force field and semiempirical molecular orbital techniques (*3–5*). Next we select the most stable form of the phase and of the analyte to compute the structure and the

0003-2700/87/0359-1731$01.50/0 © 1987 American Chemical Society

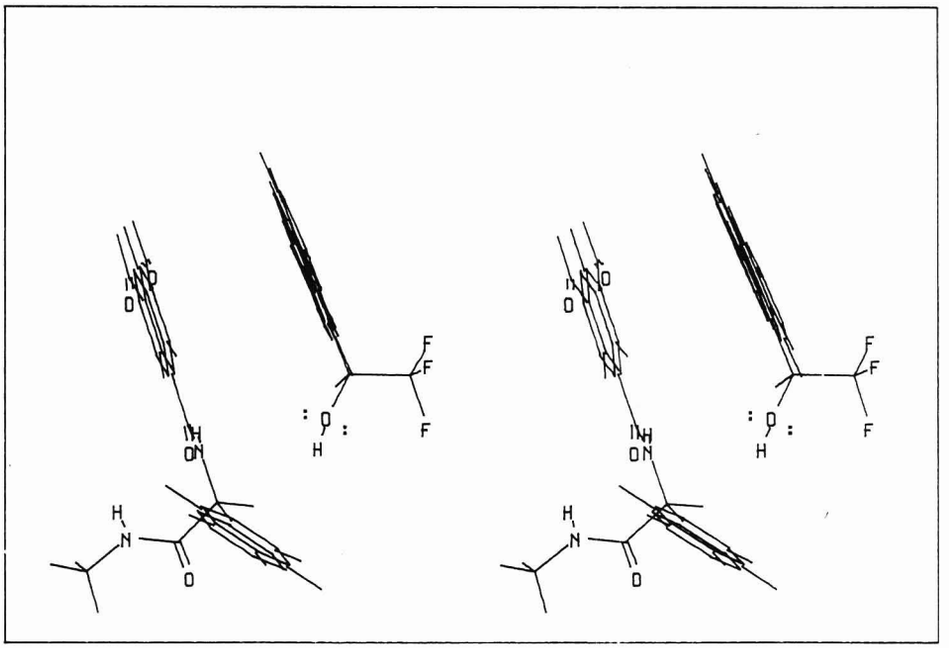

Figure 3. Stereoview of the lowest energy *RR* structure.

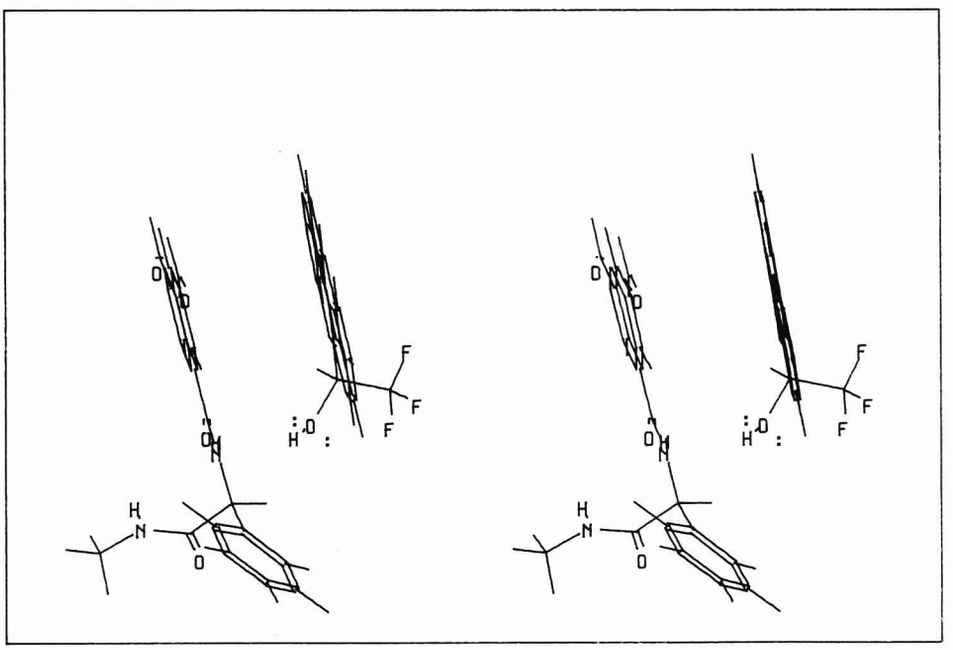

Figure 4. Stereoview of the lowest energy *RS* structure.

energies of the diastereomeric complexes. Details of our computational procedure will be reported in a full paper; here we outline the methodology.

The position of analyte with respect to CSP is represented in a spherical coordinate system (r, θ, ϕ). We select an origin and three orthogonal axes on the CSP. We then select an origin and a set of axes on the analyte in a way that allows us to systematically sample all orientations of the analyte with respect to the CSP. The distance, r, between origins and the latitude θ and the longitude ϕ between origins precisely defines where analyte is with respect to the CSP (Figure 1).

Now consider a rod eminating from the origin of the CSP at a fixed latitude θ and longitude ϕ. We allow the analyte to slide down the rod until the van der Waals surfaces touch, compute an intermolecular energy, reorient the analyte, slide it back down the rod, and recompute the energy at that θ and ϕ. After all orientations of the analyte have been sampled at that θ and ϕ, we move the rod to a new latitude and longitude to repeat the aforementioned procedure. Only the lowest energy structure is saved for each grid point. A plot of the lowest intermolecular energy as a function of θ and ϕ is thus generated. This plot represents the intermolecular energy between the two molecules as we tumble the analyte over the van der Waals surface of CSP. It is important to note that both analytes are treated the same way: the origins are identical, the axes are the same, and the manner in which analyte is tumbled over the CSP is precisely the same for both optical isomers.

By virtue of the size of the molecules involved as well as the extraordinary number of orientations to be sampled, we limit ourselves to the empirical force field method for computation of intermolecular energies. The force field we select is the Allinger MM2 force field (*6*) because of its versatility of treating a wide range of organic functional groups and its documented reliability to accurately predict structures and energies (*7*, *8*). All computations were performed on a VAX 11/780 computer employing the molecular modeling program previously described (*3*).

RESULTS AND DISCUSSION

Plots of the intermolecular energies of *R* and *S* alcohols **2** with CSP analogue **3** are presented in Figure 2. Note that the propyl chain of **1** has been replaced with a methyl group

in 3 for convenience and the NO_2 groups have been replaced with CHO groups because NO_2 parameters for MM2 do not yet exist. This substitution is of little consequence and the charge transfer effect is successfully modeled (vida infra). Energies were obtained by sweeping through θ = 0–180° and ϕ = 0–360° in 20° increments. The minima in the range θ = 80–160° and ϕ = 20–100° were then reinvestigated with a finer grid and with a larger number of analyte orientations at each $\theta\phi$ grid point.

Both contour maps are strikingly similar but difference plots (not shown here) highlight the differential binding of *R* vs. *S* on the CSP. As seen in Figure 2 there are two broad and shallow binding regions about the CSP favored by the analyte. One region corresponds to front-side association of analyte while the other involves rear-side association. The shallowness around each minimum assures a large number of diastereomeric structures exist; each of which may contribute to the overall retention of the analyte. The energy difference between the two global minima is 0.3426 kcal mol^{-1}, favoring retention of the *S* analyte. The *R* enantiomer experimentally has the shorter retention time; hence for this example theory and experiment agree. The small difference in binding energy was anticipated and is consistent with α = 1.33. These minima correspond to CSP and analyte rigidly locked in their preferred conformations. Preliminary work suggests that when all degrees of freedom are relaxed so that CSP can alter its conformation to better accommodate analyte and the analyte can alter its shape to better bind to CSP that the difference in binding energy is somewhat larger but still favoring retention of the *S* analyte.

A chiral recognition model for analyte binding to CSP 1 exists (*2*). We have not located structures corresponding to those expected from such a model. While we are not yet in a position to confirm nor deny the validity of the established mechanism, snapshots of analyte orientations taken from near the global minima in Figure 2 reveal a consistent pattern of binding.

The most highly retained *S* analyte is found to maintain structures like the one shown in Figure 3 while the *R* analyte binds like that depicted in Figure 4. In both diastereomeric complexes we find a π acid–π base interaction between the aryl rings (the existing model has this feature) and a hydrogen bond between CSP and analyte (the existing model also has this feature). The difference between binding of *R* and *S* analytes involves the direction of analyte as it docks with the CSP and how it utilizes the hydroxyl group. For the *R* enantiomer the hydroxyl serves as a hydrogen bond donor coordinating with the amide carbonyl oxygen on the CSP. For the *S* enantiomer, in contrast, the analyte is rotated 180° and the analyte serves as a hydrogen-bond acceptor. In this orientation the N–H of the CSP amide is directed toward the lone pair of electrons on the oxygen of the analyte's hydroxyl group. In both instances the phenyl group on the CSP serves only as a steric barrier to keep analytes from strongly binding to the rearside.

In this communication we have demonstrated a novel approach to the problem of predicting which of two optical analytes is the most retained on a chiral column. We have provided insight about where on the CSP aryl alcohol **2** prefers to bind, and we have presented an alternative mechanism by which enantioselection may take place.

Our results are preliminary; they are not meant to credit nor discredit the existing chiral recognition model. In this communication we simply demonstrate that modern computation along with molecular graphics can furnish information heretofore not available and we can provide insight to problems that are important in separation science.

ACKNOWLEDGMENT

We thank Bill Pirkle for his hospitality and stimulating discussions.

LITERATURE CITED

(1) Souter, Rex W. *Chromatographic Separation of Stereoisomers*; CRC Press: Boca Raton, FL, 1985.
(2) Pirkle, W. H.; House, D. W.; Finn, J. M. *J. Chromatogr.* **1980**, *192*, 143–158.
(3) Lipkowitz, K. B.; Landwer, J. M.; Darden, T. *Anal. Chem.* **1986**, *58*, 1611–1617.
(4) Lipkowitz, K. B.; Malik, D. J.; Darden, T. *Tetrahedron Lett.* **1986**, *27*(16), 1759–1762.
(5) Lipkowitz, K. B.; Demeter, D. A.; Parish, C. A.; Landwer, J. M.; Darden, T. *J. Comput. Chem.*, in press.
(6) Allinger, N. L. *J. Am. Chem. Soc.* **1977**, *99*, 8127.
(7) Burkert, U.; Allinger, N. L. *Molecular Mechanics*; American Chemical Society, Monograph 177; American Chemical Society: Washington, DC, 1982.
(8) Clark, T. *A Handbook of Computational Chemistry: A Practical Guide to Chemical Structure and Energy Calculations*; Wiley-Interscience: New York, 1985.

Kenny B. Lipkowitz*
David A. Demeter
Carol A. Parish

Department of Chemistry
Indiana–Purdue University
Indianapolis, Indiana 46223

Thomas Darden

Laboratory of Molecular Biophysics
National Institute of Environmental Health Science
P.O. Box 12233
Research Triangle Park, North Carolina 27709

RECEIVED for review February 2, 1987. Accepted April 1, 1987. This work was funded by the donors of the Petroleum Research Fund, administered by the American Chemical Society.

Pulsed-Laser Photothermal Refraction Detection in Capillary Liquid Chromatography

Sir: The absence of detectors that are versatile and sensitive and have extremely low volumes has impeded the development and utilization of capillary liquid chromatography (LC) separation techniques in chemical analysis (*1*, *2*). Commercially available spectrophotometric (absorbance-based) detectors are used extensively in analytical-scale LC. However, the majority of these detectors are not compatible with LC due to the large volumes (ca. 10 μL) of their flow cells. The volumes of solute bands eluted by capillary LC columns range from low nanoliters for true open capillary columns to high nanoliters for the slurry-packed capillary columns employed in this work (*3*). While the flow cells of some commercial spectrophotometric detectors have been modified to accomodate certain capillary columns (*4*, *5*), these modified detectors generally suffer from poor sensitivity (due to short optical path lengths), relatively large amounts of stray light, and poor light throughput.

The intense, highly collimated outputs of lasers can be focused to produce large photon densities, in extremely low-volume flow cells, without large amounts of stray radiation.

0003-2700/87/0359-1733$01.50/0 © 1987 American Chemical Society

This often provides for sensitive fluorescence detection in capillary LC (*6*), which, whenever possible, should be performed "on-column" (*7, 8*). The effective flow-cell volume of a laser beam focused to a 10-μm spot at the end of a 20-μm-i.d. capillary column is a mere 3 pL. Unfortunately fluorometry is not a particularly versatile technique, due to the small percentage of analytes that possess appreciable fluorescence quantum efficiencies. Methods based on the measurement of absorbance are much more versatile but, when applied to capillary LC detection, exhibit the aforementioned problems.

Recently, attention has been given to developing laser-based thermal optical detection techniques for LC (*8–13*). These techniques provide for sensitive absorbance-based measurements by relying for their signals on temperature increases in a sample, generated by the nonradiative dissipation of absorbed laser radiation. The techniques that have been used most in LC are thermal lens (*8–10*) and photothermal refraction (*11*) and deflection (*12*) detection. Signal generation with these techniques is critically dependent on the spatial properties of the laser beams that are employed. When a laser beam with a Gaussian spatial distribution of light intensity is passed through an absorbing sample, Gaussian temperature and refractive index gradients are created in the sample. With the thermal lens technique a probe laser beam is focused through the sample collinear with an absorbed laser beam. This probe beam will experience a lensing effect, which can be monitored in the far field with a pinhole and a photodetector. The photothermal refraction technique differs in that the absorbed and probe beams are perpendicularly intersected in the sample and the optical element experienced by the probe beam is that of a cylindrical, rather than spherical, lens. Because the volume probed within the sample is the volume of the intersected beams, the photothermal refraction technique is constrained to measuring absorbances in very small volumes. Photothermal beam deflection involves monitoring the deflection (as opposed to the divergence) of the probe laser beam. With this technique the absorbed and probe beams typically intersect within the sample at an angle that is less than that of the perpendicular offset used in photothermal refraction, although in one report a crossed beam configuration has been successfully employed for photothermal deflection (*14*).

Previous applications of these techniques to LC detection have involved the use of continuous wave (CW) lasers. These lasers offer excellent beam properties and high average powers, but they do not readily offer access to the analytically important ultraviolet (UV) portion of the electromagnetic spectrum. A pulsed, pumped-dye laser, using the appropriate dyes and harmonic generation optics, offers a convenient means to access any wavelength in the UV for detection purposes. The uses of pulsed-laser thermal lens detection for flowing liquid samples (*13*) and pulsed-laser photothermal deflection for gas chromatography detection (*15*) have been reported. In this report we discuss our use of pulsed-laser photothermal refraction detection in capillary LC. Separations are performed with slurry-packed capillary columns. The technique is illustrated for the separation of nitrated pyrene isomers in a synthetic coal fly ash extract. CW laser, photothermal refraction detection has provided for the sensitive measurement of dabsyl–amino acids (dabsyl = (dimethylamino)azobenzenesulfonyl), following separation with a microbore LC column (*11*). The work presented herein differs in that we (1) employ for detection an excimer pumped-dye laser tuned to the near-UV absorbance maximum of the underivatized analyte of interest and (2) employ for the separation true capillary LC using slurry-packed capillary columns. Eliminating the need to derivatize the sample in order to match the wavelength of the laser, we do not have to be concerned with whether derivatization was complete and also do not have to resolve the analytes of interest from unreacted and hydrolyzed derivatizing reagent, which may be present in the sample. The capillary columns provide excellent efficiency in this application and afford the possibility of injecting extremely small sample volumes.

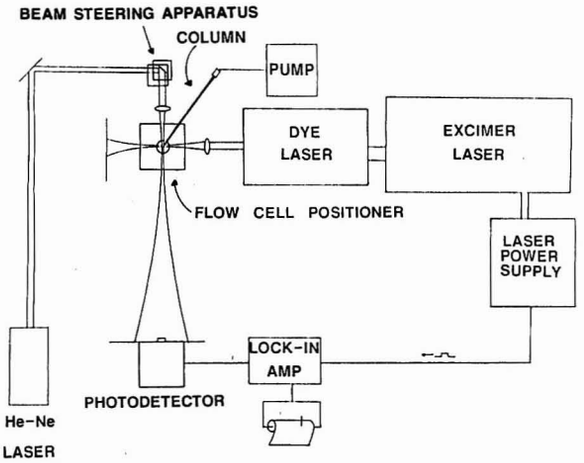

Figure 1. Experimental apparatus for pulsed-laser photothermal refraction detection is capillary liquid chromatography.

EXPERIMENTAL SECTION

Apparatus. A block diagram of the equipment used in this work is shown in Figure 1. The photothermal refraction detector consisted of a Lambda Physik FL 2000 dye laser pumped by a Lambda Physik EMG 50 excimer laser. The excimer uses a Xe/HCl gas fill to pump the 2-(4-biphenylyl)-6-phenylbenzoxazole (PBBO) dye (Lambda Physik LC 4000) at 308 nm. The dye laser, which produces the absorbed beam, was tuned to 400.0 nm. The energy of the laser pulses was 30 μJ and a repetition rate of 23 Hz was employed. The probe laser was a Spectra-Physics Model 145-01 helium–neon laser. The absorbed laser beam was focused with a 25-mm-focal-length (*f*) quartz biconvex lens. The probe laser beam was focused with a 22-mm-*f* lens. The intensity of the probe beam at beam center was monitored with a Clairex Model CL707HM photoconductive cell placed 67 cm from the flow cell. An Ithaco, Model 391A lock-in amplifier, referenced to the synchronous output of the excimer laser, was employed to monitor and amplify the photocell signal. A sensitivity of 300 μV and time constant of 4 s were typically used. The lock-in output was monitored with a Cole-Parmer Model 8376-20 recorder. The entire system was rigidly mounted on a pneumatically stabilized optical table (Modern Optics), which served to minimize vibration induced contributions to the background.

Chromatography. The slurry-packed microcolumns were constructed and packed following the procedure of Gluckman and co-workers (*3*). The columns were 200-μm-i.d. fused silica (Scientific Glass Engineering, Austin, TX) and were packed with 5-μm CPS-Hypersil particles (Shandon Southern Products, Ltd., Cheshire, England). The particles were slurry packed at 5000 psi with a Haskel Model 17502 pneumatic amplifier pump employing acetone as the slurry and packing solvent. Porous Teflon frits, 20 μm thick, were employed as exit frits and were held in place by a 1 cm length of 50-μm-i.d. fused-silica capillary, which was secured with epoxy into the end of the column. Detection was performed in a short length of 200-μm-i.d. fused silica from which the polyimide coating had been removed. This short length of tubing was attached to the 50-μm-i.d. fused silica at the terminus of the column by means of epoxy. Injection was performed as described in ref 3. The injection volume was approximately 20 nL. The mobile phase, 95/5 *n*-hexane/2-propanol, was pumped by the aforementioned Haskel pump, generally at 1000 psi.

Reagents. All solvents used for separations were Mallinckrodt Chrom AR grade. 1-Nitropyrene and dinitropyrene isomers were received from the NCI Chemical Carcinogen Reference Standard Depository, a function of the Division of Cancer Etiology, NCI, NIH, Bethesda, MD. The sample analyzed was an extract of coal fly ash that had been coated with pyrene and subsequently ex-

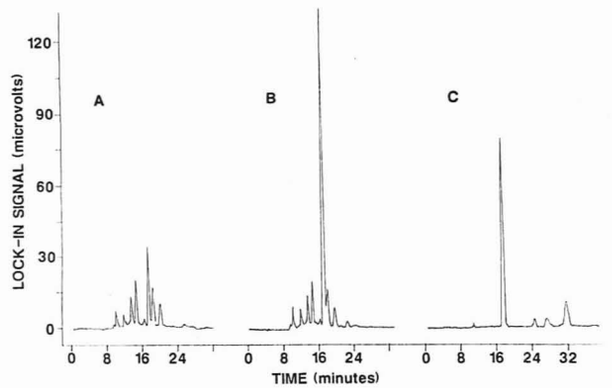

Figure 2. Chromatograms of synthetic sample extracts (A and B) and 1-NP and dinitropyrene isomers standard mixture (C).

posed to an atmosphere of NO_2 (*16*). The fly ash was then extracted in a Soxhlet apparatus with toluene, concentrated, and injected onto the column.

RESULTS AND DISCUSSION

Pulsed-laser photothermal measurements do offer advantages when compared with CW-laser-based methods. The shorter rise time of the signal that results when a pulsed laser is used allows for a shorter signal collection time and reduced errors (*15*). The use of a pulsed laser for thermal lens measurements in a flowing liquid (*14*) illustrated that there was no dependence of signal on flow rate while CW-laser-based thermal lens measurements have shown a significant dependence on flow rate (*8*). The theoretical enhancement offered by pulsed-laser thermal lens measurements compared to CW-laser thermal lens has been reviewed (*17*). The pulsed method is favored for small samples, rapid analyses, and gas-phase samples. For this application of pulsed-laser photothermal refraction detection the primary advantage is the tunability of the dye laser employed. The slow flow rate encountered when using capillary liquid chromatography columns would probably not have a deleterious effect on either CW or pulsed laser measurements. The ability to tune the source provides the opportunity to detect analytes at a wavelength corresponding to their maximum absorption coefficient. The near-UV wavelength of 400.0 nm used in these experiments was the optimum wavelength for detection of 1-nitropyrene in the mobile phase employed. Measurements at wavelengths further into the UV require a change of dye or frequency doubling. Frequency doubling was not required in order to perform measurements at 400.0 nm.

We employ the crossed-beam photothermal refraction configuration because of its proven ability to make sensitive absorption measurements in small volumes (*18*) and its ease of alignment relative to thermal lens detection, which employs collinearly aligned laser beams. Once aligned and optimized, the photothermal refraction detector remains aligned from day to day, requiring only occasional "tweaking" of the signal. This is readily achieved by replacing the capillary column flow cell with a flow cell attached to a syringe pump. The syringe pump delivers a test solution to the flow cell at a reproducible flow rate so that the signal level can be set to the same value as previous alignments. The crossed-beam technique makes the process of switching and aligning flow cells fairly easy. Placing the flow cell at the intersection of the two beams is simply a matter of observing the image of the two lasers in the far field as the flow cell is translated into the intersection point. With some practice, the flow cell can be reproducibly placed at the intersection point of the beams.

Nitro-substituted polynuclear aromatic hydrocarbons have received considerable attention in recent years due to their mutagenic and carcinogenic activity (*19–22*). Figure 2 contains a series of chromatograms illustrating the use of a slurry-packed silica column with pulsed-laser photothermal refraction detection to indicate the presence of nitropyrene isomers in the sample previously described. The column employed was 200 μm i.d. × 62 cm packed with 5-μm CPS-Hypersil particles. Isocratic elution with a mobile phase of 95/5 *n*-hexane/2-propanol was accomplished with a constant inlet pressure of 1000 psi. Chromatograms A and B are separations of the sample. Chromatogram C of the figure is the separation of a standard mixture of (in elution order) 3.0 ng of 1-nitropyrene (1-NP), 0.31 ng of 1,3-dinitropyrene (1,3-DNP), 0.80 ng of 1,6-dinitropyrene (1,6-DNP), and 1.3 ng of 1,8-dinitropyrene (1,8-DNP). This chromatogram illustrates the separation capability of slurry-packed capillary columns under isocratic elution conditions (analytical scale separations of this mixture typically require gradient conditions). The ability to accomplish this separation under isocratic conditions preserves the thermooptical properties of the mobile phase and, hence, serves to maintain a constant photothermal refraction background signal (*23*).

The small injection volume used (20 nL) for these separations is also advantageous. The complex mixtures resulting from extractions of air particulate matter, soil samples, and other naturally occurring samples often contain many components that are at concentrations below the limit of detection. Concentration of extracts to microliter volumes prior to injection can often enhance the opportunity to detect these trace components. This was the case with the synthetic fly ash sample investigated in this work. The original 80-mL extraction volume was reduced to 10 μL before the chromatograms in Figure 2 could be accomplished. The use of split injection techniques provides minimal band broadening and the greatest flexibility concerning the quantity injected. Unfortunately, when sample sizes are extremely small, as in this case, split injection is not possible.

All three chromatograms in Figure 2 were obtained by using the same column and conditions. The tallest peak of chromatogram A was suspected of being 1-NP due to its match in retention time with 1-NP in the standard mixture. Spiking the extract with 1-NP provided an increase in peak height for the suspect peak while the remaining peaks remained the same height (Figure 2B). The presence of 1-NP in this extract has been confirmed by direct inlet probe mass spectrometry (*16*). The additional peaks in the chromatogram could include different positional isomers of nitrated pyrene.

The analytical utility of photothermal refraction detection is dependent on the relationship of signal to concentration. A linear calibration curve was constructed for photothermal refraction signal response to different concentrations of 1-NP in *n*-hexane, flowing in a 200-μm fused-silica flow cell. The linear dynamic range for the plot extended from 4×10^{-6} to 6×10^{-4} M with a correlation coefficient of 0.997. The reproducibility of response for chromatographic detection is illustrated by the detector response to the amount of 1-NP added to the complex mixture. The chromatogram of the standard mixture containing 3.0 ng of 1-NP (Figure 2C) yielded a lock-in amplifier response of 80.0 μV, or a response factor of 26.7 μV/ng injected. The separation of the unspiked sample (Figure 2A) yielded a 1-NP peak of 34.5 μV. A spike of 3.9 ng/injection yielded a 1-NP peak of 137 μV after separation (see Figure 2B). Taking the difference of the detector response for 1-NP for the spiked and unspiked chromatograms yields a response factor of 26.2 μV/ng. This good correlation indicates the possibility of employing standard addition in order to quantify analytes present in a sample when using this type of detection.

The photothermal refraction measurement is independent of path length (*23*). Rather than attempt to relate these

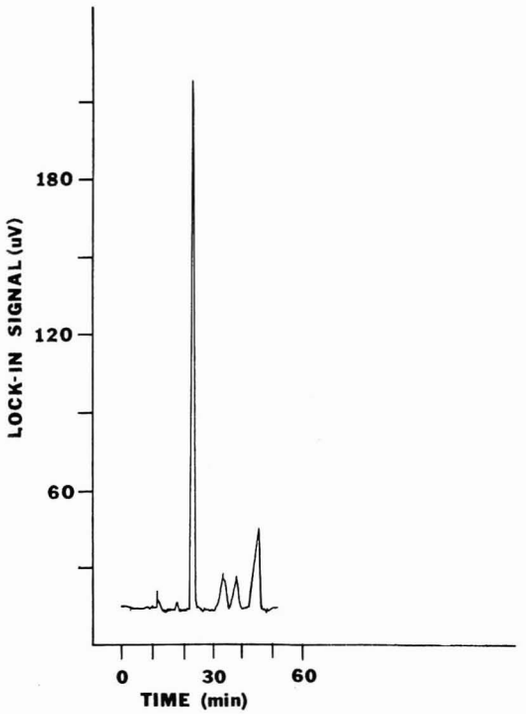

Figure 3. Chromatogram of 1-NP and dinitropyrene isomers standard mixture (higher laser power than that used in Figure 2).

measurements to Beer's law absorbances, the measurements at the limit of detection are best expressed as the product of concentration and molar absorptivity (ϵC). The 1-NP peak in Figure 2C has a Gaussian profile and therefore the concentration at peak center for the 3 ng injected is calculated to be 2.7×10^{-5} M. Assuming a direct proportionality between signal and amount injected, the limit of detection at a signal to noise ratio (S/N) of 3 is $\epsilon C = 7.4 \times 10^{-3}$ cm^{-1}. This value is relatively poor with respect to previously reported values (*11*, *18*) and with good reason. One problem in using a highly focused pulsed laser is the destructive effects of the large power density involved. In order to obtain the maximum signal, it is advantageous to maximize the power of the absorbed laser beam due to its direct relationship to signal (*23*). Unfortunately, high incident power can destroy flow cells. The average power used to obtain the chromatograms in Figure 2 was 0.6 mW. Figure 3 shows a chromatogram of the synthetic mixture of 1-NP and dinitropyrene isomers with an improved S/N. A 200-μm × 90-cm column was employed with isocratic elution at 1500 psi with a 95/5 hexane/2-propanol mobile phase. The injected quantitites were the same as in Figure 2C. Detection was obtained by using an average power of approximately 1.0 mW, which corresponds to a peak power density of approximately 0.2 GW/cm^2. This incident power eventually burned a hole through the thin-wall fused-silica flow cell. Extrapolation of the signal for the 3.0-ng injection of 1-NP for this chromatogram to a S/N of 3 yields $\epsilon C = 4.6 \times 10^{-3}$ cm^{-1}, which corresponds to an absorbance of 9×10^{-5}. We have successfully employed heavy-walled 500-μm-i.d. square quartz flow cells and have obtained a limit of detection of $\epsilon C = 2.7 \times 10^{-4}$ cm^{-1}. While this value exceeds the value obtained with pulsed-laser thermal lens detection of flowing liquids (*13*), it is a factor of 50 less than the extrapolated value of 5×10^{-6} cm^{-1} reported by Dovichi and co-workers for detection of dabsyl–glycine when using CW laser excitation (*11*).

Tunability, compatibility with low-volume flow cells, and the potential for high sensitivity characterize the pulsed-laser-based photothermal refraction detector discussed herein. The development of a an ultraviolet–visible (UV–vis) absorbance detector that can provide high sensitivity and low detector-related solute band dispersion should aid in the growth of capillary LC. While the sensitivity obtained in this work is slightly better than that for previously reported work with pulsed-laser thermal optical detection for flowing liquid samples, it is only approximately equivalent to that reported for conventional absorbance detectors that had been designed or modified for detection in capillary LC (*24*). In order for the large (several orders of magnitude for the laser system employed in this work) theoretical enhancements in sensitivity over normal Beer's law measurements to be realized, several practical problems associated with the use of pulsed lasers must be solved or reduced. Further development of this detection method should include the use of lower wavelength UV excitation, continuous tuning of the dye laser output for maximization of analyte detection, and the combination of the technique with time-resolved fluorescence detection to provide additional analytical information. Improvements in sensitivity should be possible if more durable flow cells that can tolerate higher laser powers are developed. Sheath flow cells may prove useful in this matter (*25*, *26*). More sophisticated laser systems, which provide output pointing and intensity stabilities that are superior to the system employed in this work, could also result in significant improvements in sensitivity.

LITERATURE CITED

(1) Knox, J. H.; Gilbert, M. T. *J. Chromatogr.* **1979**, *186*, 405–418.
(2) Scott, R. P. W. *J. Chromatogr. Sci.* **1980**, *18*, 49–54.
(3) Gluckman, J. C.; Hirose, A.; McGuffin, V. L.; Novotny, M. *Chromatographia* **1983**, *17*, 303–309.
(4) Kok, W. Th.; Brinkman, U. A. Th.; Frei, R. W.; Hanekamp, H. B.; Nooitgedacht, F.; Poppe, H. *J. Chromatogr.* **1977**, *144*, 157–163.
(5) Yang, F. J. *HRC CC, J. High Res. Chromatogr., Chromatogr. Commun.* **1981**, *4*, 83–89.
(6) Murray, G. M.; Sepaniak, M. J. *J. Liq. Chromatogr.* **1983**, *6*, 931–938.
(7) Guthrie, E. J.; Jorgenson, J. W.; Dluzneski, P. R. *J. Chromatogr. Sci.* **1984**, *22*, 171–176.
(8) Sepaniak, M. J.; Vargo, J. D.; Kettler, C. N.; Maskarinec, M. P. *Anal. Chem.* **1984**, *56*, 1252–1257.
(9) Leach, R. A.; Harris, J. M. *J. Chromatogr.* **1981**, *218*, 15–19.
(10) Buffett, C. E.; Morris, M. D. *Anal. Chem.* **1982**, *54*, 1824–1825.
(11) Nolan, T. G.; Hart, B. K.; Dovichi, N. J. *Anal. Chem.* **1985**, *57*, 2703–2705.
(12) Collette, T. W.; Parekh, N. J.; Griffin, J. H.; Carreira, L. A.; Rogers, L. B. *Appl. Spectrosc.* **1986**, *40*, 164–169.
(13) Nickolaisen, S. L.; Bialkowski, S. E. *Anal. Chem.* **1986**, *58*, 215–220.
(14) Westel, G. C.; Stotts, S. A. *Appl. Phys. Lett.* **1983**, *42*, 931–933.
(15) Nickolaisen, S. L.; Bialkowski, S. E. *J. Chromatogr.* **1986**, *366*, 127–133.
(16) Yokley, R. A. Ph.D. Dissertation, Chemistry Department, University of Tennessee, 1985.
(17) Bialkowski, S. E. *Spectroscopy (Springfield, Oreg.)* **1986**, *1*, 26–48.
(18) Nolan, T. G.; Weimer, W. A.; Dovichi, N. J. *Anal. Chem.* **1984**, *56*, 1704–1707.
(19) Wang, Y. Y.; Rappaport, S. M.; Sawyer, R. F. Talcott, R. E.; Wei, E. T. *Cancer Lett. (Shannon, Irel.)* **1978**, *5*, 39–47.
(20) Salmeen, I.; Durisin, A. M.; Prater, T. J.; Riley, T.; Schuetzle, D. *Mutat. Res.* **1982**, *104*, 17–23.
(21) Wei, E. T.; Shu, H. P. *Am. J. Public Health* **1983**, *79*, 1085–1088.
(22) Rosenkrantz, H. S. *Mutat. Res.* **1984**, *140*, 1–6.
(23) Dovichi, N. J.; Nolan, T. G.; Weimer, W. A. *Anal. Chem.* **1984**, *56*, 1700–1704.
(24) Walbroehl, Y.; Jorgenson, J. W. *J. Chromatogr.* **1984**, *315*, 135–143.
(25) Zarrin, F.; Dovichi, N. J. *Anal. Chem.* **1985**, *57*, 2690–2692.
(26) Van Liet, H. P. M.; Poppe, H. *J. Chromatogr.* **1985**, *346*, 149–160.

C. N. Kettler
M. J. Sepaniak*

Department of Chemistry
University of Tennessee
Knoxville, Tennessee 37996-1600

RECEIVED for review December 5, 1986. Accepted March 30, 1987. This research was sponsored by the Division of Chemical Sciences, Office of Basic Energy Sciences, U.S. Department of Energy, under Contract DE-FG05-8613613 with the University of Tennessee, Knoxville, TN.

AIDS FOR ANALYTICAL CHEMISTS

Composite Ion Exchanger for Removal of Sodium-24 in Neutron Activation Analysis of Biological Materials

Aleksander Bilewicz, Barbara Bartoš, and Jerzy Narbutt*

Department of Radiochemistry, Institute of Nuclear Chemistry and Technology, 03-195 Warsaw, Poland

Halina Polkowska-Motrenko

Department of Analytical Chemistry, Institute of Nuclear Chemistry and Technology, 03-195 Warsaw, Poland

Sodium-24, predominating in the γ spectra of neutron-irradiated samples of biological materials, ought to be removed from the samples, making it possible to detect other radionuclides of analytical interest. Crystalline hydrated antimony pentaoxide (HAP) is commonly used for this purpose. The procedure consists of passing a hydrochloric acid solution of an irradiated sample through a small column filled with HAP grains on which sodium ions are selectively adsorbed (*1*).

However, like other inorganic ion exchangers, crystalline HAP exhibits some serious shortcomings which limit its application. Poor mechanical stability of the HAP grains results in clogging the column with pulverized HAP particles in the course of eluting, especially with more concentrated HCl solutions (*2*). The process of ion exchange on HAP is characteristic of poorer kinetics than that on ion exchange resins. The retention capacity, below 2 mequiv of Na^+/g of HAP, lower than the calculated value of 5.06 mequiv/g (*3*), indicates that only a fraction of the ion-exchange sites participates in the process of sodium retention. The HAP grains are of irregular shapes, which increases the flow resistance of the sorbent bed. Finally, the common procedures of HAP synthesis yield rather low fractions of the grains of the size appropriate for column operation.

In order to improve some of the properties of the sorbent, crystalline HAP was powdered and implanted into a matrix of an ion-exchanger resin. A new composite ion exchanger has been thus obtained.

EXPERIMENTAL SECTION

Crystalline HAP, obtained in the way described in ref 1, was powdered to grains of dimensions below 0.03 mm and then added in a calculated proportion to a viscous reaction mixture of sulfonated phenol with formaldehyde, commonly used in synthesizing polycondensation resins (*4*). The resulting suspension was dispersed in Apiezon oil heated up to 90 °C. Small drops of this suspension, formed as a result of vigorous stirring, hardened within a couple of minutes. Spherical beads of the composite sorbent obtained that way were then separated from oil, degreased, and dried (*5*).

Retention of metal ions on the composite ion exchanger was studied under dynamic conditions from 8 M HCl. The diameter of the column was 4 mm and the bed height was 50 mm, the flow rate being 0.75 cm^3/min. The following radionuclides, either supplied by the Isotope Production and Reactor Centre at Swierk near Warsaw or obtained by neutron irradiation of spectrally pure compounds, were used as radiotracers: ^{22}Na, ^{24}Na, ^{76}As, ^{198}Au, ^{115}Cd, ^{64}Cu, ^{59}Fe, ^{197}Hg, ^{114}In, ^{42}K, ^{54}Mn, ^{99m}Tc, and ^{65}Zn. A Ge(Li) detector (Schlumberger, active volume of 70 cm^3, resolution of 3.1 keV for the ^{60}Co 1332-keV peak), coupled to a 4096-channel pulse height analyzer Didac-4000 (Intertechnique) was used. Distribution coefficients of sodium ions were measured in batch experiments. Retention capacities of the sorbents were determined under dynamic conditions by passing a Na^+ (1.5 mg/cm^3) solution in 5 M HCl through standard columns filled with 0.5 g of each sorbent studied, at a rate of 0.3 cm^3/min.

Table I. Some Properties of Pure Crystalline HAP and the Composite Ion Exchanger Containing 60% HAP

parameter	pure HAP	composite HAP
grain shape	irregular	spherical (beads)
grain size (diameter), mm	0.1–0.3	0.1–0.3
distribution coeff of Na^+ in 5 M HCl, cm^3/g	3×10^2	2×10^3
retention capacity for Na^+, mg/g	29	23
adsorption rate ($t_{1/2}$), min	4	3
flow resistance	high	low
resistance to:		
5–8 M HCl	low[a]	high
5–7 M HNO_3	low	low[b]

[a] Peptization. [b] The material slowly decays because of oxidation of the matrix.

Table II. Elution of Sodium and Some Other Elements with 8 N HCl Solution from the Bed of HAP-Composite Ion Exchanger[a]

element	% rel content of the elements in the effluent 0–15 cm^3	0–30 cm^3
Na	0	0
As	43.4	49.1
Au	95.0	98.5
Cd	100	100
Cu	94.8	95.0
Fe	100	100
Hg	96.9	96.9
In	98.3	98.3
K	94.2	100
Mn	100	100
Tc	100	100
Zn	100	100

[a] Column diameter, 4 mm; bed height, 50 mm; diameter of beads, 0.1–0.3 mm; flow rate, 0.75 cm^3/min; room temperature.

RESULTS

Spherical beads of the composite ion exchanger containing 60% HAP in a phenolsulfonic–formaldehyde matrix, 0.05–0.5 mm in diameter, were synthesized. The fraction of dimensions from 0.1 to 0.3 mm was selected for the experiments (Figure 1). High yield of this fraction (over 50%) was attained; moreover, the granulation can easily be controlled in a broad range. The beads are of good mechanical stability comparable to that of ion-exchange resins. The comparison of some properties of crystalline and composite HAP is given in Table I. It is noteworthy that the composite ion exchanger con-

0003-2700/87/0359-1737$01.50/0 © 1987 American Chemical Society

Table III. Results of Cu and Mn Determination in Standard Reference Biological Materials

std material	Cu content,[a] μg/g			Mn content,[a] μg/g		
	analyt result	mean value	recommended value	analyt result	mean value	recommended value
bovine liver, NBS 1577	172	184	193 ± 10	9.4	9.3	10.3 ± 1.0
	173			8.9		
	180			9.6		
	212			9.3		
rye flour, IAEA V-8	0.97	0.98	0.95 ± 0.19	2.19	2.07	2.06 ± 0.12
	0.97			2.12		
	1.01			1.92		

[a] Dry weight.

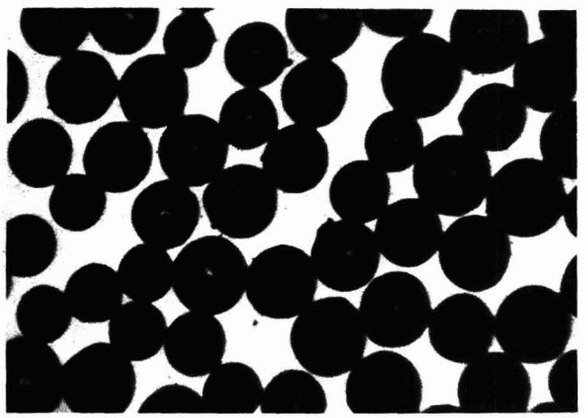

Figure 1. Beads (0.1–0.3 mm) of the composite ion exchanger containing 60% HAP in phenolsulfonic–formaldehyde matrix.

taining a bare 60% of the active sorbent (HAP) has a higher distribution coefficient for Na^+ than the pure crystalline material. Also the retention capacity of the composite ion exchanger, when related to the content of the active sorbent, is greater than that of the pure crystalline HAP. Both observations can be explained assuming an increase of the number of active sites available for sodium ions in the composite material, obviously caused by reducing the sizes of the implanted HAP grains when compared to the pure HAP crystals.

Improved kinetics of the ion exchange and decreased flow resistance of the composite sorbent make it possible to increase the flow rate of the effluent and reduce the time of the analysis. Due to the increased resistance of the composite material to hydrochloric acid, the HCl solutions of higher concentration can be used, decreasing the retention of some other elements of analytical interest.

Examination of the retention of a number of metal ions often determined in biological samples (Table II) shows that none of the elements tested, except arsenic, is retained on the HAP-composite sorbent from 8 M HCl (also selenium and tungsten are partly retained under these conditions (*6*)), while the retention of sodium-24 is quantitative, even at 50 bed volumes of the effluent. This makes it possible to use the HAP-composite ion exchanger for removing ^{24}Na from neutron-activated biological samples more efficiently than pure crystalline HAP. The analytical application of the composite sorbent can be illustrated by the results of the determination of copper and manganese in two standard reference biological materials specified in Table III. The irradiated samples (30–100 mg) were decomposed under heating in the mixture of HNO_3 and $HClO_4$ and then repeatedly evaporated to dryness with 8 M HCl. The residue was dissolved in a small amount of 8 M HCl and the solution obtained was transferred into a column filled with the composite ion exchanger. The elution was carried out with 15 cm^3 of 8 M HCl. Sodium-24 was completely retained on the sorbent bed, while copper and manganese quantitatively passed to the effluent. The results of the determination of both elements do agree with the recommended values (Table III).

The above procedure can be used as well to determine other nonvolatile elements not retainable on the composite ion exchanger from hydrochloric acid solutions. The composite sorbent can hardly be used in nitric acid solutions, not only due to worse selectivity of sodium separation but also because of poor resistance of the phenolsulfonic–formaldehyde matrix to the oxidizing medium (Table I).

It is worth mentioning that also other inorganic ion exchangers of both analytical and technological interest, exhibiting poor mechanical stability but resistant to more concentrated solutions of sulfuric acid, can be transformed into stable beads of the composite sorbents (*5*, *7*).

Registry No. ^{24}Na, 13982-04-2; Sb_2O_5, 1314-60-9.

LITERATURE CITED

(1) Girardi, F.; Sabbioni, E. *J. Radioanal. Chem.* **1968**, *1*, 169–178.
(2) Amman, K.; Knöchel, A. *Microchim. Acta* **1984**, 385–391.
(3) Abe, M. In *Inorganic Ion Exchange Materials*; Clearifield, A., Ed.; CRS Press: Boca Raton, FL, 1982; Chapter 6, p 226.
(4) Rabek, T. I. *Teoretyczne podstawy syntezy polielektrolitów i wymieniaczy jonowych*; PWN: Warszawa, 1960; p 354.
(5) Narbutt, J.; Bartoš, B.; Bilewicz, A.; Szeglowski, Z. European Patent Appl 86111963.4, 1986.
(6) Kučera, J., Nuclear Research Institute, Řež, Czechoslovakia, personal communication, 1986.
(7) Narbutt, J.; Siwiński, J.; Bartoš, B.; Bilewicz, A. *J. Radioanal. Nucl. Chem.* **1986**, *101*, 41–49.

RECEIVED for review November 14, 1986. Accepted February 2, 1987. The work was supported by the Central Research Programme CPBP 01.09.

Recovery of Picloram and 2,4-Dichlorophenoxyacetic Acid from Aqueous Samples by Reversed-Phase Solid-Phase Extraction

Martha J. M. Wells*[1] and Jerry L. Michael

U.S. Forest Service, Southern Forest Experiment Station, Auburn University, Alabama 36849

Extensive preparation of samples before chromatographic analysis is usually the most time-consuming process in the determination of many organic compounds in environmental matrices. In the past, removal of some organics from aqueous solution was commonly done by liquid/liquid extraction. However, the introduction of stable, covalently bonded reversed-phase sorbents now allows efficient removal of hydrophobic compounds from aqueous solution by adsorption on a chromatographic support. Solid-phase extraction is not a new technique. However, the procedure is more convenient today because of the commercial availability of ancillary equipment and prepackaged disposable adsorption cartridges in a variety of sorbents (*1*, *2*).

Solid-phase extraction on bonded-phase organosilica based sorbents is an emerging technology for the analysis of chemicals of environmental significance. Environmental applications of solid-phase extraction for organic pollutant determinations in water have included the isolation of chlorophenolics (*3*, *4*), azaarenes (*5*), priority pollutants (*6*, *7*), PAH and PCB's (*8*), and the trace enrichment of oil- or jet-fuel-contaminated water (*9*, *10*).

Pesticide residue determinations in water by solid-phase extraction have been published for the insecticides lindane, heptachlor, aldrin, endosulfan, dieldrin, DDT, and zolone (*11*), aldicarb (*12*), and carbaryl (*13*, *14*) and for the herbicides paraquat (*15*), paraquat and diquat (*16*), fluridone (*17*, *18*), pyrazon (*19*), 2,4-D, 2,4,5-T, and silvex (*20*), atrazine, simazine, 2,4-D, silvex, and 2,4,5-T (*21*), and certain triazines (*22*). A solid-phase extraction method for the analysis of endrin, lindane, methoxychlor, and toxaphene has been submitted as an alternative test procedure to the current EPA (Environmental Protection Agency) approved method (*23*). If approved, the proposed technique would amend the National Primary Drinking Water Regulations to eliminate the liquid/liquid extraction step in the current USEPA test procedure for these four organochlorine pesticides, replacing it with a solid-phase extraction technique. Comprehensive reviews of analytical procedures for pesticide analysis from water have been published (*24–26*).

In the procedure presented herein, the herbicides picloram (4-amino-3,5,6-trichloropicolinic acid) and 2,4-dichlorophenoxyacetic acid (2,4-D) are recovered from aqueous samples via solid-phase extraction on reversed-phase sorbents as an alternative to liquid/liquid extraction. Previously, solid-phase extraction on reversed-phase sorbents was used to effect purification of picloram-containing samples that had first been concentrated by partitioning with diethyl ether (*6*, *7*). Current modification of earlier methods accomplishes both sample purification and sample concentration.

While this report was in preparation, two solid-phase extraction methods for chlorophenoxy acid herbicides, including 2,4-D, were published by Hoke et al. (*20*) and Sherma (*21*). However, neither of these procedures included picloram and thereby did not address samples that could contain both picloram and 2,4-D.

In this report, differential elution from the bonded-phase sorbent is used to cleanly separate picloram and 2,4-D from each other. Such a multistage process is not limited to herbicide analysis and should find application to any multiresidue samples sorbed on reversed-phase supports and differing sufficiently in hydrophobicity as do picloram and 2,4-D.

EXPERIMENTAL SECTION

Apparatus. The liquid chromatograph consisted of a Waters Model 6000A solvent pump equipped with a Model 720 system controller, Model 710B intelligent sample processor, automated solvent switching valve, a Model 440 UV absorbance detector, and a Laboratory Data Control SpectroMonitor III variable wavelength UV absorbance detector, a Houston Instrument strip-chart recorder, and a Perkin-Elmer Sigma 10B data handling system.

Reagents and Chemicals. Spectrophotometric grade acetonitrile (ACN) and methanol (MeOH) were purchased from Burdick and Jackson Laboratories, Inc., and spectrophotometric grade glacial acetic acid (HOAc) was purchased from J. T. Baker Chemical Co. Potassium permanganate ($KMnO_4$), ACS grade, was purchased from Fisher Scientific and sodium hydrogen sulfite ($NaHSO_3$), ACS grade, from Alfa Products. The analytical standards, picloram, 99.0% purity and 2,4-D, 99+% purity, were obtained from Dow Chemical Co. and PolyScience Corp., respectively.

Liquid Chromatographic Conditions. An Ultrasphere ODS, 5 μm, spherical porous particle column, 15 cm by 4.6 mm i.d., 2UE5354N, from Altex Scientific, Inc., was used in this study with a CO:PELL ODS, 30–38 μm, 7 cm by 2.1 mm i.d. guard column from Whatman, Inc. The liquid chromatographic mobile phases were acetic acid (4%)/acetonitrile (95:5 v/v) monitored at 254 nm for picloram or acetic acid (4%)/acetonitrile (60:40 v/v) monitored at 280 nm for 2,4–D and were pumped at a flow rate of 1.5 mL/min. (Note: Never allow these phases to remain idle in the system.)

Equipment for Solid-Phase Extraction. C_{18} disposable extraction columns, part no. 7020-3, solvent reservoirs, adaptors, and a vacuum manifold were purchased from J. T. Baker Chemical Co. Polyethylene frits, 20 μm, $1^1/_{16}$ in. diameter, were purchased from Analytichem International and a low-form Filtrator was purchased from Fisher Scientific.

Sample Fortification. Fortified samples were prepared by dissolving pure picloram and 2,4-D standards into separate water solutions. Appropriate amounts of each of these stock solutions were added together to aqueous samples to produce desired concentrations or the solutions were further diluted to produce the test concentrations.

Determination. Aqueous samples were acidified to pH 2 with concentrated sulfuric acid. Two Baker C_{18} columns, each containing about 500 mg of sorbent in a disposable polypropylene column, were connected via adaptors in tandem with each other and with a 75 mL capacity polypropylene sample reservoir. A $1^1/_{16}$ in. polyethylene frit was placed at the bottom of the solvent reservoir. The apparatus was fitted into a side-arm filtering flask. Five milliliters of ACN followed by 10 mL of 4% HOAc in water were added separately and pulled through the adsorbent with vacuum (530 mmHg) at a flow rate of 10–12 mL/min. Before the adsorbent could dry, the sample was passed through the column, followed by 2 mL of 4% HOAc. The frit was removed from the solvent reservoir. Picloram was eluted with 9.0 mL of 25% HOAc directly into a 10-mL volumetric flask contained in a Fisher Filtrator or Baker vacuum manifold. To this eluted fraction, 0.5 mL of saturated aqueous $KMnO_4$ was added, and the mixture was allowed to remain at room temperature for 5 min. A 5 M solution of $NaHSO_3$ was added dropwise to reduce excess permanganate. The sample was diluted to 10.0 mL with 25% HOAc. The 2,4-D still remaining on the adsorbent was serially

[1] Current address: Research Center, West Point Pepperell, PO Box 398, Valley, AL 36876.

This article not subject to U.S. Copyright. Published 1987 by the American Chemical Society

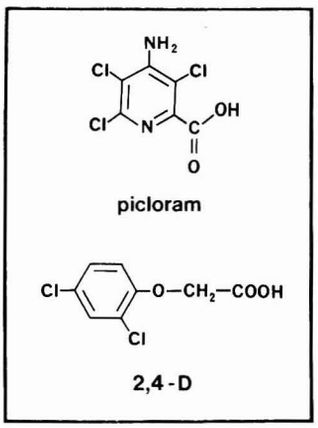

Figure 1. Chemical structures of the herbicides picloram and 2,4-D.

eluted with 4.5 mL of MeOH directly into a 5-mL volumetric flask contained in a Fisher Filtrator or Baker vacuum manifold. This fraction was diluted to 5.0 mL with MeOH. A 50-μL aliquot of each fraction was injected into the chromatograph under the conditions appropriate for each as described above. External standard solutions were prepared by dissolving pure picloram and 2,4-D standards into separate methanol solutions. Appropriate dilutions of these stock solutions were prepared to obtain standards with a range of concentrations. These standards were randomly selected and injected as every fourth sample by the autosampler.

Caution: Pesticides can be injurious to humans, domestic animals, desirable plants, and fish or other wildlife—if they are not handled or applied properly. Use all pesticides selectively and carefully. Follow recommended practices for the disposal of surplus pesticides and pesticide containers.

RESULTS AND DISCUSSION

Picloram and 2,4-D (Figure 1) are formulated together in some of the herbicidal preparations that bear the trade name Tordon. Concomitant analysis for the presence of trace residues of picloram and 2,4-D in environmental waters necessitates development of a rapid, reliable, and sensitive analytical protocol. Solid-phase extraction of these compounds on reversed-phase sorbents is an attractive alternative to more traditional methods that utilize liquid/liquid extraction for the removal of these herbicides from aqueous samples.

Picloram is a much polar compound than 2,4-D. Being less hydrophobic, its extraction from environmental water samples requires a greater amount of reversed-phase sorbent than that needed for 2,4-D. One column of 500 mg is insufficient to produce desirable recovery of picloram. A two-column tandem assembly is necessary to provide 1.0 g of sorbent (500 mg each) for sufficient recovery from 200-mL samples. A similar effect was noted by Rostad et al. (*3*) in their report of the recoveries of 27 phenols, PAH's, and sulfur, oxygen, and nitrogen heterocycles from 500 mg of cyclohexyl bonded phases. They too observed limited recovery for very water-soluble, very polar compounds. They minimized this problem by reducing the sample volume applied to the 500 mg cyclohexyl column. But reducing sample volume adversely affects the amount of substance detectable. For the analysis of picloram and 2,4-D, it was preferable to increase the amount of sorbent, to allow sufficient recovery from 200-mL samples.

The parameters of sample volume, sorbent mass, and solute hydrophobicity are interrelated. For methods development of environmental samples on reversed-phase sorbents, a 200-mL sample volume, 100 ppb sample concentration, and 1.0 g of sorbent are recommended starting values (*1*). The C_{18} sorbent used in this report is now available prepackaged in 1000 mg (1.0 g) quantities per cartridge, which can effectively replace the two-column tandem assembly with a single column.

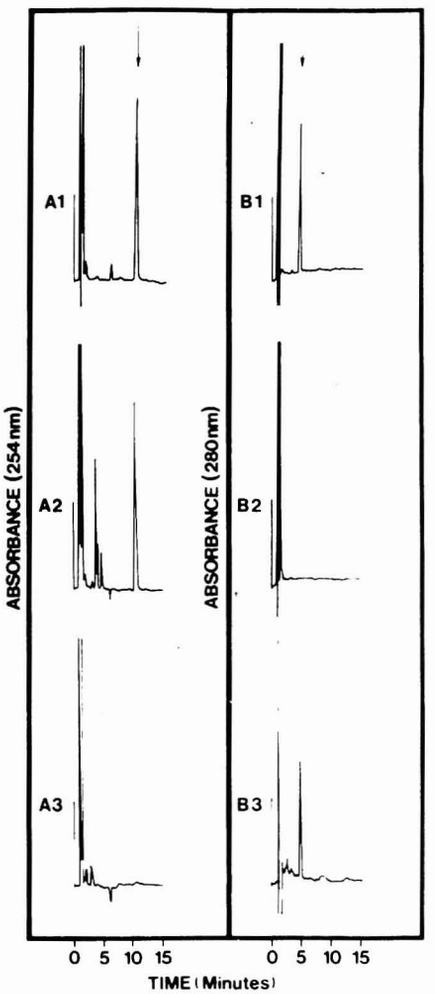

Figure 2. Chromatograms of picloram (A1) 44.2 ng and 2,4-D (B1) 46.5 ng standards; the first fraction desorbed by 25% acetic acid (A2 and B2); the second fraction desorbed by methanol (A3 and B3). The "A" chromatograms were obtained under conditions appropriate for the detection of picloram and the "B" chromatograms for 2,4-D.

Because picloram and 2,4-D differ sufficiently in hydrophobicity, selective desorption of the individual compounds from the extraction sorbent is possible. Variation in solvent eluotropic strength is utilized in the technique presented here to accomplish preferential desorption of the solutes picloram and 2,4-D when simultaneously sorbed on an extraction column. Figure 2 illustrates the chromatographic results. The chromatograms A1 and B1 depict the elution of picloram and 2,4-D standards obtained under the conditions of isocratic mobile-phase composition and detector wavelength appropriate for each component. The four remaining chromatograms, A2, B2, A3, and B3, all stem from a single 200-mL distilled water sample that was spiked with 50 ppb each of picloram and 2,4-D. A2 and B2 are chromatograms of the same elution fraction (i.e., the first desorption with 25% acetic acid) injected under the proper conditions for detecting picloram (A2) or 2,4-D (B2). A3 and B3 are chromatograms of the second fraction eluted with methanol and chromatographed under conditions appropriate for picloram (A3) or 2,4-D (B3). The figure clearly shows that picloram and 2,4-D are cleanly separated in a serial elution by 25% acetic acid followed by methanol from the reversed-phase sorbent. No 2,4-D is detected (B2) in the picloram-containing fraction (25% HOAc) nor is picloram detected (A3) in the 2,4-D-containing fraction (MeOH).

Figure 3 illustrates results typical of natural stream water samples. The chromatograms C1 and D1 depict the elution of picloram and 2,4-D standards obtained under the conditions

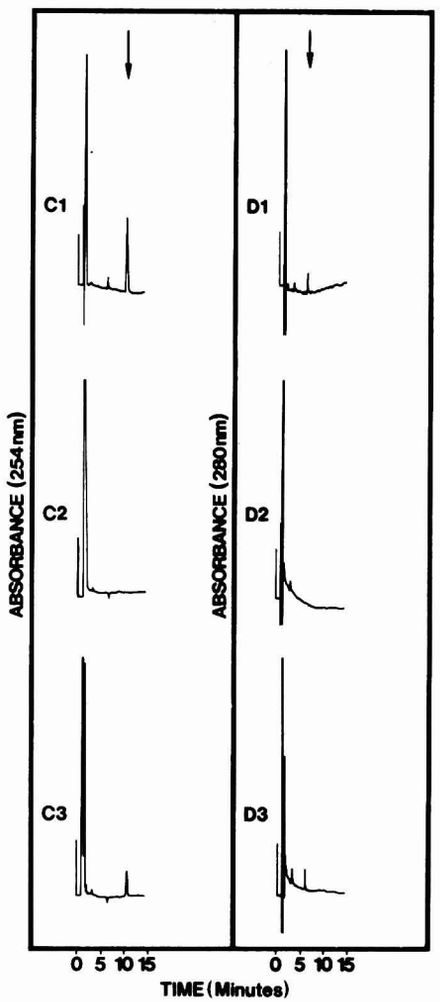

Figure 3. Chromatograms of picloram (C1) 67.5 ng and 2,4-D (D1) 22.9 ng standards; an unfortified natural water sample serially desorbed first by 25% acetic acid (C2) followed by methanol (D2); a fortified natural water sample serially desorbed first by 25% acetic acid (C3) followed by methanol (D3). The "C" chromatograms were obtained under conditions appropriate for the detection of picloram and the "D" chromatograms for 2,4-D.

of isocratic mobile-phase composition and detector wavelength appropriate for each component. The center chromatograms in Figure 3, C2 and D2, demonstrate the background absorbance from an unfortified natural water sample serially desorbed first by 25% acetic acid (C3) followed by methanol (D3). The lower pair of chromatograms in Figure 3, C3 and D3, portray the recovery of picloram and 2,4-D, respectively, from a 200-mL natural water sample that was fortified with 24.3 ppb of each of these two herbicides.

The two-stage desorption of aqueous samples (200 mL) simultaneously spiked with picloram and 2,4-D at four fortification levels (250, 50, 25, and 5 ppb) yielded an overall recovery level of 98.2% (3.9% standard deviation) for picloram and 91.9% (10.7% standard deviation) for 2,4-D (Table I). Single-stage desorption by the solvent of greater eluting strength (i.e., MeOH) produces equivalent recoveries of each solute into the same fraction. However, collecting picloram and 2,4-D into the same fraction from the reversed-phase solid-phase extraction column also includes coeluting contaminants that would have retention times longer than that of picloram and shorter than that of 2,4-D on the reversed-phase analytical column. The elution order of picloram and 2,4-D from a reversed-phase analytical column is analogous to the desorption order from a reversed-phase solid-phase extraction column. Therefore, complete separation of the two components is desirable because it improves the subsequent analytical results.

Table I. Recovery of Variable Molar Amounts of Picloram and 2,4-D from Fortified Water Samples of Constant Volume (200 mL)

		% average recovery	
fortification, ppb	n	2,4-D	picloram
5.0	2	96	102
25.0	3	91.7	101.1
50.0	4	88.2	97.2
250.0	3	94.4	94.1
	overall	91.9	98.2
	SD	10.7	3.9

[a] There is no statistical difference among the means for recovery of 2,4-D or picloram ($\alpha = 0.01$) by Tukey's Studentized range test (HSD).

Registry No. 2,4-D, 94-75-7; picloram, 1918-02-1; H_2O, 7732-18-5.

LITERATURE CITED

(1) Wells, M. J. M. "General Procedures for the Development of Adsorption Trapping Methods used in Herbicide Residue Analysis". In *Proceedings of the Second Annual International Symposium on Sample Preparation and Isolation Using Bonded Silicas*; Analytichem International: Harbor City, CA, 1985.
(2) Wells, M. J. M. "Off-line Multistage Extraction Chromatography for Ultraselective Herbicide Residue Isolation". In *Proceedings of the Third Annual International Symposium on Sample Preparation and Isolation Using Bonded Silicas*; Analytichem International: Harbor City, CA, 1986.
(3) Rostad, C. E.; Pereira, W. E.; Ratcliff, S. M. *Anal. Chem.* **1984**, *56*, 2856–2860.
(4) Renberg, L.; Lindstrom, K. *J. Chromatogr.* **1981**, *214*, 327–334.
(5) Steinheimer, T. R.; Ondrus, M. G. *Anal. Chem.* **1986**, *58*, 1839–1844.
(6) Chladek, E.; Marano, R. S. *J. Chromatogr. Sci.* **1984**, *22*, 313–320.
(7) Chladek, E.; Marano, R. S. "Use of Bonded Phase Silica Sorbents for the Sampling of Priority Pollutants in Wastewaters". In *Proceedings of the Second Annual International Symposium on Sample Preparation and Isolation Using Bonded Silicas*; Analytichem International: Harbor City, CA, 1985.
(8) Benjamin, J. "Use of Bonded Silica Sorbents for Selective Isolation of PAH and PCB at Low Level in Various Water Samples"; In *Proceedings of the Second Annual International Symposium on Sample Preparation and Isolation Using Bonded Silicas*; Analytichem International: Harbor City, CA, 1985.
(9) Saner, W. A.; Jadamec, J.R.; Sager, R. W.; Killeen, T. J. *Anal. Chem.* **1979**, *51*, 2180–2188.
(10) Puyear, R. L.; Fleckenstein, K. J.; Montz, W. E., Jr.; Brammer, J. D. *Bull. Environ. Contam. Toxicol.* **1981**, *27*, 790–797.
(11) Andrews, J. S.; Good, T. J. *Am. Lab. (Fairfield, Conn.)* **1982**, *14*, 70, 73–75.
(12) Spalik, J.; Janauer, G. E.; Lau, M.; Lemley, A. T. *J. Chromatogr.* **1982**, *253*, 289–294.
(13) Bushway, R. J. *J. Chromatogr.* **1981**, *211*, 135–143.
(14) Jones, A. S.; Jones, L. A.; Hastings, F. L. *J. Agric. Food Chem.* **1982**, *30*, 997–999.
(15) Ahmad, I. *J. Assoc. Off. Anal. Chem.* **1983**, *66*, 663–666.
(16) Badesso, R. J. "Solid Phase Extraction of Herbicides from Aqueous and Solid Samples". In *Proceedings of the Second Annual International Symposium on Sample Preparation and Isolation Using Bonded Silicas*; Analytichem International: Harbor City, CA, 1985.
(17) West, S. D.; Day, E. W., Jr. *J. Assoc. Off. Anal. Chem.* **1981**, *64*, 1205–1207.
(18) West, S. D.; Parka, S. J. *J. Agric. Food Chem.* **1981**, *29*, 223–226.
(19) Nyagah, G. *J. Chromatogr. Sci.* **1981**, *19*, 500–502.
(20) Hoke, S. H.; Brueggemann, E. E.; Baxter, L. J.; Trybus, T. *J. Chromatogr.* **1986**, *357*, 429–432.
(21) Sherma, J. *J. Liq. Chromatogr.* **1986**, *9*, 3433–3438.
(22) Steinheimer, T. R.; Brooks, M. G. *Int. J. Environ. Anal. Chem.* **1984**, *17*, 97–111.
(23) *Fed. Regist.* **1986**, *51*, 37608–37612.
(24) Chau, A. S. Y.; Afghan, B. K. *Analysis of Pesticides in Water. Vol. 1. Significance, Principles, Techniques, and Chemistry of Pesticides*. CRC Press, Inc.: Boca Raton, Florida, 1982.
(25) Elgar, K. E. "Pesticide Residues in Water—An Appraisal". In *Pesticide Chemistry: Human Welfare and the Environment. Vol. 4. Pesticide Residues and Formulation Chemistry*; Greenhalgh, R., Drescher, N., Eds.; Pergamon: New York, 1982.
(26) Nash, R. G.; Wells, M. J. M.; Smith, A. E.; Van Wambeke, E. "Pesticide Residues In Environmental Samples". In *Analytical Methods for Pesticides and Plant Growth Regulators*; Zweig, G., Sherma, J., Eds.; Academic: Orlando, FL, 1986; Vol. XV.

RECEIVED for review June 30, 1986. Resubmitted February

17, 1987. Accepted February 26, 1987. Methods development described in this paper was funded in part by the National Agricultural Pesticide Impact Assessment Program. The use of trade, firm, or corporation names in this publication is for the information and convenience of the reader. Such use does not constitute an official endorsement or approval by the U.S. Department of Agriculture of any product or service to the exclusion of others which may be suitable.

Design and Evaluation of a Capillary Gas Chromatography–Atomic Absorption Spectrometer Interface

Donald S. Forsyth

Food Research Division, Food Directorate, Health Protection Branch, Ottawa, Ontario, Canada K1A 0L2

Quartz tube atomizers have been frequently used in organometallic speciation studies (*1–4*). A variety of tube material (*5, 6*), heating methods (*6, 7*), and interfaces (*4, 5, 8*) have been reported, but few systematic studies to improve the quartz tube atomizer, particularly the gas chromatographic interface, have been done.

Tubal dimensions should minimize analyte dilution before reaching the optical pathway of the atomic absorption spectrophotometer, yet maximize residence time in the light pathway. Ebdon et al. (*6*) found that a long narrow tube configuration gave the best sensitivity. Several studies have shown that H_2 enhances sensitivity (*1, 4, 9*), likely by hydrogen radicals (formed by catalytic activity of the quartz surface (*7*)) mediating analyte atomization (*4, 9*).

A gas chromatograph (GC)–atomic absorption spectrometer (AAS) interface should (a) preserve and transport the analyte compounds to the atomization region of the furnace in a minimum gas volume and (b) introduce the furnace support gases; this allows the use of a simple quartz T-tube design.

The purpose of this study was to improve an existing interface design (*4*) to allow efficient coupling of a capillary column to the quartz T-tube atomizer.

EXPERIMENTAL SECTION

Apparatus. The analytical system was assembled with a Varian 3400 gas chromatograph (GC), a quartz furnace (assembled at Health and Welfare Canada), an Instrumentation Laboratory Model 751 atomic absorption spectrometer (AAS), and a recording integrator (Varian Model 4270).

The GC was equipped with a split/splitless injector and a 15 m × 0.32 mm DB-5 fused silica column (J&W Scientific, Inc.). Operating conditions were as follows: carrier gas, helium, 1.5 mL min^{-1}; injector temperature, 200 °C, splitless mode, 1 min post-injection solvent vent at 30 mL min^{-1}, temperature program isothermal at 50 °C for 1 min followed by linear ramping at 10 °C min^{-1} to 175 °C (held for 0.5 min).

About 60 cm of the fused silica column was extended from the GC oven to the AAS through an insulated, heated $^1/_4$ in. (0.64 cm) o.d. copper transfer tube. The transfer tube temperature (200 °C) was maintained by a heating tape (Cole Palmer Co.), which was controlled by a time proportional temperature controller (Model 6100, Omega Engineering, Inc.). The temperature was monitored by a digital temperature indicator (Model 115, Omega Engineering, Inc.).

The atomic absorption spectrometer was equipped with a Pb hollow cathode lamp (IL Visimax). Operating conditions were as follows: hollow cathode lamp current, 3 mA; wavelength, 283.3 nm; band-pass, 0.5 nm; photomultiplier tube voltage, 700 V; single beam mode.

The quartz furnaces (Figure 1 and Figure 1 of ref 4) consisted of a quartz T-tube (upper tube 10 cm × 9 mm o.d., 7 mm i.d.; lower tube 4 cm × 6.25 mm o.d., 4 mm i.d.) heated electrically with 3.1 m of 25 gauge Chromel 875 resistance wire (Hoskins Alloys of Canada) coiled around the upper tube (furnace A, Figure 1, ref 4) or with 6.7 m of 26 gauge Chromel 875 wire coiled and embedded into the two refractory brick sections (furnace B, Figure 1) with refractory cement (Alundum cement, Fisher Sci. Co.). A layer of Fiberfrax ceramic fiber (The Carborundum Co.) insulated the quartz tube in furnace A, whereas none was used in furnace B. Insulation was removed around the inlet region of furnace A for air circulation. In furnace B, the insulation and heating elements were extended to the edge of the detector casing. The four Swagelok $^1/_8$ in. (0.32 cm) NPT to $^1/_8$ in. (0.32 cm) tube connections were mounted in the furnace casing (11 cm × 4.8 cm o.d., 4 cm i.d.) as ports for electrical connections to the heating elements and to position two type K (chromel–alumel) thermocouples. Ceramic tubing (Omega Engineering, Inc.) mounted within the Swagelok connectors was used as electrical insulation. The furnace casing was held together with an aluminum mounting bracket. The furnace was positioned within the optical path of the AAS by an adjustable ball joint affixed to the mounting bracket.

Furnace temperature was controlled by a Model 6100 proportional temperature controller (Omega Engineering, Inc.) and monitored by a digital temperature indicator (Model 115, Omega Engineering, Inc.).

The interface between the capillary column and the quartz furnace utilized readily available parts (Figure 2, ref 4). A $^1/_4$ in. (0.64 cm) to $^1/_8$ in. (0.32 cm) Swagelok reducing union, modified with an attached $^1/_{16}$ in. (0.16 cm) stainless steel tubing gas inlet (E, Figure 2, ref 4), positioned either a section of ceramic tubing (8 cm × $^1/_8$ in. (0.32 cm) o.d., $^1/_{16}$ in. (0.16 cm) i.d.) or quartz tube lined ceramic insert within the lower tube of the quartz furnace. A $^1/_8$ in. (0.32 cm) to $^1/_{16}$ in. (0.16 cm) Swagelok reducing union similarly modified with an attached $^1/_{16}$ in. (0.16 cm) stainless steel tubing gas inlet (J, Figure 2, ref 4) was mounted to the ceramic tube/insert as a gas tight connection for the capillary column. The quartz tube lined ceramic inserts were constructed from 0.53 mm deactivated fused silica (J&W Scientific, Inc.) centered within the ceramic tube with refractory cement (Alundum cement, Fisher Scientific Co.) and the interspace was sealed with sodium silicate.

Three interfaces were examined. Interface I used the ceramic tube. The end of the GC column was positioned 5 mm in front of the ceramic tube, at the T-tube junction.

Interface II used a ceramic insert which was 8 cm long (ceramic tube) with the fused silica extending out 5 mm from both ends. The tip of the insert was positioned at the T-tube junction. The GC column was backed up 6–7 mm from the tip, just outside the insulated region of the furnace.

Interface III used a ceramic insert which was 6.5 cm long (ceramic tube) with the fused silica extending out 17 mm at the end inserted into the furnace with 5 mm of fused silica at the other end. The 5-mm extension of fused silica at the GC column end of the insert simplified insertion of the 0.32-mm fused silica column through the insert. The air inlet (G, Figure 2, ref 4) was sealed and the air introduced by routing both the H_2 and air through a tee union into the H_2#1 inlet. The insert tip was positioned at the T-tube junction. The end of the GC column was positioned 18–19 mm from the tip, just outside the insulated (and heated) region of furnace type B.

A timed furnace gas purge cycle was controlled by the GC electronics (Figure 2). The H_2 flow (45 mL min^{-1}) to H_2#1 inlet of the GC–AAS interface was vented to a fume hood for the initial

0003-2700/87/0359-1742$01.50/0 Published 1987 by the American Chemical Society

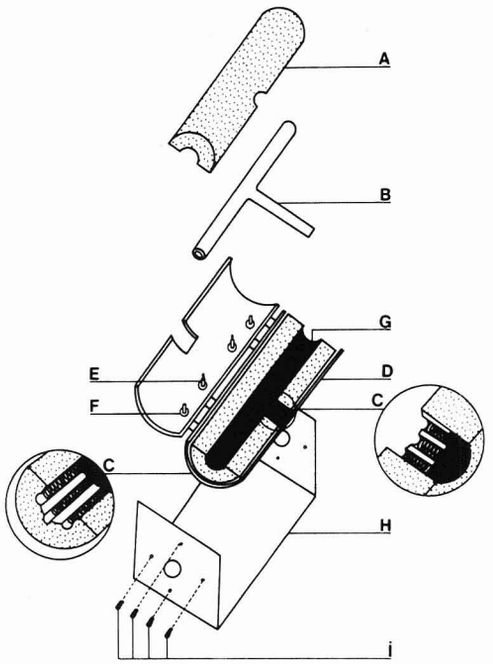

Figure 1. Exploded view of quartz T-tube furnace: A, shaped firebrick, upper casing; B, quartz T-tube; C, Alloy 875 wire embedded within the firebrick; D, hinged aluminum casing; E, type K thermocouples; F, Swagelok connectors with ceramic tubing inserts; G, shaped firebrick with refractory cement covering heating elements; H, aluminum mounting bracket; I, machine (6-32) screws.

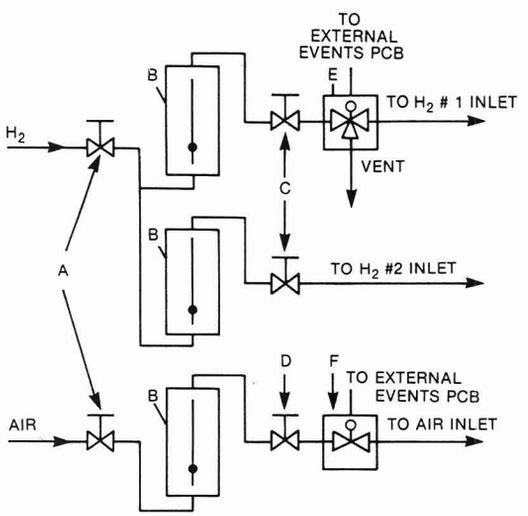

Figure 2. GC–AAS interface pneumatic schematic: A, toggle shut-off valves; B, gas rotameters; C, flow controllers; D, metering valve; E, three-way solenoid valve; F, two-way solenoid valve.

2 min of the chromatographic run by using a three-way solenoid valve (Asco Model U83251). Air entered the furnace at 200 mL min^{-1} during this period via a two-way solenoid valve (Asco Model U82252). After 2 min, the air solenoid was deactivated, shutting off the air flow entering the furnace. Hydrogen (30 mL min^{-1}) also entered the furnace continuously through the H_2#2 inlet of the GC–AAS interface to sweep the lower tube void volume.

Reagents. All compressed gases were prepurified grade or better with the exception of the air (medical grade). Gas flow rates were measured by soap bubble flowmeter. A solution containing trimethylbutyllead (4.6×10^{-6} g mL^{-1}), dimethyldibutyllead (4.6×10^{-6} g mL^{-1}), triethylbutyllead (2.5×10^{-6} g mL^{-1}), and diethyldibutyllead (2.5×10^{-6} g mL^{-1}) in isooctane was used. The alkylbutyllead standards were previously synthesized (*4*).

Procedure. Furnace A was tested with interfaces I and II. Furnace B was tested with interface III. The furnace temperature was varied from 900 to 1200 °C in 100 °C increments. Quadruplicate sample injections (1 μL) were performed by hand. Peak area and peak height were recorded.

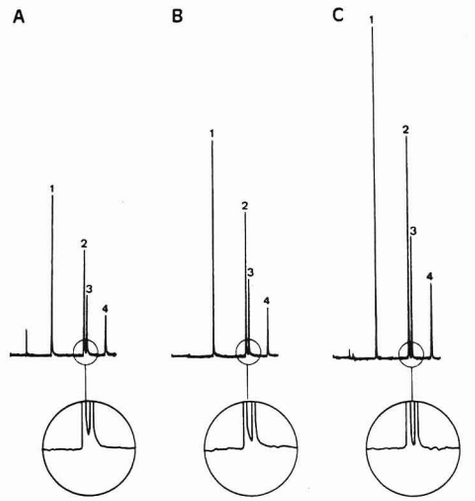

Figure 3. GC–AAS chromatograms of: (1) Me_3BuPb, (2) Me_2Bu_2Pb, (3) Et_3BuPb, and (4) Et_2Bu_2Pb with A, interface I and furnace A; B, interface II and furnace A; C, interface III and furnace B. Furnace Temperature was 900 °C.

RESULTS AND DISCUSSION

The furnace A and interface type I combination produced generally the lowest analyte response and largest area to height ratio (an approximation of half height peak width(s)). Peak tailing was clearly present (Figure 3A) at 900 °C indicating analyte interaction somewhere in the chromatographic system. Preliminary work using a ^{63}Ni electron capture detector produced symmetrical peaks, so the problem was likely in the GC–AAS interface. Previous work with a similar furnace and interface (*4*) showed better response and minimal analyte tailing when used with a packed column (flow rate 35 mL min^{-1}) connected to a short section of fused silica column transfer line. The linear velocity through the GC–AAS interface in that system (ca. 700 cm s^{-1}) was much greater than that with the capillary column (ca. 31 cm s^{-1}) in the present system. Lower linear velocity may enhance analyte decomposition outside the atomization region of the furnace. Increasing the furnace temperature enhanced peak area response and improved peak shape, but no maxima were observed within the operating limits of the furnace (Figure 4A). Sustained operation above 1000 °C would also be detrimental to the heating element and particularly the thermocouple lifespan.

The furnace A and interface II combination improved system performance slightly (Figure 3B). The linear velocity of the analytes through the GC–AAS interface was increased to ca. 350 cm s^{-1} by mixing the effluent of the GC capillary column (positioned within the interface just outside the heated region of furnace A) with the H_2 flow (45 mL min^{-1}) entering through the H_2#1 inlet. Although some peak area enhancement occurred at 900 °C, performance at higher temperatures was similar to interface I (Figure 4B). Peak shape, however, noticeably improved (Figure 3B) with decreased area to height ratio values (Figure 4B). Sample effluent linear velocity is, therefore, a factor in system performance. However, the improvement in peak area response with increasing furnace temperature suggested that another factor was involved.

Many organometallic compounds decompose at temperatures much below the volatilization temperature of the elemental metal (*9*). It was, therefore, important to have the temperature gradient (from transfer to atomization temperatures) over a minimal distance along the lower tube of the furnace to prevent premature decomposition. The removal of insulation around the inlet region of furnace A allowed air circulation but produced a large surface area which radiated heat, reducing the lower tube temperature gradient. Increasing

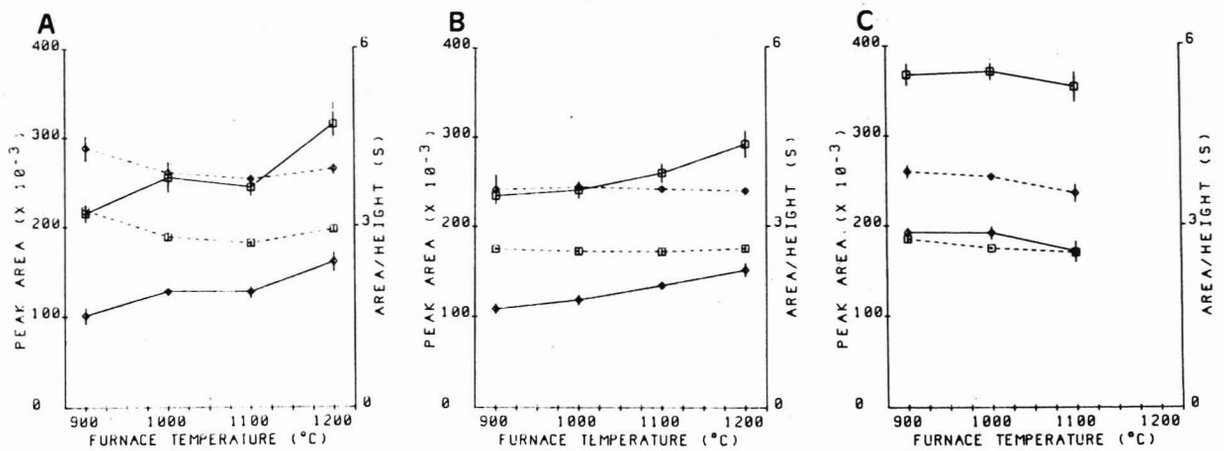

Figure 4. Response of (——) peak area and (- - -), area to height ratio of (□) Me_3BuPb and (◇) Et_3BuPb to changes in furnace temperature with A, interface I and furnace A; B, interface II and furnace A and C, interface III and furnace B. Error bars represent ±1 standard deviation of four replicate determinations.

the furnace A temperature likely enhanced the temperature gradient, resulting in improved peak area response.

The furnace B–interface III combination produced the largest peak area response (Figure 4C) and minimum peak tailing (Figure 3C). System sensitivity was very similar to earlier work (*4*) even though the less sensitive 283.3-nm lead line was used. The peak area response did not increase with furnace temperature (although the area to height ratio did improve slightly) (Figure 4C) indicating that the furnace temperature was not a critical parameter. In furnace B, the extension of the insulation and heating elements to the edge of the detector casing (in the lower tube region) allowed the insulation–air interface to form a temperature gradient along the lower tube of the furnace. Also, lower tube exposure to radiated heat prior to entry into the heated zone of the furnace was minimized by eliminating the large exposed insulation surface area present in furnace A. Since furnace temperature had little effect on system performance, the temperature gradient was optimized. A lower furnace operating temperature could, therefore, be used ensuring better system reliability.

However, optimizing the lower tube temperature gradient resulted in approximately 15 mm of the lower tube being heated to atomization temperatures. As the analytes could no longer be preserved for atomization in the upper tube of the quartz T-tube furnace, interface III was designed to act as an in situ hydride generator. Lead hydrides were produced when the analytes (mixed with H_2) passed through the quartz tube of ceramic insert B at furnace temperatures via reactions proposed in previous studies (*4*, *9*). The lead hydrides then entered the optical pathway of the AAS. Also, the ceramic insert quartz tube has little thermal mass, minimizing thermal conduction to cooler parts of the interface.

The life span of the quartz T-tube in furnace B was approximately 300–400 h because the alumina cement caused extensive recrystallization. However, if the heating elements were held with small deposits of alumina or silicate cement rather than being totally embedded, the T-tube life span would likely be greatly increased.

Metallic lead and/or carbonaceous deposits were noted at the tip of the capillary column in interface I and the quartz tip of interface II. Deposits in the interface or furnace may cause a slow degradation of system response. However, the timed purging of the inner surface of the quartz tube of the ceramic insert in interface III with air prevented the deposition. Elimination of deposits within the system should minimize routine maintenance requirements in automated operation.

The quartz T-tube furnace and GC–AAS interface previously reported (*4*) are not suitable for use with capillary gas chromatography. In the present work, design features that improved system performance were (a) extension of the heating elements to the edge of the detector casing (enhanced the temperature gradient along the lower tube), (b) addition of a heated quartz lined ceramic insert (acted as an in situ hydride generator), and (c) transference of the analytes as hydrides into the upper tube of the quartz T-tube. Also, automated air purging of the interface eliminated deposition formation during prolonged system usage. The GC–AAS system will be further characterized and applications for other organometallic compounds examined.

ACKNOWLEDGMENT

The author thanks J. F. Lawrence and J. J. Ryan for helpful discussions during the preparation of the manuscript and P. L'Abbé (National Research Council, Ottawa, Canada) for providing glassblowing services.

Registry No. Me_3BuPb, 54964-75-9; Me_2Bu_2Pb, 65151-01-1; Et_3BuPb, 64346-32-3; Et_2Bu_2Pb, 65121-94-0.

LITERATURE CITED

(1) Chakraborti, D.; De Jonghe, W. R. A.; Van Mol, W. E.; Van Cleuvenbergen, R. J. A.; Adams, F. C. *Anal. Chem.* **1984**, *56*, 2692–2697.
(2) Chau, Y. K.; Wong, P. T. S.; Kramar, O. *Anal. Chim. Acta* **1983**, *146*, 211–217.
(3) Chau, Y. K.; Wong, P. T. S.; Bengert, G. A.; Dunn, J. L. *Anal. Chem.* **1984**, *56*, 271–274.
(4) Forsyth, D. S.; Marshall, W. D. *Anal. Chem.* **1985**, *57*, 1299–1305.
(5) Chau, Y. K.; Wong, P. T. S.; Goulden, P. D. Proceedings of the International Conference on Heavy Metals in the Environment, 1975, Toronto, Vol. 1, pp 295–302.
(6) Ebdon, L.; Ward, R. W.; Leathard, D. A. *Analyst (London)* **1982**, *107*, 129–143.
(7) Welz, B.; Melcher, M. *Analyst (London)* **1983**, *108*, 213–224.
(8) Van Loon, J. C.; Radziuk, B. *Can. J. Spectrosc.* **1976**, *21*, 46–50.
(9) Parris, G. E.; Blair, W. R.; Brinckman, F. E. *Anal. Chem.* **1977**, *49*, 378–386.

RECEIVED for review December 29, 1986. Accepted March 25, 1987.

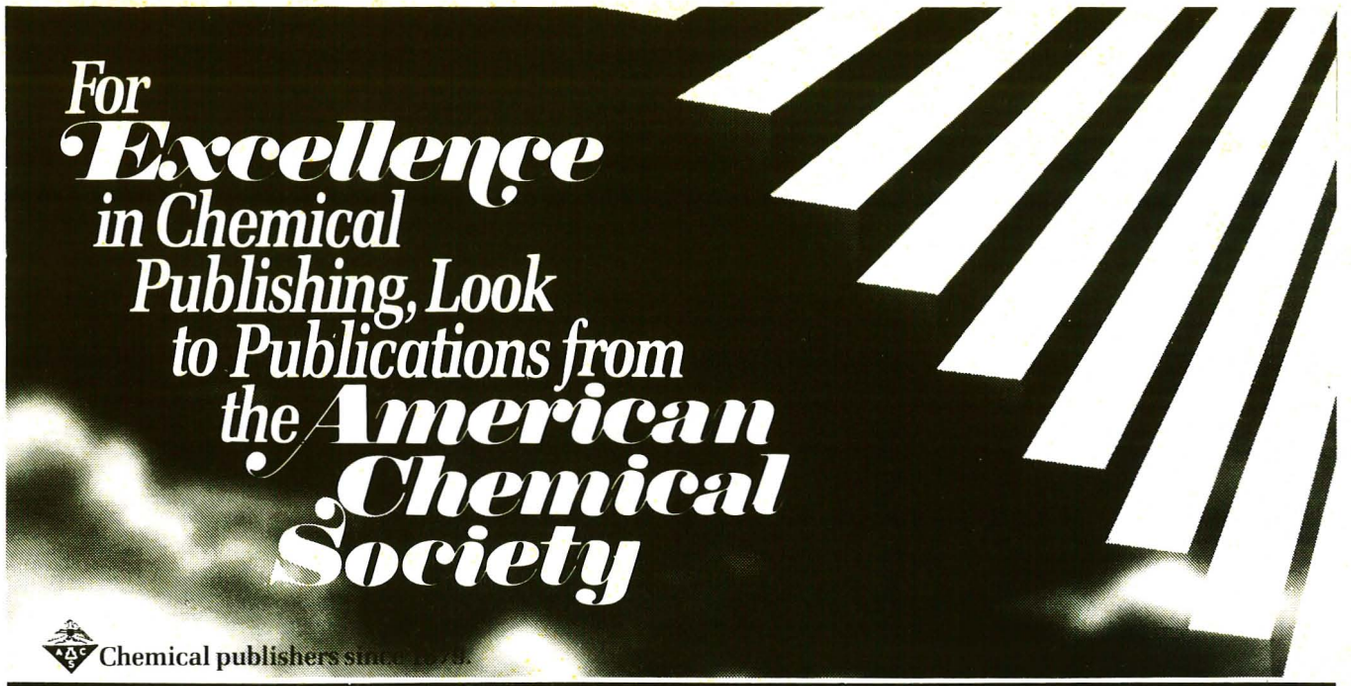

❑ ACCOUNTS OF CHEMICAL RESEARCH
Editor, F.W. McLafferty
Cornell University
12 issues a year. ISSN 0001-4842
Member $23 Nonmember $99

❑ ANALYTICAL CHEMISTRY
Editor, George H. Morrison
Cornell University
24 issues a year. ISSN 0003-2700
Member $25 Nonmember $37

❑ BIOCHEMISTRY
Editor, Hans Neurath
University of Washington
26 issues a year. ISSN 0006-2960
Member $75 Nonmember $386

❑ CHEMICAL & ENGINEERING NEWS
Editor, Michael Heylin
51 issues a year. ISSN 0009-2347
Nonmember $44

❑ CHEMICAL REVIEWS
Editor, Josef Michl
University of Texas
6 issues a year. ISSN 0009-2665
Member $22 Nonmember $99

❑ CHEMTECH
Editor, Benjamin J. Luberoff
12 issues a year. ISSN 0009-2703
Member $34 Nonmember (Pers.) **$44**
Nonmember (Inst.) **$244**

❑ ENERGY & FUELS
Editor, John W. Larsen
Lehigh University
6 issues a year. ISSN 0887-0624
Member $46 Nonmember $269

❑ ENVIRONMENTAL SCIENCE & TECHNOLOGY
Editor, Russell F. Christman
University of North Carolina, Chapel Hill
12 issues a year. ISSN 0013-936X
Member $30 Nonmember (Pers.) **$45**
Nonmember (Inst.) **$176**

❑ INDUSTRIAL & ENGINEERING CHEMISTRY RESEARCH
Editor, Donald R. Paul
University of Texas, Austin
12 issues a year. ISSN 0888-5885
Member $52 Nonmember $286

❑ INORGANIC CHEMISTRY
Editor, M. Frederick Hawthorne
University of California, Los Angeles
26 issues a year. ISSN 0020-1669
Member $79 Nonmember $422

❑ JOURNAL OF AGRICULTURAL AND FOOD CHEMISTRY
Editor, Irvin E. Liener
University of Minnesota
6 issues a year. ISSN 0021-8561
Member $24 Nonmember $126

❑ JOURNAL OF THE AMERICAN CHEMICAL SOCIETY
Editor, Allen J. Bard
University of Texas
26 issues a year. ISSN 0002-7863
Member $70 Nonmember $350

❑ JOURNAL OF CHEMICAL AND ENGINEERING DATA
Editor, Bruno J. Zwolinski
Texas A&M University
4 issues a year. ISSN 0021-9568
Member $29 Nonmember $160

Call Toll Free (U.S.)

800-424-6747

Telex: 440159 ACSP UI or
892582 ACSPUBS
Cable Address: JIECHEM
Telecopier (SANYO Group 1,2,3): 202-872-4615

American Chemical Society
Marketing Communications Department
1155 Sixteenth St., N.W.
Washington, D.C. 20036
U.S.A.

❑ JOURNAL OF CHEMICAL INFORMATION AND COMPUTER SCIENCES
Editor, Thomas L. Isenhour
Utah State University
4 issues a year. ISSN 0095-2338
Member $17 Nonmember $90

❑ JOURNAL OF MEDICINAL CHEMISTRY
Editor, Philip S. Portoghese
University of Minnesota
12 issues a year. ISSN 0022-2623
Member $40 Nonmember $208

❑ THE JOURNAL OF ORGANIC CHEMISTRY
Editor, Frederick D. Greene
Massachusetts Institute of Technology
26 issues a year. ISSN 0022-3263
Member $53 Nonmember $276

❑ JOURNAL OF PHYSICAL AND CHEMICAL REFERENCE DATA
Editor, David R. Lide, Jr.
National Bureau of Standards
4 issues a year. ISSN 0047-2689
Member $55 Nonmember $240

❑ THE JOURNAL OF PHYSICAL CHEMISTRY
Editor, Mostafa A. El-Sayed
University of California, Los Angeles
26 issues a year. ISSN 0022-3654
Member $65 Nonmember $387

❑ LANGMUIR
Editor, Arthur W. Adamson
University of Southern California
6 issues a year. ISSN 0743-7463
Member $55 Nonmember $329

❑ MACROMOLECULES
Editor, Field H. Winslow
AT&T Bell Laboratories
12 issues a year. ISSN 0024-9297
Member $53 Nonmember $306

❑ ORGANOMETALLICS
Editor, Dietmar Seyferth
Massachusetts Institute of Technology
12 issues a year. ISSN 0276-7333
Member $55 Nonmember $330

❑ SINGLE ARTICLE ANNOUNCEMENT
24 issues a year. ISSN 0044-7587
Member $63 Nonmember $126

Rates listed are for 1987 U.S. subscriptions. For subscription rates outside the U.S., contact American Chemical Society or your subscription agency. Member rates are for personal use only. For nonmember subscriptions in Japan, write Maruzen Co., Ltd.

For the Most Efficient Means of Nitrogen/Protein Analysis, Look for the

LECO® FP-228 Nitrogen/ Protein Determinator

- **Rapid analysis - 160 seconds or less**
- **No toxic or corrosive reagents required**
- **Direct result display as nitrogen or protein**
- **Built-in printer for permanent records**
- **Self-diagnostics for minimum downtime**

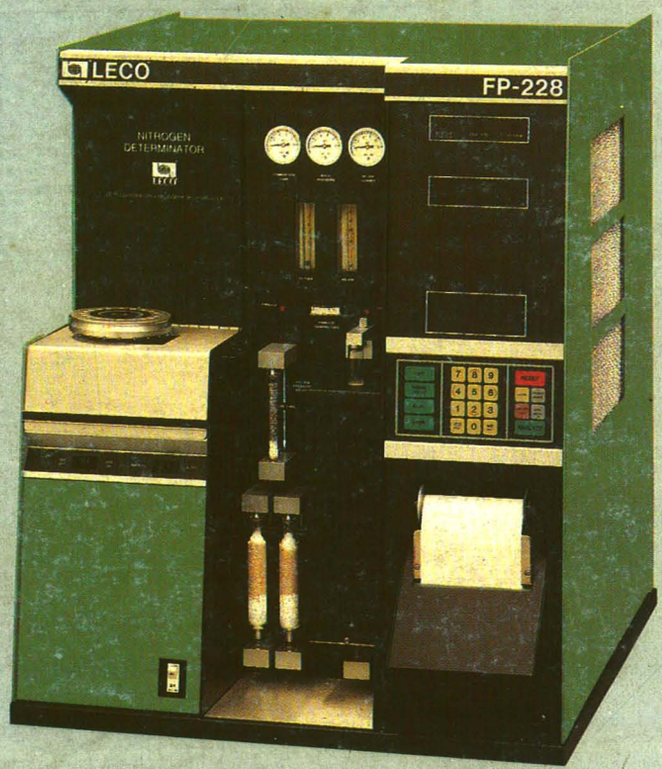

The **LECO®** FP-228 Nitrogen/Protein Determinator is designed to handle a wide variety of materials, from grains, stock feed, and meat, to fertilizer, rubber and soil. The FP-228 has unsurpassed accuracy, speed, and ease of operation. Protein or nitrogen is reliably determined with an accuracy of ±2% or better. After the sample has been weighed, the fully automatic analysis requires no further attention from the operator. The encapsulated sample is combusted in oxygen in the resistance furnace. The products of combustion are carried through scrubbers to a thermal conductivity cell for measurement. The final result is directly displayed and printed as percent nitrogen or percent protein, as selected. Analysis requires only 160 seconds. The instrument is programmed to compensate for the moisture content of the sample when it is known. Calibration is quickly performed, automatically calculated and very stable. Sensitive blank determination promotes accuracy. Self-diagnostics keep downtime to a minimum. A 19 or 49 sample-capacity automatic sample carousel is available for unattended operation to increase operator efficiency and daily sample throughput.

For full details regarding this new LECO® instrument, call or write today!

LECO CORPORATION
3000 Lakeview Avenue
St. Joseph, MI 49085-2396 U.S.A.

Phone: (616) 983-5531
Telex: 211605
Facsimile: (616) 983-3850

LECO® ***PRODUCTS FOR EARTH SCIENCE***

CIRCLE 90 ON READER SERVICE CARD